SAPIENZA

University of Rome

PhD Programme in Life Sciences

XXXII cycle

Different Strategies to Target the Epigenome

Daniela Tomaselli

Tutor and Supervisor
Prof. Antonello Mai

Coordinator
Prof. Marco Tripodi

Director of PhD program

Professor **Marco Tripodi** Ph.D.
Department of Cellular Biotechnology and Heamatology, "Sapienza" University of Rome, P.le Aldo Moro, 5 - 00185 – Rome, Italy.

Supervisors

Professor **Antonello Mai** Ph.D. (tutor and main supervisor)
Department of Drug Chemistry and Technology, "Sapienza" University of Rome, P.le Aldo Moro, 5 - 00185 – Rome, Italy.

Professor **Alessio Ciulli** Ph.D. (foreign supervisor)
School of Life Sciences, University of Dundee, Dow Street - DD1 5EH – Dundee, Scotland, United Kingdom.

LIST OF PUBLICATIONS:

1. Carafa, V.; Poziello, A.; Della Torre, L.; Giovannelli, P.; Di Donato, M.; Safadeh, E.; Yu, Z.; Baldi, A.; Castoria, G.; **Tomaselli, D.**; Mai, A.; Rotili, D.; Nebbioso, A.; Altucci, A. Enzymatic and biological characterization of novel sirtuin modulators against cancer. *J. Exp. Clin. Cancer Res.*, **2019**. doi: 10.3390/ijms20225654

2. Monaldi, D.; Rotili, D.; Lancelot, J.; Marek, M.; Wössner, N.; Lucidi, A.; **Tomaselli, D**.; Ramos-Morales, E.; Romier, C.; Pierce, R.; Mai, A.; Jung, M. Structure-Reactivity Relationships on Substrates and Inhibitors of the Lysine Deacylase Sirtuin 2 from Shistosoma Mansoni (SmSIRT2). *J. Med. Chem*, **2019**. doi: 10.1021/acs.jmedchem.9b00638

3. **Tomaselli, D**.; Lucidi, A.; Rotili, D.; Mai, A. Epigenetic polypharmacology: A new frontier for epi-drug discovery. *Med. Res. Rev.*, **2019**, doi: 10.1002/med.21600

4. Lucidi, A.; **Tomaselli, D.**; Rotili, D.; Mai, A. Book: The DNA, RNA, and Histone Methylomes, Title of the Chapter: DNA Methylation: Biological Implications and Modulation of Its Aberrant Dysregulation. *Springer Editor*, **2019**, doi: 10.1007/978-3-030-14792-1_12

5. Nocentini, A.; Lucidi, A; Perut, F.; Massa, A.; **Tomaselli, D.**; Gratteri, P.; Baldini, N.; Rotili, D.; Mai, A.; Supuran, CT. α,γ-Diketocarboxylic Acids and Their Esters Act as Carbonic Anhydrase IX and XII Selective Inhibitors. *ACS Med. Chem. Lett.*, **2019**, 10(4):661-665. doi: 10.1021/acsmedchemlett.9b00023

6. Nawrozkij, MB.; Forgione, M.; Yablokov, AS.; Lucidi, A.; **Tomaselli, D.**; Patsilinakos, A; Panella, C.; Hailu, GS.; Kirillov, IA.; Badia, R.; Riveira-Muñoz, E.; Crespan, E.; Armijos Rivera, JI.; Cirilli, R.; Ragno, R.; Esté, JA.; Maga, G.; Mai, A.; Rotili, D. Effect of α-Methoxy Substitution on the Anti-HIV Activity of Dihydropyrimidin-4(3 H)-ones. *J. Med. Chem.*, **2019**, 62(2):604-621. doi: 10.1021/acs.jmedchem.8b01238

7. Blanquart, C.; Linot, C.; Cartron PF.; **Tomaselli, D.**; Mai, A.; Bertrand, P. Epigenetic metalloenzymes. *Curr. Med. Chem.*, **2018**, doi: 10.2174/0929867325666180706105903

8. Milelli, A.; Marchetti, C.; Turrini, E.; Catanzaro, E.; Mazzone, R.; **Tomaselli, D**.; Fimognari, C.; Tumiatti, V.; Minarini, A. Novel polyamine-based Histone deacetylases-Lysine demethylase 1 dual binding inhibitors. *Bioorg. Med. Chem. Lett.*, **2018**, 28(6):1001-1004. doi: 10.1016/j.bmcl.2018.02.034

9. Sabatino, M.; Rotili, D.; Patsilinakos, A.; Forgione, M.; **Tomaselli, D.;** Alby, F.; Arimondo, P.; Mai, A.; Ragno, R. Disruptor of telomeric silencing 1-like (DOT1L): disclosing a new class of non-nucleoside inhibitors by means of ligand-based and structure-based approaches. *J. Comput. Aided. Mol. Des.*, **2018**, 32(3):435-458. doi: 10.1007/s10822-018-0096-z

Abbreviations

2-OG, 2-oxoglutarate;
AASIS, amino-acid-stimulated insulin secretion;
Ac_2O, acetic anhydride
ACC, acetyl-CoA carboxylase;
AcOEt, ethyl acetate;
AD, Alzheimer's disease;
ADM, adrenomedullin;
ADPr, Adenosine diphosphate ribose;
AEBP2, Adipocyte Enhancer-Binding Protein 2;
AMC, 7-aminomethylcoumarin;
AML, acute myeloid leukemia;
ANG II, Angiotensin II;
ANT2, adenine nucleotide translocator 2;
AR, androgen receptor;
ATP, Adenosine triphosphate;
BAH, bromo-adjacent homology;
BCL, B-cell lymphoma;
BDNF, brain-derived neurotrophic factor;
BET, Bromodomain and extra-terminal domain;
BL, Burkitt's lymphoma;
Bp, base pair;
CaMKs, Ca^{2+}/calmodulin-dependent kinases;
Carbon tetrabromide CBr4
CdLS, Cornelia de Lange syndrome;
CH_3CN, acetonitrile;
CH_3COOH, acetic acid
$CHCl_3$, chloroform;
CHD, Chromodomain-Helicase-DNA binding;
ChIP, Chromatin immunoprecipitation;
CLL, chronic lymphocytic leukemia;
CoA, Coenzyme A;
Cortactin, cortical actin-binding protein;
CPS1, carbamoyl phosphate synthetase 1;
CPT1, carnitine palmitoyl transferase 1;
CRBN, Cereblon;
CREB2, cAMP response element-binding protein 2;
CRPC, Castration-resistant Prostate Cancer;
CSE, cigarette smoke extract;
CtBP, C-terminal binding protein;
CTCL, refractory cutaneous T-cell lymphoma;
DCC, *N,N'*-dicicloesilcarbodiimmide
DCM, dichloromethane;
DIPEA, *N,N*-diisopropylethylamine;
DLAT, dihydrolipoyllysine acetyltransferase;
DLBCL, diffuse large B-cell lymphoma;
DNMT3L, DNMT3-Like protein;
DNMTi, DNMT inhibitors;
DNMTs, DNA methyltransferases;
Dot1, disruptor of telomeric silencing;
DOT1-L, the disruptor of telomeric silencing-1-like;

EGFR, epidermal growth factor receptor;
GCN5, general control non-derepressible 5;
K, lysine;
KDMs, histone demethylases;
KMTs, lysine methyltransferases;
KO, knockout;
KOAc, potassium acetate
$LiALH_4$ lithium aluminum hydride
LiOH, lithium hyroxyde
LNCaP, human prostatic adenocarcinoma cell line;
LPS, lipopolysaccharide;
LSCC, laryngeal squamous cells carcinoma
LSD1, lysine-specific histone demethylase 1A;
MAOi, MAO inhibitors;
MAOs, known monoamine oxidases;
MAPK1, mitogen-activated protein kinase;
MARI, mating-type regulator 1;
MBPs, methyl-binding proteins
MC, 3-methylcrotonyl-CoA;
MCCC, methylcrotonyl carboxylase complex;
MCD, malonyl-CoA decarboxylase;
MCM, the multi-compound medication;
MDM2, mouse double minute 2 homolog;
MDS, myelodysplastic syndrome;
MEF2, myocyte enhancer factor-2;
MEFs, embryonic fibroblasts;
MeOH, methanol;
MG, 3-methylglutaryl;
MGc, 3-methylglutaconyl;
miRNAs, microRNAs;
MITR, myocyte enhancer factor-2-interacting transcriptional repressor;
MLL, mixed lineage leukemia;

MM, refractory or relapsed multiple myeloma;
MMT, the multiple-medication therapy;
MnSOD, manganese superoxide dismutase;
MTDL, multi-target-directed ligands;
mTORC1, target of rapamycin complex 1;
Na_2CO_3, sodium carbonate;
Na_2SO_4, sodium sulphate;
NAD^+, nicotinamide adenine dinucleotide;
$NaHCO_3$, sodium bicarbonate;
NaHSO4, sodium bisulphate;
NaI, sodium iodide;
NAM, nicotinamide
NAMPT, nicotinamide phosphoribosyl transferase;
NaOAc, sodium acetate
N-CoR, nuclear receptor co-repressor;
NES, nuclear export signal;
Nex A, Nexturastat A;
NF-𝜘B, nuclear factor kappa-light-chain-enhancer of activated B cells;
NHS, N-hydroxysuccinimide
NLS, nuclear localization signal;
NMP, 1-metil-2-pirrolidone
NSCs, neural stem cells;
NURD/Mi-2/CHD, Nucleosome Remodeling Deacetylase
OE, overexpression;
PAF1, polymerase associated factor;
PAR, poly(ADP-ribose);
PARG, poly(ADP-ribose)glycohydrolase;
PARPi, PARPs inhibition;
PARPs, Poli (ADP-ribose) polymerases;
Pc, Polycomb;
PCAF, P300/CBP-associated factor;
PcG, polycomb group;
PCLs, Polycomb-like proteins;
$Pd(OAc)_2$, palladium acetate
PD, Parkinson's disease;
PDGF, platelet derived growth factor;
PDGFR, platelet-derived growth factor receptor;
PDH, of pyruvate dehydrogenase;
PEG, polyethylene glycol;
PHD, plant homeodomain;
PHD, prolyl hydroxylase domain;
PhoRC, Phorepressive complex;
PI3K, The phosphatidylinositol 3-kinase;
$POCl_3$, phosphoryl chloride;
PP1, protein phosphatase 1;
PPARα, Peroxisome-activated receptor α;
pRB, retinoblastoma protein;
PRCs, Polycomb Repressive Complexes;
PR-DUB, Polycomb Repressive Deubiquitinase;

PRMTs, arginine methyltransferases;
PROTACs, Proteolysis targeting chimeras;
PTCL, refractory peripheral T-cell lymphoma;
PTMs, histone post-translational modifications;
PTP, permeability transition pore;
PWWP, Pro-Trp-Trp-Pro;
PXXP, proline rich;
R, arginine;
RbAp46/48, Retinoblastoma Associated protein 47 or 48;
RBC, reaction biology corporation
$Rh_2(OAC)_4$, Rhodium (II) acetate dimer
RNAi, RNA interference;
ROS, reactive oxygen species;
RSC, Remodeling the Structure of Chromatin;
SAH, S-adenosyl-L-homocysteine;
SAHA, suberoylanilide hydroxamic acid;
SAM, S-adenosyl-L-methionine
SCLC, small cell lung carcinoma;
SIR2's, silent information regulator;
siRNAs, small-interfering RNAs;
SIRTi, sirtuin inhibitor;
SMRT, silencing mediator for retinoic acid and thyroid hormone receptors;
SRC, steroid-receptor co-activator;
STAT3, Signal transducer and activator of transcription 3;
Structural activity relationship studies (SAR)
SUMO, small ubiquitin-like modifier;
SUZ12, Suppressor of Zeste 12;
SWI/SNF, SWItch/Sucrose Non-Fermentable;
VHL, Von Hippel-Lindau;
VPA, sodium valproate;

VCAM-1, Vascular cell adhesion protein 1;
TET, Ten-eleven translocation;
TFIIS, transcription factor S-II;
THF, tetrahydrofuran;
TKi, tyrosine kinase inhibitor;
TNKS-1, Tankirase-1;
TNKS-2, Tankirase-2;
Tosyl chloride TsCl;
TRIM24i, TRIM24 inhibitors;
TRX, thioredoxin;
TSC2, Tuberous sclerosis 2;
TSSs, transcription start sites;
TXNIP, thioredoxin-interacting protein;

UTX, ubiquitously transcribed tetratricopeptide repeat X chromosome;
UV, Ultraviolet;
WT, wild-type;
xSIRT4, *Xenopus tropicalis* SIRT4;
Z-Lys (HMG) AMC, Z-lysine-(hydroxy-3-methylglutaric)-coumarin;
Z-MAL, Z-Lys (Acetyl) AMC, Z-lysine-(acetyl)-coumarin;

Table of contents.

Chapter 1

1.1   Epigenetics

As widely known by now, the genetic information of each single eukaryotic cell is stored in DNA molecules which are condensed in a dynamic structure known as chromatin. Chromatin, which results from the physical association between DNA double helix and histone and non-histone proteins, is in dynamic balance between a decondensed and transcriptionally active form, called euchromatin and a condensed and transcriptionally repressed one, known as heterochromatin.

The basic unit of such complex, named nucleosome, is composed of a histone core (an octamer resulting of two tetramers, each consisting of histones H2A, H2B, H3 and H4) around which DNA wrapped approximately 146 base pair (bp). Nowadays, it is well known that the DNA code itself does not drive the gene expression independently, but such activity depends on different biological phenomena that have been enclosed into the category of epigenetics. Epigenetics (from the Greek words επί, over, and γεννετικός, genetics), that can be considered as the first director of the correlation between genotype and phenotype, refers to reversible and heritable changes in gene expression that cannot be justified by alterations in the DNA sequence of bases. Despite most of cells in a multicellular organism show an identical genotype, individual development generates a huge variety of cell types with distinct, yet stable, profiles of gene expression and different cellular phenotype and functions.[1] Gene expression is intimately regulated by epigenetic mechanisms which response to environmental exposures (early life experience, stress, etc).[2,3] These modifications are control by, at least, three main mechanisms: histone modifications, covalent modifications to the cytosine residues of DNA, and noncoding RNAs. Proteins taking part in chromatin remodeling complexes show the capability to reversibly add, remove, or read such covalent modifications and can be classified as "writers", "erasers" or "readers" thus offering the possibility of pharmacologically restore these effects (Figure 1.1).
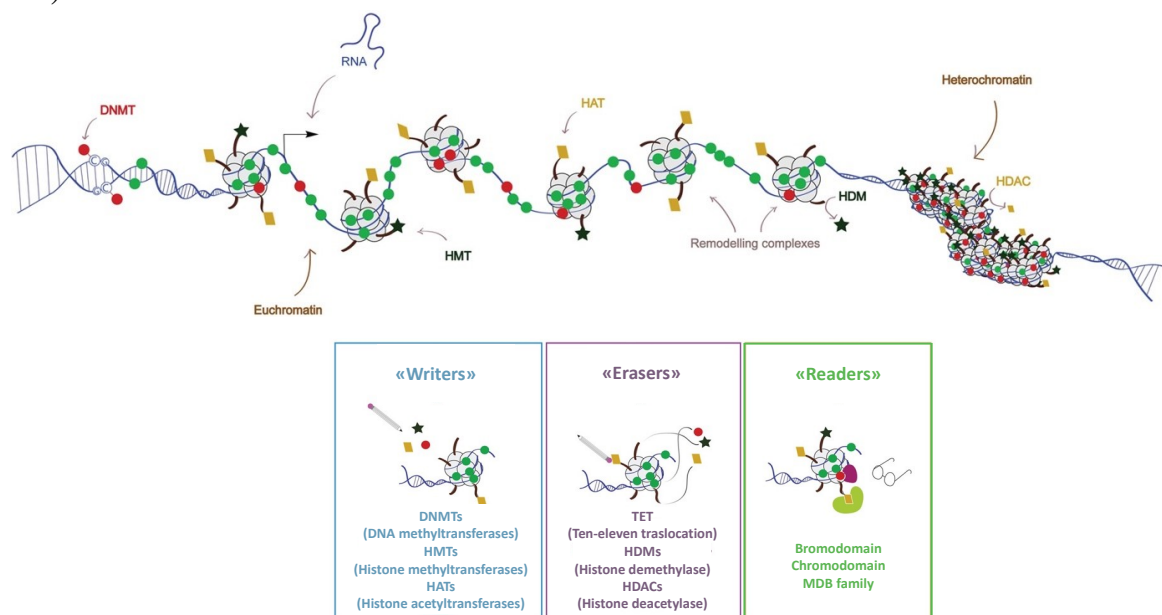
Figure 1.1. Epigenetic regulation is a dynamic process resulted from the balance between euchromatin and heterochromatin state. The main players of such condition can be classified in: "writers" (DNA methyltransferases (DNMTs), histone acetyl transferases (HATs), histone methyltransferases (HMTs), light blue box); "erasers" (histone deacetylases (HDACs), histone

demethylases (KDMs) and phosphatases, purple box); "readers" (proteins containing chromodomains, bromodomains, and Tudor domains, gree box), which respectively catalyze the introduction, the removal as well as recognize and bind these marks at histone and non-histone level. Adapted from Pechalrieu *et al*. *Biochemical Pharmacology*, 2017, 129, 1–13.[4]

In human, a wide variety of histone modifications have been discovered including methylation, acetylation, ubiquitination phosphorylation and sumoylation. DNA methylation, that can be described as the most stable epigenetic mark known in humans,[5] involves the C5 of the cytosine residue mainly in the context of 5'-CpG-3' (5'-cytosine-phosphate-guanine-3') dinucleotide and it is catalyzed by DNA methyltransferases (DNMTs) enzymes, which use *S*-adenosyl-L-methionine (SAM) as co-substrate. Methylated CpG sites are randomly distributed among the genome, whereas the unmethylated CpG are placed in the so-called "CpG island", predominantly localize into the promoter region of over 50% of all human genes.[6] DNA methylation is widely known to play a repressive role as it is able to arrest transcriptional initiation, either by preventing the binding of specific transcription factors or by recruiting methyl-binding proteins (MBPs).

Simplifying, if the interested promoter shows this mark, the transcription of the corresponding gene is repressed. It is important to emphasize that, all the epigenetic mechanisms mentioned so far, do not work independently of each other but create a deep network of interconnections known as "epigenetic crosstalk",[7] cooperating in the establishment of an inactive or active transcriptional chromatin state. DNA methylation, for example, has a direct influence on both histone methylation and acetylation processes.[8] In this framework, the repressed chromatin state induced by the recruitment of MBPs is principally due to the implication of histone methyltransferases (HMTs) and/or histone deacetylases (HDACs) enzymes. These enzymes catalyze the addition of methyl units (HMTs) or the removal of acetyl groups (HDACs) at histone tails level, allowing the recognition and binding of chromatin silencers and the transition to the heterochromatin state (Figure 1.2).[9]
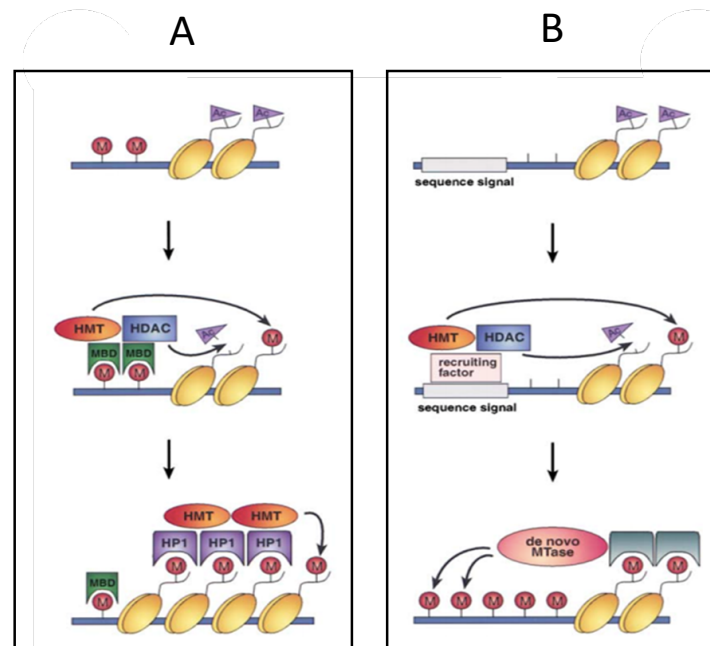
Figure 1.2. Mechanisms of epigenetic crosstalk: (A) DNA methylation and consequent chromatin silencing. Methyl marks (M) on the DNA are recognize and bind by MBDs, which recruit HDACs and HMTs that catalyze the removal of acetyl (Ac) and the addition methyl (M) units respectively, thus allowing the recognition and bound of chromatin silencers such as HP1. This transcriptionally

silenced state of chromatin can be further propagated by the recruitment of HMTs by HP1. (B) Suggested mechanism of DNA methylation induced by chromatin signals. A first mark, probably within the DNA sequence, is bound by a factor that could recruit HMTs and HDACs. Such modified histones can be recognized by factors that bring about DNA methylation, most probably through recruitment of a *de novo* DNMT. Adapted from Ben-Porath *et al*. *Mol*. *Cell*, 2001, 8 (5), 933–935.[9]

As previously mentioned, the regulatory pathways related to small non-coding RNA molecules, known as RNA interference (RNAi), can be considered as the third type of epigenetic modifications. RNAi can be mediated by endogenous molecules of RNA, such as microRNAs (miRNAs) or by exogenous RNA molecules known as small-interfering RNAs (siRNAs).[11] miRNAs are long non-coding RNA containing about 22 nucleotides, which bind the 3' untranslated region of mRNA controlling, in this way, the post translational gene expression in a negative way increasing mRNA degradation or suppressing its translation.[11,12] Several proofs showed that miRNAs can act both as tumor suppression genes or oncogenes resulting altered in different human cancers.[12,13]

Despite the overriding importance of the role covers by the epigenetic modifications in the control of several cellular processes such as differentiation and development, dysfunctional genes regulation and relative expression are responsible for the onset of many human diseases, first of all cancer. The modulation of epigenetic processes is presently and strongly considered an innovative and challenging therapeutic strategy.[14]

1.2 *Histone post-translational modifications and chromatin remodeling*

Nucleosomes are the basic repeating structural and functional unit of chromatin that consist of two copies each of the four core histone proteins (H2A, H2B, H3 and H4), around which, approximately, 1.7 turns of DNA (or about 146 bp) is wrapped. Unlike the other histones, histone H1 does not makes up the nucleosome "bead", in fact it sits on top of the structure improving DNA adhesion to the histone octamer thereby increasing the degree of compaction. In addition to nucleosome binding, the histone H1 also interacts with the "linker DNA" region between nucleosomes, taking part in the stabilization of the zig-zagged 30 nm chromatin fiber. Histones appear as globular proteins, except in the unstructured *N*-terminal portions consisting of about 25-30 residues. The *N*-terminal region of histone tails result the place where the largest number of epigenetic modifications happen. The basic nature of histone proteins is a consequence of the strong presence of physiologically positively charged arginine and lysine residues that favorably interact with the negative charges of phosphate groups of the DNA double strand, thus allowing the establishment of a stable association within the nucleosome. The conserved domain of histone proteins, of about 70 amino acids, consists of three α-helix regions, named histone-fold, and is responsible for the formation of the two head to tail H3-H4 and H2A-H2B heterodimers interaction. While under physiological conditions chromatin appears as a 30 nm fiber characterized by a helical structure consisting in six nucleosomes per coil, under low ionic strength, coupled with the absence of histone H1, the chromatin switch to the less condensed structure of 10 nm.[15]

It is widely known that the three-dimensional chromatin structure strongly affects different fundamental cellular processes such as recombination, replication, mitotic condensation and transcription. The generally repressive nature of chromatin structure has long been appreciated in transcription regulation, indeed, histones collaborate with transcription factors to provide gene depression. Nevertheless, sometimes, chromatin organization can facilitate the activation of specific genes as proved by the fact that the bending and

supercoiling of DNA on a nucleosome, can promote the binding of transcription factors or the enhancement of the interactions between different partner proteins.[16]

The major mechanism involved in the modulation of chromatin structure and function is represented by the histone post-translational modifications (PTMs). To date a huge number of PTMs have been identified: lysine and arginine methylation, lysine acetylation, lysine ubiquitination, lysine sumoylation, arginine citrullination ADP-ribosylation, proline isomerization, and serine/threonine/tyrosine phosphorylation (Figure 1.3).
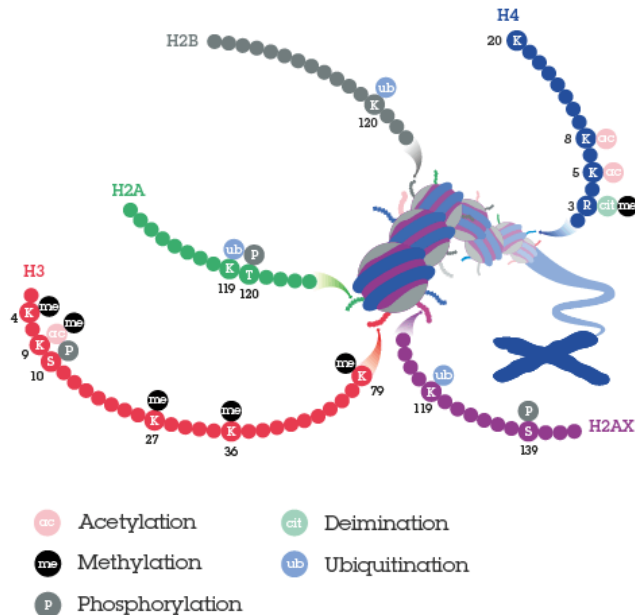
Figure 1.3. Schematic representation of histone post-translational modifications.

Promising progresses in understanding histone PTMs functions have been reached thanks to the identification of the protein machineries that allow the introduction (writers), removal (erasers), and binding (readers) of histone PTMs. Two landmark discoveries in this regard were the identifications in 1996 of HDAC1/Rpd3 and p55/Gcn5 as transcription associated histone deacetylases[17] and acetyltransferases,[18] respectively. PTMs might work individually or in combination (on the same or distinct histone tails) thus providing the distinct outcome-(s) associated with them. In fact, in addition to induce direct physical effect on chromatin structure (that is typical for lysine acetylation, that counteract the positive charge of histone proteins), PTMs could also act through the selective recruitment of readers protein that recognize and bind specific epigenetic marks thus mediating their distinctive effects on the chromatin structure. In this framework, one of the major turning point was the discovery of the bromodomain motif as an acetyl-lysine reader domain.[19] This result not only paved the way for subsequent characterization of this important family of chromatin effectors,[20] but also opened new perspectives that motivated further efforts for the identification of other reader protein domains. Moreover, it has become absolutely clear that many chromatin-associated factors are characterized by multiple histone binding domains, within a single simple protein as well as within distinct component of enzymatic complexes. This evidence offers a diverse and exciting potential for multivalent histone engagement[21] (Figure 1.4) that adds further consistence of specificity to histone PTM recognition. Several closely spaced histone binding domains relative to single proteins have been identified to interact with histone PTM marks on a histone tail, termed *cis* interactions, or on neighbours or spanning histones and DNA, thus being colled *trans* interactions.[22]
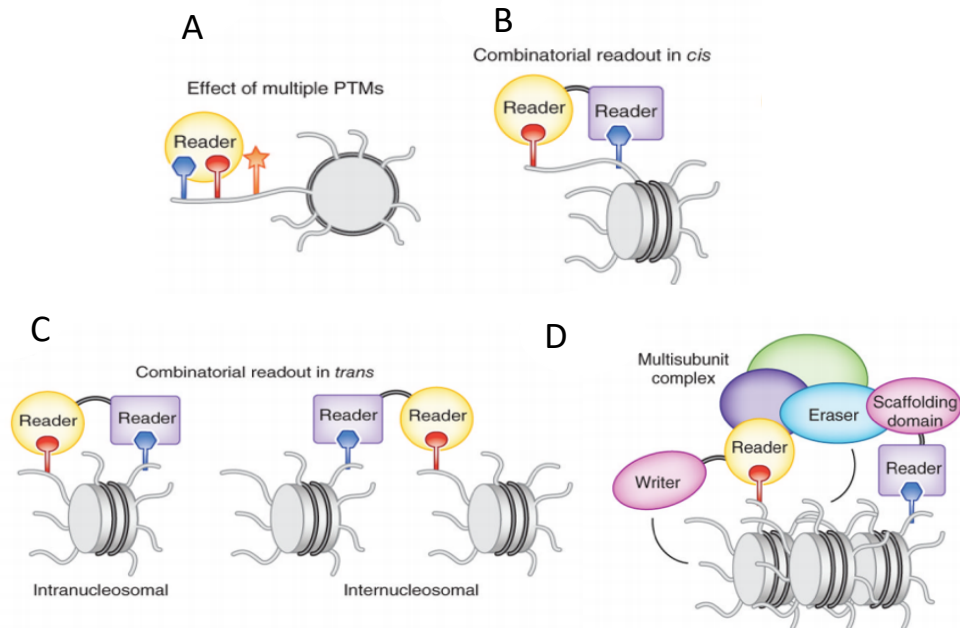
Figure 1.4. Linked protein domains coordinate the addition (writer), removal (eraser), and recognition (reader) of histone PTMs, creating a dynamic and variable chromatin environment. (**a**) Recognition and bind of a specific PTM is influenced by neighboring PTMs involving the same histone tail; (**b**) *Cis* indicates multivalent events which take place on the same histone; (**c**) *Trans* relates to multivalent events happening on neighboring histones or histones and DNA, either within the same nucleosome or on adjacent nucleosomes. (**d**) The reader can also by be characterized by a catalytic (which act as eraser or writer) or scaffolding domains that connect the other parts of the complex with their host proteins. Adapted from Musselman *et al*. *Nat Struct Mol Biol.*, 2012, 19,1218–1227.[23]

Adenosine triphosphate (ATP)-dependent highly conserved chromatin multi components (of between 4 and 17 subunits) remodeling complexes (>1 MDa) are characterized by the presence of an ATPase subunit belonging to the superfamily II helicase-related proteins.[24] Based on the additional presence of unique domains within or adjacent to the ATPase subunit, in addition, such class can be classified into at least four distinct families: SWItch/Sucrose Non-Fermentable (SWI/SNF), ISWI, INO80 and Nucleosome Remodeling Deacetylase (NURD/Mi-2/CHD). The SWI/SNF family is the most studied and includes RSC (Remodeling the Structure of Chromatin), that recognize, bind and remodel the nucleosomes and function in the sliding and eviction of nucleosomes. ISWI regulates nucleosome assembly and spacing and seems to have also functions in higher-level chromatin organization. Chromodomain-Helicase-DNA binding (CHD) remodelers correlate with nucleosome sliding, eviction, spacing, and nucleosome assembly. The main role of the INO80 family consist in the nucleosome restructuring.[25–27]

1.2.1 Histone ADP-ribosylation

Poli (ADP-ribose) polymerases (PARPs) are NAD^+-dependent enzyme responsible for the production of ADP-ribose polymers involving glutamic or aspartic acid residues of targeted proteins.[28] The poly(ADP-ribosyl)ation is a post translational modification regulating the chromatin dynamism in response to both physiological and pathological events.[29] Like the others PTMs, also the poly(ADP-ribosyl)ation is a reversible mark, since it can be

modulated by the catalytic activity of poly(ADP-ribose)glycohydrolase (PARG) enzymes. Moreover, this mark is really flexible, indeed it may differ by extension, branching, polymer binding and protein acceptor.[30] PARP family consists of 18 members, among which PARP1-6 are able to catalyze the synthesis of poly(ADP-ribose) (PAR). While the subtypes 9 and 13 lack polymerase activity, the rest can move only one ADP-ribose unit.[31] From a functional point of view, it can be useful to distinguish two main groups: the first containing the subtypes 1, 2 and 3, which are characterized by a nuclear localization and a DNA-dependent activity (since they start to perform their task in response to DNA damaging events), and the second including PARP5a and PARP5b, better known as Tankirase-1 (TNKS-1) and Tankirase-2 (TNKS-2) respectively, that, despite mainly work in order to maintain the telomere integrity,[32] resulted also involved in the regulation of the Wnt/β-catenin signaling pathway by stimulating the degradation of axin.[33] However, within this framework, the most important issue to be faced is the recognition of PARPs as epigenetic targets. Until today, different pieces of evidence support the belonging of these enzymes to the epigenetic category. In fact, regardless of the specific subtype function, PARPs activation has, as primary effect, the chromatin remodeling through the modification of nucleosome structure or the recruitment of proteins responsible for the chromatin asset.[31,34] Indeed, recent studies demonstrate that PARP1 interacts with the histone H1, and determines its dissociation from promoters PARP1-dependent.[35] Furthermore, while low concentration of nicotinamide adenine dinucleotide (NAD$^+$) causing chromatin condensation and the consequent inhibition of transcription (PARP1 strictly interacts with the chromatin), high levels of NAD$^+$, through auto(ADP-ribosyl)ation, dissociates PARP1 from chromatin, making the double helix accessible for the transcriptional machinery.[34,36] Other evidence testify the crosstalk between the poly(ADP-ribosyl)ation and both the histone acetylation and the DNA methylation processes.[37] Starting from these findings and considering the definition of epigenetics, it is possible to assume that even the poly(ADP-ribosyl)ation can be considered as a new player in the epigenetic landscape.[29] A great deal of recent data showed that PARPs inhibition (PARPi) have shown to be effective in the treatment of stroke and neurodegenerative diseases acting as promising weapon in the fight against cancer. As proof of this, PARPi can be used as chemo-potentiator since they block the PARP-mediated DNA repair mechanism (triggered by the DNA damaging effect of the anticancer agents used in combination with it), as well as a standalone therapy for tumors in which the DNA repair mechanisms do not work in the correct way.[38]

1.2.2 Histone Phosphorylation

Phosphorylation of histones can be defined as a highly dynamic process which takes place on threonine and tyrosine residues, mainly, but not exlusively, at histone level. The state of such histone mark results from the balanced activities of two class of enzymes that work in an opposite way: kinases and phosphatases, which respectively catalyze the introduction and the removal such modification. All the identified histone kinases catalyze the transfer of a phosphate group from ATP to the hydroxyl group of the target amino-acid side chain conferring a significant negative charge to histones that strongly physically influences the three-dimensional chromatin structure. However, for most kinases, it is unclear how the enzyme is properly recruited to its chromatin site of action. For example, the mammalian mitogen-activated protein kinase (MAPK) enzyme is characterized by an intrinsic DNA-binding domain through which it is recruited to the DNA.[39] Even if most histone phosphorylation sites appear in the the *N*-terminal tails, also sites into the core regions must be present. Despite little il known about the role of the non-receptor tyrosine kinase Janus kinase 2 (JAK2) which is responsible for the phosphorylation of H3Y41,[40] surely, given the

sorely rapid turnover registered for specific histone phosphorylation, also a high phosphatase activity within the nucleus do exist. Histone phosphorylation covers an important role in several fundamental cellular processes such as transcription, apoptosis, DNA repair, and chromosome condensation. Histone phosphorylation, by involving Ser10 of histone H3, is critical during the interphase because it transcriptionally activates several genes depending on upstream signaling pathways. Moreover, the location of Ser10 residue in proximity to other residues which may be the subject of other epigenetic changes in the H3 tail, allows a variety of crosstalk between phosphorylation and other modifications such as acetylation and methylation. In this framework, it is well known that H3S10 phosphorylation inhibits H3K9 methylation, triggering, at the same moment, H3K4 methylation as well as H3K14 acetylation, which further induce a chromatin decondensation state. A lot of H3S10 kinases, including Aurora B, are involved in this signaling plot.[41] Furthermore, during androgen receptor (AR)-dependent gene activation process is notable a strong crosstalk between phosphorylation and methylation. Importantly, protein kinase C (PKC)-dependent phosphorylation of H3T6 inhibits the demethylation of H3K4 whereas accelerates the demethylation of H3K9 by altering LSD1 substrate specificity. Furthermore, increased levels of the histone H3Ser28 phosphorylation mark were found in brain ischemia, indeed this dysregulation, by altering the function and the genomic localization of chromatin remodeling complexes, leads to neuronal necrosis.[42]

1.2.3 Histone ubiquitination

Recent pieces of evidence showed that the histones H2A and H2B are the most common substrates of ubiquitination (also known as ubiquitylation), which are converted into their monoubiquitinated form (H2Aub and H2Bub). H2Aub was mapped to the highly conserved residue Lys119 and comprise between 5% and 15% of the available H2A, while H2B is modified on the Lys123 in yeast and on the Lys120 in vertebrates.[43] Results obtained from Chromatin immunoprecipitation (ChIP) experiments proved that enriched monoubiquitinated H2A levels were found in the genome satellite regions, while monoubiquitinated H2B increased levels are typical of transcription active genes body.[44] Differently to the other histone modifications which result in fairly small molecular changes, ubiquitination correlates with a much larger covalent modification of the ε-NH$_2$ histone terminal tails. In fact, ubiquitin itself consists of a polypeptide of 76-amino acids that is introduce to lysine residues *via* the sequentially activity of three specific enzymes: ubiquitin-activating enzymes, ubiquitin-conjugating enzymes and ubiquitin ligases.[45] Enzyme complexes control both the substrate specificity (which lysine is targeted) and the extend of ubiquitination (either mono- or poly-ubiquitylated). As just mentioned, two of the well-characterized sites for histone ubiquitination involve the histones H2A and H2B: H2AK119ub1 correlates with the repression of gene expression, whereas H2BK123ub1 covers a main role in transcriptional initiation and elongation.[46,47] The removal of ubiquitination mark is performed by the action of isopeptidases called de-ubiquitinating enzymes (DUBs) involved in both transcriptional activation and silencing. In addition to H2A and H2B, the other core histones H3, H4, as well as histone H1, have also been reported to be modified by ubiquitin. For example, H3 and H4 were polyubiquitinated *in vivo* by CUL4–DDB–RBX1 ubiquitin ligase complex after Ultraviolet (UV) irradiation.[48] However, to date, the biological role of such modifications has not been fully understood. Beyond their mono-ubiquitination, histone H2A and H2B can be modified by ubiquitin chains.[49] Ubiquitination of H2B is mainly regulated by the the RNF20/RNF40 ubiquitin ligase complex and the ubiquitin-conjugating enzyme E2A (UBE2A or RAD6A). Altered expression of UBE2A and RNF20/RNF40 may contributes to the onset and progression of different kind of tumors. Recent studies show that H2B ubiquitination is involved in DNA

damage repair.[46] Furthermore, cells in which either RNF20 or RNF40 were independently or simultaneously silenced, exhibit a strong increase of DNA double strand breaks (DSBs) which specifically links H2Bub1 to DSB repair.[50] In addition to the decreased cellular monoubiquitinated H2B level, RNF20 depletion correlates with the enhanced expression of specific proto-oncogenes and growth-related genes including *c*-Fos and *c*-myc. Further study reported that RNF20 represses gene expression by disrupting the interaction between polymerase associated factor (PAF1) elongation complex and transcription factor S-II (TFIIS) and by inhibiting transcriptional elongation. In addition, RNF20 depleted cells are characterized by a reduced expression of the tumor suppressor p53, as well as by an increased cell migration thus resulting in the development of features typical cell malignant transformation. Moreover, hypermethylation involving the promoter of RNF20 was registered in differen tumor samples, suggesting that H2B ubiquitin ligase RNF20 is a putative tumor suppressor agent.[51]

1.2.4 Histone SUMOylation

Sumoylation is PTMs related to ubiquitylation,[52] and provides the covalent introduction of SUMO (small ubiquitin-like modifier) proteins to histone lysine through the activity of ubiquitin-activating, conjugating and ligases enzymes. In mammals are known four SUMO paralogues. SUMO-1 has been independently isolated by different research groups as a binding partner of the RAD51/52 nucleoprotein filament proteins.[53] SUMO-2 and -3, which approximately share only 50% similarity with SUMO-1, instead, differ from each other by only three *N*-terminal residues and are often collectively considered as SUMO-2/3. Despite SUMO-1 chains have been proved *in vitro*,[54] *in vivo* seems that SUMO-1 could act as a chain terminator on SUMO-2/3 polymers.[55] A DNA sequence analysis predicted the isoform SUMO-4 as a 95-residues protein with a similarity of 87% in the amino acid chain with SUMO-2. SUMO proteins are produced as inactive precursors that must first subjected to a *C*-terminal cleavage allowed by the SENP (sentrin/SUMO-specific protease) family enzymes. This process provides the exposure of a di-glycine motif that allows the conjugation of SUMO with lysine residues whitin the target proteins. The same SENP enzymes are responsible for the reverse of protein SUMOylation that therefore acquires the characteristic of highly dynamic process.[56] Sumoylation process has been registered for all four core histones and seems to act as an antagonist of ubiquitylation and acetylation that otherwise could involve the same lysine residue.[57,58] Although on the basis of these pieces of evidence it may appear that this process is related to a repressive outcome, more informations about SUMO proteins molecular mechanism(s) are still needed to proprerly understand their role in the chromatin contex.

1.2.5 Histone methylation

The reversible histone methylation process covers a fundamental role in the epigenetic regulation of gene expression mainly affecting lysine and arginine residues of histones H3 and H4.

Histone methylation, unlike histone acetylation which always corresponds to transcriptional activation, can modulate gene expression in both directions, depending on the specific residues involved as well as on the extent of methylation (Figure 1.5).
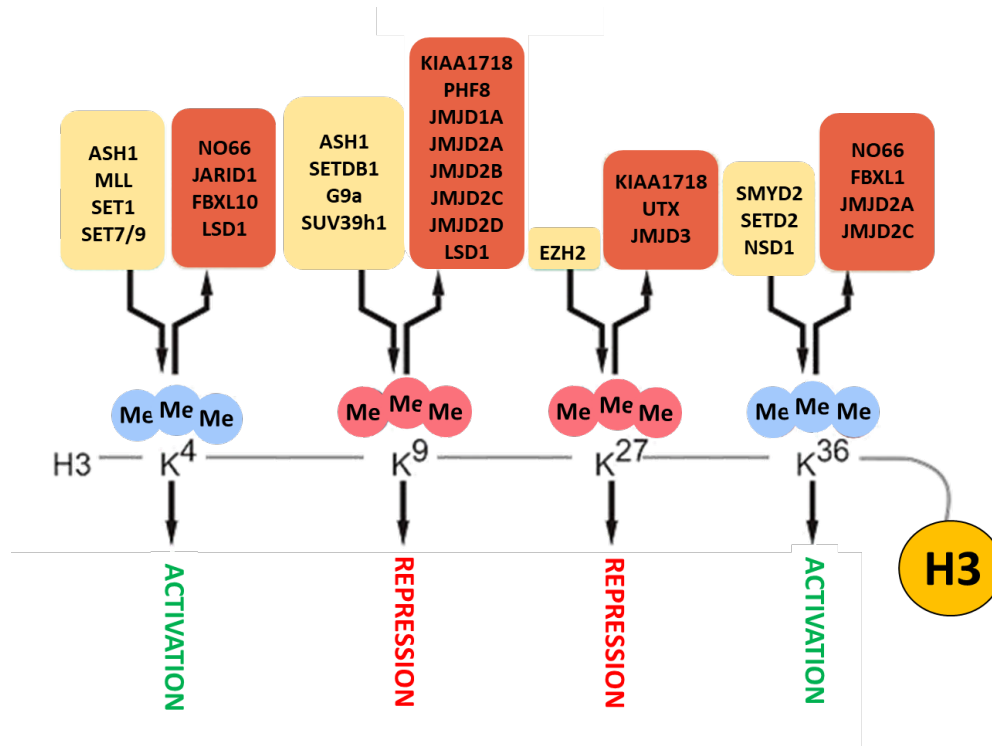
Figure 1.5. Overview of the effects induced by different states of methylation involving distinct lysine residues of H3. The lysine methylation pattern resulted from the balanced activity of HMTs (in the pale-yellow boxes) and KDMs (in the orange boxes) enzymes.

As previously mentioned, the maintenance of a balanced methylation status is assured by HMTs and KDMs enzymes.[59]

The source of methyl group is SAM, which is converted to *S*-adenosyl-L-homocysteine (SAH) during the histone methylation process. In particular, lysine can be mono-, di- or trimethylated by lysine methyltransferases (KMTs) (Figure 1.6A) while arginine residues can be monomethylated, symmetrically or asymmetrically dimethylated by arginine methyltransferases (PRMTs) (Figure 1.6B). Moreover, also histidine has been reported to be monomethylated, although this methylation appears to be rare and has not been further characterized.[60]

A
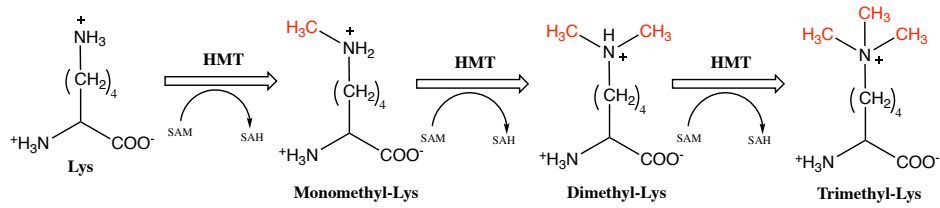
B
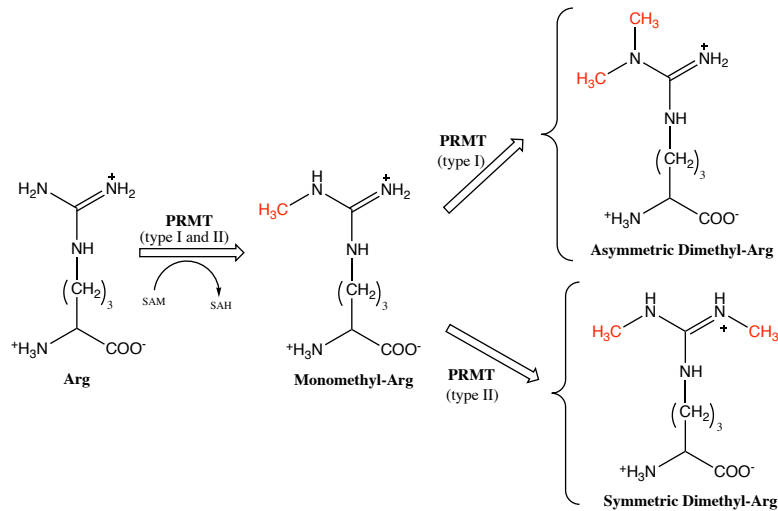
Figure 1.6. Chemical characterization of (**A**) (mono-, di-, and tri) lysine and (**B**) (asymmetric and symmetric) arginine methylation.

The most studied lysine (K) methylation sites include H3K9, H3K4, H3K27, H3K36, H3K79 and H4K20. Arginine (R) methylation mainly involves H3R2, H3R8, H3R17, H3R26 and H4R3.[61] However, mass spectrometry studies and quantitative proteomic analyses also identified many other basic residues within H1, H2A, H2B, H3 and H4 as further possible methylation sites. The number of targetable histone lysine residues and the extend of methylation involving each methylation site correlates with a highly complex variety of potential functional outputs. For example, while methylation of H3K4, H3K36, and H3K79 allows the occurrence of a transcriptionally active state, methylation of H4K20, H3K9, H3K27 residues leads to an "off" transcription state.[62,63] Histone methylation marks do not work in isolation but rather in cooperation with other histone modifications. Deregulation of both methylation and demethylation events may be responsible for the alteration of the expression level of tumor-promoting and tumor-suppressor genes, allowing the onset and progression of different kinds of cancer.[64]

Histone methylation marks do not work alone but rather in cooperation with other histone modifications. Histone lysine methylation is known to be involved in several important cellular processes including transcription, cell identity and genome stability. Aberration in histone lysine methylation-controlled regulatory cues are frequently observed in cancer.[65]

Several pieces of evidence highlighted that KDMs mutation or overexpression (OE) correlates with many types of cancer,[66,67] thus KDMs are an attractive target to inhibit with small epigenetic modulators.

1.2.5.1 Histone Lysine Methyltransferases

More than 50 KMTs have been reported to literature so far. Such enzymes show high selectivity among the targeted histone lysine residues, as well as among the extend of methylation that they can lead. Based on their catalytic domain sequence, two different families of KMTs have been identified: the disruptor of telomeric silencing-1-like (DOT1L) proteins and the SET domain-containing proteins. The acronym SET originates from the *Drosophila* polycomb proteins in which such domain was firstly identified, known as Enhancer of zeste (E(z)), Suppressor of variegation 3–9 (Su(var)3–9), and Trithorax (Trx).[68–70] SET-domain containing proteins catalyze the transfer of a methyl unit from SAM to the lysine ε-amino group, releasing a methylated lysine residue and the byproduct SAH. As previously mentioned, methylation of specific histone lysine residues precisely modulates the gene expression acting as "marker" for the recruitment of chromatin remodeling complexes. Moreover, KMTs activity covers both histones and non-histone substrates.[71] The KMT SET7/9, for example, can stabilize the tumor suppressor p53 by methylation of its K372, as well as DNMT1, estrogen receptor alpha (ERα), and nuclear factor kappa-light-chain-enhancer of activated B cells (NF-ϰB).[72] In contrast, the other classes of human KMTs are not characterized by a SET domain, but show only an evolutionarily conserved protein called Dot1 (disruptor of telomeric silencing; also known as Kmt4)[69], that specifically catalyzes the methylation of histone H3 at lysine 79.[73,74] Dot1 and its homologs contain a catalytic cleft resembling that of the arginine methyltransferases.[75–77] The most interesting histone lysine methylation sites are H3K4, H3K27, H3K9, H3K79, H3K36, and H4K20 (Figure 1.6), even if other lysine residues object of methylation have been identified also in further positions within H3 and H4 as well as in H1, H2A, H2B.

Despite some lysine methylation marks specifically correlate with euchromatin thus promoting the activation of gene expression (H3K4, H3K36, and H3K79) or with the heterochromatin state and consequent gene silencing (H3K9, H3K27, and H4K20),[78] more often the final output on chromatin is influenced by the contemporary interplay of various histone modifications ("histone crosstalk").[79] As previously exposed, an aleterated histone covalent modification pattern leads to a dysregulated expression of oncogenes and tumor suppressor genes and is often associated with cancer.[65] In this framework, Fraga et *al*. showed that the reduced Lys16 acetylation and/or Lys20me3 levels of H4, rapresented a typical "cancer signature".[80] Furthermore, aberrant histone methylation has been related not only with cancer but also with aging and mental retardation.[81–83]

SET methyltransferases have been classified into four different families based on the similarity of their SET domain sequence and adjacent protein region into SET1, SET2, SUV39 and RIZ, that commonly take part in multiprotein complexes[84] where the SET methyltransferase enzyme are the catalytic domain and the accessory proteins are responsible for the activity and selectivity of the whole complex. Despite the SET1 family harboring the SET domain, plus, commonly, a post-SET domain, the two well-known EZH1 (Enhancer of Zeste 1) and EZH2 (Enhancer of Zeste 2), do not show such portion. To the SET2 family belong a SET domain that is always between an AWS domain and a post-SET resulting rich in cysteine, the nuclear receptor binding SET domain-containing proteins NSD1-3, the SMYD and the SETD2 family proteins. All members of the SUV39 family (G9a, GLP, SUV39H1, SUV39H2, CLLL8 and ESET) show a pre-SET domain, which result fundamental for their enzymatic activity.[60] To conclude, the RIZ family members, PFM, BLIMP1 and RIZ1 harbor the SET domain at the level of the amino-terminal region.[85] NSD1 is a large protein containing several motifs involved in transcriptional regulation, including a SET domain and five PHD fingers. The mechanism and the role that this protein cover in differentiation and cell proliferation still need to be

clarified. However, NSD1 is essential for normal development, since homozygous mutant *Nsd1*−/− embryos die during gastrulation is characterized by high apoptosis levels.[86] The NUP98-NSD1 fusion protein can be a driving oncogene in acute myeloid leukemia in mice.[87] Expression of the fusion protein is enough to support the self-renewal of myeloid stem cells *in vitro* and to raise the expression of the homeobox (Hox)A7, HoxA9, HoxA10 and the Meis1 proto-oncogenes. The NSD2 protein contains a SET domain, a plant homeodomain (PHD) finger, a Pro-Trp-Trp-Pro (PWWP) domain and a high-mobility Group (HMG) box. NSD2 trimethylates H3K4 and H4K20, to mono- and trimethylates H3K27, and to mono-, di- and trimethylates H3K36. This protein is known to interact with different transcriptional factors and chromatin modifying enzymes such as HDAC1, HDAC2, SIN3A as well as with lysine-specific histone demethylase 1A (LSD1). These data suggest that NSD2 could be involved in cell fate decisions.[88] NSD3 probably catalyzes the methylation of H3K36. It is overexpressed in a few cases of breast carcinomas and in acute myeloid leukemia is present as fusion protein NUP98–NSD3.

EZH2 represents the catalytic subunit of Polycomb Repressive Complexes (PRCs). EZH2 and its related homolog EZH1 are KMTs catalyze mono- di- and trimethylation of H3K27 and play a main role in transcriptional regulation.[88] EHMT1 (GLP) and EHMT2 (G9a) are members of the Suv39h subgroup of SET domain-containing molecules. In contrast to the H3K9 tri-methyl-specific KMTs, EHMTs catalyze H3K9 mono- and di-methylation. G9a and GLP function as a part of heterodimeric complex in the regulation of transcriptional repression and activation, influencing essential cellular developmental processes. EHMTs physically interact with DNMTs and PRC2 contributing to transcriptional repression. EHMTs are not significantly mutated in cancer but G9a results overexpressed in lung and bladder cancers.[89,90]

Dot1 was firstly discovered in *Saccharomyces cerevisiae* through a genetic screen to identify proteins whose OE leads to impaired telomeric silencing.[72] The main enzymatic function of Dot1 is its histone methyltransferase activity upon its substrate, H3K79.[69,74,91] Dot1 is evolutionary conserved in mammals, known as DOT1L, and shows enzymatic activities analogue to that of its yeast homologue. As previously mentioned, Dot1 differs from other histone lysine methyltransferases in several ways: i) it is unique in being the only non-*SET* domain containing methyltransferase identified to date; ii) it methylate histone H3 in the globular domain on Lys79, (this residue is located on the nucleosome surface and is accessible to chromatin binding factors, but is an unusual site for histone methylation which most frequently occurs in *N*-terminal histone tails); iii) it adds methyl groups to lysine residues in a non-processive manner (Dot1 must dissociate and re-associate with Lys79 to allow cofactor exchange and formation of higher levels of methylation); iv) it requires a chromatin substrate, and is not active on free histones and v) it is the only enzyme known to be responsible for all forms of H3K79 methylation, suggesting that only this protein would need to be targeted in diseases involving aberrant H3K79 methylation.[92,93] Several lines of evidence suggested that H3K79 methylation was indeed reversible and subjected to dynamic regulation, but the identity of a specific demethylase has not yet been revealed. Dot1 lacks a SET domain and possesses an SAM binding motif similar to class-I methyltransferases.[94–96]

Mixed-lineage leukemia (MLL) is a multi-domain protein showing different putative DNA-binding portions at the *C*- and *N*- terminal SET domain specific for H4K3me1/2/3 and is known to be responsible for the modulation of the transcription of developmental genes including the HOX ones.[97]

Rearrangements of the MLL gene correlates with the onset of different kinds of incurable cancers including leukemias of myeloid, lymphoid, or mixed/ indeterminant lineage as well as infant acute leukemias.[85,97–99]

Most of tumors related to MLL translocation identified so far were associated with oncogenic fusion proteins characterized by the replacement of the proper methyltransferase domain with sequences derived from ENL, AF10, AF9, AF4. Such sequences can take part into direct or indirect interaction with DOT1L facilitating transcriptional elongation.

In this scenario, several pieces of evidence proved that DOT1L, as well as the H3K79me2/3 mark, play a main role in the onset and and maintenance of MLL-rearranged leukemia. In fact, preclinical and clinical (NCT03724084, NCT03701295) data collected after DOT1Li-based treatments of MLL-rearranged leukemia (as well as other type of leukemia) resulted very promising.[100,101,110,102–109] SMYD proteins belong to the KMT sub-family with a divergent SET domain. The substrate specificity of this class of enzymes is not clear, but H3K4, H4K20 and H4K5 have all been described as targets for SMYD3 and H3K4 and H3K36 for SMYD2. SMYD2 also methylate non-histone substrates such as HSP90, TP53, RB1 and ER. Both SMYD2 and SMYD3 result overexpressed in various types of cancer and some studies suggest also their involvement in cancer cell proliferation.

Since methylation of lysine residues does not alter their charge, such histone modification leads to the modulation of the chromatin organization allowing the binding of different proteins that mediate downstream effects. Recent studies on histone methylation identified at least three protein motifs: the CHD,[10,111–114] the Tudor domain[115] and the WD40-repeat domain,[116] capable of specific interactions with methylated lysine residues. For example, the chromodomain of heterochromatin protein 1 (HP1) specifically interacts with methylated H3K9, whereas that one of Polycomb (Pc) particularly interacts with methylated H3K27 (Figure 1.7).[117]
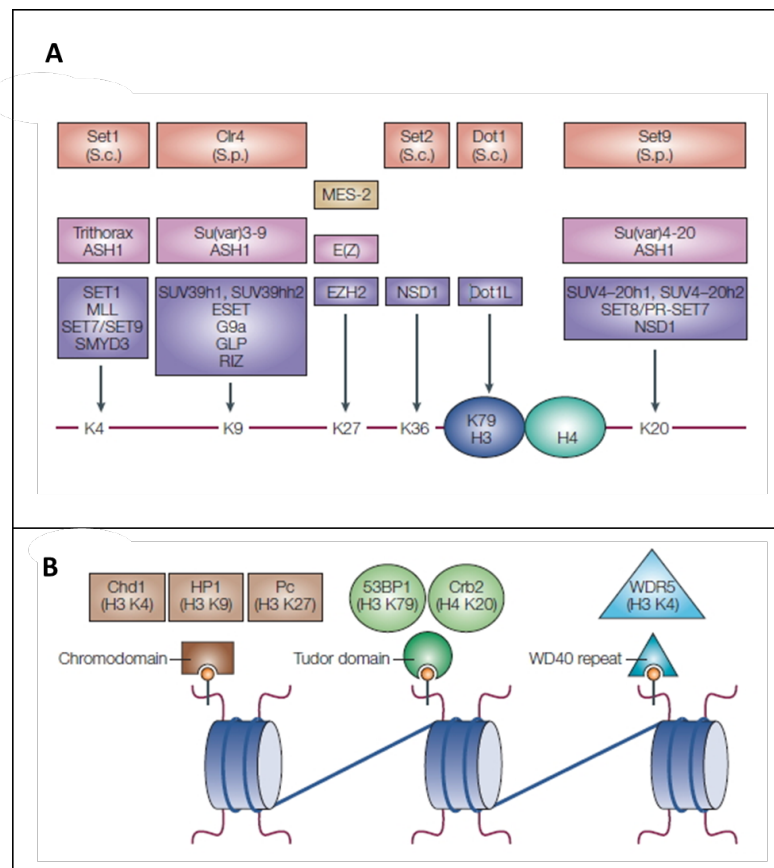
Figure 1.7. (a) The lysine methyltransferases are classified based to the specific lysine residue involved and the specific box color is different according to their origin: worm, yellow; yeast, red; mammalian, purple; fly, pink. HMTs are indicated as S.p. and S.c. and for *Schizosaccharomyces pombe* and *Saccharomyces cerevisiae*, respectively. The histone tails are depicted as straight lines

while the globular domains are represented as ovals. (**b**) Schematic representation of methyl-lysine binding proteins containing the chromodomain (brown rectangle), the Tudor domain (green circle) or the WD40-repeat domain (blue triangle). Adapted from Martin *et al.*, *Nat Rev Mol Cell Biol*, 2005, 6, 838–849.[117]

1.2.5.1.1 Polycomb repressive complex 2 (PRC2) and its components

After their identification in the fruit fly *Drosophila melanogaster* as crucial repressive regulators of developmental genes (e.g. HOX genes),[118] the polycomb group (PcG) proteins were later described as highly evolutionary conserved, from unicellular organisms to humans.[119] PcG proteins, assembled in multiprotein PRCs, control gene silencing mainly, but not only, through histone PTMs. Two main polycomb group complexes are described in mammals: PRC1 and PRC2. Additionally, also the phorepressive complex (PhoRC) and the polycomb repressive deubiquitinase (PR-DUB9) have been identified.[120–122] The PRCs possess histone modifying activities. While PRC1 monoubiquitinates H2AK119 and can compact chromatin by binding to nucleosomes, PRC2 catalyzes up to tri-methylation of H3K27 (H3K27me3), a repressive chromatin mark.[122–124] As all the other epigenetic marks, also H3K27 methylation is reversible due to the activity of the histone demethylases ubiquitously transcribed tetratricopeptide repeat, X chromosome (UTX) and Jumonji D3 (JMJD3) (Figure 1.8).[125–129]
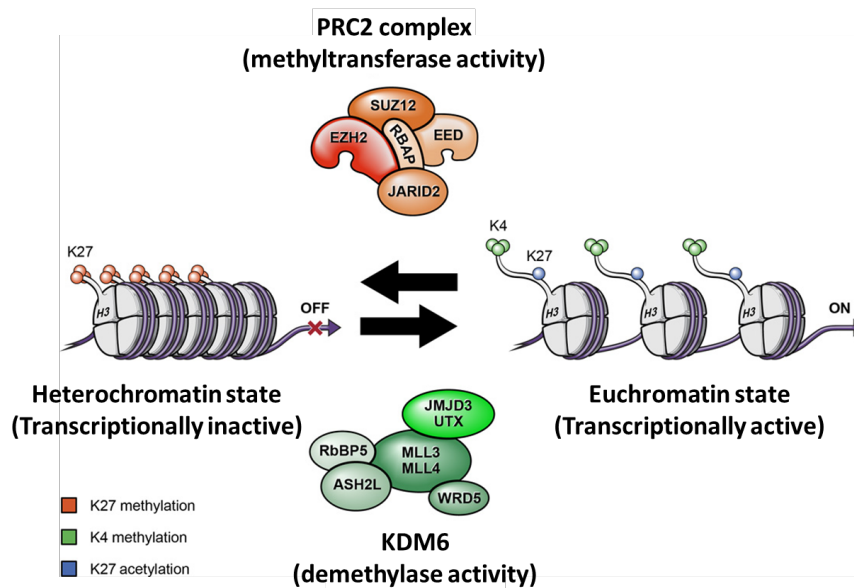
Figure 1.8. PRC2 histone methyl transferase activity on H3K27 (H3K27me3) correlates with the repression of gene expression. UTX and JMJD3, instead, catalyze the opposite reaction activating the transcription state. Adapted from Lulla *et al*. *Sci*. *Adv*., 2016.[130]

Interestingly, PRC1 has been shown to recognize and bind H3K27me3 and PRC2 is able to recognize H3K27me3 as well as H2AK119ub1.[113,114,131,132] In this way PRC1 and PRC2, being recruited at specific genomic *loci*, can cooperate in silencing gene expression.[133]
The minimal PRC2 core complex, endowed with a catalytic activity, include the following subunits (Figure 1.9): EZH1 or EZH2, suppressor of zeste 12 (SUZ12), and embryonic ectoderm development (EED). Additional protein subunits such as retinoblastoma associated protein 47 or 48 (RbAp46/48, also named RBBP4/7), adipocyte enhancer-binding protein 2 (AEBP2), polycomb-like proteins (PCLs), jumonji interaction domain 2 (JARID2) and AT-rich domain have been reported to play a key role in the PRC2 complex,

thereby modulating its activity in different contexts. Specifically, each PRC2 subunit carries out a specific function(s) that allow to complete the whole process of gene suppression through methylation modifications.[133]

EZH1 and EZH2 contain the conserved catalytic SET domain found in many other KMTs, and they both use SAM as a co-substrate. Even though EZH1 and EZH2 are charachterized by a high sequence similarity, with 76 % overall identity and 96 % sequence identity in their catalytic SET domains, such proteins show diverse catalytic efficiencies, distinct chromatin binding properties and expression patterns. In particular, while EZH1 is expressed both in dividing and non-proliferative differentiated adult cells, EZH2 is only active in dividing cells.[134] EZH1-containing PRC2 (PRC2-EZH1) provided a less effective methyltransferase activity than PRC2-EZH2.[135] Several pieces of evidence suggest that PRC2-EZH2 should establish cellular H3K27me1/2/3 levels, while PRC2-EZH1 is involved in restoring H3K27me1/2/3 that could have been lost through demethylase activity or upon histone exchange.[135] By themselves, EZH1 and EZH2 resulted unable to mediates the catalysis of H3K27 methylation, since both require the co-presence of at least two other component of the PRC2 complex: EED and SUZ12.[136–138] PRC2-independent functions have been discovered for EZH2, which resulted involved in the methylation of different non-histone substrates, including the transcription factors GATA4 and PLZF.[139,140] The non-PRC2 activity of EZH2 may involve activation but also repression of gene expression.[141]

After the EZH2-mediated catalysis of H3K27me3, EED is able to bind H3K27me3 marks through its WD40 domain resulting in a conformational change, which boots the enzymatic activity of EZH2, referred to as allosteric activation.[142] In this way, binding its own product *via* the WD40 domain of EED, PRC2 complex can spread to neighboring nucleosomes to deposit a new H3K27me3 mark, thus maintaining the repression of gene expression[143–145] SUZ12, instead, acts as a stabilization factor for PRC2 *via* its VEFS domain.[146] RBBP4 and RBBP7 are needed for PRC2 binding to unmodified nucleosomes and are required for a full methyltransferase activity.[136,147]

Despite both the EED and the SUZ12 subunits facilitate the stabilization of the complex though the binding with H3 *N*-terminal tail together with H3K27me3, the stabilization induced by SUZ12 plays a major role in promoting the completion of the triple-methylation process. The mechanism by which PRC2 is recruits on target genes is not properly clarified yet, but several studies showed that PRC2 shows a strong tendency to be present at the level of CpG island typical of the promoter regions of lowly transcribed or inactive genes. In particular, the recognition of this genomic region is allowed by AEP12 thanks to its "G-C rich" binding domain.[148,149]

JARID2, instead, specifically binds the EED subunit and contains four different domains: two DNA binding domains, a zinc-finger domain, an AT-rich interaction domain and two Jumonji domains, JmjC and JmjN.[150,151]

In addition, JARID2 acts as both inhibitor and activator of PRC2 in relationship to different levels of intracellular methylation. Moreover, JARID2 covers the role of PRC2 stabilizer interacting with nucleosome entities through its zinc-finger domain (Figure 1.9).[150–152]

Different pieces of evidences showed that the step involving the switch from H3K27me2 to H3K27me3 has the slowest conversion time in comparison with the other two methylation states of H3K27, thus highlighting how extensive time and stabilization is necessary for PRC2 to effectively conduct a complete methylation process.[153]
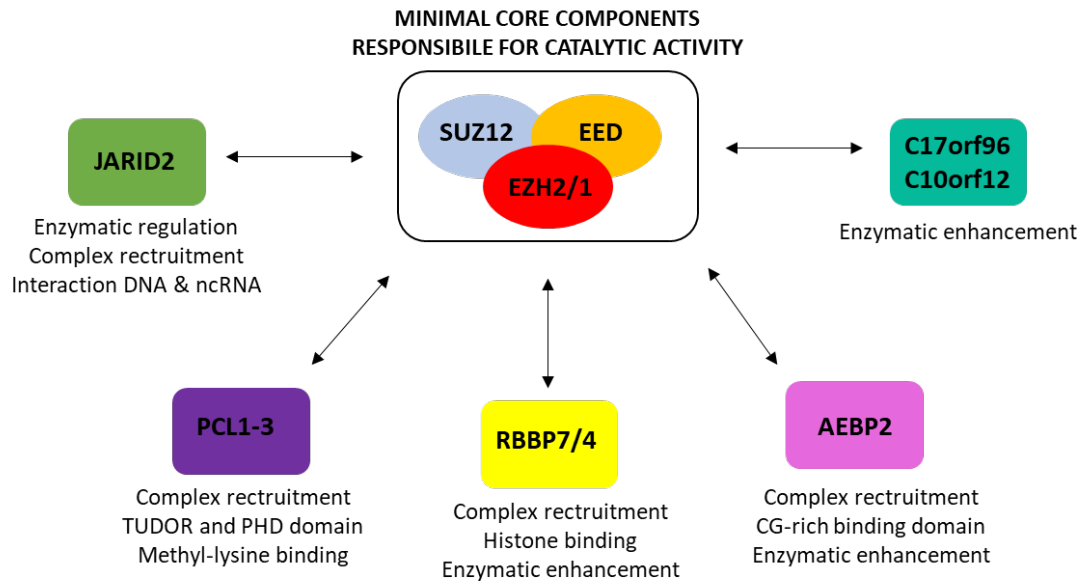
MINIMAL CORE COMPONENTS RESPONSIBILE FOR CATALYTIC ACTIVITY

JARID2

Enzymatic regulation
Complex rectruitment
Interaction DNA & ncRNA

SUZ12 EED
EZH2/1

C17orf96
C10orf12

Enzymatic enhancement

PCL1-3

Complex rectruitment
TUDOR and PHD domain
Methyl-lysine binding

RBBP7/4

Complex rectruitment
Histone binding
Enzymatic enhancement

AEBP2

Complex rectruitment
CG-rich binding domain
Enzymatic enhancement

Figure 1.9. Schematic representation of PRC2 complex, its subunits and their roles.

1.2.5.1.2 Relevance of EZH2 in cancer

The different biological roles covered by EZH2 and, specifically, its deep involvement in the regulation of cell cycle progression and different cellular pathways, easily explain the reason why its dysfunctions result associated with several solid or hematological tumors. A consistent number of literature examples show its dysregulation in cancers, as well as its involvement in stem cell maintenance and tumor development.[140,154,155] EZH2 OE has been related to increased H3K27me3 levels involved in the repression of tumor suppressor genes,[156,157] as well as to the establishment of specific methylation patterns driving a global epigenetic reprogramming.[158] EZH2 OE in cancer was reported for the first time in prostate[159] and breast[160] cancers. Its OE in prostate cancer was associated with aggressiveness and metastasis[161] and, similarly in endometrial, melanoma and bladder cancer, it correlates with invasiveness and poor outcome.[159,161–164] Moreover, EZH2 ectopic expression in primary cells was associated with proliferative advantage.[162] However, it was found that the sole EZH2 OE is not sufficient to cause leukemia, but can prevent hematopoietic stem cells exhaustion.[165] Additionally, EZH2 knock-in leads to the development of myeloproliferative disorders in mice.[166] Tanaka *et al*. found that EZH2 KO in the MLL-AF9 acute myeloid leukemia (AML) mouse model slowed leukemia progression *in vivo*, and compromised leukemia cell proliferation *in vitro*.[167] Conversely, a recent work by Vo *et al*. showed that, in a mouse model of *c*-Myc-driven group of medulloblastoma, EZH2 inactivation accelerated tumor initiation and progression. In particular they found that EZH2 normally represses Gfi 1 proto-oncogene expression, but in case of EZH2 inactivation Gfi 1 is overexpressed and collaborates with *c*-Myc, inducing the tumor development.[167] Even though EZH2 is involved in regulating the epithelial-mesenchymal transition (EMT), its role in this process is still debated. In laryngeal squamous cells carcinoma (LSCC), EZH2 promotes EMT mediating the down-regulation of E-cadherin (Ca^{2+} dependent cell adhesion molecule E), and up-regulation of H3K27me3 *in vitro* and *in vivo*,[168] but, on the other hand, in ovarian cancer cells, it was recently described as essential for the maintaince of an epithelial phenotype.[168] These evidences could also indicate a different role for EZH2 in relation to the cell/cancer type. Recently, EZH2 was described as crucial regulator of multiple myeloma (MM) progression *via* the

modulation of different factors, including the oncogenes IRF-4, XBP-1, PRDM1/BLIMP-1 (also described as immune response regulators),[169–172] c-Myc as well as the tumor suppressor microRNAs miR-125a-3p and miR-320c.[173] As previously mentioned, EZH2 has PRC2 independent functions, but also non-canonical functions, whose mechanism is not yet fully understood. However, also these unconventional activities seem to play a role in cancers (See section 4.3.2). For example, in natural killer/T-cell lymphoma EZH2 acts as transcriptional activator. Its activity is methylation-independent, based on binding and activation of the CCND1 promoter.[174] Some examples of non-histone targets methylation in cancers are given by androgen receptor (AR) in prostate cancer,[175] and signal transducer and activator of transcription 3 (STAT3) in glioblastoma.[176]

1.2.5.1.3 EZH2 mutations (gain or loss of function)

Activating or inactivating somatic EZH2 mutations and deletions have been found in 22% of germinal-center diffuse large B-cell lymphoma (DLBCL), 7% of follicular lymphomas, and 12–23% of patients having myelodysplastic and myeloproliferative disorders. These mutations have been found within the SET domain and include Y641F, Y641N, Y641S, Y641H, Y641C 128, A677G[177] and A687V.[178] The Y641 mutations were initially reported as involved in the inactivation of the catalytic activity of the PRC2 complex *in vitro*, which was in contrast with the hyper-methylated state reported in EZH2-mutated cancers. Further studies demonstrated that wild-type (WT) EZH2 mostly mono-methylate H3K27, whereas the Y641 mutants display increased efficiency for H3K27 di- and tri-methylation. In fact, all the reported Y641 mutations are heterozygous, thus the mutant allele is always associated with a WT allele. Hence, mutation of Y641 may cooperate with WT EZH2 to increase H3K27 methylation, thus providing a condition similar to that one registered after EZH2 OE.[179] In T-cell acute lymphoblastic leukemia, myeloproliferative disorders and myeloid malignancies a significant number of missense, nonsense and frameshift EZH2 heterozygous or homozygous mutations have been recorded.[180–182] These mutations have been associated with loss of methyltransferase activity, leading, in particular cases, to an enhancement of NOTCH1 or RUNX1 oncogenic signaling. These evidences suggest that also loss of EZH2 can contribute to tumor development. Even though there are a huge number of data about EZH2 mutations in hematological cancers, not much have been investigated about such mutations in solid cancers. In conclusion, since that both gain and loss of function EZH2 mutations have been identified in cancers, we could conclude that EZH2 could act in turn as an oncogene or as an onco-suppressor, in relation to the context. However, in each condition, a balanced EZH2 activity is required to keep homeostasis.[159]

1.2.5.1.4 EZH2 in cancer and non-cancer cell stemness

The role of EZH2 in maintaining the self-renewal potential in adult and embryonic stem cells (ESC) has been pointed out by numerous studies. Already in 2006, it has been reported that PRC2 was able to maintain pluripotency in ESCs by targeting and repressing a special set of developmental genes (including OCT4, SOX2, NANOG), whose expression could induce differentiation.[183] Both the PRCs are involved in a spatial and temporal control of epigenetic processes in stem cells, repressing undesirable differentiation conditions, while selectively and stepwise establishing a specific terminal differentiation program.[184] A recent study by Shan *et al.* provided new insights in the role played by EZH2/PRC2 in cell fate decision in ESC.[185] Interestingly, they have shown that PRC2 is differently required for maintaining pluripotency in ESC, being essential for the primed state of ESC, but dispensable in naïve state cells. A direct correlation between ESC and poorly differentiated

cancer cells has been highlighted by a shared gene expression signature of PRC2 target genes.[186] Accordingly, EZH2 resulted crucial for cancer stem cell formation as well as for the expansion of an aggressive cancer stem cell population that correlates with cancer progression.[187] In this framework, it is evident that EZH2 is primarily regarded as a target in cancer. However, EZH2 activity is also affecting thymopoiesis and lymphopoiesis as well as hematopoietic stem cell proliferation and differentiation.[188] Several studies also assessed EZH2 as regulator of plasticity and T-cell differentiation, as well as of the development of graft-versus-host disease (GVHD) and autoimmune pathologies. These data indicate that the modulation of histone methylation may have key roles in the development of novel therapeutic strategies for the treatment of GVHD or other T cell-mediated inflammatory disorders.[188]

The capability of EZH2 to maintain the multipotent identity has been proved also in non-cancer adult stem cells, including muscle cell precursors (myoblasts)[189] and neural stem cells (NSCs).[190] In NSCs, EZH2 OE correlates with an increased oligodendrocytes and decreased astrocytes differentiation.[190] Recently, EZH2 has been described to be fundamental for astroglial differentiation in adult mice through the ink4a (p16)/Arf (p19) and Olig2 inhibition.[191,192] On the other hand, EZH2 KO during mice cerebral development is responsible for the reduction of H3K27me3 level in cortical progenitor cells, leading to a direct (into neurons) or indirect (in the cerebral cortex) differentiation. [192] Aberrant EZH2 expression has been registered also in muscular disorders. For example, in Duchenne muscular dystrophy, raised amount of TNF$-\alpha$ from myotubes inhibited the regenerative potential of satellite cells mediating the epigenetic silencing of the Notch-1 signaling, through the NF-ϰB-stimulated recruitment of DNMT3b and EZH2 on Notch1 gene promoter.[193] It has been shown that Pax7 activation and satellite cells proliferation is promoted by pharmacological inhibition or genetic knockdown of either p38a kinase or EZH2, with subsequent muscles regeneration in dystrophic or normal mice.[194] Proliferation of β$-$cells in pancreatic islets plays a pivotal role in self-renewal and in adaptive islet expansion. In this context, EZH2 has been described to repress Ink4a/Arf in β-cells.[195] EZH2 induced Ink4a repression in young adult mice was sufficient to increase replication and regeneration of β-cells.[196] Additionally, EZH2 was found involved in osteogenesis and adipogenesis. Human mesenchymal stem cells (hMSCs) can be activated for osteogenesis, after EZH2 inactivation by cyclin-dependent kinase 1-mediated phosphorylation.[197] Dissociation of EZH2 from the promoter region of myocyte enhancer factor-2-interacting transcriptional repressor (MITR) gene results in its upregulation and consequent association with PPARγ 2, counteracting its activity thus preventing adipogenesis, wheares enhancing osteogenic differentiation from hMSCs.[198] On the other hand, EZH2 supports adipogenesis by disrupting the Wnt/β-catenin signaling through its direct interaction with the Wnt genes promoter to repress their expression.[199]

1.2.5.2 Histone Lysine Demethylases

Based on their catalytic mechanisms (Figure 1.10) as well as sequence homologies, two main families of KDMs have been identified (Table 1.1).[200]

The LSD-family members are flavin adenine dinucleotide (FAD)-dependent amine oxidases (Figure 1.10) and demethylate mono and di-methylated but not tri-methylated lysines[68] and show closed homology to the well-known monoamine oxidases (MAOs).[64]

The second class embraces the JmjC domain-containing proteins (JmjC) and consists of more than 30 human dioxygenases classified in turn into seven different subfamilies KDM2-8 (depending on their histone sequence and homology of their JmjC domains, as well as on their methylation state selectivity), and catalyze the demethylation event in a Fe^{2+}/2-oxoglutarate (2-OG) dependent manner.[201,202] Their catalytic mechanism is begings with the formation of a superoxide radical by the complex Fe^{2+}/2-OG, which affects the carbon in position -2 of 2-OG, thus allowing the establishment of a Fe^{4+}-oxo specie and the consequent decarboxylation of 2-OG to succinate. The Fe^{4+} abstract a hydrogen atom from the *N*-methyl group of the amine substrate and it being thus reduced to Fe^{3+}. The last two steps lead to the generation of a carbinolamine species on the substrate, which leaves the demethylated product releasing formaldehyde (Figure 1.10).

Since their mechanism does not require an imine formation, JmjC KDMs, in contrast to what happen for KDM1, are also able to remove the methyl mark from quaternary lysine (Figure 1.10).[201–203]
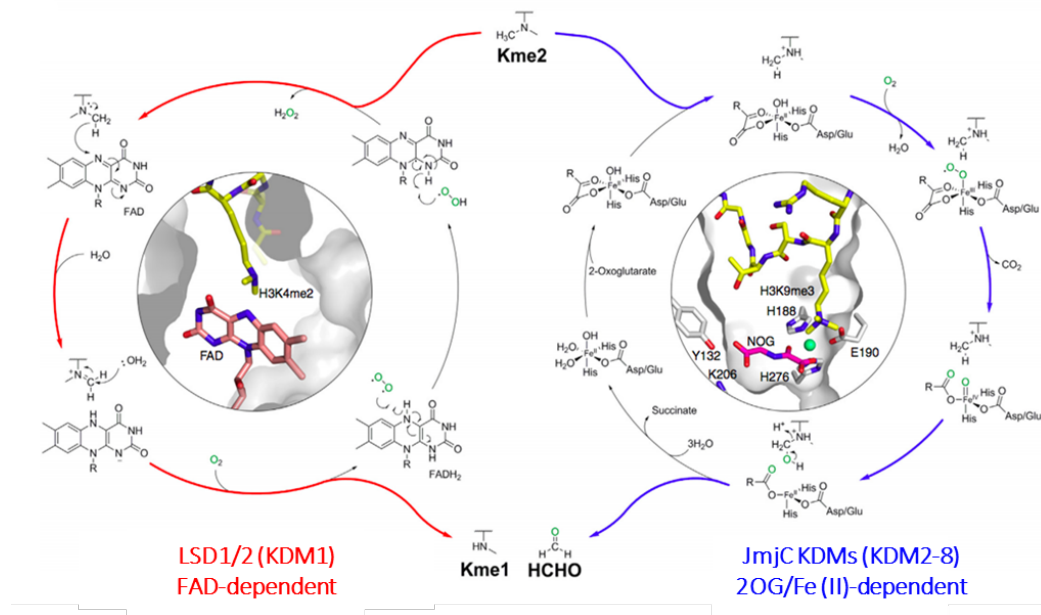
Figure 1.10. Catalytic mechanisms of KDM1 (LSD1, LSD2) and KDM2-7 (JmjC) enzymes. Adapted from Thinnes *et al*. *Biochimica et Biophysica Acta 1839*, 2014, 1416–1432.[204]

Class of KDMs	Official Symbol	Others Name	Histone Substrates	Up-regulation	Down-regulation
Flavin-dependent lysine-specific demethylases (LSDs or KDM1s)	**KDM1A**	LSD1, KDM1, AOF2, BHC110	H3K4me1/me2, H3K9me1/me2	ER-negative breast cancer, bladder, colorectal, small cell lung cancer	ganglioneuroblastoma/ganglioneuroma
	KDM1B	LSD2, AOF1, C6orf193	H3K4me1/me2	?	?
	KDM2A	JHDM1A, FBXL11, CXXC8, FBL11, FBL7, LILINA	H3K36me1/me2	lung, breast, gastric cancer	glioblastoma, prostate cancer
	KDM2B	JHDM18 CXXC2, FBXL10, fbl10, PCCX2	H3K4me3, H3K36me1/me2	pancreatic ductal adenocarcinoma, leukemia, bladder cancer	glioblastoma, prostate cancer
JmjC domain-containing proteins	**KDM3A**	JHDM2A, JHMD2A, JMJD1, JMJD1A, TSGA	H3K9me1/me2	breast, colorectal, renal, prostate, hepatocellular cancer	?
	KDM3B	JMJD18, NET22, 5Qnca, C5orf7	H3K9me1/me2	?	?
	KDM3C	JMJD1C, TRIP8	H3K9me1/me2	?	?
	KDM4A	JMJD2A, JMJD2, JHDM3A, TDRD14B	H3K9me2/me3, H3K36me2/me, H14K26/me2/me3	breast cancer	bladder cancer
	KDM4B	JMJD2B, TDRD148	H3K9me2/me3, H3K36me2/me, H14K26me2/me3	peripheral nerve sheath tumor	?
	KDM4C	JMJD2C, JHDM3C, GASC1, TDRD14C	H3K9me2/me3, H3K36me2/me, H14K26me2/me3	esophageal, squamous, prostate, B-cell lymphoma, medulloblastoma, breast cancer	?
	KDM4D	JMJD2D	H3K9me2/me3, H14K26me2/me3	?	?
	KDM4E	JMJD2E, KDN4DL	H3K9me2/me3, H3K56me3	?	?
	KDM5A	JARID1A, RBBP-2, RBBP2, RBP2	H3K4me2/me3	lung, hemopoietic cancer	melanoma
	KDM5B	JARID1B, PUT1, RBBP2H1A CT31, PLU-1	H3K4me2/me3	prostate, breast, bladder	?
	KDM5C	JARD1C, MRXSJ, SMCX, XE 169, MRXJ, MRXSCJ	H3K4me2/me3	Prostate	renal carcinoma (mutated)
	KDM5D	JARID1D, SMCY, HY, HYA	H3K4me2/me3	?	prostate (deleted)

27

KDM6A	UTX, KABUK2	H3K27me2/me3	breast	lung (mutated), renal clear cell carcinoma, esophageal squamous, liver multiple myeloma, chronic myelomonocytic leukemia, transitional cell carcinoma of bladder
KDM6B	JMJD3	H3K27me2/me3	prostate, leukemia, lung, liver	?
KDM7A	JHDM1D	H3K9me1/me2, H3K27me2/me3	?	?
KDM7B	PHF8, MRSXSSD, ZNF422, JHDM1F	H3K9me1/me2, H3K20me1	prostate, laryngopharyngeal squamous cell carcinoma, esophageal squamous cell carcinoma, non-small-cell lung cancer	?
KDM7C	PHF2, JHDM1E, CENP-35, GRC5	H3K9me2	esophageal squamous cell carcinoma	stomach, colorectal, breast, head and neck-squamous cell cancer
MINA	MINA53, ROX, NO52, MDIG, FLI14393	H3K9me3	non-small cell lung cancer	?
NO66	ROX, MAPJD, NO66	H3K4me1/me3, H3K36me2	non-small cell lung cancer	?
KDM8	JMJD5	H3K36me2	?	?

? = role yet unknown

Table 1.1. Histone lysine demethylases (KDMs) classification, specificity and potential role in cancer.[200]

1.2.5.2.1 Histone Lysine Demethylase: LSD-family members

LSD1 removes methyl groups from H3K4 when mono- or di-methylated (H3K4me1/2) at the ε-position. Metzger and coworkers demonstrated that the specificity of action for LSD1 can change from mono- to dimethylated H3K9 (H3K9me1/2) when co-localized with the AR. In addition, LSD1 is known to be able to demethylate also non-histone targets, such as p53, DNMT1 and E2F1. LSD2 (also called AOF1 or KDM1B), seems, so far, been only involved in the demethylation of H3K4me1/me2. SWIRM domain of LSD2 takes part in an interaction with glyoxylate reductase 1 homolog (GLYR1; also known as NPAC), which positively stimulates its demethylase activity. Such interaction is mediated through a unique coiled loop typical of LSD2, thus NPAC does not associate with LSD1. In fact, beyond sharing the AO and SWIRM domains, LSD1 and LSD2 are characterized by different domain architectures which correlate with specific proteins showing distinct genomic distribution profiles. For example, LSD1 takes part in CoRepressor for Element-1-Silencing Transcription factor (CoREST) complex and this interaction is due to the presence of a coiled-coil 'Tower' domain inserted into the AO domain of LSD1, which is replaced, in LSD2 structure, with a unique *N*-terminal zinc finger domain with unknown function.[205,206]

A genome-wide analysis showed that LSD2 is mainly located in the intragenic regions of actively expressed genes, thus inducing their activation perhaps through the association with transcriptional elongation factors.[207] Different pieces of evidence showed that LSD2 seems to be not crucial for mouse development. However, the DNA methylation of several imprinted genes is lost in oocytes from LSD2-deleted females. Consequently, the embryos derived from these oocytes are characterized by biallelic expression or silencing (i.e., loss of monoallelic expression) of the affected imprinted genes and died before midgestation.[208] The molecular mechanism involving the functional link between H3K4 demethylation and DNA methylation for expression of imprinted genes is still to be clarified.

1.2.5.2.2 Histone Lysine Demethylase: JmjC domain-family members

The JmjC domain was first idividuated in a gene trap screen for factors taking part in neural tube formation. Homozygous mutant mice were characterized by abnormal groove formation on the neural plate and a defect in neural tube closure. Takeuchi *et al*. called such mutation "Jmj", since homozygous mutant mice usually have an additional groove at the future midbrain-hindbrain boundary that cross the normal neural groove, creating a ''cross'' shaped cut on the neural plate (in Japanese the word "Jumonji" means "cruciform").[209] The JmjC domain is typical of 31 human proteins, among which about 20 have been identified as able to catalyze the demethylation of specific histone lysine. Depending on the homology of the JmjC domain as well as on the presence of other domains, such enzymes can be further classified into seven distinct subfamilies (Figure 1.11).[64] The first JmjC domain-containing protein identified as a histone lysine demethylase was FBXL11 (F-box and leucine-rich repeat protein 11). In particular, FBXL11 and FBLX10 have been proved to catalyze the H3K36me2/me1 demethylation process [210] and FBXL10 seems to act also as H3K4me3 demethylase, but this activity is still controversial.[211] In addition of its catalytic domain, FBXL10 harbor a F-box (which is a signature domain for a component of SCF (SKP1–cullin-1–F-box) E3 ligases) and a CXXC DNA-binding domain.[212] Recently has been highlighted that FBXL10 controls the expression of Polycomb target genes, indicating that FBXL10 could also contribute to tumorigenesis.

Figure 1.11. Phylogenetic tree of JmjC domain-containing proteins. Proteins known to be HDMs are marked in bold and the methylation-levels of their targeted residues closely reported. Histone H3 are represented with orange circles while H4 with green ones. Asterisk referred to proteins showing a non-canonical amino acid at the cofactor binding portion probabibily responsible for the catalytic inactivity. Adapted from Højfeldt, *et al*. *Nat*. *Rev*. *Drug Discov*. 2013, 12 (12), 917–930.[213]

JMJD1A is a histone demethylase selective for H3K9me2/me1[214] and two homologues of the latter have been identified in human cells: JMJD1B and JMJD1C. JMJD1A shows a characteristic LXXLL motif that is involved in nuclear receptor interactions and results implicated in demethylation of H3K9me2 at the level of AR target genes. Indeed, JMJD1A was also found to interact with the AR in a ligand-dependent way. Studies of knockout (KO) mice have proved essential roles for this histone demethylase in germ cell development and metabolism.[215,216] JMJD1A resulted implicated in the transcriptional control of metabolic genes in adipose tissues and muscle since JMJD1A KO mice showed an adult onset obesity phenotype. In addition, JMJD1A is dynamically and strongly expressed during spermatogenesis: male JMJD1A KO mice result infertile, presenting a severe reduction in sperm count as well as small testes. This defect seems to be connected to a JMJD1A-dependent regulation of the expression of genes responsible for maturation and sperm chromatin condensation through the catalysis H3K9me2/me1 demethylation. During hypoxia JMJD1A stimulates the expression of hypoxia-inducible factors (HIFs) target genes such as adrenomedullin (ADM). Krieg *et al*. demonstrated that, in colon cancer, under hypoxia condition, the expression of ADM is regulated by JMJD1A and ADM favors the growth of colon carcinoma cells. However, this pathway still need to be elucidated in breast cancer cells and hepatocellular carcinoma (HCC).[217,218] The often observed deletion of 5q31 locating JMJD1B gene as well as the registered reduced expression of JMJD1C in various malignancies, seems to indicate potential roles of JMJD1 proteins in tumor suppression.[219]

JMJD2 subfamily, that consists of four expressed members, JMJD2A-2D, selectively demethylates di and triple-methylated lysines on histone H3. Different members of such family show slightly differences in term of substrate preference.[220] For example, JMJD2D

catalyze the demethylation of H3K9me2/me3, but not of H3K36me2/me3. Sequence alignment of JMJD2A and JMJD2D proves that a variable Ser/Ala position in the binding pocket is responsible for this different selectivity and the generation of Ala291Ser and Ser288Ala mutations in JMJD2D and JMJD2A, respectively, modulates the substrate specificity of these enzymes. Important genetic data collected in a mouse model of T cell lymphoma, showed that the loss (or the decreased level) of H3K9me3 seems to favor carcinogenesis.[221] Given the evidence that proved that the JMJD2 family catalyze the H3K9me2/3 demethylation, it is rational to hypnotize that an OE of these proteins would result in analogues outcome. Furthermore, different studies have dimostrated that JMJD2C is required for growth in varius cancer cell lines, including squamous cell carcinoma, breast carcinoma, prostate carcinoma and diffuse large B cell lymphoma.[222]

JARID1 subfamily members (JARID1A-D) demethylates H3K4me2/me3 marks. JARID1A regulates circadian clock length, not *via* its catalytic demethylase activity, but inducing the inhibition of HDAC1. JARID1A takes part in a complex with CLOCK and BMAL1, which are well-known transcription factors fundamental for the modulation of animal circadian rhythms. In mammalian cells, deletion of JARID1A correlates with a reduced activation of circadian genes as well as with a short circadian rhythm, in addition to a reduced histone H3K9 acetylation. Moreover, JARID1A has been described as a a key effector of retinoblastoma protein (pRB) mediated cell cycle withdrawal and differentiation by interacting with the tumor suppressor pRB.[223] JARID1B catalyze the demethylation of H3K4me2 and H3K4me3, which resulted strongly associated with coding regions and transcription start sites (TSSs) in embryonic stem cells.[224] Knockdown of JARID1B correlates with an average of 2.2 fold increased H3K4me3 level at JARID1B targets. However, after its deplation, only 3.4% of JARID1B targeted appeared differentially expressed. In addition, JARID1B correlates with a non productive initiate ectodermal differentiation *in vitro*. Thus, it has been proposed that the function of JARID1B is to maintain the H3K4me3 status of its targeted genes at intermediate/low levels ensuring the proper execution of cell differentiation programmes.[224] Such KDMs results overexpressed in different cancers, including prostate, melanoma breast and bladder carcinoma.[225–229] In addition to its implication in epilepsy and X-linked mental retardation, JARID1C is also connected to the pathogenesis of human papillomavirus (HPV)-associated cancers since resulted one of the E2-dependent regulators of HPV oncogene expression.[230]

The JmjC domain-containing proteins, JMJD3 and UTX, were found able to specifically catalyze the removal of di- and trimethyl units from H3K27 and, thereby counteract PcG-mediated histone modification by EZH2. After lipopolysaccharide (LPS) treatment of macrophages, JMJD3 is recruited to promoters that show increased H3K4me3 levels.[129,231] Specifically, most of the promoters bound by JMJD3 resulted not associated with H3K27me3 before JMJD3 binding and only a few number of these promoters shows decreased levels of H3K27me3 following LPS treatment. Moreover, JMJD3 depletion only alters the expression of relatively few genes and does not correlates with an increased H3K27me3 levels. Thus, JMJD3 could be described as a safeguard against further H3K27 methylation events, ensuring the activation of specific genes after LPS treatment. UTX is associated with MLL3/4 complexes and was the first reported mutated histone demethylase gene associated with cancer.[127,232] Biallelic somatic mutations of UTX have been identified in several tumors (mainlyin multiple myeloma), clearly suggesting that UTX has a tumor suppressor role.[233]

Concluding, the role of the JmjC KDMs in cancer has not yet been fully understood, in fact, as reported, some evidences shows that JmjC KDMs can be both genetically amplified and translocated, up-regulated, deleted or genetically mutated and afterwards down-regulated in cancer (Table 1.1).[213,234,235]

1.2.6 Histone Acetylation

The acetylation of histone and non-histone proteins modulate a large variety of cellular processes, thus affecting the entire organism.

As previously mentioned, histone acetylation involves the ε-amino group of histone lysine resulting from the opposite activity of HATs and HDACs (Figure 1.12).[236,237]
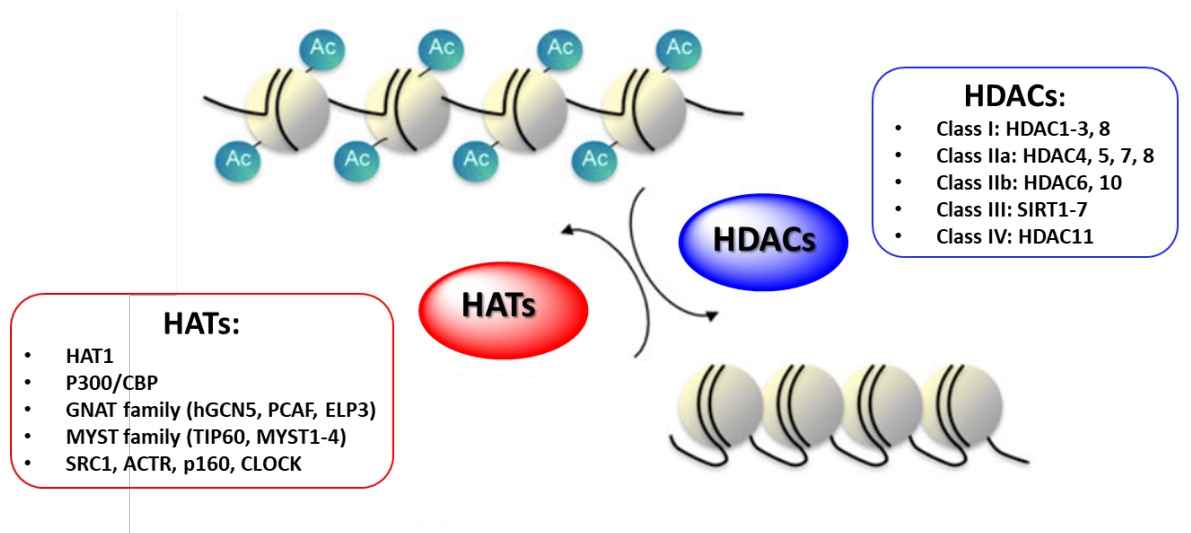

Figure 1.12. HATs and HDACs families. Illustration of the switching of the chromatin conformation as a result of the HATs/HDACs activity. Adapted from Schneider *et al*. *Neurotherapeutics*, 2013, 10(4).[238]

HATs, using acetyl-coenzyme-A (Acetyl-CoA) as an acetyl group donor, neutralize the positive charge of the ε-amino group of histone lysine residues thus counteracting the electrostatic interaction physiologically present with the negatively charged phosphate groups typical of DNA. The resulted euchromatin state allows more access of transcriptional factors, transcriptional regulatory complexes and RNA polymerases to DNA promoter regions.[238] Conversely, HDACs catalyze the removal of acetyl groups from histone lysine restoring the positive charge and leading, in this case, to the occurrence of the heterochromatin state which correlates with the "turn off" of the gene transcription.[239,240] HATs and HDACs are the main actors responsible for the regulation of the balanced acetylation levels of histones but also non-histone substrates, modulating proliferation, apoptosis, angiogenesis, differentiation thus playing a fundamental role in cancer and neuroprotection and inflammatory conditions.

1.2.6.1 Histone acetyltransferases (HATs)

HATs can be organized into four different families, based on primary-structure homology: the general control non-derepressible 5 (GCN5)-related *N*-acetyltransferase (GNAT) family (KAT2); the p300/CBP (CREB binding protein) family (KAT3); the MYST family (KAT6) and the Rtt109 family, named for identification as regulator of Ty1 transposition gene product 109 (KAT11).

Several pieces of evidence also showed that different transcription factors, as well as over a dozen of proteins (for example, TAFII250/TAFII130, and the steroid-receptor co-activator (SRC) families), possess intrinsic HAT activity.[241–243] GCN5 is the first identify member of GNATs which includes, in addition to the latter, P300/CBP-associated factor (PCAF), Elp3, Hat1, Hpa2 and Nut1. The MYST HATs family name results from the acronym of its members: MOZ, Sas2, Tip60 and Ybf2/Sas3.[244] HATs are often part of multi-subunit protein complexes that influence their catalytic activity and binding selectivity. Bromodomains, chromodomains, WD40 repeats, Tudor domains and PHD fingers cooperate to recruit HATs to the appropriate location in the genome. For example, GCN5 contains a bromodomain motif that is important for the binding, recognition and retention of SAGA on acetylated promoter nucleosomes. Since HATs are responsible for both transcriptional activation and repression effect, further analyses are needed to understand how these single enzymes associated with other proteins, can regulate this switch. The gene transcription role of HATs can be also schematized into gene-specific results and global effects. While histone acetylation of promoter regions regulates activation or repression of specific genes, histone acetylation over large chromatin regions, including non-promoter and coding regions, mediate a global gene expression effect. Specifically, global histone modification levels are predictive of cancer recurrence.[245]

Recent proteomic analysis showed that several proteins contain acetylated lysine residues, many of which are metabolic enzymes. Almost every enzyme in glycolysis, tricarboxylic acid, glycogen and fatty acid metabolism, as well as the and urea cycles enzymes, was found to be acetylated in human liver tissue. Importantly, p300/CBP acetylates the tumor suppressor p53.[246] It is now known that binding of p53 to p300/CBP through its proline rich (PXXP) domain mediates the DNA-dependent acetylation of p53, thereby stabilizing the acetylated p53-p300/CBP complex.[247]

Based on their cellular origin and functions, HATs can also be divided in two classes: i) type-A HATs are nuclear enzyme and catalyze transcription-related acetylation events and are, therefore, responsible for generating the epigenetic code;[27] ii) type-B, instead, are cytoplasmic enzymes and catalyze acetylation events linked to the transport of newly synthesized histones from the cytoplasm to the nucleus for deposition onto newly replicated DNA.

1.2.6.2 Histone deacetylase (HDACs)

18 mammalian deacetylase enzymes have been identified so far, which are classified as follows: class I, II, IV and III, based on their sequence homology to their yeast orthologues Rpd3, HdaI and Sir2, respectively (Table 1.2).[248–250]

CLASS	HDAC	INTERACTION	CELLULAR LOCALIZATION	TISSUE EXPRESSION
I **(Homologue to yeast Rpd3)**	**HDAC1**	DNMT1, ATM, BRCA1, MECP2, MyoD, p53, pRb, NF-kB	Nucleus	Ubiquitous
	HDAC2	DNMT1, BRCA1, pRb, NF-kB, GATA-2, Bcl-6	Nucleus	Ubiquitous
	HDAC3	pRb, NF-kB	n/c	Ubiquitous
	HDAC8	p53, ERRα, cortactin	n/c	Ubiquitous
IIA **(Homologues to yeast Hda1)**	**HDAC4**	14-3-3, MEF2, calmodulin, GCMa, GATA-1, HP-1	Shuttling n/c	Heart, muscle, brain
	HDAC5	14-3-3, MEF2, calmodulin, Smad7, HP-1, GCMa	Shuttling n/c	Heart, muscle, brain
	HDAC7	14-3-3, MEF2, calmodulin, FLAG1&2, HIFa, Bcl-6	Shuttling n/c	Heart, placenta, pancreas, muscle
	HDAC9	FOX3P	Shuttling n/c	Muscle, brain
IIB	**HDAC6**	a-tubulin, HSP90, SHP, Smad7	Cytoplasm	Kidney, liver, heart, pancreas
	HDAC10	HSP90, PP1, LcoR	Cytoplasm	Spleen, kidney, liver
IV **(Similar to both Class I and II)**	**HDAC11**	HDAC6	n/c	Heart, muscle, kidney, brain

n/c: Nucleus and Cytoplasm

Table 1.2. Classification of HDACs (class I, II, IV) enzymes.

Nucleus-located Class I members (HDAC1, 2, 3, 8) are ubiquitously expressed in various cell lines. Based on sequence homology among their deacetylase domains, class II results in turn divided into two subclasses: IIa (HDAC4,5,7,9, which seems to shuttle between nucleus and cytoplasm) and IIb (HDAC6,10, which contain two catalytic domains, despite are preferably expressed in the cytoplasm seems , also in this case, able to shuttle between nucleus and cytoplasm).[251–253] Class IV, instead, consists only of one member, HDAC11, about which little is known.[254] The deacetylase activity of all these isoforms is Zn^{2+}-dependent.[255]

The proposed deacetylation mechanism involves an acetylated lysine residue (shown in red in Figure 1.13) which coordinates the zinc cation in the active site thus allowing the establishment of a tetrahedral intermediate by nucleophilic attack of the water molecule,

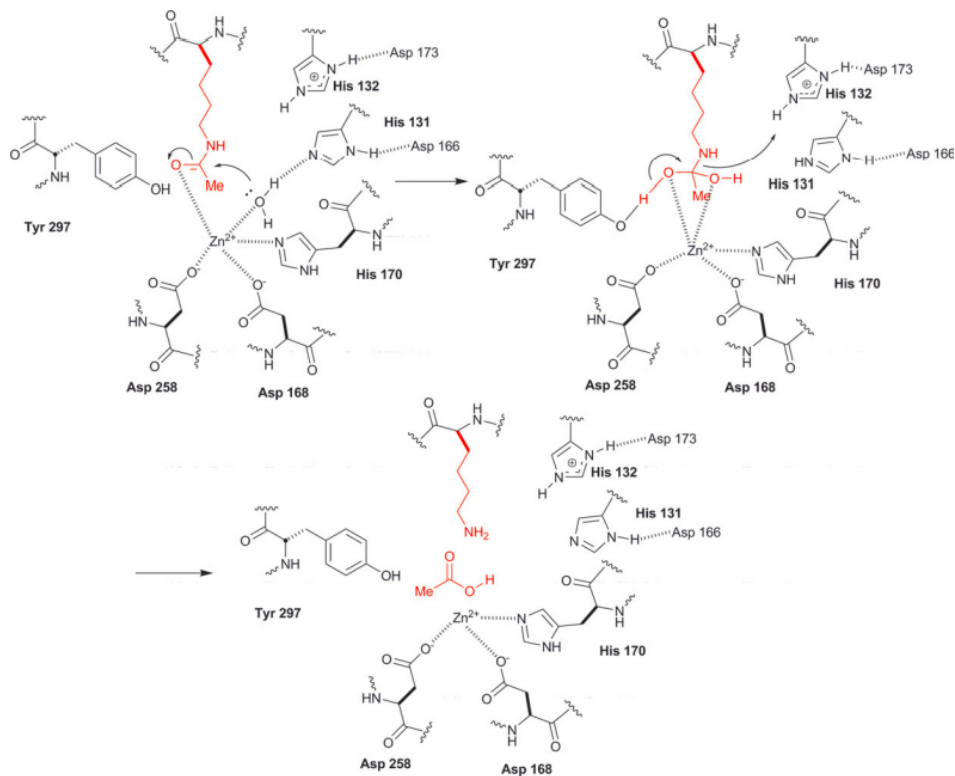after which the intermediate collapses to release the deacetylated lysine residue and a acetic acid molecule.[256]

Figure 1.13. Proposed mechanism of action of Zn^{2+}- dependent HDACs.[256]

These enzymes possess a highly conserved catalytic domain of approximately 390 amino acids, but, in particular, the class II of these proteins are two to three times larger in size than the class I proteins (120-130 kDa and 42-55 kDa, respectively) and there are certain conserved sequence motifs in the catalytic domain that differ between the two classes. Members of class I and II are subunits of multiprotein nuclear complexes that play a crucial role in repression of DNA transcription. HDAC1 and 2 have been found in the CoREST complex that inactivates the expression of neuronal genes in non-neuronal tissues and also as components of NURD and SIN3 repressor complexes.[257,258]

The cellular trafficking of class IIa members (HDAC4, 5, 7, 9) are defined by intrinsic nuclear import and export signals as well as binding sites for 14-3-3 proteins, indeed these isoforms contain three conserved 14-3-3 binding sites. Binding of the 14-3-3 proteins stimulate the nuclear export or cytoplasmic retention of the class IIa HDACs in a phosphorylation dependent manner that consequently regulates the activity of transcription factors like the myocyte enhancer factor-2 (MEF2).[254,259,260] Moreover the phosphorylation of these 14-3-3 binding sites depend on several signaling pathways including salt-inducible kinases,[261] microtubule affinity-regulating kinases[262] and Ca^{2+}/calmodulin-dependent kinases (CaMKs).[259] In addition, class II HDACs differ from class I proteins depending on their tissue expression, subcellular localization and consequently biological roles. Class I HDACs are ubiquitously expressed, whereas class II enzymes display tissue-specific expression in humans and mice.[263] The Class III isoform is known also as sirtuin family. Humans contain seven different sirtuins, all share a conserved catalytic core domain of about 275 amino acids and operate by a different mechanism that requires NAD^+ as cosubstrate.[264] Based on phylogenetic analysis of their sequence, mammalian sirtuins have been divided into four classes: SIRT1-3 belong to class I, SIRT4 to class II, SIRT5 to class III, and SIRT6 and SIRT7 to class IV.[265]

1.2.6.2.1 Class I HDACs

Class I HDACs are components of multiprotein complexes. HDAC1 and HDAC2 show a high degree of homology, with an overall sequence identity of approximately 85% and have undergone little functional divergence, although specific and distinct roles have also been identified for each of them.[266] In a recent series of 140 colorectal cancer samples, high HDAC1, 2, 3 expression levels correlated with significantly reduced patient survival, with HDAC2 expression being an independent prognostic factor.[267] In hepatocellular carcinoma, high HDAC1 expression was associated with cancer cell invasion into the portal vein. Most studies show that HDAC1 OE appears especially common in cancers of the gastrointestinal system and is associated with enhanced proliferation, invasion, advanced disease and poor prognosis. However, these studies mostly investigated only HDAC1 and no other HDAC family member. In cancer cells, since HDAC1 is involved in controlling cell proliferation, HDAC1 knock down resulted in inhibition of cell proliferation of HeLa cells, whereas knockdown of HDAC4 and 7 did not lead to decreased cell numbers.[268] In addition, knockdown of HDAC1 provided an arrest either in the G1 phase or in the G2/M transition of the cell cycle, thus leading to cell growth inhibition, loss of mitotic cells as well as an increased percentage of apoptotic events in breast cancer and osteosarcoma. HDAC2 knockdown, instead, showed no such effects in these cells[269] but, in cervical cancer cells causes a differentiated phenotype and subsequently induces apoptosis associated with increased expression levels of the cell cycle inhibitor p21$^{Cip1/WAF1}$ that was independent of p53. In breast cancer cells if HDAC2 is knockdown, the functional DNA binding activity of p53 increases, thus leading to the inhibition of proliferation and induction of cellular senescence.[270]

Together with HDAC1,2, also HDAC3 expression was significantly associated with poor prognosis in gastric, prostate and colorectal cancer samples. HDAC3 shares 63% identical amino acids with HDAC1,2 and has 43% overall sequence identity to HDAC8. In addition, the nuclear localization signal (NLS) that other class I HDACs possess, has a NES (nuclear export signal) associated to its ability to localize both to the nucleus as well as to the cytoplasm. HDAC3 is the catalytic component of the SMRT (silencing mediator for retinoic acid and thyroid hormone receptors) and N-CoR (nuclear receptor co-repressor) complex. Both act as co-repressors and have a conserved deacetylase activating domain for HDAC3 activation.[271,272]

HDAC8 is most recently identified among the members that belong to HDAC of class I. It contains 377 amino acids (42 kDa), is ubiquitously expressed and can localize to either the nucleus (primary site) or the cytoplasm. HDAC8 can deacetylate both histone and non-histone substrates, such as a tetrapeptide derived from p53. HDAC8 resulted detached from other members of class I in the early evolution, probability proving a discrete functional specialization.[250] Some particular non-histone proteins including ERα, cortical actin-binding protein (cortactin) or cohesin, have been found to be connected with HDAC8. This HDAC, in addition, play a main role in the regulation of different events such energy homeostasis, sister chromatid separation, muscle contraction and microtubule integrity, as well as covering a multifaceted role in human pathophysiology. In Cornelia de Lange syndrome (CdLS), mutations involving its catalytic portion result in the loss of its activity. [273] In addition to its registered deregulated interactions with specific transcription factors, HDAC8 OE was highlighted in different kind of tumors covering an important role mainly in gastric cancer, T cell lymphoma, childhood neuroblastoma.[274,275] HDAC8 was also reported to be involved in viral infection and parasitic diseases.[276–278]

1.2.6.2.2 Class II HDACs

At the level of their regulatory *N*-terminal domains, HDACs of Class IIa (HDAC4,5,7,9) are characterized by the presence of two or three conserved serine residues subject to reversible phosphorylation, thus leading to the binding of the 14-3-3 proteins and the consequent nuclear export of HDACs as well as derepression of their targeted genes. A range of kinases and phosphatases, acting downstream of diverse biological pathways, have been identified to regulate the nucleus-cytoplasmic distribution of class IIa HDACs.[279]
HDAC4, 5 and 7 have their catalytic domain in the *C*-terminal half of the protein, and the NLS is situated close to the *N*-terminus. Binding domains for *C*-terminal binding protein (CtBP), MEF2 and 14-3-3 proteins are conserved in all three HDACs on the N-terminus. The initial examination of the sequences surrounding the conserved phosphorylation residues in class IIa HDACs revealed that they are closely related to consensus phosphorylation sites for the CaMKs. CaMK I and CaMK IV phosphorylate all four class IIa HDACs and in cell-culture models CaMKs induced the re-localization of class IIa HDACs from the nucleus to the cytoplasm.[280]
As shown by the phylogenetic tree, HDAC9 splice variants are reported as a separate group related to HDAC4, 5 and 7 within class II of the classical HDAC family. The HDAC9 catalytic domain is located on the *N*-terminus, as for the class I HDACs. HDAC9 interacts with MEF2, CaMK and 14-3-3 proteins, indicating that HDAC9 may have an important function in muscle differentiation.
HDAC6 is evolutionarily most closely related to HDAC10, indeed they belong to the so-called Class IIb. In 2010, Mandana *et al.* reported that, after the selective inhibition of HDAC6 reached with tubacin, cell death induced by suberoylanilide hydroxamic acid (SAHA) and etoposide may be significantly enhanced in MCF-7 breast cancer cell line and human prostatic adenocarcinoma cell line (LNCaP). In addition, HDAC6 exerts cellular functions independently from its deacetylase activity. The binding to ubiquitin *via* its zinc finger domain regulates aggresomal function, autophagy, heat shock factor-1 (HSF-1) and platelet derived growth factor (PDGF) function.[281,282]
Finally, HDAC10 is structurally related to HDAC6, but contains one additional catalytically inactive domain. HDAC10 was found in both the nucleus and cytoplasm. HDAC10 knockdown correlates with an increased thioredoxin-interacting protein (TXNIP) expression in SNU-620 gastric cancer cells, while HDAC1, 2 and 6 knockdowns did not induce the same effect. TXNIP is the endogenous inhibitor of the cellular antioxidant thioredoxin (TRX). In addition, HDAC10 inhibition induce the release of cytochrome C and activate apoptotic signaling molecules through accumulation of ROS (reactive oxygen species).[283]

1.2.6.2.3 Class IV HDACs

HDAC11 has sequence similarity to classes I and II HDACs. Beyond its evolutionary conservation that suggest a vital role across diverse species, different pieces of evidence proved a role for this HDAC in the decision between immune tolerance and immune activation. However, little is known about HDAC11 functions.[252,284] Recently, HDAC11 OE has been reported in several carcinomas and its depletion resulted enough to induce cell death inhibithing metabolic activity in SKOV-3 ovarian, MCF-7 breast, HCT-116 colon and PC-3 prostate cancer cell lines. An anticancer effect can be registered by enhancing the expression of a catalytically impaired variant of HDAC11, suggesting that the application of HDAC11 inhibitors could provide the desired phenotypic changes.[285]

1.2.6.2.4 Class III HDACs: Sirtuin family

In 1979 the first sirtuin Sir2 from *Saccharomyces cerevisiae* originally known as mating-type regulator 1 (MARI) has been discovered by Klar and co-workers.[286] Ten years later, Gottlieb and Esposito[287] proved that silent information regulator's (SIR2) function is not restricted to control mating type expression but also may function in excluding the rDNA region from the general recombination system.[288] In 1991 Gottschling *et al*.[289] showed that SIR genes take part in different mechanisms for silencing chromosomal domains in *Saccharomyces cerevisiae* by providing a complete silencing at Hidden MAT Right (HMR) and Hidden MAT Left (HML) thus blocking the switching from the silent transcription state to the active one. After two years, in 1993, Braunstein[290] demonstrate that the silencing of silent mating-type cassettes and telomeres is strictly associated with acetylation of the ε−amino groups of lysine in the amino-terminal domains of three of the four core histones. The SIR2 OE induced a substantial histone deacetylation, an additional characteristic that distinguished SIR2 from other SIR genes. In 1995 Brachmann[291] and Derbyshire[292] discovered four *Saccharomyces cerevisiae* homologs of the SIR2 silencing gene (HSTs), as well as conservation of this gene family from bacteria to mammals. They hihlighted that HST1, showing 71% sequence identity over 84% of its length, resulted closely related to SIR2. In addition, through the polymerase chain reaction using degenerate primers on *Saccharomyces cerevisiae* DNA, three additional SIR2-related genes, known as HST2,3,4 have been identified. In particular, HST3 and HST4 together modulate cell cycle progression and genomic stability, providing new connections between these fundamental cellular processes and silencing. In 1999 and 2000 Frye[264,293] discovered seven human sirtuins (SIRT1-7) among which SIRT1 showed the closest homology to the *Saccharomyces cerevisiae* Sir2p. As previously highlighted, sirtuins family functions result principally related to changes in acylation proteins state. In addition to the acetyl moiety, in fact, other acyl groups such as succinyl, glutaryl, malonyl, myristoyl, carbamoyl etc. can also be removed by sirtuins. As previously mentioned, the seven isoforms of this family, namely as SIRT1-SIRT7[294] are commonly divided into different classes in relation to their subcellular localization: while SIRT1, SIRT6 and SIRT7 are almost located in the nucleus, SIRT3, SIRT4 and SIRT5 have a mitochondrial distribution and SIRT2 is the main component in the cytoplasm (Table 1.3). However, this classification is flexible since, for example, some cells showed cytoplasmic expression of SIRT1[295] and SIRT2 proactively shuttled between the nucleus and cytoplasm.[296] Multiple cell localizations were also found for SIRT7 and SIRT3.[297,298] As just mentioned, in addition to deacetylation, other enzymatic activities have been described for sirtuins. In fact, while SIRT1-3 and SIRT7 are primarily lysine deacetylases,[299,300] SIRT4 acts as both an ADP-ribosyl transferase and lysine deacylase,[301,302] SIRT5 provides lysine demalonylation,[303] desuccinylation[304] and deglutarylation,[305] and SIRT6 is an ADP-ribosyl transferase and deacetylase.[306,307] Several sirtuins targets have been identified during the last years, including different histones and non-histones proteins (Table 1.3). Since these substrates are involved in different physiological and/or pathological processes, sirtuins regulation may have therapeutic potential for specific diseases. After 37 years more than three thousand publications that touch the sirtuins from pharmacology, biology, biochemistry to medicinal chemistry have been written, but much still needs to be discovered.

| Sirtuin	Localiz-ation	Substrates	Catalytic activity	Functions	Pathology
SIRT1	Nucleus, Cytosol	PGC1α, eNOS, FOXO, NF-kB, MyoD, PPARα, H1 K26ac, H3K9ac, H4K16ac	NAD$^+$-dependent protein deacetylation	Cell survival, insulin, signaling, inflammation, metabolism regulation, lifespan regulation, oxidative stress response	Colon, prostate, ovarian, lung and breast cancer, glioma, melanoma, lung adenocarcinoma, acute myeloid leukemia (AML)*;* neurodegenerative diseases
SIRT2	Nucleus, Cytosol	H3K56ac, H4K16ac, α-tubulin, Foxo3a, p53, G6PD, MYC	NAD$^+$-dependent protein deacetylation	Cell cycle regulation, nervous system development	Glioma; Neurodegenerative diseases
SIRT3	Nucleus, Mitochondria	AceC2, ShdhA, SOD2, PDMC1a, IDH2, GOT2, FoxO3a	NAD$^+$-dependent protein deacetylation	Regulation of mitochondrial energetic metabolism	B-cell chronic lymphocytic leukemia (CLL), mantle cell lymphoma, (MCL), breast and gastric cancer; Neurodegenerative diseases
SIRT4	Mitochondria	GDH, MCD, PDH	NAD$^+$-dependent protein deacylation (acyl, lipoyl and 3-hydroxymethyglutaryl) & ADP-ribosylation	Regulation of mitochondrial energetic metabolism, fatty acid oxidation and insulin secretion	Breast, colorectal cancer and esophageal squamous cell carcinoma (ESCC)
SIRT5	Mitochondria	Histone H4, CPS1, cyt c	NAD$^+$-dependent deacylation (succinyl, malonyl and glutaryl)	Urea cycle and apoptosis regulation	Breast, pancreatic, non-small cell lung carcinoma
SIRT6	Nucleus	H3K9ac H3K56ac, PARP1	NAD$^+$-dependent protein deacylation (acyl and	Genome stability, DNA repair, nutrient-dependent	Breast and colon cancer

			long-chain fatty acyl) & Mono- ADP-ribosyl transferase	metabolism regulation	
SIRT7	Nucleus	RNA pol I, p53, H3K18ac	NAD$^+$-dependent protein deacetylation	Regulation of rRNA transcription and cell cycle	Liver, spleen, testis, thyroid and breast cancer

Table 1.3. Seven mammalian sirtuins characterization.[308]

1.2.6.2.4.1 Sirtuins: NAD$^+$-dependent deacetylase mechanism

Sirtuins share a common NAD$^+$-binding catalytic domain (of ~275 amino acids), catalysing proteins deacylation by breaking the bonds between NAD$^+$ and nicotinamide (NAM) ribosomes, thus transferring the acylated groups from proteins to ADP-ribose, then releasing the deacylated products. Therefore, NAM can be considered an endogenous inhibitor of sirtuins through a feed-back mechanism (Figure 1.14A,B).[309,310]
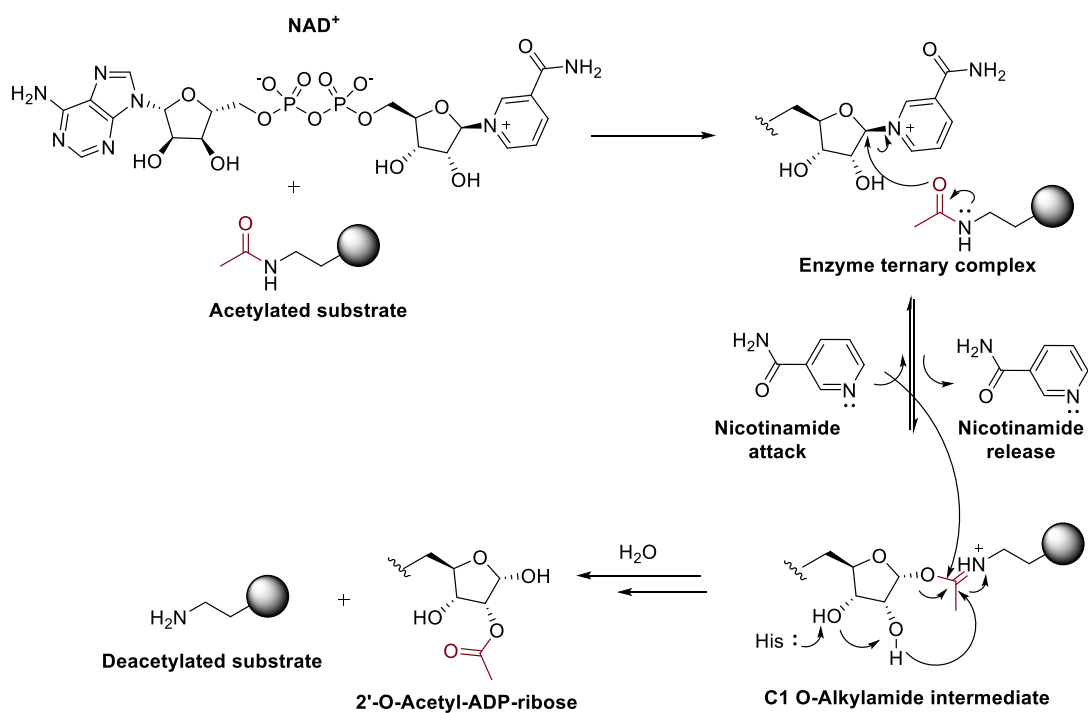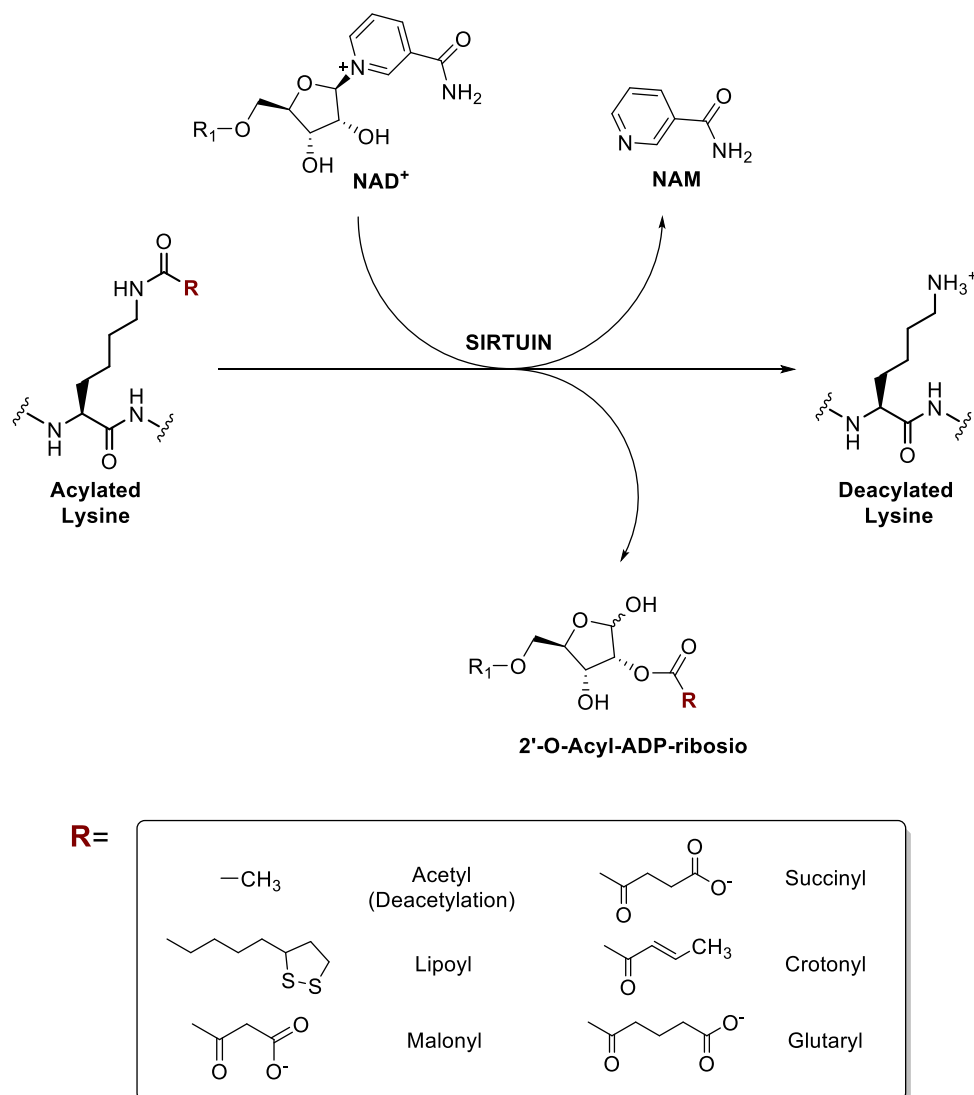
B

Figure 1.14. Mechanism of sirtuins deacylation (**A, B**). Deacetylation process is highlited on the top of the figure (**A**).

The accepted deacetylation mechanism (Figure 1.14A) begins with Michaelis complex formation (when both NAD$^+$ and substrate are bound) and starts with a nucleophilic attack of 1' NAM ribose moiety by the carbonyl oxygen of the lysine substrate through SN$_2$ mechanism that led to the NAM cleavage and the 1'-O-alkylamidate intermediate formation. Once the NAM has been released it can rebind in the C-pocket and react with the intermediate to reform NAD$^+$. In this step, Phe33 appears to play a role as gatekeeper in the nicotinamide exchange reaction in which it helps to shield the O-alkylamidate intermediate from free NAM. After the formation of 1'-O-alkylamidate intermediate, the 2'-hydroxyl group of the ribose is activated by a conserved His116 providing the 1', 2'-cyclic intermediate. Then a protonated histidine can act as acid protonating the amino-acetal, thus releasing the free deacetylated substrate. Finally, an activated water molecule, attacks the cyclic intermediate to furnish 2'-O-acetyl-ADP ribose (might be in equilibrium with its corresponding 3' isomer).[311]

1.2.6.2.4.2 Sirtuins Architecture

The analysis of the reported high-resolution structures of human sirt1-6 in apo- or (co)substrate/inhibitor-bound complexes revealed their NAD⁺-dependent catalytic mechanism.[312,313] The overall structures is composed of the large Rossmann-fold domain and the small domain which includes the α-helical and the Zn^{2+} binding subdomains (Figure 1.15). These two portions are connected by four loops that arise from the Rossmann fold and include a flexible loop called the co-factor binding loop. The most interesting part of sirtuins structure is the cleft between the large and small domain. The substrate and NAD⁺ are inserted, from opposite sides, into a hydrophobic portion within the cleft, where catalysis takes place. This catalytic core adopts an oval-shaped fold which contribute to the active site cleft between the subdomains.[314] Unlike what happens for the other "classical" HDACs, the zinc ion does not participate to the catalysis because it is too far from sirtuins active site but it is essential for structural stability as well as for the coordination with four conserved cysteines holding the three β-strands together. In fact, the removal of zinc ion (by using chelating reagent or through mutation of the coordinating cysteine induce a partial collapse of the structure), correlates with the lack of the deacetylase activity, in fact the subsequent supplementation of zinc restores activity.[315] The large domain has a classical open α/β Rossmann-fold structure for NAD⁺ binding. It consists of a central β-sheet with six parallel β-strands sandwiched by several α-helices on each side (the number of those helices depends upon the different sirtuins).[316]
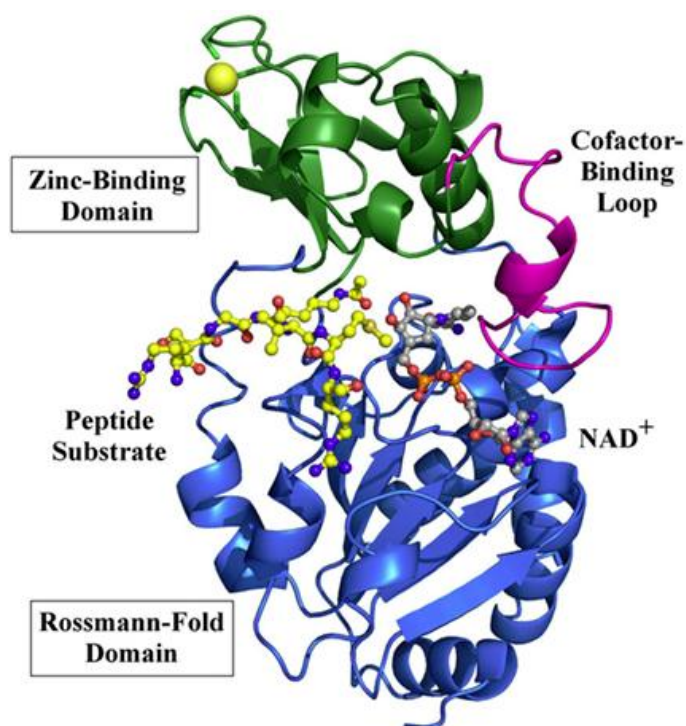

Figure 1.15. Overall sirtuins structure represented by human Sirt3 bonding NAD⁺ analogue and AceCS2 (acetylCoA synthetase 2) peptide. Sirt3 structure (PDB entry 3glr) is represented as a cartoon model with Zinc-binding domain and Rossmann-fold domain depicted in green and blue, respectively. The cofactor binding loop (that it colored in magenta) is in a closed conformation and binds a carba-NAD⁺ molecule (represented in gray), which was introduced to the given model based on a superposition with the structure of an Hst2/carba-NAD structure (1szc). The active site cleft consists also of the peptide substrate AceCS2 (depicted in yellow) with the acetylated lysine which point toward the active site.[313]

The four loops connecting the large and the small domains establish the cleft that acts as enzyme active site. The elongated NAD^+ molecule introduces its NAM ribose moiety into the cleft, poses the pyrophosphate portion along the edge of the β-sheet in a positively charged groove, and lays the adenine group in a remoted pocket from the cleft. The orientation of NAD^+ here is inverted compared with most Rossmann fold-containing enzymes, where the adenine base of NAD^+ binds to the *C*-terminal half, and the nicotinamide group of NAD^+ binds to the *N*-terminal half of the β-sheet.[317] The specific orientations of the Rossmann-fold and small domains, despite differ in known sirtuins structures, seem to be related to the absence or presence of substrates. The so-called "cofactor binding loop" is characterized by high flexibility and its conformation was shown to evolve in close relation to the catalytic events.[314] Collected data about different substrates or substrate analogue complexes for sirtuins show that, upon the substrate binding, the cofactor binding loop gets ordered thus changing to a more closed conformation after the transfer of the acetyl moiety, probably taking part in expelling the first reaction product, nicotinamide.[265,318] In addition, a reorientation of two domains relative to each other have been also observed upon the acetyl-lysine substrate binding inducing the closure of the cleft.[319]

Despite structural rearrangements proving the dynamic structure of this class of enzymes have been discovered, individual sirtuins are characterized by specific preferences in sequence related to variables in their electrostatics properties peptide binding groove shape (Figure 1.16).[314,319] The capability of sirtuins to recognize a huge number of substrate moieties, prove their high adaptability.
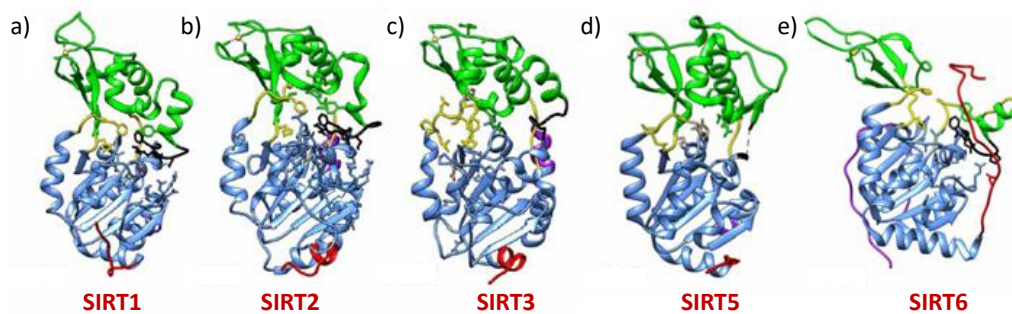

Figure 1.16. Crystal structure of human SIRT1-3,5,6. (a) H. sapiens sirt1 (PDB: 4IF6). (b) H. sapiens SIRT2 (PDB: 3ZGV). (c) H. sapiens SIRT3 (PDB: 3GLR). (d) H. sapiens SIRT5 (PDB: 4F4U). (e) H. sapiens SIRT6 (PDB: 3ZG6). The Rossman-fold domain in represented in blue, the small domain is coloured in green, the cofactor binding loop in black, the connection loops in yellow, while the *N*-terminal in red and the *C*-terminal in magenta.

It is well-know that sirtuins can adopt different conformational states. Moniot *et al*.[320] showed how SIRT2 is able to switch from an open conformation to a closed one (PDB entry: 3ZGV) after ADPr and pocket binding and, a similar phenomenon, have been observed also in SIRT1, SIRT3 and SIRT5 isoforms.[43,321–323] SIRT6 and SIRT7 are reported to lack the helical module in the small domain mentioned in the above shared active center.[299] As previously mentioned, SIRT5 shows a very weak deacetylation intensity and a strong demalonylase/desuccinylase capability. Such specificity may be related to the exclusive presence of Tyr102/Arg105 residues in its catalytic core which ae capable of produce specific polar interaction with succinate and malonate substrates.[324]

1.2.6.2.4.3 Sirtuins in physiology and pathology: an overview

All sirtuins are thought to be closely related to specific aging diseases such as cardiovascular disorders, neurodegeneration, and tumors.[308,325–327] In particular, recent pieces of evidence showed that different members of this family often play opposite roles in tumor onset,[326] both promoting and inhibiting tumor formation and progression.[328,329] For example, despite SIRT1 results highly expressed in colon, prostate, gastric and skin cancer suggesting a role in tumor promoting, its expression appears, instead, reduced in breast cancer.[330–334] In addition, SIRT1 is involved in many neuronal processes[335,336] prompted further investigations into its role in neurological disorders such as Alzheimer's disease (AD), Parkinson's disease (PD), and Huntington's disease (HD).[337–339] SIRT1 shows a neuroprotective role taking part in the regulation of survival, neuropathology and in the expression of brain-derived neurotrophic factor (BDNF). In a mouse model of HD, SIRT1 KO correlates with a pathology exacerbation, while its re-expression provides neuroprotective effects.[340] Recently, a correlation between nicotinamide phosphoribosyl transferase (NAMPT) and SIRT1 has been highlighted. NAMPT is known to be a challenging therapeutic target against ischemic stroke, acting in neurogenesis and vascular repair. SIRT1 is involved in NAMPT deacetylation (Lys53) thus increasing its activity and secretion.[341] The first evidence linking SIRT1 to tumorigenesis derived from two studies which proved that p53 deacetylation and consequent inhibition,[342,343] correlates with cancer cell death. As just mentioned, SIRT1 seems to play a contradictory role in tumorigenesis acting both as a tumor promoter and suppressor.[344,345] Since SIRT1 regulates the expression of many tumor suppressors and DNA repair genes,[346–349] thereby results clear the reason why SIRT1 upregulation is described in many human malignancies.[350] In addition, recent collected data proved that patients expressing high levels of SIRT1 had a higher possibility of result resistant to chemotherapy treatment than patients with low expression of this sirtuin. One report highlighted a role for SIRT1 in the onset and maintainance of melanoma suggesting the use of SIRTs inhibitors (such as tenovins, EX-527, and sirtinol), either alone or in combination. Such inhibitors hit different SIRTs, promoting the idea that the simultaneous inhibition of different sirtuin isoforms could contribute to the counteract of malignant growth.[351] SIRT2 seems to exert a neurodegenerative action in neurological disease.[352] Indeed, pharmacological or genetic inhibition of SIRT2 blocks α-Syn-mediated toxicity.[353] SIRT2 takes part in the control of apoptosis events through the regulation of p53-related process. Different pieces of evidence proved that SIRT2 is also involved in the control of cell cycle progression at different levels and in different metabolism processes, including adipogenesis.[354] SIRT2 deacetylates glucokinase (GCK), which is essential for the maintainance of glucose homeostasis, physiologically modulated by the binding of the glucokinase regulatory protein (GKRP). Different data showed that, acetylated state of GKRP is connected to diabetes mellitus.[355]

Concerning the three mitochondrial SIRTs (SIRT3, 4, and 5), some proofs correlates SIRT3 with neurodegenerative disease. SIRT3 seems to protect cochlea neurons from oxidative damage in response to calorie restriction[356] and to stress-regulating mitochondrial antioxidant manganese superoxide dismutase (MnSOD) in microglia.[357] Since SIRT3 deacetylase and activates different mitochondrial protein regulating differentiation proliferation and survival, a role for SIRT3 has been hypnotized in cancer. In this framework, SIRT3 seems to act as a tumor suppressor *via* the deacetylation and activation of pyruvate dehydrogenase (PDH). In addition, SIRT3 was found to strongly inhibit mitochondrial ROS production.[358,359] Much less is known about the remaining mitochondrial sirtuins. Unlike other family members, SIRT4 lacks a significant NAD⁺-dependent deacetylase activity *in vitro*, but its capability to inhibit the malonyl-CoA-decarboxylase (MCD) through its deacylation has been registered. However, SIRT4 is

principally known for its ADP-ribosyltransferase and lipoamidase activities towards glutamate dehydrogenase (GDH) and PDH, respectively. In addition, a new deacylase activity has been recently discovered.[360] SIRT4 is involved in a variety of mitochondrial metabolic processes such as insulin secretion, lipid synthesis, redox state, apoptosis and ATP homeostasis. For the reasons just mentioned, SIRT4 covers a main role in the onset of different metabolic disease including diabetes and obesity.[361] SIRT4 is induced by DNA damage including γ-irradiation and chemotherapy inducing the cell cycle arrest by inhibiting mitochondrial glutamine metabolism. SIRT4 inhibits proliferation, invasion, and migration in colorectal cancer cells, and its low expression correlates with worse prognosis. However, the role of SIRT4 in cancer is still subject of debate.[362] SIRT5 is reported to interact with carbamoyl phosphate synthetase 1 (CPS1), inducing its deacetylation. Despite the role of SIRT5 in carcinogenesis is still not clear, a recent study reported its OE in non-small cell lung cancer tissue as a marker of poor prognosis.[363] SIRT6 is known to modulates cellular homeostasis, metabolism and telomere maintenance thus acting as an epigenetic DNA repair agent as well as a guardian for cellular differentiation.[364] The capability of SIRT7 to catalyze the selective deacetylation of an epigenetic biomarker of aggressive tumors, H3K18, thus modulating the expression and transcription of varius tumor suppressor genes, makes this sirtuin an interesting target for anticancer therapy. As proof of this, OE of SIRT7 have been individuated in aggressive cancers and correlates with low survival.[365] A recent report showed that chlorpromazine-based treatment of rat glioma cells inhibit cell cycle progression thus inducing autophagic cell death. In other words, the FDA approved drug for the treatment of bipolar disorder and schizophrenia, also increases Lys382 acetylation level of p53, thanks to its capability to induce SIRT1 inhibition.[366]

In condition of nutritional deficiency, sirtuin deacylase activity increases when levels of NAD^+ are high.[367] Recents evidence showed that after a metabolic stress, an enhanced acetylation state for metabolic proteins, including tricarboxylic acid cycle (TCA) enzymes and fatty acid oxidation enzymes, has been registered.[368,369] In fact, increased level of mitochondrial NAD^+ has a protective effect in cell survival upon genotoxic stress through SIRT4 and SIRT3.[367] Physical exercise modulate the NAD^+/NADH ratio increasing the NADH skeletal muscle level, thereby improving mitochondrial functions, as well as it may alter the content and activity of some sirtuins, first of all of those belonging to the mitochondrial matrix.[370] To conclude, sirtuins principally control stress responses and metabolism and are being considered therapeutic targets for aging-related diseases.

1.2.6.2.5 SIRT4

SIRT4 was first described in 1999 as member of the mitochondrial subtype of sirtuins.[301,371] SIRT4 mRNA levels have been proved to be abundant in a wide range of tissues, including brain, heart, liver, kidney and skeletal muscle.[292] As previously reported, unlike the other mitochondrial sirtuins that show deacetylase (SIRT3) and desuccinylase (SIRT5) capability, no prominent deacetylase or deacylase activity as well as structural information were, until recently, available for SIRT4. Trials to crystallize human SIRT4 (hSIRT4) protein construct (which consists of the catalytic core and native *C*-terminus but lacks 24 residues proper of the *N*-terminal mitochondrial localization sequence) were not successful. In 2017, Pannek et *al*.[360] reported specific acyl substrates and crystal structures for SIRT4 demonstrating isoform-specific acyl selectivity.

Their crystal structure of SIRT4 from *Xenopus tropicalis* (xSIRT4) (xSIRT4, hSIRT4 similarity 81%) (Figure 1.17) shows a particular acyl binding site with an additional access channel which could explain its activities, as well as a conserved, isoform-specific SIRT4 loop that folds into the active site to potentially regulate catalysis.
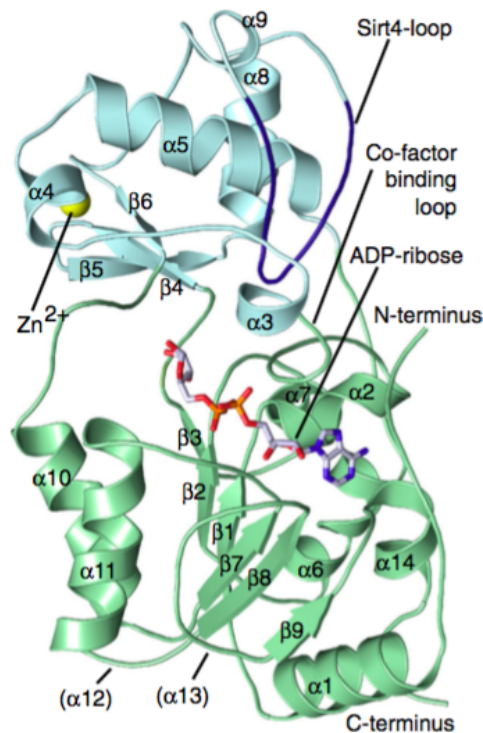

Figure 1.17. Overall structure of the xSirt4/ADPr complex, in which the Zn^{2+}-binding domains, Rossmann-fold domain, and a Sirt4-specific loop are coloured in cyan, green and blue, respectively. ADPr is represented as sticks, painted according to atom type. Elements missing in xSirt4 secondary structures are indicated by brackets, while the others are numbered equivalent to other sirtuins.[360]

As just mentioned, sirtuins share a conserved catalytic core of ~275 amino acids[372] and differ for the *N*- and *C*- terminal domains that contribute to the localization and activity specificity.[373,374]

Is known that, the catalytic core of SIRT4 has only a short ~28 residue *N*-terminal extension (that acts as mitochondrial localization sequence) and no *C*-terminal appendage.[373,375]

Substrate specificity among the different sirtuins isoforms is consequent to the binding of the acyl moiety to an active site channel with isoform-specific characteristics.

Given the little to no detectable deacetylase SIRT4 activity against acetylated histone *in vitro*,[376,377] alternative deacylase activities have been investigated. In particular, SIRT4 was

found to catalyze the deacylation of lysine decorated with glutaryl (G), 3-methylglutaryl (MG), 3-methylglutaconyl (MGc) or 3-hydroxy-3-methylglutaryl (HMG), or group *in vivo* and *in vitro*.[360]

HMG- Coenzyme A (CoA) and MGc-CoA substrates result from leucine catabolism while MC-CoA is a product of the reduction of MGc-CoA.[378] SIRT4 interacts with proteins that take part in branched chain amino acids catabolism and in particular with component of the methylcrotonyl carboxylase complex (MCCC) which convert 3-methylcrotonyl-CoA (MC) into MGc (Figure 1.18).[302,379]
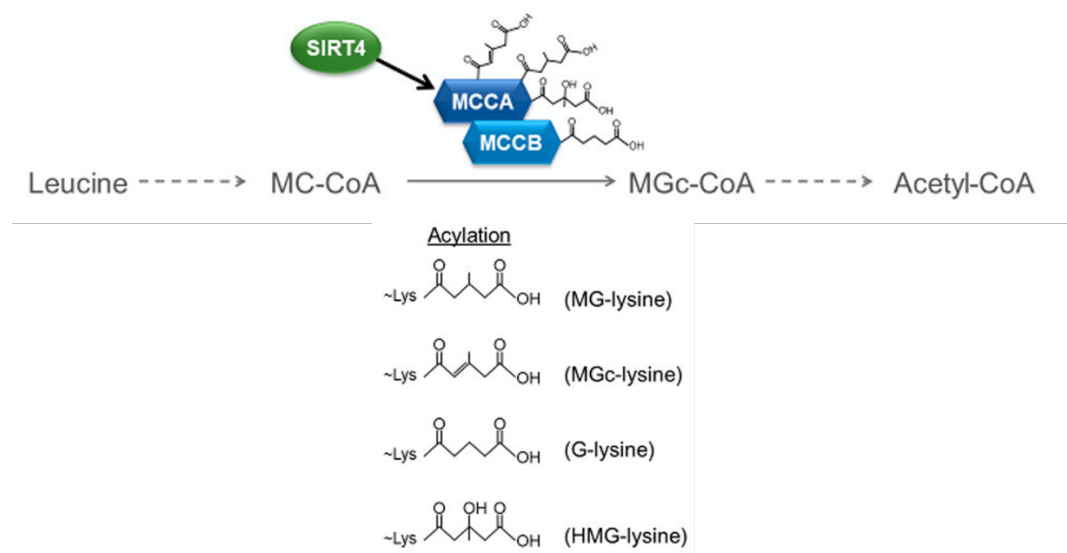
Figure 1.18. Deacylation processes mediated by SIRT4 and its substrates. Adapted from Betsinger *et al*. *J. Proteome Res*., 2019, 18, 1929–1938.[380]

Evidence collected by Pannek et al.[360] highlighted that SIRT4 deacylase activity is mainly focused on the removal of the HMG residue. Strictly, SIRT4 shares this deacylase activity with SIRT5 but does not shows any desucciylase activity (which is typical of the latter) or other activities own of the other mitochondrial sirtuin SIRT3. In particular, despite the α-5 centre contributes to acyl recognition (as it happens for SIRT5), in SIRT4 even the remote α-5 *N*-terminus takes part in this event. In the crystal structure proposed by Pannek et al.,[360] the SIRT4-loop for the NAD+ binding assumes at least two state and it has to rearrange to provide a productive NAD+ interaction thus inducing a conformational change in the acyl site: the shift of the residue Asp201 away from the conventional acyl binding pocket may support the binding of dicarboxylic substrates such as HMG.

An analogous procedure of the well-known "Fluor-de-Lys" (FdL) deacetylation assay widley used for SIRT1-3,[381] has been proposed to highlight the novel SIRT4 deacylase activity. In particular, our collaboration with the research group of Professor Steegborn, provided the synthesis of an "ad-hoc" SIRT4 substrate. Specifically, the replacement of the acetyl group of the SIRT1–3 substrate Z-MAL **1**[382] with the desired HMG provided the HMG-FdL SIRT4 substrate (Z-Lys(HMG)AMC, MC3659, **2**), that allowed the fluorescence monitoring deriving from the FdL procedure also for SIRT4 (this topic is accurately exposed in Chapter 3) (Figure 1.19).[381]
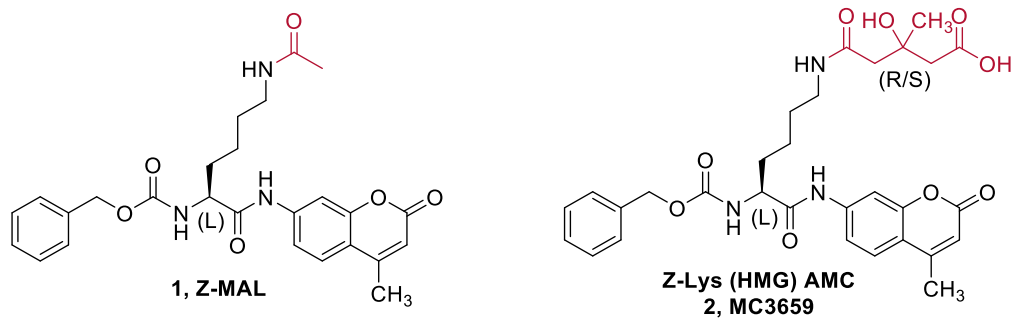
Figure 1.19. Structure of the SIRT4 substrate Z-lys(HMG)-AMC synthetized in Prof. Mai laboratory.

Suramin, a pan-sirtuins inhibitor has been used to confirm the recognition and deacylation of MC3659 **2** by SIRT4. Increased levels of HMG-CoA (recreated through a HMG-CoA-lyase deficiency model) correlates with an enhanced protein HMG-ylation.[378] Comparable changes are expected during ketogenic protein catabolism and under fasting condition highlighting that de-HMGylating enzymes, like SIRT4, may regulate target functions during starvation.

As previously mentioned, through its weak deacetylation activity, SIRT4 inhibits MCD, which promotes lipid anabolism and represses fatty acid oxidation.[301,375]

SIRT4 is mainly known for its capability to inhibit PDH by its delipoylation,[379] and for its ADP-ribosyltransferase activity on GDH mediating its inhibition thus regulating the insulin secretion (Figure 1.20).[301,375]
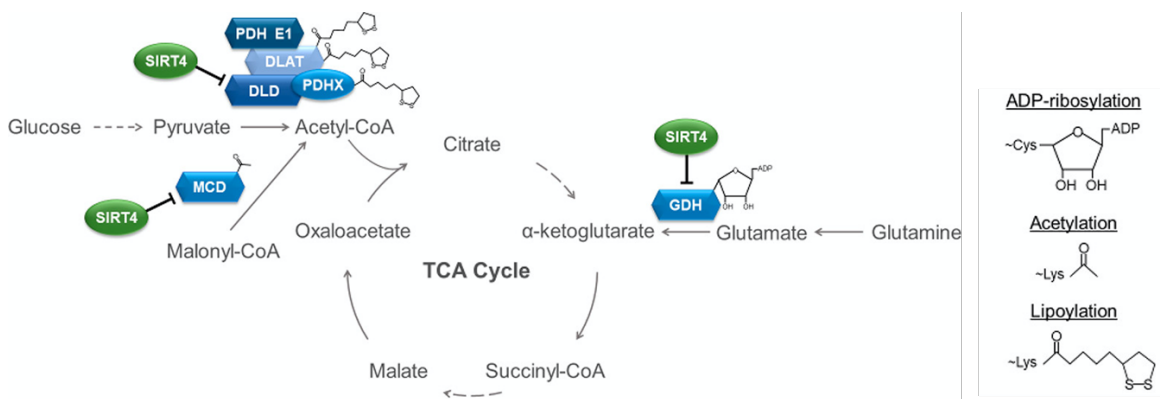

Figure 1.20. Main biological functions of SIRT4. Betsinger *et al*. *J. Proteome Res*., 2019, 18, 1929–1938.[380]

These evidences support the key roles that SIRT4 covers in the modulation of metabolic enzymes, antioxidant defence mechanism and mitochondria metabolism in response to exercise. In particular, SIRT4 depresses the insulin secretion amino acids-mediated in pancreatic β-cells, promotes lipogenesis and fatty acid oxidation and regulates the mitochondrial ATP homeostasis as well as apoptosis. Fatty acid oxidation can stimulate ROS (mainly hydrogen peroxide H_2O_2) production consequently to the upregulation of electron transport chain activity. Given its role in the regulation of ATP levels and lipid metabolism, has been speculated that SIRT4 might be associated with different mitochondrial dysfunction-related pathologies, such as non-alcoholic fatty liver disease, diabetes, diet induced obesity, neurodegeneration, heart disease, aging, inflammatory vascular disease, apoptosis and cancer.[383–386] In particular, while recent pieces of evidence indicate that SIRT4 may act as tumor suppressor by regulating the glutamine

metabolism,[362,387–391] other studies have also highlighted the potential oncogenic activity of SIRT4 (Figure 1.21).[392,393]
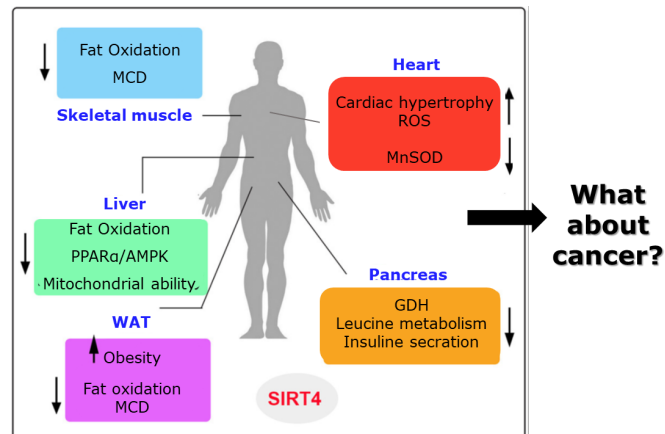

Figure 1.21. Schematic representation of the metabolic roles of SIRT4 in different organs. Adapted from Min *et al*. *Front*. *Endocrinol.2019,9:783*.[394]

As exposed in Table 1.4, knock-down of SIRT4 in mouse model showed increased MCD activity with an enhanced exercise tolerance and protection against diet-induced obesity.[384] SIRT4 inhibition correlates with an upregulation of the expression of genes enconcoding for fatty acid and mitochondrial metabolism-related enzymes.[395] The decrease of SIRT4 levels in insulinoma cells, instead, activate GDH, thus leading to the increase insulin secretion.

Genotype	Phenotype	Process	Activities
SIRT4 OE cells	Inhibition of insulin secretion in pancreatic β cells	Inhibition of GDH	ADP-ribosylation
SIRT4 KO cells	Activation of GDH & stimulation of insulin secretion in pancreatic β cells	Activation of GDH	ADP-ribosylation
SIRT4 KO mice	Stimulation of insulin secretion in pancreatic β cells	Activation of GDH	ADP-ribosylation
SIRT4 KO mice	Deregulated leucine metabolism and aging	Dysregulated leucine oxidation	Deacetylation
SIRT4 OE cells	Increased lipogenesis and decreased FAO in myocyte and adipocyte cells	Inhibition of MCD	Deacetylation
SIRT4 KO cells	Increased FAO in WAT and muscle cells	Activation of MCD	Deacetylation

SIRT4 KO mice	Elevated FAO and resistance to obesity and exercise	Activation of GDH	Deacetylation
SIRT4 OE cells	Depressed FAO in liver cells	Repression of PPARα transcriptional activation by SIRT1	-
SIRT4 KO cells	Increased FAO rate	Activation of PPARα	-
SIRT4 KO mice	Increased FAO rate and PPARα pathway	Activation of FAO by SIRT1 and PPARα	-

OE, over expression; KO, knock-out

Table 1.4. Summary of the effect consequent to an OE or KO of SIRT4 in cell metabolism.[394]

In addition to the previously mentioned enzymatic activities, recent proofs also supported that SIRT4 takes part in different mitochondrial processes in a non-enzymatic way. In mice liver, hepatoma cells, fibroblast and kidney an OE of SIRT4, in fact, correlates with the repression of the activity of the transcription factor PPARα,[396] wich promotes the expression of mitochondrial fatty acid oxidation genes. SIRT4 is also able to inhibit adenine nucleotide translocator 2 (ANT2) increasing ATP levels in different mouse tissues thus leading to a decreased AMPK activity and consequent fatty acid oxidation.[397] In addition, it is also known that SIRT4 compete with MnSOD for binding to SIRT3.[398] Recently, SIRT4 has been identified as a coronary artery disease biomarker as a consequence of its correlation with increased mitochondrial ROS.

Given the emerging role of SIRT4 in the onset of different disease, a full understanding of the enzymatic role of this sirtuin in metabolism is crucial for developing novel epigenetic modulators.

1.2.6.2.5.1. SIRT4 suppresses glutamate dehydrogenase (GDH) activity

Insulin secretion can be stimulated by glucose or amino acids.[399] In the second case, amino acids are catabolize into TCA intermediates generating ATP thus enhancing insulin release. Glutamine is initially hydrolysed by glutamate synthase (GLS) to glutamate, which is then subsequently converted, by GDH, into the Krebs cycle intermediate α-ketoglutarate.[384] In pancreatic β-cells, SIRT4 interacts with GDH catalysing its ADP-ribosylation thus repressing its activity. Pancreatic islets isolated from Sirt4 KO mice showed an increased GDH activity compared with controls. In pancreatic β-cells, SIRT4-mediated inhibition of GDH provides the repression of amino-acid-stimulated insulin secretion (AASIS), indeed Sirt4 KO mice are characterized by increased circulating insulin levels. SIRT4 regulation of ANT2 activity and leucine catabolism also contribute to insulin secretion. Leucine is an allosteric activator of GDH, therefore SIRT4 promotion of leucine catabolism through the SIRT4-mediated activation of MCC may correlates with a decreased release of insulin. In this framework, Sirt4 KO mice develop, in addition to hyperinsulinemia, also insulin resistance and glucose intolerance confirming the involvement of SIRT4 in diabetes of type II.[380] Sirt4 KO mice, in addition, showed abnormal leucine metabolism which correlates with a chronic increased insulin production triggering senescence-induced insulin resistance.[302] SIRT4 also interacts with insulin-degrading enzyme thus reducing insulin secretion in response to glucose,[400] indicating that it acts as a general nutrient sensor controlling insulin release (Figure 1.22).

While quiescent cells exploit the TCA to obtain energy from glucose, proliferating cells manly use it as a carbon source for lipogenesis through the mitochondrial efflux of citric acid. This efflux need to be replaced by an influx of TCA intermediates, known as anaplerosis. Of relevance, glutamine is the main source for TCA anaplerosis in proliferating cells.[401] Furthermore, SIRT4 modulates the opening of mitochondrial permeability transition pore (PTP),[402] a crucial step in mitochondria-mediated apoptosis events, also interacting with ANT proteins,[400] which are known to take part in this event. Inhibition of SIRT4, along with SIRT3, was proved to mediate the protective effect of nicotinamide on high glucose/palmitate-induced cell death in INS-1 β-cells,[403] showing that, in pancreatic cells, it modulates mitochondria-mediated apoptosis, thus supporting that SIRT4 inhibition could be helpful for the treatment of metabolic diseases. A recent study by Jeong et al.[404] shows a new relation between DNA damage and metabolism. Through metabolic analyses of cells in the presence or absence of DNA damage, Jeong and coworkers proved that DNA damage increments the flux within the pentose phosphate pathway.[387,405] In addition, they registered an unpredicted decreased glutamine uptake, as well as in intermediates of TCA. These initial evidence were focused on the connection between DNA damage, glutamine, and the TCA. Jeong et al.[387,392] characterized how several types of DNA damages block glutamine anaplerosis in proliferating cells. Increased SIRT4 mRNA levels have been registered upon different types of DNA damage, more than other sirtuins already known to be related to the DNA damage response, (for example SIRT1 and SIRT3). SIRT4-mediated inhibition of glutamine anaplerosis is crucial for a productive cell cycle arrest upon DNA damage. In the framework, the lack of SIRT4, does not ensure an efficient cell cycle arrest inducing a delayed DNA repair mechanism as well as increased chromosomal aneuploidies. SIRT4-deficient primary fibroblasts are characterized by aberrant levels of polyploidy, highlighting that SIRT4 results essential not only in response to exogenous-induced DNA damage, playing also a protective role from spontaneous damage. All these data prove that, due to its capability to mediate a blockade of glutamine anaplerosis, SIRT4 seems to act as a tumor suppressor. In this scenario, pieces of evidence showing that SIRT4-deficient fibroblasts grow faster than their WT counterparts have been collected. In addition, neoplastic SIRT4-deficient fibroblasts are characterized by a less dependence from glucose forming bigger allograft tumors compared to those typical of SIRT4-proficient cells. However, in these conditions, physiological phenotypes were restored when such cells were treated with GDH or GLS1 inhibitors as well as with upon ectopic expression of catalytically active SIRT4.

Different human cancers show reduced mRNA levels of SIRT4, and this condition may correlate with a poorer outcome in lung adenocarcinomas.[404]

Csibi et al.[388] demonstrated that the target of rapamycin complex 1 (mTORC1) mediates transcriptional repression of SIRT4 thus inducing the glutamine anaplerosis as a consequence of GDH activation. Specifically, the mTORC1-mediated protesome destabilization of CREB2 is responsible for the repression of SIRT4.
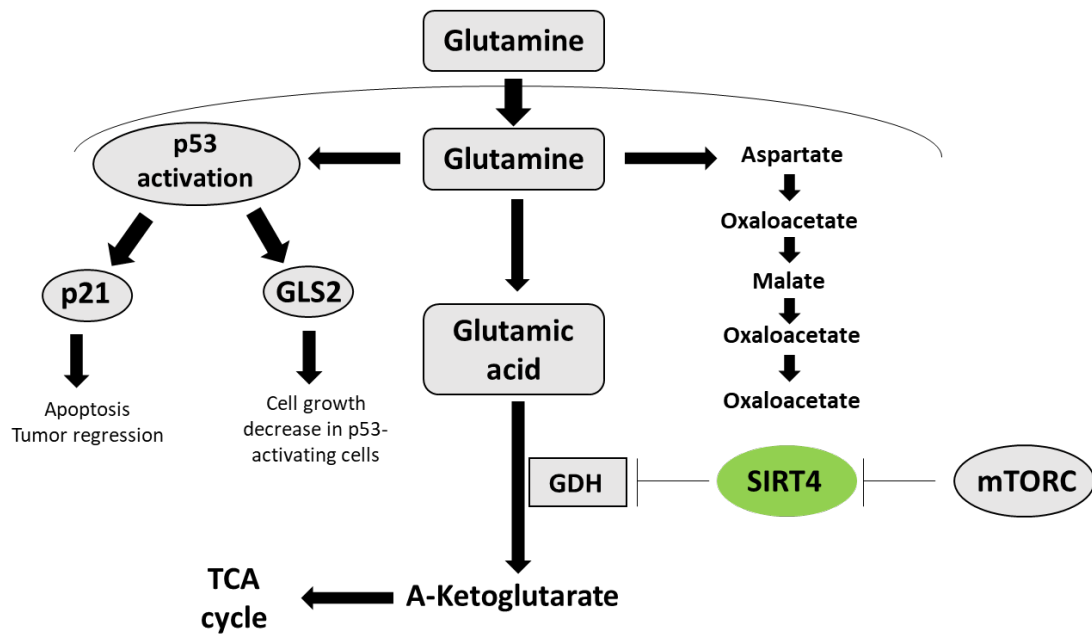
Figure 1.22. Overview of the glutamine metabolism and SIRT4-mediated regulation.

1.2.6.2.5.2 The role of SIRT4 in lipid metabolism

Lipid metabolism precisely respond to the nutritional organism status. In fact, while nutrient deprivation promotes fat oxidation, nutrient-rich conditions correlates with an increased lipogenesis. One of the main steps at the base of lipid homeostasis is the interconversion of malonyl-CoA to acetyl-CoA, since malonyl-CoA promotes fat synthesis and inhibits fat oxidation and it is regulated by two main enzymes which constitute a highly responsive control system: acetyl-CoA carboxylase (ACC) converts acetyl-CoA to malonyl-CoA and MCD which converts the latter back to acetyl-CoA. SIRT4 is considered one of the most critical regulator of the lipid metabolism (Figure 1.23). SIRT4, in fact, deacetylates and inhibits MCD.[384] Malonyl-CoA, in turn, allosterically inhibits the activity of carnitine palmitoyl transferase 1 (CPT1), the enzyme that catalyzes mitochondrial uptake of fatty acids for β-oxidation.[406] During nutrient-rich conditions, SIRT4 deacetylates MCD, thus countering its activity. While SIRT4 OE in adipocytes and myocytes correletes with the reduction of the MCD activity, white adipose tissues and muscles from Sirt4 KO mice ara characterized by increased MCD activity as well as reduced malonyl-CoA levels. Therefore, in skeletal muscle, SIRT4 represses fatty acid oxidation stimulating, in white adipose tissue, the lipogenesis process, thus proving that such sirtuin can modulate the balance between fat synthesis and oxidation. In fact, in Sirt4 KO mice increased level of fatty acid oxidation associated with enhanced exercise capacity and resistance to diet-induced obesity have been registered.[375]

PPARα is a ligand-activated transcription factor that induces the expression of genes taking part in the regulation of fatty acid catabolism.[407,408]

SIRT4 also suppress fatty acids oxidation by decreasing PPARα activity and the expression of PPARα-related genes. Worthy of note is, in this framework, the crosstalk that exists between nuclear and mitochondrial sirtuins. Deletion of SIRT4, in fact, activates PPARα activity through activation of SIRT1 consequent to the increased NAD⁺ levels.[409] Other studies showed the capability of SIRT1 to activate PPARα, and this event is repressed by SIRT4 OE.[395] Collectively, both studies demonstrated that SIRT4 is a suppressor of fatty acid oxidation by inhibiting SIRT1-mediated activation of PPARα.

AMPK covers a crucial role in promoting fatty acid oxidation, through the phosphorylation and inhibition of ACC. The consequent reduced malonyl-CoA levels, correlates with an increased CPT1-mediated mitochondrial fatty acid uptake.[406,410,411] A recent study dimostrated that, during fasting, increased SIRT4 levels have been registered thus inhibiting the AMPK activity and suppressing the fatty acid oxidation process.[412] In addition, AMPK is also known for its capability to activate the transcriptional co-activator of fatty acid oxidation genes PGC-1α.[413]As proof of these data, Sirt4 KO mice livers presented elevated levels of active AMPK, resulting in increased phosphorylation of ACC and consequent PGC1-α induction.[412] As previously mentioned ANT2 is a mitochondrial protein associated with the internal mitochondrial membrane that catalyses the exchange of ATP generated in the mitochondria with cytosolic ADP.[397] ANT2 knockdown in SIRT4-overexpressing cells correlates with decreased AMPK activity, highlighting that ANT2 plays an essential role in SIRT4-dependent AMPK modulation.[412] To conclude, SIRT4 suppresses fatty acid oxidation by regulating the activity of MCD, AMPK and PPARα.
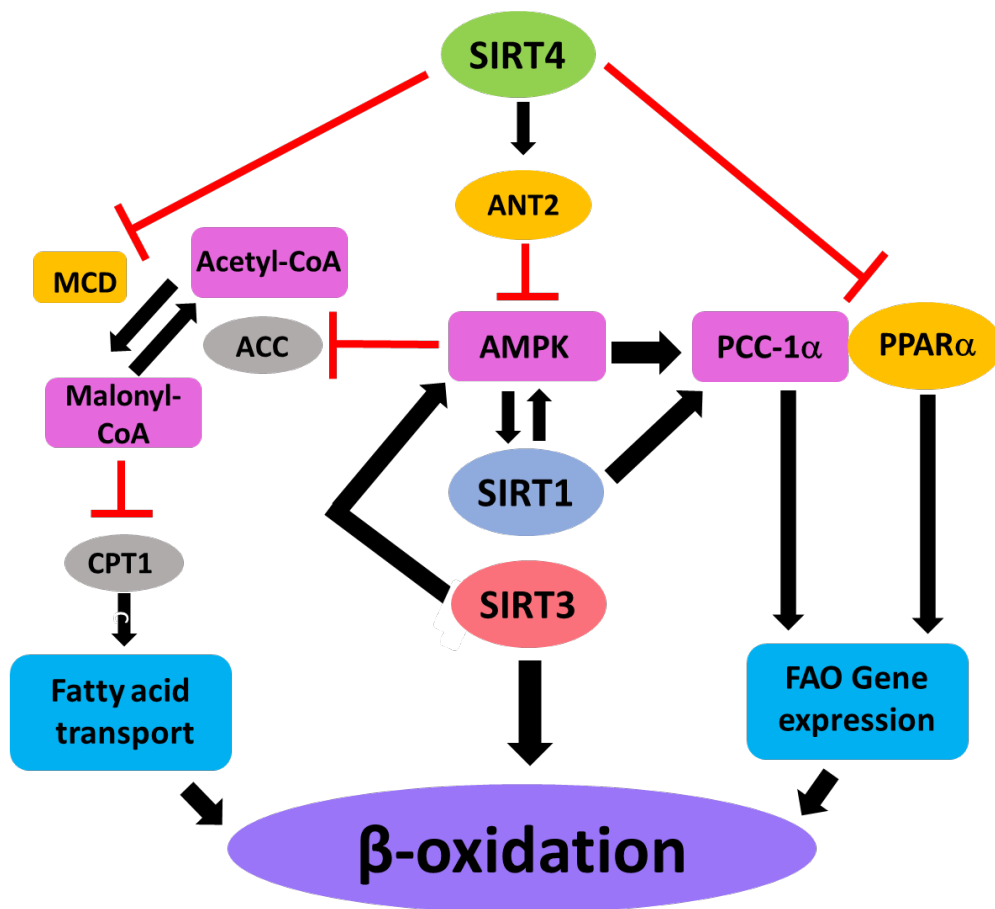

Figure 1.23. Overview of substrates taking part in fatty acid oxidation process and relative roles covered by SIRT1 and by the mitochondrial sirtuins SIRT3 and SIRT4. SIRT4 directly (orange ovals) and indirectly (pink rectangles) modulates the activity of different targets.

1.2.6.2.5.3 SIRT4 regulate pyruvate dehydrogenase complex (PDH) activity

The mitocondrial multi-component PDH complex consists of five subunits, among which, three are involved in its catalytic activity and are known as E1 (pyruvate decarboxylase), E2 (dihydrolipoyl lysine acetyltransferase, DLAT) and E3 (dihydrolipoyl dehydrogenase), two are regulatory subunits (PDH phosphatase and PDH kinase) and the PDH-binding component X, PDHX covers instead, a structural role.[414] The catalytic activity of such complex involves the oxidative decarboxylation of pyruvate to provide acetyl-CoA, thus representing a bridge between the glycolysis and the TCA processes. The reversible phosphorylation of the E1 subunit, mediated by specific PDH kinases, correlates with its inactivation.[415,416] Mathias et al.[379] demonstrated that SIRT4 shows a biotinyl- and lipoyl- more efficient removed capability (from lysine) compared to the deacetylation process toward the PDH complex. SIRT4, in fact, catalyze the hydrolysis of the lipoamide cofactors from the DLAT E2 component in a phosphorylation-independent manner, thus repressing the whole enzymatic activity of the complex. In addition, glutamine stimulation enhance the SIRT4 lipoamidase activity, triggering a decreased PDH and DLAT activity. Since the PDH complex activity indirectly modulate a large variety of downstream effects, these pieces of evidence show that SIRT4 is one of the main regulators of cellular metabolism.

1.2.6.2.5.4 SIRT4 and manganese superoxide dismutase (MnSOD)

Despite SIRT4 results highly expressed in the heart, its role remains almost unknown. Luo et al.[398] recently reported that SIRT4 induces oxidative stress upon pathological stimulation, which resulted in an enhanced hypertrophic response. Oxidative stress covers a crucial role in the pathogenesis of cardiac hypertrophy and heart failure. Angiotensin II (Ang II), a well-known hypertrophic agonist, induces increased mitochondrial ROS levels in cardiomyocytes, thus contributing to cardiac hypertrophy. To protect cells against oxidative damage, mitochondrial antioxidant enzymes such as MnSOD, glutathione and mitochondrial thioredoxin take part to a tricky defense system to detoxify mitochondrial ROS.[398,417] These antioxidant enzymes are the main heart guardians from oxidative injury and cardiac dysfunction.[418–420]

Strictly, upon Ang II treatment, cardiac decompensation resulted dramatically triggered by the SIRT4 cardiac (Sirt4-Tg) OE. In contrast, cardiac function of Sirt4 KO mice was preserved and no particular difference was registered between saline and Ang II treatments.[421] These results proved the capability of SIRT4 to mediate cardiac performance sensitivity to hypertrophic stress. ROS affect all of the main hallmark typical of cardiac maladaptation, including the contractile dysfunction, extracellular matrix remodeling, hypertrophic response and arrhythmia.[301] SIRT4 boots ROS accumulation in the myocardium upon hypertrophic stress. Mitochondria generate ROS during oxidative phosphorylation, and prolonged oxidative stress correlates with the possibility of causing damage mitochondria. To prevent ROS over-accumulation in the mitochondria, MnSOD catalyzes the production of H_2O_2 from O_2^-, and H_2O_2 is immediately converted to H_2O by other specific antioxidant enzymes, including catalase.[422] In humans, mutations of mitochondrial antioxidant enzyme (e.g. MnSOD, catalase, GPx, and TrxR) boost the risk of cardiovascular pathologies.[423–426] As widely known, MnSOD is crucial for a physiological heart function and even just a little reduction in the activity of MnSOD might results in cardiac dysfunction.[418] In human, increased risks for non-familial idiopathic dilated cardiomyopathy seems to be correlated with mutations in MnSOD.[423] In addition, decreased protein level and activity of MnSOD, have been registered in murine

hypertrophic hearts and human failing myocardia.[427,428] Ang II-based treatment induces a reduction of MnSOD acetylation level, thus modulating its activity. The registered enhanced SIRT3 binding to MnSOD, could correlates with decreased MnSOD acetylated level in response to Ang II, since MnSOD resulted to be directly deacetylated by SIRT3. SIRT4 counteracts the interaction between SIRT3 and MnSOD in order to reach increased MnSOD acetylation levels after Ang II treatment. In addition, SIRT4 influences SIRT3 expression levels in mouse liver[358] and an interaction between SIRT4 and SIRT3 was highlighted in HEK293 cells. In the heart, despite none effect of SIRT4 on SIRT3 expression was detected, a SIRT4-SIRT3 interaction was registered in cardiomyocytes. In particular, in hypertrophic cardiomyocytes, such interaction resulted decreased and SIRT4 lost controls the activity as well as the protein levels of SIRT3. Therefore, given the collected data, it is possible to assume that SIRT4 competes with MnSOD for binding with SIRT3, and SIRT4 OE correlates with increased MnSOD acetylation levels during cardiac hypertrophy. Nonetheless, the MnSOD knockdown blocks the effects of SIRT4 on mitochondrial ROS as well as hypertrophy.

1.2.6.2.5.5 How does SIRT4 function either as both tumor suppressor or oncogene?

SIRT4 mRNA levels are reduced in several human cancers, such as liver, lung, pancreatic, ovarian, prostate, renal, endometrial tumor as well as blood cancers.[387,391,429,430] Lower level of sirt4 expression in tumor cells is often associated with inferior survival and SIRT4 KO mice displayed increased incidence of spontaneous tumors.[387,431–434]

Worthy of note is the role covered by glutamine metabolism in the proliferation of cancer cells. Glutamine is a crucial amino acid playing a main role in various intracellular processes including macromolecular synthesis, redox homeostasis, oxidative metabolism, and many others. Although most mammalian cells can produce glutamine by their-self, during rapid cell proliferation (typical of cancer), a steady extracellular source of glutamine results fundamental. Glutamine acts as an anaplerotic substrate by replenishing the Krebs cycle *via* α-ketoglutarate, a product of glutamine catabolism. Different cancer cells can be defined ''glutamine addicted', since require exogenous glutamine to promote survival and proliferation.[433] For example, cell cycle progression in HeLa cells is intimately dependent on glutamine.[402] Recent studies proved that SIRT4 seems to act as a tumor suppressor thanks to its capability to repress the glutamine metabolism thus promoting genomic stability.[388,430,435]

The tumor-suppressor activity of SIRT4 was also studied in the context of *c*-Myc-driven human Burkitt lymphoma cells.[388] *c*-Myc is a well known transcription factor that represses specific microRNA (miR-23a and miR-23b) increasing the expression of glutaminase an consequent greater conversion of glutamine to glutamate.[433] *c*-Myc driven cancers which typically show marked glutamine dependence.[436,437] In Burkitt lymphoma cells, SIRT4 OE reduces glutamine utilization, thus inhibiting their proliferation sensitizing them to glucose depletion. In addition, in a mouse model of Burkitt lymphoma, SIRT4 loss induce lymphomagenesis and mortality. Malignant B cells from these mice show increased glutamine uptake and GDH activity.[388]

Csibi et *al*.[388] demonstrated that the mechanistic mTORC1 negatively controls SIRT4 expression by promoting proteasome-mediated degradation of the SIRT4 transcriptional regulator cAMP response element-binding protein 2 (CREB2). This evidence could explain the decreased expression of SIRT4 in cancer cells. Tuberous sclerosis 2 (TSC2) is a negative regulator of mTORC1. Tsc2 KO mouse embryonic fibroblasts (MEFs) show increased mTORC1 activation. In Tsc2 KO cells, rapamycin mediated-mTORC1 inhibition correlates with increased SIRT4 expression and reduced GDH activity. SIRT4 OE

counteracts transformation and proliferation characteristics of Tsc2 KO MEFs *in vitro* and delays tumor development in xenograft models. Sirt4 KO in MEF cells enhanced the entry of glutamine-derived metabolites into the Krebs cycle, resulting unable to counteract the DNA damage-induced glutamine uptake inside cells. In addition, these cells show an increased proliferation rate, an effect effectively abrogated by treatment based on glutamine metabolism inhibitors, thus proving their glutamine-dependent proliferation.

In addition to the role that SIRT4 covers in the regulation of glutamine in cancer, noteworthy is also its capability to modulate several other processes involved in cancer such as cell cycle progression, tumor growth, apoptosis and metastasis. In fact, SIRT4 can also regulates the EMT at the base on the tumor metastatization mediating the upregulation of E-cadherin which promote cell-cell adhesion thus preventing tumor invasion. It was also showed that, such upregulation correlates with the SIRT4-mediated inhibition of the glutamine metabolism, since an addition of α-ketoglutarate decreased E-cadherin expression.[362]

Defective apoptosis is known to be one of the primary causes of tumor onset and progression. Caspases are a family of cysteine proteases that cover crucial roles in the regulation of apoptosis. SIRT4 OE correlates with a decreased activities of caspases 3/7 under hypoxic conditions and it also reduces the hypoxia-mediated induction of caspases 3/9. Recently, SIRT4 resulted able to inhibit the activity of NF-ϰB mediating the arrest of the IkBα degradation. NF-ϰB is a transcription factor that modulates the inflammatory responses and transcriptionally controls the expression of surface adhesion molecules, including VCAM-1 and E-selectin.[438] Treatment based on cigarette smoke extract (CSE), strongly induces the expression of vascular cell adhesion protein 1 (VCAM-1) and E-selectin in human pulmonary microvascular endothelial cells (HPMECs). In addition, SIRT4 OE in HPMECs blocks the CSE-induced expression of such surface adhesion molecules and mononuclear cell adhesion (Figure 1.24).[439]
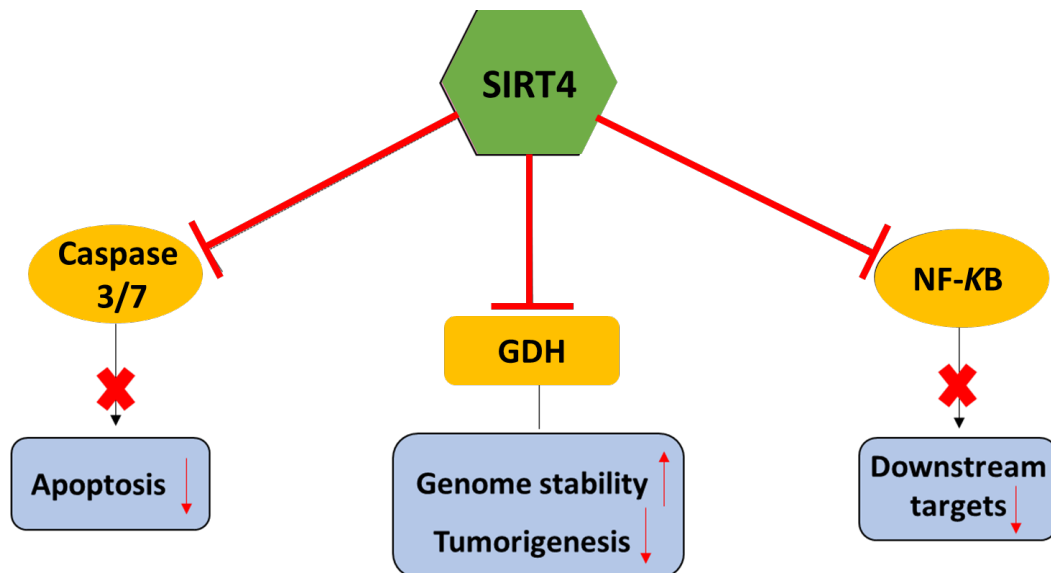

Figure 1.24. Overview of SIRT4 target substrates and tumor suppressor functions. SIRT4 show the direct (orange rectangle) or indirect (orange ellipses) capability to regulate the activity of various target substrates which play crucial roles in other cellular processes (blue rectangles). Upward and downward red arrows indicate the promotion or suppression of a particular condition, gene expression, or physiological activity.

Jeong et *al*. proved that genotoxic stress, which is responsible for the arrest of cell cycle progression thus allowing a correct repair of DNA damage, induces SIRT4 expression, that,

in turn, counteracts mitochondrial glutamine metabolism.[387] In summary, in non-cancer cell, SIRT4 protected from the accumulation of DNA damage thus acting as a tumor suppressor.[389] Since SIRT4 delayed cell cycle in DNA-damaging condition,[387] recent data proved that SIRT4 can decrease the sensitivity of cancer cells to chemotherapy treatment. For example, some evidence showed that OE of SIRT4 increase the colony rate formation during cisplatin treatment.[392]

Indeed, alterations in DNA damage response are associated with tumorigenesis and are observed in many tumor cells.[440,441] In fact, on the other site, cancer cells abuse these critical cellular mechanisms modulating their stress response pathways to escape the therapeutic cytotoxic effect thus acquiring resistance to the antitumor treatment.

Since SIRT4 responds to genotoxic stress regulating the mitochondrial metabolism,[442] it has been proposed that SIRT4 controls stress resistance of cancer cells. Jeong et al.[392] showed that SIRT4 loss correlates with a decreased cell survival and tumor growth after DNA damage, highlighting the important role that SIRT4 covers in cell survival after oncogene expression and oncogenic stresses, thus suggesting the oncogenic function of this sirtuin.

Therefore, SIRT4 supports tumor cell growth and survival in response to different cellular stresses. It is not surprising, in fact, that genes known for their tumor suppressive roles, can act as oncogenes in relation of genetic context, tumor type and stage.

A recent study conducted by Lai et al.[393] showed that cytoplasmic protein levels of SIRT4 in esophageal squamous cell carcinoma (ESCC) tissues in Chinese patients were higher than the correspondent normal tissues, and in particular, this data seems to be more pronounced in woman patients. The OE of such sirtuin correlates, in addition, with a shorter survival time suggesting that SIRT4 may participate in the development of ESCC.

In addition, as a key regulator of the connection between glycolysis and TCA cycle, SIRT4 can also contribute to the tumor onset and progression by regulating PDH activity.

In conclusion, a better mechanistic understanding of how SIRT4 contributes to cancer, and, in general, to human disease is certainly necessary (Figure 1.25).
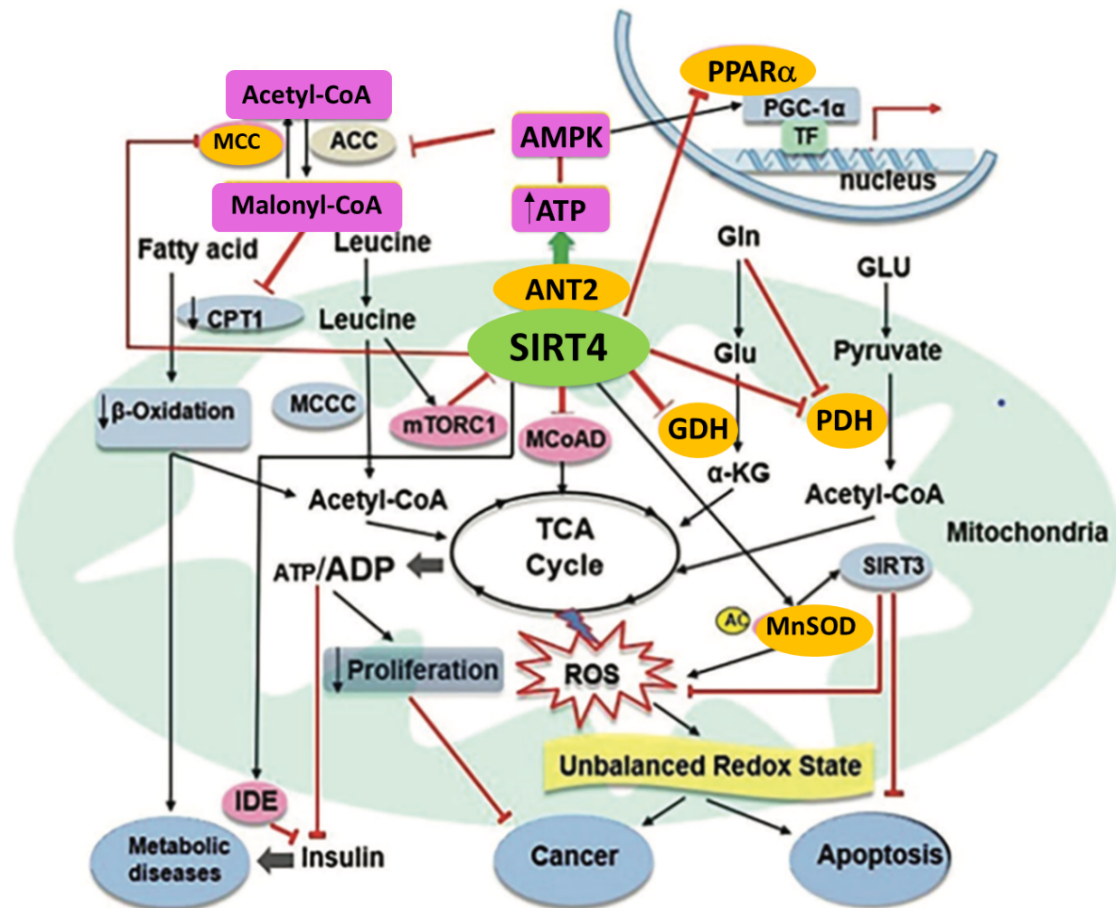
Figure 1.25. Overview of SIRT4 functions, its direct and indirect targets and relative downstream effect. Adapter from Han et al. Front. Physiol. 2019.[361]

1.2.6.2.5.6 Other SIRT4 targets

SIRT4 plays also a role in the development of brain astrocytes, in fact, GDH inhibition induced by SIRT4 seems to regulate the development of glial cells.[443] An excess of glutamate at synapses level prevents efficient neurotransmission resulting in excitotoxicity, cell death and neurodegenerative disease.[444] SIRT4 was found to be upregulated in response to excitotoxins, and, increased activity of GDH (due to a decreased ADP-ribosyl transferase activity of SIRT4) correlates with neurological disorders observed in patients with congenital hyperinsulinism-hyperammonemia syndrome thus suggesting a new role for SIRT4 as neuroprotective agents.[380,443]

SIRT4 was shown to be upregulated in different cell lines following senescence during aging. Different evidences showed that SIRT4 transcript levels resulted increased with increased age in a specific area of the brain, the preoptic one, which regulates the release of hormones that are important for reproduction. Such event may suggest also a role for SIRT4 in the modulation (decrease) of serotonin and testosterone levels during aging.[380,445]

To conclude, recent studies showed that SIRT4 could be also implicated in protecting cells against virus and bacteria pathogens.[380]

Despite the recently growing body of literature elucidating the role of SIRT4 in different patho/physiological condition, a full understanding of the mechanisms that drive the role of SIRT4 in human diseases is still necessary in order to better evaluate the potential of SIRT4 as new therapeutic epigenetic target.

1.3 DNA methylation

DNA methylation is probably the most extensively studied epigenetic mark. The establishment and maintenance of DNA methylation level is governed, as previously mentioned, by a class of enzymes called DNMT.[446] In mammals, DNMTs comprise four members divided in two families that are structurally and functionally distinct. While the DNMT3 family is resposable for the initial CpG methylation mark introduction, DNMT1 maintains this pattern during chromosome repair and replication.[447] The DNMT3 family includes two active methyltransferases, DNMT3A and DNMT3B as well as a regulatory factor, DNMT3-Like protein (DNMT3L). DNMT1 shows preference for hemimethylated DNA *in vitro*, which is consistent with its role as a maintenance DNMT, whereas DNMT3A and DNMT3B methylate unmethylated and methylated DNA at an equal rate, which is consistent with a *de novo* DNMT role. DNMT enzymes mechanism of action is focused on the catalysis of the transfer of a methyl group from the co-substrate SAM (that allosterically regulates DNMTs activity) to the C5 of cytosine. Three are the key actors involved in the DNA methylation: DNMT, DNA and the co-substrate SAM (that allow the transfer of monocarboxylic units at the lower oxidation state). It is necessary to underline that, in standard conditions, cytosine residues result unable to enter in the catalytic pocket of the enzyme because it engages hydrogen bond with its coupled base, thus stabilizing the double helix as postulated by Watson and Crick. What energetically allowed this process is: i) the substrate-enzyme interaction (that is promote by the dissolution of the hydrogen bond between cytosine and guanine); ii) the simultaneous formation of π-interactions with the adjacent base; iii) the cytosine nuchelophilicity. Upon the recognition of the methylable CpG site by the enzyme, it is able to pull out the deoxycytidine directing it to the catalytic pocket through a process known as "base flipping". The next step sees the binding of a specific DNMTs cysteine (Cys1226, Cys711 and Cys652 for DNMT1, 3A and 3B, respectively) to the C6 of the involved cytosine leading to the corresponding enamine, allowed by the transient protonation of the nitrogen atom in the third position (N3) permitted by a glutamate residue, thus breaking the pyrimidine aromaticity. Next, the transfer of the methyl group to the C5 is promoted by its delocalized electrons that are involved in such specific nucleophilic attack to the SAM methyl unit. To conclude, the release of the cysteine *via* a β-elimination reaction (allowed by the deprotonation of the C5 by a basic aminoacidic residue typical of each DNMT isoform) restore the aromaticity of the cytosine leading to SAH and to the free DNMT enzyme which is ready for a new catalytic cycle (Figure 1.26).[448,449] As already discussed, the introduction of such methyl unit trigger the recruitment of different regulatory proteins.
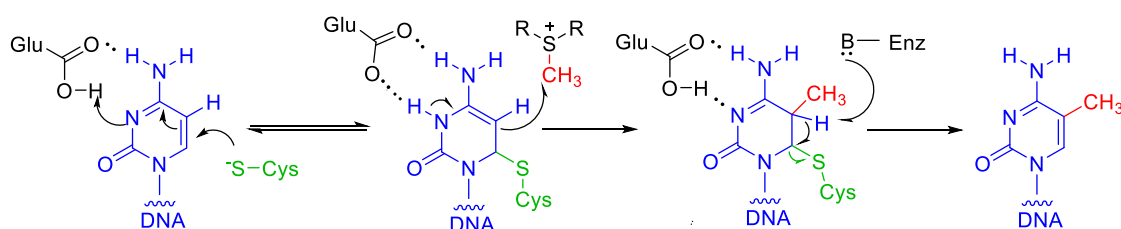

Figure 1.26. Schematization of DNA cytosine methylation mechanism catalyzed by DNMT enzymes.[450]

As it is inherent in the definition of epigenetic modification, the methylation mark is reversibly maintained during mitosis without altering the genetic sequence. As previously discussed, when this process arises at the level of the CpG island, the gene interested resulted silenced, dynamically modulating the gene expression.[451] DNA methylation plays a main role in genomic imprinting, DNA repair, X-chromosome inactivation and in the silencing of retrotransposons, repetitive elements and tissue-specific genes. In humans, DNA methylation mainly involves the CpG dinucleotides clustered in ~1 kb regions, called CpG islands (Figure 1.27a).[452–454] In addition, this process also occurs at regions with lower CpG density that lie in close proximity (~2 kb), known as "CpG island shores" (Figure 1.27b).[455] DNA methylation is poorly associated with transcriptional activation, as when, for exaple, it occurs at gene bodies (Figure 1.27c). Gene body methylation is commonly registered in ubiquitously expressed genes and positively correlates with gene expression.[456] It has been proposed that it might be correlated with prevention of spurious initiations of transcription as well as with elongation efficiency.[457]

Ten-eleven translocation (TET) are methylcytosine dioxygenases enzymes which plays a main role in the modulation of the balance of DNA methylation providing its demethylation.[458] This family consists of three members (TET1-3) that catalyse the hydroxylation of DNA converting the methyl cytosine mark into 5-hydroxymethylcytosine that can be subject to further oxidation obtaining 5-formylcytosine and 5-carboxymethylcytosine. During the methylation process, these last oxidized state of cytosine are excised by thymine DNA glycosylase and then replaced by unmodified cytosine *via* base exision repair mechanisms[459,460] High levels of 5-hydroxymethylcytosine have been detected in adult neuronal cells and ESCs and its levels seems to decrease during differentiation. In this framework, vatious evidence proved that, in some tissues, 5-hydroxymethylcytosine has a low turnover acting not only as an intermediate state of oxidation but also as an independent epigenetic mark probability modulating the the local chromatin environment through the displacement or recruitment of specific proteins.[461–464]

A significant fraction of deeply methylated CpGs is found in repetitive elements (Figure 1.27d). This DNA methylation is required to protect chromosomal integrity, that is reached by counteracting the reactivation of endoparasitic sequences responsible for chromosomal instability, gene disruption and translocations.[465]
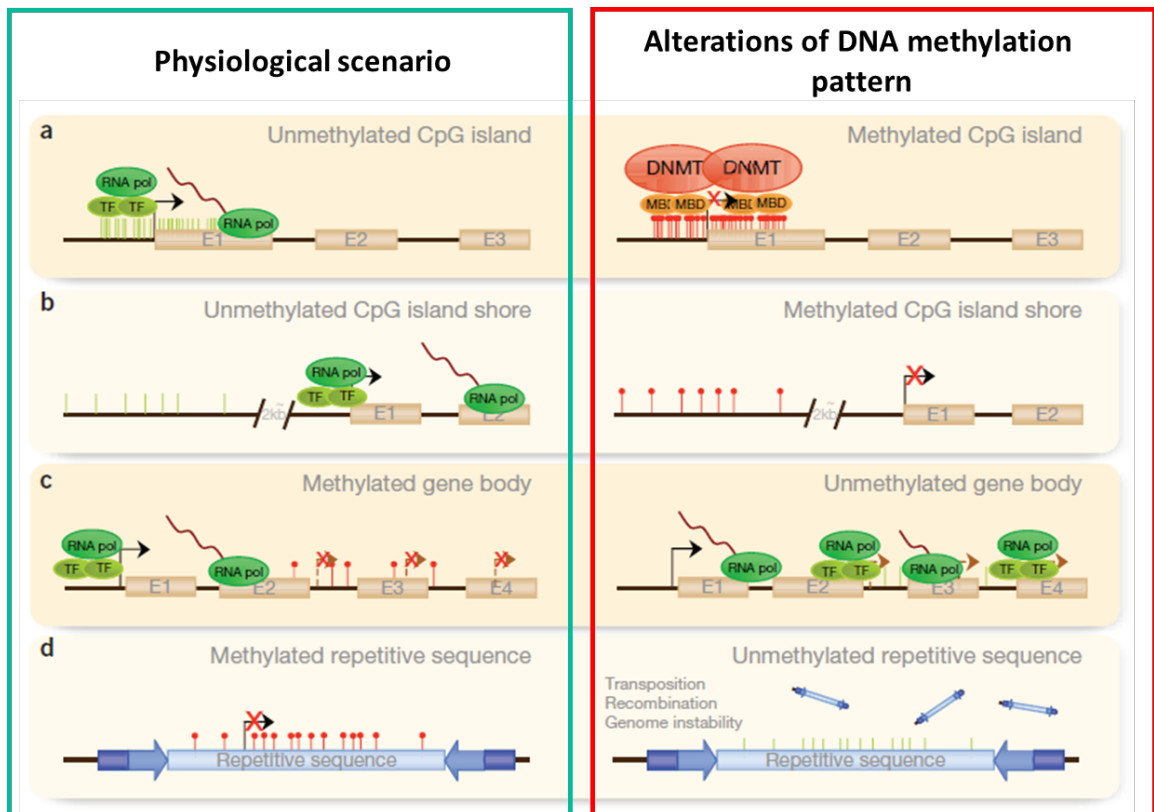
Figure 1.27. (**a**) In physiological condition CpG islands at gene promoter regions are unmethylated, allowing gene expression and transcription. Aberrant hypermethylation of these regions leads to transcriptional inactivation. (**b**) The same condition is registered for GpG island shores (located up to 2 kb upstream of the CpG island). (**c**) Methylation of gene body facilitates transcription; in different diseases, instead, gene bodies tends to demethylate allowing spurious transcription. (**d**) In normal condition, repetitive sequences resulted to be hypermethylated, thus preventing chromosomal instability, gene disruption and translocations. Adapted from Portela *et al*. *Nat Biotechnol*, 2010, 28,1057–1068. [454]

Only < 80% of the methylatable CpG population, which correlates with over 50% of promoters, resulted methylated. Different CpG sites are methylated in various tissues, establishing a gene and tissue specific pattern of methylation[466] which leads to a layer of information which allow the assignment of specific cell type identity. While transcriptional active chromatin regions correlates with hypomethylated DNA, hypermethylated DNA is packaged in inactive chromatin, which is associated with the silencing of gene expression. DNA methylation is a fundamental mechanism for the establishment of a silenced pattern of gene expression in plants and vertebrates, or by the modulation of of transcription factors binding, or by the recruitment of MBDs, which, in turn recruit other histone modifying enzymes.[467]

During the onset and development of cancers, a genome-wide demethylation takes place potentially promoting genome instability through the activation of silenced retrotransposons.[6] On the other hand, focal hypermethylation of CpG islands has been strongly evaluated in cancer. In fact, all types of tumor show transcriptional inactivation of specific tumor suppressor genes due to DNA hypermethylation.[13] However, the exact mechanism at the base of the appearance of DNA methylation in a given promoter still need to be understood.

1.4 PTMs recognition: The Readers

In this chapter, the most significant epigenetic mechanisms that influence the gene expression have been discussed. As previously mentioned, these modifications can induce changes in the chromatin compaction state directly or indirectly through protein modules that read the message written in form of chemical code. These modules are termed readers, and are specific for each PTMs, degree of modification (for example mono-, di- or trimethylated residues) as well as position inside the histone peptide.[468] The interaction between the histone mark and its partner can be considered as a generic protein-protein interaction, in which the key feature is the reader surface groove. However, many pieces of evidence suggest that the concept "one domain-one mark" is outmoded. Indeed, a single PTM can recall different readers, protein modules with opposite effects can bear the same binding motif, and above all, the same domain can bind several PTMs. Moreover, it is possible to rank the readers on the base of their functional outcomes: i) chromatin architectural proteins induce chromatin compaction by binding multiple nucleosomes; ii) chromatin remodelers are responsible for the chromatin relaxation determined by shifting the nucleosomes on different positions; iii) the recognition of specific PTMs by the chromatin modifiers triggers a further modification of the original PTM; iv) finally, the adaptors recruit machineries involved in several DNA metabolism pathways (transcription, recombination, replication, repairs etc.) (Figure 1.28).[469]
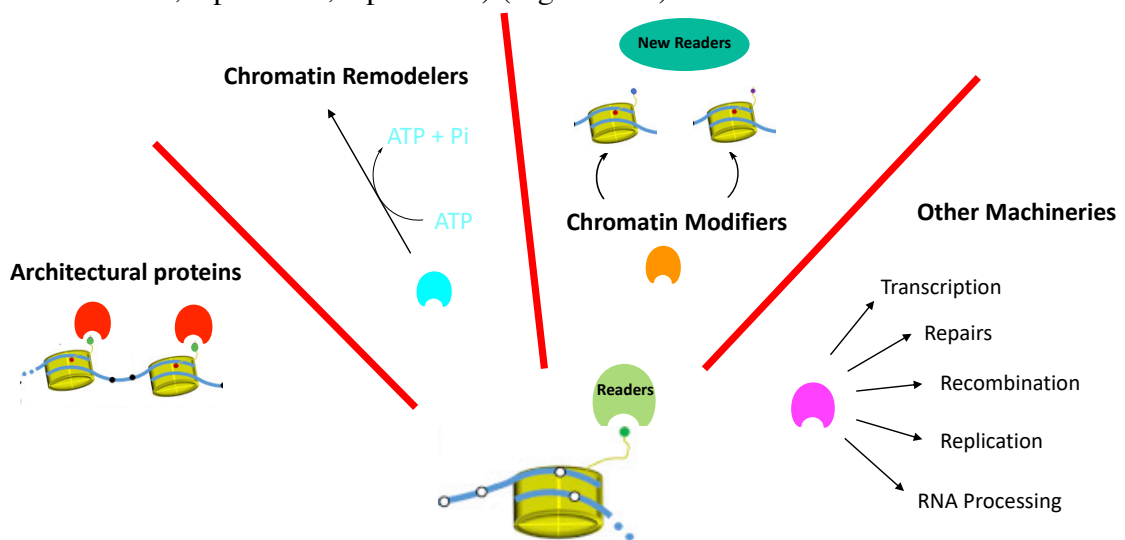

Figure 1.28. Schematization of "readers" functional outcomes.

Nowadays a large number of readers for acetylated lysine, methylated lysine or arginine, and phosphorylated serine or threonine residues have been identified.[470] Bromodomains are protein modules, located in chromatin associated protein complexes or into the peptide structure of HATs, that recognize the acetylated lysines. Conversely, since the methylation state influences the physical-chemical properties of lysines, the recognition of this mark requires a large variety of effector modules thus allowing state-specific readouts. Indeed, while histone acetylation process neutralize the lysines charge, all lysine methylated forms are cationic at physiological pH. While the addition of methyl group(s) correlates with increased hydrophobicity, on the other hand ε-NH$_2$ lysine group ability to donate hydrogen bonds simultaneously results decreased. In general, it is possible to distinguish the royal superfamily, the plant homeodomain (PHD) zinc finger, WD40 repeat, ankyrin repeat, bromo-adjacent homology (BAH)-containing proteins as different classes of protein folds that share the common feature of use aromatic cage for the placement of the methylated

lysine.[468] Such aromatic cages engage the quaternary ammonium functional groups, with cation-π–type interactions dominating the energetics and hydrophobic desolvation effects having an appreciable but lesser role[471] for recognition of lower methylation states (me2 and me1), hydrogen-bonding and steric exclusion are increasingly important.[472] Aberrant dysfunction of this recognition domains may affect the normal cellular functioning, thus generating the favorable conditions for the onset of diseases, especially cancer.

The first Bromodomain associated with the concept of reader was the HAT PCAF domain, which has been found to bind acetylated lysine residues. About 61 bromodomains have been then identified in many different nuclear bromodomain containing proteins (BCPs), all sharing a 110 amino acids module, organized in a left-handed bundle of four α-helices, which together compose the hydrophobic surface interacting with the histone modified lysine. The recognition event is driven by the hydrogen bond between the carbonyl oxygen of acetylated lysine and an asparagine residue of the helix B, reinforced by several additional hydrogen bonds between water molecules and other histone peptide residues.[473]

Among BCPs, Bromodomain and extra-terminal domain (BET) bromodomain containing proteins have been the most widely investigated for their role in transcriptional elongation, cell-cycle regulation,[470] and viral infections. BET subfamily includes BRD2, BRD3, BRD4 and BRDT and, as the name suggest, they contain two bromodomains (BD1 and BD2) followed by an extra terminal (ET) domain, that confers to the protein the ability to associate with pluri-modified H3 and H4 histone tails.[474] BET proteins functions are member specific: BRD4 is involved in the maintenance of epigenetic memory by labeling chromosomes during cell division, whereas BRD3 performs the recognition of acetylated GATA1, a transcription factor implicated in hematopoiesis. Finally, while BRD2 plays an important role in cell-cycle progression, BRDT is a testis specific BET protein responsible for the spermatogenic gene regulation.[475]

BET- containing proteins have been identified in the last few years as a promising novel target group for the cancer treatment. In particular, the best studied BET member BRD4, is known to be implicated in various solid and hematological tumors since it modulates the transcription elongation of essential genes that play a crucial role in apoptosis and cell cycle such as BCL2 and *c*-Myc.[476]

1.5   An overview of epigenetic modulators

Recently, a huge number of small molecules characterized by reversible high affinity binding for a selected epigenetic target have been published, resulting in seven approved new anticancer agents and numerous clinical candidates (Table 1.5).[477] DNMT inhibitors (DNMTi) azacytidine **3** and decitabine **4** (Table 1.5) were the first epigenetic modulators reaching the Food and Drug Administration (FDA) approval in 2004 and 2006, respectively, for the treatment of haematological malignancies.

The potential applicability of DNMTi in the fight against cancer consists in their ability to reactivate silenced tumor suppressor genes.[478,479] Azacitidine **3** and decitabine **4**, are nucleoside analogues characterized by a 1,3,5-triazine ring and, after triple phosphorylation, such prodrugs are metabolically converted into the correspondent active species, allowing their incorportation into DNA, being also accepted as DNMT substrates. Upon the nucleophilic attack of the enzyme to the triazine C6 position and the introduction of the methyl group at N5 from the co-substrate SAM, azacitidine **3** and decitabine **4** counteract the final elimination step as a consequence of the lack of a proton at the N5 position, leaving the enzyme covalently and irreversibly inhibited.[480] As simply understandable from their mechanism of action, such drugs, despite their high efficacy, suffer from toxic side-effects as a consequence of the lack of selectivity, showing, in addition, chemical instability and poor bioavailability. Given these evidences, non-nucleoside DNMTi, since they do not need to be incorporated into DNA, are promising candidate to avoid the onset of this kind of toxicity. Unfortunately, many members of this class display low potency, poor target selectivity, and unknown mechanisms of inhibition. However, despite the limitations just described, azacitidine **3** and decitabine **4** are approved for the treatment of myelodysplastic syndrome (MDS), that often progresses to AML.

Among histone modifications, lysine acetylation and methylation are the main object of interest. One of the most promising classes is those of HDAC inhibitors (HDACi), which are molecules able to reactivate signalling pathways silenced by deacetylation processes, in cancer and non-cancer diseases. A pharmacophoric model for HDACi characterized by three different portions can be described. It is composed by: (i) a partially solvent exposed cap binding group (ii) a spacer that mimics the substrate lysine side-chain, and (iii) a moiety able to chelate the zinc ion, that is known to be crucial for the HDAC catalytic action.[481] Vorinostat **5** (SAHA, Table 1.5) was the first pan-HDACi approved by the FDA for the treatment of refractory cutaneous T-cell lymphoma (CTCL) and it consists of an anilide cap group, a six-methylene unit linear spacer and a hydroxamate function as zinc ion binder. Romidepsin **6** (FK-228, Table 1.5), instead, is a natural prodrug approved by FDA for the treatment of refractory CTCL decorated by a disulfide bridge that is reduced *in vivo* thus leading to the thiol zinc binding moiety. Unlike vorinostat **5,** romidepsin **6** is not a pan-HDACi but shows but shows selectivity of inhibition towards class I HDACs. Belinostat **7** and panobinostat **8** (Table 1.5) are two other hydroxamate-containing pan-HDAC inhibitors approved by FDA for the treatment of refractory peripheral T-cell lymphoma (PTCL) and refractory or relapsed MM, respectively. Tucidinostat **9** (chidamide, Table 1.5) is, instead, the first benzamide-based HDACi, was approved by Chinese FDA, for treatment of PTCL resulting active against HDAC1/2/3/10. The well-known antiepileptic drug sodium valproate (VPA) **10** (Table 1.5) selectively inhibits class I HDACs and decreases tumor growth and metastatization in various animal models of cancer. Mocetinostat **11** and entinostat **12** (Table 1.5) are two benzamide based class I-selective HDACi in clinical trials for the treatment of numerous solid tumors. Abexinostat **13**, pracinostat **14**, rocilinostat **15,** resminostat **16**, quisinostat **17** and givinostat **18** (Table 1.5) are hydroxamates based pan-HDACi (except for **15,** which is quite selective for HDAC6) currently in clinical trials for the treatment of different hematological (**13-14, 16-17**, and **15**) and solid tumors (**16**). In
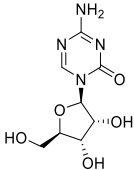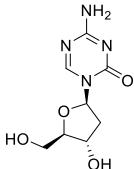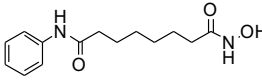
particular, pracinostat **14**, resminostat **16**, and givinostat **18** granted the status of orphan drugs for AML, hepatocellular carcinoma, and Duchenne muscular dystrophy, respectively.[482,483] Until today, nicotinamide **19** is the only sirtuin inhibitor (SIRTi) currently used in clinics for the treatment of solid tumors (Table 1.5). Recently, clinical candidates have been discovered for other epigenetic targets such as KMTs, KDM, PRMTs, and BRDs.
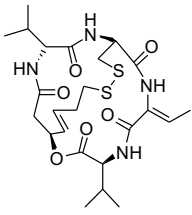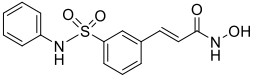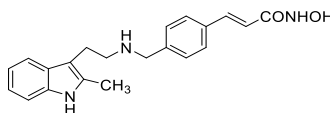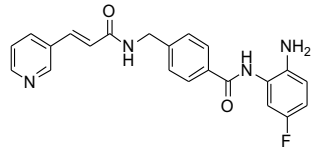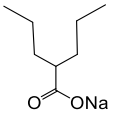
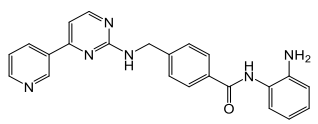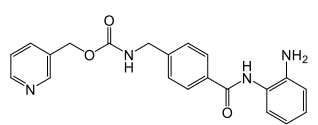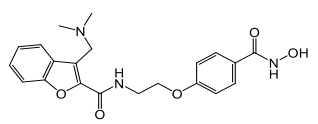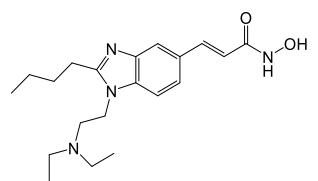GSK126 **20** (also known as GSK2816126), tazemetostat **21**, and CPI-1205 **22** (Table 1.5) are selective inhibitors of both WT and mutant forms of EZH2, currently in clinical trials in patients with MM, various lymphomas and solid tumors.[484,485] Pinometostat **23** (Table 1.5), instead, is a picomolar selective (more than 30 000-fold selectivity against other KMTs) DOT1L inhibitor (DOT1Li). When used in rearranged-MLL cells and xenograft models,[486] it decreases H3K79 methylation level, thus increasing the expression of MLL target genes expression inducing a selective leukemia cell death.[487,488]
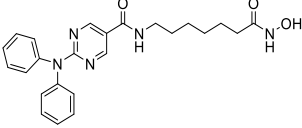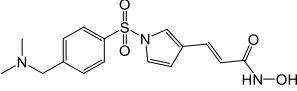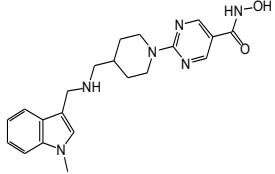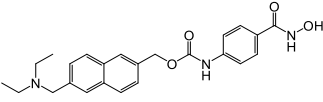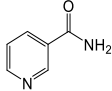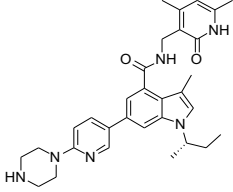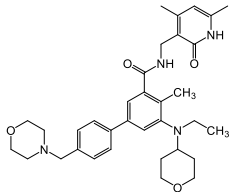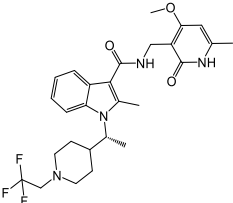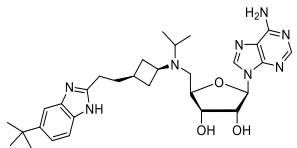
Despite the majority of MAO inhibitors (MAOi) failed to inhibit LSD1, tranylcypromine (TCP) **24** (Table 1.5) results able to irreversibly inhibit LSD1 in the micromolar range, through a radical species obtained from the opening of the cyclopropane ring.[489] ORY-1001 **25** and GSK2879552 **26** (Table 1.5), are two TCP analogs that shows high selectivity for LSD1 over MAOs keeping an inhibitory potency in the nanomolar range. ORY-1001 **25** and GSK2879552 **26** are currently in clinical trials for the treatment of leukemia and small cell lung carcinoma (SCLC).[490]
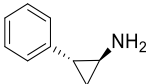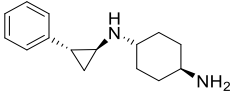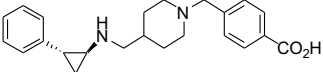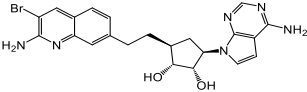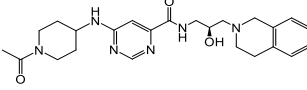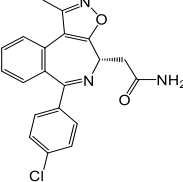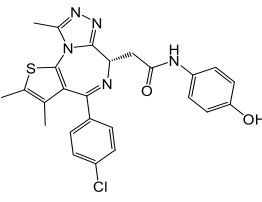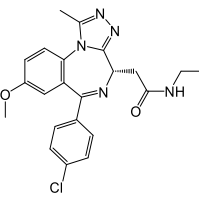
JNJ-64619178 **27**[491] and GSK3326595 **28**[492] (Table 1.5) are two potent and selective PRMT5 inhibitors, recently entered in clinical trials, that induce tumor regression in both hematologic malignancies and solid tumors.

The BETi CPI-0610 **29**, OTX015 **30** and GSK525762 **31** (Table 1.5) are currently tested in clinical trials for a variety of cancers including acute leukemia, MM, NUT midline carcinoma and triple negative breast cancer, respectively.[493,494]

Compound	Structure	Epi-Target	Clinical implication	Status	Clinical trial number
3 Azacytidine		**DNMT**	acute myeloid leukemia, myelodysplastic syndrome	FDA-approved, 2004	-
4 Decitabine		**DNMT**	acute myeloid leukemia, myelodysplastic syndrome	FDA-approved, 2006	-
5 Vorinostat		**HDAC**	cutaneous T-cell lymphoma	FDA-approved, 2006	-

#	Structure	Target	Indication	Status	Clinical Trial
6 **Romidepsin**		**HDAC**	cutaneous T-cell lymphoma	FDA-approved, 2009	-
7 **Belinostat**		**HDAC**	peripheral T-cell lymphoma	FDA-approved, 2014	-
8 **Panobinostat**		**HDAC**	multiple myeloma	FDA-approved, 2015	-
9 **Tucidinostat (Chidamide)**		**HDAC**	peripheral T-cell lymphoma	Chinese FDA-approved, 2015	-
10 **Sodium Valproate**		**HDAC**	progressive, non-metastatic prostate cancer breast cancer solid tumors	Phase I/II	NCT 00670046 NCT 01007695 NCT 00107458
11 **Mocetinostat**		**HDAC**	solid tumors, Hodgkin's and non-Hodgkin's lymphoma, leukemia	Phase I/II	NCT 02236195 NCT 00358982 NCT 00323934 NCT 00324194
12 **Entinostat**		**HDAC**	breast cancer invasive breast cancer ER-negative, PR-negative, HER2-negative (triple negative) breast cancer	Phase I/II	NCT 00828854 NCT 03361800
13 **Abexinostat**		**HDAC**	Hodgkin's and non-Hodgkin's lymphoma, multiple myeloma, leukemia, lymphocytic B-cell lymphoma	Phase I/II	NCT 01149668 NCT 00724984
14 **Pracinostat**		**HDAC**	solid tumors, hematologic malignancies, myelodysplastic syndrome	Phase I	NCT 00741234

15 **Rocilinostat**		**HDAC6**	lymphoma, lymphoid malignancies, multiple myeloma	Phase I/II	NCT 02091063 NCT 01323751
16 **Resminostat**		**HDAC**	advanced colorectal carcinoma	Phase I/II	NCT 01277406
17 **Quisinostat**		**HDAC**	cutaneous T-cell lymphoma	Phase I/II	NCT 01486277 NCT 00677105
18 **Givinostat**		**HDAC**	myeloproliferative diseases, Hodgkin's lymphoma	Phase I/II	NCT 00606307 NCT 00496431
19 **Nicotinamide**		**Sirtuins**	solid tumors	Phase II/III	NCT 00360867
20 **GSK126** **(GSK2816126)**		**EZH2**	acute myeloid leukemia, non-Hodgkin lymphoma, multiple myeloma	Phase I/II	NCT 02082977
21 **Tazemetostat**		**EZH2**	different kinds of lymphomas and solid tumors	Phase I/II	NCT 02875548 NCT 03009344 NCT 02601950
22 **CPI-1205**		**EZH2**	B-cell lymphoma	Phase I	NCT 02395601
23 **Pinometostat**		**DOT1L**	Mixed-lineage leukemia	Phase I	NCT 03724084* NCT 03701295*

		Target	Indication	Phase	Clinical trial
24 **Tranylcypromine**		**LSD1**	Acute myelogenous leukemia	Phase I/II	NCT 02261779 NCT 02717884
25 **ORY-1001**		**LSD1**	myeloid leukemia, small cell lung cancer, relapsed or refractory acute leukemia	Phase I/II	UDRACT n° 2013-002447-29 2018-000482-36 2018-000469-35
26 **GSK2879552**		**LSD1**	myelodysplastic syndrome leukemia small cell lung carcinoma	Phase II/I	NCT 02929498 NCT 02177812 NCT 02034123
27 **JNJ-64619178**		**PRMT5**	relapsed/refractory B cell non-Hodgkin lymphoma, advanced solid tumors	Phase I	NCT 03573310
28 **GSK3326595**		**PRMT5**	selected solid tumors and non-Hodgkin's lymphomas, neoplasms	Phase I	NCT 02783300 NCT 03614728
29 **CPI-0610**		**BRD family**	multiple myeloma, lymphoma	Phase I	NCT 02157636 NCT 01949883
30 **OTX015**		**BRD family**	glioblastoma multiforme, triple negative breast cancer and other solid tumors, acute leukemia	Phase II/I	NCT 02296476 NCT 01713582
31 **GSK525762**		**BRD family**	relapsed refractory hematological malignancies, midline carcinoma	Phase I	NCT 01943851 NCT 01587703

*Only in combination with azacytidine **1** or cytarabine, daunorubicin hydrochloride and pinometostat **21**.
**Only in combination with tretinoin or all-*trans* retinoic acid and cytarabine.

Table 1.5. Clinically approved and clinical candidates among epigenetic modulators.[477]

The inefficiency of the single (epi-) target approach in anticancer treatments is mainly due to the emergence of pharmacological resistance. The constant changes over the time of the

complex network of signals at the base of neoplastic disease are responsible for the onset of phenotypic aberrations and consequent treatment resistance.

In particular, epigenetic dysregulations play a main role in cell plasticity observed during tumorigenesis, potentially providing drug resistance to the adopted treatment.[495,496]

In fact, despite the promising results reached with HDACi and DNMTi-based treatment of haematological malignancies, such drugs could potentially hit a huge number of targets providing the genome-wide re-expression of physiologically and aberrantly regulated genes and consequent conflicting therapeutic effects.[497] Among the most representative examples,[498–505] DNA hypermethylation state induced by DNMTi has been associated with hypometilation of promoter regions of drug efflux, DNA-repair as well as pro-apoptotic genes thus repressing their expression contributing to the development of resistance.[506]

For the reasons just mentioned, the aim of (epi-)drug discovery is moving toward the identification of network-active compounds with multitargeting properties thus overcoming the old trend focused on the design of high selective compounds. The main concept is that: an effective anticancer therapy may not be focused only on a single target of interest, but on the entire biological system.[507] This approach, known as polypharmacology, has the goal to specifically and simultaneously hit related targets that participate to the onset and development of the same pathology, although at different levels, in order to get a synergistic effect against the considered dysregulation.[477] Such approach can be reached *via* three different strategies: (i) the multiple-medication therapy (MMT) based on drug combination; (ii) the multi-compound medication (MCM) which result from the association of selected active principles in the same formulation; (iii) or the new promising multi-target-directed ligands (MTDL) approach focused on the design of multi-targeting compounds. For example, the well-known MMT strategy could increase or maintain the desired therapeutic efficacy potentially needing a lower dose of each individual drug, virtually minimizing toxicity and drug resistance compared to the related single-target based-treatment.[508] On the other hand, one of the main disadvantages of such approach, also called "drug cocktails", is the negative impact on patient compliance, that could be compensated, instead, by the correlate MCM approach that provides a "polyvalent-pill" in which two or more agents are associated in a single tablet.[509] However, both strategies are characterized by potential pharmacodynamic/pharmacokinetic disadvantages, including the possible drug-drug interactions and potential different solubility of the selected molecules that could interfere with the bloodstream uptake. In addition, when drugs are used in combination or association, regulatory agencies generally require the safety demonstration of each individual agent before clinical trials. If the selected drugs are owned by different pharmaceutical companies, it can require a longer period of time.[510,511]

As widely accepted, each tumor, as well as each patient anticancer therapy response, is different from each other. In this framework, one of the main advantages of the MMT approach consists in the possibility to choose different dosages, establishing a prolonged administration of drugs, thus potentially adopting a real personalized treatment.[507,512]

MTDLs result from the conjugation of two or more warheads that individually own a known activity against specific target. This can be achieved in three different ways:[477] (i) by connecting molecules with a physiologically cleavable linker (mutual pro-drugs); (ii) by connecting molecules with a stable linker, allowing each element to interact with its specific target without interfering with the activity of its counterpart; (iii) connecting and preserving only the relative pharmacological moiety of the selected molecules.

Epi-MTDLs reported to literature so far specifically act towards one epi-target and another one that could be, or not, related to epigenetics, thus hitting molecular factors belonging to the same or different cellular pathways.

Most of the epi-MTDLs developed are hybrid molecules resulting from the connection of the scaffold of a selected HDACi to another drug able to hit a cancer related target(s), such as other epi-drugs as well as conventional tyrosine kinase inhibitor (TKi) or cytotoxic agents.[477] A simple analysis about the state of the art can explain the preference of HDACi's structural elements among various epi-drugs to design MDLs: i) from 2000 to now, a huge number of paper on HDACi has been reported by academic or industrial medicinal chemists; ii) the cap group that characterizes all the HDACi points out of the catalytic tunnel of the enzymes and is tolerant of high degree of structural variation without losing the pharmacological activity thus allowing the introduction, at this level, of a specific warhead able to interact with another selected target.[513,514]

To date, two dual HDACi/TKi, CUDC-101 **32** (Figure 1.29) and CUDC-907 **33** (Figure 1.29) are currently in advanced stage of clinical trials for the treatment of different hematological and solid tumors.[515–522] As commonly happens, also in the TKi drugs discovery process, the initial aim has been focused on the design of highly selective molecules. Today, instead, seems that better results can be reached using TKi able to selectively and simultaneously interact with specific kinases. In fact, if it is true for some types of tumor that the deregulation of a specific kinase could be the driving force, this single agent-based treatment commonly culminates in the loss of its efficacy due to the onset of new mutations and redundancies in biological networks. Starting from these findings, the simultaneous inhibition of different kinases has been recently considered the best choice.[513,523] Co-administration of HDACi and TKi *in vitro* and *in vivo* models have shown synergistic effects suggesting that the design of dual HDACi/TKi could result a very promising approach.[524,525] CUDC-101 **32**, is an hydroxamate derivative of the well-known TKi erlotinib **34** (Figure 1.29). The hydroxamic acid Zn^{2+} chelating group is spaced from the quinazoline scaffold by a hexamethylene linker, the same present in the structure of vorinostat **5**. CUDC-101 **32** resulted able to inhibit HDACs enzymes as well as epidermal growth factor receptor (EGFR), the human epidermal receptor 2 (HER2) and the platelet-derived growth factor receptor (PDGFR) reaching the nanomolar range.[515,517]

As previously mentioned, CUDC-101 **32** is actually in phase I clinical trials to evaluate its oral tolerability and safety in cancer patients (NCT01702285), and in phase Ib open label study in patients with advanced neck and head (alone or in combination with cisplatin and radiotherapy NCT01384799),[518] liver, gastric, and breast cancer (NCT01171924), as well as NSCLC (NCT01171924).[517,519]

The phosphatidylinositol 3-kinase (PI3K) plays an essential role in differentiation, proliferation, motility, protein synthesis and apoptosis.[520] On the other hand, when activated, such kinase is also responsible for the onset of different tumors such as indolent B-cell lymphoma (BCL) and aggressive BCL. Single-based drug treatments for diffuse large BCL with either HDACi or PI3Ki were often ineffective and it is due to the simultaneous activation of other growth and survival- related pathways. Concurrent inhibition of these two targets, instead, displayed a synergistic effect.[526,527] CUDC-907 **33**[521] (Figure 1.29), is a dual PI3K/HDAC inhibitor obtained from chemical manipulation of the structure of the PI3Ki pictilisib **35** (Figure 1.29). CUDC-907 **33** provides a, potent, oral dual inhibitory activity against both PI3Ks and results effective against chronic lymphocytic leukemia (CLL) through PI3K/HDAC inhibition that join to the repression of STAT3 and RAF/MEK/ERK signaling, thus reducing the expression of anti-apoptotic BCL2-family members, BCL-xL, BCL-2 and MCL-1. Treatment based on CUDC-907 **33** gave a reduction in *c*-MYC gene expression in *c*-Myc driven-tumor model, in which c-Myc OE has been reported to be among the worst prognostic factors in relapsed, refractory DLBCL. To date, CUDC-907 **33** is currently in phase I clinical trials for the treatment of lymphomas and solid tumors (NCT02674750, NCT0230724, NCT0290977, NCT03002623).[521]

34
erlotinib
EGFR 2 nM

32
CUDC-101

HDAC 4 nM
EGFR 2 nM
HER2 16 nM

35
pictilisib
PI3Ka 3 nM
PI3Kd 33 nM

33
CUDC-907

PI3K 19 nM
PI3Kb 54 nM

HDAC1 1.7 nM
HDAC2 5 nM
HDAC3 1.8 nM
HDAC10 2.8 nM
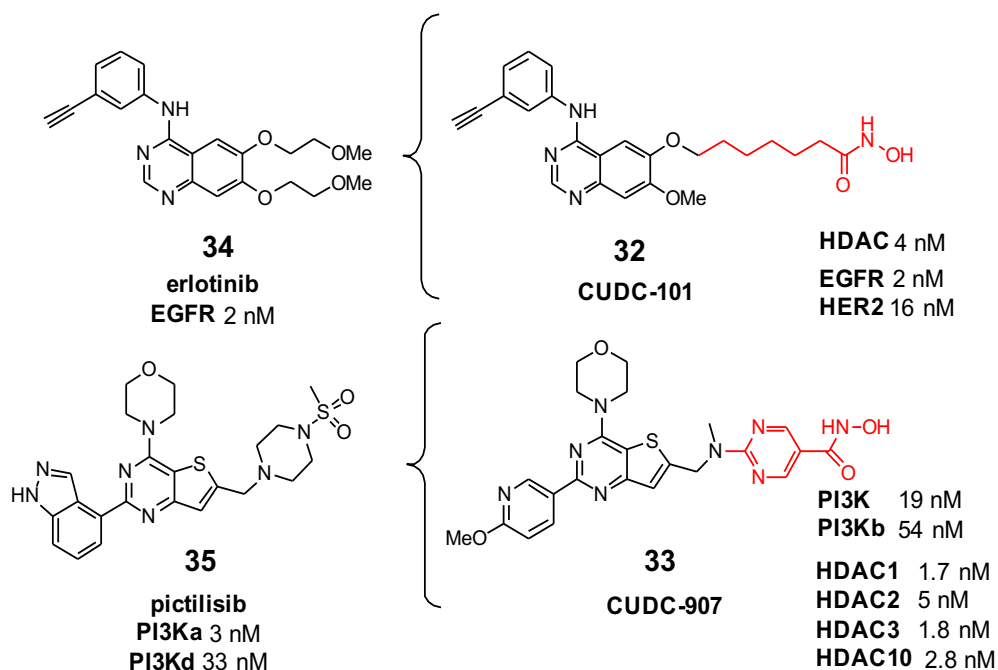
Figure 1.29. Rational design of the dual HDACi/TKi CUDC-101 **32** and CUDC-907 **33**, in clinical trial for the treatment of cancer. IC_{50} values for the different targets are indicated, when available. The HDAC inhibitory portions are depicted in red.

As just exposed, the possibility of provide combined effect restoring specific epigenetic processes in addition to disease-related dysregulations, correlates with potential reprogramming of the entire epi-genome of tumor cells towards physiological condition avoiding a non selective cytotoxic effect.[528]
Despite the success connected to the simple applicability and flexibility of MMT approach at both pre-clinical and clinical stage, the drug-drug interactions, potential formulation problems and consequent toxicity suggest that the MTDL strategy could be the new frontier of polypharmacology given the potentially reachable possibility of induce the simultaneous inhibition of carefully chosen targets. In this scenario, a novel and special type of MTDLs is represented by proteolysis targeting chimeras (PROTACs).[529–531]

Chapter 2

2.1   Proteolysis targeting chimeras (PROTACs) approach applied to epigenetic targets

As previously discussed, medicinal chemists have usually focused their attention on the development of small molecules targeting a (epigenetic-)protein of interest ((e-)POI) by binding and blocking a functional region of the latter (Figure 2.1A). In this scenario, it is worthy of note the emerging role of PROTACs,[530–532] which are molecules composed of two portions connected with a linker that combine an E3 ligase recognition sequence with a moiety that targets a (e-)POI. The key aspect of PROTACs mechanism of action provides the selective induction of the degradation of its target protein at sub-stoichiometric concentrations through the recruitment of the ubiquitin-proteasome system (UPS),[533] thus modulating the targeted protein levels instead of its function (Figure 2.1B).
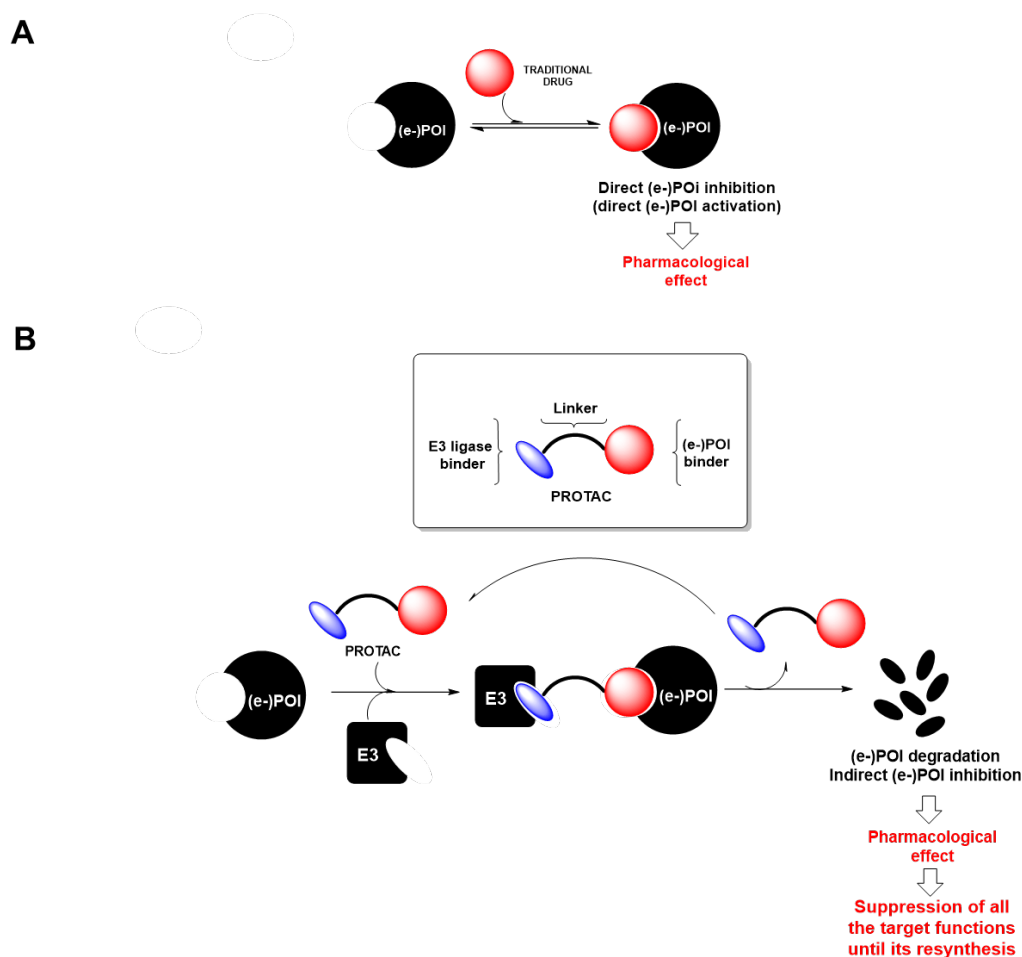
Figure 2.1. (**A**) (e-)POI functions modulation by traditional drugs. (**B**) Schematic representation of PROTAC structure and its pharmacological effects ((e-)POI degradation). Adapted from Itoh *et al. Chem Rec.* 2018, 18(12):1681-1700.[534]

Recent studies have also highlighted that this approach showed encouraging data not only *in vitro* but also *in vivo*, resulting promising for the treatment of several human illness.[535–537] Protein knockdown by PROTACs could be applied also in epigenetic area given the

recent proofs which support that mutation and/or OE of specific e-POI, as well as related non-enzymatic activities of the latter, are responsible for the onset of numerous human diseases, including cancer. On these bases, a full-blockade of the functions of a selected e-POI rather than just inhibit its catalytic activity, is a rational strategy and a new weapon to fight numerous disorders. Compared to classical epi-small molecules, this approach could evolve in the possibility to reach an increased potency and prolonged action which may be enhanced by achieving a potential higher selectivity towards the different isoforms that belong to every single class of epigenetic proteins, for which specific modulators are not yet available.[534]

As the role of the PROTAC is merely to facilitate the interaction between the E3 ligase complex and target protein, upon the conclusion of the substrate ubiquitination, PROTAC is released and is ready to induce the degradation of a new molecule (protein), acting as a true catalyst (Figure 2.1A). A fundamental characteristic of PROTACs, concerns the possibility of being effective also against proteins that are not involved in receptor or enzymatic functions, such as, for example, proteins anchoring protein complexes as well as unfolded proteins. In fact, PROTACs approach open up the potential possibility to induce knockdown of previously thought "undruggable" targets (including factors as *c*-Myc, β-catenin, Gli, as well as scaffolding proteins such as Gab family, KSR, BCL10, AKAPs, β-arrestin),[538] because PROTACs only need to bind the (e-)POI rather than inhibit a specific function, since any affinity probe able to bind any orthostatic or other site with sufficient affinity could result as a starting point for PROTACs design. Considering these findings, PROTACs could allow, in principle, to hit proteins which do not have any functional binding site. Another important goal achieved by this approach include the possibility to target mutated and overexpressed (e-)POIs, inducing a prolonged pharmacodynamic effect beyond drug exposure.[539] The system of degradation induced by PROTACs mimics, as mentioned before, the physiological mechanism of proteins degradation, which consists of three main steps: the first is the ATP-dependent activation of ubiquitin by the ubiquitin-activating enzyme 1 (E1), which leads to the formation of a conjugate with E1 through the reaction between the carboxylic group of ubiquitin and the thiol group of cysteine of E1; followed by the transfer of ubiquitin to conjugating enzyme (E2) and finally the recognition by the ligase (E3) of the substrate protein, which is thus ubiquitinate, leads to its proteasomal degradation. (Figure 2.2A). As mentioned above, a PROTAC molecule bring the E3 ligase and the targeted (e-)POI in close proximity, triggering the multiple transfer of ubiquitin units to the (e-)protein thus mediating its protosomal degradation (Figure 2.2B).
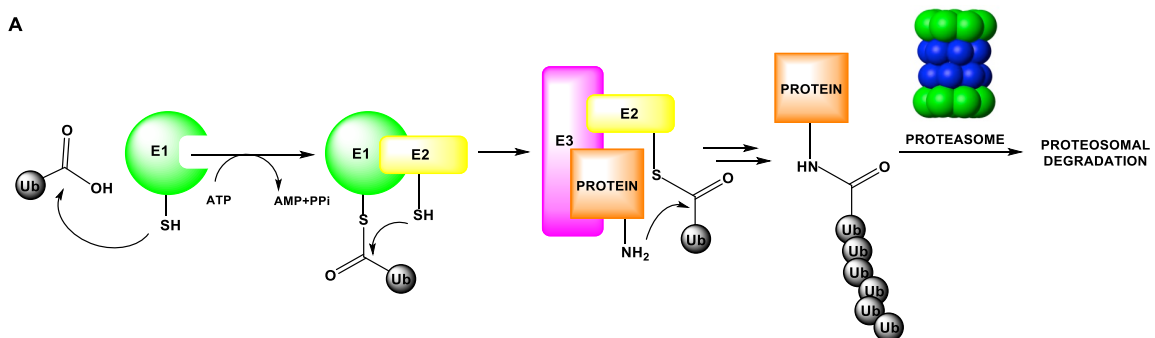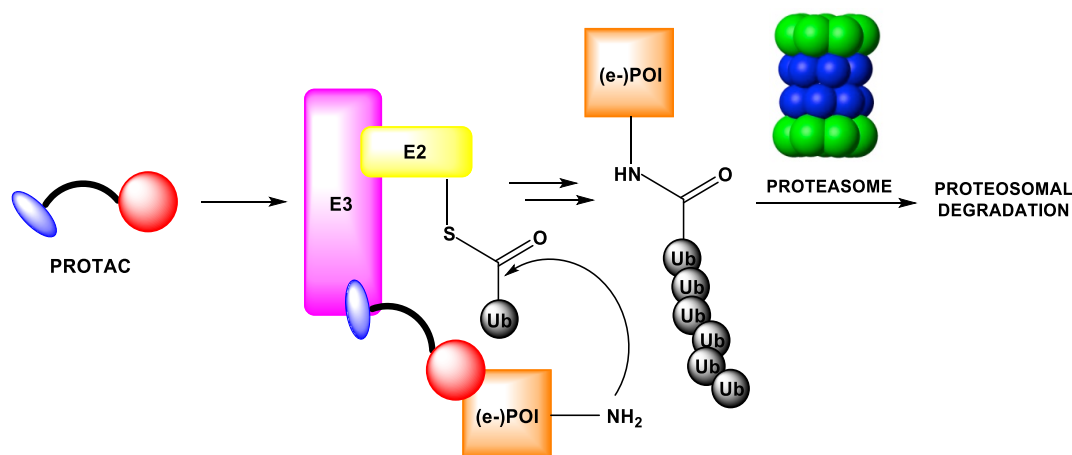
B

Figure 2.2. A) Overview of the ubiquitin system; B) PROTAC-mediated ubiquitination and proteasomal degradation.

To date, about 600 different types of E3 ligases have been identified, which differ in terms of their characteristics and specificity. Particularly, most attempt has focused on the quartet of ligase binders comprising Cereblon (CRBN), Von Hippel-Lindau (VHL), mouse double minute 2 homolog (MDM2) and Inhibitor of Apoptosis (IAP) (Figure 2.3). Especially, CRBN is the substrate adapter for the Cullin 4a E3 ligase complex and lots of immunomodulatory imide drug, including thalidomide (**36a**, Figure 2.3) and its analogs pomalidomide (**36b**, Figure 2.3) and lenalidomide (**36c**, Figure 2.3), as well as the thalidomide chemically and biologically most manageable derivatives (**36d,e** Figure 2.3) and its hydroxy-derivatives (**36f,g** Figure 2.3), have been reported to bind CRBN inducing the degradation of different types of proteins including Ikaros (IKZF1) and Aiolos (IKZF3).[540–542] VHL is instead the substrate adapter for the Cullin 2 E3 ligase complex and induces the complete degradation of its substrate HIF-α. Hydroxyproline moiety is the key recognition sequence of small molecule targeting the VHL E3 ligase. Post-translational hydroxylation of HIF-1α proline residues by prolyl hydroxylase domain (PHD) oxygen-dependent enzymes result at the base of the specific recognition of HIF-α by VHL.[543–545] Under low oxygen condition, HIF-α remain un-hydroxylated, avoiding in this way the VHL recognition and consequent mediated degradation, forming heterodimer complexes with HIF-β that bind to DNA hypoxia response elements (HREs).[546] When HIFs are transcriptionally active, the expression of a wide range of genes taking part in cell proliferation, angiogenesis, glucose uptake, anaerobic and anaerobic metabolism occur, promoting a hypoxic response.[539,547–551] Recently, Soares *et al.*,[550] reported VH298 (**37b**, Figure 2.3) as the first ligand able to achieve double-digit nanomolar affinity for VHL acting as a potent inhibitor of the VHL:HIF-α PPI inside cells thus improving the conventional chemical tools (PHD inhibitors or iron chelators) that are characterized by broad spectrum activities. VH298 **37b** strongly and selectively engages with VHL inducing an on-target accumulation of hydroxylated HIF-α in a time- and concentration-dependent manner leading to an upregulation of HIF-target genes in different cell lines. VH298 **37b** was designed starting from the X-ray crystal structure of the complex composed of VHL, elongin B, and elongin C with the already known VHL ligand VH032 (**37a**, Figure 2.3)[552] in order to improve the cell membrane passive permeability, cellular activity as well as binding affinity. VH298 **37b** was obtained *via* the replacement of the terminally methyl group typical of VH032 **37a** with a cyano-cyclopropyl fragment, keeping the carbonyl group in order to maintain the hydrogen bond between such residue and a structural water in the VHL pocket. The design strategy was focused on the subsequent replacement of the

three hydrogen atoms of the acetamide residue, one a time, with different alkyl group to better occupy the binding pocket and on the introduction of electron withdrawing groups at the amide α position, in order to lock the conformation.[553,554] However, substitution of two hydrogens with a restrained cyclopropyl group resulted in an improvement in both aspects as well as the introduction of the cyano electron-withdrawing which forms a hydrogen bond with a water molecule that allows the formation of an effective water network. Overall, the greater lipophilicity of VH298 **37b** in comparison to VH032 **37a**, contributed to its higher cellular permeability and intracellular free compound concentration leading to the registered higher cellular potency.[538] During the last years, in order to better explore the different orientations that a selected ternary complex could potentially assume, VHL ligase binders characterized by different derivatization point, in term of nature and position, have been developed.[539,552]

In fact, despite the amidation of a terminal *tert*-Leu (**37f**) of the VHL ligand VH032 **37a** is extensively exploited conjugation possibility for PROTACs,[555] recently even other strategies turned out to be promising including: i) the introduction of a phenolic attachment point followed by the replacing of the cyano-cyclopropyl group (typical of VH298 **37b**) with a fluorine-cyclopropyl group thus obtaining a more potent VHL ligand (as previously exposed by structural activity relationship (SAR) studies conducted by Soares *et. al*[550]), known as VH101 **37c**;[550,556] 2) the introduction of a thioether linkage out of the *tert*-butyl group of the VHL ligand, in which the *tert*-Leu group is replaced with a penicillamine moiety, also decorated with a terminal acetyl group **37d**[557] or with a terminal fluorine-cyclopropyl residue **37e**.[541]

Moreover, in addition to the choice of ligand and relative attachment point, also the selected linker play a main role in the PROTACs design and biological activity in fact, also small changes in both physico-chemical nature (polyethylene glycol (PEG) versus alkylic as well as mixtures thereof), and length can impact degradation activity as well selectivity in an unpredictable manner.[556,558,559]
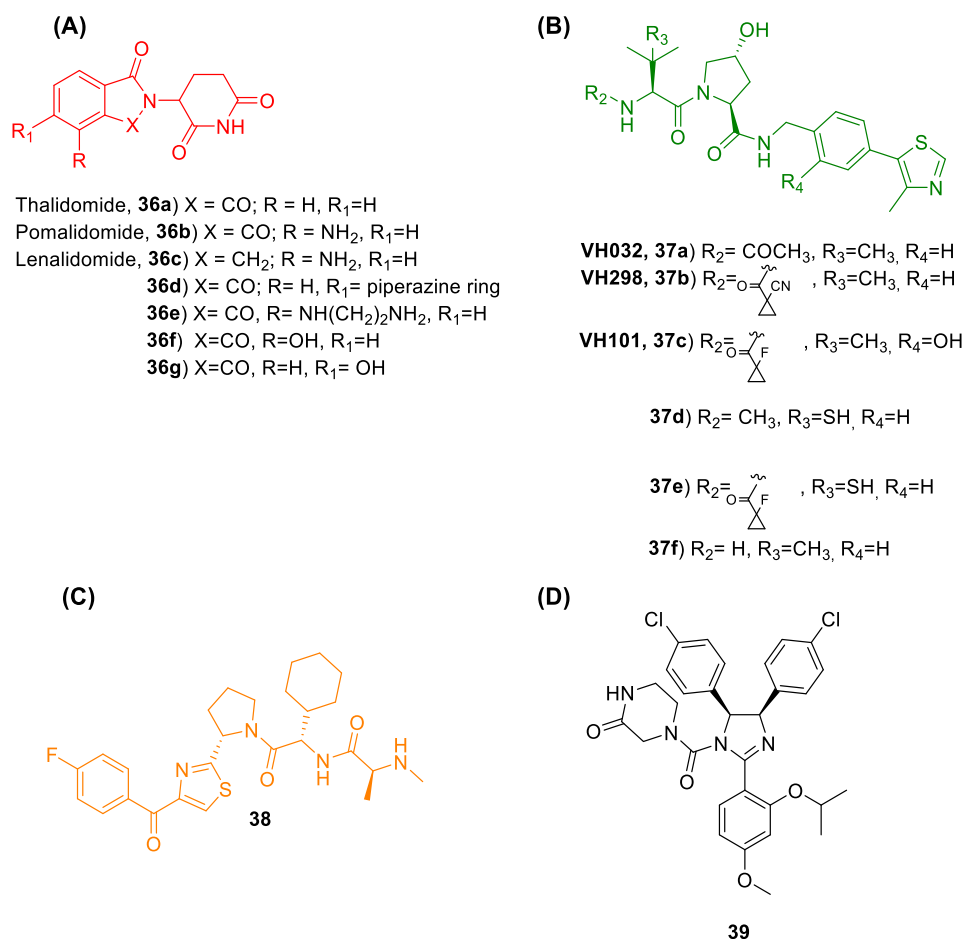
Figure 2.3. (A) Structure of the CRNB ligands thalidomide (**36a**), pomalidomide (**36b**), lenalidomide (**36c**) and thalidomide derivatives (**36d-g**); (B) Example of VHL ligands (**37a-f**); (C) IAP recognition moiety (LCL 161-based structure) **38;** (D) MDM2 recognition moiety (Nutlin-3 based structure) **39**.

As just mentioned, one of the main advantages of (epi-)PROTACs in comparison with classical small molecules, commonly selected as (epi-)warheads, consist in their catalytic nature which results in an increased potency as well as in the possibility to be administered in sub-stoichiometric amounts. This condition can always be performed, except in the case of the use of irreversible or very slow-on/off molecule as (epi-)POI ligands.[529] The prolonged pharmacodynamics effect beyond drug exposure resulting from the chemical knock-down induced by (epi-)PROTACs[539] could be compared with the durable mRNA knockdown proper of RNA interfering (RNAi) molecules, in respect of those (epi-)PROTACs show chemical and metabolic stability as well as better pharmacokinetic characteristics.[560] The potential increased selectivity of action of (epi-)PROTACs can be explained by examining their mechanism of action which is composed, as previously mentioned, by two main steps: 1) the formation of the bond between the (epi-)PROTAC and the (epi-)POI; 2) the activation of the UPS which transfers ubiquitin to the exposed lysine(s) residue(s) on the (epi-)POI. While the first step is limited by the capability to generate a selective ligand for the specific (epi-)POI, the second one, depends on the (epi-)POI lysine positioning, can be tuned even among closely related proteins.[529] In other terms, the selectivity is the result of different interactions complementarities of the (epi-)POI with the E3 ligase.[531,561] This feature is likely could be very promising in the epigenetic field, because of the several isoforms that belong to every single class of epigenetic proteins, for which no selective modulators are reported in literature yet. For example, studies by Ciulli

and co-workers have shown that the BET pan-selective inhibitor JQ1 **44b** can be converted into a VHL-based PROTAC (MZ1, **44a**)[561] that unexpectedly leads to a selective knock-down of BRD4, leaving the BRD2 and BRD3 homologous family members unmodified. While PROTACs resulting from the connection of the structure of JQ1 **44b** with those of thalidomide CRNB ligand with the appropriate linker, led to pan-selective degradation of all BET proteins.[562,563] In addition, (epi-)PROTACs offer the possibility to use them as pharmacological tools to study not only the functional but also the structural roles that the target proteins play within multiprotein complexes, that quite often are not fully clarified in epigenetics. In principle, the mechanism of action of (epi-)PROTACs opens up the possibility to induce the degradation not only of the targeted protein recognized by the selected warheads, but also of different proteins taking part in the same multiprotein complex. As potential drugs, (epi-)PROTAC, if compared to actual epigenetic small molecules, could show increased potency and prolonged action and higher target selectivity. On the other hand, potentially induced (epi-)POI degradation could be beneficial or detrimental by a therapeutic point of view depending on the specific structural roles of the targeted (epi-)POI within its multiprotein complexes. Since Crews, Deshaies and co-workers published the first report on protein degradation induced by PROTACs in 2001,[564] the design of new molecules has undergone to a strong acceleration, which has led to new molecules inducing the degradation of epi and non-epi targets.

2.2   PROTACs targeting major epigenetic players

2.2.1 Epi-PROTACs hitting "writers": the case of PRC2 complex

In 2019, Potjewyd *et al.*[565] reported a first-in-class chemical PRC2 degrader. UNC6852 **40a** (Figure 2.4) is composed by an EED ligand (EED226, **40b**, Figure 2.4)[566] connected through an alkyl linker of three methylene units to the VHL ligand binder **37f**. As previously mentioned, (epi-)PROTACs approach opens the possibility to induce the degradation not only of the targeted protein recognized by the selected warhead, but also of different proteins taking part in the same multiprotein complex. In fact, in this particular case, UNC6852 **40a**, in addition to induce the degradation of EED (D=80%) after 24h treatment at 5μM, also degrades the catalytic component of PRC2, EZH2 (D=76%), decreasing, in addition, the H3K27me3 levels (51%, 72h treatment at 5 μM) as well as proliferation in HeLa and DLBCL cells as a result of the lack of EZH2 activity.

40a
UNC6852
EED, D= 80%
EZH2, D= 76%
(HeLa cells, 24h @ 5μM)
EED, IC$_{50}$= 247 nM
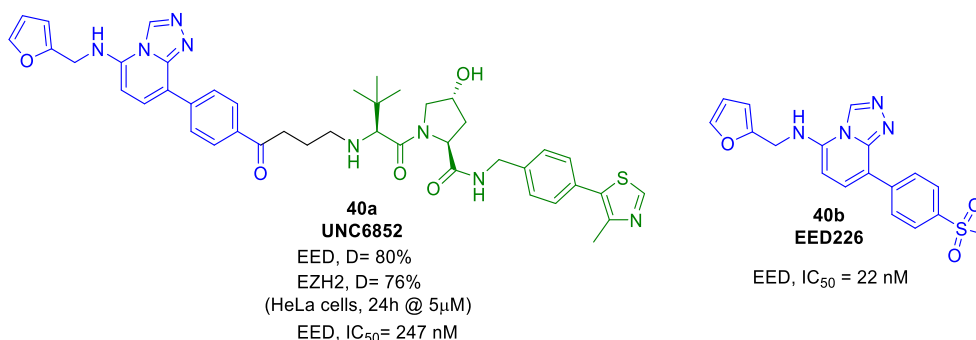
40b
EED226
EED, IC$_{50}$ = 22 nM

Figure 2.4. Structure of the PRC2 targeting PROTAC UNC6852 **40a** based on the scaffold of the selective EED inhibitor EED226 **40b** which is highlighted in blue, those of VHL ligand binder VH032 **37f** is depicted in green.

2.2.2 Epi-PROTACs hitting "erasers"
2.2.2.1 The case of HDAC6

As previously reported, HDAC6 in addition to play a main role in the deacetylation process, also takes part in HSP90 and α-tubulin modulation, protein trafficking and degradation, migration and cell shape.[567] Is not surprising, in fact, that the deregulation of HDAC6 correlates with different diseases such as pathological immune response, neurodegenerative disease, as well as, cancer. In this framework, the PROTACs technology could be very useful to reach the "knock-out" of this endogenous disease-causing protein. In 2018, Yang *et al*.[568] reported the first small molecule HDAC6 degrader (**41a**, Figure 2.5), which resulted the best compounds of a designed series obtained from the conjugation of the previously reported pan-HDACi **41b** (Figure 2.5)[569,570] with the scaffold of the CRBN binder pomalidomide **36b**,[571] connected with several different linkers. **41b** showed a high, dose-dependent degradation activity against HDAC6 [572,573] after MCF-7 breast cancer cell treatment with a DC_{50} of 34 nM and a maximum percentage of degradation collected of 70.5%. Increased levels of acetylated-tubulin were also registered after **41b**-based treatments as well as an enhanced acetylated levels of histone H3, that is likely due to nuclear class II HDAC inhibition, thus indicating that the bifunctional molecule **41b** showed the capability of inhibit HDACs in addition to induce the degradation of the cytoplasmatic target HDAC6. **41b** was also tested against MM.1S multiple myeloma cell lines and the maximal effect of degradation was observed after 6h of treatment at concentrations of 80 nM and above. Such pieces of evidence showed that MM.1S cell lines resulted more sensitive than the MCF-7 one to the **41b**-based treatment. In 2019, another pomalidomide **36b**-based HDAC6 targeting PROTAC was reported by An and Lv.[574] The introduction of the pomalidomide **36b** moiety onto the end of the aliphatic chain of the structure of the already known selective HDAC6i Nexturastat A (Nex A, Figure 2.5) **42a**, Figure 2.5)[575] through a particular pegylated linker leads to NP8 **42b**(Figure 2.5), which showed a significant degradation of HDAC6 after 24h of treatment in different cell lines (in particular in the MM.1S cell lines, DC_{50} (HDAC6) = 3.8 nmol/L). NP8 **42b** manteins the selectivity of action among the different HDACs isoforms inducing, in addition, an efficient inhibition of cell proliferation.

41a
IC_{50} (HDAC1) = 2.28 nmol/L
IC_{50} (HDAC2) = 3.12 nmol/L
IC_{50} (HDAC3) = 1.82 nmol/L
IC_{50} (HDAC6) = 35.80 nmol/L
IC_{50} (HDAC8) = 60.32 nmol/L
IC_{50} (HDAC10) = 11.05 nmol/L

41b
DC_{50} (HDAC6) = 34 nM
(MCF-7 cell lines)

42a
Nex A
IC_{50} (HDAC6) = 5 nM

42b
NP8
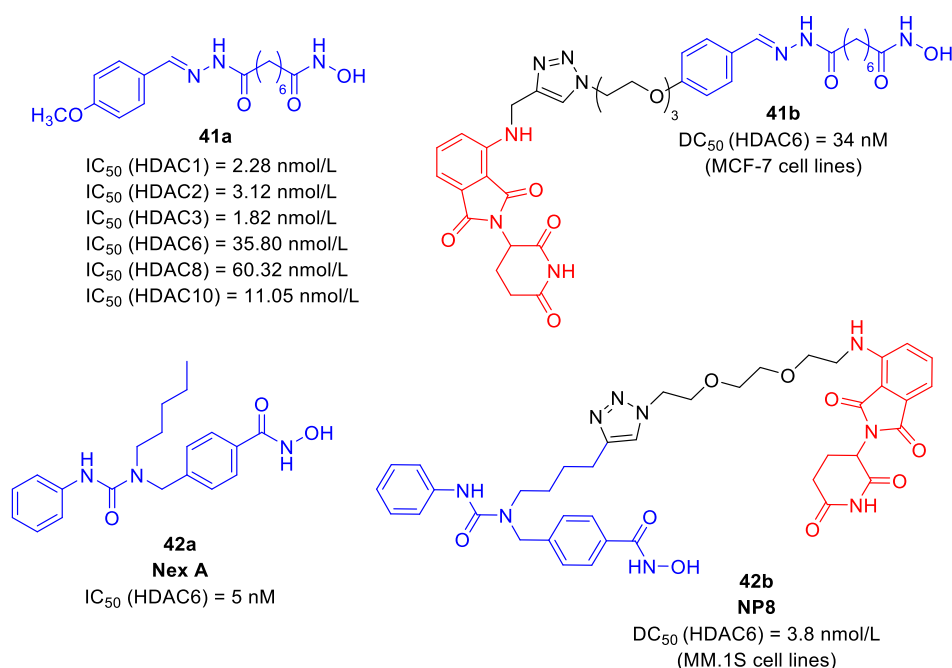DC_{50} (HDAC6) = 3.8 nmol/L
(MM.1S cell lines)

Figure 2.5 Structures of HDAC6 **41b** and **42b** targeting PROTACs based on the scaffold of the HDACis **41a**, NexA **42a** which are highlighted in blue, those of CRBN binder pomalidomide **36b** is depicted in red. IC_{50} and DC_{50} values are indicated where available.

2.2.2.2. The case of SIRT2

Sirt2 dysregulation has been registered in different pathological conditions including diabetes of type II, neurodegenerative diseases, bacterial infections and cancer, thus making this sirtuin a challenging target also for the PROTACs approach.[576–579] **43a** (Figure 2.6) is the first example reported to literature of PROTAC that acts by involving the degradation of sirtuins, in particular of SIRT2.[580] **43a**, resulted by the conjugation of the structure of the SIRT2i SirReal2 **43b** (Figure 2.6) with **36f** (Figure 2.6). When tested against HeLa cell lines, **43a** induced, in addition to an isotype selective SIRT2 degradation, a hyperacetylation of microtubules network associated with enhanced protein process elongation.

43a
IC_{50} (Sirt1): >100 μM
IC_{50} (Sirt2): 0.25 μM
IC_{50} (Sirt3): >100 μM

43b
IC_{50} (Sirt1): >100 μM
IC_{50} (Sirt2): 0.12 μM
IC_{50} (Sirt3): >100 μM
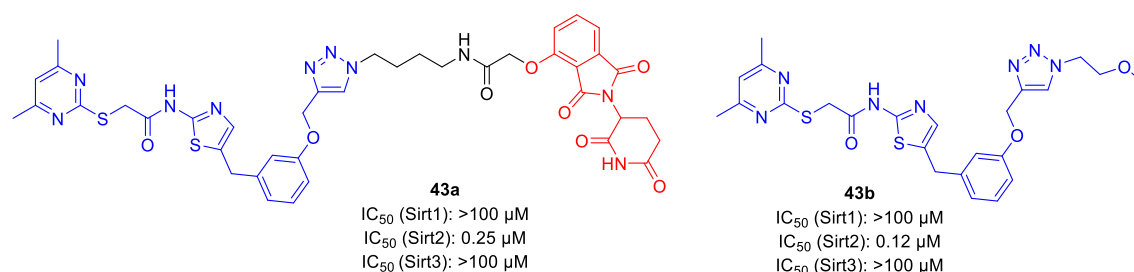
Figure 2.6. Structure the SIRT2 **43a** targeting PROTAC based on the scaffold of SIRTi SirREal2 **43b** which is highlighted in blue, those of CRBN binder **36f** is depicted in red. IC_{50} and DC_{50} values are indicated where available.

2.3 Epi-PROTACs hitting "readers"
2.3.1 The case of the bromodomains and extra-terminal domain (BET) family proteins

In addition to the classical small-molecule strategy, also PROTACs targeting bromodomain and BET proteins have been designed. Giving the main role covers by the deregulation of these epigenetic proteins in different pathologies, a consistent number of CRBN-, VHL- and IAP-based Bromodomain/BET degraders have been reported.[475,534] Among the BET family members, BRD4 has been strongly related to cancer and inflammatory diseases, thus motivating why the main effort in BET-targeting PROTACs design are focused on the latter.[581]

MZ1 **44a** (Figure 2.7) is one of the most interesting BRD4-targeting PROTACs reported so far. As previously mentioned, Zengerle et al.[561] designed this molecule in 2015 as result of the introduction of the scaffold of the VHL ligase binder **37f** onto the solvent exposed (not involved in key interactions) tert-butyl ester group of the well-known pan-BETi JQ1 **44b** (Figure 2.7) through a three units pegylated linker.

MZ1 **44a** results a rapid, effective, and prolonged intracellular degrader of BRD4, with no detectable protein observed after 24h of treatment in HeLa cell lines. MZ1 **44a** showed DC_{50} values for BRD4 degradation of 8 and 23 nM in H661 and H838 cells, respectively, as well as a potent antiproliferative and cytotoxic effects in AML cell lines (pEC_{50} = 7.6 in Mv4-11 cells). In addition, MZ1 **44a** well as JQ1 **44b** also induced the downregulation of

c-Myc and the upregulation of AREG and P21 expression after 12-24h of treatment. As previously discussed, MZ1 **44a** is an example of how the PROTACs approach could be promising in the epigenetic field: starting from a pan-BETi (JQ1 **44b**), a molecule able to lead a selective knockdown of BRD4, leaving the BRD2 and BRD3 homologous family members unmodified despite binding the different BET bromodomains with comparable affinities, has been obtained. The exact reason why this PROTAC shows a high selectivity against BRD4 is not yet clearly understood, but the most probable hypothesis concerns the role of the linker as well as the combination of the selected E3 ligase with the choosen ligand for the e-POI. A new PROTACs, AT1 **44c** (Figure 2.7), has been designed starting from the rational analysis of ternary complex crystal structure of MZ1 **44a** with human VHL and the Brd4 bromodomain (Brd4[BD2]).[557] From a chemical point of view, AT1**44c**, despite keeping the JQ1 **44b** structure as warhead, is characterized by an another VHL binders **37d** decorated with a different (in term of nature and position) attachment point as well as a different (alkyl) linker. AT1 **44c** showed an enhanced selectivity for BRD4 degradation (in cells at 1-3 μM) over BR2 and BRD3. Having shown that the aryl ring of thalidomide as well as the carboxyl group on JQ1 **44b** can bear chemical modification, the highly selective cereblon-based BRD4 degrader, dBET1 **44d** (Figure 2.7),[562] has been designed. *In vitro* and *in vivo* collected data highlighted its capability to strongly delayed leukemia progression also exhibiting modest effect on *c*-Myc and PIM1 expression. As a proof of this evidence, BRD4 resulted completely degraded after 100nM dBET1 **44d**-based 2h treatment. Moreover, dBET1 **44d** is also responsible for a greater and more potent apoptosis induction in AML cells than the warhead JQ1**44b** in both xenograft mouse models and cell-based assay. Since BETi have shown growth-inhibitory activity in preclinical models of castrate resistant prostate cancer (CRPC), Raina *et al*. hypothesized that a BET degrader would have a more effective activity in term of growth and/or survival suppression of CRPC cells in comparison to the already known BETi. ARV-771 **44e** (Figure 2.7) is the first PROTACs that shows efficacy in a solid-tumor malignancy thus potentially representing an important therapeutic advance in the treatment of CRPC. [582] ARV-771 **44e** potently degrades BET proteins (BRD2/3/4) in 22Rv1 prostate cancer cell lines, (with a DC_{50} less than 5 nM), showing strong antiproliferative effect on VCaP, 22Rv1, and LnCaP95 cell lines, resulting, in addition, in a strong depletion of *c*-Myc level.
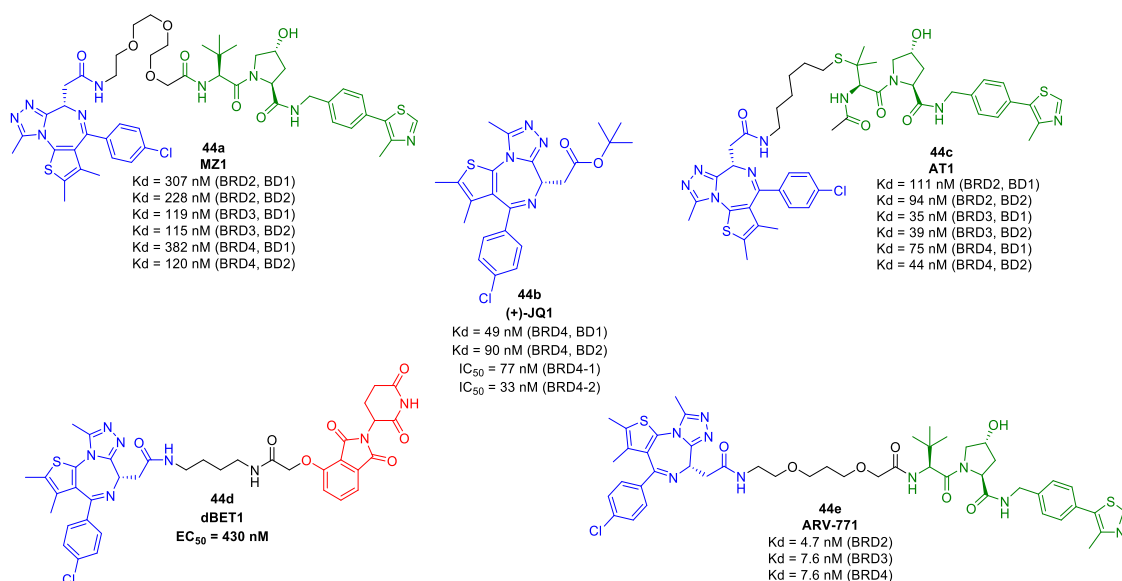

Figure 2.7. Structures of BET targeting PROTACs **44a, 44c-e** based on those of pan-BETi JQ1 **44b** which is highlighted in blue, VHL binders **37f** and **37e** are depicted in green and CRBN binder **36f** in red. IC_{50} and DC_{50} values are indicated where available.

Worthy of note are also other BET-targeting PROTACs based on BET binder moiety different from those of JQ1 **44b**.

Crews and co-workers, for example, designed the BET degrader ARV-825 **45a** (Figure 2.8) which results from the connection of the BETi OTX015 **30** (Figure 2.8), which shares the same triazolo-diazepine acetamide binding moiety seen for JQ1 **44b**, with the CRBN binder pomalidomide **35b** by a flexible polyethyleneglycol linker. ARV-825 **45a** induces an efficient, fast as well as prolonged degradation of BRD4 in Burkitt's lymphoma (BL) cell lines, suppressing, as already shown for others BETi or BET-targeting PROTACs, the *c*-Myc level which culminated in the inhibition of cell proliferation and apoptosis induction.[563]

Worthy of note is the case of the BET targeting PROTACs decorated by the structure of the potent tetrahydroquinoline-based BETi I-BET726[583] **46a** (Figure 2.8) as warheads, known as MZP-54 **46b** (Figure 2.8).[558] Crystal structure of I-BET726 **46a** bound to BET bromodomains highlighted that the carboxylic acid portion of I-BET726 **46a** is solvent exposed and does not take part in key interactions[583,584] allowing the conjugation of this portion, though an amide bond formation, to a pegylated linker of three units, thus chemically connected the structure of the selected BETi with those of **37f**.

In fact, despite tetrahydroquinoline based BETis result more effective in term of BET inhibition than the triazolodiazepine JQ1 **44b** (Kd for Brd4 tandem bromodomain is 4 nM for I-BET726 **46a** compared to Kd of 100 nM for JQ1 **44b**), the latter exhibits better capability in cooperative of ternary complex formation inducing a stronger target degradation. This particular evidence emphasizes that, the choice of a more potent inhibitor, does not always overlap with even more effective PROTAC. However, MZP-54 **46b** provides an interesting antiproliferative effects in the BET-sensitive cell lines HL60 and MV4;11. In 2018, Wang and co-workers,[573] reported ZBC260 **47a** (Figure 2.8) as a new BET-targeting PROTACs which induce the complete degradation of BRD2, BRD3 and BRD4 proteins in leukemia cancer cells at sub-nanomolar concentrations. ZBC260 **47a**, provides the degradation of the targets thanks to chemical manipulations on the 2-carboxamide group attached to the [6,5,6] tricyclic system of the azacarbazole-based BET inhibitor HJB97 **47b** (Figure 2.8), which resulting solvent exposed, represents a suitable site for tethering to lenalidomide **36b** moiety via an alkylic linker. ZBC260 **47a** strongly decrease BET proteins levels at concentrations as low as 30 pM in the RS4;11 leukemia cell line, reaching an IC_{50} value of 51 pM in inhibition of RS4;11 cell growth, exhibiting, in addition, rapid tumor regression *in vivo* of about 90% in RS4;11 xenograft tumors.

In the same year, Wang and co-workers,[585] also reported the discovery of the most potent [1,4]-oxazepines-based BET degrader QCA570 **48a** (Figure 2.8) reported to date, which acts in the lower picomolar range in leukemia cell lines (MV4;11, RS4;11 and MOLM-13 with IC_{50} values of 8.3, 62 and 32 pM, respectively) achieving a complete and durable tumor regression in leukemia xenograft mice models. QCA570 **48a**-based treatment reduced the levels of BRD2, BRD3, and BRD4 proteins at concentration of 30-100 pM, and, in addition, at concentrations as low as 10 pM in RS4;11 and 30 pM in MV4;11 cell lines resulted capable to reduce also *c*-Myc levels.

Their modeling of their previously synthetized BETi QCA-276 **48b** (Figure 2.8) complexed with BRD4 (BD1) highlighted that the 1-methyl-1*H*-pyrazole group is solvent exposed making it a promising point for the linker introduction, connecting, in this way, the selected CRBN binder moiety thus providing QCA570 **48a**.
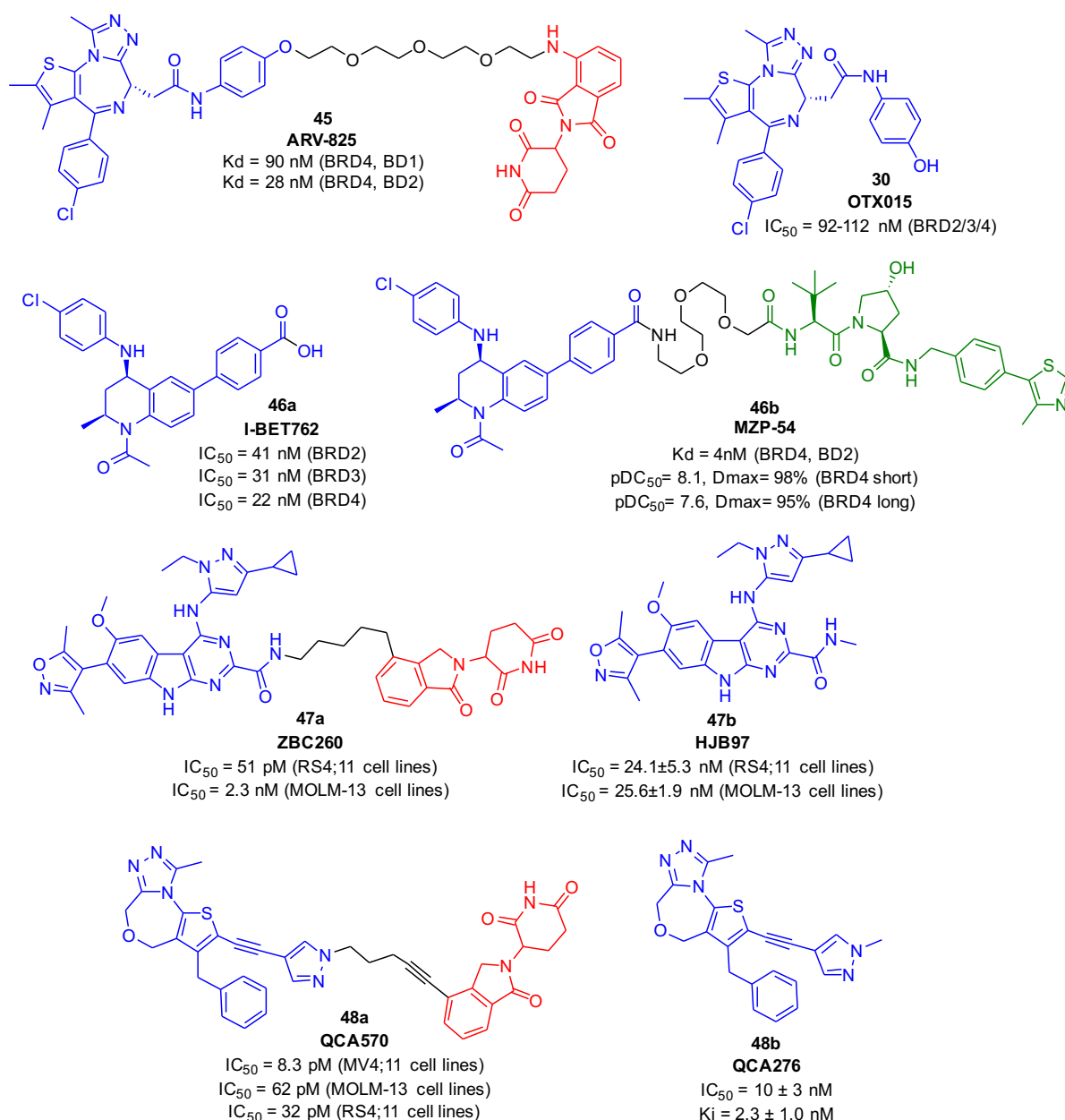
Figure 2.8. Structures of BET targeting PROTACs **45, 46b, 46a, 48a** based on those of other BETi such as OTX015 **30**, I-BET62 **46a**, HJB97 **47b** and QCA276 **48b** which are highlighted in blue, those of VHL binder **37f** is depicted in green and CRBN binders in red. IC_{50} and DC_{50} values are indicated where available.

Despite a conspicuous number of BET targeting PROTACs have been developed with the main aim to induce the degradation of BRD4, also BRD9, a subunit of the human BAF (SWI/SNF) nucleosome remodelling complex, has emerged as promising target, either for the role that it plays in cancer but also for better understand which are the roles of this protein beyond the acetylation recognition, that are not clearly described so far.

dBRD9 **49a** (Figure 2.9) is the first BRD9 degrader reported to literature and derives from the moiety of the BRD9i BI-7273 **49b** (Figure 2.8) connected with a pegylated bridge to those of the CRBN binder pomalidomide **36a**.[586] dBRD9 **49a** was found to induce strong degradation of BRD9 ($ > 90\%$ degradation after 4 h treatment at100 nM in MOLM-13 and EOL-1 cell lines) over a broad range of concentrations (from 50 nM to 5μM in MOLM-13 cell lines) with an increased selectivity against BRD9 over other BET family members (dBRD9 **49a** does not degrade BRD4 or BRD7 at concentrations down to 5 μM).

In 2019, Zoppi *et al.*[587] identified a novel BrdL1-based dual BRD7/BRD9 targeting PROTACs, called VZ185 **50a** (Figure 2.9) as a result of the stepwise design and optimization of a series of VHL-based degraders. VZ185 **50a** is characterized by a DC_{50} value in the single-digit nanomolar range (with a slight preference for BRD9 (DC_{50}= 1.8 nM) over its close homolog BRD7 (IC_{50}= 4.5 nM) and profound Dmax greater than 90%.

From a chemical point of view, VZ185 **50a** derived from the conjugation of the structure of the BRD7/9 ligand BrdL1 **50b** (Figure 2.9) in which the piperazine ring, resulting solvent exposed and not involved in key interaction, has been use as attachment point for the pegylated linker introduction, thus connecting the selected warhead with the structure of VHL ligand **37d.**

TRIM24 is a multidomain protein that belongs to the TRIM/RBCC protein family that has been reported as a co-regulator of transcription since the RING domain of TRIM24 seems to be involved in the ubiquitination and consequent degradation of p53.[588,589]

Recent pieces of evidence showed that chromatin localization of TRIM24 is mediated, at least in part, by a tandem PHD-bromodomains, able to recognize and bind the H3K23ac and H3K4me0 histone modification.[590]

The role that TRIM24 covers in tumors, has supported the developing of TRIM24 inhibitors (TRIM24i), such as the potent dimethylbenzimidazolone IACS-9571 **51a** (Figure 2.9). Despite its inhibitory potency, IACS-9571 **51a** do not exert effective anti-proliferative responses.[591]

The TRIM24 targeting PROTAC dTRIM24 **51b** (Figure 2.9) based on the scaffold of the TRIM24 binder IACS-7e **51c** (Figure 2.9), an analogue of IACS-9571 **51a**, has been designed to overcome this limit and to analyse the dynamic genome-wide consequent to TRIM24 loss on chromatin localization and gene control.[592]

TRIM24 PROTAC-induced degradation versus bromodomain inhibition showed a superior anti-proliferative activity due to an enhanced effect on genome wide transcription at TRIM24 targeted genes, uncovering TRIM24 as a novel dependency in leukemia. dTRIM24 **51b** was designed using the solvent exposed sulfonamide tail of IACS-7e **51c** as linker attachment point, thus connecting its moiety with those of the VHL binder **37f**. Both time- and dose-dependent degradation of TRIM24 have been observed, with maximum degradation apparent at 5 μM. Marked degradation is evident after 4 h of treatment, and TRIM24 depletion is maintained through 72h with continuous drug treatment.

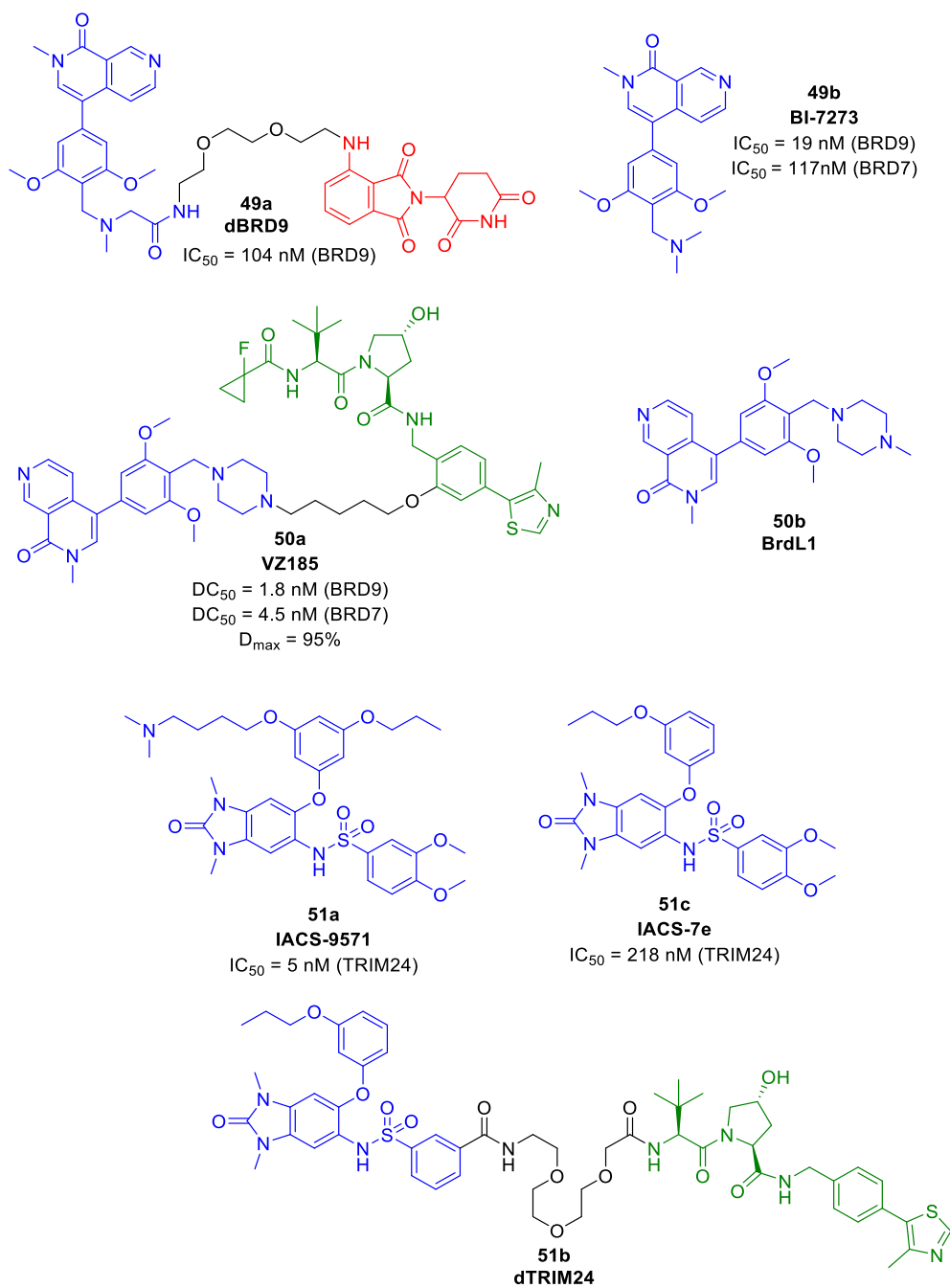**Figure 2.9**. Structures of BRD7/BRD9 and TRIM24 targeting PROTACs **49a, 50a, 51b** based on the structure of BRD7/BRD9 inhibitors BI-7273 **49b**, BrdL1 **50b** and TRIM24i IACS-9571 **51a** and IACS-7e **51c** which are highlighted in blue, those of VHL binders **37f** and **37d** are depicted in green and pomalidomide **36a** in red. IC_{50} and DC_{50} values are indicated where available.

2.2.3.2 *The case of PCAF/GCN5*

As previously mentioned, PCAF and GCN5[593] can be considered almost epigenetic proteins, as they both have an acetyltransferase and an "acetyl-reader" (bromodomain) activity. Because of these characteristics, their functions are related to the modulation of chromatin, thus playing a main role in several cellular processes, such as proliferation and differentiation as well as in the regulation of certain metabolic pathways and DNA damage repair mechanisms. PCAF/GCN5 are also involved, as far as the immune system is concerned, in several inflammatory processes.[245,594,595] In particular, PCAF has been implicated in the production of inflammatory cytokines, including TNF and IL-6. Such evidence supported that its inhibition could be useful for the treatment of different inflammatory diseases.[596,597] In 2018, starting from GSK4027 **52a** (Figure 2.10), a potent and selective inhibitor targeting the bromodomains of PCAF and GCN5[598] ($IC_{50\,=}$ 60 nM), Bassi *et al*.[599] designed GSK983 **52b** (Figure 2.10), a potent, cell penetrant anti-inflammatory thalidomide-based PCAF/GCN5 targeting PROTAC, which induced a concentration-dependent degradation of PCAF and GCN5 in the human monocytic cell line THP1 cells with DC_{50} value of 1.5 nM and 3 nM, respectively. PCAF/GCN5 degradation quickly occur after treatment with 30 nM of **52b**, in fact, levels of both proteins resulted reduced by 80% within 10 minutes of addition of GSK983 **52b** to human peripheral blood mononuclear cells. GSK983 **52b** was also able to modulate the expression of several cellular mediators (such as IL-6, IL-8 and TNF) involved in different inflammatory processes both in macrophages and dendritic cells stimulated by LPS.

52a
GSK4027
IC_{50} = 60 nM (BRD of PCAF and GCN5)
(HEK293 cell lines)

52b
GSK983
PCAF, DC_{50} = 1.5 nM
GCN5, DC_{50} = 3.0 nM
(THP1 cell lines)
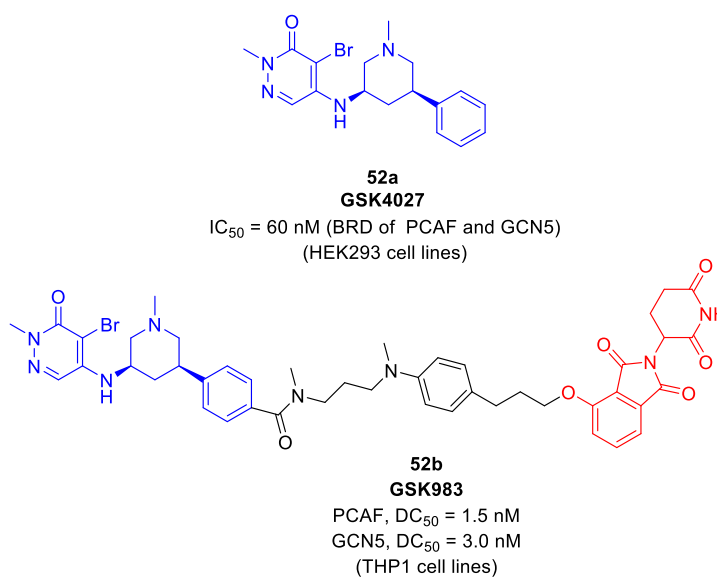
Figure 2.10. Structure of PCAF/GCN5 targeting PROTAC GSK983 **52b** based on the scaffold of the GSK4027 **52a** which is highlighted in blue, **36f** is depicted in red. IC_{50} and DC_{50} values are indicated.

2.3 Future challenges and applicability of PROTACs

The possibility of design a compound that can work in a catalytic manner, offering a long-lasting effect by suppressing the selected target until its re-synthesis, makes PROTACs a promising class of molecules.[600] Furthermore, if a "classical" inhibitor blocks only one function, the degradation of the target protein disturbs all functions including allosteric and structural ones. As mentioned above, this could be a "double-edged blade", particularly in epigenetics, considering the roles that epi-proteins could play within their multicomponent complexes. Moreover, as previously mentioned, protein knockdown approach can be extended to various proteins, including those targets previously considerate as "undruggable". Targeted degradation may also prove useful in drug-resistance mechanisms that involve a compensatory increase in the expression of inhibited proteins or mutations that result in the loss of inhibition despite maintained target engagement. In the epigenetics field, PROTACs result very promising thanks to their increased potency, prolonged action, and potential selectivity towards the different isoforms that characterize all the epi-targets. Despite of these advantages, considering their molecular weight crumbling into the 700-1000 Da range, their bioavailability, the delivery of PROTACs still remain one of the largest glitches on their way to clinic. However, notwithstanding at present no epi-PROTACs are in the clinical phase, this particular kind of small molecules could result very promising for the treatment of different human diseases, in the near future.

Chapter 3

3.1 Design, Synthesis and Biological Validation of novel SIRT4 Inhibitors Research project

As previously discussed, the emerging role of the human mitochondrial SIRT4 generated considerable interest, because could offer new therapeutic opportunities in various disorders such as obesity,[375] diabetes,[371] cardiac hypertrophy[398] and, although the role of SIRT4 is entirely in discussion in this disease, in cancer.[362,387,392,393,432,601]

In this framework, little is known about SIRT4 modulators. Like for all other isoforms, the physiological pan-sirtuin inhibitors NAM **19** (IC_{50} = 13 μM) and NADH (IC_{50} = 126 μM) provide the SIRT4 inhibition.[602] While NAM **19**-mediated SIRT4 inhibition is comparable to other sirtuins, NADH inhibits SIRT4 ten-fold stronger than any other isoform and renders SIRT4 a sensor for physiological NAD^+/NADH ratio.[603] In addition, the antiprotozoal drug suramin competitively inhibits SIRT4 by occupying the entire active-site, but other sirtuin family members are affected with comparable potency.[308] No specific and potent SIRT4 inhibitors (SIRT4i) have been reported so far. Starting from a docking screen focused on a library of 1.3 million compounds and a homology model of SIRT4 (based on SIRT5) (Figure 3.1), the research group of our collaborator prof. Sippl (Martin Luther Universitat of Halle Wittenberg, Germany), identified two inhibitor scaffolds and three hit candidates. The selected compounds were tested in orthogonal assay systems to exclude false positive results, which are well-known in sirtuin drug screening.
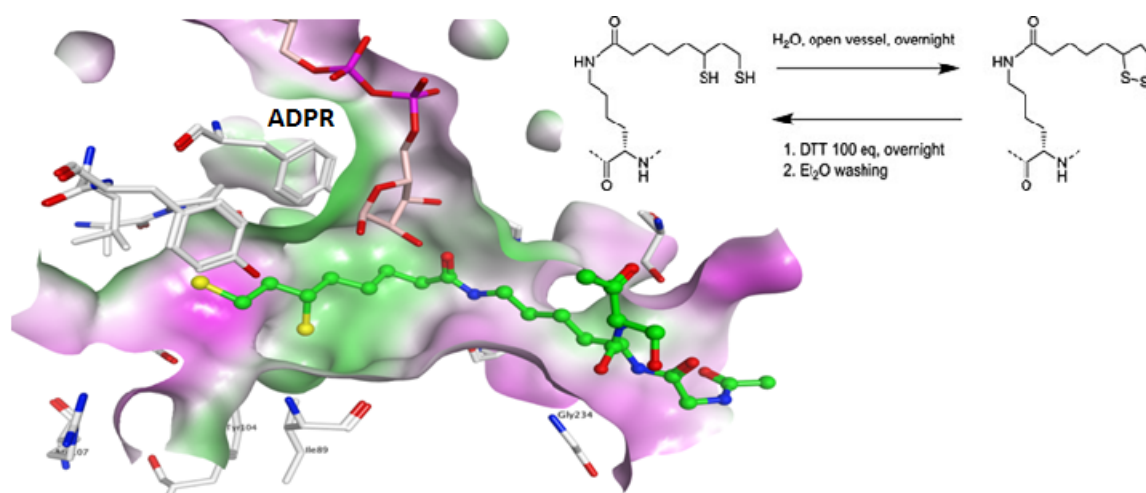
Figure 3.1. Sirt4 Homology model, substrate: lipoyl-Lys in ring-opened form.

As previously described in the section dedicated to SIRT4 (section 1.2.6.2.5), Prof. Steegborn and coworkers (University of Bayreuth, Germany), instead, highlighted the SIRT4 capability to recognize and remove the 3-hydroxy-3-methylglutaric residue if linked to the amino group of a lysine, in addition to the already accepted ADP-rybosyltransferase, delipoylase and weak deacetylase activity.[360] These two findings were the starting point of this project. In addition, the recently solved Sirt4 structure of the highly homologous X*enopus tropicalis* orthologue (hSIRT4 similarity 81%) reported by Pannek *et al*. (Figure 1.17) showed, as previously discussed (section 1.2.6.2.5) a potentially regulatory loop as well as an unusual acyl binding site with an additional acces channel which could explain its activities.[360] Since SIRT4 shows little to no detectable deacetylase activity against

acetylated histone *in vitro*, the synthesis of a substrate was needed in order to perform enzymatic assays to evaluate the potential inhibitory capability of the developed SIRT4i. Exploiting the new discovery, we designed an analog of the SIRT1-3 substrate Z-MAL (Z-Lys (Acetyl) AMC, **1**) which, instead of being characterized by an acetyl moiety linked to the ε-amino group of lysine, has the HMG residue (Z-Lys (HMG) AMC, **2**), toward which, indeed, the mitochondrial sirtuin SIRT4 shows a new deacylating activity (that is shared with SIRT5) (Figure 3.2).
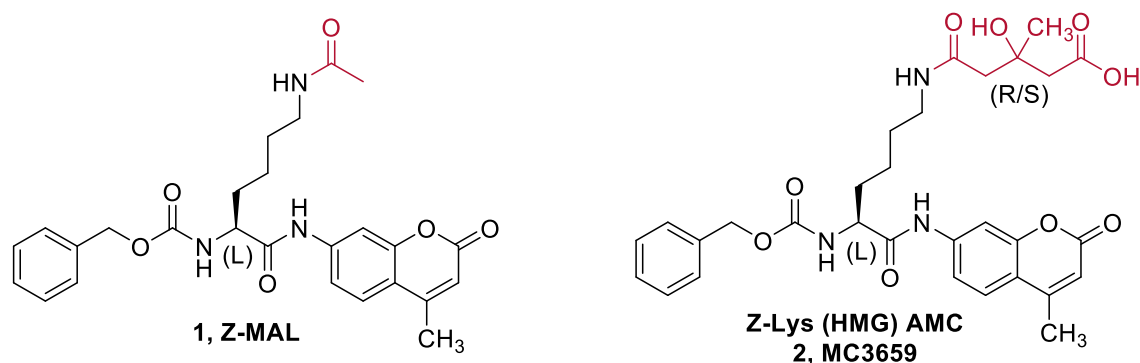
Figure 3.2. Structures of new pseudopeptidic SIRT4 substrate MC3659 **2** compared to the SIRT1-3 substrated ZMAL **1**.

The endogenous substrate characterized by the HMG portion is not yet been identified but it is known that this moiety is typical of the HMG-CoA, an important intermediate for the synthesis of cholesterol and ketone bodies (produced in a reaction catalyzed by the enzyme HMG-CoA synthase between acetoacetic acid, acetyl-CoA and water).

HMG-CoA lyase deficit model induced an increased level of HMG-CoA as well as increased protein HMG-ylation. Similar changes are predicted under ketogenic protein catabolism and fasting condition suggesting that de-HMG enzymes may modulate target functions during starvation.[378]

Further investigations are therefore necessary to determine whether SIRT4 actually has the ability to intervene in the regulation of this pathway, in fact, thioester bond is known to be characterize by a high-energy, therefore this aspect may favor the activity of SIRT4 even if a lysine residue is not present.[360]

Analyses of docking poses of the hit compounds indicated that they fill the substrate binding pocket of hSIRT4. Three compounds, characterized by two different chemical scaffolds were identified as particular promising starting points for chemical optimization (UBCS191 **53a**, UBCS178 **54a** and UBCS313 **54b**, Figure 3.3).

UBCS-0191
53a
IC$_{50}$= 66.7 µM

UBCS-0178
54a
IC$_{50}$= 45.6 µM

UBCS-0313
54b
IC$_{50}$= 54.7 µM
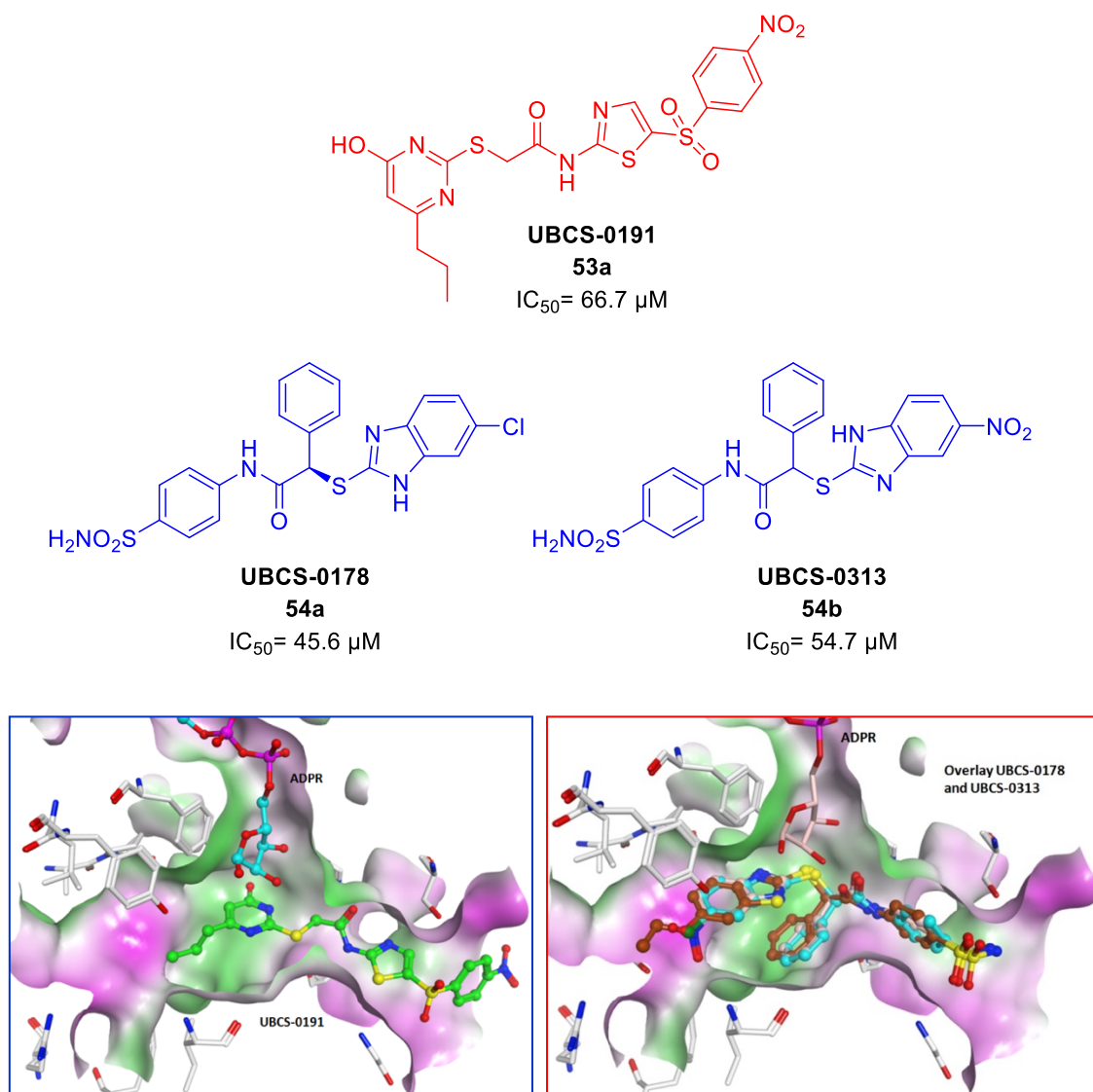
Figure 3.3. Structures of hit compounds (UBCS-0191 **53a**, UBCS-0178 **54a** and UBCS-0313 **54b)**, collected from Sippl's docking screen and their orientation (and overlay for **54a,54b**) inside the hydrophobic surface of SIRT4 active site.

UBCS-0191 **53a** (Figure 3.3, 3.4), shows an IC$_{50}$ of 66.7 μM towards SIRT4, and is characterized by a N-(5-((4-nitrophenyl)sulfonyl)thiazol-2-yl)amide portion, in which the amide group is donating a hydrogen bond to the Thr231 whereas the thiazole ring takes part to π-stacking interaction with Phe233. In addition, such hit compound contains a 2-mercapto-6-propyl-pyrimidin-4(*3H*)-one ring that establish hydrophobic interactions with Pro88 in the Sirt4-acyl pocket. Docking analysis seems to indicate that the replacement of the *n*-propyl chain at the level of the C6 of the 2-mercapto-6-propyl-pyrimidin-4(*3H*)-ones with bulkier substituent can be tolerate, potentially increasing the inhibitory activity towards SIRT4.
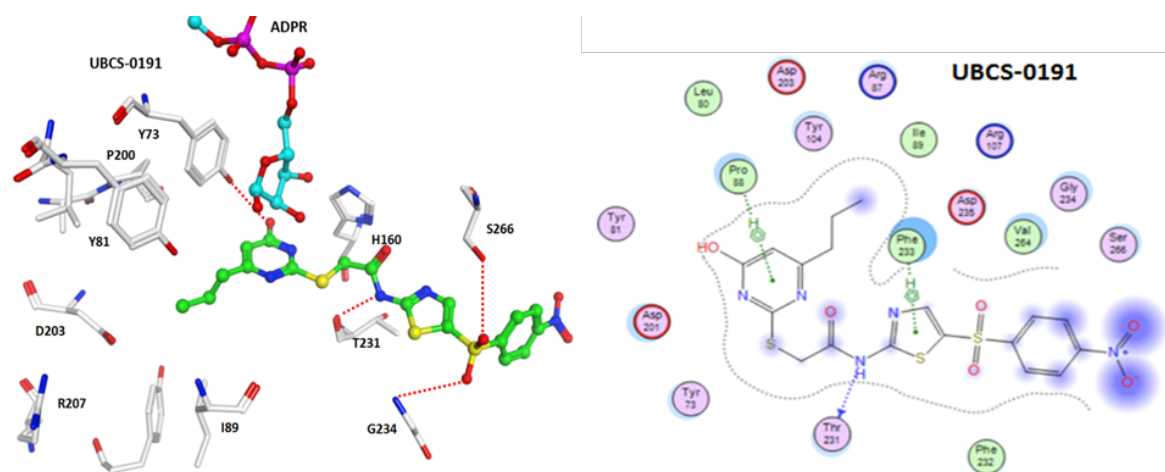
Figure 3.4 Interaction inside the SIRT4 active site of UBCS-0191 **53a**.

Analysis of UBCS-0313 **54b** (Figure 3.3, 3.5, IC_{50} (SIRT4)= 54.7 μM), the -NO$_2$ homologous of UBCS-0178 **54a** (Figure 3.3, 3.5, IC_{50} (SIRT4)= 45.6 μM), highlighted the establishment of different type of interactions at the level of the benzimidazole moiety: i) π-stacking interactions with Tyr81, Tyr73 and Tyr104 residues; ii) hydrophobic interactions with Ile89, Pro88 and Leu80 residues; iii) electrostatic interactions between oxygen atoms of the -NO$_2$ group (which present a delocalized negative charge) and Arg86/87 residues as well as between the nitrogen of such group (which presents, instead, a partial positive charge) and Asp203; iv) Pro88, Phe 233 and Ser 266 residues take part in hydrophobic interactions with the phenyl moiety in α to the amide carbonyl. Fundamental seems the hydrogen bond established between the -NH group of the amide bond and Thr231, as well as those between the free amino group of sulfonamide and Asp235. Worthy of note is, also, the hydrogen bonds interactions between a molecule of water which, at the same time, coordinates the residues of Arg269, Val237 as well as one of the oxygen atoms of the sulfonamide moiety.
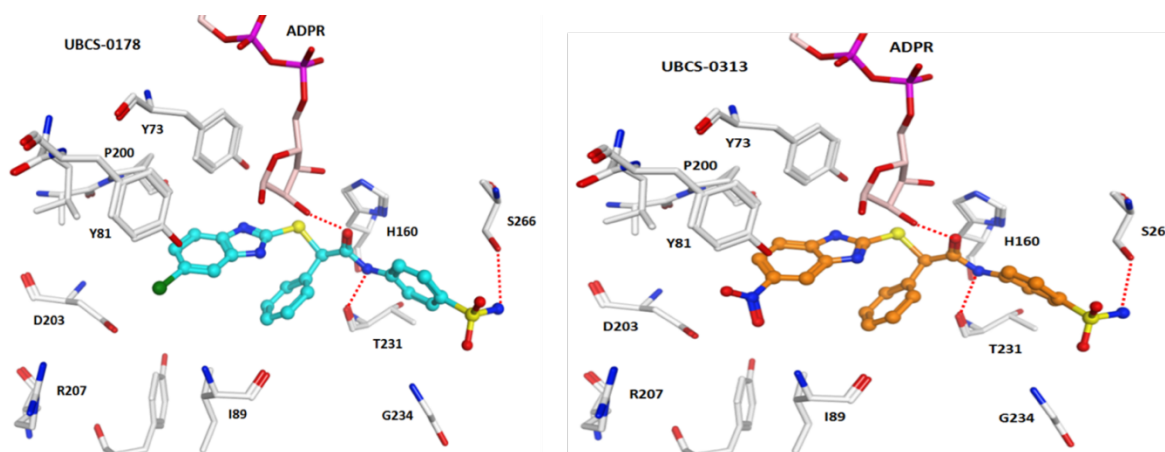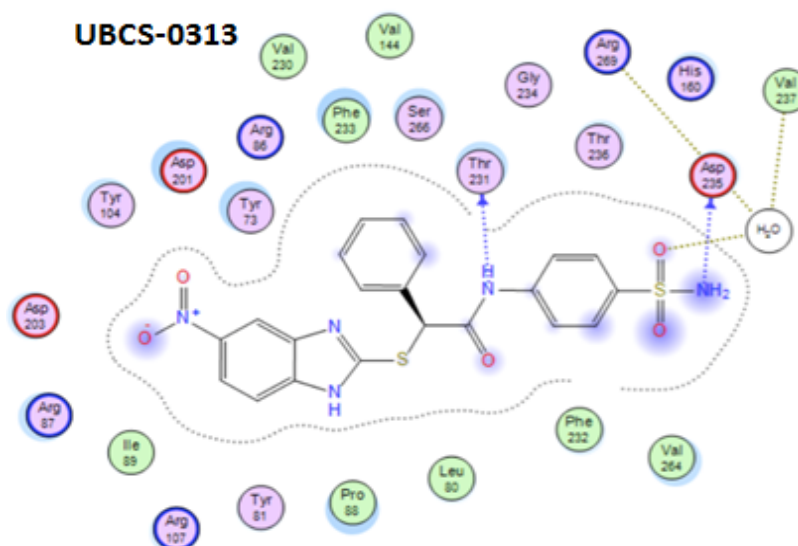
Figure 3.5. Interaction inside the SIRT4 active site of UBCS-0178 **54a** and UBCS-0313 **54b**.

Starting from all these findings, we were able to design and synthetized analogues of both the two main scaffolds as well as a series of hybrid compounds between them (Figure 3.6). Chemical modifications of UBCS-0191 **53a** involved: i) the propyl chain at the position -6 of the 2-mercapto-pyrimidin-4(*3H*)-one, which was replaced both with shorter chains, such as methyl, and longer and bulky substituents with the aim of better occupy the hydrophobic pocket of the active site (such as phenyl, benzyl and similar); ii) the α-position of the carbonyl amide, in which both a phenyl, typical of the UBCS-0178 **54a** scaffold, or methyl unit have been introduced; iii) the 2-mercapto-6-propyl-pyrimidin-4(*3H*)-one was replaced with a phenyl, *p*-NH$_2$-phenyl or a quinazolin-4-one ring in order to induce a molecular simplification and, following the same idea of structural simplification, also the central thiazole ring has been replaced with a simple phenyl ring.

Structural changes in UBCS-0178 **54a** were focused on: i) the -C5 position of the benzimidazole portion, in which -Cl was replaced with an -NH$_2$ group, with the aim to verify if, in that position, the achievement of a potential additional hydrogen bonds instead of an electrostatic interaction could improve the activity, modulating, consequently, the overall lipophilicity of the molecule; ii) as a result of a molecular simplification attempt, the benzimidazole moiety was replaced with a *p*-NH$_2$-phenyl in order to try to keep π-stacking interactions, establishing a new putative hydrogen bond. Another approach for designing potentially improved SIRT4i was focused on the merging of the features from both hit compounds thus obtaining a series of hybrids derivatives. The designed chimeric compounds are characterized by the typical 5-substituted benzimidazole portion present in the UBCS-0178 **54a** as well as by the 5-((4-nitrophenyl)sulfonyl)thiazol-2-amide fragment typical of UBCS-0191 **53a**. The -Cl atom in position -5 of the benzimidazole was also substituted with a -NO$_2$ (typical of UBCS-0313 **54b**) or -NH$_2$ group, to further investigate how such replacement could influence new putative interactions as well as the molecular polarity. Finally, the phenyl ring in α-position (typical of UBCS-0191 **53a**) of the carbonyl amide was introduced even in the hybrid series.

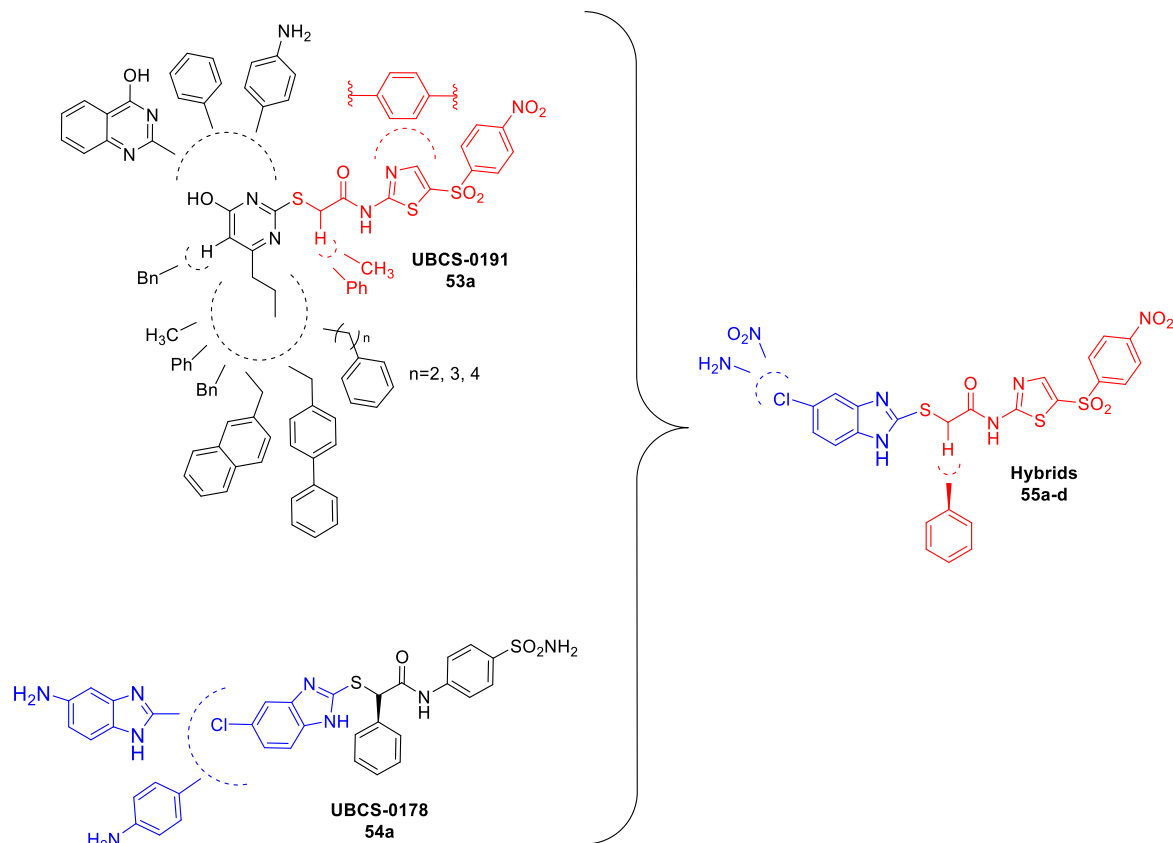**Figure 3.6.** Overview of the whole synthetic project. A series of a analogues has been synthetized for each identified hit compound (UBCS-0191 **53a** and UBCS-0178 **54a**) as well as hybrids compounds among them.

Daniela Tomaselli

3.2 Chemistry

Routes used for synthesis of substrate MC3659 Z-Lys(HMG)AMC **2**, proper alkyl halide **63a-e**, 2-mercapto-6-substituited-pyrimidin-4(*3H*)-ones **65a-c**, and compounds **53b-p**, **54c,d** and **55a-d** are depicted in Scheme 3.1-3.3. The pseudopeptidic substrate MC3659 **2** (Scheme 3.1) was synthesized starting from a coupling reaction between the commercial Z-Lys(BOC)COOH **56** and the AMC **57** in presence of POCl₃ in dry pyridine thus affording Z-Lys(BOC)AMC **58**, which was treated with HCl 4N in dioxane for the removal of the protecting BOC group. Hydrochloride derivative was first stirred in saturated solution of Na₂CO₃ to obtain the free base **59**, and then coupled with 4-hydroxy-4-methyldihydro-2H-pyran-2,6(*3H*)-dione **60** in dry THF, in presence of DIPEA, thus leading to compound Z-Lys(HMG)AMC **2** (Scheme 3.1).

Desired alkyl halide **63a-e** were obtained from the simultaneous and dropped addition of the requisite acetyl halide **61a-c** and DIPEA to the solution of the proper amine **62a-c** in dry THF (Scheme 3.2A). 2-mercapto-6-substituited-pyrimidin-4(*3H*)-ones **65a-c** were prepared starting from the cyclization of the correspondent β-ketoesters **64a-c** which were provided as reported to literature (Scheme 3.2B).[604–606] Suitable conditions of S-alkylation of the proper aryl-thiols **65a-k**, **67** and **68a-c** with the required alkyl halide **63a-e** led to desired final compounds **53b-n,p**, **54c,d** and **55a-d** (Scheme 3.3A-C). Coupling reaction between both commercially available 2-(phenylthio)acetic acid **66** and 5-((4-nitrophenyl)sulfonyl)thiazol-2-amine **62c**, in presence of POCl₃ in dry pyridine, provided the compound N-(5-((4-nitrophenyl)sulfonyl)thiazol-2-yl)-2-(phenylthio)acetamide **53o** (Scheme 3.2B). 2-mercapto-5,6-substituited-pyrimidin-4(*3H*)-ones **65d** and **65f-j** were synthetized according to the procedures reported to literature.[607–610] Z-Lys(BOC)COOH **56,** AMC **57,** 4-hydroxy-4-methyldihydro-2H-pyran-2,6(3H)-dione **60,** aryl-thiols 2-mercapto-6-propylpyrimidin-4(3H)-one **65e,** 2-mercaptoquinazolin-4(3H)-one **65k**, **67** and **68a-c**, amines **62a-c** and 2-(phenylthio)acetic acid **66** are commercially available. Chemical-physical data are reported in Tables 3.1

Scheme 3.1. Synthesis of the SIRT4 substrate (Z-Lys (HMG) AMC), MC3659, 2.[a]
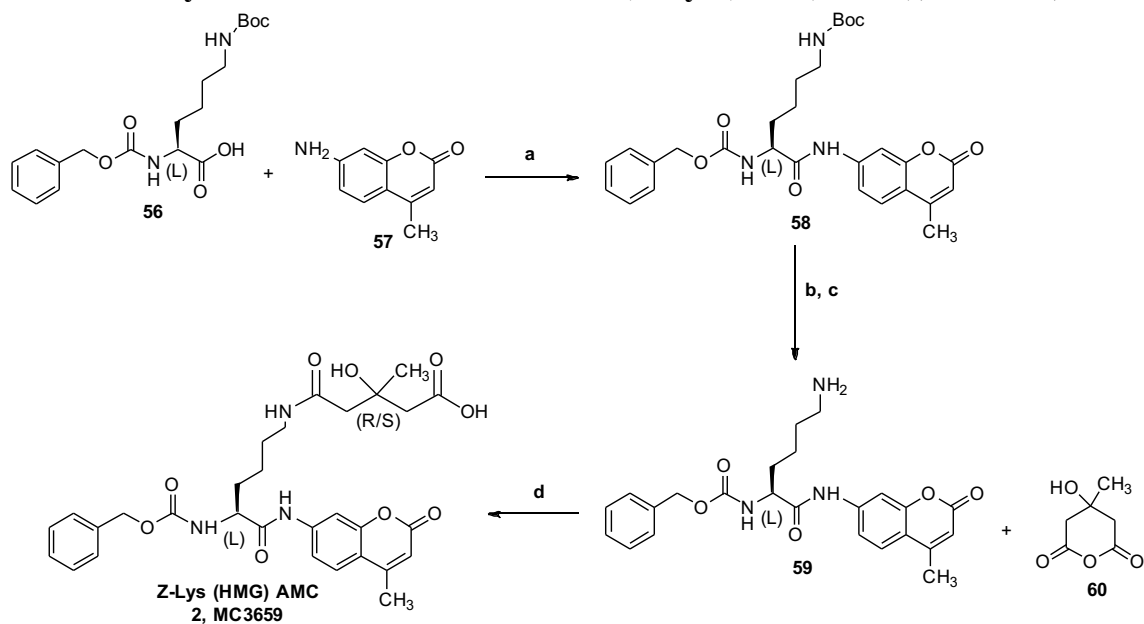
[a]Reagents and conditions: (a) POCl₃, dry pyridine, 4h, -15°C, N₂; (b) HCl 4N solution in dioxane, dry DCM, 24h, 0°C→ rt; (c) saturated solution of Na₂CO₃, 0°C→ rt; (d) DIPEA, N₂, dry THF, 19h, 0°C→ rt.

Scheme 3.2. Synthesis of intermediates 63a-e and 65a-c.[a]

A

R₁, R₃= Cl, Br
R₂= H, Me, Ph

$R_4 =$

B

n=1, 3, 4
R₅= H, Ph
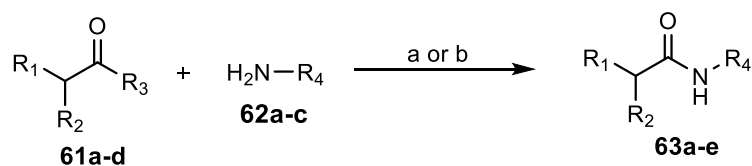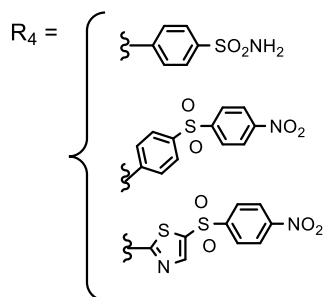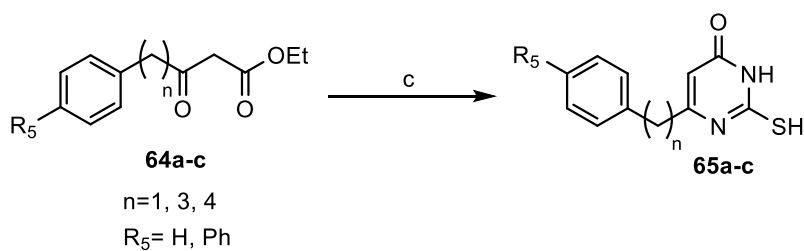
[a]Reagents and conditions: (a) if $R_1=R_3=$ Cl, R_2 = H, or CH_3 or Ph: DIPEA, dry THF, 4h 30 min, 0°C→ rt; (b) 2-bromoacetyl bromide, DIPEA, dry THF, 4h 30 min -20°C; (c) thiourea, sodium metal, dry EtOH, reflux, 16-18 h.

Scheme 3.3. Synthesis of Compounds 53b-p, 54c-d and 55a-d.[a]

[a]Reagents and conditions: (a) **63e**, K_2CO_3, dry DMF, 6h 30 min, rt; (b) required alkyl halide (**63a, c, d**), K_2CO_3, NaI, dry DMF, 6-31h, rt; (c) **63b**, K_2CO_3, dry DMF, 3h, 90°C; (d) **62c**, $POCl_3$, dry pyridine, 3h 30min, -15°C, N_2.
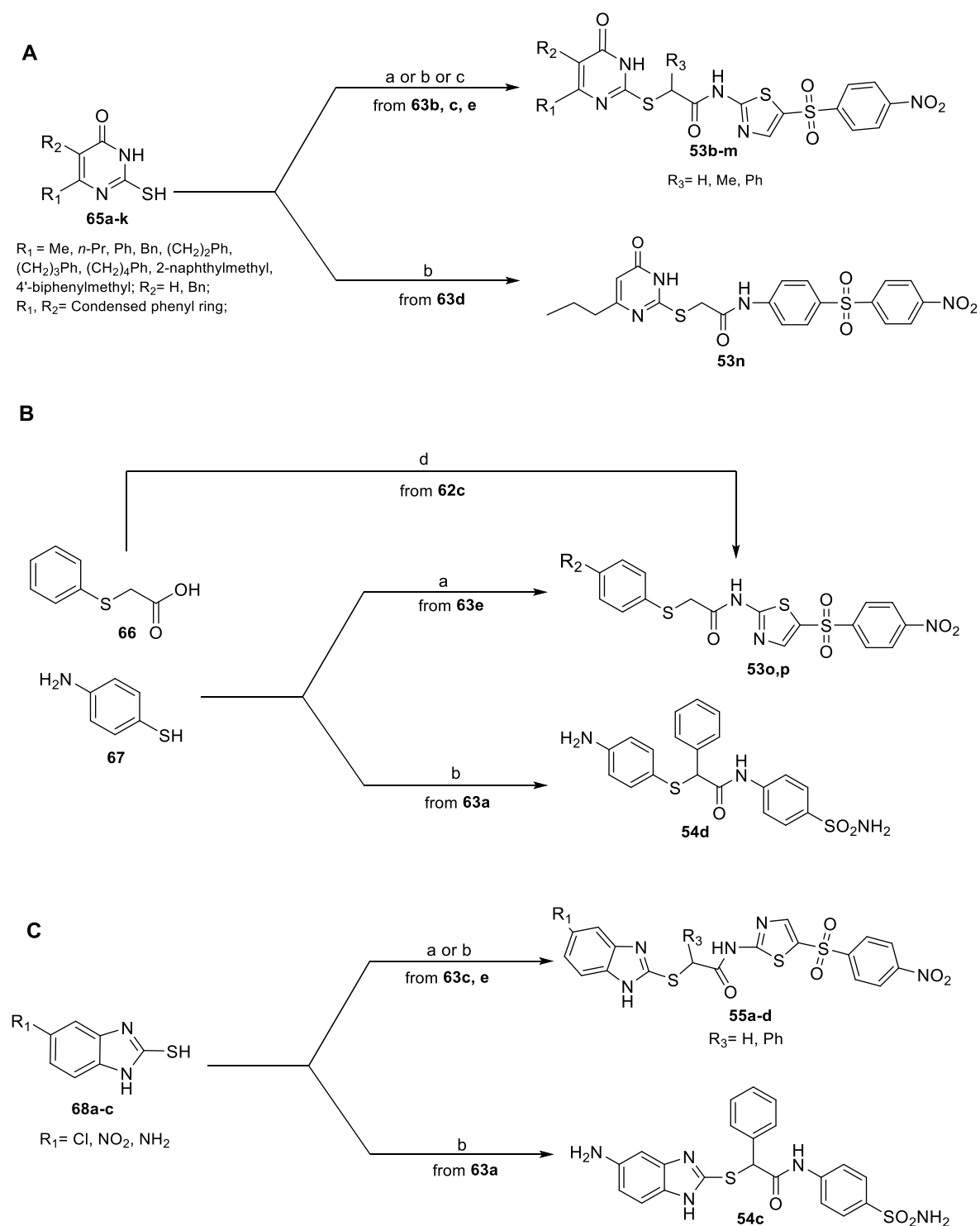
3.2.1 Experimental section

Melting points were determined using a Buchi 530 melting point apparatus. ^{1}H-NMR spectra were recorded at 400 with a Bruker AC 400 spectrometer, by reporting chemical shifts in δ (ppm) units relative to the internal reference tetramethylsilane. All compounds were routinely checked by TLC, ^{1}H-NMR. TLC was performed on aluminum-backed silica gel plates (Merck DC, Alufolien Kieselgel 60 F_{254}) with spots visualized by UV light. Yields of all reactions refer to the purified products. All chemicals were from Sigma-Aldrich srl, Milan (Italy), and were of the highest available purity. Mass spectra were recorded with an API-TOF Mariner by Perspective Biosystem (Stratford, TX, USA); samples were injected by a Harvard pump using a flow rate of 5-10 μL/min with electrospray ionization. Elemental analysis was used to determine the purity of compounds which in all cases was >95%; all analytical results were within ±0.40% of the theoretical values.

Synthesis of Z-Lys(HMG)AMC, MC3659, 2.

To a stirring mixture of the commercial Z-Lys(BOC)COOH **56** (1.31mmol, 1.05eq) and AMC **57** (1.25 mmol, 1eq) in dry pyridine (9 mL), $POCl_3$ (3.38 mmol, 2.7eq) was added dropwise at -15°C and the resulting mixture was stirred for 4h. After the disappearance of starting materials (checked by TLC), the reaction was poured in ice/water, stirred for 15 min and the obtained aqueous phase was extracted with AcOEt (80 mL x 4). The organic phases were combined and washed in order with 5% p/p solution of $NaHCO_3$ (30 mL x 3), $NaHSO_4$ 1N solution (30 mL x 5) and brine (20 mL x 2), dried over anhydrous Na_2SO_4, filtered and evaporated under vacuum, affording pure Z-Lys(BOC)AMC **58** as a yellow spongy solid.

To a cooled solution (0°C) of Z-Lys(BOC)AMC **58** (0.558 mmol, 1eq) in dry DCM, HCl 4N solution in dioxane (5.58 mmol, 10eq) was added and the resulting solution was stirred for 24h at rt, allowing the precipitation of the hydrochloride salt as a white solid. At completion, the suspension was filtered under vacuum, giving the hydrochloride derivative which was first stirred, after cooling at 0°C, in saturated solution of Na_2CO_3 at rt and then extracted with DCM (30 mL x 10). Combined organic phases were dried over anhydrous Na_2SO_4, filtered and evaporated under reduced pressure thus obtaining the pure free amine **59**. **59** (0.388 mmol, 1eq) was dissolved in dry THF, cooled at 0°C, and, 4-hydroxy-4-methyldihydro-2H-pyran-2,6(3H)-dione **60** (0.47 mmol, 1.2eq), followed by DIPEA (0.78 mmol, 2eq) were added under nitrogen atmosphere. The resulting mixture was stirred at rt for 19h, then quenched with water, acidified with $KHSO_4$ 1M solution and extracted with AcOEt (10 mL x 7). The combined organic phases were washed with brine (3 mL), dried over anhydrous Na_2SO_4, filtered and the solvent removed under reduced pressure, thus leading to the desired Z-Lys(HMG)AMC **2** as a crude purified through silica flash chromathografy (Biotage Isolera SNAP 25) eluted with a gradient of methanol MeOH in $CHCl_3$. Evaporation of the fractions containing the target compounds gave the analytically pure Z-Lys(HMG)AMC, MC3659, **2**.

Z-Lys(BOC)AMC, 58. Yield, 95%. **^{1}H-NMR** (400MHz; CDCl₃) δ 1.44 (s, 9H, -C(C*H₃*)₃), 1.46-1.56 (m, 4H, -CH₂-C*H₂*-C*H₂*-CH₂-NHCO-), 1.71-1.75, 1.98-2.00 (m, 2H, -C*H₂*-CH₂-CH₂-CH₂-NHCO-), 3.09-3.20 (m, 2H, -CH₂-CH₂-CH₂-C*H₂*-NHCO-), 4.25-4.33 (m, 1H, -NH-C*H*-CONH-), 4.62-4.66 (m, 1H, -CH₂-N*H*-CO-), 5.14 (s, 2H, Ph-C*H₂*-), 5.55-5.60 (m, 1H, -CH-N*H*-CO), 6.23 (s, 1H, -C-*H* coumarin ring), 6.36 (s, 1H, -C*H₃*), 7.38-7.55 (m, 5H, C-*H* phenyl ring), 7.65 (m, 3H, C-*H* coumarin ring), 10.49 (s, 1H, -CON*H*-coumarin ring).

Z-Lys(NH₂)AMC, 59. Yield, 93%. **¹H-NMR** (400MHz; DMSO-d_6) δ 1.22-1.27, 1.49-1.54 (m, 4H, -CH₂-C*H₂*-C*H₂*-CH₂-NH₂), 1.82-1.87 (m, 2H, -C*H₂*-CH₂-CH₂-CH₂-NH₂), 3.36-3.38 (m, 2H, -CH₂-CH₂-CH₂-C*H₂*-NH₂), 4.17 (s, 1H, -NH-C*H*-CONH-), 5.05 (s, 2H, Ph-C*H₂*-), 6.23 (s, 1H, -C-*H* coumarin ring), 6.34 (s, 1H, -C*H₃*), 7.37 (m, 5H, C-*H* phenyl ring), 7.42 (s, 1H, -CH-N*H*-CO), 7.62-7.67 (m, 3H, C-*H* coumarin ring), 7.86-7.95 (m, 3H, -N*H₂*·*H*Cl), 7.92 (s, 1H, -CH₂-N*H*-CO-), 10.49 (s, 1H, -CON*H*-coumarin ring).

Z-Lys(HMG)AMC, MC3659, 2. Yield, 32%. **¹H-NMR** (400MHz; DMSO-d_6) δ 1.20 (s, 3H, -C*H₃* HMG), 1.25-1.29, 1.50-1.56 (m, 4H, -CH₂-C*H₂*-C*H₂*-CH₂-NH₂), 1.83-1.89 (m, 2H, -C*H₂*-CH₂-CH₂-CH₂-NH₂), 2.36-2.38 (m, 2H, -CH₂-CH₂-CH₂-C*H₂*-NH₂), 2.42 (s, 2H, -C*H₂*-COOH), 3.34 (s, 2H, -C*H₂*-CO-NH-), 4.15 (s, 1H, -NH-C*H*-CONH-), 5.05 (s, 2H, -O-C*H₂*-Ph), 6.23 (s, 1H, C-*H* coumarin ring), 6.34 (s, 1H, *H*O-C-CH₃), 7.37 (m, 5H, C-*H* phenyl ring), 7.42 (s, 1H, -N*H*-CO-O-) 7.62-7.67 (m, 3H, C-*H* coumarin ring), 7.92 (s, 1H, -CH₂-N*H*-CO-), 10.52 (s, 1H, CO-N*H*-coumarin ring), 12.01 (s, 1H, -COO*H*). **¹³C-NMR** (DMSO-d_6) δ: 174.2, 172.6, 170.9, 161.4, 156.5, 154.2, 153.5, 142.5, 136.8, 128.6 (2C), 128.2 (2C), 127.8, 124.5, 116.7, 112.5, 110.7, 105.2, 71.5, 66.8, 54.1, 47.6, 46.9, 39.1, 30.5, 29.7, 27.4, 22.5, 18.9. **MS (ESI)**, *m/z:* 580 (M−H)⁻.

General Procedure for the synthesis of alkyl halide 63a-e.

General procedure a. The appropriate amine **62a,b** (0.701 mmol, 1eq) was dissolved in dry THF (7.5 mL) and the solution was then cooled at 0°C. DIPEA (2.63 mmol, 2.5eq) and the requisite acetyl chloride **61a-c** (1.90 mmol, 1.8eq) were added simultaneously and dropwise. The resulting mixture was stirred and kept under cooling for the first 30 min then at rt for further 4h. The reaction was then diluted with AcOEt (10 mL for each mL of THF) and washed with KHSO₄ 0.1 N (15 mL x 2) and distilled water (15 mL x 2). The organic phase was dried over anhydrous Na₂SO₄, filtered and evaporated under reduced pressure, affording **63a-d** as a crude purified trough trituration from Et₂O furnishing the analytically pure required substance by filtration as white solid.

General procedure b. 5-((4-nitrophenyl)sulfonyl)thiazol-2-amine **62c** (0.701 mmol, 1eq) was dissolved in dry THF (7.5mL), the solution was then cooled at -20°C and DIPEA (0.981 mmol, 1.4eq) and 2-bromo acetylbromide (1.90 mmol, 1.8eq) were added simultaneously and dropwise. The resulting mixture was stirred and kept under cooling for the first 30 min then at rt for further 4h. The reaction was then diluted with AcOEt (10 mL for each mL of THF) and washed with KHSO₄ 0.1 N (15 mL x 2) and distilled water (15 mL x 2). The organic phase was dried over anhydrous Na₂SO₄, filtered and evaporated under reduced pressure, affording **63e** as a crude purified trough trituration from AcOEt/*n*-hexane. The resulting precipitate was isolated by filtration providing the analytically pure substance.

2-chloro-2-phenyl-N-(4-sulfamoylphenyl)acetamide, 63a. Yield, 85%, mp 176-180°C. **¹H-NMR** (400MHz; DMSO-d_6) δ 5.80 (s, 1H, -C*H*-Cl), 7.29 (s, 2H, -N*H₂*), 7.38-7.46 (m, 3H, -C*H* phenyl ring), 7.59-7.61 (d, 2H, -C*H* phenyl ring), 7.74-7.81 (m, 4H, -C*H* 4-sulfamoylphenyl), 10.89 (s, 1H, -CO-N*H*-).

2-chloro-N-(5-((4-nitrophenyl)sulfonyl)thiazol-2-yl)propenamide, 63b. Yield, 94%, mp 195-198°C. **¹H-NMR** (400MHz; DMSO-d_6) δ 1.58 (d, 3H, -C*H₃*), 4.8 (q, 1H, -C*H*-CH₃), 8.26-8.28 (d, 2H, -C*H* phenyl ring), 8.4 (s, 1H, -C*H* thiazole), 8.42-8.44 (d, 2H, -C*H* phenyl ring), 13.4 (s, 1H, -CO-N*H*-).

2-chloro-N-(5-((4-nitrophenyl)sulfonyl)thiazol-2-yl)-2-phenylacetamide, 63c. Yield, 89%, mp 198-202°C. **¹H-NMR** (400MHz; DMSO-d_6) δ 5.80 (s, 1H, -C*H*-Cl), 7.40-7.55 (dd, 5H, -C*H* phenyl ring), 8.24-8.26 (d, 2H, -C*H* 4-nitrophenyl), 8.38 (s, 1H, -C*H* thiazole), 8.40-8.42 (d, 2H, -C*H* 4-nitrophenyl), 13.72 (s, 1H, -CO-N*H*-).

2-chloro-((4-nitrophenyl)sulfonyl)phenyl)acetamide, 63d. Yield, 66%, mp 204-208°C. **¹H-NMR** (400MHz; DMSO-d_6) δ 4.31 (s, 2H,-C*H₂*-), 7.83-7.85 (d, 2H, -C*H* phenyl ring), 7.99-8.01 (d, 2H, -C*H* phenyl ring), 8.19- 8.21 (d, 2H,-C*H* 4-nitrophenyl), 8.39-8.41 (d, 2H, C*H* 4-nitrophenyl),10.81 (s, 1H, -CO-N*H-).*

2-bromo-N-(5-((4-nitrophenyl)sulfonyl)thiazol-2-yl)acetamide, 63e. Yield, 86%, mp 171-173°C, **¹H-NMR** (400MHz; DMSO-d_6) δ 4.20 (s, 2H, -C*H₂*-), 8.20-8.27 (m, 2H, -C*H* phenyl ring), 8.40 (s, 1H, -C*H* thiazole), 8.42-8.49 (m, 2H, -C*H* phenyl ring), 13.4 (s, 1H, -CON*H-).*

General Procedure for the synthesis of 2-mercapto-6-substituited-pyrimidin-4(3H)-ones 65a-c.

To a perfectly clear solution of sodium ethoxide (20mmol, 2eq of sodium metal has been dissolved in 23 mL of dry EtOH, initially at 0°C and then at rt) thiourea (14 mmol, 1.4eq) was added followed by the appropriate β-ketoester **64a-c** (10 mmol, 1 eq) at rt. The reaction was left stirring under reflux conditions for 16-18h. Upon the conclusion of the reaction (checked by TLC), the mixture was left at rt until cooling, then the solvent was evaporated and the obtained solid dissolved in the minimum amount of water. The aqueous solution was then acidified with HCl 2N (till red of the pH indicator) obtaining a white solid precipitate which was filtered, washed with water and dried to afford the desired 2-mercapto-6-substituited-pyrimidin-4(*3H*)-one **65a-c**, which was finally triturated from Et₂O, thus filtered to furnish analytically pure required compound.

2-mercapto-6-(3-phenylpropyl)pyrimidin-4(3H)-one, 65a. Yield 87%, mp 201-202°C. **¹H-NMR** (400MHz; DMSO-d_6) δ 1.85-1.87 (m, 2H, Ph-CH₂-C*H₂*-CH₂-), 2.39 (t, 2H, Ph-CH₂-CH₂-C*H₂*-), 2.60 (t, 2H, Ph-C*H₂*-CH₂-CH₂-), 5.69 (s, 1H, -C*H* thiouracil ring), 7.20-2.29 (t, 5H, -C*H* phenyl ring), 12.27 (s, 1H, -N*H* thiouracil ring).

2-mercapto-6-(4-phenylbutyl)pyrimidin-4(3H)-one, 65b. Yield, 88%, mp 171-174 °C. **¹H-NMR** (400MHz; DMSO-d_6) δ 1.27-1.29 (m, 4H, Ph-CH₂-C*H₂*-C*H₂*-CH₂-), 1.98-2.01 (t, 2H, Ph-CH₂-C*H₂*-CH₂-CH₂-), 2.21-2.25 (t, 2H, Ph-CH₂-CH₂-CH₂-C*H₂*-), 5.92 (s, 1H, -C*H* thiouracil ring), 6.87 (d, 2H, -C*H* phenyl ring), 7.11 (t, 1H, -C*H* phenyl ring), 7.17 (t, 2H, -C*H* phenyl ring), 12.3 (s, 1H, -N*H* thiouracil ring).

6-([1,1'-biphenyl]-4-ylmethyl)-2-mercaptopyrimidin-4(3H)-one, 65c. *Yield 85%*, mp *262-265°C*. **¹H-NMR** (400MHz; DMSO-d_6) δ 3.76 (s, 2H, -C*H₂*-), 5.66 (s, 1H, -C*H* thiouracil ring), 7.34-74 (m, 5H, -C*H* phenyl ring), 7.64-7.68 (m, 4H, -C*H* phenyl ring), 12.17 (s, 1H, -N*H* thiouracil ring).

General Procedure for the synthesis of compounds 53b-p, 54c,d and 55a-d.

General procedure a. Appropriate alkyl halide **63d,e** (0.207 mmol, 1eq), requisite aryl-thiol (0.207 mmol, 1eq) and anhydrous K_2CO_3 (0.227 mmol, 1.1eq) were suspended in dry DMF (0.5 mL) and stirred for 6h 30 min at rt. When TLC showed the disappearance of starting material, K_2CO_3 was decanted using a mixture THF/MeOH and the obtained solution was evaporated under vacuum. Water was added (5 mL) and the resulting suspension was filtered under vacuum or extracted with AcOEt (10 mL x 4) thus dried over anhydrous Na_2SO_4, filtered and evaporated under reduced pressure. The resulting crude was purified by column chromatography on silica gel eluting with the suitable mixture of $CHCl_3$/MeOH or $CHCl_3$/THF/MeOH or AcOEt/*n*-hexane. Evaporation of the fractions containing the target compound gave a product that was finally purified by recrystallization from the appropriate solvent system (Table 3.1) to give **53b-k,n,p** and **55a-c**.

General procedure b. Proper alkyl halide **63a,c** (0.228 mmol, 1 eq), required ary-thiol (0.228 mmol, 1eq), anhydrous K_2CO_3 (0.251mmmol, 1.1eq) and NaI (0.228 mmol, 1eq), were suspended in dry DMF (0.5 mL) and stirred for 6-31h at rt until the complete conversion of the starting material in the desired compound (monitored by TLC). K_2CO_3 was decanted using a mixture of THF/MeOH and the resulting solution was stripped down from the solvent under reduced pressure. Water (5 mL) was added and the resulting precipitate was isolate by filtration, washed over the filter with water and purified by column chromatography on silica gel eluting with the suitable mixture of $CHCl_3$/THF/MeOH or AcOEt/*n*-hexane. Evaporation of the fractions containing the desired compound gave a crude that was finally purified by recrystallization from the appropriate solvent system to give **53m, 54c,d** and **55d.**

General procedure c. For the synthesis of the compound **53l**, alkyl halide **63b** (0.532 mmol, 1eq), commercially available 2-mercapto-6-propylpyrimidin-4(3H)-one **65e** (32 mmol, 1eq) and anhydrous K_2CO_3 (0.585 mmol, 1.1eq) were suspended in dry DMF (1 mL) thus stirred for 3h at 90°C. Upon the conclusion of the reaction, the solvent was evaporated under vacuum. Water (8 mL) and brine (2 mL) were added, and the resultant aqueous phase was extracted with AcOEt (10 mL x 6). The organic layer was then washed with brine (4 mL x 2) dried over anhydrous Na_2SO_4, filtered and evaporated under reduced pressure providing a crude that was purified by column chromatography on silica gel eluting with a mixture of $CHCl_3$/AcOEt and then $CHCl_3$/THF. The obtained product was finally purified by recrystallization from CH_3CN to furnish the pure compound *2-((4-hydroxy-6-propylpyrimidin-2-yl)thio)-N-(5-((4-nitrophenyl)sulfonyl)thiazol-2-yl)propanamide* **53l**.

General procedure d. A solution of commercially available 2-(phenylthio)acetic acid **66** (0.350 mmol, 1eq) and 5-((4-nitrophenyl)sulfonyl)thiazol-2-amine **62c** (0.350 mmol, 1eq) in dry pyridine (3 mL) was cooled at around -15°C (using a mixture ethylene glycol/CO_2) and, under a nitrogen atmosphere, $POCl_3$ (0.946 mmol, 2.7eq) was added dropwise. The reaction was stirred for 3h 30 min at -15°C, then poured on ice/water and stirred for 20 min. The obtained basic aqueous phase was extracted with AcOEt (20 mL x 4) and the organic layer was washed with brine (5 mL x 2), dried over anhydrous Na_2SO_4, filtered and evaporated under reduced pressure, affording **53o** as a crude which was purified through column chromatography on silica gel eluted with a mixture $CHCl_3$/THF. Evaporation of the fractions containing the target compound gave a solid that was finally purified by recrystallization from toluene.

2-((4-hydroxy-6-methylpyrimidin-2-yl)thio)-N-(5-((4-nitrophenyl)sulfonyl)thiazol-2-yl)acetamide, 53b, MC3998. **¹H-NMR** (400MHz; DMSO-d_6) δ 2.01 (s, 3H, -C*H$_3$* thiouracil ring), 4.15 (s, 2H, -S-C*H$_2$*-CO-), 6.04 (s, 1H, -C*H* thiouracil ring), 8.23-8.25 (d, 2H, -C*H* phenyl ring), 8.32 (s, 1H, -C*H*-thiazole ring), 8.34-8.43 (d, 2H, -C*H* phenyl ring), 12.4 (s, 1H, -N*H* thiouracil ring), 12.8 (s, 1H, -CH$_2$-CO-N*H*-). **¹³C-NMR** (100 MHz, DMSO-d_6) δ 23.92, 33.88, 104.2, 125.09, 128.03, 134.01, 143.77, 147.12, 149.54, 161.03, 164.18, 167.23, 168.09, 168.32. Exact. Mass: 467, **MS (ESI)**, *m/z*: 468 [M + H]$^+$.

2-((4-hydroxy-6-phenylpyrimidin-2-yl)thio)-N-(5-((4-nitrophenyl)sulfonyl)thiazol-2-yl)acetamide, 53c, MC4055. **¹H-NMR** (400MHz; DMSO-d_6) δ 4.28 (s, 2H, -S-C*H$_2$*-CO-), 6.67 (s, 1H, -C*H* thiouracil ring), 7.07-7.11 (t, 2H, -C*H* phenyl ring), 7.25-7.30 (t, 1H, -C*H* phenyl ring), 7.80-7.82 (d, 2H, -C*H* phenyl ring), 8.20-8.27 (m, 2H, -C*H* 4-nitrophenyl ring), 8.37 (s, 1H, -C*H* thiazole), 8.39-8.41 (m, 2H, -C*H* 4-nitrophenyl ring), 13.17 (s, 1H, -N*H* thiouracil ring), 13.45 (s, 1H, -CH$_2$-CO-N*H*-). **¹³C-NMR** (100 MHz, DMSO-d_6) δ 33.92, 99.33, 126.06, 128.11, 128.25, 128.88, 129.81, 133.72, 135.75, 143.68, 147.23, 149.55, 159.25, 161.03, 166.41, 167.82, 168.34. Exact. Mass: 529.02, **MS (ESI)**, *m/z*: 530 [M + H]$^+$.

2-((4-benzyl-6-hydroxypyrimidin-2-yl)thio)-N-(5-((4-nitrophenyl)sulfonyl)thiazol-2-yl)acetamide, 53d, MC4056. **¹H-NMR** (400MHz; DMSO-d_6) δ 3.58 (s, 2H, -C*H$_2$*-Ph), 4.18 (s, 2H, -S-C*H$_2$*-CO-), 6.01 (s, 1H, -C*H* thiouracil ring), 6.75 (m, 1H, -C*H* benzyl ring), 6.85-6.88 (t, 2H, -C*H* benzyl ring), 7.04-7.06 (d, 2H, C*H* benzyl ring), 8.28-8.30, 8.45-8.47 (d, 4H, -C*H* phenyl ring), 8.40 (s, 1H, -C*H* thiazole), 13.02 (s, 1H, -N*H* thiouracil ring), 13.37 (s, 1H, -CH$_2$-CO-N*H*-). **¹³C-NMR** (100 MHz, DMSO-d_6) δ 33.95, 42.05, 102.06, 125.09, 127.03, 128.08, 128.87, 128.99, 133.82, 138.37, 143.69, 147.15, 149.55, 160.92, 160.99, 166.15 167.19, 168.35. Exact. Mass: 543.03, **MS (ESI)**, *m/z*: 544 [M + H]$^+$.

2-((4-hydroxy-6-phenethylpyrimidin-2-yl)thio)-N-(5-((4-nitrophenyl)sulfonyl)thiazol-2-yl)acetamide, 53e, MC4063. **¹H-NMR** (400MHz; THF-d_8) δ 2.56-2.58 (m, 2H, -C*H$_2$*-C*H$_2$*-Ph), 2.59-2.63 (m, 2H, -C*H$_2$*-C*H$_2$*-Ph), 3.96 (s, 2H, -S-C*H$_2$*-CO-), 5.79 (s, 1H, -C*H* thiouracil ring), 6.86-7.05 (m, 5H, -C*H* phenyl ring), 7.96 (s, 1H, -C*H* thiazole ring) 8.0-8.03 (d, 2H, -C*H* 4-nitrophenyl), 8.16-8.21 (d, 2H, -C*H* 4-nitrophenyl), 10.9 (s, 1H, -N*H* thiouracil ring), 13.47 (s, 1H, -CH$_2$-CO-N*H*-). **¹³C-NMR** (100 MHz, DMSO-d_6) δ 33.96, 35.01, 38.35, 103.03 125.09, 126.63, 128.50, 128.69, 128.75, 133.71, 141.16, 143.78, 147.15, 149.55, 160.99, 164.01, 166.58, 167.89, 168.32. Exact. Mass: 557.05, **MS (ESI)**, *m/z*: 558 [M + H]$^+$.

2-((4-hydroxy-6-(3-phenylpropyl)pyrimidin-2-yl)thio)-N-(5-((4-nitrophenyl) sulfonyl) thiazol-2-yl)acetamide, 53f, MC4135. **¹H-NMR** (400MHz; DMSO-d_6) δ 1.60-1.66 (m, 2H, -CH$_2$-C*H$_2$*-CH$_2$-Ph), 2.21-2.23 (m, 4H, -C*H$_2$*-CH$_2$-C*H$_2$*-Ph), 4.10 (s, 2H, -S-C*H$_2$*-CO-), 5.91 (s, 1H, -C*H* thiouracil ring), 7.03-7.17 (m, 4H, -C*H* phenyl ring), 8.21-8.24 (m, 2H, -C*H* 4-nitrophenyl), 8.38 (s, 1H, -C*H* thiazole ring), 8.59 (m, 2H, -C*H* 4-nitrophenyl), 12.64 (s, 1H, -N*H* thiouracil ring), 13.02 (s, 1H, -CH$_2$-CO-N*H*-). **¹³C-NMR** (100 MHz, DMSO-d_6) δ 29.81, 33.99, 34.58, 35.15, 102.31, 125.08, 126.65, 128.11, 128.53, 128.65, 133.72, 142.11, 143.68, 147.12, 149.62, 161.05, 165.23, 166.58, 167.57, 168.77. Exact. Mass: 571.07, **MS (ESI)**, *m/z*: 572 [M + H]$^+$.

2-((4-hydroxy-6-(4-phenylbutyl)pyrimidin-2-yl)thio)-N-(5-((4-nitrophenyl)sulfonyl)thiazol-2-yl)acetamide, 53g, MC414. **¹H-NMR** (400MHz; DMSO-d_6) δ 1.19-1.24 (m, 4H, Ph-CH$_2$-C*H$_2$*-C*H$_2$*-CH$_2$-), 2.01-2.03 (t, 2H, Ph-C*H$_2$*-CH$_2$-CH$_2$-CH$_2$-), 2.21-2.25 (t, 2H, Ph-CH$_2$-CH$_2$-CH$_2$-C*H$_2$*-), 4.14 (s, 2H, -S-C*H$_2$*-CO-), 5.9 (s, 1H, -C*H* thiouracil ring), 6.87-6.89 (d, 2H, -C*H* phenyl ring), 7.11 (t, 1H, -C*H* phenyl ring), 7.11-

7.18 (t, 2H, -C*H* phenyl ring), 8.16-8.18 (d, 2H, -C*H* 4-nitrophenyl), 8.24-8.27 (d, 2H, -C*H* 4-nitrophenyl), 8.37 (s, 1H, -C*H* thiazole ring), 12.3 (s, 1H, -N*H* thiouracil ring), 13.2 (s, 1H, -CH₂-CO-N*H*-). **¹³C-NMR** (100 MHz, DMSO-d_6) δ 27.71, 29.88, 33.99, 35.52, 36.79, 103.01, 125.11, 126.68, 128.04, 128.52, 128.99, 133.75, 141.80, 143.65, 147.13, 150.02, 161.75, 165.27, 166.72, 167.75, 168.40. Exact. Mass: 585.08, **MS (ESI)**, *m/z*: 586 [M + H]⁺.

2-((4-hydroxy-6-(naphthalen-2-ylmethyl)pyrimidin-2-yl)thio)-N-(5-((4 nitrophenyl)sulfonyl)thiazol-2-yl)acetamide, 53h, MC4131.

¹H-NMR (400MHz; DMSO-d_6) δ 3,79 (s, 2H, -C*H₂*-naphthyl), 4.11 (s, 2H, -S-C*H₂*-CO-), 6.06 (s, 1H, -C*H* thiouracil ring), 7.28,7.29 (d, 1H, -C*H* naphthyl ring), 7.34-7.40 (m, 2H, -C*H* naphthyl ring), 7.52-7.54 (d, 1H, -C*H* naphthyl ring), 7.63-7.72 (m, 3H, -C*H* naphthyl ring), 8.25-8.27 (d, 2H, -C*H* 4-nitrophenyl), 8.38 (s, 1H, -C*H* thiazole), 8.41 -8.43 (d, 2H, -C*H* 4-nitrophenyl), 13.17 (s, 1H, -N*H* thiouracil ring), 13.38 (s, 1H, -CH₂-CO-N*H*-). **¹³C-NMR** (100 MHz, DMSO-d_6) δ 34.01, 42.08, 102.09, 125.11, 126.25, 126.44, 126.66, 127.42, 127.44, 127.81, 128.05, 133.42, 133.88, 134.09, 136.35, 143.62, 147.15, 149.55, 160.71, 161.09, 166.11, 167.15, 168.34. Exact. Mass: 593.05, **MS (ESI)**, *m/z*: 594 [M + H]⁺.

2-((4-([1,1'-biphenyl]-4-ylmethyl)-6-hydroxypyrimidin-2-yl)thio)-N-(5-((4-nitrophenyl)sulfonyl)thiazol-2-yl)acetamide, 53i, MC4130.

¹H-NMR (400MHz; DMSO-d_6) δ 3.67 (s, 2H, -C*H₂*-Ph-Ph), 3.35 (s, 2H, -S-C*H₂*-CO-), 6.06 (s, 1H, -C*H* thiouracil ring), 7.25-7.27 (d, 2H, -C*H* -CH₂-<u>Ph</u>-Ph), 7.33-7.36, 7.38-7.56 (t, 5H, C*H* -CH₂-Ph-<u>Ph</u>), 7.53-7.60 (d, 2H, -C*H* -CH₂-<u>Ph</u>-Ph), 8.22-8.24 (d, 2H, C*H* 4-nitrophenyl), 8.36 (s, 1H, -C*H* thiazole ring), 8.38-8.39 (d, 2H, C*H* 4-nitrophenyl), 13.15 (s, 1H, -N*H* thiouracil ring), 13.22 (s, 1H, -CH₂-CO-N*H*-). **¹³C-NMR** (100 MHz, DMSO-d_6) δ 33.94, 41.95, 102.08, 125.11, 127.23, 127.79, 127.93, 128.03, 128.72, 129.04, 133.73, 137.63, 139.15, 140.83, 143.65, 147.12, 149.55, 160.93, 161.03, 166.13, 167.22, 168.35. Exact. Mass: 691.07, **MS (ESI)**, *m/z*: 620 [M + H]⁺.

2-((4-hydroxyquinazolin-2-yl)thio)-N-(5-((4-nitrophenyl)sulfonyl)thiazol-2-yl)acetamide, 53j, MC4064.

¹H-NMR (400MHz; DMSO-d_6) δ 4.28 (s, 2H, -S-C*H₂*-CO-), 7.24-7.26 (d, 1H, -C*H* quinazoline ring), 7.36-7.39 (t, 1H, -C*H* quinazoline ring), 7.65-7.68 (t, 1H, -C*H* quinazoline ring), 7.99-8.00 (d, 1H, -C*H* quinazoline ring), 8.22-8.24 (d, 2H, -C*H* phenyl ring), 8.38 (s, 1H, -C*H* thiazole ring), 8.439-4.41 (d, 2H, -C*H* phenyl ring), 12.87 (s, 1H, -N*H* quinazoline ring), 13.30 (s, 1H, -CH₂-CO-N*H*-). **¹³C-NMR** (100 MHz, DMSO-d_6) δ 33.93, 114.93, 123.68, 124.85, 125.11, 125.44, 128.02, 131.71, 133.73, 143.65, 147.15, 148.71, 149.55, 161.04, 165.62, 167.52, 168.33. Exact. Mass: 503, **MS (ESI)**, *m/z*: 504 [M + H]⁺.

2-((5-benzyl-4-hydroxy-6-methylpyrimidin-2-yl)thio)-N-(5-((4-nitrophenyl)sulfonyl)thiazol-2-yl)acetamide, 53k, MC4073.

¹H-NMR (400MHz; DMSO-d_6) δ 2.51 (s, 3H, -C*H₃* thiouracil ring), 3.68 (s, 2H,-C*H₂*-Ph), 4.15 (s, 2H, -S-C*H₂*-CO-), 7.12-7.14 (m, 3H, -C*H* phenyl ring), 7.21-7.23 (m, 2H, -C*H* phenyl ring), 8.23-8.25 (d, 2H, C*H* 4-nitrophenyl), 8.35 (s, 1H, -C*H* thiazole ring), 8.40-8.43 (d, 2H, 4-nitrophenyl), 12.8 (s, 1H, -N*H* thiouracil ring), 13.33 (s, 1H, -CH₂-CO-N*H*-). **¹³C-NMR** (100 MHz, DMSO-d_6) δ 22.15, 32.33, 33.96, 115.68, 125.35, 126.99, 128.04, 128.19, 133.75, 138.01, 143.67, 147.14, 149.55, 160.45, 16.05, 166.38, 167.55, 168.33. Exact. Mass: 557.05, **MS (ESI)**, *m/z*: 558 [M + H]⁺.

2-((4-hydroxy-6-propylpyrimidin-2-yl)thio)-N-(5-((4-nitrophenyl)sulfonyl)thiazol-2-yl)propenamide, 53l, MC4084. **¹H-NMR** (400MHz; DMSO-d_6) δ 0.46 (s, 3H, CH_3-CH$_2$-CH$_2$-), 1.24-1.25 (m, 2H, CH$_3$-CH_2-CH$_2$-), 1.48-1.50 (d, 3H, -S-CH-CH_3), 2.16 (m, 2H, CH$_3$-CH$_2$-CH_2-), 4.57 (m, 1H, -S-CH-CH$_3$), 5.93 (s, 1H, -CH thiouracil ring), 8.23-8.26 (d, 2H, -CH phenyl ring), 8.37 (s, 1H, -CH thiazole ring), 8.41-8.43 (d, 2H, -CH phenyl ring), 12.60 (s, 1H, -NH thiouracil ring), 13.03 (s, 1H, -CH-CO-NH-). **¹³C-NMR** (100 MHz, DMSO-d_6) δ 13.79, 22.14, 38.65, 102.77, 121.49, 125.11, 128.01, 129.04, 133.75, 143.99, 147.12, 149.54, 161.02, 165.68, 166.15, 166.73, 166.78. Mass: 509.05, **MS (ESI)**, m/z: 510 [M + H]⁺.

N-(5-((4-nitrophenyl)sulfonyl)thiazol-2-yl)-2-((6-oxo-4-propyl-1,6-dihydropyrimidin-2-yl)thio)-2-phenylacetamide, 53m, MC4089. **¹H-NMR** (400MHz; DMSO-d_6) δ 0.39 (m, 3H, CH_3-CH$_2$-CH$_2$-), 1.24 (m, 2H, CH$_3$-CH_2-CH$_2$-), 2.01 (m, 2H, CH$_3$-CH$_2$-CH_2-), 5.70 (s, 1H, -S-CH-CH$_3$), 5.93 (s, 1H, -CH thiouracil ring), 7.30-7.43 (m, 3H, -CH phenyl ring), 7.49-7.50 (d, 2H, -CH phenyl ring), 8.22-8.24 (d, 2H, -CH 4-nitrophenyl), 8.34 (s, 1H, -CH thiazole ring), 8.40-8.42 (d, 2H, -CH 4-nitrophenyl), 12.73 (s, 1H, -NH thiouracil ring), 12.95 (s, 1H, -CH-CO-NH-). **¹³C-NMR** (100 MHz, DMSO-d_6) δ 13.85, 20.99, 36.58, 56.79, 105.25, 125.11, 128.04, 128.08, 128.75, 129.53, 133.74, 138.15, 143.62, 147.14, 149.55, 159.75, 160.92, 164.13, 164.85, 172.15. Exact. Mass: 571.07, **MS (ESI)**, m/z: 572 [M + H]⁺.

2-((4-hydroxy-6-propylpyrimidin-2-yl)thio)-N-(4-((4-nitrophenyl)sulfonyl)phenyl) acetamide, 53n, MC4082. **¹H-NMR** (400MHz; DMSO-d_6) δ 0.69-0.72 (t, 3H, CH_3-CH$_2$-CH$_2$), 1.40-1.49 (m, 2H, CH$_3$-CH_2-CH$_2$-), 2.17-2.21 (t, 2H, CH$_3$-CH$_2$-CH_2-), 4.18 (s, 2H, -S-CH_2-CO-), 5.68 (s, 1H, -CH thiouracil ring) 7.88-7.95 (m, 4H, -CH phenyl ring) 8.16-8.19 (d, 2H, -CH 4-nitrophenyl), 8.37-8.39 (d, 2H, CH 4-nitrophenyl), 12.21 (s, 1H, -NH thiouracil ring), 12.3 (s, 1H, -CH$_2$-CO-NH-). **¹³C-NMR** (100 MHz, DMSO-d_6) δ 13.78, 22.15, 33.89, 38.85, 101.91, 120.03, 124.85, 128.89, 131.41, 135.22, 140.41, 145.01, 149.44, 165.61, 166.55, 167.05, 167.49. Exact. Mass: 488.08, **MS (ESI)**, m/z: 489 [M + H]⁺.

N-(5-((4-nitrophenyl)sulfonyl)thiazol-2-yl)-2-(phenylthio)acetamide, 53o, MC4078. **¹H-NMR** (400MHz; DMSO-d_6) δ 4.01 (s, 2H, -S-CH_2-CO-), 7.15-7.38 (m, 5H, -CH thiophenol ring), 8.23-8.26 (d, 2H, -CH phenyl ring), 8.35 (s, 1H, -CH thiazole ring), 8.40-8.42 (d, 2H, -CH phenyl ring), 13.19 (s, 1H, -CH$_2$-CO-NH-).**¹³C-NMR** (100 MHz, DMSO-d_6) δ 38.52, 125.09, 127.13, 128.08, 129.31, 129.93, 133.75, 135.82, 143.65, 147.13, 149.55, 160.91, 168.77. Exact. Mass: 435, **MS (ESI)**, m/z: 436[M + H]⁺.

2-((4-aminophenyl)thio)-N-(5-((4-nitrophenyl)sulfonyl)thiazol-2-yl)acetamide, 53p, MC4112. **¹H-NMR** (400MHz; DMSO-d_6) δ 3.65 (s, 2H, -S-CH_2-CO-), 5.34 (s, 2H, -NH_2), 6.46-6.48 (d, 2H, -CH 4-amino-phenyl), 7.07-7.09 (d, 2H, -CH 4-amino-phenyl), 8.24-8.26 (d, 2H, -CH phenyl ring), 8.32 (s, 1H, -CH thiazole ring), 8.42-8.44 (d, 2H, -CH phenyl ring), 12.98 (s, 1H, -CH$_2$-CO-NH-). **¹³C-NMR** (100 MHz, DMSO-d_6) δ 38.55, 115.29, 125.08, 128.03, 128.15, 128.54, 133.78, 143.66, 146.03, 147.12, 149.55, 160.91, 168.67. Exact. Mass: 450.01, **MS (ESI)**, m/z: 451 [M + H]⁺.

2-((5-amino-1H-benzo[d]imidazol-2-yl)thio)-2-phenyl-N-(4-sulfamoylphenyl)acetamide, 54c, MC4096. **¹H-NMR** (400MHz; DMSO-d_6) δ 4.84 (s, 2H, -NH_2 benzimidazole ring), 5.94 (s, 1H, -S-CH-), 6.44-6.46 (d, 1H, -CH benzimidazole ring), 6.55 (s, 1H, -CH benzimidazole ring), 7.13 (s, 1H, -CH benzimidazole ring), 7.33-7.39 (m, 5H, -CH phenyl ring), 7.58-7.59 (d, 2H, -SO$_2$-NH_2), 7.72-7.77 (m, 4H, -CH 4-nitrophenyl), 10.95 (s, 1H, -CH-CO-NH-), 12.05 (s, 1H, -NH benzimidazole ring). **¹³C-**

NMR (100 MHz, DMSO-d_6) δ 56.82, 101.11, 111.92, 112.08, 120.08, 127.93, 128.08, 128.95, 129.50, 132.28, 136.74, 139.04, 139.79, 139.88, 144.65, 149.11, 170.34. Exact. Mass: 453.09, **MS (ESI)**, *m/z*: 454 [M + H]+.

2-((4-aminophenyl)thio)-2-phenyl-N-(4-sulfamoylphenyl)acetamide, 54d, MC4100. **¹H-NMR** (400MHz; DMSO-d_6) δ 4.93 (s, 1H, -S-C*H*-), 5.35 (s, 2H, -N*H₂* thiophenol ring), 6.44 (d, 2H, -SO₂-N*H₂*), 7.05-7.07 (d, 2H, -C*H* thiophenol ring), 7.29-7.35 (m, 5H, C-*H* phenyl ring), 7.55-7.58 (d, 2H, -C*H* thiophenol ring), 7.67-7.76 (m, 4H, -C*H* phenyl ring), 10.52 (s, 1H, -CH-CO-N*H*-). **¹³C-NMR** (100 MHz, DMSO-d_6) δ 60.35, 115.62, 119.88, 126.05, 127.84, 128.44, 128.99, 129.63, 131.05, 136.77, 138.92, 139.55, 146.43, 170.99. Exact. Mass: 413.09, **MS (ESI)**, *m/z*: 414 [M + H]+.

2-((5-chloro-1H-benzo[d]imidazol-2-yl)thio)-N-(5-((4-nitrophenyl)sulfonyl)thiazol-2-yl)acetamide, 55a, MC4092. **¹H-NMR** (400MHz; DMSO-d_6) δ 4.41 (s, 2H, -S-C*H₂*-CO-), 7.13-7.15 (d, 1H, -C*H* benzimidazole ring), 7.40-7.47 (m, 2H, -C*H* benzimidazole ring), 8.23-8.25 (d, 2H, -C*H* phenyl ring), 8.37 (s, 1H, -C*H* thiazole ring), 8.39-8.42 (d, 2H, -C*H* phenyl ring), 13.32 (s, 1H, -N*H* benzimidazole ring), 13.52 (s, 1H, -CH₂-CO-N*H*-). **¹³C-NMR** (100 MHz, DMSO-d_6) δ 34.45, 111.48, 117.25, 125.09, 125.33, 128.02, 129.65, 133.78, 136.62, 139.34, 143.68, 147.12, 149.55, 152.44, 161.04, 168.54. Exact. Mass: 508.97, MS (ESI), *m/z*: 510 [M + H]+.
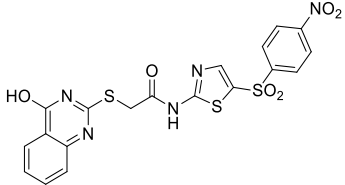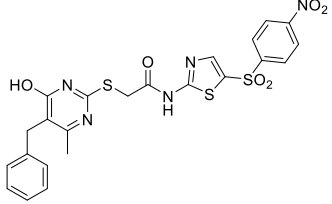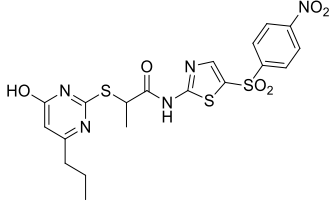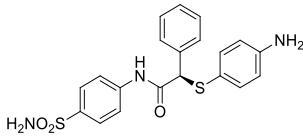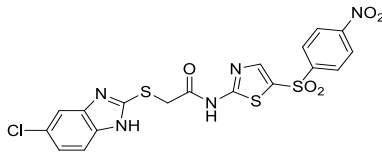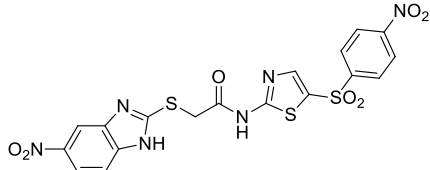
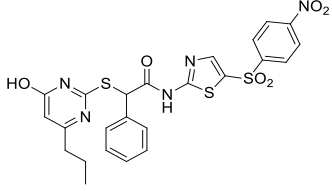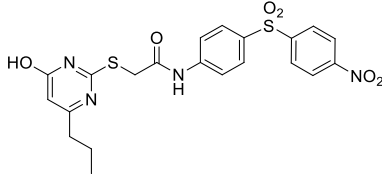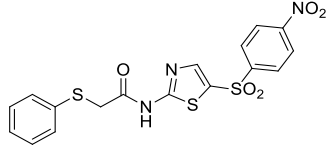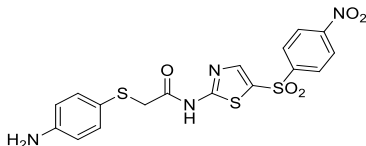***2-((5-nitro-1H-benzo[d]imidazol-2-yl)thio)-N-(5-((4-nitrophenyl)sulfonyl)thiazol-2-yl)acetamide, 55b, MC4091.*** **¹H-NMR** (400MHz; DMSO-d_6) δ 4.47 (s, 2H, -S-C*H₂*-CO-), 7.57-7.60 (d, 1H, -C*H* benzimidazole ring), 8.04-8.06 (d, 1H, -C*H* benzimidazole ring), 8.22-8.24 (d, 2H, -C*H* phenyl ring), 8.27 (s, 1H, -C*H* thiazole ring), 8.38 (s, 1H, -C*H* benzimidazole ring), 8.39-8.41 (d, 2H, -C*H* phenyl ring), 13.32 (s, 1H, -N*H* benzimidazole ring), 13.54 (s, 1H, -CH₂-CO-N*H*-). **¹³C-NMR** (100 MHz, DMSO-d_6) δ 34.55, 111.59, 112.57, 120.86, 125.11, 128.03, 133.94, 141.08, 141.13, 143.55, 143.72, 147.15, 149.56, 152.80, 161.05, 168.55. Exact. Mass: 519.99, **MS (ESI)**, *m/z*: 521 [M + H]+.
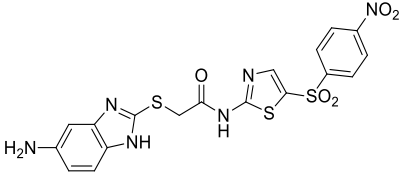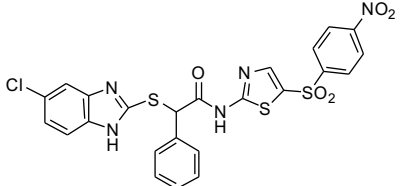
2-((5-amino-1H-benzo[d]imidazol-2-yl)thio)-N-(5-((4-nitrophenyl)sulfonyl)thiazol-2-yl)acetamide, 55c, MC4098. **¹H-NMR** (400MHz; DMSO-d_6) δ 4.26 (s, 2H, -S-C*H₂*-CO-), 5.28 (s, 2H, -N*H₂* benzoimidazole ring), 6.43-6.45 (d, 1H, -C*H* benzimidazole ring), 6.55 (s, 1H, -C*H* benzimidazole ring), 7.08-7.09 (d, 1H, -C*H* benzimidazole ring), 8.22-8.24 (d, 2H, -C*H* phenyl ring), 8.35 (s, 1H, -C*H* thiazole ring), 8.39-8.42 (d, 2H, -C*H* phenyl ring), 12.49 (s, 1H, -N*H* benzimidazole ring), 12.74 (s, 1H, -CH₂-CO-N*H*-). **¹³C-NMR** (100 MHz, DMSO-d_6) δ 35.01, 102.09, 111.99, 112.08, 125.11, 128.04, 132.45, 134.01, 139.67, 143.52, 145.01, 147.15, 149.53, 152.04, 161.05, 169.01. Exact. Mass: 490.02, **MS (ESI)**, *m/z*: 491 [M + H]+.

2-((5-chloro-1H-benzo[d]imidazol-2-yl)thio)-N-(5-((4-nitrophenyl)sulfonyl)thiazol-2-yl)-2-phenylacetamide, 55d, MC4122. **¹H-NMR** (400MHz; DMSO-d_6) δ 6.03 (s, 1H, -S-C*H*-Ph), 7.03-7.06 (d, 1H, -C*H* benzimidazole ring), 7.30-7.36 (m, 5H, -C*H* phenyl ring), 7.44-7.46 (d, 2H, -C*H* benzimidazole ring), 8.12-8.15 (d, 2H, -C*H* 4-nitrophenyl), 8.27-8.29 (d, 2H, -C*H* 4-nitrophenyl), 8.44 (s, 1H, -C*H* thiazole ring), 13.05 (s, 1H, -N*H* benzimidazole ring), 13.54 (s, 1H, -CH-CO-N*H*-). **¹³C-NMR** (100 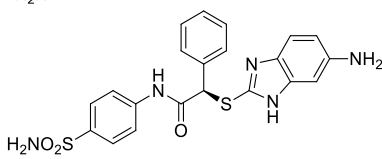MHz, DMSO-d_6) δ 56.88, 111.43, 117.23, 125.23 125.45, 128.01, 128.09, 128.75, 129.67, 129.77, 133.72, 136.38, 139.16, 139.55, 143.72, 147.14, 149.55, 149.77, 161.01 172.87. Exact. Mass: 585, **MS (ESI)**, *m/z*: 586 [M + H]+.

Melting Point and Yield Data for Compounds 53b-p, 54c,d and 55a-d

Compd	Structure	Mp (°C)	Recryst. system[a]	% Yield
53b MC3998		215-218	A	71
53c MC4055		220-223	A	51
53d MC4056		222-225	A	80
53e MC4063		193-198	B	60
53f MC4135		189-190	B	25
53g MC4140		180-182	B	30
53h MC4131		208-210	B	77
53i MC4130		192-195	A	53

Compound	Structure			
53j **MC4064**		203-206	B	89
53k **MC4073**		208-210	B	75
53l **MC4084**		201-204	A	26
53m **MC4089**		181-183	B	28
53n **MC4082**		223-227	B	26
53o **MC4078**		198-201	C	26
53p **MC4112**		91-93	C	36
54c **MC4096**		151-159	D	61
54d **MC4100**		176-180	D	51
55a **MC4092**		158-161	B	80
55b **MC4091**		232-235	A	30

55c **MC4098**		175-178	B	34
55d **MC4122**		166-168	D	27

[a]A: THF/CH₃CN/MeOH; B: CH₃CN/MeOH; C: toluene; D: CH₃CN

Table 3.1. Melting point and Yield data for compounds 53b-p, **54c,d** and **55a-d.**

3.3 Biological evaluation, results and discussion

Prof. Steegborn and his research group carried out an enzymatic assay, using our substrate MC3659 **2** in presence and in absence of the novel SIRT4i synthesized. Such assay was used to obtain information primarily on the SIRT4 ability to recognize and deacylate the HMG residue linked to the lysine of MC3659 **2**, showing, in this way that MC3659 **2** can be considered to all effects a new substrate for SIRT4, and secondly to evaluate the inhibitory activities of the SIRT4i developed. Samples used contained: hSirt4 (1 μM), NAD⁺ (500 μM), Z-Lys(HMG)AMC, MC3659, **2** (500 μM), the potential SIRT4i synthetized (at 10, 25 and 100 μM), the FdL-developer (Trypsin 5 mg/mL) in DMSO. The theoretical concept at the base of such assay is focused on the capability of SIRT4 to recognize and deacylate **2**, thus leading to the free lysine amino-terminal group, which is, in turn, recognized only in its deacylate state, by trypsin. Trypsin mediates the lysis of amide bond, leading therefore to the release of AMC **57**, which is fluorescent (λex= 365 nm, λem= 465 nm). The just described sample without the inhibitor was used a negative control (in this case SIRT4 will deacylate lysine and trypsin will split the peptide bond) and the positive control instead sees only the presence of NAM **19** (which acts as SIRT4i), finally, the only enzyme in DMSO was used as blank, in order to identify hypothetical contaminations. Summarizing, 20 compounds, among which 14 are analogues of **53a** UBCS191, 2 are analogues of **54a** UBCS178 and 4 are hybrid between **54a** UBCS178 and **53a** UBCS191 (**55a-d**) have been synthetized (Table 5.1).

As shown in Figure 3.7, most of the analyzed compounds displayed a strong inhibitory activity against SIRT4 at 100 μM (blue histograms) and many of these also kept a moderate inhibition at 25 μM (red histograms). This prescreen allowed us to identify the most promising inhibitors of this first series: **53h-j** (MC4131, MC4130, MC4064), **53l** (MC4084), **53m** (MC4089), **55a-d** (MC4092, MC4091, MC4098, MC4122) but also the worst: **54c** (MC4092), **54d** (MC4100) and **53p** (MC4112) that have very poor inhibitory activity.
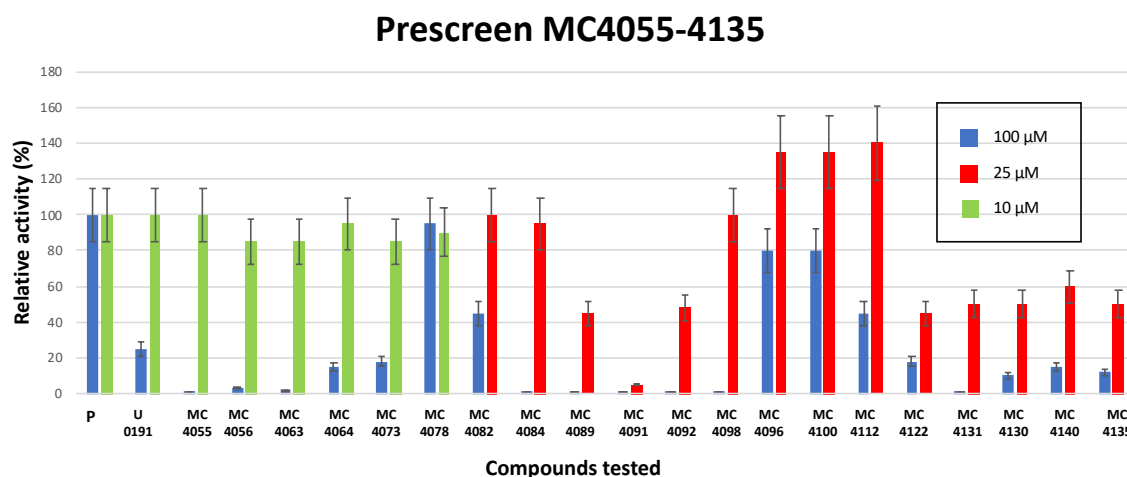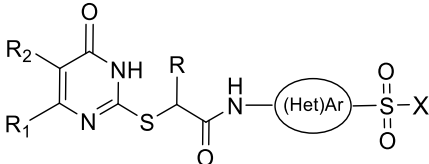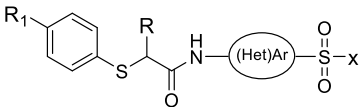
Figure 3.7. Prescreen of compounds MC4055—135 at 100 μM (blue histograms), 25 μM (red histogram, for MC4082, MC4084, MC4089, MC04091, MC4092, MC4089, MC4100, MC4112, MC4131, MC4130, MC4140, MC4135) or 10 μM (green histograms, for P, UBCS0191, MC4055, MC4056, MC4064, MC4078). Compounds been testested as a biological duplicate. Relative activity (%) is normalized to reaction without any compounds in presence of same DMSO concentration (indicated with "P"= "positive").

IC$_{50}$ of the most active compounds were following determined (Table 3.2) using dilutions from 500 to 0 μM for each inhibitor. In this assay, Prof. Steegborn and coworkers used

hSirt4 (1μM), FdL–substrate (MC3659 **2**, 500 μM), NAD+ (500 μM) at fixed 5% DMSO and tested a serial dilution from 500 to 8 μM (and 0 μM cmpd, with DMSO added only). They took 8 data points and measured a biological duplicate at least, except for MC4089 **53m**, for which more data points and replicates were necessary since it initially showed noisy results.

Comments	BAYREUTH CODE	COMMERCIAL/ MAI'S GROUP CODE	R	R1	R2	(HET) Ar	X	RESIDUAL ACTIVITY @100 μM	RESIDUAL ACTIVITY @10/25 μM	IC$_{50}$ (μM)
From virtual screening	UBCS-0191	OSSK_671780 53a	H	n-Pr	H	thiazole	4-NO$_2$ Ph	29.5	98.8	66.7 ± 7.9
Analogues of UBCS-0191		MC3998 53b	H	Me	H	thiazole	4-NO$_2$ Ph	56.9	Not tested	
	UBCS-0370	MC4055 53c	H	Ph	H	thiazole	4-NO$_2$ Ph	-2.2 ± 34.6	103 (single determination)	35.8 ± 3.7
	UBCS-0371	MC4056 53d	H	Bn	H	thiazole	4-NO$_2$ Ph	8.9 ± 31.5	83 (single determination)	76.4 ± 12.0
	UBCS-0372	MC4063 53e	H	(CH$_2$)$_2$Ph	H	thiazole	4-NO$_2$ Ph	-12.5	84.3	69.0 ± 6.3
	UBCS-0389	MC4135 53f	H	(CH$_2$)$_3$Ph	H	thiazole	4-NO$_2$ Ph	14.3 ± 1.3	60.0+-1.2	41.8 +- 2.7
	UBCS-0388	MC4140 53g	H	(CH$_2$)$_4$Ph	H	thiazole	4-NO$_2$ Ph	19.9 ± 11.3	66.0 ± 5.1	82.2 ± 4.1
	UBCS-0386	MC4131 53h	H	2Naphtyl -methyl	H	thiazole	4-NO$_2$ Ph	3.8 ± 17.6	55.4 ± 4.1	24.1 +- 6.1
	UBCS-0387	MC4130 53i	H	4'Biphenyl -methyl	H	thiazole	4-NO$_2$ Ph	23.2 ± 19.8	53.9 ± 12.1	20.1 +- 4.5
	UBCS-0373	MC4064 53j	H	Condensed phenyl ring		thiazole	4-NO$_2$ Ph	7.9	97	15.9 ± 1.0
	UBCS-0374	MC4073 53k	H	Me	Bn	thiazole	4-NO$_2$ Ph	12.3	83.5	84.4 ± 25.9
	UBCS-0377	MC4084 53l	Me	n-Pr	H	thiazole	4-NO$_2$ Ph	-62.5 ± 17.5	70.0 ± 35.5	33.4 ± 6.9
	UBCS-0378	MC4089 53m	Ph	n-Pr	H	thiazole	4-NO$_2$ Ph	-28.3 ± 43.7	50.1 ± 15.2	9.6 ± 1.9
	UBCS-0376	MC4082 53n	H	n-Pr	H	Ph	4-NO$_2$ Ph	47.0 ± 40.3	107.9 ± 26.9	

Comments	BAYREUTH CODE	COMMERCIAL/ MAI'S GROUP CODE	R	R1	R2	(HET) Ar	X	RESIDUAL ACTIVITY @100 μM	RESIDUAL ACTIVITY @10/25 μM	IC$_{50}$ (μM)
Analogues of UBCS-0191	UBCS-0375	MC4078 53o	H	H	-	thiazole	4-NO$_2$ Ph	103.5	93.7	
	UBCS-0384	MC4112 53p	H	NH$_2$	-	thiazole	4-NO$_2$ Ph	52.6 ± 42.7	165.4 ± 49.4	
Analogues of UBCS-0178	UBCS-0383	MC4100 54d	Ph	NH$_2$	-	Ph	NH$_2$	69.0 ± 51.3	154.2 ± 38.3	
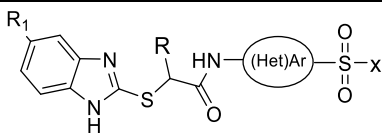
			R_1	R	-	(Het)Ar	X			
From virtual screening	UBCS-0178	OSSK_979070 54a	Ph	Cl	-	Ph	NH$_2$	30.2		**45.6 ± 10**
	UBCS-0313	OSSK_766801 54b	Ph	NO$_2$	-	Ph	NH$_2$	27.3		**54.7 ± 6.0**
Analogues of UBCS-0178	UBCS-0382	MC4096 54c	Ph	NH$_2$	-	Ph	NH$_2$	78.1 ± 61.5	149.5 ± 32.9	
Chimeric compds between the two prototypes UBCS-0178 & UBCS-0191	UBCS-380	MC4092 55a	H	Cl	-	thiazole	4-NO$_2$ Ph	-25.3 ± 35.4	58.8 ± 32.4	**14.0 ± 1.3**
	UBCS-379	MC4091 55b	H	NO$_2$	-	thiazole	4-NO$_2$ Ph	-0.3 ± 15.2	15.0 ± 28.7	**33.3 ± 2.5**
	UBCS-381	MC4098 55c	H	NH$_2$	-	thiazole	4-NO$_2$ Ph	-12.1 ± 53.7	107.0 ± 100.0	**39.0 ± 3.1**
	UBCS-0385	MC4122 55d	Ph	Cl	-	thiazole	4-NO$_2$ Ph	16.2 ± 4.0	40.4 ± 15.4	**0.9± 0.3**

Table 3.2. Residual activities of final compounds registered at 100, 25, 10 μM and IC$_{50}$ values of the most promising SIRT4i.

Most of the compounds synthesized displayed a lower IC$_{50}$ value compared with their corresponding prototype, in particular, **53a** UBCS-0191 analogues **53m** MC4089, **53j** MC4064, **53i** MC4130, **53h** MC4131 exhibit an IC$_{50}$ between 9.6-24.1 µM (Table 3.2 and Figure 3.8).
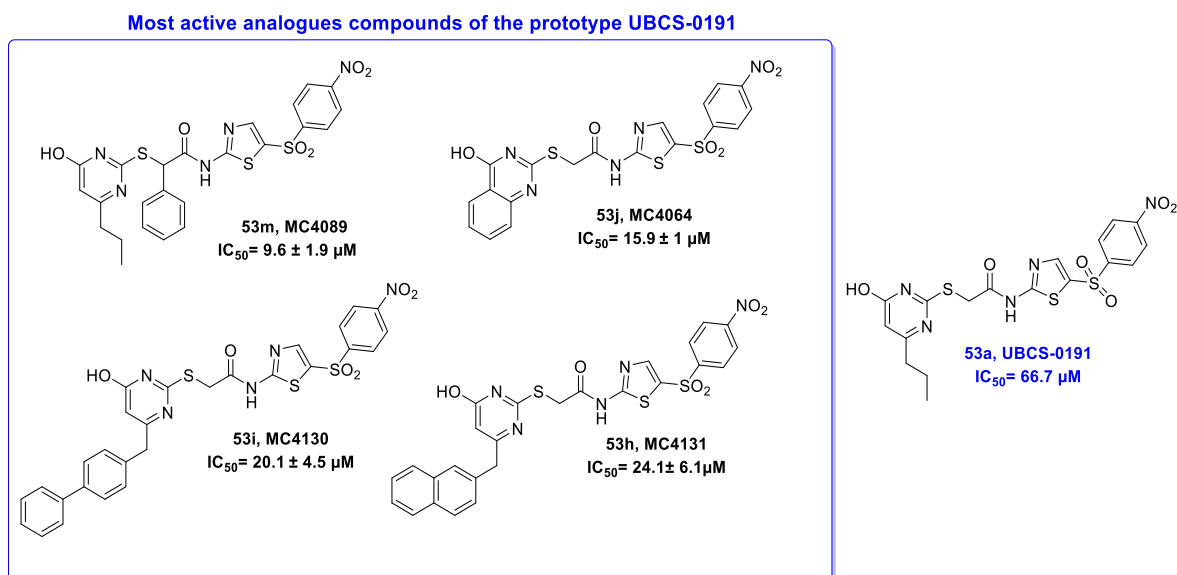
Figure 3.8 Structures of the most active **53a** UBC-0191 analogues **53m** MC4089, **53j** MC406, **53i** MC4130, **53h** MC4131 synthetized and their relative IC$_{50}$ values.

As shown in Figure 3.9 and Table 3.2, also **55d** MC4122, **55a** MC4092, that belong to the series of hybrid compounds between the two prototypes **53a** UBCS-0191 and **54a** UBCS-0178, provided very promising results. **55d** MC4122 showed, in particular, the best inhibitory capability since its IC$_{50}$ reach the low micromolar range (IC$_{50}$= 0.9 ± 0.3 µM).
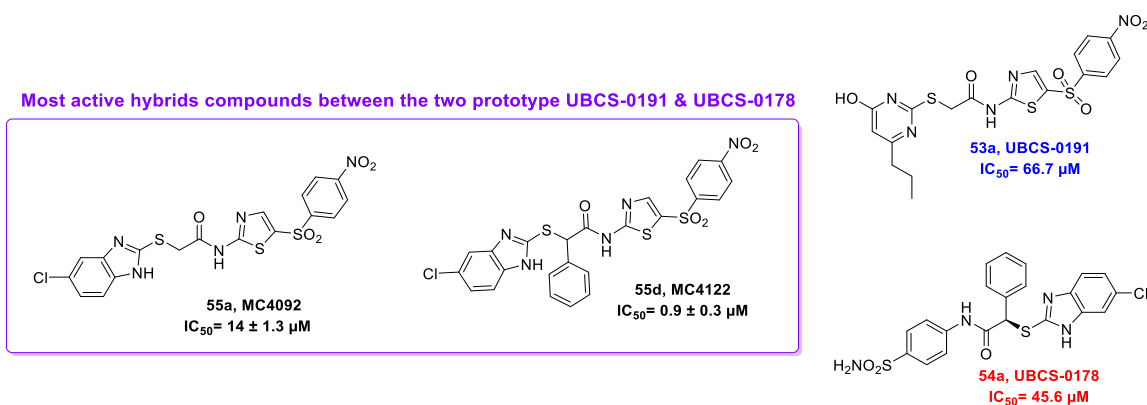
Figure 3.9. Structures of the most active hybrids compounds **55a** MC4092 and **55d** MC4122 between the two prototypes **53a** UBC-0191 and **54a** UBCS-0178 and their relative IC$_{50}$ values.

To determine sirtuin isoforms selectivity of the most active SIRT4i synthetized (Figure 3.8, 3.9), such compounds were tested against SIRT1-3,5,6 using acetylated SIRT-FdL-substrate **1** (for SIRT1-3,6) or succinylated FdL-substrate (for SIRT5), respectively, since all the sirtuins, with the exception of SIRT5, showed a strong capability to recognized and remove the acetyl group. **53j** MC4064, **53m** MC4089, **54a** MC4092 and **55d** MC4112 were analyzed at the K$_M$ value of their respective substrate, which was determined at 2 mM NAD$^+$, to make the data comparable to the SIRT4 IC$_{50}$ measurements with the Z-Lys(HMG)AMC, MC3659, **2** substrate. Testing 0, 10, 50, and 200 μM of each compound, a significant inhibition of SIRT2 by **55d** MC4122 (data not shown), **53m** MC4089, and **55a** MC4092 and for the latter two, also effects on SIRT1, have been registered (activation and inhibition, respectively). In addition, **55d** MC4122 seems to interact with SIRT3 (data not shown), and **53m** MC4089 on SIRT6 as activator, although the effects were weak and not dose-dependent. Considering that IC$_{50}$ values against SIRT4 are below 20 μM, analysis conducted at up to 50 μM are most relevant for the comparison. Under these conditions, the most potent SIRT4i, **55d** MC4122, also inhibits SIRT2 and SIRT3 (data not shown). **53j** MC4064, on the other hand, despite shows a slightly lower potency in SIRT4 inhibition then **55d** MC4122, resulted high selective, with no significant effects on other sirtuin isoforms. Thus, **55d** MC4122 can serve as a lead for SIRT4i development but requires improvement of specificity, while **53j** MC4064 can serve as a lead for SIRT4-specific inhibition yet needs to be improved in its potency.
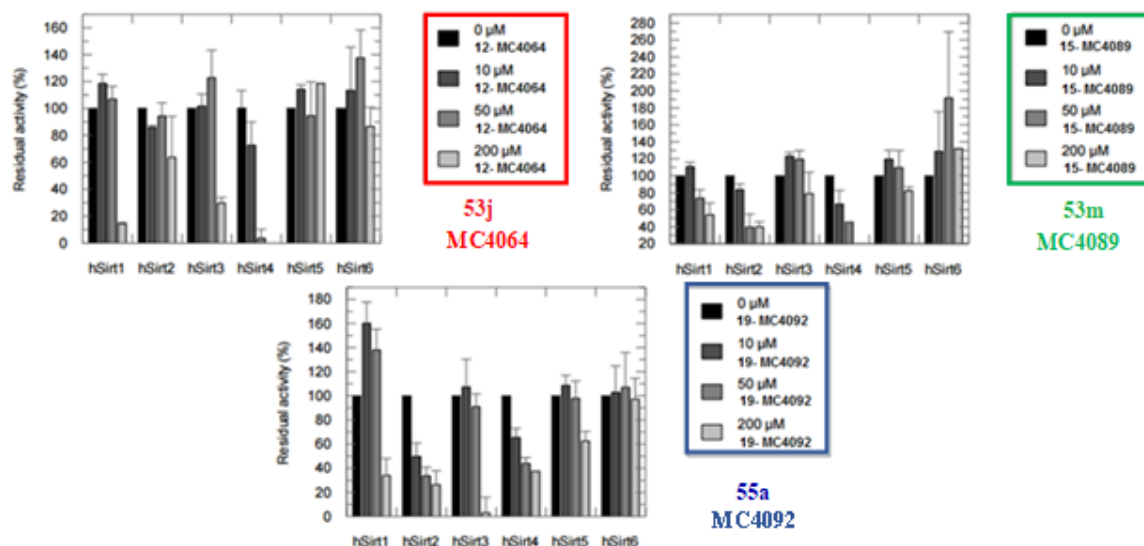
Figure 3.10. Selectivity results among different sirtuins isoforms for **53j** MC4064, **55a** MC4092 and **53m** MC4089.

3.4. Conclusions and future perspectives

Considering that this is an early stage project, it is still premature to talk about SAR, but we can make some observations about:

- Analogues of the hit compound **53a** UBCS-0191:
  - The position 6 of the 2-mercapto-pyrimidin-4(*3H*)-one ring seems to well tolerate small alkyl chain (like *n*-propyl) or bulky substituent with low conformational freedom (like 2-naphthylmethyl, 4'-biphenylmethyl) which contribute to a higher activity compared to bulky substituent with high conformational freedom (such as benzyl, phenylpropyl or phenybutyl);
  - The introduction of a phenyl group (typical of **54a** UBCS-0178) in α- position of the acetamide moiety seems to increase the inhibitory activity.

- Hybrids compounds:
  - -Cl seems to be better tolerated compared to the -NO_2 and -NH_2 group at position -5 of benzimidazole ring.

Further biological results, which will direct us towards most promising adoptable replacement or structural changes are ongoing.
However, given the chemical and enzymatic information collected so far, could be helpful to better understand our achievements provide a:

- Enantiomeric separation and potential eutomer identification since the most active SIRT4i **55d** MC4122 as well as **53m** MC4089 were obtained as racemic mixtures;
- -NO_2 group replacement given its well-known related toxicity (*in vivo* is reduced to the strong reactive species hydroxylamine, potentially inducing carcinogenesis);
- Bioisosteric replacement of the aromatic rings with heterocyclic systems in order to evaluate the electronic request;
- Increase in the length of the molecule through the introduction of further methylene in the chain in the α-position of the acetamide moiety, to better occupy the active site cavity of the enzyme rising the molecular stability and potency;
- -OH group typical of compound **53j** MC4064 and **53m** MC4089 could be alkylated in order to exploit new hydrophobic interactions since seems that such group is not involved in key hydrogen bond interaction;
- Introduction of the phenyl ring in in the α-position of the acetamide moiety also in **53j** MC4064 (Figure 3.11) to better investigate its inhibitory capability and selectivity among the sirtuins family.
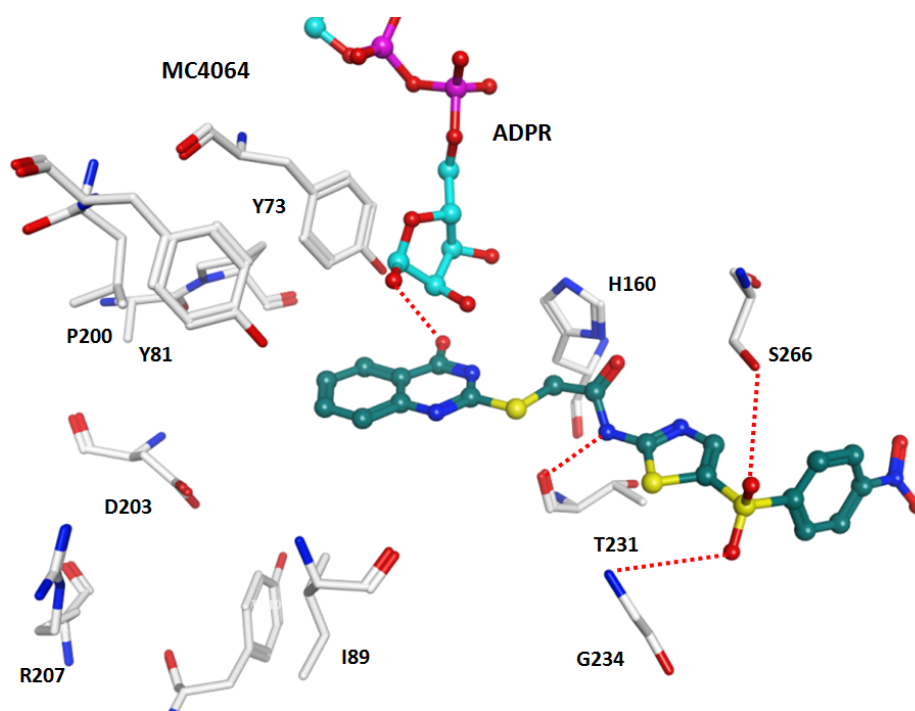
Figure 3.11. Docking of the most selective synthetized SIRT4i **53j** MC4064 inside SIRT4 active site.

3.5 Methods

Inhibitors assays were conducted with a high-throughput fluorescence-based assay using Z-Lys(HMG)AMC, MC3659, **2** as SIRT4 substrate. 1 μM hSirt4 was mixed with the assay buffer (25 mM Tris/HCl 150 mM NaCl, pH= 7.5), NAD$^+$ (final assay concentration reached 500 μM), MC3659 **2** (final assay concentration reached 500 μM) and the respective SIRT4i **53b-p**, **54c,d** and **55a-d** in DMSO at various concentrations (10-100 μM) or DMSO as a negative control (final DMSO concentration 5–20% (v/v)). The mixture was incubated at 37 °C for 20 min, with agitation at 150 r.p.m. The potential deacylation was then highlighted by the addition of FdL-developer trypsin (final concentration reached 10 mg/mL Trypsin + 2 mM NAM **19)** to cleave **57** AMC from **2** MC3659 after SIRT4-mediated removal of the HMG portion from the lysine residue to yield the fluorescence signal. NAM **19** was then added in order to block further sirtuin reactions during development and the mixture was then incubated for tryptic digestion of the deacylated product to release the fluorophore (45 min at rt). The fluorescence intensity was measured in a microplate reader (BMG Polarstar, λ_{ex} 365 nm, λ_{em} 465 nm). The amount of inhibition was determined using the mixture with only DMSO as standard. IC$_{50}$ values were determined with GraphPad Prism software using a non-linear regression to fit the dose–response curve. FdL assay procedure is schematically represented in Fig. 3.12
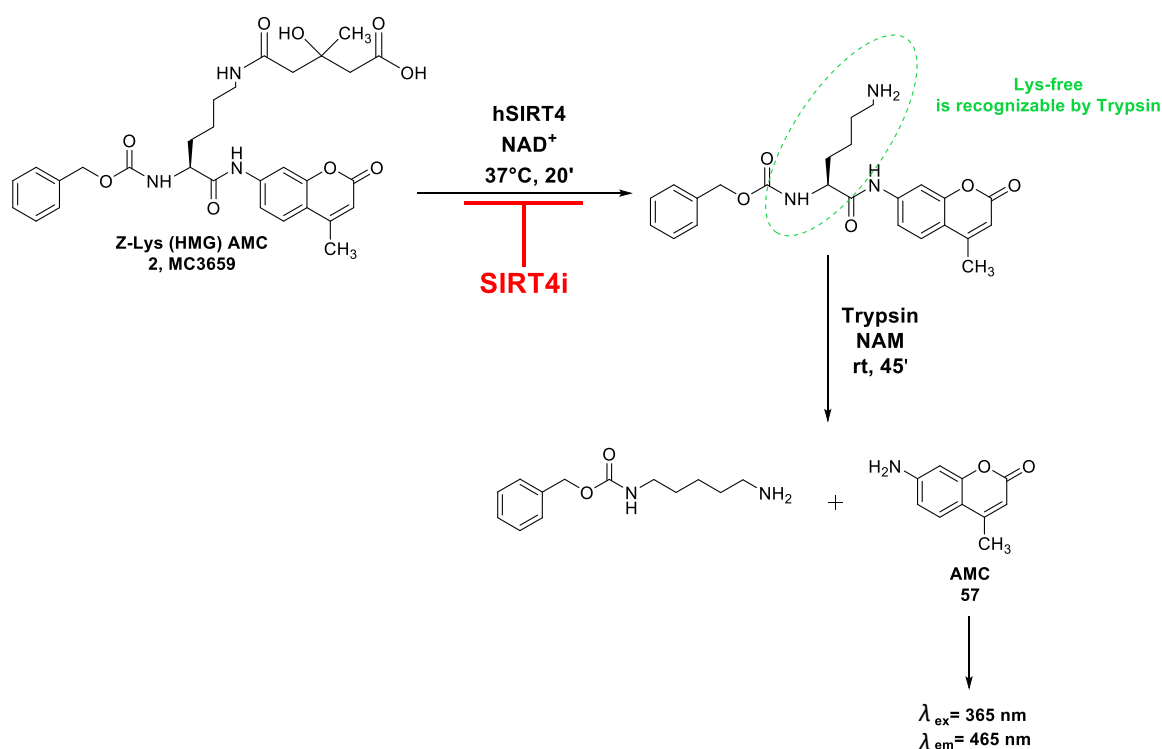
Figure 3.12. Graphic representation of the deacylation of the substrate MC3659 **2** and consequent fluorescent emission during the assay. If a tested molecule (**53b-p**, **54c,d** and **55a-d**) acts as SIRT4i, the deacetylation process will be less efficient and will result in a lower fluorescent emission.

Concerning selectivity studies for **53j** MC4064, **53m** MC4089, **54a** MC4092 and **55d** MC4112, assays with hSIRT1, hSIRT2, hSIRT3 and hSIRT5 were performed with the same concentration of NAD$^+$, but FdL substrate concentrations were adapted to the K$_M$ for each sirtuin/substrate pair. hSIRT1, hSIRT2, hSIRT3 and hSIRT6 were assayed using 50, 200, 40 and 300 μM FdL1, respectively. hSIRT5 was tested using 40 μM succ-FdL5.

Reaction times were decreased to 7 min for all sirtuins except hSIRT6, for which reaction time was elongated to 30 min due its weak activity.

Chapter 4

4.1 Epi-PROTACs approach applied to new epigenetic targets Research project

As previously discussed in Chapter 2, the degradation of disease-related proteins mediated by PROTACs is emerging as a novel promising therapeutic method.

The most revolutionary aspect of such chimeric molecules is their capability to work in a catalytic manner inducing a long-lasting effect as well as the suppression of all the target functions until its resynthesis.[600] Furthermore, if a "classical" inhibitor blocks only one function, POI degradation provide a strong impact towards all its functions including allosteric and structural ones.

As mentioned above, PROTACs technology could be particularly promising in epigenetics, in fact, in addition to reach a potential selectivity towards the different isoforms that characterize the selected epi-targets, opens the possibility to investigate the (structural) roles that the targeted epi-POI could play, also within specific multicomponent complexes. In this framework, only degraders of bromodomains and BET family members,[557,558,561,562,573,582,585,592,611,612] PCAF and GCN5,[599] SIRT2,[580] and HDAC6,[568,574] EED/PRC2[535] are reported to literature so far.

In order to overcome these limits, we focused our efforts on the design and synthesis of novel epi-PROTACs able to induce the degradation of epi-targets for which no PROTACs degraders have been yet designed. In addition to potentially reach an increased potency, selectivity and time of action compared to classical epigenetic modulators, such novel chimeric compounds could be use as biological tools to deeply evaluate the effects consequent to the induced degradation of the e-POI in a specific biological system.

In this section, our recent progresses regarding the application of PROTACs in the epigenetic field will be discussed, specifically concerning the design of LSD1, Jmjc KDMs, p300 and EZH2 targeting PROTACs.

4.2 Novel epi-PROTACs hitting "erasers"
4.2.1 The case of LSD1

As previously described, LSD1 is a FAD-dependent amine oxidase which removes methyl moieties from histone H3K4me1/2 (an active transcriptional mark) and H3K9me1/2 (a repressive transcriptional mark) as part of the CoREST complex, along with CoREST1 and HDAC1. Histone methylation pattern covers a main role in genetic stability and gene regulation processes and its dysregulation has been registered in different types of tumor. Several pieces of evidence highlighted that an OE of LSD1 is closely associated with stem cell biology, EMT, cell differentiation, malignant transformations, autophagy, senescence, metabolism and neurodegenerative diseases.[613,614]

As shown in Figure 4.1a, LSD1 is recruited at the level of target genes by a different number of transcription factors such as SNAIL, HP1, NuRD, CoREST etc. promoting the transcriptional repression *via* the demethylation of the H3K4me2 which act as an activation mark. In addition, LSD1 also provide the demethylation of the repressive mark H3K9me2 as coactivator with the AR or ER (Figure 4.1b).
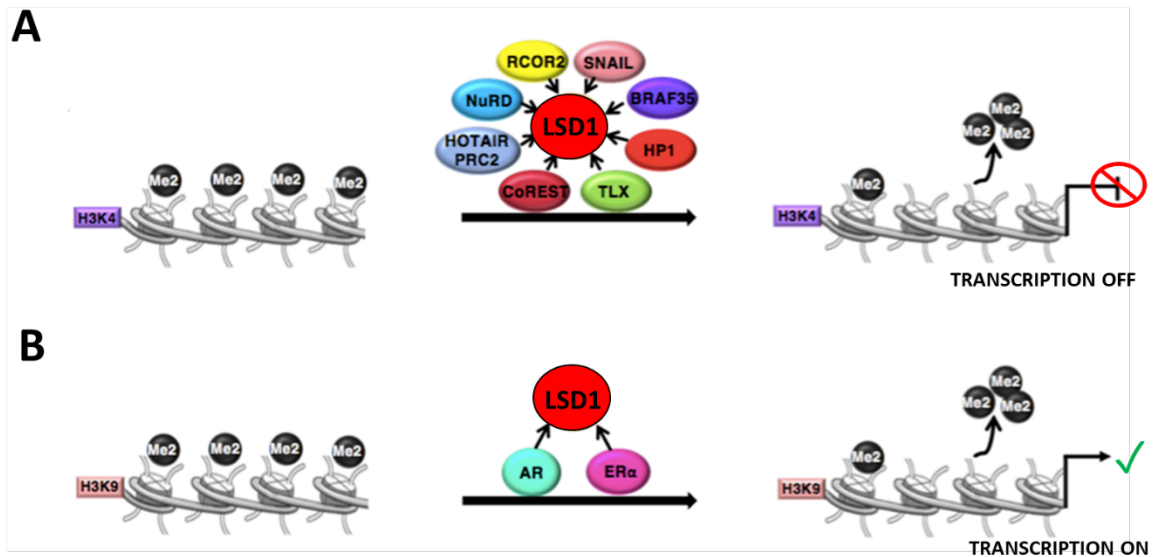
Figure 4.1 Role of LSD1 in the regulation of the H3K4me1/2 (a) and H3K9me1/2 (b) patterns. Adapted from Majello *et al*. *Cancers*, 2019.[614]

LSD1 is target of different post-translational modifications that alter its stability or activity expanding the roles that this protein can cover in the regulation of transcription and gene expression.[615,616] While LSD1 Ser112 phosphorylation catalysed by the PKCα (Protein kinase C alpha) seems to be crucial for its recruitment on E-cadherin promoter,[617] LSD1 acetylation by the acetyltransferase MOF is a specific marks of epithelial cells and may be critically involved in LSD1-induced EMT.[618]

LSD1 is also responsible for the demethylation of specific lysine residues of different non-histones proteins such as p53, STAT3, DNMT1, RB1, E2F1, MTA1, MEFD2 HSP90, HIF-1α, ERα and AGO2 (Figure 4.2) thus modulating both the function and stability of the aforementioned proteins.[619] In particular, for example, LSD1 enhances p53 and STAT3 functional activity without inducing changes in their expression levels; it stabilizes E2F1, MEFD2 and HIF-1α and destabilizes the MYPT1 protein. How LSD1 influences different cellular processes by the non-histone methylation events is not yet clearly understood.
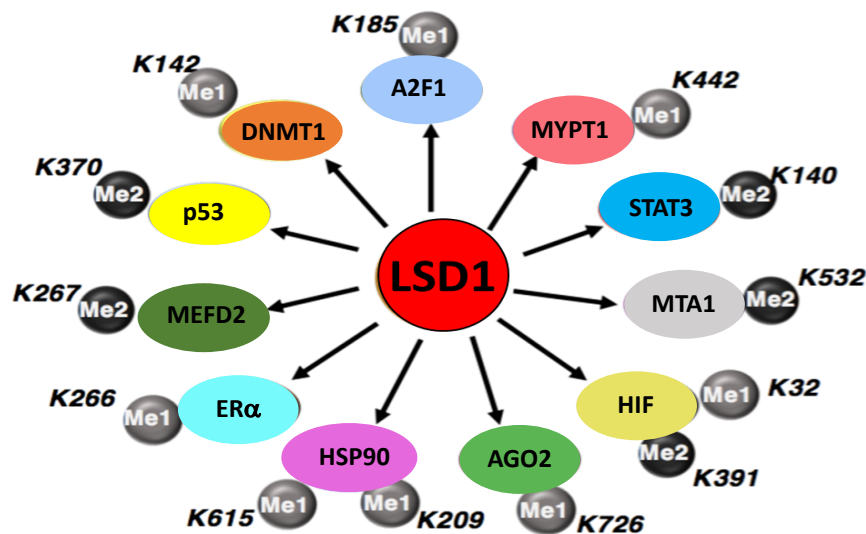
Figure 4.2 Schematic representation of non-histone LSD1 demethylating targets. Adapted from Majello *et al*. *Cancers*, 2019.[614]

Since its OE in both hematologic (AML) and solid tumors (brain, lung, prostate, breast cancer) correlates with poor prognosis, LSD1 has been proposed as a druggable target.

In 2018, Sehrawat et al.[620] have proven that, in prostate cancer, LSD1 promotes survival of CRPC cells in a demethylase independent manner. Inactivation of LSD1 enhanced the expression of a set of prostate cancer lethal genes (mitosis, cell-cycle and ESC identity genes) highlighting its role as a driver of proliferation and survival in this condition.

Sehrawat and co-workers also showed that irreversible LSDi based-treatments failed to suppress the survival of prostate cancer cells which resulted, instead, sensitive to LSD1 RNAi treatment. On the contrary, treatment based on the LSD1 allosteric inhibitor SP-2509[621,622] provided the reduction of cell viability in such tested models as well as increased caspases activity and apoptosis events.

This evidence was supported by further *in silico* computation docking analysis with SP-2509 and LSD1 which showed that, in addition to act as an allosteric inhibitor of LSD1, SP-2509 also reduces the half-life of LSD1 measured after treatment based on the inhibitor of the protein synthesis cycloheximide, explained by the fact that SP-2509 also decreases LSD1 protein stability. In addition, SP-2509 blocks the interaction between LSD1 and one of the key regulators of tumorigenesis ZNF217, an effect typically unreachable with the other LSD1i but visible after LSD1 RNAi based-treatment.

The mechanism allowing the upregulation of LSD1 in tumors in still not clearly clarified. A unbiased siRNA screening against all the human deubiquitinases conducted by Wu and co-workers[623] identified USP28 as a *bona fide* LSD1 deubiquitinases. USP28 interacts and stabilizes LSD1 through its deubiquitination, in fact, if an OE of LSD1 correlates with an OE of USP28, a knockdown of UPS28 resulted in consequent LSD1 destabilization, thus providing the suppression of stemness characteristics *in vitro* as well as the repression of tumorigenicity *in vivo* (which can be rescued by ectopic LSD1 expression).

Importantly, these recent works suggest that, decide to target LSD1 protein stability and indirectly its demethylase-independent functions, rather than only its catalytic activity, is a rational strategy and new weapon to fight prostate cancer. However, until today, excluding SP-2509 for which further studies have been required, this goal is not achievable with currently known therapies, suggesting that PROTACs approach could be strongly promising in this field. Until now, a huge number of both reversible or irreversible LSD1i has been reported to literature.[624]

Among these, worthy of note is a the well-known MAO/LSD1 inhibitor TCP **24** (Figure 4.3) as well as one of its most promising *N*-alkylated derivative GSK2879552 **26** (Figure 4.3), which were previously mentioned in the Chapter 1 (section 1.5) since both are in clinical trial (Table 1.5).[625] TCP **24** is in phase I/II for the treatment of acute myelogeneous leukemia (NCT02261779, NCT02717884) and GSK2879552 **26** was in phase I clinical trial for the treatment of SCLC (NCT02034123) and AML (NCT02177812) until January 2019, but the correlated risks, in both cases, did not support the prosecution of the clinical study. Kinetic data showed that the inhibition mechanism of these molecules involves the establishment of a first reversible interaction with the active site of LSD1 that evolves toward an irreversible and time-dependent inactivation of such enzyme providing an irreversible adduct with the FAD moiety. However, despite the similarity between MAOs and LSD1, inactivation mechanism of such enzymes mediates by TCP **24** involves the formation of different adduct with FAD. In particular, the phenyl ring of the adduct FAD-TCP **24** in LSD1 is located in hydrophobic pocket and does not take part in interactions with surrounding residues. This evidence suggest that TCP **24** analogues characterized by additional hydrophobic substitutions on the phenyl ring could reach a more potent and selective LSD1 inhibition.

The orally active LSD1i GSK2879552 **26** is highly selective for LSD1 (Ki= 1.7 μM) over LSD2 and MAOs. The antitumor activity of GSK2879552 **26** resulted particularly pronounced in AML and SCLC cell lines, in which, in fact, an OE of LSD1 is widely reported.[626,627]

Structural analysis of GSK2879552 **26** pointed out that, while the removal of carboxylic acid function does not affect its inhibitory activity in both term of efficiency and selectivity, the acetylation of the -NH group connected to the cyclopropane ring correlates with the lack of the activity. Starting from these findings we decided to functionalize the irreversible LSD1i GSK2879552 **26** at the level of its carboxylic acid residue for the attachment of the E3 ligase ligand 4-hydroxythalidomide **36f** moiety though pegylated linkers of different lengths in order to obtain a series of **36f** CRBN-based LSD1 targeting PROTACs (**70a,b**, Figure 4.3) potentially able not only to induce the degradation of LSD1, but also the indirect disruption of the entire CoREST complex. In addition, in order to achieve the same results, a more chemically manageable derivative of TCP **24** harboring an -NH$_2$ group in the *para* position of its phenyl ring (*p*-NH$_2$, TCP, **69,** Figure 4.3), which resulted functionalisable for the introduction of the same linkers mentioned above, has been used as warhead for the synthesis of another series (**71a,b**, Figure 4.3) of **36f** CRBN base LSD1-targeting PROTACs.

24, TCP
irreversible LSD1/MAOi

69, *p*-NH$_2$-TCP
irreversible LSD1/MAOi

26, GSK2879552
Ki= 1.7 μM
irreversible LSD1i
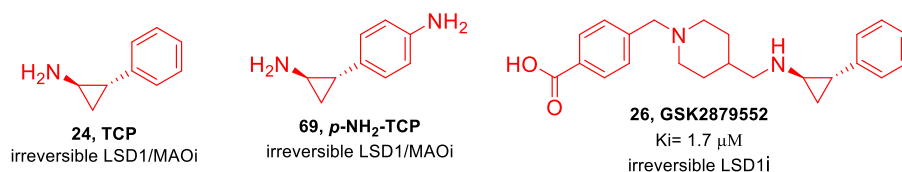
CRBN-based LSD1 targeting PROTACs with different pegylates linkers

Warhead: GSK2879552

70a,b

Warhead: *p*-NH$_2$-TCP

71a,b

LINKERS:

n=1,2
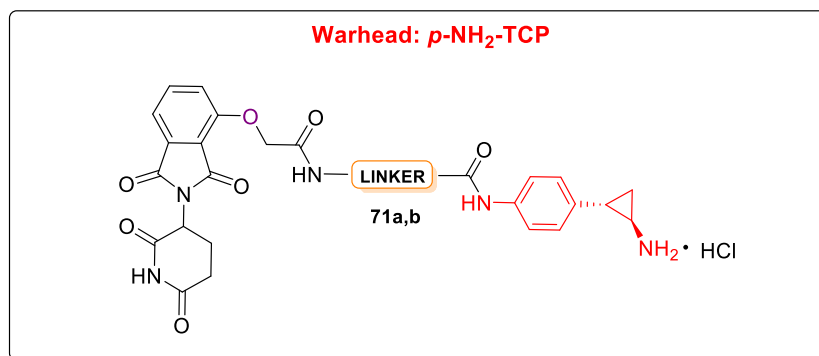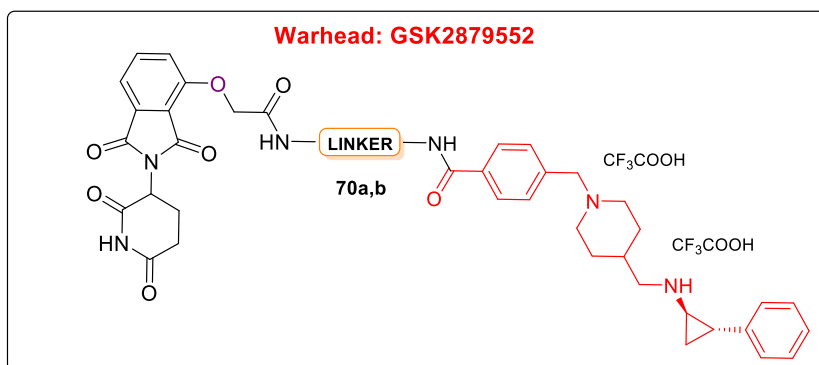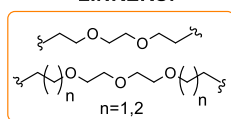
Figure 4.3 New CRBN-based LSD1 targeting PROTACs deriving from the structures of the TCP **24** analogues GSK2879552 **26** and p-NH$_2$-TCP **69**.

119

In order to avoid the possibility of loss the catalytic profile typical of PROTACs approach, we also selected a reversible LSD1i, known as GSK-690[628] **72** (Figure 4.4) as new warhead for the design of another series of **36f** CRBN-based LSD1 targeting PROTACs (**73a,b**, Figure 4.4). GSK-690 **72** resulted from systematic modification and replacement involving the scaffold of the irreversible LSD1i TCP **24**. SAR studies highlighted that the pyrrolidine ring of the GSK-690 **72** could represent a perfect portion where the two different pegylated linkers may be introduced since it does not take part in key interactions in the active site of the enzyme.

Despite its strong affinity and inhibitory capability towards LSD1, GSK-690 **72** application is limited by its lack of selectivity since it interacts also whit *h*ERG ionic channels as well as with MAOs enzymes. In this framework, PROTACs approach may be useful also to overcome the limitations connected to its promiscuous range of interaction.
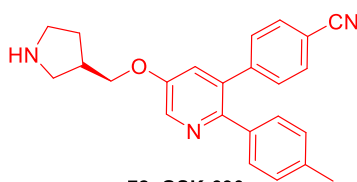
72, GSK-690
Kd=9 nM, IC$_{50}$= 37 nM
reversible LSD1i

CRBN-based LSD1 targeting PROTACS with different pegylated linkers
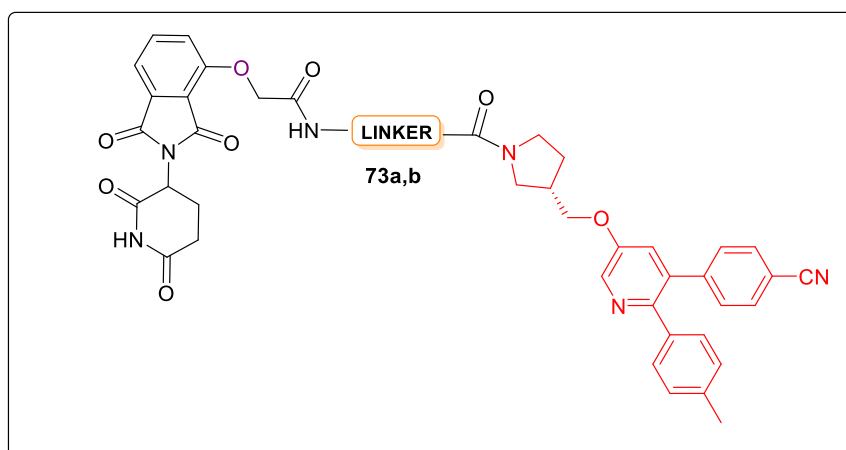
LINKERS:
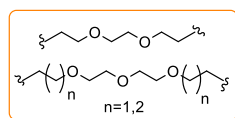
Figure 4.4 New CRBN-based LSD1 targeting PROTACs deriving from the structure of the reversible LSDi GSK-690 **72.**

4.2.2 The case of JmjC KDMs subfamilies

As previously described in the relative section (1.2.5.2.2), histones demethylation, in addition to being catalysed by the FAD-dependent KDM1, also involves the 2OG/Fe(II)-dependent JmjC KDM2-7 subfamilies, which catalyse the demethylation of mono-, di- and tri-methylated lysines at multiple sites.[201]

Several are the physiological and pathological processes regulated by JmjC KDMs such as neural function and/or development, autism, X-linked mental retardation, and midline defects.[629–632]

To date, the role of the JmjC KDMs in cancer still need to be clarified. In fact, despite not for all the Jumonji KDMs an involvement in this disease could be proven so far, some pieces of evidence have shown that JmjC KDMs can be both genetically amplified and afterwards down-regulated in cancer (Table1.1).[213,234,235]

In this scenario, further studies are still needed to clearly understand the physio/pathological role as well as the substrate specificity of the different JmjC KDM isoforms.

Several evidences support that the biological roles of KDMs enzymes cannot be simply described as "erasers" of histone methylation process. In fact, all the human KDMs are predicted to be characterize also by non-catalytic "binding" domains. Their interaction with chromatin/nucleosomes could be best considered as protein-protein/nucleic acid interactions in which the histone methylation pattern is a component.

Most, if not all JmjC-type KDMs are involved in transcriptional chromatin or complexes, showing, not only catalytic properties but also structural ones.[204]

Starting from these findings, the PROTACs approach could be an innovative strategy to hit this class of histone demethylases as well to better investigate their structural roles.

A huge number of JmjC KDMs inhibitors have been reported so far.[200] In order to obtain these results we focused our attention on the broad-spectrum 2-OG oxygenase inhibitor 5-carboxy-8 hydroxyquinoline (IOX1, Figure 4.5) **74** which belongs to one of the most studied class of KDMi characterized, precisely, by the hydroxyquinoline scaffold as a common feature. IOX1 **74** shows a (sub-)micromolar inhibition *in vitro* potency against KDM2A, KDM3A, KDM4A/C/D/E, KDM5C, KDM6A and PHF8. The mechanism of action of such KDMi is connected to its capability to chelate Fe(II) in a bidentate manner involving its phenol oxygens atom as well as its quinoline nitrogen (as highlighted in figure 4.5). The carboxylic acid function present in position -5 of the quinoline ring interacts with Lys206 and Tyr132 residues typical of the active site of this class of enzyme.[633]

GSK-J1 **75** (Figure 4.6), instead, is the first small-molecule reported to literature as selective KDM6 family (KDM6A and KDM6B) nanomolar competitive inhibitor of the two cofactors, but not of the substrate.[634] GSK-J1 **75**, in fact, is able to chelate the active site Fe(II) through the nitrogen atoms of its pyridine and pyrimidine rings (as highlighted in figure 4.6) while its propanoic acid-side chain acts as a mimetic portion of 2-OG side chain binding.

Using the carboxylic function of both just mentioned KDMi as attachment point for the introduction of pegylated linkers of different lengths, we were able to synthetize **36f** CRBN-based PROTACs **76a,b** (Figure 4.5) and **77a,b** (Figure 4.6) targeting this class of epigenetics "erasers".
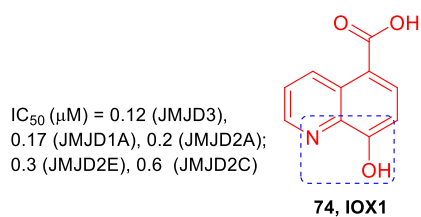
IC$_{50}$ (μM) = 0.12 (JMJD3), 0.17 (JMJD1A), 0.2 (JMJD2A); 0.3 (JMJD2E), 0.6 (JMJD2C)

74, IOX1

CRBN-based KDMs targeting PROTACs with different pegylated linkers

76a,b

LINKERS:

n=1,2
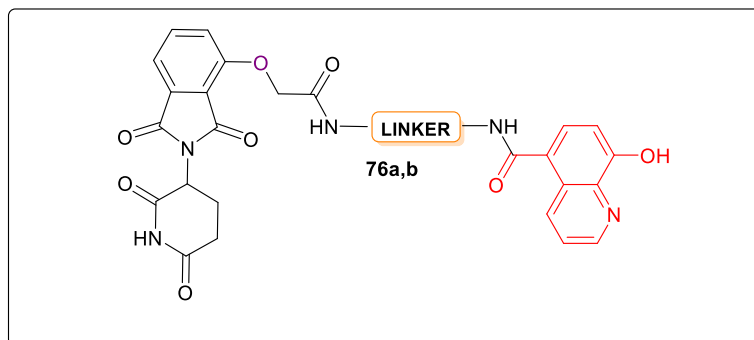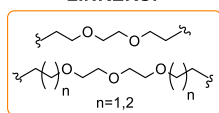
Figure 4.5. New **36f** CRBN-based KDMs targeting PROTACs **76a,b** deriving from the structure of the broad-spectrum KDMi IOX1 **74**.
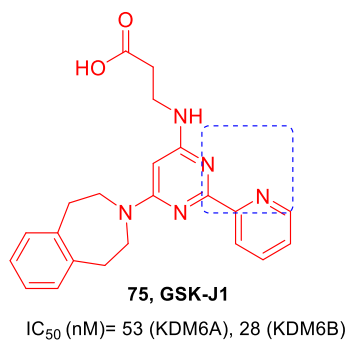
75, GSK-J1

IC$_{50}$ (nM)= 53 (KDM6A), 28 (KDM6B)

CRBN-based KDM6 targeting PROTACs with different pegylated linkers

77a,b

LINKERS:

n=1,2
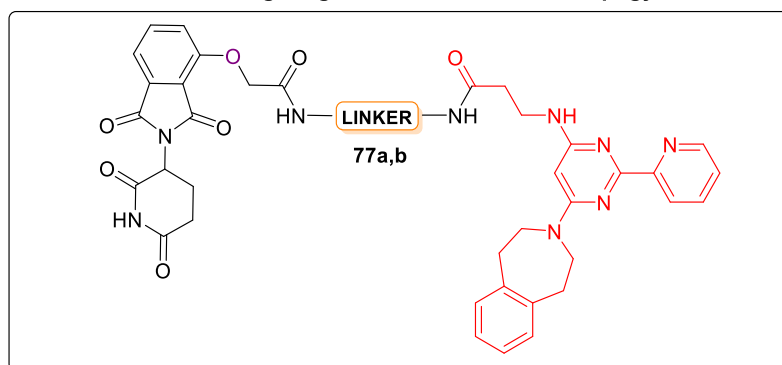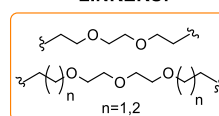
Figure 4.6. New **36f** CRBN-based KDMs targeting PROTACs **77a,b** based on the structures of the KDM6i GSK-J1 **75**.

4.3   Novel epi-PROTACs hitting "writers"

4.3.1. The case of p300

As previously described in section 1.2.6.1, PCAF[593] is characterized by an acetyltransferase and an "acetyl-reader" activity. Its functions cover a wide range of possibilities, in fact it may be related to the modulation of chromatin structure and several cellular processes including differentiation and DNA damage repair mechanisms. P300 is also involved in various inflammatory events[245,594,595] such as inflammatory cytokines production (TNF and IL-6), supporting the possibility of use p300 as a target for the treatment of different inflammatory diseases.[596,597]

The c-Myb oncogene is a sequence-specific DNA-binding transcription factor that plays a pivotal role in the regulation of hematopoiesis processes resulting highly expressed in AML. Pattabiraman et al.[635] showed that the interaction between the co-activator p300 and c-Myb is fundamental for its intrinsic transforming activity in vitro. P300 is recruited by c-Myb through its KIX domain, that is able to recognize and bind the LXXLL amino-acid motif typical of c-Myb.[636] Recently was also highlighted that p300 is required for the c-Myb induced repression of different genes involved in myelo-differentation (Figure 4.7).[637]
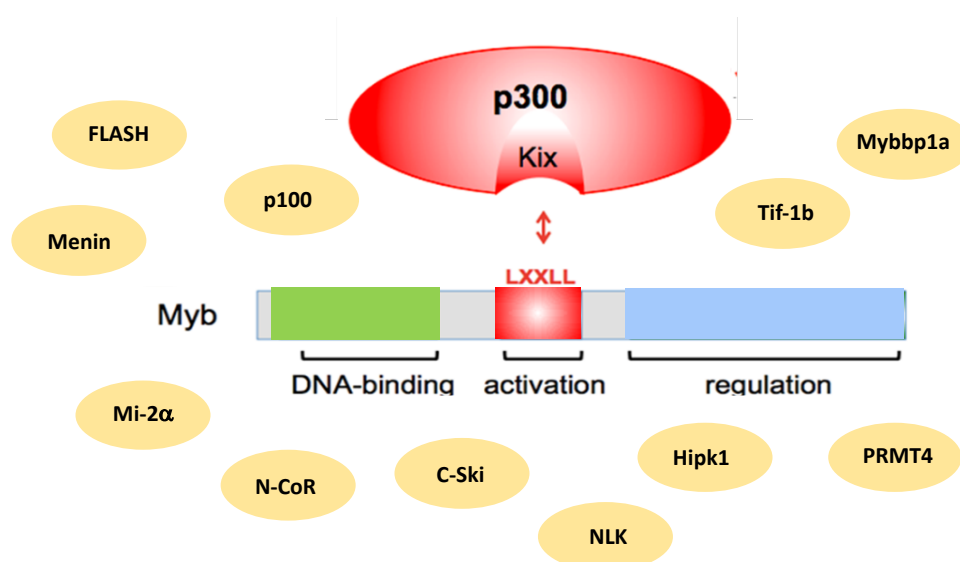
Figure 4.7. Schematic representation of the p300/c-Myb interaction showing the genes that resulted inactivated. Adapted from Uttarkar et al. Mol. Cancer Ther., 2016.[637]

Pattabiraman et al.[635] also proved the importance of this interaction in vivo using two mutant mouse models, strain Plt6[638] and Booreana,[639] that show mutation in p300 and c-Myb, respectively, thus interfering with the aforementioned c-Myb/p300 pathway.

The use of these mouse models demonstrated that the abrogation of the c-Myb/p300 association strongly blocks leukemogenesis and transformation by both MLL and AML1-ETO fusions, suggesting that targeting such interaction may be a new therapeutic anti-cancer strategy.

In 2016 Uttarkar et al.[637] reported plumbagin and different naphtoquinones as the first small molecules acting as a c-Myb inhibitors by binding the c-Myb transactivation domain thus distrupting the interaction between p300/c-Myb (Figure 4.8). These molecules suppressed the c-Myb target genes expression enhancing the differentiation state of HL60 myeloid leukemia cell line. In addition, they also reported that a triterpenoid isolated from roots of Tripterygium wilfordii (Thunder God Vine), called celastrol, is a potent inhibitor of c-

Myb/p300 interaction due to its capability to bind the hydrophobic groove on the surface of the p300 KIX domain thus acting as a competitor of *c*-Myb (Figure 4.8). Celastrol induces the down-regulation of *c*-Myb related genes in HL60 cells responsible of apoptosis and differentiations, inhibits AML proliferation in cell belonging to both mouse model and human patient, prolonging, in addition, the survival of mice in an *in vivo* model of aggressive AML.[640]

Therefore, we hypnotized that the design of p300 targeting PROTACs may be a rational approach to develop a potential and selective new therapy for the treatment of AML. In fact, the chemical nature of both plumbagin and celastrol do not ensure a full selectivity of action.
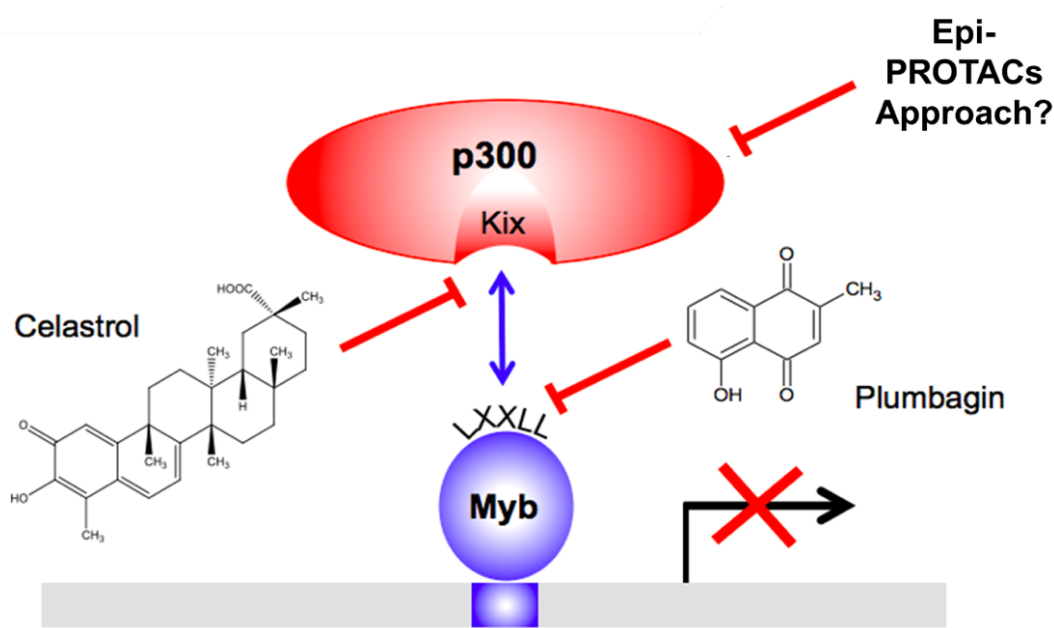
Figure 4.8. Structures and relative targets of the only small molecule (celastrol, plumbagin) reported so far able to act as disruptors of the p300/*c*-Myb interaction. In this framework the PROTACs approach could result very promising. Adapted from Uttarkar *et al*. *Mol*. *Cancer Ther*., 2016.[637]

Among all the p300i reported to date we selected the pyrazolone-based p300i C646 **78** (Figure 4.9), which results the most potent competitive non covalent p300i (Ki=460 nM and an IC_{50}=1.6 μM) known so far. C646 **78** has been discovered through structure-based virtual screening analysis focused on commercially available small molecules docked into the pocket where Lys–CoA binds p300.[641] C646 **78** strongly blocks H3 and H4 acetylation as well as proliferation in lung cancer and melanoma cell lines, inhibiting, in addition, colony formation and cell growth associated with a reduction of histone acetylation levels in AML1-ETO positive leukemia cells line.[641,642]

However, this p300i has been proved to be non-selective since it also inhibits other KDACs, thus opening the possibility that its cellular effects could be also a consequent of other putative interactions.[643] C646 **78** is also known to show strong immunomodulatory effects on macrophage in bacterial phagocytosis (down-regulating the activity levels of FcγR III/II and CR3 thus leading the phagocytic ability against *E*. *coli*) as well as in the production of LPS-induced pro-inflammatory cytokines.[644]

SAR showed that the carboxylic acid function takes part in key binding interactions. However, the loss of its activity is only consequent to the reduction or oxidation (to carbonyl) of its exomethylene residue, highlighting that the planarity and electronic characteristics of the conjugated system are critical for the activity. As previously mentioned, C646 **78** is a competitive non covalent inhibitor of p300, but its α,β unsaturation

makes it a susceptible to Michael addition. In fact, several pieces of evidence showed that C646 **78** reacts with different protein containing specific cystein residues that may contribute to its registered cells effect.[641]

Using the carboxylic function of the C646 **78** as attachment point for the introduction of pegylated linkers of different lengths, we were able to synthetize a series of **36f**-CRBN-based p300 targeting PROTACs **79a,b** (Figure 4.9).

78, C646
Ki=460 nM
IC$_{50}$=1.6 μM

CRBN-based p300 targeting PROTACs with different pegylated linkers

79a,b

LINKERS:

n=1,2
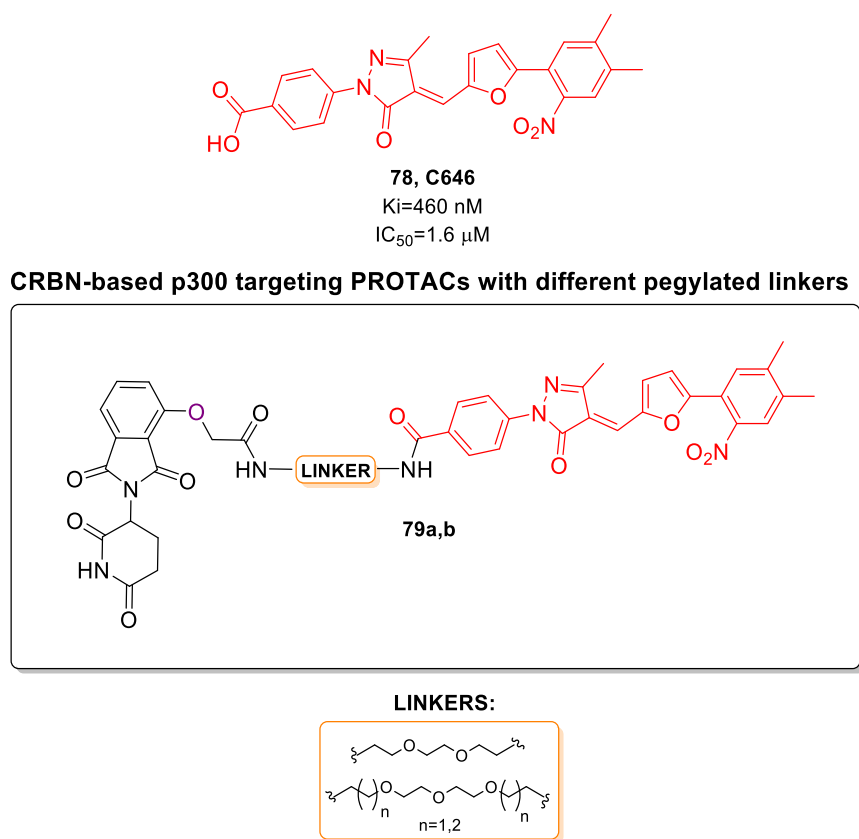
Figure 4.9 New **36f** CRBN-based p300 targeting PROTACs **79a,b** deriving from the structure of the competitive non covalent p300i C646 **78**.

4.3.2 The case of EZH2

As previously exposed (section 1.2.5.1.), EZH2 is the catalytic subunit of the PRC2 complex and is the only enzyme (known to date) able to catalyze the methylation (me1/me2/me3) of ε-NH2 group of H3K27 using SAM as a co-substrate, thus silencing the expression of targeted genes.

Despite EZH2 is essential for different physiological functions such as embryonic development and differentiation, high levels of H3K27me3 have been registered in both hematological and solid cancers, due to EZH2 OE and/or mutation which promote proliferation, cell survival, EMT, and drug resistance. Specifically, somatic heterozygous mutations of A677 and Y641 (which is the most frequently observed) residues within the catalytic SET domain of EZH2 has been registered in follicular lymphoma as well as in DLBCL.[177,645–647] EZH2 is best known as an PRC2-dependent epigenetic silencer, however, recent pieces of evidence have suggested that EZH2 might also acts in a histone and PRC2 independent manner as well as a transcriptional activator.[648] Beyond playing as a histone modifier, in fact, EZH2 can methylate non-histone proteins, for example STAT3 in glioblastoma (leading, in this way, to enhanced STAT3 phosphorylation thus promoting its tumorigenicity) or can takes part, as a co-activator, in androgen receptor associated complexes in castration-resistant prostate cancer.[141,175,176] Additionally, ER-negative basal-like breast cancer, EZH2 binds NF-*k*B forming a complex which correlates with the transcriptional activation of downstream genes involved in tumorigenesis (Figure 4.10).[649]
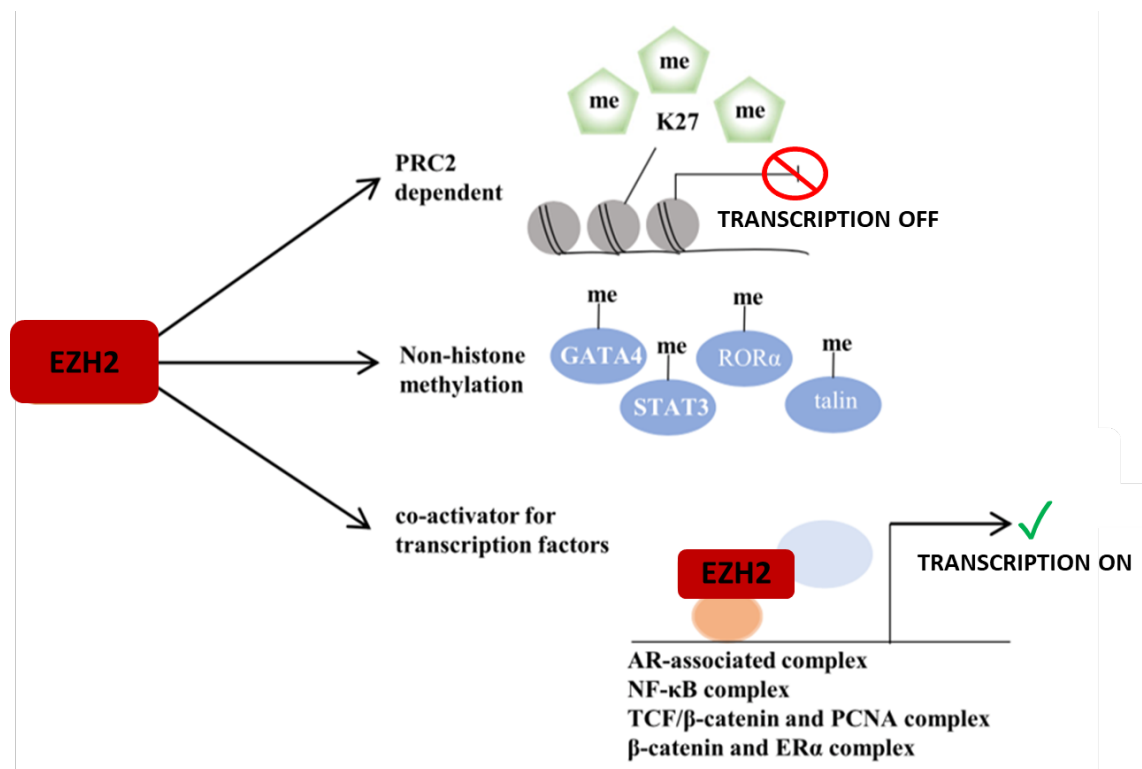
Figure 4.10. Overview of the whole known EZH2 functions. Adapted from Gan *et al*. *Biomark Res*, 2018, 6: 10.[648]

Recent proofs support the necessity of achieve a superior anticancer effect by not only inhibiting the enzymatic role of EZH2 but also promoting a full blockade of its activities in order to completely inhibit its oncogenic functions.[650]

Kim et al. [650] highlighted the above-mentioned PRC2/methyltransferase independent non-catalytic role that EZH2 covers occupying the AR promoter in PCa thus acting as a transcriptional activator.

EZH2 knockdown in C4-2B prostate cancer cell resulted more effective than its enzymatic inhibition or AR antagonist agent based-treatments in cell growth assay, thus giving proof of the necessity to induce a full blockade of EZH2 functions. Since no EZH2 degrader has been reporter to literature so far, Kim and coworkers were able to recreate the same effect by using a combination based on the EZH2 SAM-competitive inhibitor GSK126 **20** in association with the AR antagonist ezetimibe (in order to target one key downstream pattern of EZH2-activating role in PCa) thus obtaining a strong suppression of PCa progression *in vitro* and *in vivo*. These preclinical data could suggest, in addition to a possible clinical applications of AR antagonist/EZH2i combination based-treatment in in castration-resistant prostate cancer, the need to design EZH2 degrader agents.

In a wide variety of tumors, mutations of genes encoding for the subunits that compose SWI/SNF chromatin remodelling complexes have been registered due their pivotal role in remodel nucleosomes modulating the transcription process.[651] In a recent work Kim et al.[652] highlighted that EZH2 is fundamental in various cancer cell lines and xenograft harboring mutations of different subunits of SWI/SNF complexes, including ARD1A, SMARCA4 and PBRM1. Such cancer cells resulted mainly dependent upon a non-catalytic role of EZH2. To prove this, Kim and co-workers compared an approach based on the recently described stabilized alpha–helix of EZH2 (SAH–EZH2) stapled peptides which strongly blocks H3K27me3 by disrupting the interaction between EZH2 and EED within the PRC2,[653] with those focused on EZH2i (GSK126 **20**) based-treatment.

In the first case, they obtained a full inhibition of PRC2 functions due to the EZH2 degradation induced by the stapled peptide, eliminating, in this way, not only the catalytic activity related to EZH2 but also any structural contributions. This reached condition resulted in a strong decreasing of SWI/SNF mutants cancer cell lines growth, also in those (H1299 and RCC4) that were resistant to EZH2i-based treatments. Such data suggested that, in RCC4 and H1299 cell lines, cell growth is dependent upon EZH2 but independent from its catalytic activity. This evidence, in addition to prove a shared dependency of cancer with genetic alterations in SWI/SNF subunits, also suggest that EZH2i cannot fully suppress the oncogenic role of EZH2 supporting the mechanistic requirements needed for the next–generation of EZH2-targeting agents for an optimal blockade of the pathologic PRC2 activities.

In this framework, the gene encoding for the SWI/SNF subunit ARID1A, shows one of the highest mutation rate across many cancer types. For example, ARID1A is mutated in over 50% of ovarian clear cell carcinomas, for which no effective therapy is available to date. Bitler et al.[654] reported that the catalytic inhibition of EZH2 reached by EZH2i, for example by GSK126 **20**, selectively acts in a synthetic lethal manner in ARID1A- mutated ovarian cancer cells (also *in vivo*), in which, the ARID1A mutatuated condition correlated with the EZH2i-response. In particular, they highlighted that EZH2 and ARID1A are antagonistic in regulating PI3K-interacting protein 1 gene (PIK3IP1, a negative regulator of PI3K which controls cell division, motility, and survival in most cell types) expression which results upregulated after GSK126 **20**-based treatment, thus contributing to the just mentioned synthetic lethality by inhibiting PI3K-AKT signalling (a transduction pathway that promotes proliferation, metabolism, growth, cell survival, and angiogenesis in response to extracellular signals). In addition, PIK3IP1 expression was not upregulated by EZH2i treatment in ARID1A WT RMG1 cells, which is in agreement with the collected data showing that GSK126 **20** not affect RMG1 cell growth.

Restoration of ARID1A WT in ARID1A-mutated cells correlates with resistance to the EZH2i-based treatment, also without changing in EZH2 expression highlighting that the antagonism between EZH2 and ARID1A occurs at a functional level (Figure 4.11).
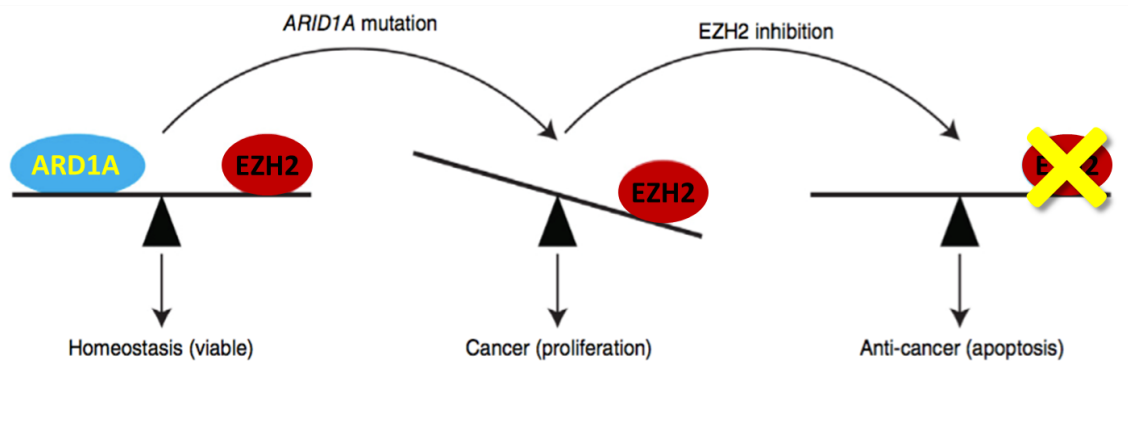
Figure 4.11. Proposed model explaining the observed synthetic lethality between inhibition of EZH2 methyltransferase activity and *ARID1A* mutation in ovarian cancer. Adapted from Bitler *et al*. *Nat. Med.* 2015.[654]

Given the recent identification of PRC2 and histone independent roles of EZH2, Wang *et al*.[655] reported an unique strategy to induce the degradation of EZH2 in order to reach a full blockade of its oncogenic functions. They identified the gambogenic acid (GNA, a natural molecule derived from gamboge known for its potent anti-cancer effect) and its derivatives as degraders of EZH2 since these molecules specifically and covalently binds the Cys668 within the EZH2-SER domain inducing the EZH2 dissociation from the PRC2 complex and in turn its degradation through COOH terminus of Hsp70-interacting protein (CHIP)-mediated ubiquitination (Figure 4.12). CHIP is a well-known actor in the protein quality control system that induces the polyubiquitination and consequent degradation of aggregated or misfolded proteins.[656,657] This effect correlates with a significantly decreased H3K27me3 levels, the reactivation of PRC2 silenced tumor suppressor genes, thus hindering the tumor growth in an EZH2-dependent manner. GN002 **80** is the most active EZH2 degrader among the series of GNA derivatives that have been synthetized by Wang and coworkers. However, further analysis are required to investigate the selectivity of action of this class of compounds since this non-specific degradation mechanism could involve also other cysteine residues of different SET-containing domain methyltransferases.
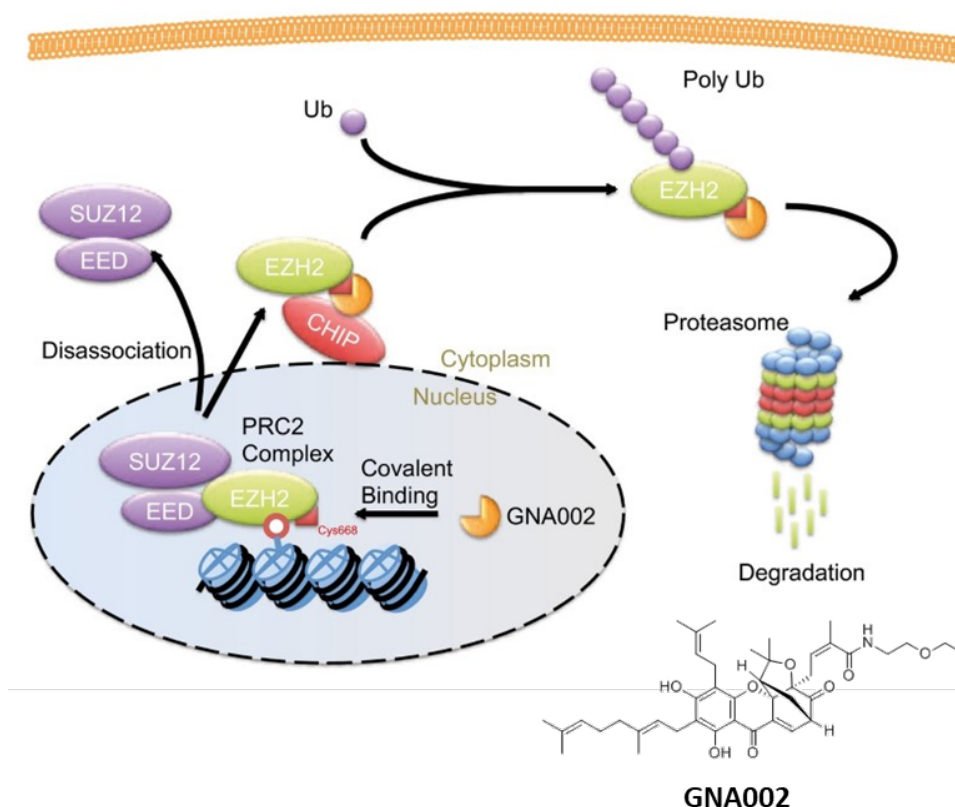
GNA002

Figure 4.12. Proposed model of the molecular mechanisms of GNA derivatives (among which the most potent resulted GNA002 **80**) as a novel class of EZH2 degrader. Adapted from Wang *et al.*, *The EMBO Journal*, 2017, 36: 1243–1260.[655]

Starting from these findings, we decided, also in this case, to apply the PROTACs approach in such scenario in order to induce the selective degradation of EZH2 which, as previously exposed in detail, may correlates with the full blockade of its oncogenic functions.

The first PRC2 degrader UNC6852 **40a** reported in 2019 has been described in Chapter 2 (section 2.2.1).[565] UNC6552 **40a** is characterized by the EED ligand EED226 **40b** as warhead and, despite induces a strong degradation of its main target EED (D=80%), and indirectly, also of EZH2 (D=74%), does not appear extremely potent (in comparison with the results commonly obtained within PROTACs field) since these effects are reached at micromolar level (5μM) after 24h treatments.

In order to achieve our goal, the well-known SAM competitive EZH2i GSK126 **20** has been selected as warhead. GSK126 **20** is one of the main promising members of the 2-pyrimidone based selective series of EZH2i (Figure 4.13). All the molecules that belong to such series are characterized by the 2-pyridone moiety (higlited in red in figure 4.13) which is connected though an amide linker to a support substructure, that can be either a bicyclic heteroaromatic ring such as indole (GSK126 **20**, CPI-1205 **22**, EI1 **84**) or indazole (GSK343 **81**, UNC1999 **82**, EPZ005687 **83**) or a simple monocyclic (hetero) aromatic ring (tazemetostat **21**). All these molecules shows, as further decoration, variable "tail" and "arm" residues attached to the bottom and top of the structure body. GSK126 **20** entered in phase I clinical trial in 2014 (as GSK2816126) for patients affected by various lymphomas, MM and solid tumors (NCT02082977). The limitation connected to its application seems to be the onset of a therapeutic resistance.[658–660] In addition, as previously reported in section 1.5 and Table 1.5, also the EZH2i tazemetostat **21** (NCT02875548, NCT03009344, NCT02601950) and CPI-1205 **22** (NCT02395601) and are in clinical trials for the treatment

of different lymphomas and solid tumors, while GSK343 **81**, UNC-1999 **82** are in the preclinical state.
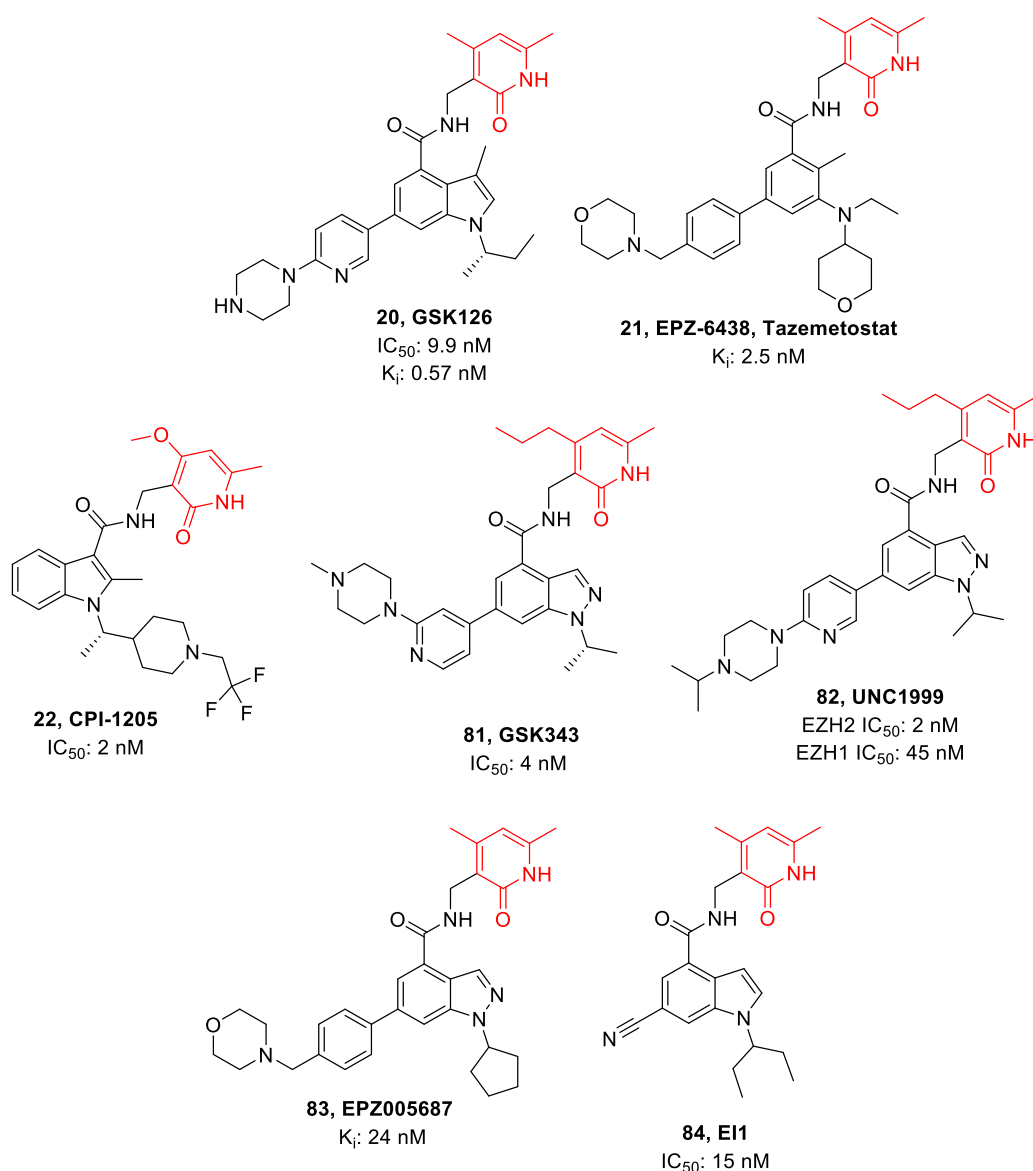
Figure 4.13. Structures and relative activities of the most promising 2-pyrimidone (highlited in red)-based EZH2i GSK126 **20**, tazemetostat **21**, CPI-1205 **22**, GSK343 **81,** UNC1999 **82,** EPZ005687 **83,** EI1 **84**.

The 2-pyridone moiety resulted crucial for a selective and effective inhibition of the enzyme since it partially occupies the site for the co-substrate SAM in the binding pocket, thus providing a SAM competitive mechanism of action. GSK126 **20** is 150-fold selective for EZH2 over its highly homologue EZH1 (76% sequence identity overall and 96% sequence identity) and 1,000-fold selective over other methyl transferase. Despite seems that the 2-pyridimidone moiety plays an important role in such registered selectivity, the structural factor mainly responsible for this feature is still unclear since multiple functional groups impacting selectivity.[77,661,662]
GSK126 **20** effectively induces both cytostatic and cytotoxic response in EZH2 mutant DLBCL cell lines and strongly arrest the growth of EZH2 mutant DLBCL xenografts in mice. The collected results showed that the inhibition of EZH2 may provide a promising treatment for EZH2 mutant lymphoma.[661] Zang *et al.* in 2017 showed that GSK126 **20** effectively decrease the H3K27me3 level in MM.1S and LP1 myeloma cells, as well as the

number of colony formation and live cells through the enhancing of the intrinsic mitochondrial apoptosis pathway. They also reported that GSK126 **20** decrease the stem-like myeloma cells destroying the Wnt/β-catenin pathway and its *in vivo* anti-tumor effect was proved by using RPMI8226 myeloma cells in a xenograft mouse model.[663]

In 2018 Bratkowski *et al*. solved the crystal structures of hPRC2 bound to GSK126 **20** (Figure 4.14)[664] highlighting that the amine and carbonyl groups of the pyridone ring of GSK126 **20** mimic the amine and carboxylate ones of SAM. More in detail, the carbonyl oxygen and the amide nitrogen of the pyridone taking part in distorted hydrogen bonds with the main chain amide nitrogen and carbonyl oxygen, respectively, of residue W624 of EZH2 thus acting in a SAM- competitive way. The pyridine and piperazine rings of the tail regions of GSK126 **20** point outward toward the solvent and do not take part in keys interactions with the active site of the enzyme.
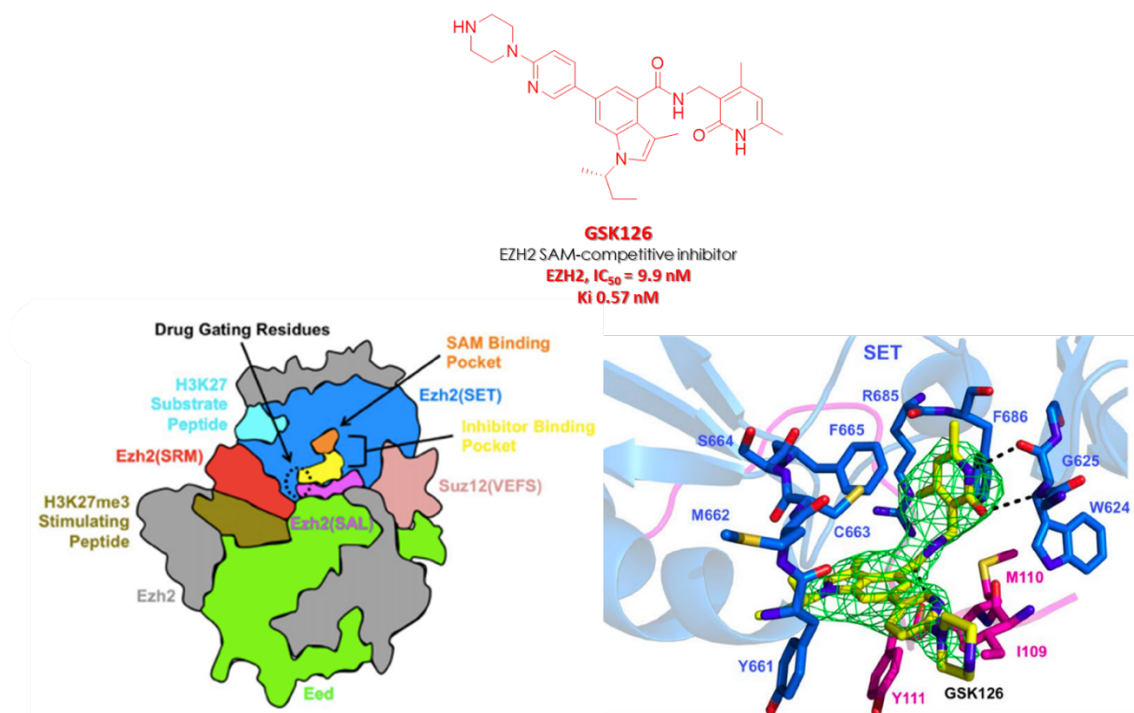
Figure 4.14. GSK126 **20** structure (on the top), schematic representation of PRC2 with important regions color-coded (bottom left) and structure of hPRC2 in complex with GSK126 **20** (yellow sticks, bottom right). Adapted from Bratkowski *et al*. *Scientific reports*, 2018, 8:9092.[664]

Starting from these findings, we decided to design a series of EZH2-targeting PROTACs resulting from the functionalization of the -NH group of the GSK126 **20** piperazine ring as linker attachment point.

The collaboration with Professor Alessio Ciulli (School of Life Sciences, University of Dundee, Scotland, UK) has added value to the project since it was focused, not only on the design of 4-hydroxythalidomide **36f** CRBN based EZH2 targeting PROTACs , but also on the evaluation of different CRBN (**36d, 36g**) and VHL (**37f**, VH101 **37c** and **37e**) ligase binders which were connected *via* various pegylated and not-pegylated linkers, to the scaffold of GSK126 **20** (Figure 4.15).

Specifically, the CRBN-based EZH2-targeting PROTACs that have been synthetized were characterize not only by the 4-hydroxy thalidomide moiety **36f** (**85a,b**) but also by its analogue in which the -OH group is moved to the position -5 **36g** (which seems to be more stable in cells) (**86a-d**) as well as by the biologically and chemically most manageable pomalidomide **36b** derivative **36d** (**87a-d**) (Figure 4.15A). Concerning the VHL-based

EZH2 targeting PROTACs (Figure 4.15B), various VHL binders characterized by different attachment point in both term of position and nature were selected: i) the well-known VHL ligand **37f** (**88a-d**); ii) VH101 **37c** which, in addition to result a more potent VHL binder thanks to the increased hydrophobic interaction carry out by the introduction the fluorine-cyclo-propyl group (see section 2.1), also shows a new phenolic attachment point (**89a-d**); iii) the VHL binder which derived from the introduction of a thioether linkage out of the *tert*-butyl group of the VHL ligand **3f**, in which the *tert*-Leu group is replaced with a penicillamine one, harbouring, as seen for VH101 **37c**, a terminal fluorine-cyclopropyl group **37e** (**90a-d**).

A
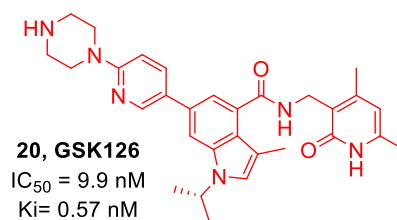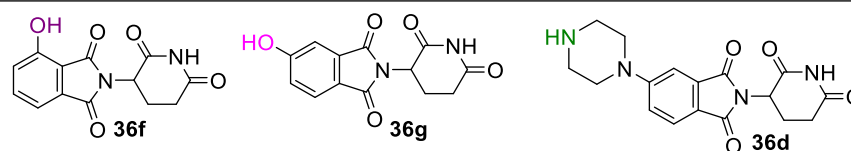
20, GSK126
IC$_{50}$ = 9.9 nM
Ki= 0.57 nM

Selected CRBN ligands

36f   **36g**   **36d**

CRBN-based EZH2 targeting PROTACs with different attachment points and linkers

85a,b

LINKERS:

n=1,2

86a-d

87a-d

LINKERS:

B

20, GSK126
IC$_{50}$ = 9.9 nM
Ki= 0.57 nM

Selected VHL-ligands

37f

37c, VH101

37e

VHL-based EZH2 targeting PROTACs with different attachment points and linkers

88a-d

89a-d
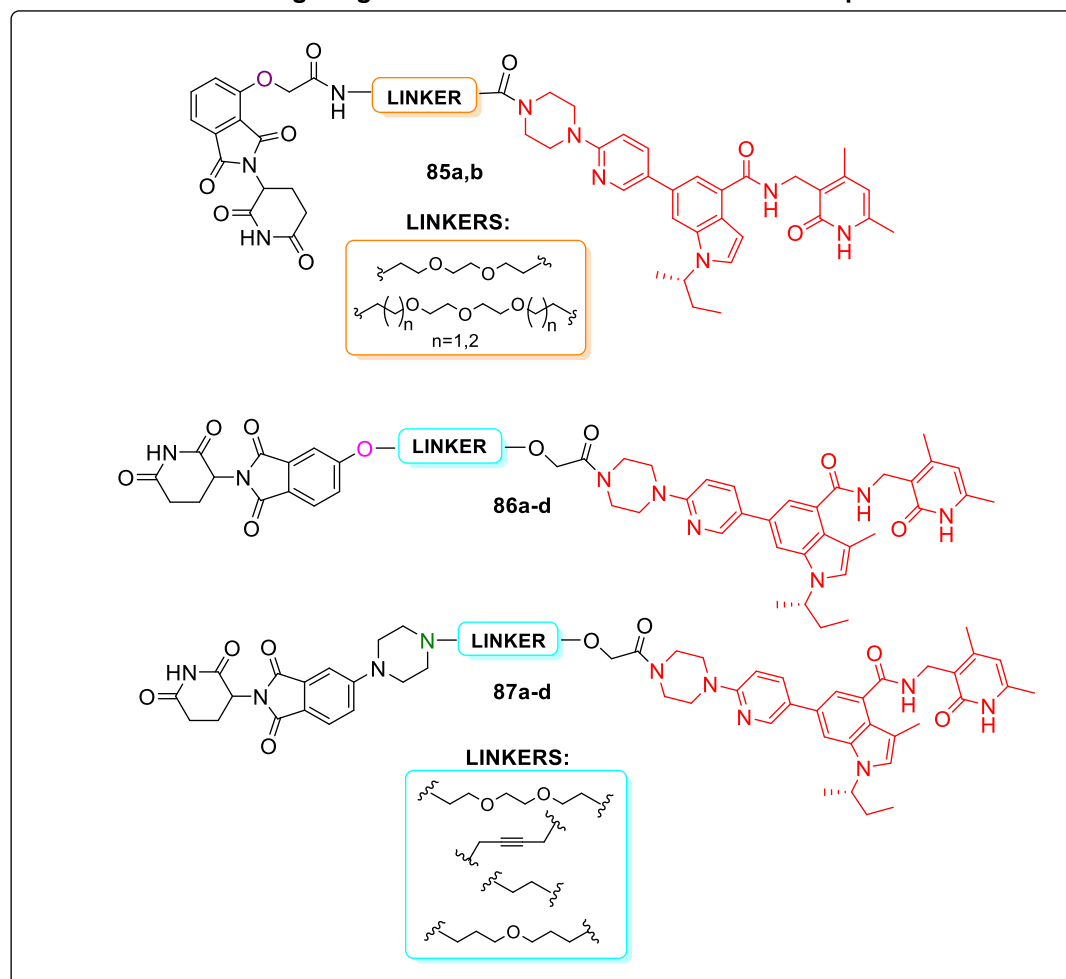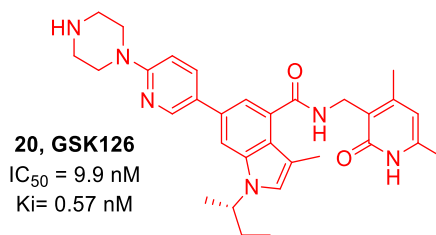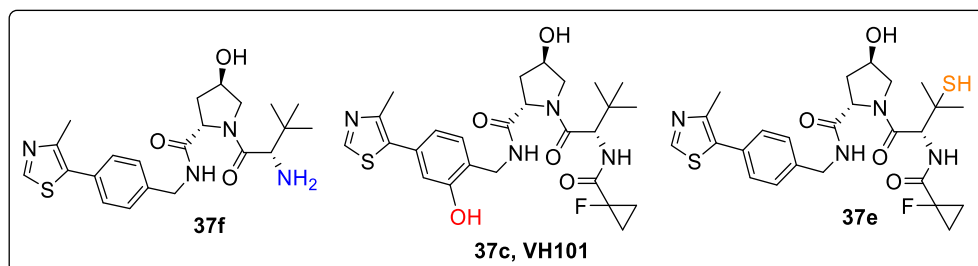
90a-d

LINKERS:
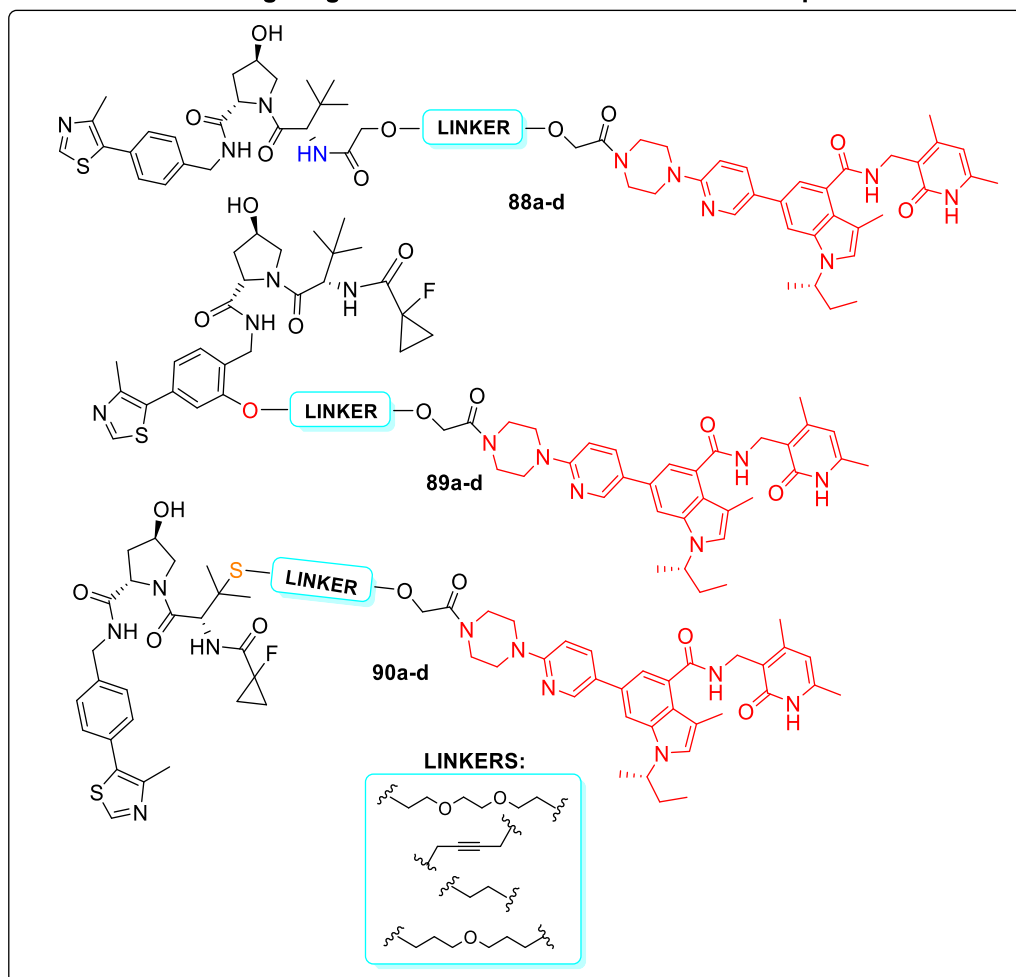
Figure 4.15. New CRBN- (A) and VHL- (B) based EZH2 targeting PROTACs based on the structure of the SAM- competitive EZH2i GSK126 **20**.

4.4 Overview of the whole Epi-PROTACs Project

As just mentioned, 34 novel Epi-PROTACs targeting different epigenetic targets in the category of "erasers" (such as LSD1 and JmjC KDMs) and "writers" (such as p300 and EZH2) characterized by different E3 ligase binders and pegylated and non-pegylated linkers have been developed.

The whole epi-PROTACs project has been schematized in the following picture:
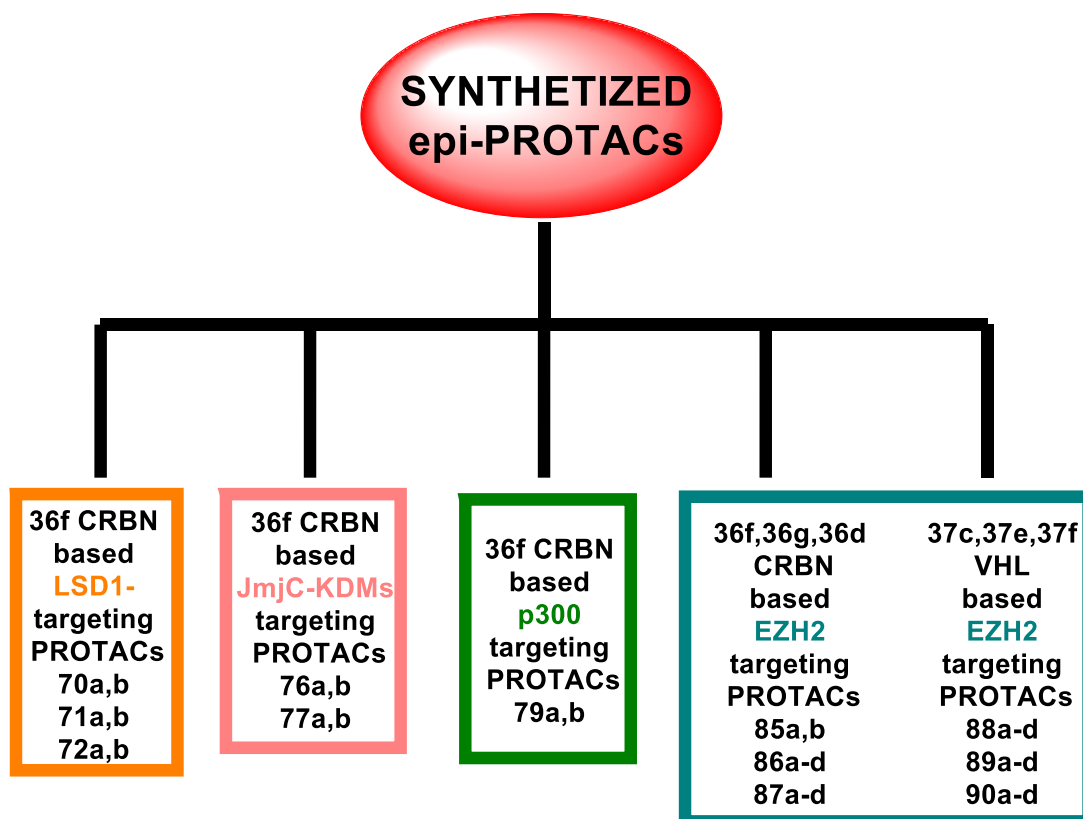
Figure 4.16. Schematic representation of the epi-PROTACs project. Epi-PROTACs targeting LSD1 (**70a,b**, **71a,b**, **72a,b**), JmjC-KDMs (**76a,b**, **77a,b**), p300 (**79a,b**), EZH2 (**85a,b**, **86a-d**, **87a-d**, **88a-d**, **89a-d**, **90a-d**) are reported in the orange, pink, green and blue box, respectively.

4.5 Chemistry

Routes for the synthesis of linkers **114a,b,d**, **116a-d**, CRBN **36f**, **36g**, **36d** and VHL **37c** binders, as well as final compounds **70a,b** (and their negative controls **135a,b**), **71a,b** (and their negative controls **137a,b**), **73a,b**, **76a,b** (and their negative controls **140a,b**), **77a,b,** **79a,b**, **85a,b, 86a-d, 87a-d, 88a-d, 89a-d, 90a-d** are depicted in Scheme 4.1-4.6. CRBN binder **36f** was synthetized starting from the intramolecular cyclization of Nα-BOC-L-Glutamine **91** in presence of CDI and DMAP as a catalyst in dry THF thus providing the 3-amino BOC-protected 2,6-dioxo piperidine **92,** which was deprotected using TFA to allow the consequent reaction with the 4-hydroxyisobenzofurane 1,3 dione **94** in dry pyridine thus obtaining **36f**. **36f** was subjected to OH-alkylation using *tert*-butyl bromoacetate and K_2CO_3 as base in dry DMF, providing the acid derivative **96** after TFA mediated *tert*-butyl-ester deprotection of **95** (Scheme 4.1A). **36g** also results from the intramolecular cyclization of the 4-hydroxyptalic acid **97** after the protection of its -OH group in basic condition with benzyl bromide yielding **99** using Ac_2O as catalyst. The following reaction between the title compound **99** and the 3-amino piperidine-2,6-dione hydrochloride in presence of glacial CH_3COOH and NaOAc provided **100**. Debenzylation under H_2 atmosphere using Pd/C furnished the -OH free group of **36g** (Scheme 4.1B). Reaction between 4-fluoropthalic anhydride **101** and 3-amino piperidine-2,6-dione hydrochloride, following the same conditions used to obtain **100**, provided **102** which was treated with 1-BOC piperazine and DIPEA in NMP obtaining compound **103**, which gave the desired **36d** after deprotection mediated by HCl 4N dioxane using a mixture of DCM/MeOH as solvent (Scheme 4.1B). The first step for the synthesis of **37c** required a cross coupling reaction between the 5-bromo-2-isocyanophenol **104** and the 4-methylthiazole **105** in presence of Pd(OAc)₂ and KOAc in DMA providing the cyano-derivative **106**, which was reduced to the correspondent amine **107** using $LiALH_4$ in dry THF. Coupling reaction involving **107** and *N*-BOC-trans-4-hyroxy-L-proline using Pyoxim as coupling reagent and DIPEA as base in dry DMF provided **108**, which was then deprotected with HCl 4N in dioxane and subjected again to a coupling reaction with BOC-L-tert-Leu using the same condition followed for **108**. Last deprotection with HCl 4N in dioxane gave **111** and conclusive coupling reaction, following the conditions just exposed, between the latter and the 1-fluorocyclopropane-1-carboxylic acid gave VH101 **37c** (Scheme 4.2). For the synthesis of linkers **114a,b** and **116a-c,** the opportune diol **112a-c** was treated with *tert*-butyl bromoacetate in presence of NaH 60% min oil in dry DMF using different ratio of the two reagents in order to obtain the mono **115a-c** (scheme 4.3A) or di-alkylated product **113a-c** (scheme 4.3B). The -OH group of the mono ester derivative **115a-c** was converted in a good leaving group like tosyl or bromine through the reaction with TsCl and TEA in dry DMF or CBr₄ and PPh₃ in dry DCM, respectively (Scheme 4.3B), thus yielding **116a-c.** Di-alkylated intermediates **113a,b** were deprotected using a mixture of TFA and DCM thus obtaining the correspondent di-acid derivatives **114a,b**. **114d** and **116d** were prepared starting from the 3-(benzyloxy)propan-1-ol **117** which was subjected first to tosylation (using the same condition just exposed), followed by a nucleophilic substitution with propane-1,3-diol in presence of NaH 60% min oil in dry DMF, to provide the required 3-(3-(benzyloxy)propoxy)propan-1-ol **119**. **119** was alkylated to yield the correspondent *tert*-butyl ester **120** using N₂CHCOOtBu in presence of Rh₂(OAc)₄ in dry DCM. Upon H_2, Pd/C mediated debenzylation of **120**, the obtained compound **115d** was converted into **114d** and **116d** following the same condition used for **120** and **116a-c** (Scheme 4.3C). Linkers **121a-d** introduction to the scaffold of **96** required a coupling reaction using HATU, DIPEA in dry DMF thus providing **112a-d** which were then deprotected using TFA in dry DCM affording the proper amine or acid **123a-d** derivatives (Scheme 4.4A). The opportune dicarboxylic acid linker **114a-d** was first converted in the

correspondent NHS-ester **128a-d** using NHS and DCC in dry DCM. The required activated acid linker **128a-d** was subjected to a coupling reaction with the VHL binder **37f** in presence of DIPEA in dry DMF thus obtaining the relative intermediates **129a-d** harbouring the proper linker (Scheme 4.5A).

Linkers characterized by a good leaving group like **116a-d** were introduced to the scaffold of the CRBN binders **36g** and **36e** as well as to those of VHL ligands **37c** and **37e** using nucleophilic substitutions involving the opportune base (K_2CO_3 or DIPEA) in dry DMF at the required temperature thus providing **125a-d**, **127a-d**, **131a-d** and **133a-d** after *tert*-butyl ester deprotection through a mixture of TFA:TIPS:DCM (Scheme 4.4B,C and 4.5 B,C).

Final coupling reaction using the appropriate intermediate **123a-d**, **, 125a-d**, **127a-d**, **129a-d, 131a-d, 133a-d,** the required epigenetic modulator (o its protected form) **20**, **72**, **75**, **78**, **134**, **136**, **139**, Pyoxym or HATU as coupling reagent and DIPEA as base in dry DMF provided the desired final compounds **70a,b** (and their negative controls **135a,b**), **71a,b** (and their negative controls **137a,b**), **73a,b**, **76a,b** (and their negative controls **140a,b**), **77a,b, 79a,b**, **85a,b, 86a-d, 87a-d, 88a-d, 89a-d, 90a-d** (Scheme 4.6).

Amine **106a-d**, 3-(benzyloxy)propan-1-ol **117**, 2,2'-(ethane-1,2-diylbis(oxy))diacetic acid **114c** and 3-amino piperidine-2,6-dione hydrochloride are commercially available.

All the ^{1}H-NMR and ^{13}C-NMR spectra relative to compounds **106-111** and VH101 **37c** are consistent with those published.[541] VHL ligands **37f** and **37e** were prepared in according with the reported procedure and all the ^{1}H-NMR and ^{13}C-NMR spectra are consistent with those already reported to literature.[541,552]

The ^{1}H-NMR spectra of hydrochloride salts **36d** is in according for those described for its relative BOC-protected form **103.**

The ^{1}H-NMR spectra of the acid derivatives **125a-d, 127a-d, 131a-d** and **133a-d** are consistent with those reported for their relative ester **124a-d**, **126a-d, 130a-d** and **132a-d**, respectively.

Scheme 4.1 Synthesis of CRBN binders 36f (A), 36g (B), 36d (C) and 96 (A).[a]

[a]Reagent and condition: (a) CDI, DMAP, THF, 90°C, 24h, N_2; (b) TFA, 0°C → rt, 2h; (c) dry pyridine, 110°C, 24h; (d) *tert*-butyl bromoacetate, K_2CO_3, dry DMF, rt, 24h; (e) TFA: H_2O: TIS, 0°C → rt, 6h 30min; (f) BnBr, KOH, H_2O, 120 °C, 16h; (g) Ac_2O, reflux, 2h; (h) 3-aminopiperidine-2,6-dione hydrochloride, NaAcO, glacial CH_3COOH, 120 °C, 16h; (i)
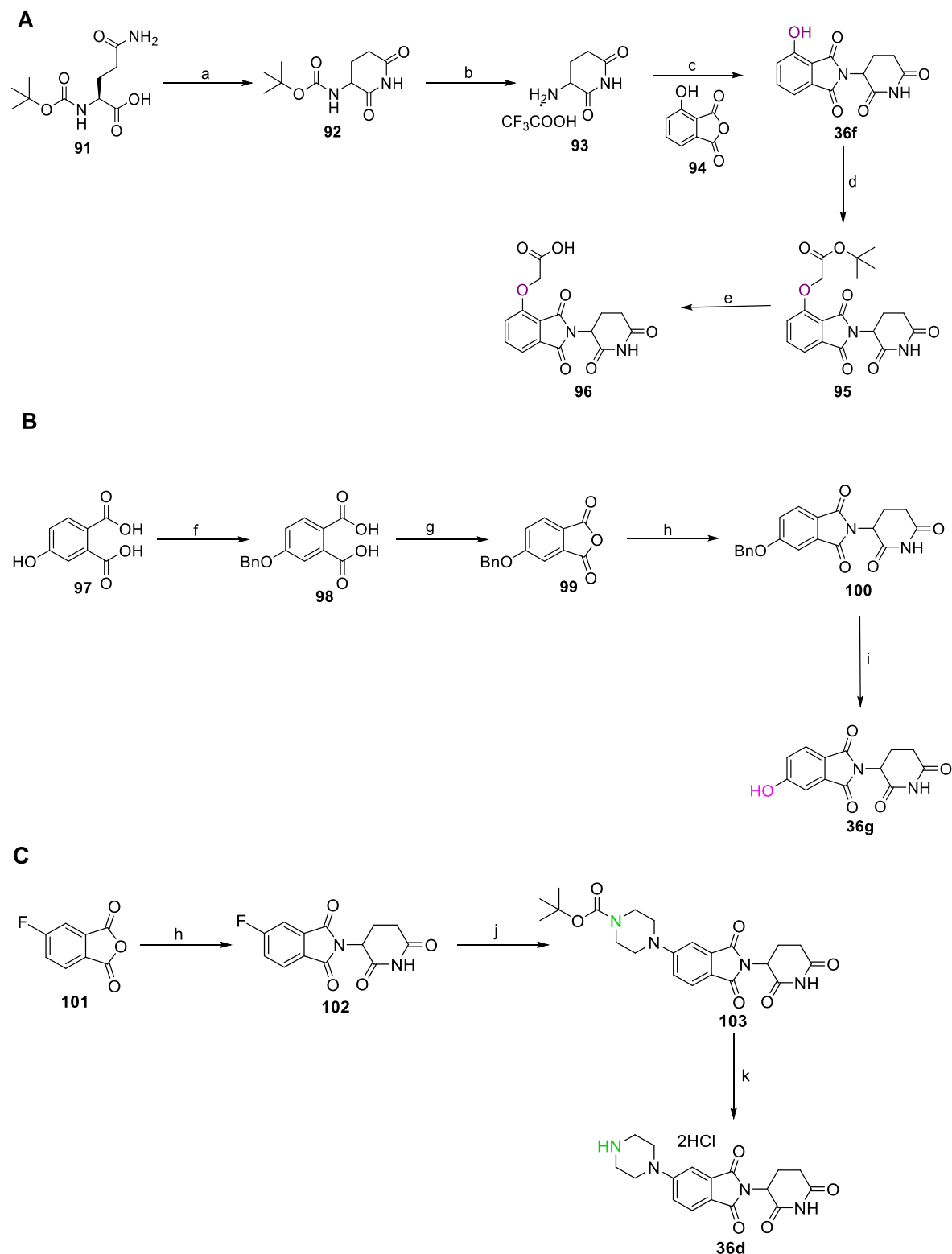
H$_2$, Pd/C 10 %, MeOH, rt, 16h; (j) 1-Boc-piperazine, NMP, DIPEA, 90 °C, 16h; (l) HCl 4M in dioxane, DCM/MeOH 0°C → rt, 2h.

Scheme 4.2. Synthesis of VHL ligand VH101 37c.[a]
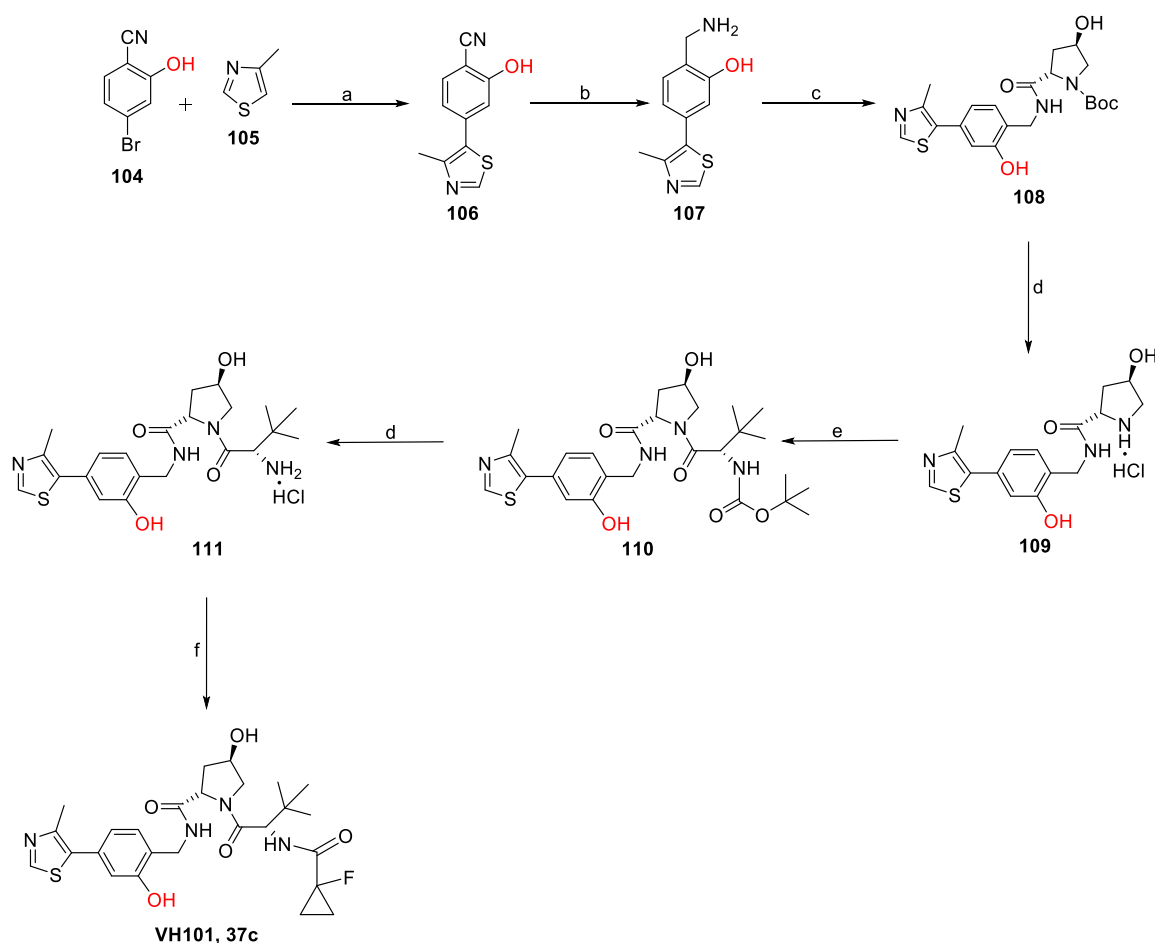
[a]Reagents and conditions: (a) Pd(OAc)$_2$, KOAc, DMA, 150°C, 16h, Yield 74% (b) LiAlH$_4$, dry THF, 150°C, 16h, N$_2$, Yield 30%; (c) *N*-Boc-trans-4-hydroxy-L-proline, PyOxim, DIPEA, dry DMF, 0°C --> rt; 3h, Yield 22%; (d) HCl 4N in dioxane, DCM, 16h, Yield quantitative; (e) Boc-L-Tert-Leu, PyOxim, DIPEA, DMF, rt, 16h, Yield 90%; (f) 1-fluorocyclopropane-1-carboxylic acid, Pyoxym, DIPEA, dry DMF, rt, 2h, Yield 94%.

Scheme 4.3. Synthesis of linkers 114a-c and 116a-d.[a]

A

B

C
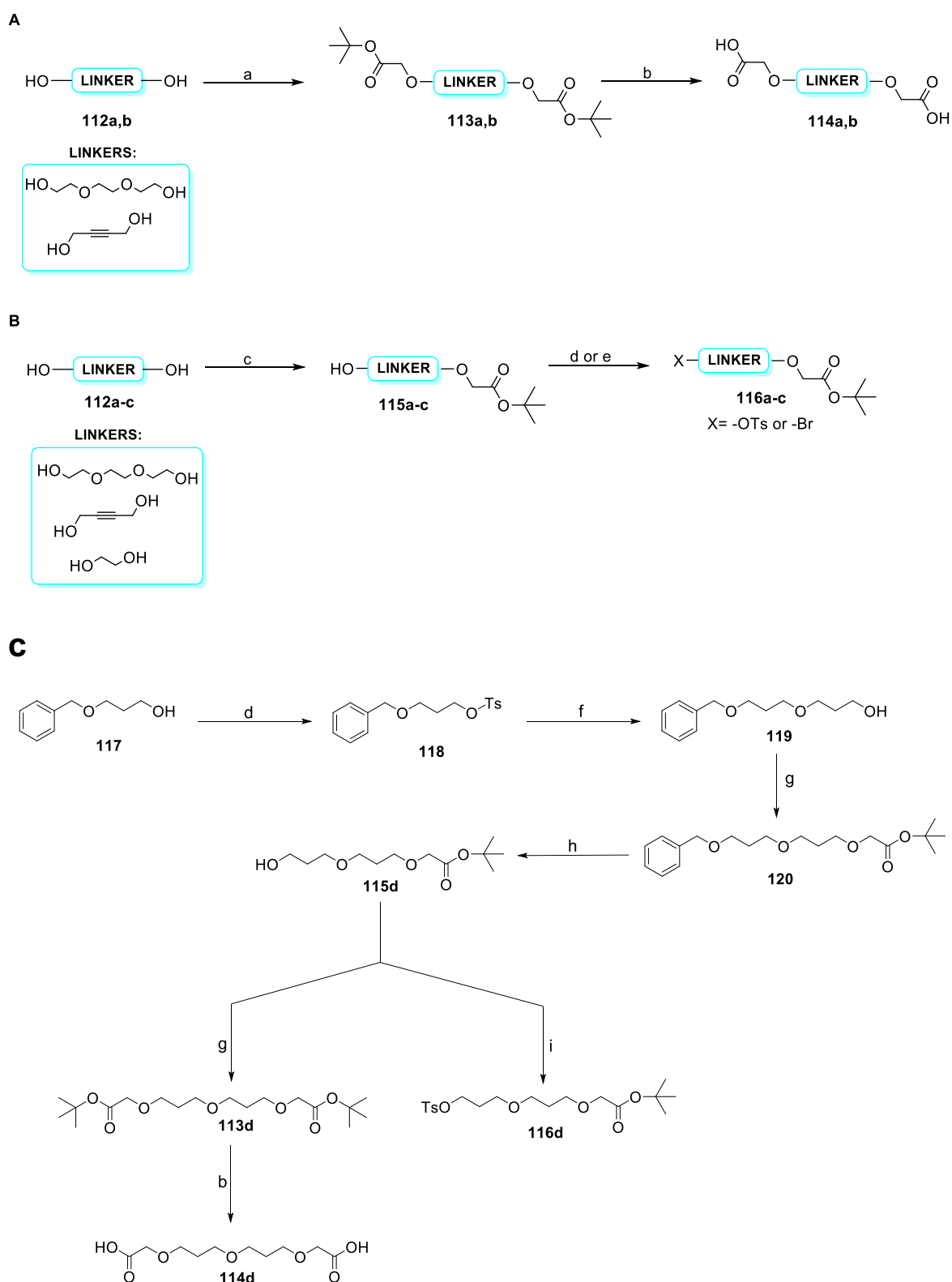
[a]Reagent and conditions: (a) *tert*-butyl bromoacetate, NaH 60% min oil, dry DMF, 0°C→rt, 16h, N$_2$; (b) TFA, DCM, 0°C→rt, 2h; (c) *tert*-butyl bromoacetate, NaH 60% min oil, dry DMF, 0°C→rt, 16h, N$_2$; (d) TsCl, TEA, dry DCM, rt, 16h, N$_2$; (e) PPh$_3$, CBr$_4$, dry DCM, 0°C→rt, 16h; (f) propane-1,3-diol, NaH, dry DMF, 0°C→rt, 16h, N$_2$; (g) N$_2$CHCOOtBu,

Rh$_2$(OAc)$_4$, dry DCM, 0°C→rt, 16h, N$_2$; (h) H$_2$, Pd/C, MeOH, rt, 16h; (i) TsCl, DMAP, TEA, rt, 16h.

Scheme 4.4 Synthesis of the intermediates 123a-d (A), 125a-d (B), 127a-d (C).[a]

A
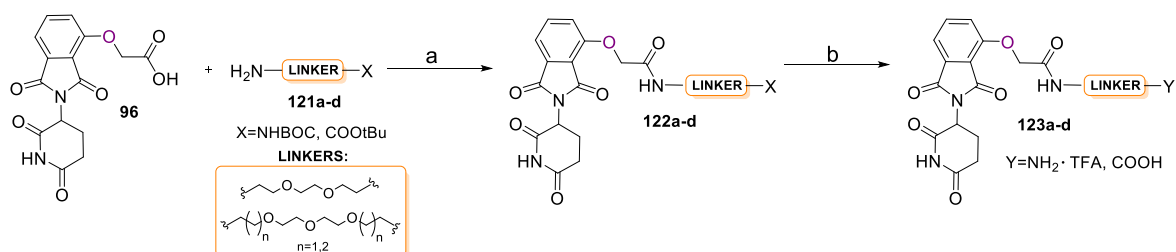
B
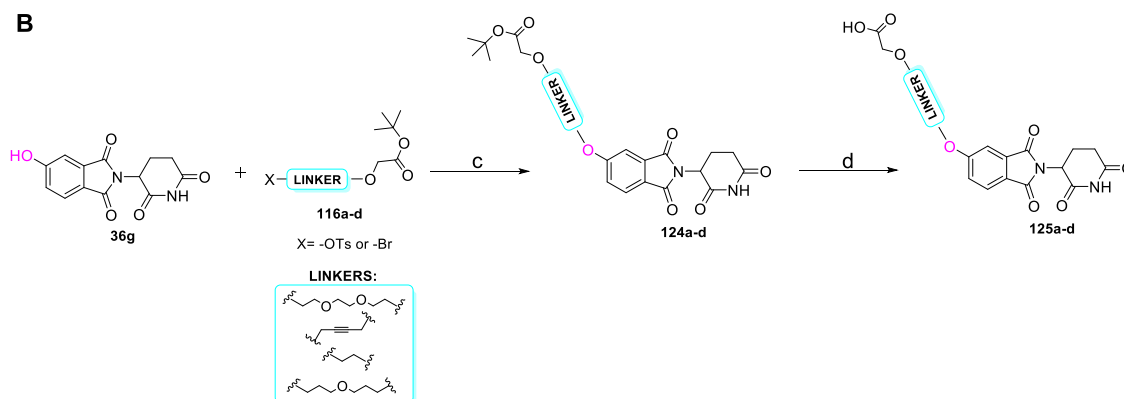
C
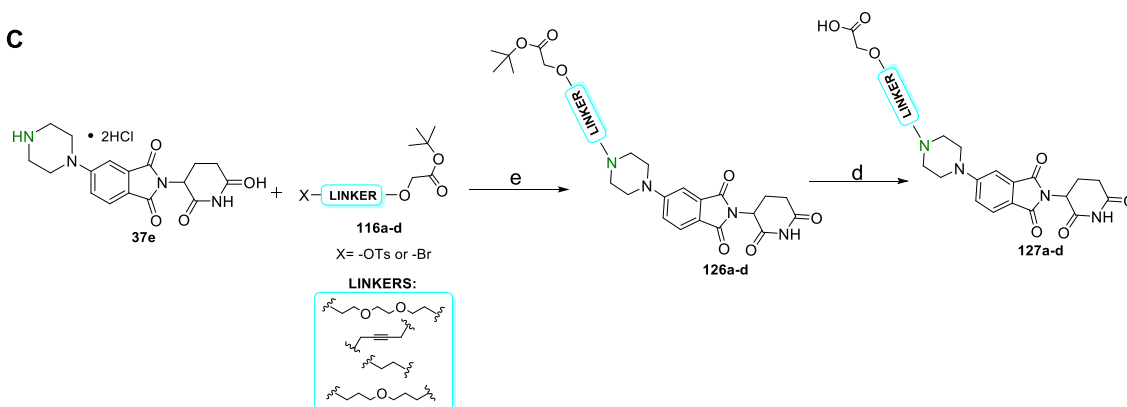
[a]Reagents and conditions: (a) DIPEA, HATU, DMF, rt, 7h, N$_2$; (b) TFA:DCM, 0°C→rt, 7h; (c) K$_2$CO$_3$, KI, dry DMF, 100°C, 48h; (d) DCM:TFA:TIPS, 0°C→rt, 2h; (e) DIPEA, dry DMF, 100°C, 24h.

Scheme 4.5. Synthesis of intermediates 129a-d (A), 131a-d (B) and 133a-d (C).[a]
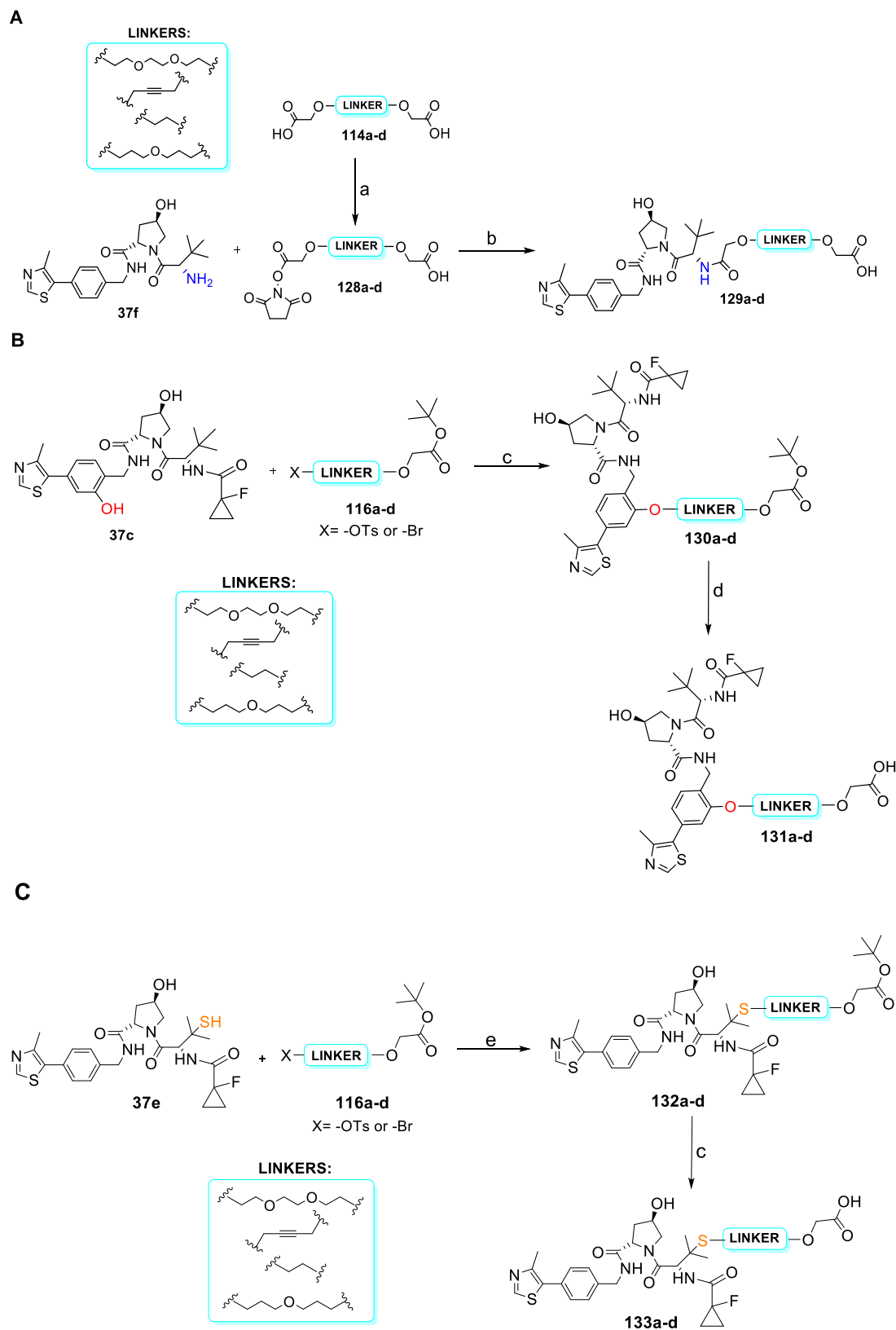
[a]*Reagent and conditions:* (a) NHS, DCC, dry DCM, rt, 16h; (b) DIPEA, dry DMF, rt, 2h; (c) K_2CO_3, dry DMF, 70°C, 16h; (d) DCM:TFA:TIPS, 0°C→rt, 2h; (e) K_2CO_3, dry DMF, rt, 16h, N_2.

Scheme 4.6 Synthesis of 36f CRBN based PROTACs 70a,b (A), 71a,b (B), 76a,b (C), 77a,b, 79a,b (D), 73a,b, 79a,b (E).[a]

A

B

C

D

E

LINKERS:

n=1,2

72, GSK-690
reversible LSD1i

73a,b

20, GSK126
EZH2i

85a,b

123c,d

b
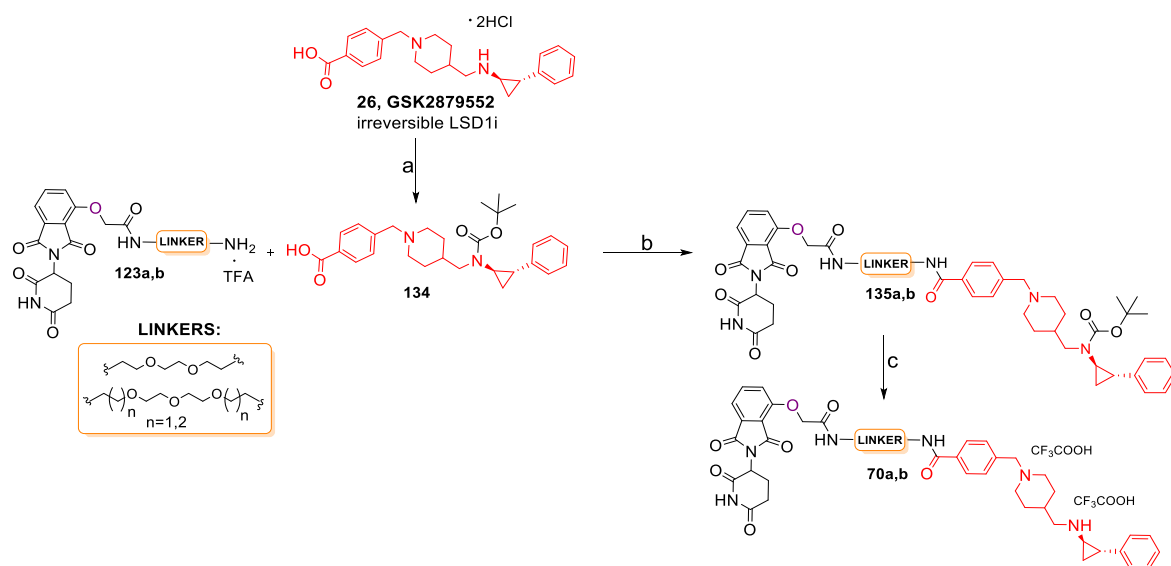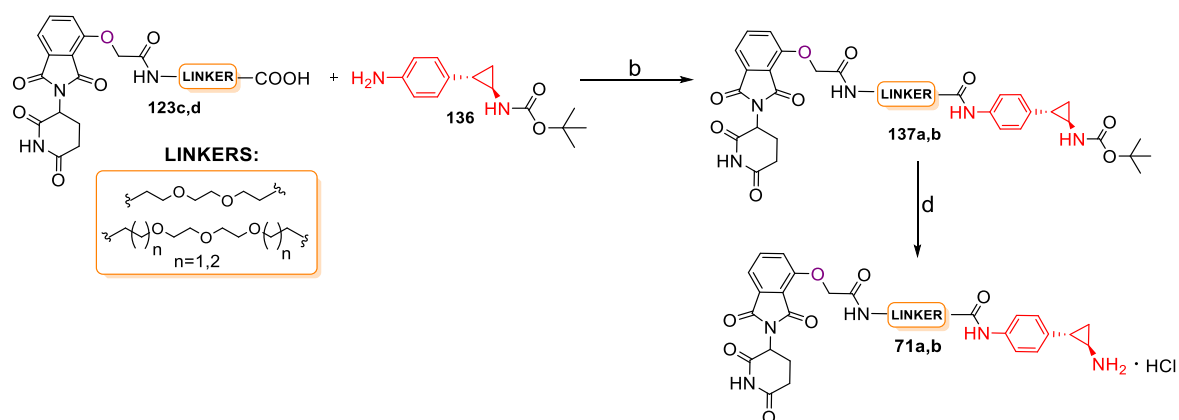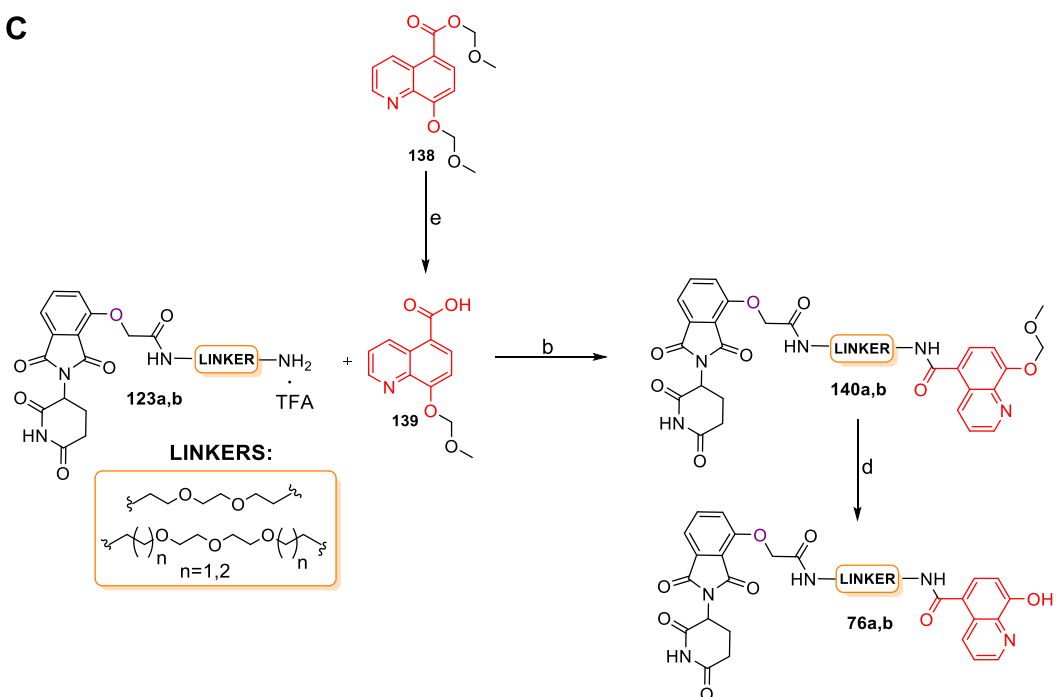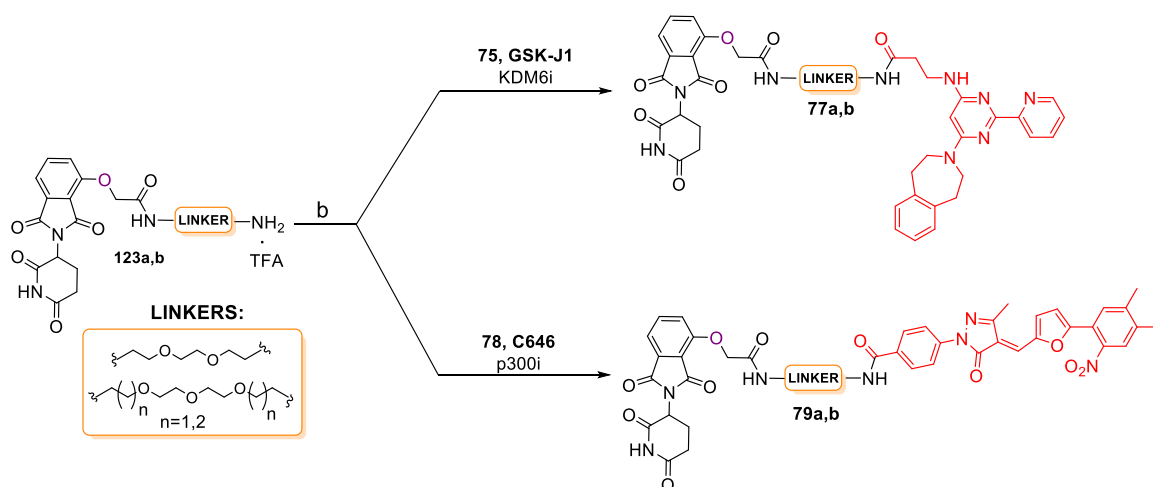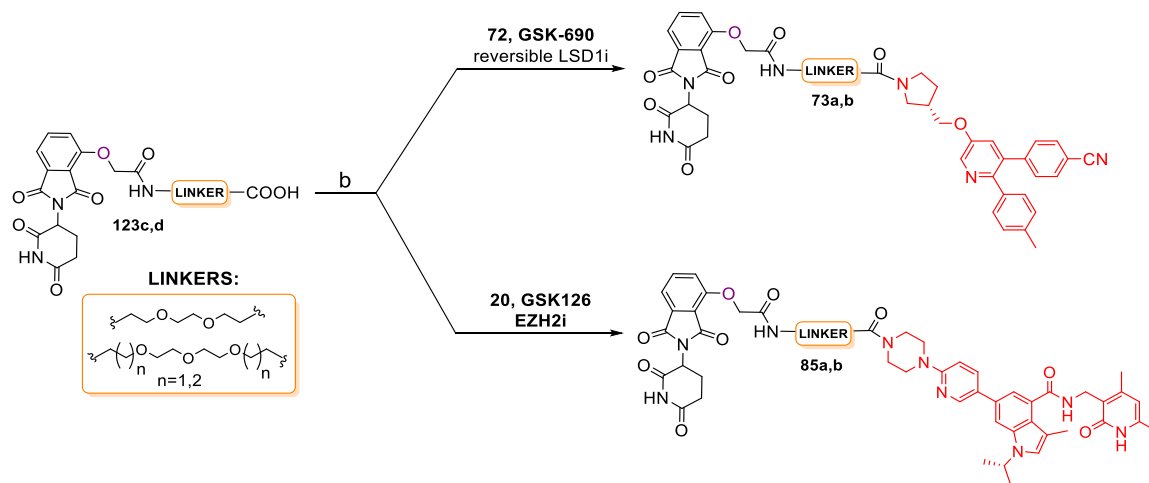
aReagents and conditions. (a) NaOH 1M, di-*tert*-butyl dicarbonate, dioxane: H$_2$O, 0°C→rt, 24h; (b) DIPEA, HATU, dry DMF, rt, 6h; (c) DCM: TFA:TIS, 0°C→rt, 5h; (d) HCl 4N in dioxane, THF, 0°C→rt, 48h; (e) LiOH·H$_2$O, THF, 0°C→rt, 6h.

Scheme 4.7. Synthesis of 36d, 36g CRBN and 37f, 37c, 37e VHL based PROTACs targeting EZH2 86a-d (A), 87a-d (B), 88a-d (C), 89a-d (D), 90a-d (E).[a]

C

LINKERS:

129a-d

+

20, GSK126

a

88a-d

D

131a-d

LINKERS:

+

20, GSK126

a

89a-d

E
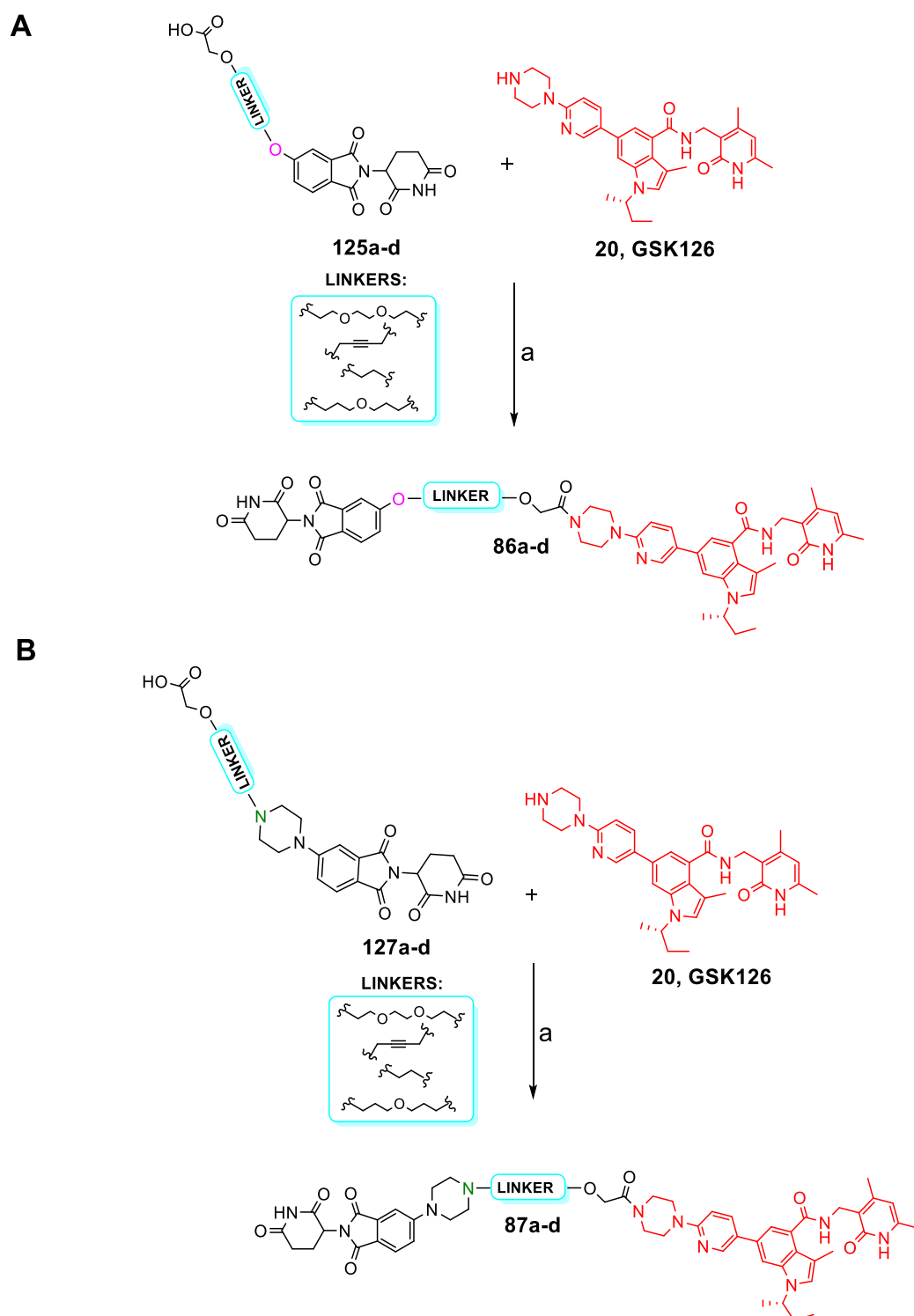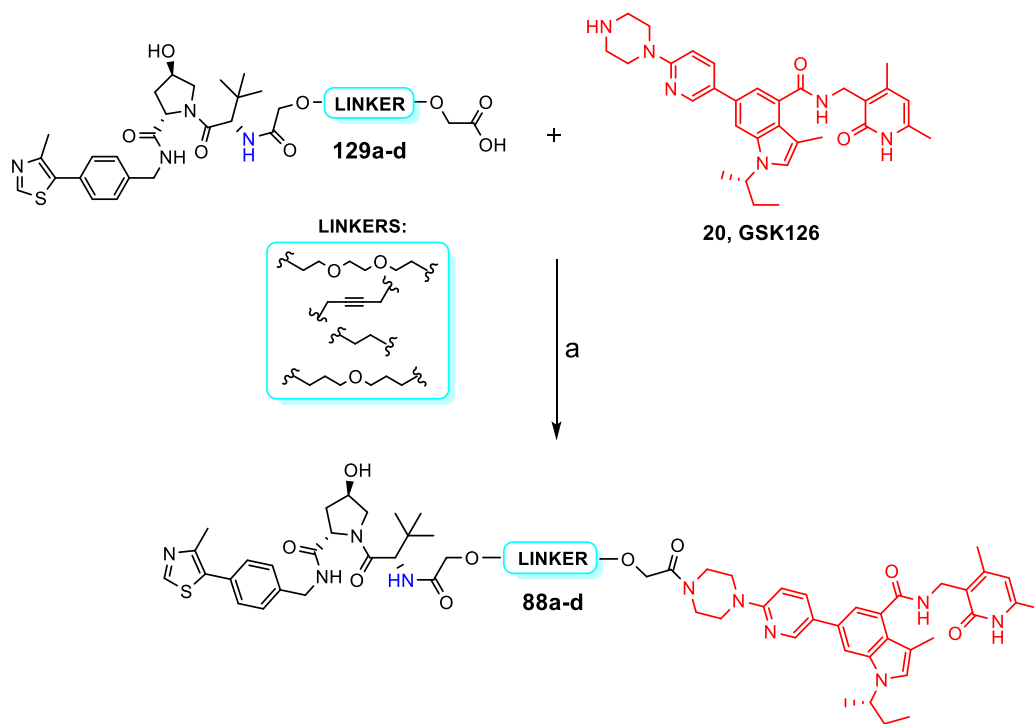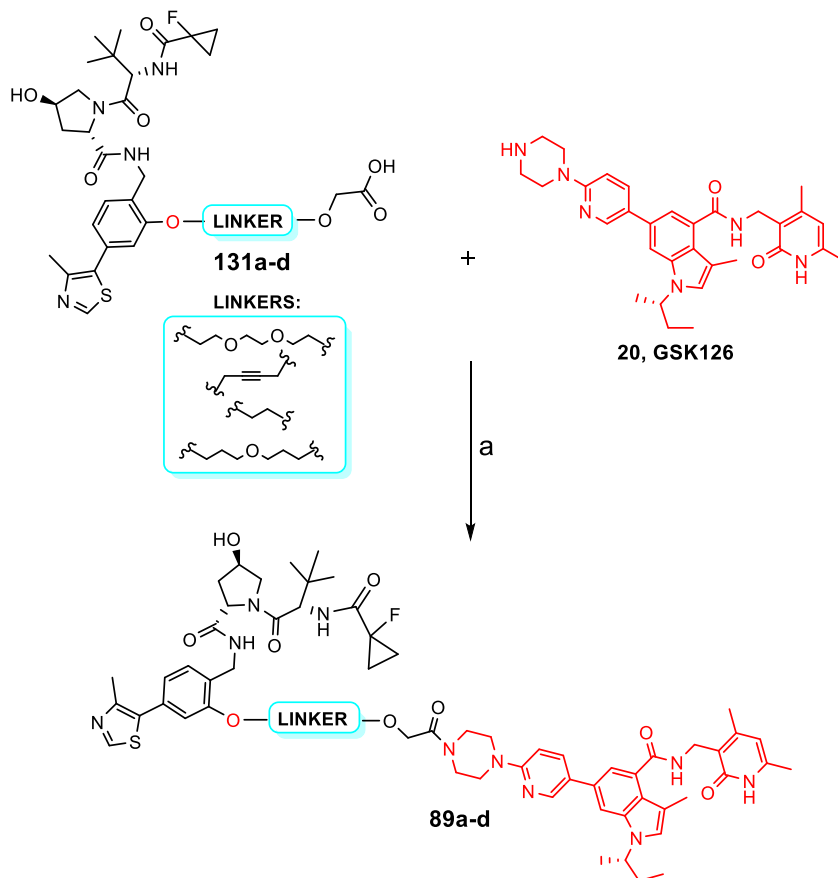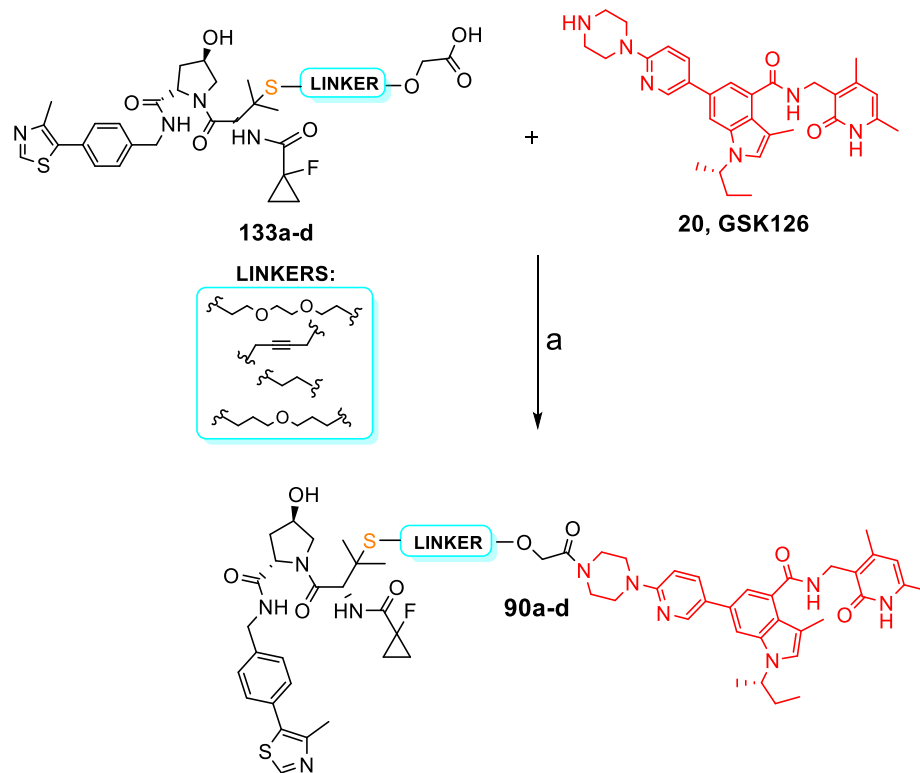
Reagents and conditions: (a) Pyoxim, DIPEA, dry DMF, rt, 1-2h.

4.5.1 Experimental section

Commercially available chemicals were purchased from Apollo Scientific, Sigma-Aldrich, Fluorochem, or Manchester Organics and used without any further purification. All reactions were carried out using anhydrous solvents. Melting points were determined using a Buchi 530 melting point apparatus. TLC was performed on precoated TLC plates (layer 0.20 mm silica gel 60 with fluorescent indicator (UV 254: Merck). The TLC plates were air-dried and revealed under UV lamp (254/365 nm). Flash column chromatography was performed using 12 prepacked silica gel cartridges (230–400 mesh, 40–63 mm; SiliCycle) using a Teledyne ISCO Combiflash Companion or Combiflash Retrieve using the solvent mixtures stated for each synthesis as mobile phase. Preparative HPLC was performed on a Gilson preparative HPLC with a Waters X-Bridge C18 column (100 mm x 19 mm; 5 μm particle size, flow rate 25 ml/min). Liquid chromatography–mass spectrometry (LC-MS) analyses were performed with either an Agilent HPLC 1100 series connected to a Bruker Daltonics MicroTOF or an Agilent Technologies 1200 series HPLC connected to an Agilent Technologies 6130 quadrupole spectrometer. For LC-MS the analytical column used was a Waters X-bridge C18 column (50 mm × 2.1 mm × 3.5 mm particle size); flow rate, 0.5 mL/min with a mobile phase of water/MeCN + 0.01% NH_4OH (basic analytical method) or water/MeCN + 0.01% HCOOH (acidic analytical method); 95/5 water/MeCN was initially held for 0.5 min followed by a linear gradient from 95/5 to 5/95 water/MeCN over 3.5 min which was then held for 2 min. The purity of all the compounds was evaluated using the analytical LC-MS system described before, and purity was >95%. ^{1}H NMR and ^{13}C NMR spectra were recorded on a Bruker Avance II 500 spectrometer (^{1}H at 500.1 MHz, ^{13}C at 125.8 MHz) or on a Bruker DPX-400 spectrometer (^{1}H at 400.1 MHz, ^{13}C at 101 MHz). Chemical shifts (δ) are expressed in ppm reported using residual solvent as the internal reference in all cases. Signal splitting patterns are described as singlet (s), doublet (d), triplet (t), multiplet (m), or a combination thereof. Coupling constants (*J*) are quoted to the nearest 0.1 Hz.

Synthesis of 2-((2-(2,6-dioxopiperidin-3-yl)-1,3-dioxoisoindolin-4-yl)oxy)acetic acid 96 (Scheme 4.1A).

Nα-BOC-L-Glutamine **91** (16.24 mmol, 1eq), CDI (17.2 mmol, 1.06eq) and DMAP cat. were dissolved in dry THF (40 mL) and the resulting mixture stirred for 24h at 90°C under a nitrogen atmosphere. Upon the conclusion of the reaction monitored by TLC, the mixture was left at rt for 1h in order to allow the precipitation of the desired product, which was filtered under vacuum and washed with dry THF first and then with petroleum ether thus furnishing the analytically pure **92** as white solid. TFA (178 mmol, 15eq) was added at 0°C to **92** and the resulting solution left to stir for 2h at rt. TFA salt **93** was obtained as a pink solid after the evaporation of TFA under vacuum followed by washes with a mixture of MeOH and Et_2O. 4-hydroxyisobenzofuran-1,3-dione **94** (11.05 mmol, 1eq) and **93** (11.05 mmol, 1eq) were dissolved in dry pyridine (35 mL) and left stirring for 24h at 110°C under a nitrogen atmosphere. Pyridine was evaporated under vacuum and water (10 mL) and HCl 2N solution (10 mL) were added to the obtained residue. The aqueous phase was extracted with warm AcOEt (30 mL x 10) and the combined organic layers were evaporated under reduced pressure, affording **36f** as a crude which was purified by column chromatography on silica gel eluting with a mixture $CHCl_3$/MeOH. The obtained product was finally purified trough trituration from a mixture of Et_2O/$CHCl_3$ furnishing the analytically pure **36f** by filtration as pale-yellow solid. **36f** (2.31mmol, 1eq) and K_2CO_3 (3.46mmol, 1.5eq) were suspended in dry DMF (3.5 mL), then *tert*-butyl bromoacetate (2.42mmol, 1.5eq) was added and the obtained mixture was stirred for 24h at rt. TLC showed the disappearance of starting material and water (7 mL) and AcOEt (140 mL) were added. The organic phase

was washed with brine (7 mL x 2) and then dried over anhydrous NaSO₄, filtered and evaporated under reduced pressure providing a crude that was purified by flash column chromatography eluting with a mixture AcOEt/*n*-hexane. Evaporation of the fractions containing **95** gave the analytically pure product which was then deprotected using a mixture of TFA:H₂O:TIS 95:2.5:2.5 at 0°C. After 6h 30min stirring at rt, TLC showed the completion of the reaction, volatiles were evaporated, and the obtained residue washed with DCM and Et₂O providing the correspondent acid **96** as white solid.

Synthesis of 2-(2,6-dioxopiperidin-3-yl)-5-hydroxyisoindoline-1,3-dione, 36g, (Scheme 4.1B).

To a solution of 4-hydroxyphtalic acid **97** (5.5mmol, 1eq) in KOH 1.7M aqueous solution (27.5 mmol, 5eq) benzyl bromide (6.05 mmol, 1.1eq) was added. The reaction mixture was heated at 120 °C and left to stir for 16h. When LC-MS analysis (acidic method) showed the disappearance of the starting material, HCl 2M was added until the obtaining of a precipitate, which was filtered under vacuum and washed over the filter with toluene to afford the title compound **98** as white solid. Compound **98** (5.9 mmol, 1eq) was dissolved in Ac₂O (34 mL) and the mixture was refluxed for 2h. The solvent was evaporated, and the required product **99** was obtained after crystallization from Ac₂O at -20 °C and used as a crude for the next step. **99** (2.6 mmol, 1 eq) was dissolved in glacial CH₃COOH (10 mL) and then 3-aminopiperidine-2,6-dione hydrochloride (2.6 mmol, 1eq) followed by NaAcO (3.12 mmol, 1.2eq) were added. The reaction was refluxed for 16h and after that time it was judge complete by LC-MS analysis (acidic method). After cooling, the mixture was poured into water (60 mL) and the solid formed filtered under vacuum. The solid over the filter was washed with water and petroleum ether to give the title compound **100** as light purple solid which was first dissolved in MeOH (5 mL), then the system was degassed (N₂), and Pd/C 10 % was added. The resulting mixture was stirred for 16h under H₂ atmosphere. The title compound **36g** was obtained after filtration on celite to remove palladium and evaporated under reduced pressure.

Synthesis of 2-(2,6-dioxopiperidin-3-yl)-5-(piperazin-1-yl)isoindoline-1,3-dione hydrochloride salt 36d (Scheme 4.1C).

4-fluorophtalic anhydride **101** (3.038 mmol, 1eq) was dissolved in CH₃COOH (10 mL) and 3-aminopiperidine-2,6-dione hydrochloride (3.038 mmol, 1eq) followed by NaAcO (3.646 mmol, 1.2eq) were added. The reaction mixture was refluxed for 16h and checked by LC-MS (acidic method). After cooling, the reaction mixture was poured into water (60 mL) and the solid formed filtered under vacuum. The solid over the filter was washed with water and petroleum ether to give the title compound **102** as light purple solid. To a stirring solution of **102** (2.33 mmol, 1eq) in NMP (4.5 mL), 1-Boc-piperazine (4.66 mmol, 2eq) followed by DIPEA (1.86 mmol, 0.4eq) were added and the resulting mixture was stirred at 90 °C for 16h. Upon the completion of the reaction checked by LC-MS (acidic method), water (6 mL) was added and then extracted with AcOEt (20 mL x 2). The organic layer was washed with brine and then died over anhydrous MgSO₄ thus filtered and evaporated under vacuum to obtain a crude that was purified with flash column chromatography eluting with a mixture in gradient with Heptane/AcOEt to yield the desired compound **103** as a yellow solid. **103** was dissolved in a solution of DCM/MeOH (9:1, 8.2 mL/0.9 mL) and HCl 4N in dioxane (9.1 mL) was added at 0°C. The reaction mixture was stirred at rt for 2h (checked by LC-MS, acidic method) and then volatile components were removed under reduced pressure providing the correspondent hydrochloride salt **36d** as a yellow solid.

Tert-butyl (2,6-dioxopiperidin-3-yl)carbamate, 92. Yield, 74%. **¹H-NMR** (400MHz; DMSO-d_6) δ 1.40 (s, 9H, -C(CH_3)$_3$), 1.89-1.91, 2.68-2.71 (m, 4H, -CH_2-CH_2-dioxopiperidine), 4.21-4.24 (m, 1H, -CH dioxopiperidine), 7.13 (d, 1H, -NH-COC(CH$_3$)$_3$), 10.75 (s, 1H, -NH dioxopiperidine).

3-aminopiperidine-2,6-dione trifluoroacetic salt, 93. Yield, quantitative. **¹H-NMR** (400MHz; DMSO-d_6) δ 2.00-2.13, 2.62-2.69 (m, 4H, -CH_2-CH_2- dioxopiperidine), 4.18-4.21 (m, 1H, -CH dioxopiperidine), 8.40 (s, 1H, -NH_2), 11.29 (s, 1H, -NH dioxopiperidine).

2-(2,6-dioxopiperidin-3-yl)-4-hydroxyisoindoline-1,3-dione, 36f. Yield, 84%.**¹H-NMR** (400MHz; DMSO-d_6) δ 1.95-2.06, 2.53-2.61 (m, 4H, -CH_2-CH_2- dioxopiperidine), 5.05-5.10 (m, 1H, -CH dioxopiperidine), 7.24-7.32 (m, 2H, -CH 4-hydroxyisoindoline-1,3-dione), 7.63-7.67 (m, 2H, -CH 4-hydroxyisoindoline-1,3-dione), 11.09 (s, 1H, -NH dioxopiperidine), 15.4 (s, 1H, -OH, 4-hydroxyisoindoline-1,3-dione).

Tert-butyl 2-((2-(2,6-dioxopiperidin-3-yl)-1,3-dioxoisoindolin-4-yl)oxy)acetate, 95. Yield, 92%. **¹H-NMR** (400MHz; DMSO-d_6) δ 1.41 (s, 9H, -C(CH_3)$_3$), 2.04-2.08, 2.62-2.86 (m, 4H, -CH_2-CH_2- dioxopiperidine), 4.72 (s, 2H, -CO-CH_2-O-), 4.88-4.92 (m, 1H, -CH dioxopiperidine), 7.03-7.05 (d, 1H, -CH 4-hydroxyisoindoline-1,3-dione), 7.44-7.46 (d, 1H, -CH 4-hydroxyisoindoline-1,3-dione), 7.58-7.62 (t, 1H, -CH 4-hydroxyisoindoline-1,3-dione), 7.92 (s, 1H, -NH dioxopiperidine).

2-((2-(2,6-dioxopiperidin-3-yl)-1,3-dioxoisoindolin-4-yl)oxy)acetic acid, 96. Yield, quantitative. **¹H-NMR** (400MHz; DMSO-d_6) δ 2.03-2.06, 2.57-2.62 2.86-2.94 (m, 4H, -CH_2-CH_2- dioxopiperidine), 5.76 (m, 1H, -CH dioxopiperidine), 7.39-7.41 (d, 1H, -CH 4-hydroxyisoindoline-1,3-dione), 7.47-7.49 (d, 1H, -CH 4-hydroxyisoindoline-1,3-dione), 7.78-7.80 (t, 1H, -CH 4-hydroxyisoindoline-1,3-dione), 11.11 (s, 1H, -NH dioxopiperidine), 13.05-13.49 (bs, 1H, -COOH).

4-(benzyloxy)phthalic acid, 98. Yield, 54%. **¹H-NMR** (400MHz; DMSO-d_6) δ 5.20 (s, 2H, -CH_2-Ph), 7.13-7.16 (d, 1H, -CH Ph), 7.32-7.45 (m, 5H, -CH Bn), 7.53 (s, 1H, -CH Ph), 7.78-7.80 (d, 1H, -CH Ph), 13.37 (s, 2H, -COOH).

5-(benzyloxy)isobenzofuran-1,3-dione, 99. Yield, quantitative. **¹H-NMR** (400MHz; DMSO-d_6) δ 5.14 (s, 2H, -CH_2-Ph), 7.48-7.49 (d, 1H, -CH isobenzofurane), 7.32-7.47 (m, 5H, -CH Bn), 7.88-7.89 (s, 1H, -CH Ph), 7.90-7.92 (d, 1H, -CH Ph).

5-(benzyloxy)-2-(2,6-dioxopiperidin-3-yl)isoindoline-1,3-dione, 100. Yield, 77%. **¹H-NMR** (400MHz; DMSO-d_6) δ 2.11-2.27 (m, 4H, -CH_2-CH_2- dioxopiperidine), 4.44-4.46 (m, 1H, -CH dioxopiperidine), 5.20 (s, 2H, -CH_2-Ph), 7.32-7.48 (m, 5H, -CH Bn), 7.55-7.59 (t, 2H, -CH hydroxyisoindoline-1,3-dione), 7.74-7.81 (t, 2H, -CH hydroxyisoindoline-1,3-dione), 10.95 (s, 1H, -NH dioxopiperidine).

2-(2,6-dioxopiperidin-3-yl)-5-hydroxyisoindoline-1,3-dione, 36g. Yield, quantitative. **¹H-NMR** (400MHz; DMSO-d_6) δ 2.02-2.10, 2.52-2.65, 2.83-2.95 (m, 4H, -CH_2-CH_2-dioxopiperidine), 5.1 (m, 1H, -CH dioxopiperidine), 7.15-7.21 (t, 2H, -CH hydroxyisoindoline-1,3-dione), 7.72-7.81 (t, 2H, -CH hydroxyisoindoline-1,3-dione), 10.98 (s, 1H, -NH dioxopiperidine), 11.05, (s, 1H, -OH, 4-hydroxyisoindoline-1,3-dione).

2-(2,6-dioxopiperidin-3-yl)-5-fluoroisoindoline-1,3-dione, 102. Yield, 77%. **¹H-NMR** (400MHz; DMSO-*d₆*) δ 2.51-2.64 (m, 4H, -C*H₂*-C*H₂*- dioxopiperidine), 5.13-5.18 (m, 1H, -C*H* dioxopiperidine), 7.69-7.74 (t, 1H, -C*H* 5-fluoroisoindoline-1,3-dione), 7.81-7.82 (d, 1H, -C*H* 5-fluoroisoindoline-1,3-dione), 7.99-8.0 (d, 1H, -C*H* 5-fluoroisoindoline-1,3-dione), 11.04 (s, 1H, -N*H* dioxopiperidine).

tert-butyl 4-(2-(2,6-dioxopiperidin-3-yl)-1,3-dioxoisoindolin-5-yl)piperazine-1-carboxylate, 103. Yield, 80%. **¹H-NMR** (400MHz; DMSO-*d₆*) δ 1.4 (s, 9H, -C(C*H₃*)₃, 1.99-2.04, 2.54-2.61 (m, 4H, -C*H₂*-C*H₂*- dioxopiperidine), 3.47-3.49 (m, 8H, -C*H₂*-C*H₂*- piperazine), 5.06-5.10 (m, 1H, -C*H* dioxopiperidine), 7.23-7.26 (d, 1H, -C*H* isoindoline-1,3-dione), 7.35 (s, 1H, C-*H* isoindoline-1,3-dione), 7.69-7.71 (d, 1H, -C*H* isoindoline-1,3-dione), 11.08 (s, 1H, -N*H* dioxopiperidine).

Synthesis of (2S,4R)-1-((S)-2-(1-fluorocyclopropane-1-carboxamido)-3,3-dimethylbutanoyl)-4-hydroxy-N-(((S)-6-hydroxy-4-(4-methylthiazol-5-yl)cyclohexa-1,3-dien-1-yl) methyl) pyrrolidine-2-carboxamide, 37c (Scheme 4.2).

To a stirring solution of 4-bromo-2-hydroxybenzonitrile **104** (19.23 mmol, 1eq), Pd(OAc)₂ (0.39 mmol, 0.02eq) and KOAc (38.5 mmol, 2eq) in DMA (20 mL), 4-methylthiazole **105** (38.5 mmol, 2eq) was added. The resulting mixture was heated to 150°C and stirred for 16h. Upon the completion of the reaction checked by LC-MS (acidic method), the mixture was cooled and quenched with water (10 mL) and brine (2 mL) thus extracted with AcOEt (20 mL x 3). The organic layers were combined and dried over anhydrous MgSO₄, filtered and evaporated under reduced pressure. The obtained crude was purified by flash column chromatography using a gradient of Heptane/AcOEt to yield the final compound as yellow solid. To a cooled (0°C) LiAlH₄ (67.90 mmol, 6eq, 28.3 mL) 2.4M THF solution, **106** (11.32 mmol, 1 eq) in THF (30 mL) was added drop by drop and the mixture turned from orange to dark red. The reaction was stirred at the beginning at rt and then heated at 50°C for 16h. After that time, the mixture was cooled at 0 °C and quenched with water and NaOH 3M (pH check): the resulting precipitate was filtered under vacuum and washed over the filter with THF and then with a solution of DCM/MeOH 8:2. The organic phases were collected and concentrated under vacuum giving a crude that was purified by flash column chromatography using a SNAP KP-NH eluting in gradient with DCM/MeOH to yield **107** as orange solid. To a solution of **107** (3.14 mmol, 1eq) in dry DMF (5 mL), *N*-Boc-trans-4-hydroxy-L-proline (3.14 mmol, 1eq) followed by DIPEA (9.43 mmol, 3eq) were added. The mixture was cooled at 0°C and PyOxim (3.14 mmol, 1eq) was added. The mixture was warmed to rt and left to stir for 3h, after which LC-MS check (acidic method) showed the disappearance of the starting material. DMF was evaporated and then water (3 mL) and brine (2 mL) were added to the obtained residue. The aqueous phase was extracted with DCM (8 mL x 3) and the organic layer washed with a saturated solution of NaHCO₃, dried over anhydrous MgSO₄, filtered and concentrated under reduced pressure obtaining a crude that was purified by flash column chromatography eluting with a mixture in gradient of DCM/MeOH providing the analytically pure desired compound **108**. **108** was dissolved in a mixture of DCM:MeOH (9 ml: 46 mL, 20:1) and then HCl 4N in dioxane (6.80 mmol, 10 eq) was added at 0°C. The reaction was stirred for 16h and the day after no starting material was detected by LC-MS check (acidic method). Volatile components were removed under vacuum providing the correspondent hydrochloride salt **109.** To a stirring solution of **109** (0.680 mmol, 1eq) in dry DMF (2 mL), *N*-BOC-L-Tert-Leu (0.680 mmol, 1eq) followed by DIPEA (2.04 mmol, 3eq) were added. The solution was cooled at 0°C and the PyOxim (0.680 mmol, 1eq) was added and the reaction was stirred for 16h. After that time, LC-MS (acidic method) check proved the completion of the reaction which was quenched with

water (3 mL) and extracted with DCM (3 mL x 5). The organic layer was washed with a saturated solution of NaHCO₃ (3 mL x 4) and then dried over anhydrous MgSO₄, filtered and evaporated under reduced pressure to give a crude that was purified by flash column chromatography eluting with a mixture in gradient of DCM/MeOH providing the expected compound **110**. Compound **111** was obtained starting from **110** and following the same procedure used for **109**. The obtained hydrochloride salt **111** (0.680 mmol, 1eq) and 1-fluorocyclopropane-1-carboxylic acid (0.680 mmol, 1eq) were dissolved in dry DMF (3.4 mL, 0.2M) and then DIPEA (3.4 mmol, 5 eq) was added (pH was checked, basic). The reaction was cooled at 0°C and PyOxim (0.680 mmol, 1eq) was added. After 2h under stirring, LC-MS (acidic method) showed the disappearance of the staring material. DMF was evaporated under vacuum and then brine (3 mL) was added to the obtained residue. The resulting aqueous phase was extracted with DCM (5mL x 3) and the organic layer washed with a saturated solution of NaHCO₃ and then dried over anhydrous MgSO₄, filtered and evaporated under reduced pressure providing a crude that was purified by C18 reverse phase column from 10 to 95%, H₂O HCOOH 2%: ACN over 22 min, obtaining the desired compound **37c**.

General procedure for the synthesis of linkers 114a,b,d and 116a-d (Scheme 4.3).

General procedure a. In a dried flask the opportune diol **112a,b** (3.33 mmol, 1eq) was dissolved in dry DMF (5 mL) and then NaH 60% min oil (9.99 mmol, 3eq) was added at 0°C under a nitrogen atmosphere. After 1h stirring, *tert*-buthyl bromoacetate (9.99 mmol, 3eq) was added dropwise at 0°C. After 16h, TLC showed the disappearance of starting materials. The obtained mixture was concentrated under vacuum and water (5 mL) was added and extracted with AcOEt (15 mL x 3). The combined organic phases were washed with a saturated solution of NH₄Cl (5 mL x 2) and then dried over anhydrous MgSO₄, filtered and evaporated under reduced pressure providing a crude that was purified by flash column chromatography eluting in gradient with a mixture AcOEt/Heptane obtaining the analytically pure **113a,b.**

General procedure b. *Tert*-butyl ester (**113a,b,d**) deprotection was achieved by treating the starting material with a solution of TFA in DCM (50% v/v) for 2h. The reaxtion was checked by LC-MS (acidic method), volatile components were removed and the crude mixture was left under vacuum to remove any excess of TFA leading to the desired dicarboxylic acid linker (**114a,b,d**).

General procedure c. In a dried flask the opportune diol **112a-c** (23.23 mmol, 3eq) was dissolved in dry DMF (9 mL) and then NaH 60% min oil (9.29 mmol, 1.2eq) was added at 0°C under a nitrogen atmosphere. After 1h stirring, *tert*-buthyl bromoacetate (7.74 mmol, 1eq) was added dropwise at 0°C. After 16h stirring at rt, TLC check showed the disappearance of starting materials. The obtained mixture was concentrated under vacuum and water (5 mL) was added and extracted with AcOEt (15 mL x 3). The combined organic phases were washed with a saturated solution of NH₄Cl (5 mL x 2) and then dried over anhydrous MgSO₄, filtered and evaporated under reduced pressure providing a crude that was purified by flash column chromatography eluting in gradient with a mixture AcOEt/Heptane obtaining the analytically pure **115a-c.**

General procedure d. The required alcohol **115a,c**, **117** (1.39 mmol, 1eq) was solubilized in dry DCM (10 mL) and then TEA (1.66 mmol, 1.2 eq) followed by TsCl (1.66 mmol, 1.2 eq) were added under nitrogen atmosphere and the obtained solution was stirred for 16h at rt. Upon the completion of the reaction monitored by TLC, water was added (5 mL) and then extracted with DCM (10 mL x 3). Combined organic layers were washed with a saturated solution of NH₄Cl (3 mL x 2) and then dried over anhydroys MgSO₄, filtered and evaporated under reduced pressure providing a crude that was purified by flash column

chromatography eluting in gradient with a mixture AcOEt/Heptane obtaining the desired pure compound **116a,c** and **118** as colorless oil.

General procedure e. **115b** (2.56 mmol, 1eq) was dissolved in dry DCM (5 mL) and PPh$_3$ (2.8 mmol, 1.1 eq) followed by CBr$_4$ (1.56 mmol, 1eq) were added at 0°C. The solution was left stirring at rt for 16h until the complete conversion of the starting material in the desired product was proved by TLC check. The mixture was directly purified by flash column chromatography eluting in gradient with a mixture AcOEt/Heptane obtaining the desired pure compound **116b** as a colorless oil.

General procedure f. In a dried flask propan-1,3-diol **112d** (30.03 mmol, 3eq) was dissolved in dry DMF (10 mL) and then NaH 60% mineral oil (12.01 mmol, 1.2eq) was added at 0°C under a nitrogen atmosphere. After 1h stirring, **118** (10.01 mmol, 1eq) was added dropwise at 0°C. After 16h TLC showed the completion of the reaction. The obtained mixture was concentrated under vacuum and water (5 mL) was added and extracted with AcOEt (15 mL x 3). The combined organic phases were washed with a saturated solution of NH$_4$Cl (5 mL x 2) and then dried over anhydroys MgSO$_4$, filtered and evaporated under reduced pressure providing a crude that was purified by flash column chromatography eluting in gradient with a mixture AcOEt/Heptane obtaining the analytically pure **119** as a colorless oil.

General procedure g. In a dried flask the appropriate alcohol **115d, 119** (2.12 mmol, 1eq) and RhOAc (0.107 mmol, 0.05eq) were dissolved in dry DCM (5 mL) under nitrogen atmosphere. The resulting green suspension was cooled at 0°C and N$_2$CHCOOtBu (3.18 mmol, 1.5eq) was added very slowly drop by drop to the stirred mixture keeping a nitrogen flux and left to stir at rt. 16h later, upon the disappearance of the starting material highlited by TLC, the green mixture was purified by flash column chromatography eluting in gradient with a mixture AcOEt/Heptane. Evaporation of the fractions containing **113c, 120** gave the desired analytically pure colorless oil.

General procedure h. **120** (0.786 mmol, 1eq) was dissolved in MeOH (8 mL) and the system was degassed (N$_2$). Pd/C 10% p/p was added, and the mixture was stirred for 16h under H$_2$. After that time, the reaction was judge complete by TLC analysis. The suspension was filter on filter paper to remove palladium and evaporated under reduced pressure to afford **115d** as a colorless oil.

General procedure i. **115d** (0.39 mmol, 1eq) was solubilized in dry DCM (5 mL) and then TEA (1.35 mmol, 3.5eq) followed by DMAP (0.023 mmol, 0.06eq) and TsCl (0.5 mmol, 1.2eq) were added under nitrogen atmosphere. The obtained solution was stirred for 16h at rt and checked by TLC. Water was added (3 mL), extracted with DCM (5 mL x 3) and the combined organic layers were washed with a saturated solution of NH$_4$Cl (2 mL x 2) and then dried over anhydrous MgSO$_4$, filtered and evaporated under reduced pressure providing a crude that was purified by flash column chromatography eluting in gradient with a mixture AcOEt/Heptane thus obtaining the desired pure compound **116d** as a colorless oil.

Di-tert-butyl 3,6,9,12-tetraoxatetradecanedioate, 113a. Yield, 96%. **^{1}H-NMR** (400MHz; CDCl$_3$) δ 1.5 (s, 18H, -C(CC*H$_3$*)$_3$), 3.65-3.82 (m, 12H, -O-C*H$_2$*-C*H$_2$*-O-), 4.05 (s, 4H, -O-C*H$_2$*-CO-).

Di-tert-butyl 2,2'-(but-2-yne-1,4-diylbis(oxy))diacetate, 113b. Yield, 40%. **^{1}H-NMR** (400MHz; CDCl$_3$) δ 1.5 (s, 18H, -C(CC*H$_3$*)$_3$), 4.05 (s, 4H, -C*H$_2$*-O-), 4.35 (s, 4H, -O-C*H$_2$*-CO-).

Di-tert-butyl 2,2'-((oxybis(propane-3,1-diyl))bis(oxy))diacetate, 113d. Yield, 54%. **¹H-NMR** (400MHz; CDCl$_3$) δ 1.4 (s, 18H, -C(CC*H$_3$*)$_3$), 1.77-1-84 (m, 4H, -CH$_2$-C*H$_2$*-CH$_2$-), 3.44-3.54 (m, 8H, -C*H$_2$*-CH$_2$-C*H$_2$*-), 3.87-3.88 (d, 4H, -O-C*H$_2$*-CO-).

3,6,9,12-tetraoxatetradecanedioic acid, 114a. Yield, quantitative. **¹H-NMR** (400MHz; CDCl$_3$) δ 3.65-3.85 (m, 12H, -O-C*H$_2$*-C*H$_2$*-O-), 4.2 (s, 4H, -O-C*H$_2$*-CO-), 10.5 (s, 2H, -COO*H*)

2,2'-(but-2-yne-1,4-diylbis(oxy))diacetic acid, 114b. Yield, quantitative. **¹H-NMR** (400MHz; DMSO-*d$_6$*) δ 4.05 (s, 4H, -C*H$_2$*-O-), 4.30 (s, 4H, -O-C*H$_2$*-CO-), 12.8 (s, 2H, -COO*H*).

2,2'-((oxybis(propane-3,1-diyl))bis(oxy))diacetic acid, 114d. Yield, quantitative. **¹H-NMR** (400MHz; DMSO-*d$_6$*) δ 1.79-1-85 (m, 4H, -CH$_2$-C*H$_2$*-CH$_2$-), 3.48-3.57 (m, 8H, -C*H$_2$*-CH$_2$-C*H$_2$*-), 4.31-4.33 (s, 4H, -O-C*H$_2$*-CO-), 12.85 (s, 2H, -COO*H*).

tert-butyl 2-(2-(2-(2-hydroxyethoxy)ethoxy)ethoxy)acetate, 115a. Yield, 77%. **¹H-NMR** (400MHz; CDCl$_3$) δ 1.5 (s, 9H, -C(CC*H$_3$*)$_3$), 3.63-3.76 (m, 12H, -C*H$_2$*-C*H$_2$*-) 4.05 (s, 2H, -O-C*H$_2$*-CO-), 5.5 (s, 1H, -O*H*).

tert-butyl 2-((4-hydroxybut-2-yn-1-yl)oxy)acetate, 115b. Yield, 55%. **¹H-NMR** (400MHz; CDCl$_3$) δ 1.5 (s, 9H, -C(CC*H$_3$*)$_3$), 1,8 (s, 1H, -O*H*), 4.1 (s, 2H, -O-C*H$_2$*-CO-), 4.45 (s, 4H, -O-C*H$_2$*-C-).

tert-butyl 2-(2-hydroxyethoxy)acetate, 115c. Yield, 15%. **¹H-NMR** (400MHz; CDCl$_3$) δ 1.5 (s, 9H, -C(CC*H$_3$*)$_3$), 3.68-3.70 (m, 4H, HO-C*H$_2$*-C*H$_2$*-O-), 4.1 (s, 2H, -O-C*H$_2$*-CO-), 1.8 (s, 1H, -O*H*).

tert-butyl 2-(3-(3-hydroxypropoxy)propoxy)acetate, 115d. Yield, 86%. **¹H-NMR** (400MHz; CDCl$_3$) δ 1.49 (s, 9H, -C(CC*H$_3$*)$_3$), 1.80-1.92 (m, 4H, -CH$_2$-C*H$_2$*-CH$_2$-), 2.47 (s, 1H, -O*H*), 3.56-3.76 (m, 6H, -C*H$_2$*-CH$_2$-C*H$_2$*-, HO-CH$_2$-CH$_2$-C*H$_2$*-), 3.76-3.79 (t, 2H, HO-CH$_2$-CH$_2$-C*H$_2$*-), 3.96 (s, 2H, -O-C*H$_2$*-C-).

tert-butyl 2-(2-(2-(2-(tosyloxy)ethoxy)ethoxy)ethoxy)acetate, 116a. Yield, 83%. **¹H-NMR** (400MHz; CDCl$_3$) δ 1.52 (s, 9H, -C(CC*H$_3$*)$_3$), 2.5 (s, 3H, -C*H$_3$*), 3.62-3.75 (m, 10H, -O-C*H$_2$*-C*H$_2$*-O-C*H$_2$*-C*H$_2$*-O-C*H$_2$*-CH$_2$-OTs), 4.05 (m, 2H, -C*H$_2$*-OTs), 7.35-7.38 (d, 2H, -C*H* tosyl), 7.75-87.83 (d, 2H, -C*H* tosyl).

tert-butyl 2-((4-bromobut-2-yn-1-yl)oxy)acetate, 116b. Yield, 55%. **¹H-NMR** (400MHz; CDCl$_3$) δ 1.5 (s, 9H, -C(CC*H$_3$*)$_3$), 3.95-3.97 (t, 2H, -C-C*H$_2$*-O-), 4.05 (s, 2H, -O-C*H$_2$*-C-), 4.37- 4.41 (t, 2H, -C-C*H$_2$*-Br).

tert-butyl 2-(2-(tosyloxy)ethoxy)acetate, 116c. Yield, 63%. **¹H-NMR** (400MHz; CDCl$_3$) δ 1.49 (s, 9H, -C(CC*H$_3$*)$_3$), 2.5 (s, 3H, -C*H$_3$*), 3.75-3.81 (m, 2H, Ts-O-CH$_2$-C*H$_2$*-O-), 3.95 (s, 2H, -O-C*H$_2$*-C-), 4.21-4.25 (m, 2H, Ts-O-C*H$_2$*-CH$_2$-O-), 7.46-7.49 (d, 2H, -C*H* tosyl), 7.81-7.85 (d, 2H, -C*H* tosyl).

tert-butyl 2-(3-(3-(tosyloxy)propoxy)propoxy)acetate, 116d. Yield, 64%. **¹H-NMR** (400MHz; CDCl$_3$) δ 1.5 (s, 9H, -C(CC*H$_3$*)$_3$), 1.79-1.85, 1.88-1.94 (m, 4H, -O-CH$_2$-C*H$_2$*-CH$_2$-O-) 2.45 (s, 3H, -C*H$_3$*), 3.43-3.47 (m, 4H, -O-C*H$_2$*-CH$_2$-C*H$_2$*-O-CH$_2$-), 3.54-3.58 (m,

2H, Ts-O-CH$_2$-CH$_2$-C*H*$_2$-O-), 3.95 (s, 2H, -O-C*H*$_2$-CO-), 4.12-4.18 (t, 2H, Ts-O-C*H*$_2$-CH$_2$-CH$_2$-O-), 7.36-7.38 (d, 2H, -C*H* tosyl), 7.79-7.82 (d, 2H, -C*H* tosyl).

3-(benzyloxy)propyl 4-methylbenzenesulfonate, 118. Yield, 84%. **¹H-NMR** (400MHz; CDCl$_3$) δ 1.95 (m, 2H, -O-CH$_2$-C*H*$_2$-CH$_2$-O-Ts), 2.5 (s, 3H, -C*H*$_3$), 3.52-3.56 (m, 2H, -O-C*H*$_2$-CH$_2$-CH$_2$-O-Ts), 4.18-4.25 (m, 2H, O-CH$_2$-CH$_2$-C*H*$_2$-O-Ts), 4.48 (s, 2H, -O-C*H*$_2$-Ph), 7.21-7.35 (5H, C-*H*, -Ph), 7.36-41 (d, 2H, -C*H* tosyl), 7.78-7.84 (d, 2H, -C*H* tosyl).

3-(3-(benzyloxy)propoxy)propan-1-ol, 119. Yield, 60%. **¹H-NMR** (400MHz; CDCl$_3$) δ 1.82-1.92 (m, 4H, -O-CH$_2$-C*H*$_2$-CH$_2$-O-, -O-CH$_2$-C*H*$_2$-CH$_2$-OH), 2.55 (s, 1H, -OH), 3.55-3.63 (m, 6H, -O-C*H*$_2$-CH$_2$-C*H*$_2$-O-, -O-C*H*$_2$-CH$_2$-CH$_2$-OH), 3.75-3.78 (t, 2H, -C*H*$_2$-OH), 4.52 (s, 2H, -O-C*H*$_2$-Ph), 7.27-7.38 (5H, -C*H*, -Ph).

tert-butyl 2-(3-(3-(benzyloxy)propoxy)propoxy)acetate, 120. Yield, 81%. **¹H-NMR** (400MHz; CDCl$_3$) δ 1.5 (s, 9H, -C(CC*H*$_3$)$_3$), 1.86-1.93 (m, 4H, -O-CH$_2$-C*H*$_2$-CH$_2$-O-), 3.52-3.62 (m, 8H, -O-C*H*$_2$-CH$_2$-C*H*$_2$-O-), 3.96 (s, 2H, -O-C*H*$_2$-CO-), 4.52 (s, 2H, -O-C*H*$_2$-Ph), 7.28-7.39 (5H, C-*H*, -Ph).

General procedure for the synthesis of intermediates 123a-d (Scheme 4.4A), 125a-d (Scheme 4.4B), 127a-d (Scheme 4.4C).

General procedure a. Acid **96** (0.451 mmol, 1eq) and the proper amine **121a-d** (0.497 mmol, 1.1eq) were dissolved in dry DMF (2 mL), then DIPEA (0.903 mmol, 2eq) followed by HATU (0.497 mmol, 1.1eq) were added under nitrogen atmosphere and the obtained solution was left to stir for 7h. After that time, TLC check showed the disappearance of the starting materials and DMF was removed under vacuum. A saturated solution of NaHCO$_3$ (12 mL) was added and the aqueous phase extracted with a mixture 4:1 CHCl$_3$: isopropanol (9 mL x 4). The resulting organic layers were washed with a saturated solution of NaHCO$_3$ (6 mL x 2) and brine (3 mL) and then dried over anhydrous Na$_2$SO$_4$, thus filtered and evaporated under reduced pressure providing a crude that was purified by column chromatography on silica gel eluting with a mixture CHCl$_3$/MeOH. Evaporation of the fractions containing the require intermediate **122a-d** gave the analytically pure product.

General procedure b. The proper intermediate **122a-d** was deprotected using a solution of TFA in DCM (50% v/v) that was added at 0°C. After 7h under stirring at rt, the reaction was judge complete by TLC and volatile components were removed under vacuum. After different washes with a mixture of DCM and Et$_2$O, the crude was left under vacuum to remove any excess of TFA leading to the desired amino-TFA salt (**123a,b**) or carboxylic acid linker (**123c,d**).

General procedure c. **36g** (0.036 mmol, 1eq) and the required linkers **116a-d** (0.044 mmol, 1eq) were dissolved in dry DMF (0.5 mL) and then K$_2$CO$_3$ (0.108 mmol, 3eq) followed by KI (0.036 mmol, 1eq) were added at rt. After 48h under stirring at 100°C, the mixture was directly purified by HPLC with gradient from 15% to 90% v/v acetonitrile with 0.01% v/v aqueous solution of HCOOH over 10 min to yield the desired compound **124a-d.**

General procedure d. The require **124a-d** and **126a-d** (0.044 mmol, 1eq) were dissolved in DCM (0.8 mL) and then the solution was cooled at 0°C and TFA (0.2mL) followed by TIPS (10.4 μL) were added. The reaction was stirred for 2h at rt and after that time the complete conversion of starting material was proved by LC-MS (acidic method). Volatile components were removed, and the obtained crude mixture was left under vacuum to remove any excess of TFA leading to the desired compounds **125a-d** and **127a-d**.

General procedure e. **36d** (0.044 mmol, 1eq) and the proper linker **116a-d** (0.046 mmol, 1.2eq) were dissolved in dry DMF (0.5 mL) and then DIPEA (0.22 mmol, 5eq) was added at rt. The reaction was stirred for 24h at 100°C and checked by LC-MS (acidic method).

The mixture was cooled at rt, then water (2 mL) was added and extracted with DCM (5 mL x 10). The combined organic layers were dried over anhydrous MgSO4, filtered and evaporated under vacuum. The obtained brown solid **126 a-d** was use for the next step without further purification.

tert-butyl (1-((2-(2,6-dioxopiperidin-3-yl)-1,3-dioxoisoindolin-4-yl)oxy)-2-oxo-7,10,13 trioxa-3-azahexadecan-16-yl)carbamate, 122a. Yield, 67%. **¹H-NMR** (400MHz; CDCl₃) δ 1.36 (s, 9H, -C(CH_3)₃), 1.67-1.77, 1.79-1.84 (m, 4H, -CH_2-CH_2- dioxopiperidine), 2.07-2.1, 2.68-2.72, 3.12-3.14, 3.44-3.59 (m, 20H, -CH_2- linker), 4.57 (s, -O-CH_2-CO-), 4.92-2.95 (m, 1H, -CH dioxopiperidine), 5.08 (s, 1H, -NHBOC), 7.12-7.14 (d, 1H, -CH dioxoisoindoline), 7.48-7.50 (d, 1H, -CH dioxoisoindoline), 7.52 (s, 1H, -CO-NH-CH₂-), 7.65-7.67 (t, 1H, -CH dioxoisoindoline), 8.6 (s, 1H, -NH dioxopiperidine).

tert-butyl(2-(2-(2-(2-((2-(2,6-dioxopiperidin-3-yl)-1,3-dioxoisoindolin-4-yl)oxy)acetamido)ethoxy)ethoxy)ethyl)carbamate, 122b. Yield, 73%. **¹H-NMR** (400MHz; CDCl₃) δ 1.36 (s, 9H, -C(CH_3)₃), 2.02-2.12, 2.64-2.88 (m, 4H, -CH_2-CH_2- dioxopiperidine), 3.22-3.29 (m, 2H, -CH_2-NH-COC(CH_3)₃), 3.46-3.59 (m, 10H, -CH_2-CH_2-O-CH_2-CH_2-O-CH_2-CH₂-NH-COC(CH_3)₃), 4.59 (s, 2H, -O-CH_2-CO-), 4.88-4.93 (m, 1H, -CH dioxopiperidine), 5.08 (s, 1H, -NH-BOC), 7.11-7.14 (d, 1H, -CH dioxoisoindoline), 7.11-7.14 (d, 1H, -CH dioxoisoindoline), 7.50-7.55 (d, 1H, -CH dioxoisoindoline), 7.65 (s, 1H, -CO-NH-CH₂-), 8.5 (s, 1H, -NH dioxopiperidine).

tert-butyl 1-((2-(2,6-dioxopiperidin-3-yl)-1,3-dioxoisoindolin-4-yl)oxy)-2-oxo-6,9,12 trioxa-3-azapentadecan-15-oate, 122c. Yield, 75%. **¹H-NMR** (400MHz; CDCl₃) δ 1.36 (s, 9H, -C(CH_3)₃), 2.07-2.09, 2.67-2.85 (m, 4H, -CH_2-CH_2- dioxopiperidine), 2.41-2.50, 3.48-3.70 (m, 16H, -CH_2- linker), 4.58 (s, 2H, -O-CH_2-CO-), 4.87-4.90 (m, 1H, -CH dioxopiperidine), 7.11-7.13 (d, 1H, -CH dioxoisoindoline), 7.47-7.49 (d, 1H, -CH dioxoisoindoline), 7.56 (s, 1H, -CO-NH-CH₂-), 7.65-7.68 (t, 1H, -CH dioxoisoindoline), 8.64 (s, 1H, -NH dioxopiperidine).

tert-butyl3-(2-(2-(2-((2-(2,6-dioxopiperidin-3-yl)-1,3-dioxoisoindolin-4-yl)oxy)acetamido)ethoxy)ethoxy)propanoate, 122d. Yield, 73%. **¹H-NMR** (400MHz; CDCl₃) δ 1.45 (s, 9H, -C(CH_3)₃), 2.17-2.18, 2.69-2.95 (m, 4H, -CH_2-CH_2- dioxopiperidine), 2.48-2.52, 3.53-3.75 (m, 10H, -CH_2-linker), 4.65 (s, 2H, -O-CH_2-CO-), 4.92-5.00 (m, 1H, -CH dioxopiperidine), 7.18-7.20 (d, 1H, C-H dioxoisoindoline), 7.54-7.56 (d, 1H, C-H dioxoisoindoline), 7.62 (s, 1H, -CO-NH-CH₂-), 7.72-7.76 (t, 1H, C-H dioxoisoindoline), 8.58 (s, 1H, NH dioxopiperidine).

N-(3-(2-(2-(3-aminopropoxy)ethoxy)ethoxy)propyl)-2-((2-(2,6-dioxopiperidin-3-yl)-1,3-dioxoisoindolin-4-yl)oxy)acetamide trifluoroacetic salt, 123a. Yield, quantitative. **¹H-NMR** (400MHz; CDCl₃) δ 1.73-1.78, 1.91-2.04 (m, 2H, -CH_2-CH_2- dioxopiperidine), 2.04-2.13, 3.17-3.18, 3.39-3.45, 3.50-3.69 (m, 20H, -CH_2-linker), 4.62 (s, 2H, -O-CH_2-CO-), 4.88-4.92 (m, 1H, -CH dioxopiperidine), 7.17-7.20 (d, 1H, -CH dioxoisoindoline), 7.48-7.51 (d, 1H, -CH dioxoisoindoline), 7.68 (s, 2H, -NH_2), 7.68-7.70 (t, 1H, -CH dioxoisoindoline), 8.5 (t, 1H, -CO-NH-CH₂-), 11.25 (s, 1H, -NH dioxopiperidine).

N-(2-(2-(2-aminoethoxy)ethoxy)ethyl)-2-((2-(2,6-dioxopiperidin-3-yl)-1,3 dioxoisoindolin-4-yl)oxy)acetamide trifluoroacetic salt, 123b. Yield, quantitative. **¹H-NMR** (400MHz; CDCl₃) δ 2.03-2.09, 2.90-2.99 (m, 4H, -CH_2-CH_2- dioxopiperidine), 2.58-2.67, 3.48-3.60 (m, 12H, -CH_2-linker), 4.80 (s, 2H, -O-CH_2-CO-), 5.10-45.14 (m, 1H, -CH dioxopiperidine), 7.41-7.43 (d, 1H, -CH dioxoisoindoline), 7.51-7.53 (d, 1H, -CH

dioxoisoindoline), 7.78 (s, 2H, -N*H₂*), 7.82-7.85 (t, 1H, -C*H* dioxoisoindoline), 7.98-8.00 (t, 1H, -CO-N*H*-CH₂-), 11.13 (s, 1H, -N*H* dioxopiperidine).

1-((2-(2,6-dioxopiperidin-3-yl)-1,3-dioxoisoindolin-4-yl)oxy)-2-oxo-6,9,12-trioxa-3-azapentadecan-15-oic acid, 123c. Yield, quantitative. **¹H-NMR** (400MHz; CDCl₃) δ 2.10-2.13, 2.82-2.89, 3.40-3.61 3.68-3.72 (m, 16H, -C*H₂*-linker), 2.50-2.54, 2.72-2.76 (m, 2H, -C*H₂*-C*H₂*- dioxopiperidine), 4.61 (s, 2H, -O-C*H₂*-CO-), 4.88-4.92 (m, 1H, -C*H* dioxopiperidine), 7.13-7.15 (d, 1H, -C*H* dioxoisoindoline), 7.45-7.50 (d, 1H, -C*H* dioxoisoindoline), 7.63-7.66 (t, 1H, -CO-N*H*-CH₂-), 7.67-7.70 (d, 1H, -C*H* dioxoisoindoline), 9.38 (s, 1H, -N*H* dioxopiperidine), 12.2 (s, 1H, -COO*H*).

3-(2-(2-(2-((2-(2,6-dioxopiperidin-3-yl)-1,3-dioxoisoindolin-4-yl)oxy)acetamido)ethoxy)ethoxy)propanoic acid 123d. Yield, quantitative. **¹H-NMR** (400MHz; CDCl₃) δ 2.02-2.1, 2.65-2.72 (m, 2H, -C*H₂*-C*H₂*- dioxopiperidine), 3.40-3-75 (m, 12H, -C*H₂*-linker), 4.63 (s, 2H, -O-C*H₂*-CO-), 4.85-4.95 (m, 1H, -C*H* dioxopiperidine), 7.14-7.16 (d, 1H, -C*H* dioxoisoindoline), 7.45-7.50 (d, 1H, -C*H* dioxoisoindoline), 7.66-7.68 (d, 1H, -C*H* dioxoisoindoline), 7.7-7.81 (t, 1H, -CO-N*H*-CH₂-), 9.12 (s, 1H, -N*H* dioxopiperidine), 12.2 (s, 1H, -COO*H*).

tert-butyl2-(2-(2-(2-((2-(2,6-dioxopiperidin-3-yl)-1,3-dioxoisoindolin-5-yl)oxy)ethoxy)ethoxy)ethoxy)acetate, 124a. Yield, 30%. **¹H-NMR** (400MHz; CDCl₃) δ 1.5 (s, 9H, -C(C*H₃*)₃), 2.15-2.20, 2.72-2.92 2 (m, 4H, -C*H₂*-C*H₂*- dioxopiperidine), 3.69-3.77, 3.91-3.94 (m, 12H, -C*H₂*-linker), 4.12 (s, 2H, -O-C*H₂*-CO-), 4.94-5.0 (m, 1H, -C*H* dioxopiperidine), 7.24-7.28 (dd, 1H, -C*H* dioxoisoindoline), 7.39-7.40 (d, 1H, -C*H* dioxoisoindoline), 7.80-7.81 (d, 1H, -C*H* dioxoisoindoline), 7.9 (s, 1H, -N*H* dioxopiperidine).

tert-butyl2-((4-((2-(2,6-dioxopiperidin-3-yl)-1,3-dioxoisoindolin-5-yl)oxy)but-2-yn-1-yl)oxy)acetate, 124b. Yield, 20%. **¹H-NMR** (400MHz; CDCl₃) δ 1.7 (s, 9H, -C(C*H₃*)₃), 2.18-2.24, 2.85-3.01 2 (m, 4H, -C*H₂*-C*H₂*- dioxopiperidine), 4.10- 4.15 (m, 4H, -CH₂-O-C*H₂*-C- linker), 4.33 (s, 2H, -O-C*H₂*-CO-), 4.55-4.60 (m, 1H, -C*H* dioxopiperidine), 4.63-4.75 (m, 4H, -C-C*H₂*- linker), 7.31-7.33 (dd, 1H, -C*H* dioxoisoindoline), 7.37-7.40 (d, 1H, -C*H* dioxoisoindoline), 7.83-7.84 (d, 1H, -C*H* dioxoisoindoline), 8.2 (s, 1H, -N*H* dioxopiperidine).

tert-butyl 2-(2-((2-(2,6-dioxopiperidin-3-yl)-1,3-dioxoisoindolin-5-yl)oxy)ethoxy)acetate, 124c. Yield, 22%. **¹H-NMR** (400MHz; CDCl₃) δ 1.5 (s, 9H, -C(C*H₃*)₃), 2.15-2.20, 2.72-2.92 2 (m, 4H, -C*H₂*-C*H₂*- dioxopiperidine), 3.98-4.00, 4.30- 4.33 (m, 4H, -C*H₂*-linker), 4.1 (s, 2H, -O-C*H₂*-CO-), 4.95-5.0 (m, 1H, -C*H* dioxopiperidine), 7.25-7.28 (dd, 1H, -C*H* dioxoisoindoline), 7.39-7.40 (d, 1H, -C*H* dioxoisoindoline), 7.80-7.81 (d, 1H, -C*H* dioxoisoindoline), 8.0 (s, 1H, -N*H* dioxopiperidine).

tert-butyl2-(3-(3-((2-(2,6-dioxopiperidin-3-yl)-1,3-dioxoisoindolin-5-yl)oxy)propoxy)propoxy)acetate, 124d. Yield, 30%. **¹H-NMR** (400MHz; CDCl₃) δ 1.49 (s, 9H, -C(C*H₃*)₃), 1.88-1.94, 2.07-2.19 (m, 4H, -C*H₂*-C*H₂*- dioxopiperidine), 2.72-2.92, 3.56-3.64, 4.20-4.23 (m, 12H, -C*H₂*-C*H₂*-C*H₂*- linker), 3.95 (s, 2H, -O-C*H₂*-CO-), 4.95-4.99 (m, 1H, -C*H* dioxopiperidine), 7.20-7.23 (d, 1H, -C*H* dioxoisoindoline), 7.37-7.38 (d, 1H, -C*H* dioxoisoindoline), 7.78-7.80 (d, 1H, -C*H* dioxoisoindoline), 8.04 (s, 1H, -N*H* dioxopiperidine).

tert-butyl2-(2-(2-(2-(4-(2-(2,6-dioxopiperidin-3-yl)-1,3-dioxoisoindolin-5-yl)piperazin-1-yl)ethoxy)ethoxy)ethoxy)acetate, 126a. Yield, quantitative. **¹H-NMR** (400MHz; CDCl₃) δ 1.4 (s, 9H, -CC*H₃*)₃), 2.04-2.07, 2.27-2.28, 2.62-2.65 (m, 4H, -C*H₂*-C*H₂*- dioxopiperidine), 2.69-2.88, 3.34-3.40, 3.49-3.51 (m, 8H, -C*H₂*-C*H₂*- piperazine), 3.54-3.70 (m, 12H, -C*H₂*-C*H₂*- linker), 3.95 (s, 2H, -O-C*H₂*-CO-), 4.84-4.90 (m, 1H, -C*H* dioxopiperidine), 6.97-7.01 (d, 1H, -C*H* dioxoisoindoline), 7.20-7.24 (d, 1H, -C*H* dioxoisoindoline), 7.60-7.71 (d, 1H, -C*H* dioxoisoindoline), 8.02 (s, 1H, -N*H* dioxopiperidine).

tert-butyl 2-((4-(4-(2-(2,6-dioxopiperidin-3-yl)-1,3-dioxoisoindolin-5-yl)piperazin-1-yl)but-2-yn-1-yl)oxy)acetate, 126b. Yield, quantitative. **¹H-NMR** (400MHz; CDCl₃) δ 1.4 (s, 9H, -C(C*H₃*)₃), 2.11-2.27 (m, 4H, -C*H₂*-C*H₂*- dioxopiperidine), 2.45-2.48, 3.44-3.47 (m, 8H, -C*H₂*-C*H₂*- piperazine), 2.73 (s, 2H, -C-C*H₂*-N- linker), 2.88 (s, 2H, -C-C*H₂*-O- linker), 3.95 (s, 2H, -O-C*H₂*-CO-), 4.85-4.89 (m, 1H, -C*H* dioxopiperidine), 6.99-7.01 (d, 1H, -C*H* dioxoisoindoline), 7.20-7.23 (d, 1H, -C*H* dioxoisoindoline), 7.61-7.63 (d, 1H, -C*H* dioxoisoindoline), 7.94 (s, 1H, -N*H* dioxopiperidine).

tert-butyl2-(2-(4-(2-(2,6-dioxopiperidin-3-yl)-1,3-dioxoisoindolin-5-yl)piperazin-1-yl)ethoxy)acetate, 126c. Yield, quantitative. **¹H-NMR** (400MHz; CDCl₃) δ 1.2 (s, 9H, -C(C*H₃*)₃), 1.35-1.37, 2.61-2.88 (m, 4H, -C*H₂*-C*H₂*- dioxopiperidine), 1.40-1.53, 2.61- 2.88 (m, 8H, -C*H₂*-C*H₂*- piperazine), 2.27-2.28, 2.29-3.05, 3.55-3.61, 3.75-3.78 (m, 4H, -C*H₂*-C*H₂*- linker), 3.90 (s, 2H, -O-C*H₂*-CO-), 4.85-4.89 (m, 1H, -C*H* dioxopiperidine), 7.01-7.1 (d, 1H, -C*H* dioxoisoindoline), 7.16-7.24 (d, 1H, -C*H* dioxoisoindoline), 7.64-7.71 (d, 1H, -C*H* dioxoisoindoline), 8.1 (s, 1H, -N*H* dioxopiperidine).

tert-butyl2-(3-(3-(4-(2-(2,6-dioxopiperidin-3-yl)-1,3-dioxoisoindolin-5-yl)piperazin-1-yl)propoxy)propoxy)acetate, 126d. Yield, quantitative. **¹H-NMR** (400MHz; CDCl₃) δ 1.4 (s, 9H, -C(C*H₃*)₃), 1.72-2.0 (m, 4H, -C*H₂*-C*H₂*- dioxopiperidine), 2.04-2.01, 2.27-2.29, 2.60-2.87, 3.0-3.13 (m, 8H, -C*H₂*-C*H₂*- piperazine), 3.21-3.74 (m, 12H, -C*H₂*-C*H₂*-C*H₂*- linker), 3.86 (s, 2H, -O-C*H₂*-CO-), 4.85-4.89 (m, 1H, -C*H* dioxopiperidine), 7.08-7.1 (d, 1H, -C*H* dioxoisoindoline), 7.22-7.24 (d, 1H, -C*H* dioxoisoindoline), 7.58-7.68 (d, 1H, -C*H* dioxoisoindoline), 8.3 (s, 1H, -N*H* dioxopiperidine).

Synthesis of intermediates 129a-d (Scheme 4.5A), 131a-d (Scheme 4.5B) and 133a-d (Scheme 4.5C).

General method a. The proper dicarboxylic acid linker **114a-d** (1.09 mmol, 1eq) and NHS (1.20 mmol, 1.1eq) were dissolved in dry DCM (6 mL). DCC (1.31 mmol, 1.2eq) was added and the reaction was left to stir at rt for 16h. After that time, TLC showed the completion of the reaction, the dicyclohexylurea was filtered off under vacuum and the solution was evaporated obtaining the desired compound **128a-d** without further purification.

General method b. The require NHS-ester **128a-d** (0.272 mmol, 1eq) was dissolved in dry DMF and the VHL ligand **37f** (0.136mmol, 0.5eq) followed by DIPEA (0.216 mmol, 3eq) were added. The mixture was left to stir at rt, and after 2h, LC-MS check (acidic method) showed no starting material. The reaction was quenched with water (0.3 mL) and purified by HPLC using a gradient from 5 to 70% v/v acetonitrile with 0.01% v/v aqueous solution of HCOOH over 10 min providing the desired compound **129a-d**.

General method c. VHL ligand **37c** (0.038 mmol, 1eq), appropriate linker hosting a good leaving group (-Ts or -Br) **116a-d** (0.056 mmol, 1.5 eq) and K₂CO₃ (0.114 mmol, 3eq) were dissolved in DMF (0.6 mL) (checked pH=9) and heated at 70°C. Complete conversion of the starting material was observed by LC-MS (acidic method) after 16h. After cooling at rt, the reaction mixture was quenched with water (0.5 mL) and extracted with DCM (3 mL x 5). Combined organic layers were collected, dried over anhydroys MgSO₄, evaporated

under reduced pressure and purified by gold flash chromatography column in gradient with DCM/MeOH to yield the desired compound **130a-d.**

General method d. *Tert*-butyl ester **130a-d** and **132a-d** deprotection was achieved by treating the obtained product with a mixture of DCM: TFA: TIPS (10:4:0.1) at 0°C. The solution was left to stir at rt for 2h and after that time, the reaction was judge complete by LC-MS (acidic-medthods) and volatile components were removed. The crude mixture was left under vacuum to remove any excess of TFA leading to the desired carboxylic acid derivative **131a-d**, **133a-d.**

General method e. VHL ligand **37e** (0.037 mmol, 1eq), appropriate linker hosting a good leaving group (-Ts or -Br) **116a-d** (0.05 mmol, 1.05eq) and K_2CO_3 (0.072 mmol, 1.5eq) were dissolved in DMF (0.6 mL) (checked pH=9) then left to stir at rt under nitrogen atmosphere for 16h and checked by LC-MS (acidic method). The reaction was quenched with water (0.2 mL) and extracted with DCM (5 mL x 5). The organic phase was dried over anhydrous $MgSO_4$ and evaporated under reduced pressure to provide the title compound **132a-d** which was used for the next step without further purification.

(S)-16-((2S,4R)-4-hydroxy-2-((4-(4-methylthiazol-5-yl)benzyl)carbamoyl)pyrrolidine-1-carbonyl)-17,17-dimethyl-14-oxo-3,6,9,12-tetraoxa-15-azaoctadecanoic acid, 129a. Yield, 30%. **¹H-NMR** (400MHz; CDCl₃) δ 0.98 (s, 9H, -C(C*H₃*)₃), 2.15-2.25, 2.38-2.48 (m, 2H, HC-C*H₂* -CHOH- hydroxyproline), 2.55 (s, 3H, -C*H₃*), 3.62-3.83 (m, 14, -C*H₂*-linker), 4.05-4.23 (m, 5H, -C*H₂*-N-, -*H*C-OH hydroxyproline, -*H*C-tBu), 4.28-4.44 (m, 2H, -Ph-C*H₂*-NH-), 4.55-4.72 (m, 3H, -C*H*-CO- hydroxyproline, -O-C*H₂*-COOH), 5.4 (s, 1H, -O*H* hyroxyproline) 7.29-7.32 (d, 1H, -C*H* Ph), 7.32-7.45 (d, 2H, -C*H* Ph), 7.55-7.60 (d, 1H, -C*H* Ph), 8.40 (s, 1H, -CH₂-N*H*-CO-), 8.7 (s, 1H, -C*H* thiazole), 8.82 (s, 1H, -CH-N*H*-CO-), 12.82 (s, 1H, -COO*H*).

2-((4-(2-(((S)-1-((2S,4R)-4-hydroxy-2-((4-(4-methylthiazol-5-yl)benzyl)carbamoyl)pyrrolidin-1-yl)-3,3-dimethyl-1-oxobutan-2-yl)amino)-2-oxoethoxy)but-2-yn-1-yl)oxy)acetic acid, 129b. Yield, 53%. **¹H-NMR** (400MHz; CDCl₃) δ 0.9 (s, 9H, -C(C*H₃*)₃), 1.98 (s, 2H, NH-CO-C*H₂*-O-) , 2.15-2.25, 2.38-2.48 (m, 2H, HC-C*H₂* -CHOH- hydroxyproline), 2.1-2.2, 2.35-2.42 (m, 2H, HC-C*H₂* -CHOH-hydroxyproline), 2.45 (s, 3H, -C*H₃*), 3.58-3.62 (m, 1H, -*H*C-tBu), 3.94-4.1 (m, 6H, -O-CH₂-C-, -C*H₂*-N-hydroxyproline), 4.42-4.55 (m, 3H, -*H*C-OH hydroxyproline, -C*H₂*-Ph), 4.63 (m, 1H, -C*H*-CO- hydroxyproline), 5.25 (s, 2H, -O-C*H₂*-COOH), 5.37 (s, 1H, -O*H* hyroxyproline), 7.32-7.34 (m, 4H, -C*H* Ph), 8.37 (s, 1H, -CH₂-N*H*-CO-), 8.65 (s, 1H, -C*H* tiazole), 8.7 (s, 1H, -CH-N*H*-CO-), 12.82 (s, 1H, -COO*H*).

2-(2-(2-(((S)-1-((2S,4R)-4-hydroxy-2-((4-(4-methylthiazol-5-yl)benzyl)carbamoyl)pyrrolidin-1-yl)-3,3-dimethyl-1-oxobutan-2-yl)amino)-2-oxoethoxy)ethoxy)acetic acid, 129c. Yield, 33%. **¹H-NMR** (400MHz; CDCl₃) δ 1.00 (s, 9H, -C(C*H₃*)₃), 2.15-2.25, 2.40-2.48 (m, 2H, HC-C*H₂* -CHOH- hydroxyproline), 2.55 (s, 3H, -C*H₃*), 3.60-3.85 (m, 6H, -O-C*H₂*-C*H₂*-O-, -*H*C-tBu), 3.95-4.18 (m, 5H, -CH₂-Ph, NH-CO-C*H₂*-O-, *H*-C-OH hydroxyproline), 5.42 (s, 1H, -O*H* hyroxyproline), 5.51-4.62 (m, 3H, -C*H₂*-COOH, *H*-C-CO hydroxyproline), 7.31-7.4 (m, 4H, -C*H* Ph), 7.55 (s, 1H, -CH₂-N*H*-CO-), 7.58 (s, 1H, -CH-N*H*-CO-), 8.65 (s, 1H, -C*H* thiazole), 12.82 (s, 1H, -COO*H*).

(S)-15-((2S,4R)-4-hydroxy-2-((4-(4-methylthiazol-5-yl)benzyl)carbamoyl)pyrrolidine-1-carbonyl)-16,16-dimethyl-13-oxo-3,7,11-trioxa-14-azaheptadecanoic acid, 129d. Yield, 50%. **¹H-NMR** (400MHz; CDCl₃) δ 0.98 (s, 9H, -C(C*H₃*)₃), 1.82-1.92 (m, 4H, -CH₂-C*H₂*-CH₂-), 2.16-2.22, 2.44-2.53 (m, 2H, HC-C*H₂* -CHOH- hydroxyproline), 2.53 (s, 3H, -C*H₃*), 3.52-3.64 (m, 8H, -C*H₂*-CH₂-C*H₂*-), 3.66-3.72 (m, 1H, -*H*C-tBu), 3.89-4.01 (m, 1H, -NH-

CO-C*H*$_2$-), 4.04-4.05 (d, 2H, -C*H*$_2$-N- hydroxyproline), 4.09-4.12 (m, 2H, -C*H*$_2$-Ph), 4.31-4.36 (m, 1H, *H*-C-OH hydroxyproline), 4.53-4.58 (m, 2H, -O-C*H*$_2$-COOOH), 4.61.4.63 (m, 1H, *H*-C-CO hydroxyproline), 6.03 (s, 1H, -O*H* hyroxyproline), 7.30-7.33 (d, 1H, -CH$_2$-N*H*-CO-), 7.35-7.37 (m, 4H, -C*H* Ph), 8.2 (s, 1H, -CH-N*H*-CO-), 8.7 (s, 1H, -C*H* thiazole), 12.9 (s, 1H, -COO*H*).

tert-butyl2-(2-(2-(2-(2-(((2S,4R)-1-((S)-2-(1-fluorocyclopropane-1-carboxamido)-3,3 dimethylbutanoyl)-4-hydroxypyrrolidine-2-carboxamido)methyl)-5-(4-methylthiazol-5 yl)phenoxy)ethoxy)ethoxy)ethoxy)acetate, 130a. Yield, quantitative. **¹H-NMR** (400MHz; CDCl$_3$) δ 0.94 (s, 9H, -C(C*H*$_3$)$_3$), 1.22-1.24 (m, 4H, -C*H*$_2$-C*H*$_2$- cyclopropane), 1.42 (s, 9H, -OC(C*H*$_3$)$_3$), 2.22 (s, 3H, -C*H*$_3$), 2.23-2.25, 2.47-2.49, (m, 2H, -C*H*$_2$-N- hydroxyproline), 3.52-3.55 (m, 8H, -O-C*H*$_2$-C*H*$_2$-O-), 3.73-3.75 (m, 2H, -C*H*$_2$-N- hydroxyproline), 4.02 (m, 1H, *H*-C-OH), 4.25 (s, 1H, *H*-C(C*H*$_3$)$_3$), 4.31-4.33 (m, 2H, Ph-O-C*H*$_2$-C-), 4.34-3.47 (m, 2H, -O-C*H*$_2$-CO-), 4.40-4.42 (m, 3H, -C*H*$_2$-Ph, *H*-C-CO hydroxyproline), 5.38 (s, 1H, -O*H* hydroxyproline), 7.32 (s, 1H, -C*H* Ph), 7.41 (d, 2H, -C*H* Ph), 8.31 (s, 1H, -CH$_2$-N*H*-CO), 8.38 (s, 1H, -CH-N*H*-CO-), 9.07 (s, 1H, -C*H* thiazole).

tert-butyl2-((4-(2-(((2S,4R)-1-((S)-2-(1-fluorocyclopropane-1-carboxamido)-3,3-dimethylbutanoyl)-4-hydroxypyrrolidine-2-carboxamido)methyl)-5-(4-methylthiazol-5-yl)phenoxy)but-2-yn-1-yl)oxy)acetate, 130b. Yield, 23%. **¹H-NMR** (400MHz; CDCl$_3$) δ 0.94 (s, 9H, -C(C*H*$_3$)$_3$), 0.99-1.24 (m, 4H, -C*H*$_2$-C*H*$_2$- cyclopropane), 1.42 (s, 9H, -OC(C*H*$_3$)$_3$), 2.03-2.07, 2.23-2.48, (m, 2H, -C*H*$_2$-N- hydroxyproline), 2.45 (s, 3H, -C*H*$_3$), 3.48-3.73 (m, 2H, HC-C*H*$_2$-CHOH- hydroxyproline), 4.10 (s, -C-C*H*$_2$-O-CH$_2$), 4.32 (s, 1H, *H*C-C(C*H*$_3$)$_3$), 4.37 (s, 2H, -C*H*$_2$-Ph), 4.4 (s, 2H, -O-C*H*$_2$-CO-), 4.47 (s, 1H, -O*H* hydroxyproline), 4.50 (s, 2H, -O-C*H*$_2$-C-), 4.53-4.55 (m, 1H, *H*C-OH), 4.58-4.60 (m, 1H, *H*C-CO hydroxyproline), 6.82 (s, 1H, -C*H* Ph), 6.89-6.92 (d, 1H, -C*H* Ph), 6.97-7.0 (m 1H, -C*H* Ph), 7.25-7.27 (m, 2H, -CH$_2$-N*H*-CO-, -CH-N*H*-CO-), 8.9 (s, 1H, -C*H* thiazole).

tert-butyl2-(2-(2-(((2S,4R)-1-((S)-2-(1-fluorocyclopropane-1-carboxamido)-3,3-dimethylbutanoyl)-4-hydroxypyrrolidine-2-carboxamido)methyl)-5-(4-methylthiazol-5-yl)phenoxy)ethoxy)acetate, 130c. Yield, 90%. **¹H-NMR** (400MHz; CDCl$_3$) δ 0.88 (s, 9H, -C(C*H*$_3$)$_3$), 1.16-1.26 (m, 4H, -C*H*$_2$-C*H*$_2$- cyclopropane), 1.4 (s, 9H, -OC(C*H*$_3$)$_3$), 2.01-2.07, 2.27-2.33 (m, 2H, -C*H*$_2$-N- hydroxyproline), 2.45 (s, 3H, -C*H*$_3$), 3.59-3.63, 3.77-3.79 (m, 2H, HC-C*H*$_2$-CHOH- hydroxyproline), 3.84-3.94 (m, 2H, -O-CH$_2$-C*H*$_2$-O-CH$_2$), 4.02 (s, 2H, -C*H*$_2$-Ph), 4.07 (s, 1H, *H*C-C(C*H*$_3$)$_3$), 4.12- 4.2 (m, 2H, -O-C*H*$_2$-CH$_2$-O-CH$_2$-), 4.4 (s, 2H, -O-C*H*$_2$-CO-), 4.47 (s, 1H, -O*H* hydroxyproline), 4.50-4.52 (m, 1H, *H*C-OH), 4.57-4.61 (m, 1H, *H*C-CO hydroxyproline), 6.83 (s, 1H, -C*H* Ph), 6.88-6.90 (dd, 1H, -C*H* Ph), 6.97-7 (m 1H, -C*H* Ph), 7.24-7.28 (m, 2H, -CH$_2$-N*H*-CO, CH-N*H*-CO-), 8.7 (s, 1H, -C*H* thiazole).

tert-butyl2-(3-(3-(2-(((2S,4R)-1-((S)-2-(1-fluorocyclopropane-1-carboxamido)-3,3-dimethylbutanoyl)-4-hydroxypyrrolidine-2-carboxamido)methyl)-5-(4-methylthiazol-5-yl)phenoxy)propoxy)propoxy)acetate, 130d. Yield, quantitative. **¹H-NMR** (400MHz; CDCl$_3$) δ 0.9 (s, 9H, -C(C*H*$_3$)$_3$), 1.19-1.26 (m, 4H, -C*H*$_2$-C*H*$_2$- cyclopropane), 1.45 (s, 9H, -OC(C*H*$_3$)$_3$), 2.03-2.08, 2.24-2.31 (m, 2H, HC-C*H*$_2$-CHOH hydroxyproline), 2.45 (s, 3H, -C*H*$_3$), 3.75-3.78, 3.83-3.85 (m, 2H, -C*H*$_2$-N- hydroxyproline), 4.05 (m, 1H, *H*C-OH), 4.22-4.25 (m, 2H, -C-C*H*$_2$-O-CO), 4.27 (s, 1H, *H*C-C(C*H*$_3$)$_3$), 4.33 (m, 2H, -O-C*H*$_2$-CO-), 4.40 (m, 3H, -C*H*$_2$-Ph, *H*-C-CO hydroxyproline), 4.65 (s, 2H, Ph-O-C*H*$_2$-C-), 4.8 (s, 1H, -O*H* hydroxyproline), 6.85 (s, 1H, -C*H* Ph), 6.89-6.90 (d, 1H, -C*H* Ph), 6.99-7.2 (m 1H, -C*H* Ph), 8.22 (s, 2H, -CH$_2$-N*H*-CO-), 8.34 (s, 2H, -CH-N*H*-CO-), 8.7 (s, 1H, -C*H* thiazole).

tert-butyl(R)-1-(1-fluorocyclopropyl)-3-((2S,4R)-4-hydroxy-2-((4-(4-methylthiazol-5-yl)benzyl)carbamoyl)pyrrolidine-1-carbonyl)-4,4-dimethyl-1-oxo-8,11,14-trioxa-5-thia-2-azahexadecan-16-oate, 132a. Yield, 57%. **¹H-NMR** (400MHz; MeOH-d_4) δ 0.99-1.1, 1.21-2.24 (m, 4H, - CH_2-CH_2- cyclopropane), 1.42 (s, 9H, -OC(CH_3)$_3$), 1.56 (s, 9H, -C(CH_3)$_3$), 2.22 (s, 3H, -CH_3), 2.23-2.48 (m, 2H, HC-CH_2 -CHOH - hydroxyproline), 3.52-3.55 (m, 8H, -O-CH_2-CH_2-O-), 3.52 (m, 2H, -CH_2-N- hydroxyproline), 3.75-3.77 (m, 4H, -O-CH_2-CH_2-S-), 4.09 (m, 1H, *H*-C-OH), 4.33 (s, 2H, -C-CH_2-O-CO-), 4.40-4.44 (m, 3H, -CH_2-Ph, *H*-C-CO- hydroxyproline), 4.62 (s, 1H, *H*C-C(CH_3)$_3$), 5.5 (s, 1H, -O*H* hydroxyproline), 7.47-7.50 (m, 2H, -C*H* Ph), 7.80-7.82 (d, 2H, -C*H* Ph), 8.32 (s, 2H, -CH$_2$-N*H*-CO-), 8.91 (s, 2H, -CH-N*H*-CO-), 9.07 (s, 1H, -C*H* thiazole).

tert-butyl 2-((4-(((R)-3-(1-fluorocyclopropane-1-carboxamido)-4-((2S,4R)-4-hydroxy-2-((4-(4-methylthiazol-5-yl)benzyl)carbamoyl)pyrrolidin-1-yl)-2-methyl-4-oxobutan-2-yl)thio)but-2-yn-1-yl)oxy)acetate, 132b. Yield, quantitative. **¹H-NMR** (400MHz; MeOH-d_4) δ 0.98-1.1, 1.22-2.25 (m, 4H, - CH_2-CH_2- cyclopropane), 1.42 (s, 9H, -OC(CH_3)$_3$), 1.55 (s, 9H, -C(CH_3)$_3$), 2.22 (s, 3H, -CH_3), 2.24-2.49 (m, 2H, HC-CH_2-CHOH - hydroxyproline), 3.13 (s, 2H, -S-CH_2-C-), 3.45-3.48, 3.51-3.55 (m, 2H, -CH_2-N- hydroxyproline), 4.0-4.07 (m, 3H, -O-CH_2-C, *H*C-OH), 4.34 (s, 2H, -O-CH_2-CO), 4.37-4.40 (m, 3H, -CH_2-Ph, *H*C-CO hydroxyproline), 4.60 (s, 1H, *H*C-C(CH_3)$_3$), 5.37 (s, 1H, -O*H* hydroxyproline), 7.42-7.47 (m, 2H, -C*H* Ph), 7.79-7.82 (d, 2H, -C*H* Ph), 8.31 (s, 2H, -CH$_2$-N*H*-CO), 8.66 (s, 2H, -CH-N*H*-CO-), 9.03 (s, 1H, -C*H* thiazole).

tert-butyl 2-(2-(((R)-3-(1-fluorocyclopropane-1-carboxamido)-4-((2S,4R)-4-hydroxy-2-((4-(4-methylthiazol-5-yl)benzyl)carbamoyl)pyrrolidin-1-yl)-2-methyl-4-oxobutan-2-yl)thio)ethoxy)acetate, 132c. Yield, 87%. **¹H-NMR** (400MHz; MeOH-d_4) δ 0.75- 0.81 (m, 4H, - CH_2-CH_2- cyclopropane), 1.18 (s, 9H, -OC(CH_3)$_3$), 1.39 (s, 9H, -C(CH_3)$_3$), 2.22 (s, 3H, -CH_3), 2.23-2.48 (m, 2H, HC-CH_2 -CHOH- hydroxyproline), 3.42-3.46, 3.51-3.54 (m, 2H, -CH_2-N- hydroxyproline), 3.72-3.74 (m, 4H -S-CH_2-CH_2-), 4.07 (s, 1H, *H*C-OH), 4.36-4.40 (m, 3H, -CH_2-Ph, *H*-C-CO hydroxyproline), 4.33 (s, 2H, -O-CH_2-CO-), 4.61 (s, 1H, *H*C-C(CH_3)$_3$), 5.32 (s, 1H, -O*H* hydroxyproline), 7.42-7.47 (m, 2H, -C*H* Ph), 7.79-7.82 (d, 2H, -C*H* Ph), 8.33 (s, 2H, -CH$_2$-N*H*-CO), 8.88 (s, 2H, -CH-N*H*-CO-), 9.02 (s, 1H, -C*H* thiazole).

tert-butyl(R)-1-(1-fluorocyclopropyl)-3-((2S,4R)-4-hydroxy-2-((4-(4-methylthiazol-5-yl)benzyl)carbamoyl)pyrrolidine-1-carbonyl)-4,4-dimethyl-1-oxo-9,13-dioxa-5-thia-2-azapentadecan-15-oate, 132d. Yield, quantitative. **¹H-NMR** (400MHz; MeOH-d_4) δ 0.97-1.14, 1.20-2.25 (m, 4H, - CH_2-CH_2- cyclopropane), 1.42 (s, 9H, -OC(CH_3)$_3$), 1.55 (s, 9H, -C(CH_3)$_3$), 1.75-1.83 (m, 4H, -CH$_2$-CH_2-CH$_2$-), 2.22 (s, 3H, -CH_3), 2.21-2.44 (m, 2H, HC-CH_2 -CHOH - hydroxyproline), 2.80-2.82 (m, 2H, -S-CH_2-), 3.35-3.38 (m, 8H, -CH_2-CH_2-CH_2-), 3.48-3.52, 3.64-3.73 (m, 2H, -CH_2-N- hydroxyproline), 4.07 (s, 1H, *H*C-OH), 4.39-4.42 (m, 3H, -CH_2-Ph, *H*C-CO- hydroxyproline), 4.35 (s, 2H, -O-CH_2-CO-), 4.64 (s, 1H, *H*C-C(CH_3)$_3$), 5.37 (s, 1H, -O*H* hydroxyproline), 7.44-7.47 (m, 2H, -C*H* Ph), 7.79-7.84 (d, 2H, -C*H* Ph), 8.32 (s, 2H, -CH$_2$-N*H*-CO-), 8.86 (s, 2H, -CH-N*H*-CO-), 9.04 (s, 1H, -C*H* thiazole).

***General procedure for the synthesis of 36f CRBN based PROTACs 70a,b
(Scheme 4.6A), 71a,b (Scheme 4.6B), 76a,b (Scheme 4.6C), 77a,b, 79a,b
(Scheme 4.6D), 73a,b, 79a,b (Scheme 4.6E).ᵃ***

General procedure a. **26** (1.08 mmol, 1eq) was dissolved in a mixture 2:1 (v/v) dioxane: water (3.25: 6.50 mL), and at 0°C, NaOH 1M solution (3.13 mmol, 2.9eq) followed by di-*tert*-butyl dicarbonate (1.5 mmol, 1.4eq) were added. After 24h stirring at rt (reaction checked by TLC), the mixture was concentrated under vacuum and water was added (11 mL) (pH checked=9) and CH₃COOH 1M was added until pH 6.5. The acqueous phase was extracted with AcOEt (20 mL x 4), and the combined organic layers were dried over anhydrous Na₂SO₄, filtered and evaporated under vacuum leading **134** without further purifications.

General procedure b. The proper acid or amino intermediate **123a-d** (0.116 mmol, 1eq) and the required amine or acid (**134, 136, 139, 75, 78, 72, 20**) (0.116 mmol, 1eq) respectively, were dissolved in dry DMF (1.5 mL) and DIPEA (0.349 mmol, 3eq) followed by HATU (0.116 mmol, 1eq) were added at rt. The reaction was left to stir for 6h under a nitrogen atmosphere and after that time judged complete by TLC. DMF was evaporated under vacuum and saturate solution of NaHCO₃ (5 mL) was added and extracted with a mixture CHCl₃: isopropanol 4:1 (5 mL x 3). The organic phase was then washed with a saturated solution of NaHCO₃ (2 mL x 2) and brine (2 mL x 2) and the combined organic layers were dried over anhydrous Na₂SO₄, filtered and evaporated under vacuum thus obtaining a crude that was purified by column chromatography silica gel eluting with the opportune mixture CHCl₃: MeOH: NH₃. Evaporation of the fractions containing the require product gave **135a,b**, **137a,b**, **140a,b 77a,b**, **79a,b**, **73a,b** and **85a,b** as an analytically pure compound.

General procedure c. The appropiate intermediate **135a,b** (0.055 mmol, 1eq) was dissolved in dry DCM (1.5 mL), the solution was cooled at 0°C and TFA (2.38 mmol, 43eq) and TIS (0.055 mmol, 1eq) were added. After 5h stirring at rt, TLC proved the complete conversion of the starting materials in the desired product. Volatile components were evaporated under vacuum and the obtained crude was washed with a mixture of DCM and Et₂O providing the formation of a white solid that was filtered and left under vacuum to remove any excess of TFA thus leading to the desired final compound **70a,b** as trifloroacetic salt.

General procedure d. The required intermediate **137a,b** (0.042mmol, 1eq) was dissolved in dry THF (1.2 mL) (adding some drops of MeOH to reach a complete dissolution if necessary) and HCl 4N in dioxane (2.94 mmol, 70eq) was added at 0°C. The obtained mixture was left to stir for 48h at rt and checked by TLC. After the complete conversion of the starting material, the reaction was evaporated and the resulting crude triturated from a mixture 2:1 of Et₂O: THF (1: 0.5 mL) and then filtered under vacuum obtaining the analytically pure desired hydrochloride salt **71a,b**.

General procedure e. Ester **138** (0.351 mmol, 1eq) was dissolved in THF (1.8 mL) and LiOH·H₂O (140 mmol, 4eq in 1.45 mL of H₂O) was added at 0°C. The reaction was left to stir for 6h at rt and checked by TLC. THF was evaporated and DCM (3.5 mL) was added followed by glacial CH₃COOH at 0°C until pH= 4. The obtained solid was filtered, washed with water and left under vacuum until dryness thus obtaining **139** as a white solid.

N-(1-((2-(2,6-dioxopiperidin-3-yl)-1,3-dioxoisoindolin-4-yl)oxy)-2-oxo-7,10,13-trioxa-3-azahexadecan-16-yl)-4-((4-((((1R,2S)-2-phenylcyclopropyl)amino)methyl)piperidin-1-yl)methyl)benzamide trifluoroacetic salt, 70a, MC4381. Yield, 76%, mp. 101-103 °C. **¹H-NMR** (400MHz; MeOH-*d4*) δ 1.29-1.42 (m, 4H, -CH_2-CH_2- cyclopropane, -CH_2-piperidine), 1.68-1.79 (m, 4H, -CH_2-CH_2-CH_2-), 1.96-2.05 (m, 4H, -CH_2-CH_2-dioxopiperidine), 2.38 (m, 1H, *H*C-Ph), 2.82-2.85 (m, 2H, -CH_2-piperidine), 2.86-2.89 (m, 1H, -C*H*-NH-), 2.86-2.88 (m, 1H, -C*H* piperidine), 2.89 (s, 1H, -N*H*-cyclopropane), 3.03-3.05 (m, 2H, -CH_2- piperidine), 3.07 (s, 2H, -CH_2-Ph), 3.13-3.15 (m, 2H, -CH_2- piperidine), 3.27-3.36 (t, 2H, -CH$_2$-CO-NH-CH_2-CH$_2$-CH$_2$-O-), 3.53 (m, 14H, -CH$_2$-CO-NH-CH$_2$-CH$_2$-CH$_2$-O-CH$_2$-CH$_2$-O-CH$_2$-CH$_2$-O-CH$_2$-CH$_2$-CH$_2$-), 4.24 (s, 2H, -NH-CH_2-piperidine), 4.75 (s, 2H, -O-CH_2-CO-), 5.02-5.06 (m, 1H, -C*H* dioxopiperidine), 7.05-7.22 (m, 5H, -C*H* Ph-cyclopropane), 7.42-7.50 (m, 4H, -C*H* Ph-CH$_2$), 7.68-7.82 (m, 3H, -C*H* dioxoisoindoline), 7.92 (s, 1H, -O-CH$_2$-CO-N*H*-), 8.5 (s, 1H, Ph-CO-N*H*-), 11.06 (s, 1H, -N*H* dioxopiperidine). **¹³C-NMR** (100 MHz, DMSO-*d₆*) δ 19.03, 24.19, 25.77, 28.95, 29.34, 29.36, 29.88, 34.25, 37.89 38.02, 41.58, 51.49, 51.72, 52.25, 60.88, 68.45, 68.58, 68.63, 70.09, 70.57, 117.01, 119.17 121.44, 126.55, 126.83, 128.45, 128.66, 129.09, 132.37, 132.63, 133.13, 142.35, 142.53, 155.48, 165.58, 166.32, 168.09, 169.34, 169.59, 172.01. Exact mass: 880.44, **MS (ESI)**, *m/z*: 881.5 [M+H]⁺.

N-(2-(2-(2-(2-((2-(2,6-dioxopiperidin-3-yl)-1,3-dioxoisoindolin-4 yl)oxy)acetamido)ethoxy)ethoxy)ethyl)-4-((4-((((1R,2S)-2 phenylcyclopropyl)amino)methyl)piperidin-1-yl)methyl)benzamide, 70b, MC4378. Yield, 76%, mp. 107-110 °C. **¹H-NMR** (400MHz; MeOH-*d4*) δ 1.40-1.61 (m, 4H, -CH_2-CH_2- cyclopropane, -CH_2- piperidine), 1.98-2.01 (m, 1H, -C*H*-Ph), 2.09-2.16 (m, 4H, -CH_2-CH_2- dioxopiperidine), 2.50-2.52 (m, 1H, -C*H* piperidine), 2.72-2.78 (m, 2H, -CH_2-piperidine) 2.89-2.98 (1H, m, -C*H*-NH), 3.0-3.08 (m, -CH_2- piperidine), 3.09 (s,1H, -N*H*-cyclopropane), 3.2 (s, 2H, -CH_2-Ph), 3.42-3.48 (m, 2H, -CH_2- piperidine), 3.53-3.68 (m, 12H, -CH_2- linker), 4.4 (s, -NH-CH_2-piperidine), 4.75 (s, 2H, -O-CH_2-CO-), 5.02-5.06 (m, 1H, -C*H* dioxopiperidine), 7.18-7.34 (m, 5H, -C*H* Ph-cyclopropane), 7.41-7.61 (m, 4H, -C*H* Ph-CH$_2$), 7.79-7.93 (m, 3H, -C*H* dioxoisoindoline), 8.1 (s, 1H, -O-CH$_2$-CO-N*H*-), 8.5 (s, 1H, Ph-CO-N*H*-), 11.06 (s, 1H, -N*H*- dioxopiperidine). **¹³C-NMR** (100 MHz, DMSO-*d₆*) δ 18.97, 24.18, 25.08, 28.94, 29.76, 34.19, 39.98, 40.21, 41.56, 51.48, 51.69, 52.22, 60.75, 68.41, 69.47, 69.54, 69.64, 69.65, 116.99, 118.70, 121.41, 126.47, 126.81, 128.46, 128.47, 129.04, 132.35, 132.64, 133.12, 142.32, 142.47, 155.43, 165.54, 166.31, 167.34, 169.33, 169.34, 171.84. Exact mass: 808.38, **MS (ESI)**, *m/z*: 809.42 [M+H]⁺.

N-(4-((1R,2S)-2-aminocyclopropyl)phenyl)-3-(2-(2-(2-(2-((2-(2,6-dioxopiperidin-3-yl)-1,3-dioxoisoindolin-4yl)oxy)acetamido)ethoxy)ethoxy)ethoxy)propanamide hydrochloride salt, 71a, MC4363. Yield, 80%, mp. 83-88 °C. **¹H-NMR** (400MHz; DMSO-*d₆*) δ 1.13-1.18, 1.29-1.34 (m, 2H, -CH_2- cyclopropane), 2.02-2.09 (m, 1H, -C*H*-Ph), 2.21-2.26, 2.51-2.62, 2.74-2.76 (m, 4H -CH_2-CH_2- dioxopiperidine), 2.88-2.90 (m, 1H, -C*H*-NH_2·HCl), 3.39-3.66 (m, 16H, -CH_2- linker), 4.8 (s, 2H, -O-CH_2-CO-), 5.09-5.14 (m, 1H, -C*H* dioxopiperidine), 7.02-7.08, 7.25-7.27, 7.77-7.93 (m, 4H, C-*H* Ph-cyclopropane), 7.50-7.60 (t, 3H, -C*H* dioxoisoindoline), 7.99 (t, 1H, -O-CH$_2$-CO-N*H*-), 8.38 (s, 3H, -NH_2·*H*Cl), 9.9 (s, 1H, Ph-CO-N*H*-), 11.1 (s, 1H, -N*H* dioxopiperidine). **¹³C-NMR** (100 MHz, DMSO-*d₆*) δ 19.55, 24.18, 25.69, 29.76, 36.01, 37.46, 39.98, 52.22, 66.17, 68.41, 69.54, 69.57, 69.68, 70.55, 70.62, 116.99, 118.70, 120.82, 121.41, 127.85, 132.35, 133.12, 137.55, 137.63, 155.43, 165.54, 166.31, 169.33, 169.34, 170.86, 171.84. Exact mass 665.27, **MS (ESI)**, *m/z*: 666.27 [M+H]⁺.

N-(4-((1R,2S)-2-aminocyclopropyl)phenyl)-3-(2-(2-(2-((2-(2,6-dioxopiperidin-3-yl)-1,3-dioxoisoindolin-4-yl)oxy)acetamido)ethoxy)ethoxy)propenamide hydrochloride salt, 71b, MC4362. Yield, 72%, mp. 101-105 °C. **^{1}H-NMR** (400MHz; DMSO-d_6) δ 1.14-1.17, 1.29-1.34 (m, 2H, -CH_2- cyclopropane), 2.03-2.09 (m, 1H, -*CH*-Ph), 2.21-2.16, 2.54-2.58, 2.73-2.76 (m, 4H -CH_2-CH_2- dioxopiperidine), 2.87-2.95 (m, 1H, -C*H*-NH$_2$·HCl), 3.44-3.65 (m, 12H, -CH_2- linker), 4.78 (s, 2H, -O-CH_2-CO-), 5.09-5.14 (m, 2H, -C*H* dioxopiperidine), 7.06-7.08, 7.38-7.40, 7.79-7.82 (m, 4H, -C*H* Ph-cyclopropane), 7.48-7.52 (t, 3H, -C*H* dioxoisoindoline), 7.99 (t, 1H, -O-CH$_2$-CO-N*H*-), 8.20 (s, 3H, -NH_2·*H*Cl), 9.9 (s, 1H, Ph-CO-N-*H*), 11.12 (s, 1H, -N*H* dioxopiperidine). **^{13}C-NMR** (100 MHz, DMSO-d_6) δ 19.59, 24.19, 26.01, 29.99, 36.04, 37.52, 39.99, 52.25, 66.19, 68.41, 69.54, 69.56, 69.67, 116.99, 118.70, 120.82, 121.41, 127.85, 132.35, 133.12, 137.55, 137.68, 155.42, 165.55, 166.32, 169.38, 169.30 171.02, 171.85. Exact mass: 621.24, **MS (ESI)**, *m/z*: 622.24 [M+H]$^+$.

N-(2-(2-(2-(3-((S)-3-(((5-(4-cyanophenyl)-6-(p-tolyl)pyridin-3-yl)oxy)methyl)pyrrolidin-1-yl)-3-oxopropoxy)ethoxy)ethoxy)ethyl)-2-((2-(2,6-dioxopiperidin-3-yl)-1,3-dioxoisoindolin-4-yl)oxy)acetamide, 73a, MC4376. Yield, 63%, mp. 101-103°C. **^{1}H-NMR** (400MHz; CDCl$_3$) δ 1.72- 1.91 (m, 1H, -C*H* pyrrolidine), 2.06-2.18 (m, 2H, -CH_2- pyrrolidine), 2.45 (s, 3H, -CH_3), 2.51-2.54, 3.50-3.68 (m, 16H, -CH_2- linker), 2.68-2.82 (m, 4H, -CH_2-CH_2- dioxopiperidine), 3.46-3.49, 3.61-3.68, 3.92-4.05 (m, 4H, -CH_2- pyrrolidine), 3.71-3.77 (t, 2H, -O-CH_2- pyrrolidine), 4.57 (s, 2H, -O-CH_2-CO-), 4.85-4.90 (m, 1H, -C*H* dioxopiperidine), 6.98-6.99, 7.10-7.12, 7.21-7.24, 7.46-7.47, 8.33-8.35 (m, 8H, -C*H* Ph-CH$_3$, -C*H* Ph-CN), 7.04-7.06, 7.49-7.51, 7.64-7.68 (m, 3H, -C*H* dioxoisoindoline), 7.60 (s, 1H, -CO-N*H*-CH$_2$-CH$_2$-), 9.2 (s, 1H, -N*H* dioxopiperidine). **^{13}C-NMR** (100 MHz, DMSO-d_6) δ 21.24, 24.19, 28.75, 28.01, 36.35, 38.49, 39.99, 46.99, 51.05, 52.28, 65.90, 68.45, 69.01, 69.55, 69.58, 69.71, 70.58, 70.65, 111.43, 115.59, 117.04, 118.25, 118.71, 121.44, 128.45, 129.02, 132.33, 132.89, 133.15, 133.79, 135.71, 137.01, 137.15, 137.39, 150.32, 155.09, 155.44, 165.66, 166.32, 169.32, 169.36, 171.85, 172.22. Exact mass: 886.3, **MS (ESI)**, *m/z*: 887.4 [M+H]$^+$.

N-(2-(2-(3S)-3-(((5-(4-cyanophenyl)-6-(p-tolyl)pyridin-3-yl)oxy)methyl)pyrrolidin-1-yl)-3-oxopropoxy)ethoxy)ethyl)-2-((2-(2,6-dioxopiperidin-3-yl)-1,3-dioxoisoindolin-4-yl)oxy)acetamide, 73b, MC4382. Yield, 65%, mp. 107-109°C. **^{1}H-NMR** (400MHz; CDCl$_3$) δ 1.71- 1.99 (m, 1H, -C*H* pyrrolidine), 2.05-2.11 (m, 2H, -C*H$_2$*- pyrrolidine), 2.25 (s, 3H, -CH_3), 2.52-2.56, 3.55-3.64 (m, 12H, -C*H$_2$*- linker), 2.68-2.80 (m, 4H, -CH_2-CH_2-dioxopiperidine), 3.62-3.79 (m, 4H, -C*H$_2$*- pyrrolidine), 3.92-4.12 (t, 2H, -O-C*H$_2$*-pyrrolidine), 4.58 (s, 2H, -O-C*H$_2$*-CO-), 4.87-4.95 (m, 1H, -C*H* dioxopiperidine), 6.98-6.98, 7.12-7.13, 7.23-7.25, 7.49-7.51, 8.32-8.35 (m, 8H, -C*H* Ph-CH$_3$, -C*H* Ph-CN), 7.10-7.11, 7.45-7.47, 7.66-7.68 (m, 3H, -C*H* dioxoisoindoline), 7.60 (s, 1H, -CO-N*H*-CH$_2$-CH$_2$-), 9.75 (s, 1H, -N*H* dioxopiperidine). **^{13}C-NMR** (100 MHz, DMSO-d_6) δ 21.25, 24.19, 28.74, 30.01, 36.35, 38.55, 39.99, 47.08, 50.95, 52.25, 65.99, 68.43, 69.01, 69.55, 69.88, 69.72, 111.42, 115.62, 117.44, 118.24, 118.72, 121.43, 128.46, 128.85, 132.43, 132.89, 133.13, 133.78, 135.78, 136.89, 137.12, 137.44, 150.32, 155.09, 155.48, 165.55, 166.33, 170.22, 170.34, 171.88, 172.25. Exact mass: 842.33, **MS (ESI)**, *m/z*: 843.4 [M+H]$^+$.

N-(1-((2-(2,6-dioxopiperidin-3-yl)-1,3-dioxoisoindolin-4-yl)oxy)-2-oxo-7,10,13-trioxa-3-azahexadecan-16-yl)-8-hydroxyquinoline-5-carboxamide, 76a, MC4366. Yield, 76%, mp. 81-84 °C. **¹H-NMR** (400MHz; MeOH-d_4) δ 1.67-1.78 (m, 4H -CH_2-CH_2-dioxopiperidine), 2.02-2.05, 2.26-2.40, 2.63-2.67, 3.21-3.63 (m, 20H, -CH_2- linker), 4.63 (s, 2H, -O-CH_2-CO-), 5.02-5.04 (m, 1H, -CH dioxopiperidine), 7.28-7.31, 7.40-7.43 (m, 3H, -CH dioxoisoindoline), 7.66-7.60, 7.88-7.90, 7.94-7.98, 8.93-8.95, 9.43-9.45 (t, 5H, -CH quinoline), 8.2 (s, 1H, -O-CH$_2$-CO-NH), 8.44 (s, 1H, -NH-CO-quinoline), 9.8 (bs, 1H, -OH), 11.6 (s, 1H, -NH dioxopiperidine). **¹³C-NMR** (100 MHz, DMSO-d_6) δ 24.19, 29.33, 29.35, 29.99, 37.85, 38.01, 52.09, 68.45, 68.59, 68.63, 70.11, 70.56, 111.55, 117.05, 118.70, 121.40, 123.26, 126.40, 127.42, 130.09, 131.82, 132.35, 133.12, 139.14, 149.32, 155.45, 155.66, 166.54, 167.29, 167.44, 169.88, 169.98, 172.09. Exact mass: 705.26, **MS (ESI)**, *m/z*: 706.3 [M+H]⁺.

N-(2-(2-(2-(2-((2-(2,6-dioxopiperidin-3-yl)-1,3-dioxoisoindolin-4-yl)oxy)acetamido)ethoxy)ethoxy)ethyl)-8 hydroxyquinoline-5-carboxamide, 76b, MC4364. Yield, 72%, mp. 71-75 °C. **¹H-NMR** (400MHz; DMSO-d_6) δ 2.03-2.06, 2.55-2.58, 2.85-2.98 (m, 4H, -CH_2-CH_2- dioxopiperidine), 3.17-3.72 (m, 12H, -CH_2- linker), 4.75 (s, 2H, -O-CH_2-CO-), 5.09-5.13 (m, 1H, -CH dioxopiperidine), 7.26-7.37, 7.44-7.47 (m, 3H, -CH dioxoisoindoline), 7.48-7.49, 7.77- 7.82, 8.0-8.02 (m, 5H, -CH, quinoline), 8.6 (s, 1H, -O-CH$_2$-CO-NH), 8.88 (s, 1H, NH-CO-quinoline), 9.1 (bs, 1H, -OH) 11.6 (s, 1H, -NH dioxopiperidine). **¹³C-NMR** (100 MHz, DMSO-d_6) δ 24.19, 30.01, 39.99, 40.11, 52.09, 69.09, 69.45, 69.58, 69.67, 69.69, 111.58, 117.11, 118.82, 121.43, 124.01, 126.45, 127.63, 130.12, 131.85, 132.44, 133.18, 138.22, 148.52, 154.91, 155.77, 166.58, 167.19, 167.49, 169.44, 169.58, 171.85. Exact mass: 633.21, **MS (ESI)**, *m/z*: 634.21 [M+H]⁺.

N-(1-((2-(2,6-dioxopiperidin-3-yl)-1,3-dioxoisoindolin-4-yl)oxy)-2-oxo-7,10,13-trioxa-3-azahexadecan-16-yl)-3-((2-(pyridin-2-yl)-6-(1,2,4,5-tetrahydro-3H-benzo[d]azepin-3-yl)pyrimidin-4-yl)amino)propenamide, 77a, MC4337. Yield, 68%, mp. 126-128°C. **¹H-NMR** (400MHz; CDCl₃) δ 1.66-1.69, 1.76-1.80 (t, 4H, -NH-CH$_2$-CH_2-CH$_2$-O-), 2.06-2.01, 2.68-2.81 (m, 4H, -CH_2-CH_2- dioxopiperidine), 2.41-2.48-3.26-3.59 (m, 20H, -NH-CH_2-CH$_2$-CH_2-O-CH_2-CH_2-O-CH_2-CH_2-O-CH_2-CH$_2$-CH_2NH-CH_2-CH_2-), 2.91-2.94, 3.83-3.85 (m, 8H, -CH_2-CH_2- diazepine), 4.54 (s, 2H, -O-CH_2-CO-), 4.89-4.91 (m, 1H, -CH dioxopiperidine), 5.4 (s, 1H, -NH pyrimidine), 5.55 (s, 1H, -CH pyrimidine), 6.89 (s, 1H, -NH-CO-CH$_2$-CH$_2$-), 7.07-7.09 (m, 4H, -CH 1,2,4,5-tetrahydro-3H-benzo[d]azepine), 7.24-7.26, 8.33-8.35, 8.66-8.67, 9.22, 9.26 (m, 4H, -CH pyridine), 7.44-7.45, 7.60-7.64, 7.69-7.73 (m, 3H, -CH dioxoisoindoline), 7.51-7.52 (s, 1H, -O-CH$_2$-CO-NH), 11.02 (s, 1H, -NH dioxopiperidine). **¹³C-NMR** (100 MHz, DMSO-d_6) δ 24.19, 29.35, 29.34, 29.82, 32.23, 36.55, 37.73, 37.99, 39.52, 48.82, 52.09, 68.48, 69.03, 68.59, 70.22, 70.87, 82.93, 117.08, 118.72, 122.40, 124.03, 124.44, 126.79, 127.55, 132.38, 133.23, 136.49, 139.45, 150.03, 152.85, 155.63, 161.97, 162.65, 162.89, 166.44, 167.36, 169.88, 169.46, 171.89, 172.23. Exact mass: 905.4, **MS (ESI)**, *m/z*: 906.41 [M+H]⁺.

N-(2-(2-(2-(2-((2-(2,6-dioxopiperidin-3-yl)-1,3-dioxoisoindolin-4-yl)oxy)acetamido)ethoxy)ethoxy)ethyl)-3-((2-(pyridin-2-yl)-6-(1,2,4,5-tetrahydro-3H-benzo[d]azepin-3-yl)pyrimidin-4-yl)amino)propenamide, 77b, MC4328. Yield, 65%, mp. 148-151°C. **¹H-NMR** (400MHz; CDCl₃) δ 2.06-2.07, 2.67-2.94 (m, 4H, -CH_2-CH_2-dioxopiperidine), 2.46-2.49, 3.36-3.60 (m, 16H, -CH_2- linker), 2.88-2.94, 3.83-3.85 (m, 8H, -CH_2-CH_2- diazepine), 4.56 (s, 2H, -O-CH_2-CO-), 4.85-4.90 (m, 1H, -CH dioxopiperidine), 5.45 (s, 1H, -NH pyrimidine), 5.51 (s, 1H, -CH pyrimidine), 6.82 (s, 1H, -NH-CO-CH$_2$-CH$_2$-), 7.07-7.09 (m, 4H, -CH 1,2,4,5-tetrahydro-3H-benzo[d]azepine), 7.23-7.25, 8.33-8.35, 8.64-8.65, 9.22, 9.26 (m, 4H, -CH pyridine), 7.44-7.46, 7.60-7.64, 7.70-7.73 (m, 3H,

-C*H* dioxoisoindoline), 7.51-7.52 (s, 1H, -O-CH$_2$-CO-N-*H*), 11.02 (s, 1H, -N*H* dioxopiperidine). **^{13}C-NMR** (100 MHz, DMSO-d_6) δ 25.17, 29.85, 32.22, 36.44, 38.01, 40.04, 40.35, 48.85, 52.24, 68.45, 69.40, 69.55, 69.72, 83.01, 117.09, 118.82, 121.45, 124.09, 124.42, 126.73, 127.60, 133.01, 133.18, 136.52, 139.49, 149.08, 152.76, 155.88, 161.92, 162.44, 163.03, 166.38, 167.18, 169.35, 169.30, 171.81, 172.02. Exact mass: 833.35, **MS (ESI)**, *m/z*: 834.4 [M+H]$^+$.

4-(4-((5-(4,5-dimethyl-2-nitrophenyl)furan-2-yl)methylene)-3-methyl-5-oxo-4,5-dihydro-1H-pyrazol-1-yl)-N-(1-((2-(2,6-dioxopiperidin-3-yl)-1,3-dioxoisoindolin-4-yl)oxy)-2-oxo-7,10,13-trioxa-3-azahexadecan-16-yl)benzamide, 79a, MC4385. Yield, 55%, mp 122-124 °C. **^{1}H-NMR** (400MHz; CDCl$_3$) δ 1.76-1.84, 3.44-3.60 (m, 20H, -C*H$_2$*-linker), 2.07-2.09, 2.64-2.84 (m, 4H, -CH$_2$-CH$_2$- dioxopiperidine), 2.23 (s, 3H, -C*H$_3$* pyrazole), 2.33-2.42 (m, 6H, -C*H$_3$* Ph), 4.53 (s, 2H, -O-C*H$_2$*-CO), 4.87-4.88 (m, 1H, -C*H* dioxopiperidine), 6.74-6.75 (d, 1H, -C*H* double bond), 7.09-7.11 (m, 2H, -C*H* dioxoisoindoline, -C*H* furane), 7.22 (d, 1H, -C*H* furane), 7.37-7.39 (m, 1H, .-C*H* dioxoisoindoline), 7.40-7.42, 7.80-7.81 (d, 4H, -C*H* Ph), 7.58 (s,1H, -C*H* dioxoisoindoline) 7.63-7.64 (s, 1H, -CO-N*H*-CH$_2$-CH$_2$-), 7.99-8.0 (d, 2H, -C*H* Ph-NO$_2$), 8.65 (s, 1H, -CO-N*H*-CH$_2$-CH$_2$-), 8.88 (d, 1H, -N*H* dioxopiperidine). **^{13}C-NMR** (100 MHz, DMSO-d_6) δ 14.82, 20.04, 20.22, 24.19, 29.45, 29.59, 29.82, 37.99, 38.05, 53.05, 68.55, 68.59, 69.44, 70.12, 70.88, 110.17, 114.63, 114.94, 117.12, 118.88, 120.65, 121.12, 121.46, 123.20, 124.99, 128.03, 129.08, 131.09, 132.37, 133.15, 135.99, 138.44, 139.58, 145.33, 149.97, 152.02, 152.95, 155.48, 165.31, 167.38, 168.17, 168.92, 169.55, 169.79, 171.85. Exact mass: 961.35, **MS (ESI)**, *m/z*: 962.35 [M+H]$^+$.

4-(4-((5-(4,5-dimethyl-2-nitrophenyl)furan-2-yl)methylene)-3-methyl-5-oxo-4,5-dihydro-1H-pyrazol-1-yl)-N-(2-(2-(2-(2-((2-(2,6-dioxopiperidin-3-yl)-1,3-dioxoisoindolin-4-yl)oxy)acetamido)ethoxy)ethoxy)ethyl)benzamide, 79b, MC4387. Yield, 64%, mp 140-142 °C. **^{1}H-NMR** (400MHz; CDCl$_3$) δ 2.16-2.18, 2.60-2.86 (m, 4H, -C*H$_2$*-CH$_2$- dioxopiperidine), 2.28 (s, 3H, -C*H$_3$* pyrazole), 2.33-2.34 (m, 6H, -C*H$_3$* Ph), 3.49-3.63 (m, 12H, -C*H$_2$*- linker), 4.55 (s, 2H, -O-C*H$_2$*-CO-), 4.84-4.87 (m, 1H, -C*H* dioxopiperidine), 6.85-6.86 (d, 1H, -C*H* double bond), 6.92- 6.95 (m, 1H, -C*H* furane), 7.06-7.08 (d, 1H, -C*H* dioxoisoindoline), 7.22 (d, 1H, -C*H* furane), 7.44-7.47, 7.60-7.64 (d, 4H, -C*H* Ph), 7.55-7.56 (m, 1H, -C*H* dioxoisoindoline), 7.78 (s,1H, -C*H* dioxoisoindoline) 7.83-7.84 (s, 1H, -CO-N*H*-CH$_2$-CH$_2$-), 7.99-8.0 (d, 2H, -C*H* Ph-NO$_2$), 8.57 (s, 1H, CO-N*H*-CH$_2$-CH$_2$-), 8.74 (d, 1H, -N*H* dioxopiperidine). **^{13}C-NMR** (100 MHz, DMSO-d_6) δ 14.75, 19.88, 20.00, 24.19, 29.82, 40.01, 40.24, 52.07, 68.51, 69.49, 69.67, 69.77, 69.81, 109.76, 114.05, 113.99, 117.25, 118.85, 120.62, 121.12, 121.43, 123.44, 124.98, 128.44, 129.08, 130.89, 132.37, 133.13, 135.87, 139.01, 139.55, 145.22, 149.00, 152.98, 155.12, 163.88, 167.36, 167.47, 167.55, 169.38, 169.45, 172.84. Exact mass: 889.29, **MS (ESI)**, *m/z*: 890 [M+H]$^+$.

1-((S)-sec-butyl)-N-((4,6-dimethyl-2-oxo-1,2-dihydropyridin-3-yl)methyl)-6-(6-(4-(1-((2-(2,6-dioxopiperidin-3-yl)-1,3-dioxoisoindolin-4-yl)oxy)-2-oxo-6,9,12-trioxa-3-azapentadecan-15-oyl)piperazin-1-yl)pyridin-3-yl)-3-methyl-1H-indole-4-carboxamide, 85a, MC4345. Yield, 62%, mp 146-148 °C. **^{1}H-NMR** (400MHz; CDCl$_3$) δ 0.89-0.93 (m, 3H, -CH$_2$-C*H$_3$*), 1.39-1.41 (s, 3H, -CH-C*H$_3$*), 1.75-1.81 (m, 2H, -C*H$_2$*-CH$_3$), 1.98-2.04, 2.68- 2.71 (m, 4H, -C*H$_2$*-CH$_2$- dioxopiperidine), 2.05 (s, 3H, -C*H$_3$* indole), 2.21, 2.34 (s, 6H, -C*H$_3$* pyridone), 2.61-2.64, 3.46-3.57 (m, 16H, -C*H$_2$*- linker), 3.43-3.49, 3.54-3.78 (m, 8H, -C*H$_2$*-CH$_2$- piperazine), 4.29-4.31 (m, 1H, CH$_3$-C-*H*-CH$_2$-), 4.53-4.55 (d, 2H, -O-C*H$_2$*-CO-), 4.58 (s, 2H, -C*H$_2$*-pyridone), 4.82-4.9 (m, 1H, -C*H* dioxopiperidine), 5.82 (s, 1H, -C*H* pyridone), 6.59-6.61 (d, 1H, -CH indole), 6.92-7.09, 7.18-7.19, 7.68-7.69 (m, 3H, -C*H*

pyridine), 7.09-7.11, 7.43-7.45, 7.60-7.62 (m, 3H, -C*H* dioxoisoindoline), 7.13-7.16, 7.35-7.36 (m, 2H, -C*H* indole), 7.53-7.55 (m, 1H, -CH$_2$-CO-N*H*-CH$_2$-), 8.36-8.37 (d, 1H, -CO-N*H*-CH$_2$-), 9.7 (s, 1H, -N*H* dioxopiperidine), 10.7 (s, 1H, -N*H* pyridone). **¹³C-NMR** (126 MHz, CDCl3) δ 173.06, 172.41, 171.98, 171.20, 167.72, 167.25, 160.39, 155.30, 154.53, 149.24, 144.76, 143.97, 140.55, 138.45, 137.11, 135.48, 132.30, 131.82, 131.05, 128.23, 126.93, 126.77, 124.76, 124.43, 123.77, 117.80, 112.82, 109.75, 109.06, 72.48, 66.87, 63.91 ,57.57 , 54.31, 51.33, 44.68, 43.38, 36.11, 32.54, 30.08, 28.15, 21.16 , 19.92, 19.03, 18.24, 17.03, 15.19, 10.95. Exact mass 1043.48, **MS (ESI)**, *m/z*: 1044.5 [M+H]⁺.

1-((S)-sec-butyl)-N-((4,6-dimethyl-2-oxo-1,2-dihydropyridin-3-yl)methyl)-6-(6-(4-(3-(2-(2-(2-((2-(2,6-dioxopiperidin-3-yl)-1,3-dioxoisoindolin-4-yl)oxy)acetamido)ethoxy)ethoxy)propanoyl)piperazin-1-yl)pyridin-3-yl)-3-methyl-1H-indole-4-carboxamide, 85b, MC4329. Yield, 52%, mp. 158-160 °C. **¹H-NMR** (400MHz; CDCl$_3$) δ 0.86-0.91 (m, 3H, -CH$_2$-C*H$_3$*), 1.39-1.41 (s, 3H, -CH-C*H$_3$*), 1.77-1.78 (m, 2H, -C*H$_2$*-CH$_3$), 1.98-2.04, 2.76- 2.81 (m, 4H, -C*H$_2$*-C*H$_2$*- dioxopiperidine), 2.06 (s, 3H, -C*H$_3$* indole), 2.22, 2.34 (s, 6H, -C*H$_3$* pyridone), 2.63-2.71, 3.49-3.68 (m, 12H, -C*H$_2$*- linker), 3.42-3.44, 3.76-3.80 (m, 8H, -C*H$_2$*-C*H$_2$*- piperazine), 4.29-4.31 (m, 1H, CH$_3$-C-*H*-CH$_2$-), 4.53-4.57 (m, 4H -O-C*H$_2$*-CO, C*H$_2$*- pyridone), 4.91-4.93 (m, 2H, -C*H* dioxopiperidine), 5.82 (s, 1H, -C*H* pyridone), 6.57-6.59 (d, 1H, -CH indole),6.91-6.93, 7.18-7.19, 7.65-7.67 (m, 3H, -C*H* pyridine), 7.09-7.11, 7.44-7.45, 7.60-7.64(m, 3H, -C*H* dioxoisoindoline), 7.13-7.16, 7.36-7.37 (m, 2H, -C*H* indole), 7.55-7.56 (m, 1H, -CH$_2$-CO- N*H*-CH$_2$-), 8.35-8.36, (d, 1H, -CO-N*H*-CH$_2$-), 9.78 (s, 1H, -N*H* dioxopiperidine), 11.05 (s, 1H, -N*H* pyridone). **¹³C NMR** (126 MHz, CDCl$_3$) δ 173.18, 172.51, 171.61, 170.38, 168.52, 166.87, 166.71, 164.70, 160.39, 154.46, 147.88, 145.62, 142.11, 141.12, 138.11, 138.01, 136.85, 133.74, 130.79, 127.75, 124.37, 122.69, 119.29, 118.04, 117.18, 116.86, 114.70, 112.09, 110.80, 109.56, 108.32, 69.48, 67.91, 67.52, 52.81, 49.35, 45.40, 41.24, 39.07, 36.20, 33.65, 31.49, 30.11, 28.53, 26.96, 22.75, 20.94, 19.71, 18.78, 15.31, 10.95. Exact mass 999.45, **MS (ESI)**, *m/z*: 1000.5 [M+H]⁺.

4-((4-(((tert-butoxycarbonyl)((1R,2S)-2-phenylcyclopropyl)amino)methyl)piperidin-1-yl)methyl)benzoic acid, 134. Yield, 30%.**¹H-NMR** (400MHz; DMSO-*d6*) δ 1.14-1.89 (m, 2H, -C*H$_2$*- cyclopropane), 1.32 (s, 9H, -C(C*H$_3$*)$_3$), 1.42-1.75 (m, 4H, -C*H$_2$*-C*H$_2$*- piperidine), 1.76-1.79 (m, 1H, *H*C-Ph), 2.05-2.01 (m, 1H, -C*H* piperidine), 2.67-2.69 (m, 1H, *H*C-N-BOC), 2.58- 3.03 (m, 4H, -C*H$_2$*-N-C*H$_2$*- piperidine), 3.66 (s, 2H, -C*H$_2$*-Ph), 4.2 (s, 2H, -C*H$_2$*-piperidine), 7.11-2.28 (m, 5H, -C*H* Ph), 7.66 (s, 2H, -C*H* Ph-COOH), 7.96-8.0 (s, 2H, -C*H* Ph-COOH), 13.07 (bs, 1H, -COO*H*).

tert-butyl((1-(4-((1-((2-(2,6-dioxopiperidin-3-yl)-1,3-dioxoisoindolin-4-yl)oxy)-2-oxo-7,10,13-trioxa-3-azahexadecan-16-yl)carbamoyl)benzyl)piperidin-4-yl)methyl)((1R,2S)-2-phenylcyclopropyl)carbamate, 135a, MC4370. Yield, 76%, mp 73-76°C. **¹H-NMR** (400MHz; MeOH-*d4*) δ 1.14-1.91 (m, 4H, -C*H$_2$*- cyclopropane, -C*H$_2$*- piperidine), 1.9 (s, 9H, -C(C*H$_3$*)$_3$), 1.51-1.57 (m, 3H, -C*H$_2$*- piperidine, *H*C-Ph), 1.68-1.78 (m, 4H, -CH$_2$-C*H$_2$*-CH$_2$-), 1.89-1.98, 2.0-2.05 (m, 4H, -C*H$_2$*-C*H$_2$*- dioxopiperidine), 2.57- 2.67 (m, 2H, -C*H$_2$*- piperidine), 2.74- 2.76 (m, 2H, -C*H$_2$*-N-BOC), 3.03-3.06 (m, 1H, *H*C-N-BOC), 3.2-3.22 (m, 1H, -C*H* piperidine), 3.26-3.29 (m, 2H, -C*H$_2$*-piperidine) 3.34-3.44 (4H, m, -C*H$_2$*-NH), 3.45-3.49 (m, 4H, -CH$_2$-C*H$_2$*-C*H$_2$*-O-), 3.50, 3.51 (m, 2H, -C*H$_2$*-Ph), 3.51- 3.53 (m, 8H, -O-C*H$_2$*-C*H$_2$*-O-C*H$_2$*-C*H$_2$*-), 4.63 (s, 2H, -O-C*H$_2$*-CO-), 5.01-5.05 (m, 1H, -C*H* dioxopiperidine), 6.99-7.13 (m, 5H, -C*H* Ph-cyclopropane), 7.29-7.43 (m, 4H, -C*H* Ph-CH$_2$), 7.64-7.69 (m, 3H, -C*H* dioxoisoindoline), 7.8 (s, 1H, -O-CH$_2$-CO-N*H*), 8.4 (s, 1H, Ph-CO-N*H*), 11.06 (s, 1H, -N*H* dioxopiperidine). **¹³C-NMR** (100 MHz, DMSO-*d$_6$*) δ 18.21, 24.04, 24.18, 28.19, 28.93, 29.32, 29.34, 29.76, 33.44, 37.88, 37.94, 42.96, 49.73,

51.69, 52.22, 60.75, 68.43, 68.56, 68.58, 70.08, 70.56, 80.85, 116.99, 118.70, 121.41, 126.53, 126.81, 128.42, 128.47, 129.04, 132.35, 132.59, 133.12, 141.73, 142.47, 154.56, 155.43, 165.54, 166.31, 168.07, 169.32, 169.56, 171.84. Exact mass 980.49, **MS (ESI)**, *m/z*: 981.5 [M+H]⁺.

tert-butyl((1-(4-((2-(2-(2-(2-((2-(2,6-dioxopiperidin-3-yl)-1,3-dioxoisoindolin-4-yl)oxy)acetamido)ethoxy)ethoxy)ethyl)carbamoyl)benzyl)piperidin-4-yl)methyl)((1R,2S)-2-phenylcyclopropyl)carbamate, 135b, MC4367. Yield, 73%, mp. 97-100 °C. **¹H-NMR** (400MHz; MeOH-*d4*) δ 1.24-1.25 (m, 4H, -C*H₂*- cyclopropane, -C*H₂*-piperidine), 1.4 (s, 9H, -C(C*H₃*)₃), 1.63-1.67 (m, 3H, -C*H₂*- piperidine, *H*C-Ph), 1.98-2.03, 2.11-2.16 (m, 4H, -C*H₂*-C*H₂*- dioxopiperidine) 2.68- 2.74 (m, 2H, -C*H₂*-piperidine), 2.77-2.88 (m, 2H, -C*H₂*-N-BOC), 3.12-3.18 (m, 1H, *H*C-N-BOC), 3.27-3.29 (m, 1H, -C*H* piperidine), 3.32-3.35 (m, 2H, -C*H₂*-piperidine), 3.49-3.50 (m, 2H, C*H₂*-Ph), 3.54-3.56 (m, 4H, -O-C*H₂*-C*H₂*-O-), 3.62-3.67 (m, 8H, -NH-C*H₂*-C*H₂*-O-), 4.75 (s, 2H, -O-C*H₂*-CO-), 5.11-5.15 (m, 1H, -C*H* dioxopiperidine), 7.12-7.28 (m, 5H, -C*H* Ph-cyclopropane), 7.39-7.53 (m, 4H, -C*H* Ph-CH₂), 7.76-7.82 (m, 3H, -C*H* dioxoisoindoline), 7.92 (s, 1H, -O-CH₂-CO-N*H*), 8.5 (s, 1H, Ph-CO-N*H*), 11.06 (s, 1H, -N*H* dioxopiperidine). **¹³C-NMR** (100 MHz, DMSO-*d₆*) δ 18.21, 24.04, 24.18, 28.19, 28.93, 29.76, 33.44, 39.98, 40.21, 42.96, 49.73, 51.69, 52.22, 60.75, 68.41, 69.47, 69.54, 69.64, 69.65, 80.85, 116.99, 118.70, 121.41, 126.53, 126.81, 128.46, 128.47, 129.04, 132.35, 132.64, 133.12, 141.73, 142.47, 154.56, 155.43, 165.54, 166.31, 167.34, 169.33, 169.34, 171.84. Exact mass 908.43, **MS (ESI)**, *m/z*: 909.4 [M+H]⁺.

tert-butyl ((1S,2R)-2-(4-(1-((2-(2,6-dioxopiperidin-3-yl)-1,3-dioxoisoindolin-4-yl)oxy)-2-oxo-6,9,12-trioxa-3-azapentadecan-15-amido)phenyl)cyclopropyl)carbamate 137a, MC4352. Yield, 60%, mp. 83-88 °C. **¹H-NMR** (400MHz; CDCl₃) δ 1.01-1.21 (t, 2H, -C*H₂*-cyclopropane), 1.55 (s, 9H, -C(C*H₃*)₃), 1.88-1.90 (m, 1H, -C*H*-Ph), 2.04-2.1, 2.65-2.82 (m, 5H, -C*H₂*-C*H₂*- dioxopiperidine, -C*H*-NHBOC), 2.51-2.62, 3.38-3.78 (m, 16H, -C*H₂*-linker), 4.58 (s, 2H, -O-C*H₂*-CO), 4.84 (m, 2H, -N*H*-BOC, -C*H* dioxopiperidine), 6.93-6.96, 7.35-7.37 (m, 4H, -C*H* Ph-cyclopropane), 7.11-7.13, 7.47-7.54, 7.65-7.90 (m, 3H, -C*H* dioxoisoindoline), 7.54 (s, 1H, -O-CH₂-CO-N*H*), 8.5 (s, 1H, Ph-CO-N*H*), 8.89 (s, 1H, -N*H* dioxopiperidine). **¹³C-NMR** (100 MHz, DMSO-*d₆*) δ 19.34, 24.18, 27.26, 28.28, 29.76, 35.21, 37.46, 39.98, 52.22, 66.17, 68.41, 69.54, 69.57, 69.68, 70.55, 70.62, 79.67, 116.99, 118.70, 120.74, 121.41, 127.13, 132.35, 133.12, 137.54, 138.39, 155.39, 155.43, 165.54, 166.31, 169.33, 169.34, 170.86, 171.84. Exact mass 765.32, **MS (ESI)**, *m/z*: 766.3 [M+H]⁺.

tert-butyl ((1S,2R)-2-(4-(3-(2-(2-(2-((2-(2,6-dioxopiperidin-3-yl)-1,3-dioxoisoindolin-4-yl)oxy)acetamido)ethoxy)ethoxy)propanamido)phenyl)cyclopropyl)carbamate, 137b, MC4341. Yield, 70%, mp. 101-105 °C. **¹H-NMR** (400MHz; CDCl₃) δ 0.80-0.99 (t, 2H, -C*H₂*- cyclopropane), 1.38 (s, 9H, -C(C*H₃*)₃), 1.88-1.91 (m, 1H, -C*H*-Ph), 2.01-2.05, 2.65-2.80 (m, 5H, -C*H₂*-C*H₂*- dioxopiperidine, -C*H*-NH-BOC), 2.51-2.55, 3.38-3.78 (m, 12H, -C*H₂*- linker), 4.79 (s, 2H, -O-C*H₂*-CO), 5.81 (m, 2H, -N*H*-BOC, C-*H* dioxopiperidine), 6.91-6.93, 7.32-7.34 (m, 4H, -C*H* Ph-cyclopropane), 7.09-7.11, 7.44-7.46, 7.63-7.67 (m, 3H, .-C*H* dioxoisoindoline), 7.55 (s, 1H, -O-CH₂-CO-N*H*), 8.4 (s, 1H, Ph-CO-N*H*), 8.59 (s, 1H, -N*H* dioxopiperidine). **¹³C-NMR** (100 MHz, DMSO-*d₆*) δ 19.34, 24.18, 27.26, 28.28, 29.76, 35.21, 37.46, 39.98, 52.22, 66.17, 68.41, 69.54, 69.56, 69.67, 79.67, 116.99, 118.70, 120.74, 121.41, 127.13, 132.35, 133.12, 137.54, 138.39, 155.39, 155.43, 165.54, 166.31, 169.33, 169.34, 170.86, 171.84. Exact mass 721.30, **MS (ESI)**, *m/z*: 722.30 [M+H]⁺.

8-(methoxymethoxy)quinoline-5-carboxylic acid, 139. Yield, quantitative. **¹H-NMR** (400MHz; MEOH-d_4) δ 3.53 (s, 3H, -O-CH$_2$-O-C*H*$_3$), 5.42 (s, 2H, -O-C*H*$_2$-O-CH$_3$), 7.33-7.35, 7.55-7.58, 7.25-7.27, 8.76-8.77, 9.46-9.48 (m, 5H, -C*H*, quinoline), 12 (s, 1H, -COO*H*).

N-(1-((2-(2,6-dioxopiperidin-3-yl)-1,3-dioxoisoindolin-4-yl)oxy)-2-oxo-7,10,13-trioxa-3-azahexadecan-16-yl)-8-(methoxymethoxy)quinoline-5-carboxamide, 140a, MC4356. Yield, 50%, mp. 81-84 °C. **¹H-NMR** (400MHz; CDCl$_3$) δ 1.71-1.84, 1.86-2.05, 3.30-3.41, 3.52-3.62 (m, 20H, -CH$_2$- linker), 2.05-2.08, 2.65-2.81 (m, 4H -C*H*$_2$-C*H*$_2$- dioxopiperidine), 3.51 (s, 3H, -O-CH$_2$-O-C*H*$_3$), 4.5 (s, 2H, -O-C*H*$_2$-CO-), 4.80-4.92 (m, 2H, -C*H* dioxopiperidine), 5.48 (s, 2H, -O-C*H*$_2$-O-CH$_3$), 6.93-6.96 (t, 1H, -O-CH$_2$-CO-N*H*-), 7.07-7.09 (d, 1H, -C*H* dioxoisoindoline), 7.27-7.29 (d, 1H, -C*H* quinoline), 7.41-7.48 (3H, m, -C*H* dioxoisoindoline, -C*H* quinoline), 7.6-7.7.67 (2H, m, -C*H* dioxoisoindoline, -C*H*, quinoline), 8.83-8.94 (m, 3H, -C*H* quinoline, -N*H*-CO-quinoline), 11.1 (s, 1H, -N*H* dioxopiperidine). **¹³C-NMR** (100 MHz, DMSO-d_6) δ 24.17, 29.32, 29.34, 29.81, 37.79, 37.88, 52.05, 56.30, 68.43, 68.56, 68.58, 70.08, 70.56, 95.74, 111.19, 117.05, 118.70, 121.40, 123.04, 126.31, 126.93, 129.11, 131.75, 132.35, 133.12, 140.04, 148.38, 152.69, 155.43, 166.36, 167.17, 167.47, 169.32, 169.56, 171.84. Exact mass 749.29, **MS (ESI)**, *m/z*: 750.32 [M+H]$^+$.

N-(2-(2-(2-(2-((2-(2,6-dioxopiperidin-3-yl)-1,3-dioxoisoindolin-4-yl)oxy)acetamido)ethoxy)ethoxy)ethyl)-8-(methoxymethoxy)quinoline-5-carboxamide, 140b, MC4357. Yield, 60%, mp. 81-84 °C. **¹H-NMR** (400MHz; CDCl$_3$) δ 2.04 -2.08, 2.59-2.75 (m, 4H -C*H*$_2$-C*H*$_2$- dioxopiperidine), 3.38-3.48, 3.53-3.59 (m, 12H, -C*H*$_2$- linker), 3.5 (s, 3H, -O-CH$_2$-O-C*H*$_3$), 4.5 (s, 2H, -O-C*H*$_2$-CO-), 4.80-4.985 (m, 2H, -C*H* dioxopiperidine), 5.48 (s, 2H, -O-C*H*$_2$-O-CH$_3$), 6.8 (s, 1H, -O-CH$_2$-CO-N*H*), 7.03-7.05 (d, 1H, -C*H* dioxoisoindoline), 7.26-7.30 (d, 1H, -C*H* quinoline), 7.39-7.41 (d, 1H, -C*H* quinoline), 7.44-7.46 (d, 1H, -C*H* dioxoisoindoline), 7.50-7.52 (m, 1H, -C*H* dioxoisoindoline), 7.61-7.66 (t, 1H, -C*H*, quinoline), 8.6 (s, 1H, -N*H*-CO-quinoline) 7.78-8.83, 8.88-8.9 (m, 2H, -C*H* quinoline), 11.2 (s, 1H, -N*H* dioxopiperidine). **¹³C-NMR** (100 MHz, DMSO-d_6) δ 24.17, 29.81, 39.98, 40.06, 52.05, 56.30, 68.41, 69.47, 69.54, 69.64, 69.65, 95.74, 111.21, 117.05, 118.70, 121.40, 123.04, 126.31, 126.93, 129.56, 131.75, 132.35, 133.12, 140.04, 148.38, 152.69, 155.43, 166.36, 167.17, 167.33, 169.33, 169.34, 171.84. Exact mass 677.23, **MS (ESI)**, *m/z*: 678.24 [M+H]$^+$.

General procedure for the synthesis of 36g, 36d CRBN and 37c, 37e, 37f VHL based PROTACs targeting EZH2 86a-d (Scheme 4.7A), 87a-d (Scheme 4.7B), 88a-d (Scheme 4.7C), 89a-d (Scheme 4.7D), 90a-d (Scheme 4.7E).
The proper acid **125a-d**, **127a-d**, **129a-d**, **131a-d**, **133a-d** (0.0195mmol, 1eq) and the GSK126 **20** (0.0195 mmol, 1eq) were dissolved in dry DMF (0.6 mL) and then DIPEA (0.078 mmol, 4eq) was added. After pH checked (around 10), PyOxym (0.0195 mmol, 1eq) was added and the resulting solution left to stir for 1-2h. After that time, LC-MS check (acidic method) showed the completion of the reaction which was purified by HPLC using a gradient from 10 to 80% v/v acetonitrile with 0.01% v/v aqueous solution of HCOOH over 10 min providing the analytically pure desired compound **86a-d, 87a-d, 88a-d, 89a-d, 90a-d.**

1-((S)-sec-butyl)-N-((4,6-dimethyl-2-oxo-1,2-dihydropyridin-3-yl)methyl)-6-(6-(4-(2-(2-(2-(2-((2-(2,6-dioxopiperidin-3-yl)-1,3-dioxoisoindolin-5-yl)oxy)ethoxy)ethoxy)ethoxy)acetyl)piperazin-1-yl)pyridin-3-yl)-3-methyl-1H-indole-4-carboxamide, 86a, DT101. Yield, 30%. **¹H-NMR** (400MHz; CDCl₃) δ 0.84-0.87 (m, 3H, -CH₂-C*H₃*), 1.48-1.49 (s, 3H, -CH-C*H₃*), 1.69-1.73 (m, 2H, -C*H₂*-CH₃), 2.19, 2.27 (s, 6H, -C*H₃* pyrimidone), 2.44 (s, 3H, -C*H₃* indole), 2.62-2.67 (m, 4H, -C*H₂*-C*H₂*- dioxopiperidine), 3.04-3.41, 3.54-3.55, 4.31-4.32 (m, 8H, -C*H₂*-C*H₂*- piperazine), 3.68-3.76 (m, 12H, -C*H₂*- linker), 3.99 (s, 2H, -C*H₂*-pyridone), 4.41-4.39 (m, 1H, CH₃-C*H*-CH₂-), 4.62 (d, 2H, -O-C*H₂*-CO-), 4.81-4.86 (m, 1H, -C*H* dioxopiperidine), 5.92 (s, 1H, -C*H* pyrimidone), 6.63-6.65 (d, 1H, -CH indole), 6.98, 7.21-7.22, 7.47-7.48 (m, 3H, -CH pyridine), 7.23-7.24, 7.35, 7.75-7.77 (m, 3H, -C*H* dioxoisoindoline), 7.81-7.83, 8.5 (m, 2H, -C*H* indole), 8.55 (s, 1H, -CH₂-N*H*-CO-), 9.97 (s, 1H, -N*H* dioxopiperidine), 10.68 (s, 1H, -N*H* pyridone). **¹³C-NMR** (126 MHz, CDCl₃) δ 173.18, 171.95, 169.64, 168.61, 168.10, 167.02, 166.88, 164.89, 164.25, 163.89, 150.73, 150.59, 142.53, 137.95, 134.19, 130.66, 127.83, 125.40, 124.45, 124.42 123.79, 123.63, 122.41, 120.76, 116.75, 110.71, 109.82 109.10, 108.44, 108.16, 70.71, 70.61, 70.51, 69.39, 68.55, 68.41, 67.95, 58.27, 52.78, 45.45, 44.51, 31.39, 30.11, 26.37, 23.39, 22.61, 19.71, 18.64, 15.31, 11.73. Exact mass 972.44, **MS (ESI),** *m/z*: 973.5 [M+H]⁺.

1-((S)-sec-butyl)-N-((4,6-dimethyl-2-oxo-1,2-dihydropyridin-3-yl)methyl)-6-(6-(4-(2-((4-((2-(2,6-dioxopiperidin-3-yl)-1,3-dioxoisoindolin-5-yl)oxy)but-2-yn-1-yl)oxy)acetyl)piperazin-1-yl)pyridin-3-yl)-3-methyl-1H-indole-4-carboxamide, 86b, DT103. Yield, 14%. **¹H-NMR** (400MHz; CDCl₃) δ 1.49-1.52 (m, 3H, -CH₂-C*H₃*), 1.18-1.93 (m, 3H, -CH-C*H₃*), 2.02, 2.23 (s, 6H, -C*H₃* pyrimidone), 2.06-2.14 (m, 2H, -C*H₂*-CH₃), 2.29 (s, 3H, -C*H₃* indole), 2.73-2.86 (m, 4H, -C*H₂*-C*H₂*- dioxopiperidine), 3.64, 3.67 (s, 4H, -C*H₂*- linker), 4.18-4.28, 4.33-4.43 (m, 8H, -C*H₂*-C*H₂*- piperazine), 4.59-4.62 (m, -C*H₂*-pyridone), 6.63-4.66 (m, 1H, CH₃-C*H*-CH₂), 4.9 (s, 2H, -O-C*H₂*-CO-), 4.93-4.95 (m, 1H, -C*H* dioxopiperidine), 6.01 (s, 1H, -C*H* pyrimidone), 6.70-6.72 (d, 1H, -CH indole), 7.00, 7.47, 8.11 (s, 3H, -CH pyridine), 7.19-7.23, 7.99-7.80, 7.81-7.84 (m, 3H, -C*H* dioxoisoindoline), 7.29-7.34, 7.48-7.51 (m, 2H, -C*H* indole), 8.49-8.50 (s, 1H, -CH₂-N*H*-CO-), 9.54 (s, 1H, -N*H* dioxopiperidine), 11.2 (s, 1H, -N*H* pyridone). **¹³C-NMR** (101 MHz, CDCl₃) δ 171.88, 171.20, 170.13 167.07, 167.58, 167.51, 167.32, 162.86, 160.18, 158.96, 155.95, 146.28, 144.31, 138.02, 136.69, 134.30, 131.47, 130.64, 129.57, 128.2, 125.58, 124.46, 124.19, 122.97, 117.08, 115.33, 112.62, 110.83, 109.66, 108.39, 80.64, 76.69, 68.51, 58.49, 57.14, 56.70, 56.11, 52.80, 45.35, 44.72, 31.42, 30.13, 28.22, 25.73, 20.94, 19.76, 18.88, 15.12, 11.84. Exact mass 908.39, **MS (ESI)**, *m/z*: 909.39 [M+H]⁺.

1-((S)-sec-butyl)-N-((4,6-dimethyl-2-oxo-1,2-dihydropyridin-3-yl)methyl)-6-(6-(4-(2-(2-((2-(2,6-dioxopiperidin-3-yl)-1,3-dioxoisoindolin-5-yl)oxy)ethoxy)acetyl)piperazin-1-yl)pyridin-3-yl)-3-methyl-1H-indole-4-carboxamide, 86c, DT102. Yield, 30%. **^{1}H-NMR** (400MHz; CDCl$_3$) δ 0.84-0.86 (m, 3H, -CH$_2$-C*H$_3$*), 1.48-1.49 (m, 3H, -CH-C*H$_3$*), 1.68-1.73 (m, 2H, -C*H$_2$*-CH$_3$), 2.19, 2.27, 2.45 (s, 6H, -C*H$_3$* pyridone), 2.45 (s, 3H, -C*H$_3$* indole), 2.55-2.89 (m, 4H, -C*H$_2$*-C*H$_2$*- dioxopiperidine), 3.54-3.55, 4.31, 4.32 (m, 8H, -C*H$_2$*-C*H$_2$*-piperazine), 3.68- 3.75 (m, 4H, -C*H$_2$*- linker), 4.02 (s, -C*H$_2$*-pyridone), 4.39-4.40 (m, 1H, CH$_3$-C*H*-CH$_2$-), 4.64 (s, 2H, -O-C*H$_2$*-CO-), 4.81-4.86 (m, 1H, -C*H* dioxopiperidine), 5.92 (s, 1H, -C*H* pyridone), 6.62-6.64 (d, 1H, -CH indole), 6.98, 7.35, 8.5 (s, 3H, -CH pyridine), 7.20-7.22, 7.75-7.77, 7.81-7.83 (m, 3H, -C*H* dioxoisoindoline), 7.22, 7.48 (s, 2H, -C*H* indole), 8.52-8.55 (s, 1H, -CH$_2$-N*H*-CO-), 9.97 (s, 1H, --N*H* dioxopiperidine), 10.80 (s, 1H, -N*H* pyridone). **^{13}C-NMR** (126 MHz, CDCl$_3$) δ 172.33, 169.58, 168.38, 167.57, 166.87, 166.81, 160.39 158.03, 155.95, 150.46, 146.31, 141.88, 137.96, 136.79, 136.57, 134.33, 132.30, 130.88, 130.66, 128.87, 128.17, 125.59, 124.28, 124.18, 124.13, 123.94, 123.65, 122.92, 120.10, 120.04, 117.11, 115.14, 110.82, 109.60, 108.46, 107.09, 69.66, 68.34, 54.55, 52.83, 49.36, 45.82, 45.39, 45.08, 44.93, 44.73, 41.63, 39.61, 36.01, 32.78, 31.41, 30.92, 30.10, 24.26, 22.67, 20.95, 20.92, 19.73, 19.15, 18.81, 15.79, 10.98. Exact mass: 884.39, **MS (ESI)**, *m/z*: 885.4 [M+H]$^+$.

1-((S)-sec-butyl)-N-((4,6-dimethyl-2-oxo-1,2-dihydropyridin-3-yl)methyl)-6-(6-(4-(2-(3-(3-((2-(2,6-dioxopiperidin-3-yl)-1,3-dioxoisoindolin-5-yl)oxy)propoxy)propoxy)acetyl)piperazin-1-yl)pyridin-3-yl)-3-methyl-1H-indole-4-carboxamide, 86d, DT115. Yield, 24%. **^{1}H-NMR** (400MHz; CDCl$_3$) δ 0.84-0.85 (s, 3H, -CH$_2$-C*H$_3$*), 1.48 (s, 3H, -CH-C*H$_3$*), 1.85-1.92, 3.62-3.76 (m, 12H, -C*H$_2$*- linker), 2.00-2.02 (m, 2H, -C*H$_2$*-CH$_3$), 2.096 (s, 3H, -C*H$_3$* pyridone), 2.25 (m, 3H, -C*H$_3$* pyridone), 2.26-2.27, 2.60-2.89 (m, 4H, -C*H$_2$*-C*H$_2$*- dioxopiperidine), 2.48-2.50 (d, 3H, -C*H$_3$* indole), 2.55-2.89 (m, 4H, -C*H$_2$*-C*H$_2$*- dioxopiperidine), 3.56, 4.19-4.21 (m, 8H, -C*H$_2$*-C*H$_2$*- piperazine), 4.22-4.23 (m, 1H, CH$_3$-C-*H*-CH$_2$-), 4.40 (s, -C*H$_2$*-pyridone), 4.63 (s, 2H, -O-C*H$_2$*-CO-), 4.91-4.92 (m, 1H, -C*H* dioxopiperidine), 6.02-6.04 (d, 1H, -C*H* pyridone), 6.69-6.73 (t, 1H, -CH indole), 6.98-7.00, 7.27-7.28, 8.08-8.1 (m, 3H, -CH pyridine), 7.1, 7.45-7.47, 7.87-7.91 (m, 3H, -C*H* dioxoisoindoline), 7.18-7.21, 7.35-7.37 (m, 2H, -C*H* indole), 8.47-8.49 (d, 1H, -CH$_2$-N*H*-CO-), 9.03 (s, 1H, -N*H* dioxopiperidine), 11.6 (s, 1H, -N*H* pyridone). **^{13}C -NMR** (126 MHz, CDCl$_3$) δ 173.05, 171.46, 169.79, 168.35, 168.06, 167.18, 167.00, 160.89, 160.60, 155.21, 149.24, 142.32, 137.97, 136.72, 136.63, 134.37, 130.75, 130.48, 127.95, 125.48, 125.15, 124.29, 123.61, 123.47, 122.54, 120.82, 116.92, 112.52, 110.60, 109.89, 108.47, 69.88, 69.12 68.40, 67.70, 66.80, 66.13, 59.84, 52.33, 44.82, 44.51, 32.43, 30.11, 29.96, 29.41, 28.70, 25.92, 19.86, 18.69, 15.24, 11.70. Exact mass:956.44, **MS (ESI)**, *m/z*: 957.5 [M+H]$^+$.

1-((S)-sec-butyl)-N-((4,6-dimethyl-2-oxo-1,2-dihydropyridin-3-yl)methyl)-6-(6-(4-(2-(2-(2-(2-(4-(2-(2,6-dioxopiperidin-3-yl)-1,3-dioxoisoindolin-5-yl)piperazin-1-yl)ethoxy)ethoxy)ethoxy)acetyl)piperazin-1-yl)pyridin-3-yl)-3-methyl-1H-indole-4-carboxamide, 87a, DT57. Yield, 12%. **^{1}H-NMR** (400MHz; CDCl$_3$) δ 0.83-0.87 (m, 3H, -CH$_2$-C*H$_3$*), 1.36-1.43 (m, 2H, -C*H$_2$*-CH$_3$), 1.48-1.50 (m, 3H, -CH-C*H$_3$*), 1.80-1.94, 2.07-2.19 (m, 8H, -C*H$_2$*-C*H$_2$*- piperazine-thalidomide), 2.19 (s, 3H, -C*H$_3$* pyridone), 2.29 (s, 3H, -C*H$_3$* pyridone), 2.35, 2.78-2.88 (m, 4H, -C*H$_2$*-C*H$_2$*- dioxopiperidine), 2.45 (s, 3H, -C*H$_3$* indole), 2.66-2.69, 3.44-3.57 (m, 12H -C*H$_2$*- linker), 3.04 (s, 1H, CH$_3$-C*H*-CH$_2$), 3.44-3.57, 4.37-4.41 (m, 8H, -C*H$_2$*-C*H$_2$*- piperazine-GSK126), 4.29 (s, -C*H$_2$*-pyridone), 4.58-4.67 (m, 2H, -O-C*H$_2$*-CO-), 4.87-4.93 (m, 1H, -C*H* dioxopiperidine), 5.92 (s, 1H, -C*H* pyridone), 6.68-6.72 (m, 1H, -CH indole), 6.99-7.00, 7.25-7.26, 7.75-7.80 (m, 3H, -CH pyridine), 7.01-7.05, 7.45-7.46, 7.66-7.68 (m, 3H, -C*H* dioxoisoindoline), 7.23-7.24, 7.29-7.30 (m,

2H, -C*H* indole), 8.46-8.47 (d, 1H, -CH$_2$-N*H*-CO-), 8.48-8.49 (s, 1H, -N*H* dioxopiperidine), 10.76 (s, 1H, -N*H* pyridone). **^{13}C-NMR** (101 MHz, CDCl$_3$) δ 173.18, 171.20, 169.63, 168.57, 167.91, 164.95, 157.93, 155.52, 150.47, 150.42, 146.30, 142.42, 137.99, 136.60, 136.31, 134.28, 130.76, 128.23, 127.82, 125.31, 124.25, 123.62, 122.51, 122.39, 117.82, 116.93, 110.69, 108.48, 108.34, 70.56, 70.41, 69.93, 69.37, 68.92, 59.31, 55.33, 52.71, 51.91, 49.16, 47.39, 45.48, 36.12, 31.46, 30.11, 22.75, 20.91, 19.73, 18.69, 11.80, 15.31, 10.97. Exact mass: 1040.51, **MS (ESI)**, *m/z*: 1041.5 [M+H]$^+$.

1-((S)-sec-butyl)-N-((4,6-dimethyl-2-oxo-1,2-dihydropyridin-3-yl)methyl)-6-(6-(4-(2-((4-(4-(2-(2,6-dioxopiperidin-3-yl)-1,3-dioxoisoindolin-5-yl)piperazin-1-yl)but-2-yn-1-yl)oxy)acetyl)piperazin-1-yl)pyridin-3-yl)-3-methyl-1H-indole-4-carboxamide, **87b, DT62.** Yield, 36%. **^{1}H-NMR** (400MHz; CDCl$_3$) δ 0.83-0.88 (m, 3H, -CH$_2$-C*H$_3$*), 1.45-1.48 (m, 3H, -CH-C*H$_3$*), 1.48-1.51 (m, 2H, -C*H$_2$*-CH$_3$), 1.81-1.91, 1,93-1.96 (m, 8H, -C*H$_2$*-C*H$_2$*-piperazine-thalidomide), 2.22 (s, 3H, -C*H$_3$* pyridone), 2.25-2.26 (d, 3H, -C*H$_3$* pyridone), 2.45 (s, 3H, C*H$_3$*-indole),), 2.74-2.81, 3.15-3.21 (m, 4H, -C*H$_2$*-C*H$_2$*- dioxopiperidine), 3.46-3.48, 3.6-3.62 (m, 8H, -C*H$_2$*-C*H$_2$*- piperazine-GSK126), 3.52, 3.75 (s, 4H, -C*H$_2$*- linker), 3.67-3.73 (m, 1H, CH$_3$-C*H*-CH$_2$), 4.32 (s, -C*H$_2$*-pyridone), 4.37 (s, 2H, -O-C*H$_2$*-CO-), 4.79-4.87 (m, 1H, -C*H* dioxopiperidine), 5.97 (s, 1H, -C*H* pyridone), 6.64-6.77 (m, 1H, -CH indole), 7.06-7.09, 7.28-7.29, 7.76-7.79 (m, 3H, -CH pyridine), 7.16-7.20, 7.45-7.46, 7.66-7.68 (m, 3H, -C*H* dioxoisoindoline), 7.26-7.27, 7.31-7.32 (m, 2H, -C*H* indole), 8.14 (s, 1H, -CH$_2$-N*H*-CO-), 8.45-8.46 (d, 1H, -N*H* dioxopiperidine), 9.16 (s, 1H, -N*H* pyridone). **^{13}C-NMR** (101 MHz, CDCl$_3$) δ 173.18, 171.73, 169.78, 168.47, 167.76, 167.36, 167.12, 165.39, 160.82, 155.45, 149.09, 148.22, 143.22, 140.93, 136.69, 132.28, 131.32, 130.76, 130.55, 128.00, 127.30, 124.17, 124.32, 123.58, 119.25, 117.23, 116.93, 112.63, 110.12, 108.76, 81.66, 80.93, 68.52, 58.69, 57.52, 52.82, 51.30, 49.14, 45.44, 44.81, 43.49, 31.42, 30.09, 22.70, 20.93, 19.80, 18.75, 12.36, 11.64, 10.98. Exact mass: 976.46, **MS (ESI)**, *m/z*: 977.5 [M+H]$^+$.

1-((S)-sec-butyl)-N-((4,6-dimethyl-2-oxo-1,2-dihydropyridin-3-yl)methyl)-6-(6-(4-(2-(2-(4-(2-(2,6-dioxopiperidin-3-yl)-1,3-dioxoisoindolin-5-yl)piperazin-1-yl)ethoxy)acetyl)piperazin-1-yl)pyridin-3-yl)-3-methyl-1H-indole-4-carboxamide, **87c, DT68.** Yield, 30%. **^{1}H-NMR** (400MHz; CDCl$_3$) δ 0.83-0.87 (t, 3H, -CH$_2$-C*H$_3$*), 1.37-1.42 (t, 2H, -C*H$_2$*-CH$_3$), 1.49-1.50 (d, 3H, -CH-C*H$_3$*), 1.82-1.94, 4.37-4.38 (m, 4H, -C*H$_2$*-C*H$_2$*-linker), 2.08- 2.14, 2.96-2.98 (m, 4H, -C*H$_2$*-C*H$_2$*- dioxopiperidine), 2.26, 2.28 (d, 6H, -C*H$_3$* pyridone), 2.50 (s, 3H, -C*H$_3$* indole), 2.81-2.82, 3.48-3.50 (m, 8H, -C*H$_2$*-C*H$_2$*- piperazine-thalidomide), 3.66-3.80 (m, 8H, -C*H$_2$*-C*H$_2$*- piperazine- GSK126), 3.59 (s, 1H, CH$_3$-C*H*-CH$_2$), 4.28 (s, -C*H$_2$*- pyridone), 4.63-4.65 (d, 2H, -O-C*H$_2$*-CO-), 4.86-4.91 (m, 1H, -C*H* dioxopiperidine), 6.04-6.06 (d, 1H, -C*H* pyridone), 6.71-6.74 (m, 1H, -CH indole), 7.00-7.01, 7.28-7.29, 8.47 (m, 3H, -CH pyridine), 7.06-7.08, 7.78-7.80, 8.16 (m, 3H, -C*H* dioxoisoindoline), 7.06-7.08, 7.70-7.71 (m, 2H, -C*H* indole), 8.47 (s, 1H, -CH$_2$-N*H*CO-), 8.57 (s, 1H, -N*H* dioxopiperidine), 11.2 (s, 1H, -N*H* pyridone). **^{13}C-NMR** (101 MHz, CDCl$_3$) δ 173.13, 171.29, 169.88, 168.34, 167.94, 165.01, 164.79, 159.10, 158.25, 149.24, 148.70, 143.97, 140.52, 136.73, 132.53, 131.44, 130.73, 130.43, 128.06, 127.33, 124.29, 124.58, 123.91, 119.96, 118.21, 116.90, 112.15, 109.71, 108.59, 69.10, 68.39, 59.26, 55.51, 53.45, 52.87, 49.20, 44.81, 44.33, 32.44, 32.11, 28.78, 25.71, 20.92, 19.88, 18.79, 14.09, 11.71. Exact mass: 952.46, **MS (ESI)**, *m/z*: 953.5[M+H]$^+$.

1-((S)-sec-butyl)-N-((4,6-dimethyl-2-oxo-1,2-dihydropyridin-3-yl)methyl)-6-(6-(4-(2-(3-(3-(4-(2-(2,6-dioxopiperidin-3-yl)-1,3-dioxoisoindolin-5-yl)piperazin-1-yl)propoxy)propoxy)acetyl)piperazin-1-yl)pyridin-3-yl)-3-methyl-1H-indole-4-carboxamide, 87d, DT114. Yield, 10%. **¹H-NMR** (400MHz; CDCl₃) δ 0.83-0.87 (t, 3H, -CH₂-C*H₃*), 1.48-1.50 (d, 3H, -CH-C*H₃*), 1.80-1.94 (m, 6H, -CH₂-C*H₂*-CH₂-, -C*H₂*-CH₃), 2.07-2.19, 2.63-2.66-2.85-2.90 (m, 4H, -C*H₂*-C*H₂*- dioxopiperidine), 2.23, 2.27 (d, 6H, -C*H₃* pyridone), 2.75-2.79, 3.49-3.62 (m, 24H, -C*H₂*-C*H₂*-CH₂-, -C*H₂*-C*H₂*- piperazine-thalidomide, -C*H₂*-C*H₂*- piperazine-GSK126), 4.23 (s, -C*H₂*-pyridone), 4.35-4.34 (m, 1H, CH₃-C*H*-CH₂-), 4.63-4.65 (d, 2H, -O-C*H₂*-CO-), 4.89-4.91 (m, 1H, -C*H* dioxopiperidine), 6.02 (d, 1H, -C*H* pyridone), 6.70-6.74 (m, 1H, -CH indole), 7.00, 7.27-7.28, 8.16 (m, 3H, -CH pyridine), 7.03-7.06, 7.67-7.69, 7.78-7.81 (m, 3H, -C*H* dioxoisoindoline), 7.1-7.13, 7.45-7.46 (m, 2H, -C*H* indole), 8.47-6.48 (m, 1H, -CH₂-N*H*-CO-), 8.68 (d, 1H, -N*H* dioxopiperidine), 11.3 (s, 1H, -N*H* pyridone). **¹³C-NMR** (101 MHz, CDCl₃) δ 173.18, 171.36, 169.78, 168.39, 168.11, 167.76, 167.13, 160.39, 155.18, 149.49, 148.21, 142.37, 140.96, 136.71, 132.27, 131.72, 130.51, 120.95, 128.37, 127.35, 124.60, 123.44, 123.09, 118.23, 117.88, 116.27, 112.65, 109.75, 109.06, 69.72, 69.12, 68.62, 68.46, 59.27, 55.26, 52.86, 52.16, 49.20, 45.55, 45.53, 32.17, 31.44, 30.10, 29.92, 28.21, 25.73, 20.91, 19.84, 18.72, 15.09, 11.70. Exact mass: 1024.52, **MS (ESI),** *m/z*: 1025.55 [M+H]⁺.

1-((S)-sec-butyl)-N-((4,6-dimethyl-2-oxo-1,2-dihydropyridin-3-yl)methyl)-6-(6-(4-((S)-16-((2S,4R)-4-hydroxy-2-((4-(4-methylthiazol-5-yl)benzyl)carbamoyl)pyrrolidine-1-carbonyl)-17,17-dimethyl-14-oxo-3,6,9,12-tetraoxa-15-azaoctadecanoyl)piperazin-1-yl)pyridin-3-yl)-3-methyl-1H-indole-4-carboxamide, 88a, DT46. Yield, 63%. **¹H-NMR** (400MHz; CDCl₃) δ 0.83-0.86 (t, 3H, -CH₂-C*H₃*), 0.98 (s, 9H, -HC(C*H₃*)₃, 1.48-1.49 (m, 3H, -CH-C*H₃*), 1.86-1.90 (m, 4H, -C*H₂*-CH₃, -CH-C*H₂*-CHOH- hydroxyproline), 2.17-2.20 (m, 3H, -C*H₃* thiazole), 2.31-2.32 (m, 3H, -C*H₃* pyridone), 2.38-2.40 (m, 3H, -C*H₃* indole), 2.42-2.43 (m, 3H, -C*H₃* pyridone), 3.42-3.46.-3.48, 3.95-4.02 (m, 8H, -C*H₂*-C*H₂*-piperazine), 3.50-3.52 (m, 2H, -NH-CO-C*H₂*-O-), 3.75-3.77 (m, 2H, -C*H₂*-N-hydroxyproline), 3.87 (s, 2H, -C*H₂*-pyridone), 4.03-4.05 (m, 1H, -C*H*-OH hydroxyproline), 4.09-4.11 (d, 1H, -*H*C-(CH₃)₃), 4.12-4.16 (m, 5H, Ph-C*H₂*-, -N-C*H*-CO, -O-C*H₂*-CO-piperazine), 4.17-4.74 (m, 12H, -C*H₂*- linker, -CH₂-C*H*-CH₃), 5.4 (s, 1H, -O*H* hydroxyproline), 5.91 (s, 1H, -C*H* pyridone), 6.73-6.74 (d, 1H, -C*H* indole), 7.01, 7.75-7.78, 7.94-7.97 (m, 3H, -C*H* pyridine), 7.27, 7.31, 7.32-7.34 (m, 4H, -C*H* Ph), 7.28, 8.46 (s, 2H, -C*H* indole), 7.45 (1H, s, -CH-N*H*-CO-), 7.66 (s, 1H, -N*H*-CH₂-Ph), 7.82 (s, 1H, -CH₂-N*H*-CO-), 8.69 (s, 1H, -C*H* thiazole), 11.06 (m, 1H, -N*H* pyridone). **¹³C-NMR** (101 MHz, CDCl₃) δ 171.32, 170.98, 170.11, 169.58, 167.59, 167.07, 160.59, 155.30, 154.53, 150.23, 144.47, 142.35, 140.42, 138.01, 138.75, 137.69, 135.39, 132.07, 131.83, 131.52, 127.59, 126.00, 126.32, 124.85, 124.77, 123.36, 117.80, 112.70, 109.75, 109.70, 70.93, 70.71, 70.55, 70.48, 70.10, 68.71, 68.61, 68.60, 68.31, 60.89, 60.56, 58.76, 56.93, 44.71, 44.14, 43.45, 36.48, 36.13, 32.52, 28.11, 26.43, 20.97, 19.74, 18.68, 17.05, 15.19, 11.88. Exact mass: 1186.59, **MS (ESI)**, *m/z*: 1187.62 [M+H]⁺.

1-((S)-sec-butyl)-N-((4,6-dimethyl-2-oxo-1,2-dihydropyridin-3-yl)methyl)-6-(6-(4-(2-((4-(2-(((S)-1-((2S,4R)-4-hydroxy-2-((4-(4-methylthiazol-5-yl)benzyl)carbamoyl)pyrrolidin-1-yl)-3,3-dimethyl-1-oxobutan-2-yl)amino)-2-oxoethoxy)but-2-yn-1-yl)oxy)acetyl)piperazin-1-yl)pyridin-3-yl)-3-methyl-1H-indole-4-carboxamide,   88b, DT48. Yield, 43%. **¹H-NMR** (400MHz; CDCl₃) δ 0.80-0.86 (t, 3H, -CH₂-C*H₃*), 0.97 (s, 9H, -HC(C*H₃*)₃), 1.45-1.47 (m, 3H, -CH-C*H₃*), 1.78-1.92 (m, 2H, -C*H₂*-CH₃), 2.12-2.18 (s, 3H, -C*H₃* thiazole), 2.28 (s, 3H, -C*H₃* pyridone), 2.33-2.38 (m, 2H, -CH-C*H₂*-CHOH-hydroxyproline) 2.42 (s, 3H, -C*H₃* indole), 2.49 (s, 3H, -C*H₃* pyridone), 3.55-3.69 (m, 8H, -C*H₂*-C*H₂*- piperazine), 3.96-4.00 (m, 2H, C*H₂*-N- hydroxyproline), 4.02-4.06 (m, 2H, -

C*H₂*-pyridone), 4.19-4.22, 4.23-4.26 (m, 4H, -C-C*H₂*-O- linker), 4.28 (s, 2H, -NH-CO-C*H₂*-O-), 4.32-4.33 (m, 1H, -CH₂-C*H*-CH₃), 4.37-4.43(m, 1H, -C*H*-OH hydroxyproline), 4.49-4.50 (m, 2H, -O-C*H₂*-CO-piperazine), 4.50-4.54 (d, 1H, -*H*C-(CH₃)₃), 4.58 (m, 2H, Ph-C*H₂*-), 4.69-4.73 (m, 1H, -N-C*H*-CO), 5.3 (1H, s, -O*H* hydroxyproline), 5.94 (s, 1H, -C*H* pyridone), 6.77-6.80 (d, 1H, -C*H* indole), 7.20-7.22, 7.46, 7.85-7.86 (m, 3H, -C*H* pyridine), 7.25-7,27, 7.28-7.32 (d, 4H, -C*H* Ph), 7.66, 8.35 (s, 2H, -C*H* indole), 8.32 (s, 1H, -N*H*-CH₂-Ph), 8.44 (s, 1H, -N*H*-CH₂-Ph), 8.68 (s, 1H, -C*H* thiazole), 8.87 -CH₂-N*H*-CO-), 11.4 (m, 1H, -N*H* pyridone). **¹³C-NMR** (101 MHz, CDCl₃) δ 172.21, 171.98, 171.20, 170.95, 167.72, 167.25, 160.39, 155.30, 154.53, 149.24, 144.76, 143.97, 140.55, 138.72, 138.45, 137.11, 135.40, 132.30, 131.82, 131.24, 128.23, 126.93, 126.77, 124.76, 124.43, 123.97, 117.80, 112.82, 109.75, 109.06, 78.45, 78.36, 70.74, 67.51, 67.43, 60.52, 60.49, 59.31, 57.92, 57.84, 54.20, 44.68, 44.42, 43.38, 36.11, 35.15, 32.54, 28.15, 26.81, 19.92, 19.03, 18.24, 17.03, 15.19, 11.05. Exact mass: 1022.54, **MS (ESI)**, *m/z*: 1023.6 [M+H]⁺.

1-((S)-sec-butyl)-N-((4,6-dimethyl-2-oxo-1,2-dihydropyridin-3-yl)methyl)-6-(6-(4-(2-(2-(2-(((S)-1-((2S,4R)-4-hydroxy-2-((4-(4-methylthiazol-5-yl)benzyl)carbamoyl)pyrrolidin-1-yl)-3,3-dimethyl-1-oxobutan-2-yl)amino)-2-oxoethoxy)ethoxy)acetyl)piperazin-1-yl)pyridin-3-yl)-3-methyl-1H-indole-4-carboxamide, 88c, DT47. Yield, 50%. **¹H-NMR** (400MHz; CDCl₃) δ 0.82-0-85 (t, 3H, -CH₂-C*H₃*), 1.01 (s, 9H, -HC(C*H₃*)₃, 1.47-1.48 (d, 3H, -CH-C*H₃*), 1.79-1.94 (m, 4H, -C*H₂*-CH₃, -CH-C*H₂*-CHOH- hydroxyproline), 2.13 (s, 3H, -C*H₃* thiazole), 2.32 (s, 3H, -C*H₃* pyridone), 2.42 (s, 3H, -C*H₃* indole), 2.48 (m, 3H, -C*H₃* pyridone), 3.15-3.19 (m, 2H, -NH-CO-C*H₂*-O-), 3.69-3.72 (m, 8H, -C*H₂*-C*H₂*-piperazine), 3.46-3.64 (m, 4H, -C*H₂*-C*H₂*- linker), 3.99 (s, 2H, -C*H₂*-pyridone), 4.05-4.15 (m, 2H, -C*H₂*-N-hydroxyproline), 4.26-4.33 (m, 1H, -CH₂-C*H*-CH₃), 4.33-4.36 (m, 1H, -C*H*-OH hydroxyproline), 4.50-4.51 (m, 2H, -O-C*H₂*-CO-piperazine), 4.57-4.61 (m, 1H, -*H*C-(CH₃)₃), 4.63.4.68 (m, 2H, Ph-C*H₂*-NH-), 4.74-4.78 (m, 1H, -N-C*H*-CO-), 5.4 (1H, bs, -O*H* hydroxyproline), 5.89 (s, 1H, -C*H* pyridone), 6.68-6.89 (d, 1H, -C*H* indole), 7.00, 7.24-7.77, 7.95-7.98 (s, 3H, -C*H* pyridine), 7.27-7.28, 7.43-7.44 (d, 4H, -C*H* Ph), 8.32 (1H, s, -CH-N*H*-CO), 8.4 (m, 2H, -C*H* indole), 8.44, (s, 1H, -N*H*-CH₂-Ph), 8.46 (s, 1H, -N*H*-CH₂-pyridone), 8.86 (s, 1H, -CH thiazole), 11.5 (bs, 1H, -N*H* pyridone). **¹³C-NMR** (101 MHz, CDCl₃) δ 172.21, 171.80, 171.20, 170.58, 167.79, 167.71, 160.39, 155.30, 154.53, 150.78, 144.73, 142.41, 140.32, 138.42, 138.05, 137.11, 135.40, 132.30, 131.82, 131.24, 128.10, 126.56, 126.46, 124.76, 124.43, 123.97, 117.32, 113.70, 110.96, 109.79, 70.31, 70.15, 68.82, 68.79, 68.60, 68.31, 60.42, 59.04, 54.71, 45.64, 44.89, 43.12, 36.15, 35.86, 32.04, 29.74, 26.95, 19.71, 19.03, 18.99, 17.85, 15.75, 11.91. Exact mass: 1099.54, **MS (ESI)**, *m/z*: 1099.5 [M+H]⁺.

1-((S)-sec-butyl)-N-((4,6-dimethyl-2-oxo-1,2-dihydropyridin-3-yl)methyl)-6-(6-(4-((S)-15-((2S,4R)-4-hydroxy-2-((4-(4-methylthiazol-5-yl)benzyl)carbamoyl)pyrrolidine-1-carbonyl)-16,16-dimethyl-13-oxo-3,7,11-trioxa-14-azaheptadecanoyl)piperazin-1-yl)pyridin-3-yl)-3-methyl-1H-indole-4-carboxamide, 88d, DT104. Yield, 61%. **¹H-NMR** (400MHz; CDCl₃) δ 0.79-0-83 (t, 3H, -CH₂-C*H₃*), 0.98 (s, 9H, -HC(C*H₃*)₃, 1.44-1.46 (d, 3H, -CH-C*H₃*), 1.80-1.82 (m, 6H, -O-CH₂-C*H₂*-CH₂-O- linker, -C*H₂*-CH₃), 2.08-2.12, 2.31-2.33 (m, 2H, -CH-C*H₂*-CHOH- hydroxyproline), 2.16 (s, 3H, -C*H₃* thiazole), 2.27 (s, 3H, -C*H₃* pyridone), 2.40 (s, 3H, -C*H₃* indole), 2.49 (m, 3H, -C*H₃* pyridone), 3.44-3.47, 3.63-3.64 (m, 8H, -C*H₂*-C*H₂*- piperazine), 3.55-56, 3.71-3.73 (m, 8H, -O-C*H₂*-CH₂-C*H₂*-O-linker), 3.82-3.94 (m, 3H, -C*H₂*-N- hydroxyproline, -C*H₂*-C*H*-CH₃), 4.02-4.05 (d, 2H, -NH-CO-C*H₂*-O-), 4.15 (s, 2H, -C*H₂*-pyridone), 4.28-4.33 (m, 1H, -C*H*-OH hydroxyproline), 4.37-4.44 (m, 2H, -C*H₂*-N), 4.48-4.51 (m, 2H, -O-C*H₂*-CO-piperazine), 4.57-4.59 (m, 2H, Ph-C*H₂*-NH-), 4.60-4.61 (m, 1H, -*H*C-(CH₃)₃), 4.68-4.72 (m, 1H, -N-C*H*-CO-), 5.3 (1H, bs, -O*H* hydroxyproline), 5.94 (s, 1H, -C*H* pyridone), 6.84-6.85 (d, 1H, -C*H* indole), 7.02,

7.47, 7.91 (m, 3H, -C*H* pyridine), 7.22-7.26, 7.28-7.32 (d, 4H, -C*H* Ph), 7.47, 8.27 (m, 2H, -C*H* indole), 8.08 (1H, s, -CH-N*H*-CO-), 8.34, (s, 1H, -N*H*-CH$_2$-Ph), 8.46 (s, 1H, -N*H*-CH$_2$-pyridone), 8.68 (s, 1H, -C*H* thiazole), 10.9 (bs, 1H, -N*H* pyridone). **¹³C-NMR** (101 MHz, CDCl$_3$) δ 172.21, 171.34, 171.04, 170.12, 169.73, 168.48, 164.98, 164.71, 151.23, 150.35, 148.30, 142.88, 138.42, 137.94, 131.73, 130.66, 130.47, 129.32, 129.32, 128.02, 127.77, 124.92, 123.97, 122.01, 116.65, 112.82, 110.60, 110.21, 109.75, 108.70, 70.28, 70.03, 68.88, 68.40, 68.61, 68.32, 60.49, 60.42, 58.94, 54.92, 52.79, 45.61, 45.43, 44.07, 36.68, 35.54, 32.54, 30.64, 30.09, 29.79, 26.41, 20.93, 19.71, 18.61, 15.98, 11.79, 10.88. Exact mass: 1170.59, **MS (ESI)**, *m/z*: 1171.6 [M+H]$^+$.

1-((S)-sec-butyl)-N-((4,6-dimethyl-2-oxo-1,2-dihydropyridin-3-yl)methyl)-6-(6-(4-(2-(2-(2-(2-(2-(((2S,4R)-1-((S)-2-(1-fluorocyclopropane-1-carboxamido)-3,3-dimethylbutanoyl)-4-hydroxypyrrolidine-2-carboxamido)methyl)-5-(4-methylthiazol-5-yl)phenoxy)ethoxy)ethoxy)ethoxy)acetyl)piperazin-1-yl)pyridin-3-yl)-3-methyl-1H-indole-4-carboxamide, 89a, DT70. Yield, 27%. **¹H-NMR** (400MHz; CDCl$_3$) δ 0.80-0.84 (t, 3H, -CH$_2$-C*H$_3$*), 0.98 (s, 9H, -HC(C*H$_3$*)$_3$), 1.20-1.38 (m, 4H, -C*H$_2$*-C*H$_2$*- cyclopropane), 1.45-1.47 (d, 3H, -CH-C*H$_3$*), 1.82-1.86 (m, 2H, -C*H$_2$*-CH$_3$), 2.01 (s, 3H, -C*H$_3$* thiazole), 2.10-2.13, 2.22-2.25 (m, 2H, -CH-C*H$_2$*-CHOH- hydroxyproline), 2.27 (s, 3H, -C*H$_3$* pyridone), 2.48 (s, 3H, -C*H$_3$* indole), 2.52 (m, 3H, -C*H$_3$* pyridone), 3.49-3.58, 3.72-3.74 (m, 8H, -C*H$_2$*-C*H$_2$*- piperazine), 3.60-3.69 (m, 8H, -O-C*H$_2$*-C*H$_2$*-O-C*H$_2$*-C*H$_2$*-O- linker), 3.87-3.96 (m, 3H, -C*H$_2$*-N- hydroxyproline, -C*H$_2$*-CH-CH$_3$), 4.17 (s, 2H, -NH-CO-C*H$_2$*-O-), 4.24(s, 2H, -C*H$_2$* pyridone), 4.25-4.26 (m, 1H, -C*H*-OH hydroxyproline), 4.44-4.46, 4.59-4.61 (m, 4H, Ph-O-C*H$_2$*-C*H$_2$*-O-), 4.38-4.40 (m, 1H, -*H*C-(CH$_3$)$_3$), 4.47-4.48 (m, 2H, -C*H$_2$*-N-), 4.63-4.65 (m, 2H, -O-C*H$_2$*-CO-piperazine), 4.67-4.69 (m, 2H, Ph-C*H$_2$*-NH), 4.75-4.76 (m, 1H, -N-C*H*-CO), 5.3 (1H, bs, -O*H* hydroxyproline), 5.94 (s, 1H, -C*H* pyridone), 6.82-6.84 (d, 1H, -C*H* indole), 6.88, 7.32-7.34, 7.88-7.90 (m, 3H, -C*H* pyridine), 6.94-6.96, 7.01, 7.10-7.13, 7.24 (m, 4H, -C*H* Ph), 7.31, 7.46 (s, 3H, -C*H* indole, -CH-N*H*-CO-), 8.09 (1H, s, 1H, -N*H*-CH$_2$-pyridone), 8.32 (s, 1H, -N*H*-CH$_2$-Ph), 8.67 (s, 1H, -C*H* thiazole), 11.2 (bs, 1H, -N*H* pyridone). **¹³C-NMR** (101 MHz, CDCl$_3$) δ 173.19, 172.93, 172.21, 172.03, 171.19, 168.40, 167.72 167.65, 160.67, 156.72, 155.30, 154.88,150.41, 145.33, 142.68, 140.95, 139.06, 137.97, 135.60 132.07, 130.53, 129.57, 127.77, 127.00, 126.08, 125.38, 124.76, 124.81, 123.95, 117.60, 113.89, 111.62, 109.08, 108.62, 79.37, 70.73, 70.47, 70.42, 70.29, 70.14, 69.65, 68.10, 59.83, 60.41, 59.82, 59.03, 54.80, 45.53, 45.34, 44.09, 41.12, 38.95, 36.96, 36.09, 35.95, 30.09, 26.37, 20.92, 19.73, 19.0318.63, 16.02, 15.19, 10.88. Exact mass: 1230.59, **MS (ESI)**, *m/z*: 1231.60 [M+H]$^+$.

1-((S)-sec-butyl)-N-((4,6-dimethyl-2-oxo-1,2-dihydropyridin-3-yl)methyl)-6-(6-(4-(2-((4-(2-(((2S,4R)-1-((S)-2-(1-fluorocyclopropane-1-carboxamido)-3,3-dimethylbutanoyl)-4-hydroxypyrrolidine-2-carboxamido)methyl)-5-(4-methylthiazol-5-yl)phenoxy)but-2-yn-1-yl)oxy)acetyl)piperazin-1-yl)pyridin-3-yl)-3-methyl-1H-indole-4-carboxamide, 89b, DT82. Yield, 32%. **¹H-NMR** (400MHz; CDCl$_3$) δ 0.79-0.82 (t, 3H, -CH$_2$-C*H$_3$*), 0.99 (s, 9H, -HC(C*H$_3$*)$_3$, 1.14-1.33 (m, 4H, -C*H$_2$*-C*H$_2$*- cyclopropane), 1.44-1.46 (s, 3H, -CH-C*H$_3$*), 1.81-1.85 (m, 2H, -C*H$_2$*-CH$_3$), 2.16-2.26 (m, 2H, -CH-C*H$_2$*-CHOH- hydroxyproline), 2.27 (s, 3H, -C*H$_3$* thiazole), 2.35 (s, 3H, -C*H$_3$* pyridone), 2.41 (s, 3H, -C*H$_3$* indole), 3.15 (m, 3H, -C*H$_3$* pyridone), 3.48 (s, 2H, -C*H$_2$*-N- hydroxyproline), 3.59-3.67 (m, 8H, -C*H$_2$*-C*H$_2$*- piperazine), 3.96-3.99 (m, 1H, -CH$_2$-C*H*-CH$_3$), 4.19 (s, -C*H$_2$* pyridone), 4.31, 4.82 (s, 4H, -C*H$_2$*-C- linker), 4.39-4.42 (m, -C*H$_2$*-CO-piperazine), 4.46 (s, 2H, -C*H$_2$*-Ph), 4.59-4.62 (m, 1H, -C*H*-OH), 4.63-4.65 (m, 1H, -*H*C-(CH$_3$)$_3$), 4.69-4.73 (m, 1H, -N-C*H*-CO), 5.9 (s, 1H, -C*H* pyridone), 6.83-6.85 (d, 1H, -C*H* indole), 6.97, 7.36, 7.47 (s, 3H, -C*H* pyridine), 6.99, 7.01, 7.12-7.14, 7.27 (m, 4H, -C*H* Ph), 7.38, 7.89-7.82 (m, 3H, -C*H* indole, -CH-N*H*-CO-), 8.08 (1H, s, 1H, -N*H*-CH$_2$-pyridone), 8.29 (s, 1H, -N*H*-CH$_2$-Ph), 8.68 (s, 1H, -C*H*

thiazole), 11.2 (bs, 1H, -N*H* pyridone). **¹³C-NMR** (101 MHz, CDCl₃) δ 173.19, 172.93, 172.21, 172.03, 171.14, 167.72, 167.03, 160.59, 156.89, 155.13, 154.12, 150.51, 145.44, 142.75, 140.96, 138.91, 138.06, 135.48, 132.30, 131.82, 131.64, 129.28, 127.76, 125.09, 124.88, 124.98, 124.43, 122.12, 116.62, 112.88, 110.65, 110.02, 108.68, 82.97, 82.20, 79.36, 76.79,70.07, 67.82,60,49, 59.82, 59.50, 59.42, 57.48, 56.72, 54.35,45.28, 43.82, 41.00, 36.77, 35.93, 32.09, 28.15, 26.38, 20.92, 21.05, 19.69, 18.60, 18.24, 17.07, 15.19, 11.05. Exact mass: 1166.54, **(ESI)**, *m/z*: 1167.55 [M+H]⁺.

1-((S)-sec-butyl)-N-((4,6-dimethyl-2-oxo-1,2-dihydropyridin-3-yl)methyl)-6-(6-(4-(2-(2-(2-(((2S,4R)-1-((S)-2-(1-fluorocyclopropane-1-carboxamido)-3,3-dimethylbutanoyl)-4-hydroxypyrrolidine-2-carboxamido)methyl)-5-(4-methylthiazol-5-yl)phenoxy)ethoxy)acetyl)piperazin-1-yl)pyridin-3-yl)-3-methyl-1H-indole-4-carboxamide, 89c, DT81. Yield, 17%. **¹H-NMR** (400MHz; CDCl₃) δ 0.79-0.81 (t, 3H, -CH₂-C*H₃*), 0.99 (s, 9H, -HC(C*H₃*)₃, 1.12-1.29 (m, 4H, -C*H₂*-C*H₂*- cyclopropane), 1.37-1.40 (s, 3H, -CH-C*H₃*), 1.80-1.85 (m, 2H, -C*H₂*-CH₃), 2.15-2.17, 2.20-2.24 (m, 2H, -CH-C*H₂*-CHOH- hydroxyproline), 2.17 (s, 3H, -C*H₃* thiazole), 2.29 (s, 3H, -C*H₃* pyridone), 2.41 (s, 3H, -C*H₃* indole), 2.52 (m, 3H, -C*H₃* pyridone), 3.64-3.67 (m, 8H, -C*H₂*-C*H₂*- piperazine), 3.95-3.99 (s, 4H, -C*H₂* pyridone, -C*H₂*-N- hydroxyproline), 4.2 (m, 3H, -C*H₂*-CO-piperazine, -C*H₂*-C*H*-CH₃), 4.30-4.32, 4.69-4.77 (m, 5H, -C*H₂*-C*H₂*- linker, C*H*-OH), 4.39-4.44 (m, 1H, -*H*C-(CH₃)₃), 4.46-4.63 (m, 1H, -N-C*H*-CO), 4.58 (m, 2H, -C*H₂*-Ph), 5.4 (s, 1H, -O*H*), 5.9 (s, 1H, -C*H* pyridone), 6.86 (s, 1H, -C*H* indole), 6.90, 7.33-7.36, 7.47 (s, 3H, -C*H* pyridine), 6.95-6.97, 7.03, 7.13-7.15 (m, 4H, -C*H* Ph), 7.33-7.35, 7.50 (m, 2H, -C*H* indole), 7.93-7.95 (s, 1H, -CH-N*H*-CO-), 8.08 (1H, s, 1H, -N*H*-CH₂-pyridone), 8.24 (s, 1H, -N*H*-CH₂-Ph), 8.68 (s, 1H, -C*H* thiazole), 11.4 (bs, 1H, -N*H* pyridone). **¹³C-NMR** (101 MHz, CDCl₃) δ 173.19, 172.93, 172.21, 172.03, 171.41, 167.84, 167.90, 160.39, 156.41, 155.30, 154.53, 150.36, 145.44, 142.74, 140.99, 138.03, 137.15, 135.48, 132.30, 131.73, 130.52, 129.06, 127.73, 126.67, 125.03, 124.14, 124.55, 123.14, 116.53, 112.40, 110.76, 110.11, 108.72, 81.61, 79.34, 70.34, 69.85, 68.78, 68.26, 60.23, 59.51, 59.33, 59.31, 54.20, 44.68, 44.42, 41.00, 36.89, 36.73, 32.09, 28.40, 26.85, 20.93, 19.69, 19.63, 19.06, 18.24, 17.07, 15.19, 11.86. Exact mass: 1142.54 **MS (ESI)**, *m/z*: 1143.6 [M+H]⁺.

1-((S)-sec-butyl)-N-((4,6-dimethyl-2-oxo-1,2-dihydropyridin-3-yl)methyl)-6-(6-(4-(2-(3-(3-(2-(((2S,4R)-1-((S)-2-(1-fluorocyclopropane-1-carboxamido)-3,3-dimethylbutanoyl)-4-hydroxypyrrolidine-2-carboxamido)methyl)-5-(4-methylthiazol-5-yl)phenoxy)propoxy)propoxy)acetyl)piperazin-1-yl)pyridin-3-yl)-3-methyl-1H-indole-4-carboxamide, 89d, DT113. Yield, 13%. **¹H-NMR** (400MHz; CDCl₃) δ 0.81-0-84 (t, 3H, -CH₂-C*H₃*), 0.98 (s, 9H, -HC(C*H₃*)₃), 1.17-1.31 (m, 4H, -C*H₂*-C*H₂*- cyclopropane), 1.46-1.47 (d, 3H, -CH-C*H₃*), 1.82-1.88 (m, 4H, -O-CH₂-C*H₂*-CH₂-O-), 2.06-2.09 (m, 2H, -C*H₂*-CH₃), 2.19 (s, 3H, -C*H₃* thiazole), 2.29 (s, 3H, -C*H₃* pyridone), 2.33-2.38 (m, 2H, -CH-C*H₂*-CHOH- hydroxyproline), 2.44 (s, 3H, -C*H₃* indole), 2.52 (m, 3H, -C*H₃* pyridone), 3.54-3.59 (m, 8H, -O-C*H₂*-CH₂-C*H₂*-O-), 3.60-3.65 (m, 8H, -C*H₂*-C*H₂*- piperazine), 3.98-4.01 (d, 1H, -CH₂-C*H*-CH₃), 4.09-4.11 (m, 2H, -C*H₂* pyridone), 4.13 (s, 2H, -C*H₂*-N-hydroxyproline), 4.33-4.44 (m, 2H, -C*H₂*-CO-piperazine,), 4.48-4.50 (m, 2H, -C*H₂*-Ph), 4.52-4.53 (m,1H, -C*H*-OH), 4.64-4.65 (m, 1H, -*H*C-(CH₃)₃), 4.71-4.75 (m, 1H, -N-C*H*-CO), 5.4 (s, 1H, -O*H*), 5.96 (s, 1H, -C*H* pyridone), 6.86 (s, 1H, -C*H* indole), 6.89, 7.24, 7.34 (s, 3H, -C*H* pyridine), 6.93-6.95, 7.03, 7.08-7.09, 7.24 (m, 4H, -C-*H* Ph), 7.32, 7.47 (s, 2H, -C*H* indole), 7.93-7.96 (d, 1H, -CH-N*H*-CO-), 8.27 (1H, s, 1H, -N*H*-CH₂-pyridone), 8.44 (s, 1H, -N*H*-CH₂-Ph), 8.69 (s, 1H, -C*H* thiazole), 11.4 (bs, 1H, -N*H* pyridone). **¹³C-NMR** (101 MHz, CDCl₃) δ 173.19, 172.93, 172.21, 172.09, 171.14, 167.72, 167.03, 160.59, 157.21, 155.30, 154.53, 149.24, 145.01, 143.97, 140.95, 138.97, 137.15, 135.48, 132.30, 131.82, 131.05, 128.03, 127.74, 126.20, 125.38, 124.76, 124.43, 123.77, 117.80,

113.02, 111.07, 109.75, 109.70, 81.61, 79.46, 70.65, 69.83, 69.17, 69.10, 68.61, 68.47, 60.41, 59.83, 59.82, 59.31, 54.29, 44.61, 44.42, 41.62, 36.16, 35.16, 32.54, 30.57, 30.28, 28.15, 26.81, 21.27, 21.05, 19.92, 19.03, 18.24, 17.07, 15.19, 11.05. Exact mass: 1214.60, **MS (ESI)**, *m/z*: 1215.60 [M+H]$^+$.

1-((S)-sec-butyl)-N-((4,6-dimethyl-2-oxo-1,2-dihydropyridin-3-yl)methyl)-6-(6-(4-((R)-1-(1-fluorocyclopropyl)-3-((2S,4R)-4-hydroxy-2-((4-(4-methylthiazol-5-yl)benzyl)carbamoyl)pyrrolidine-1-carbonyl)-4,4-dimethyl-1-oxo-8,11,14-trioxa-5-thia-2-azahexadecan-16-oyl)piperazin-1-yl)pyridin-3-yl)-3-methyl-1H-indole-4-carboxamide, 90a, DT58. Yield, 12%. **¹H-NMR** (400MHz; CDCl₃) δ 0.81-0.84 (t, 3H, -CH₂-C*H₃*), 1.15-1.26 (m, 4H, -C*H₂*-C*H₂*- cyclopropane), 1.35 (s, 3H, -CH-C*H₃*), 1.45-1.48 (d, 6H, C*H₃*-CH-S-), 2.19 (s, 3H, -C*H₃* thiazole), 2.24-2.26 (m, 2H, -C*H₂*-CH₃), 2.32 (s, 3H, -C*H₃* pyridone), 2.42 (s, 3H, -C*H₃* indole), 2.51(s, 2H, -CH-C*H₂*-CHOH- hydroxyproline), 2.53 (m, 3H, -C*H₃* pyridone), 2.73-274 (m, 2H, -C*H₂*-S- linker), 3.18-3.20 (m, 1H, -CH₂-C*H*-CH₃), 3.58 (s, 2H, -C*H₂* pyridone), 3.66-3.73 (m, 8H, -O-C*H₂*-C*H₂*-O-C*H₂*-C*H₂*-O-), 3.75-3.81 (m, 8H, -C*H₂*-C*H₂*- piperazine), 3.96-3.99 (m, 1H, C*H*-OH), 4.15-4.19 (m, 1H, -N-C*H*-CO), 4.27 (s, 2H, -C*H₂*-CO-piperazine), 4.38-4.42 (m, 2H, -C*H₂*-N-hydroxyproline), 4.48 (s, 2H, -C*H₂*-Ph), 4.74-4.69 (m, 1H, -*H*C-S-), 5.3 (s, 1H, -O*H*), 5.96 (s, 1H, -C*H* pyridone), 7.0-7.01 (d, 1H, -C*H* indole), 7.05, 7.37, 7.48 (s, 3H, -C*H* pyridine), 7.23-7.33 (m, 4H, -C*H* Ph), 7.40, 7.67 (s, 2H, -C*H* indole), 7.80-7.83 (d, 1H, -CH-N*H*-CO-), 8.05-8.07 (d, 1H, -N*H*-CH₂-pyridone), 8.18 (s, 1H, -N*H*-CH₂-Ph), 8.69 (s, 1H, -C*H* thiazole), 10.7 (bs, 1H, -N*H* pyridone). **¹³C-NMR** (101 MHz, CDCl₃) δ 173.19, 172.93, 172.53, 171.40, 169.66, 168.53, 167.03, 160.59, 155.82, 154.53, 150.94, 144.76, 142.67, 140.55, 138.31, 138.30, 137.97, 135.48, 131.68, 130.71, 130.59, 127.85, 126.32, 126.03, 124.95, 124.12, 122.12, 116.58, 113.11, 110.74, 109.98, 81.99, 79.29, 70.25, 69.89, 69.32, 68.78, 68.71, 68.60, 61.58, 61.56, 60.66, 60.41, 59.54, 59.31, 55.86, 51.83, 44.45, 44.76, 43.94, 36.24, 30.11, 32.54, 28.54, 27.73, 20.95, 20.41, 19.68, 18.66, 18.03, 17.17, 15.00, 11.83. Exact mass: 1232.56, **MS (ESI)**, *m/z*: 1233.6 [M+H]$^+$.

1-((S)-sec-butyl)-N-((4,6-dimethyl-2-oxo-1,2-dihydropyridin-3-yl)methyl)-6-(6-(4-(2-((4-(((R)-3-(1-fluorocyclopropane-1-carboxamido)-4-((2S,4R)-4-hydroxy-2-((4-(4-methylthiazol-5-yl)benzyl)carbamoyl)pyrrolidin-1-yl)-2-methyl-4-oxobutan-2-yl)thio)but-2-yn-1-yl)oxy)acetyl)piperazin-1-yl)pyridin-3-yl)-3-methyl-1H-indole-4-carboxamide, 90b, DT67. Yield, 12%. **¹H-NMR** (400MHz; CDCl₃) δ 0.80-0.84 (t, 3H, -CH₂-C*H₃*), 1.14-1.29 (m, 4H, -C*H₂*-C*H₂*- cyclopropane), 1.39 (s, 3H, -CH-C*H₃*), 1.45-1.47 (d, 6H, C*H₃*-CH-S-), 1,81-1.86 (m, 2H, -C*H₂*-CH₃), 2.19 (s, 3H, -C*H₃* thiazole), 2.23-2.26, 2.29-2.32 (s, 2H, -CH-C*H₂*-CHOH- hydroxyproline), 2.28 (s, 3H, -C*H₃* pyridone), 2.43 (s, 3H, -C*H₃* indole), 2.51 (m, 3H, -C*H₃* pyridone), 3.32-3.46 (m, 2H, -C*H₂*-S linker), 3.59-3.72 (m, 8H, -C*H₂*-C*H₂*- piperazine), 3.86-3.89 (m, 1H, -CH₂-C*H*-CH₃), 4.01-4.04 (m, 1H, -C*H*-OH), 4.22-4.27 (m, 4H, -C*H₂* pyridone, -C*H₂*-CO-piperazine),4.28-4.46 (m, 2H, -C*H₂*-O- linker), 4.55 (m, 2H, -C*H₂*-N- hydroxyproline) 4.59 (s, 2H, -C*H₂*-Ph), 4.76-4.78 (t, 1H, -N-C*H*-CO-), 5.00-5.02 (d, 1H, -*H*C-S-), 5.3 (s, 1H, -O*H*), 5.99 (s, 1H, -C*H* pyridone), 6.89-6.92 (d, 1H, -C*H* indole), 7.03, 7.24, 7.47 (s, 3H, -C*H* pyridine), 7.35-7.37 (m, 4H, -C*H* Ph), 7.47, 7.95-7.97 (m, 2H, -C*H* indole), 8.08 (s, 1H, -CH-N*H*-CO-), 8.22 (d, 1H, -N*H*-CH₂-pyridone), 8.33 (s, 1H, -N*H*-CH₂-Ph), 8.68 (s, 1H, -CH thiazole), 10.98 (bs, 1H, -N*H* pyridone).**¹³C-NMR** (101 MHz, CDCl₃) 173.19, 172.93, 172.53, 171.98, 171.14, 167.72, 167.03, 160.39, 155.30, 154.53, 149.24, 144.76, 143.97, 140.95, 138.45, 138.30, 137.11, 135.48, 132.30, 131.82, 131.05, 127.74, 126.93, 126.77, 124.76, 124.43, 123.77, 117.80, 112.82, 109.75, 109.06, 81.91, 79.76, 75.78, 75.20, 70.65, 67.51, 63.09, 63.07, 60.49, 59.31, 57.94, 54.31, 50.40, 44.68, 44.42, 43.37, 36.11, 32.54, 28.15, 27.15, 21.27,

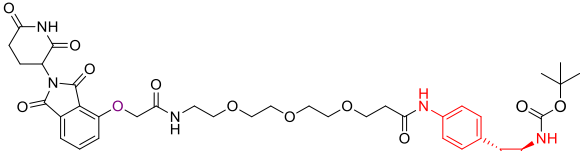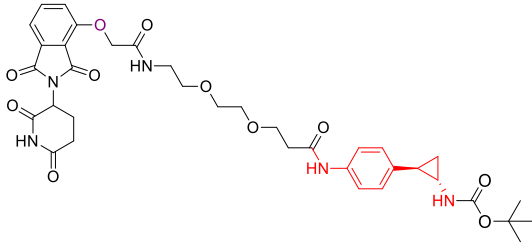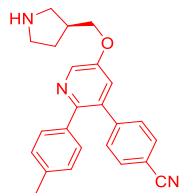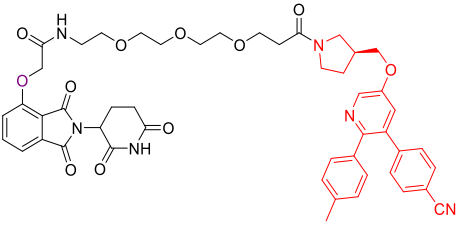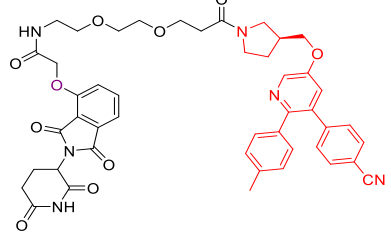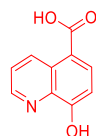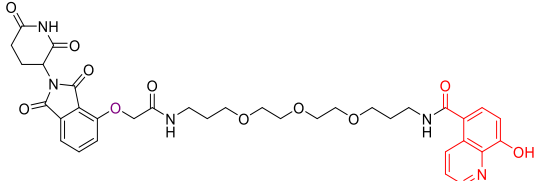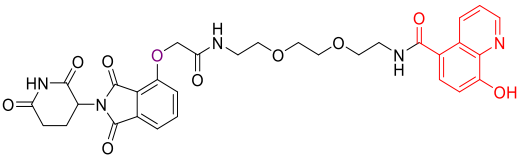21.05, 19.92, 19.03, 18.52, 18.24, 17.03, 15.19, 11.05. Exact mass: 1168.50, **MS (ESI)**, *m/z*: 1169.51[M+H]⁺.

1-((S)-sec-butyl)-N-((4,6-dimethyl-2-oxo-1,2-dihydropyridin-3-yl)methyl)-6-(6-(4-(2-(2-(((R)-3-(1-fluorocyclopropane-1-carboxamido)-4-((2S,4R)-4-hydroxy-2-((4-(4-methylthiazol-5-yl)benzyl)carbamoyl)pyrrolidin-1-yl)-2-methyl-4-oxobutan-2-yl)thio)ethoxy)acetyl)piperazin-1-yl)pyridin-3-yl)-3-methyl-1H-indole-4-carboxamide，90c，DT56. Yield, 10%. **¹H-NMR** (400MHz; CDCl₃) δ 0.83-0.87 (t, 3H, -CH₂-C*H₃*), 1.19-1.28 (m, 4H, -C*H₂*-C*H₂*- cyclopropane), 1.32-1.37 (s, 6H, C*H₃*-CH-S-), 1.46-1.50 (d, 3H, -CH-C*H₃*), 1,82-1.90 (m, 2H, -C*H₂*-CH₃), 2.21 (s, 3H, -C*H₃* thiazole), 2.23-2.25, 2.37-2.43 (s, 2H, -CH-C*H₂*-CHOH- hydroxyproline), 2.33 (s, 3H, -C*H₃* pyridone), 2.45 (s, 3H, -C*H₃* indole), 2.53 (m, 3H, -C*H₃* pyridone), 2.66-2.90 (m, 2H, -C*H₂*-S linker), 3.57 (m, 2H, -C*H₂* pyridone) 3.63-3.81 (m, 8H, -C*H₂*-C*H₂*- piperazine), 3.82 (s, 2H, -C*H₂*-CO-piperazine), 3.98-4.0 (m, 1H, -CH₂-C*H*-CH₃), 4.18 (s, 2H, -C*H₂*-Ph), 4.40-4.43 (m, 1H, -C*H*-OH), 4.45-4.49 (m, 2H, -C*H₂*-N-hydroxyproline), 4.52-4.57 (m, 2H, -C*H₂*-O linker), 4.78-4.79 (t, 1H, -N-C*H*-CO-), 4.88-4.90 (d, 1H, -*H*C-S-), 5.3 (s, 1H, -O*H*), 5.95 (s, 1H, -C*H* pyridone), 6.75-6.77 (d, 1H, -C*H* indole), 7.02 (s, 1H, -C*H* pyridine), 7.32-7.37 (m, 5H, -C*H* Ph, -C*H* pyridine), 7.38-7.39 (s, 3H, -C*H* indole, -C*H* pyridine), 7.46 (s, 1H, -CH-N*H*-CO-), 7.82-7.83 (d, 1H, -N*H*-CH₂-pyridone), 8.47 (s, 1H, -N*H*-CH₂-Ph), 8.69 (s, 1H, -CH thiazole), 10.7 (bs, 1H, -N*H* pyridone). **¹³C-NMR** (101 MHz, CDCl₃) δ 173.19, 172.93, 172.41, 171.98, 171.20, 167.72, 167.25, 160.39, 155.30, 154.53, 150.28, 144.76, 143.97, 141.59, 134.99, 132.74, 131.45, 131.14, 128.96, 126.71, 126.55, 124.76, 124.43, 123.77, 117.80, 112.82, 109.89, 109.04, 83.66, 79.33, 70.59, 70.29, 69.80, 62.87, 62.62, 60.93, 59.85, 54.25, 51.62, 44.46, 44.61, 43.52, 36.14, 32.43, 30.25, 28.47, 27.98, 21.76, 21.83, 19.99, 19.54, 18.24, 17.03, 15.19, 10.96. Exact mass: 1144.50, **MS (ESI)**, *m/z*: 1145.51 [M+H]⁺.
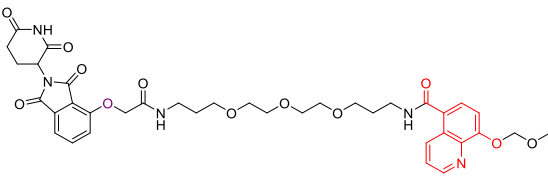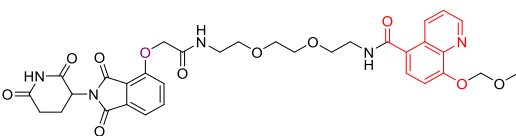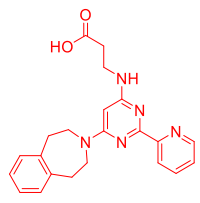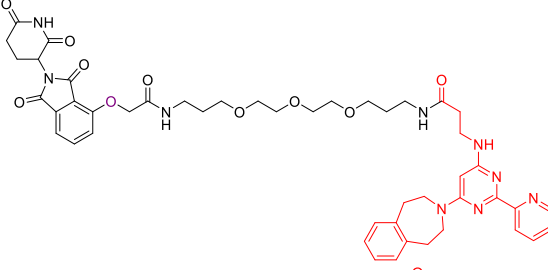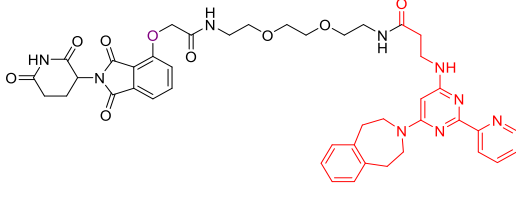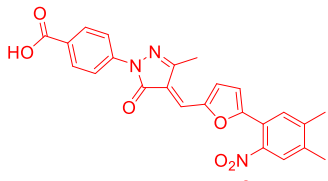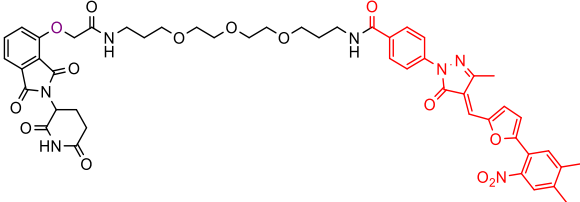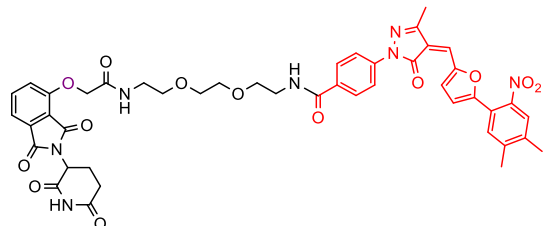
1-((S)-sec-butyl)-N-((4,6-dimethyl-2-oxo-1,2-dihydropyridin-3-yl)methyl)-6-(6-(4-((R)-1-(1-fluorocyclopropyl)-3-((2S,4R)-4-hydroxy-2-((4-(4-methylthiazol-5-yl)benzyl)carbamoyl)pyrrolidine-1-carbonyl)-4,4-dimethyl-1-oxo-9,13-dioxa-5-thia-2-azapentadecan-15-oyl)piperazin-1-yl)pyridin-3-yl)-3-methyl-1H-indole-4-carboxamide，90d，DT116. Yield, 10%. **¹H-NMR** (400MHz; CDCl₃) δ 0.81-0.84 (t, 3H, -CH₂-C*H₃*), 1.23-1.29 (m, 4H, -C*H₂*-C*H₂*- cyclopropane), 1.32 (s, 3H, -CH-C*H₃*), 1.45-1.47, 2.01 (m, 6H, C*H₃*-CH-S-), 1.71-1.72 (m, 2H, -C*H₂*-CH₃), 1.85-1.92 (m, 4H, -O-CH₂-C*H₂*-CH₂-O-, -S-CH₂-C*H₂*-CH₂-O-), 2.21-2.28 (s, 6H, -C*H₃* thiazole, -C*H₃* pyridone), 2.45-2.62 (s, 6H, -C*H₃* indole, -C*H₃* pyridone), 2.64-2.66 (s, 2H, -CH-C*H₂*-CHOH- hydroxyproline), 3.34-3.52 (m, 8H, -O-C*H₂*-CH₂-C*H₂*-O-, -S-C*H₂*-CH₂-C*H₂*-O-), 3.60-3.78 (m, 8H, -C*H₂*-C*H₂*-piperazine), 3.98-4.00 (m, 1H, -CH₂-C*H*-CH₃), 4.06 (s, 1H, -C*H*-OH), 4.19 (s, 2H, -C*H₂*-CO-piperazine), 4.43-4.44 (m, 2H, -C*H₂* pyridone), 4.52-4.55 (m, 2H, -C*H₂*-N-hydroxyproline), 4.61-3.62 (m, 2H, -C*H₂*-Ph), 4.79-4.81 (m, 1H, -N-C*H*-CO), 4.84-4.86 (m, 1H, -*H*C-S-), 5.3 (s, 1H, -O*H*), 6.00 (s, 1H, -C*H* pyridone), 6.90-6.91 (d, 1H, -C*H* indole), 7.03-7.07, 7.23, 7.62 (m, 3H, -C*H* pyridine), 7.32-7.39 (m, 4H, -C*H* Ph), 7.47, 7.95- 7.97 (m, 2H, -C*H* indole), 7.75- 7.80 (d, 1H, -CH-N*H*-CO-), 8.08 (1H, s, 1H, -N*H*-CH₂-pyridone), 8.26 (m, 1H, -N*H*-CH₂-Ph), 8.69 (s, 1H, -CH thiazole), 11.4 (bs, 1H, -N*H* pyridone). **¹³C-NMR** (126 MHz, CDCl₃) δ 173.19, 172.93, 172.53, 171.98, 171.21, 169.89, 168.49, 160.59, 155.30, 154.53, 150.37, 144.76, 143.97, 140.95, 138.24, 138.30, 137.96, 135.48, 132.30, 131.21, 129.39, 128.20, 126.93, 126.77, 124.97, 124.43, 123.77, 116.62, 110.71, 110.52, 108.75, 70.40, 69.95, 69.18, 68.61, 67.52, 63.09, 63.07, 60.41, 59.40, 54.32, 51.33, 44.61, 44.42, 43.02, 37.11, 32.10, 30.11, 29.64, 29.42, 25.48, 28.09, 27.28, 20.94, 19.76, 19.05, 18.24, 17.81, 15.78, 10.88. Exact mass: 1216.56, **MS (ESI)**, *m/z*: 1215.56 [M+H]⁺.

4.6 Biological evaluation

Before to profile the relative targets degradation, for compounds **70a,b** (and their negative controls **135a,b**), **71a,b** (and their negative controls **137a,b**), **73a,b**, **76a,b** (and their negative controls **140a,b**), **77a,b**, **79a,b** and **85a,b**, the potential maintained capability to bind and inhibit their specific targets has been evaluated in term of IC_{50} or Thermal Shift values by Prof. Mattevi and coworkers (University of Pavia) for compounds **70a,b** (and their negative controls **135a,b**), **71a,b** (and their negative controls **137a,b**), **73a,b**, **76a,b**, **77a,b** (and their negative controls **140a,b**) and by the Reaction Biology Corporation (RBC) for compounds **79a,b** and **85a,b** (Table 4.1).

WARHEADS & PROTACs ENZYMATIC ACTIVITY

TYPE	CODE	STRUCTURE	IC_{50} or ΔTm
Irreversible LSD1i	**26** GSK2879552		$Ki_{(app)}=17$ μM (LSD1)
36f CRBN-based LSD1 targeting PROTACs deriving from 26 GSK2879552	**70a** MC4381		80 nM (LSD1)
	70b MC4378		160 nM (LSD1)
36f CRBN-based LSD1 targeting PROTACs deriving from 26 GSK2879552 (negative controls)	**135a** MC4370		No inhib. (LSD1)
	135b MC4367		No inhib. (LSD1)
Irreversible LSD1i	**69** *p*-NH₂-TCP		20 μM (LSD1)
36f CRBN-based LSD1 targeting PROTACs deriving from 69 *p*-NH₂-TCP	**71a** MC4363		5 μM (LSD1)
	71b MC4362		5 μM (LSD1)

179

36f CRBN-based LSD1 targeting PROTACs deriving from 69 _p_-NH₂-TCP (negative controls)	137a MC4352		**No inhib. (LSD1)**
	137b MC4341		**No inhib. (LSD1)**
Reversible LSD1i	72 GSK-690		**37 nM (LSD1)** **+6°C Thermal Shift (LSD1)**
36f CRBN-based LSD1 targeting PROTACs deriving from 72 GSK-690	73a MC4376		**+1°C Thermal Shift (LSD1)**
	73b MC4382		**+1°C Thermal Shift (LSD1)**
JmjC KDMi	74 IOX1		**0.1-33 _μ_M (JmjC KDMs)**
36f CRBN-based JmjC KDMs targeting PROTACs deriving from 74 IOX1	76a MC4366		**81.3 _μ_M (KDM5B) 54.6 _μ_M (KDM6B) 2.3 _μ_M (KDM4A)**
	76b MC4364		**76.2 _μ_M (KDM5B) 29.3 _μ_M (KDM6B) 5.1 _μ_M (KDM4A)**

36f CRBN-based JmjC KDMs targeting PROTACs deriving from IOX1 74 (negative controls)	**140a** **MC4356**		**No inhib. (KDMs)**
	140b **MC4357**		**No inhib. (KDMs)**
KDM6i	**75** **GSK-J1**		**810 μM (KDM5B) 300 μM (KDM6B)**
36f CRBN-based KDM6 targeting PROTACs deriving from 75 GSK-J1	**77a** **MC4337**		**>100 μM (KDM5B, KDM6B) 72 μM (KDM4A)**
	77b **MC4328**		**>100 μM (KDM5B) 67 μM (KDM6B) 65 μM (KDM4A)**
P300i	**78** **C646**		**0.23 μM (p300)**
36f CRBN-based P300 targeting PROTACs deriving from 78 C646	**79a** **MC4385**		**0.95 μM (p300)**
	79b **MC4387**		**0.68 μM (p300)**

| TYPE	CODE	STRUCTURE	
EZH2i	20 GSK126		9.9 nM (EZH2)
36f CRBN-based EZH2 targeting PROTACs deriving from 20 GSK126	85a MC4345		4.4 nM (EZH2)
	85b MC4329		5.1 nM (EZH2)

Table 4.1. IC_{50} or Termal Shift values registered for compounds **70a,b** (and their negative controls **135a,b**), **71a,b** (and their negative controls **137a,b**), **73a,b**, **76a,b** (and their negative controls **140a,b**), **77a,b**, **79a,b** and **85a,b** and for their correlate warheads.

Collected enzymatic data showed that all the synthetized compounds keep the ability to bind and inhibit their specific epi-target reaching the same (micro- or nano-molar) level of their warheads, resulting, in some cases, more effective than the latter (for example the case of **85a,b** in comparison with GSK126 **20** in the inhibition of EZH2). Negative controls of **70a,b** (**135a,b**), **71a,b** (**137a,b**), **76a,b** (**140a,b**) are, as expected, inactive since their key pharmacophoric function resulted not available because chemically blocked.

However, to date, these promising enzymatic results are not supported by degradation data since their relative assays are ongoing, except for compounds **85a,b** which were evaluated, together with the other **36g, 36d** CRBN and **37c,e,f** VHL based EZH2-targeting PROTACs, **86a-d**, **87a-d**, **88a-d**, **89a-d** and **90a-d** (Table 4.2), for their potential degradation activities not only for their main target EZH2 but also towards the other components of the catalytic core of PRC2 including EED and SUZ12. The downstream effect involving the methylation state of H3K27 has been also monitored. H3 levels has been used as control.
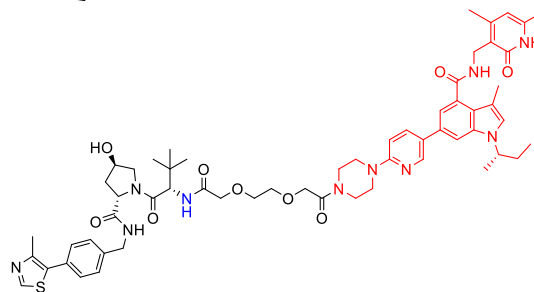
CRBN, VHL based EZH2 targeting PROTACs

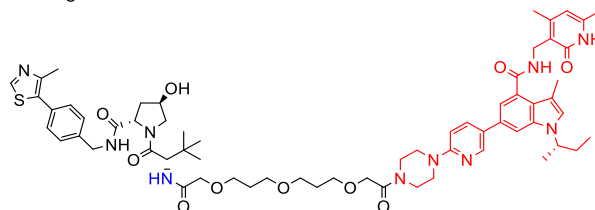| TYPE	CODE	STRUCTURE
36f CRBN-based EZH2 targeting PROTACs deriving from 20 GSK126	85a MC4345	
	85b MC4329	

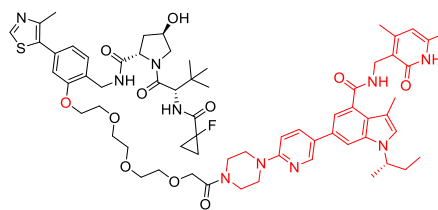|		
36g CRBN-based EZH2 targeting PROTACs deriving from 20 GSK126	**86a DT101**	
	86b DT103	
	86c DT102	
	86d DT115	
36d CRBN-based EZH2 targeting PROTACs deriving from 20 GSK126	**87a DT57**	
	87b DT62	
	87c DT68	
	87d DT114	
37f VHL-based EZH2 targeting PROTACs deriving from 20 GSK126	**88a DT46**	
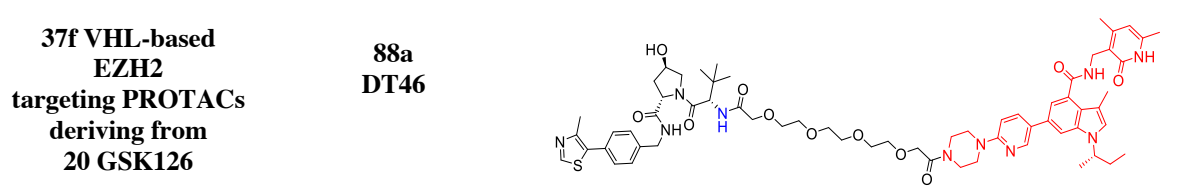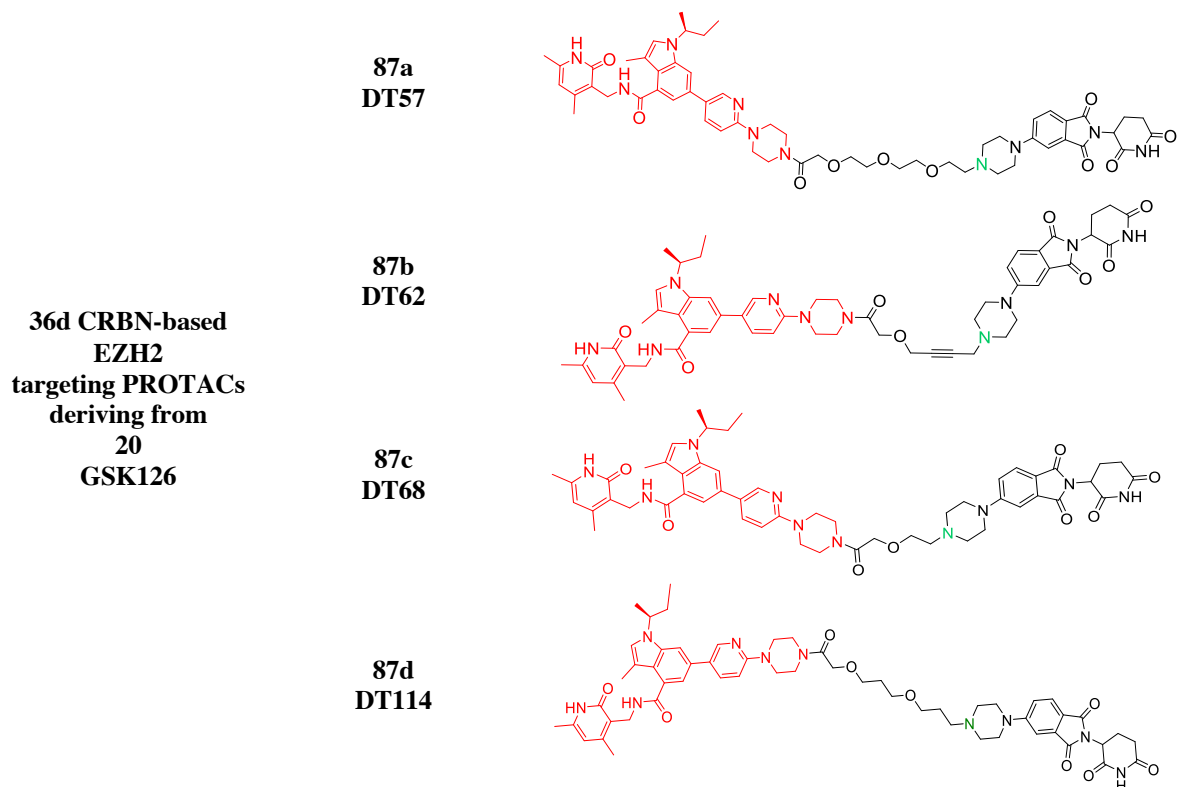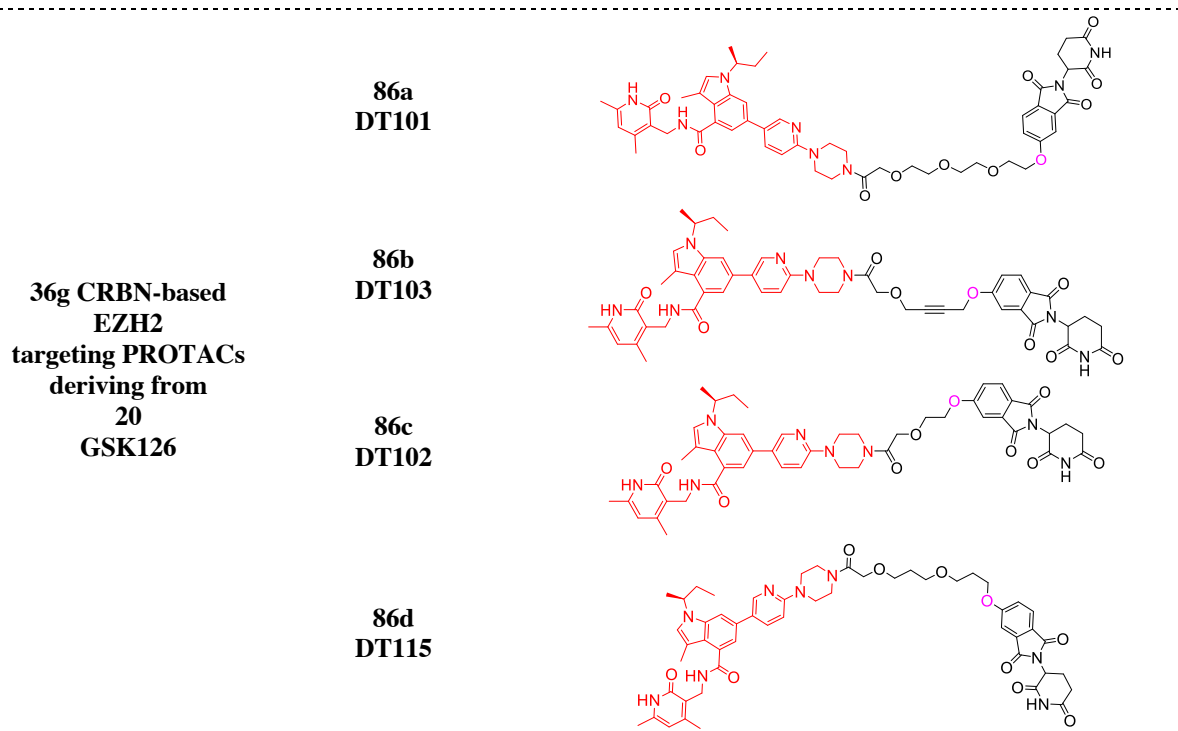
88b
DT48
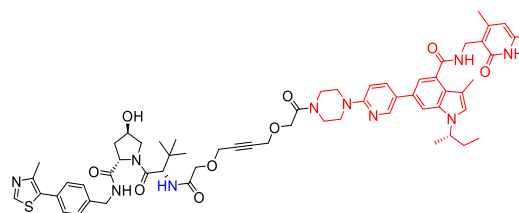
88c
DT47

88d
DT104

89a
DT70
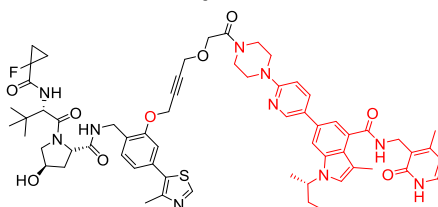
37c VHL-EZH2
targeting PROTACs
deriving from
20
GSK126

89b
DT82

89c
DT81

89d
DT113

37e VHL-EZH2 targeting PROTACs deriving from 20 GSK126	**90a DT58**
	90b DT67
	90c DT56
	90d DT116
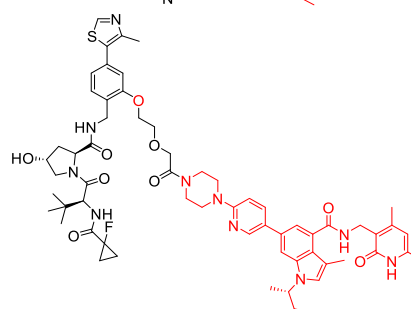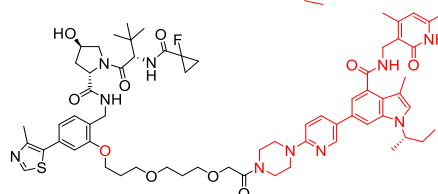
Table 4.2. List and structures of **36f, 36g, 36d** CRBN and **37f, 37c, 37e** VHL based EZH2 targeting PROTACs **36g, 36d** CRBN and **37f, 37c, 37e** VHL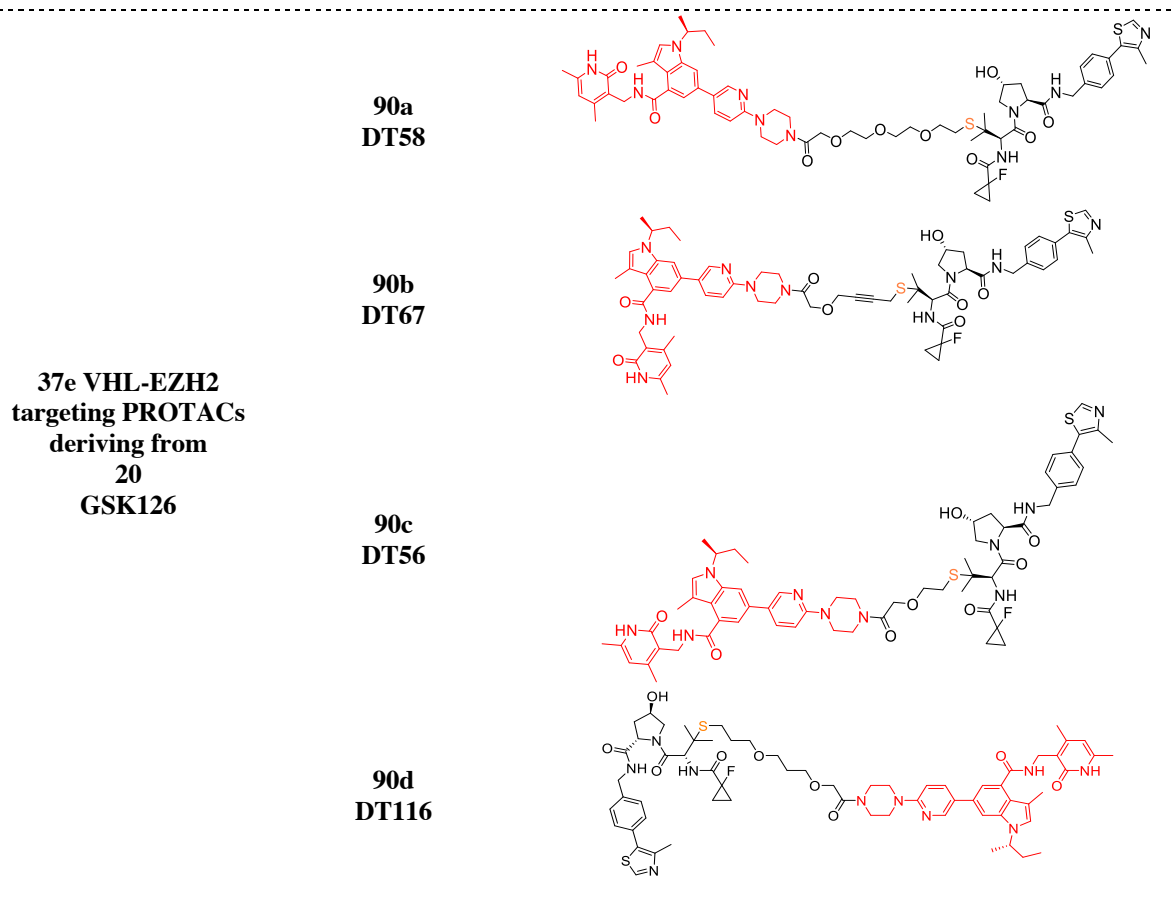 based EZH2-targeting PROTACs, **85a,b**, **86a-d**, **87a-d**, **88a-d**, **89a-d** and **90a-d** evaluated in cell assays for target(s) degradation.

To profile the degradation activities of this panel of **36** CRBN and **37c,e,f** VHL based EZH2-targeting PROTACs in HEK293 and HeLa cell lines, EZH2, EED, SUZ12, H3K27me3 and H3 protein levels were quantified by Western Blot analysis following different treatment in term of time (from 4h to 24h of treatment) and concentrations (from 0.4 nM to 5 μM) using GSK126 **20** as a negative controls for the degradation of the PRC2 components and as a positive controls for the evaluation of the downstream effects (H3K27me3 levels).

Interestingly, a modest degradation of EZH2, EED and SUZ12 was registered for few compounds.

Through the application of the siRNA technology and the consequent knockdown gene expression of EZH2, EED and SUZ12, the specific band of each targeted protein was highlighted after 72h treatment in HEK293 cell line (Figure 4.17).
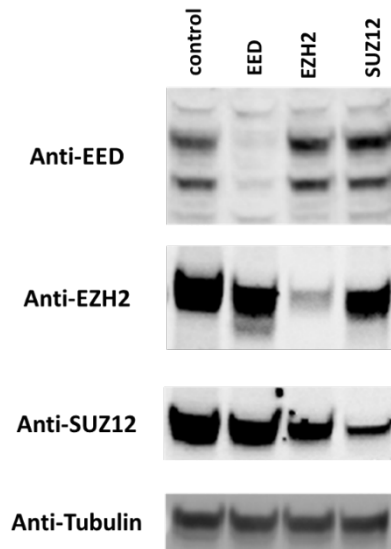
Figure 4.17. Western blot analysis of EZH2, EED, SUZ12 levels following 72h treatment of HEK293 cells with EZH2, EED or SUZ12 siRNA. The relative experimental as well as depicted results were performed by Dr Sarath Ramachandran (Prof. Alessio Ciulli research group, University of Dundee, Scotland, UK).

The first screening was focused on HEK293 cell line testing all 22 compounds (Table 4.2) at 3 different concentrations: 5 μM, 200 nM, 10 nM using GSK126 **20** (5 μM) and DMSO as controls in a 16h treatment to evaluate the degradation of EZH2 as well as the induced modulation of the H3K27me3 mark (Figure 4.18).
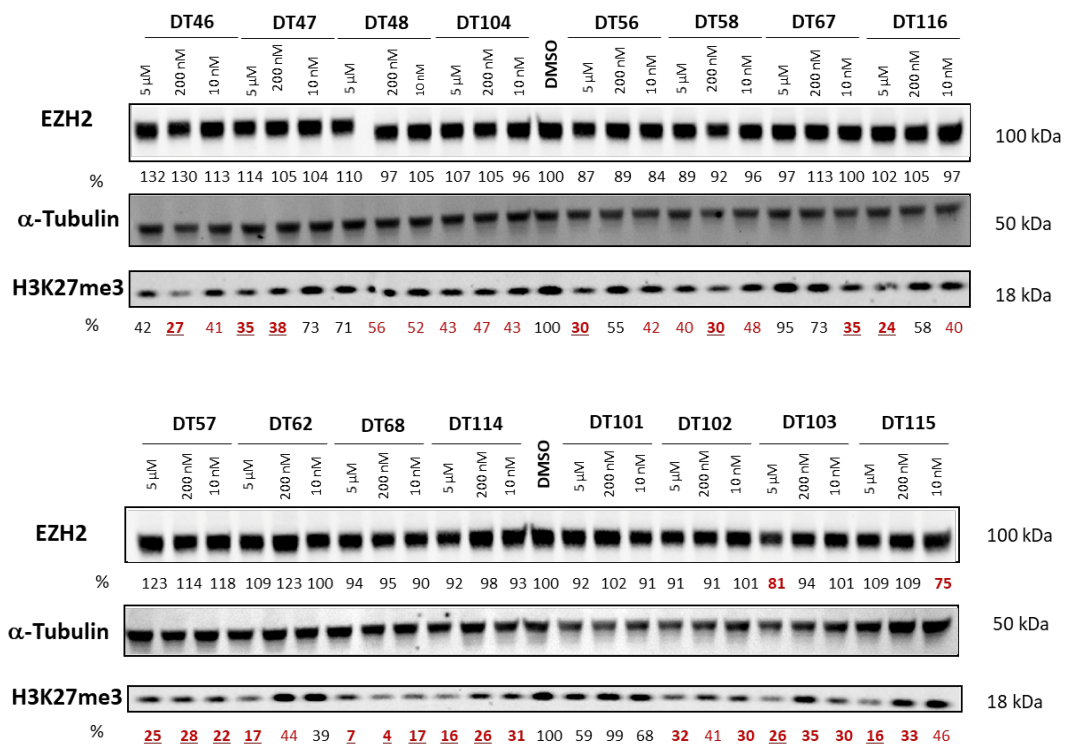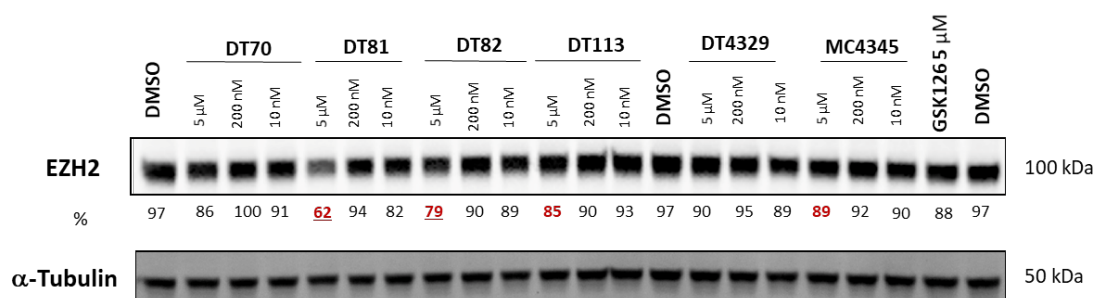
Figure 4.18. First screening of all the synthetized EZH2 targeting PROTACs (Table 4.2). Western blot analysis of EZH2 and H3K27me3 levels following 16h treatment of HEK293 cells with concentrations (5 μM, 200 nM, 10 nM) of all the synthetized CRBN and VHL based targeting PROTACs.

For the most promising compounds (**DT58, DT81, DT82, MC4345, DT68, DT62** and **DT115**) a technical replicate was also conducted to analyse the potential degradation of the other subunits of the catalytic core of PRC2, EED and SUZ12 (Figure 4.19).
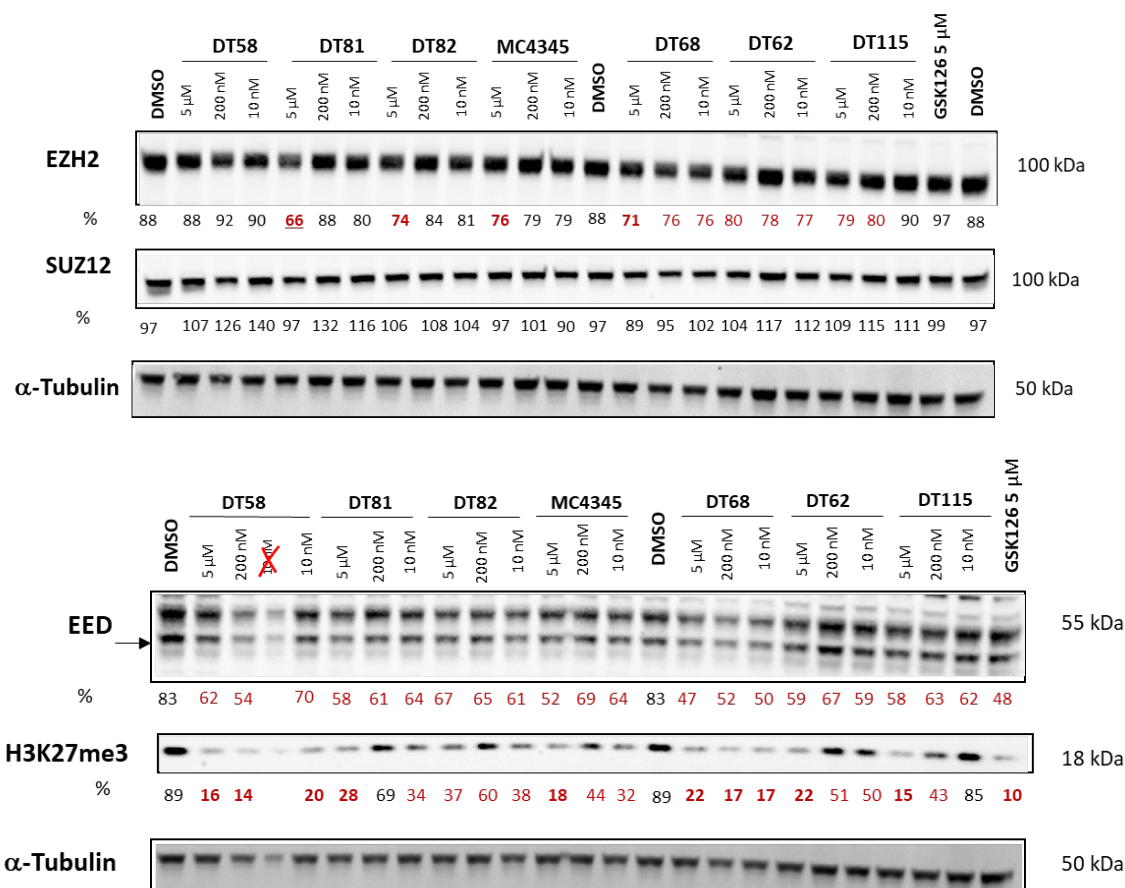
Figure 4.19. Technical replicate of the first screening. Western blot analysis of EZH2, EED, SUZ12 and H3K27me3 levels following a 16h treatment of HEK293 cells with indicated concentrations (5 μM, 200 nM, 10 nM) of the more promising compouns **DT58, DT81, DT82, MC4345, DT68, DT62** and **DT115.** The red cross for **DT58** indicate a mistake during the loading and is not to be considered.

These assays allowed the identification of 5 compounds (**DT81, DT82, DT103, DT113** and **MC4345**) that showed a modest capability to degrade EZH2 and EED at 5 μM while several compounds strongly decrease the H3K27me3 levels, which is, however, naturally

variable in the conditions adopted in our experiment (no cell cycle synchronization has been applied).

The second screening was conducted at lower concentration: 10 nM, 2 nM, 0.4 nM (Figure 4.18) in order to exclude any possible false negative potentially due to the "hook-effect" which is characteristic of bivalent molecules: whereby unproductive binary complexes preferentially form at high PROTAC concentration, which compete with and eventually suppress the formation of a productive ternary complex (Figure 4.20).[563]

188
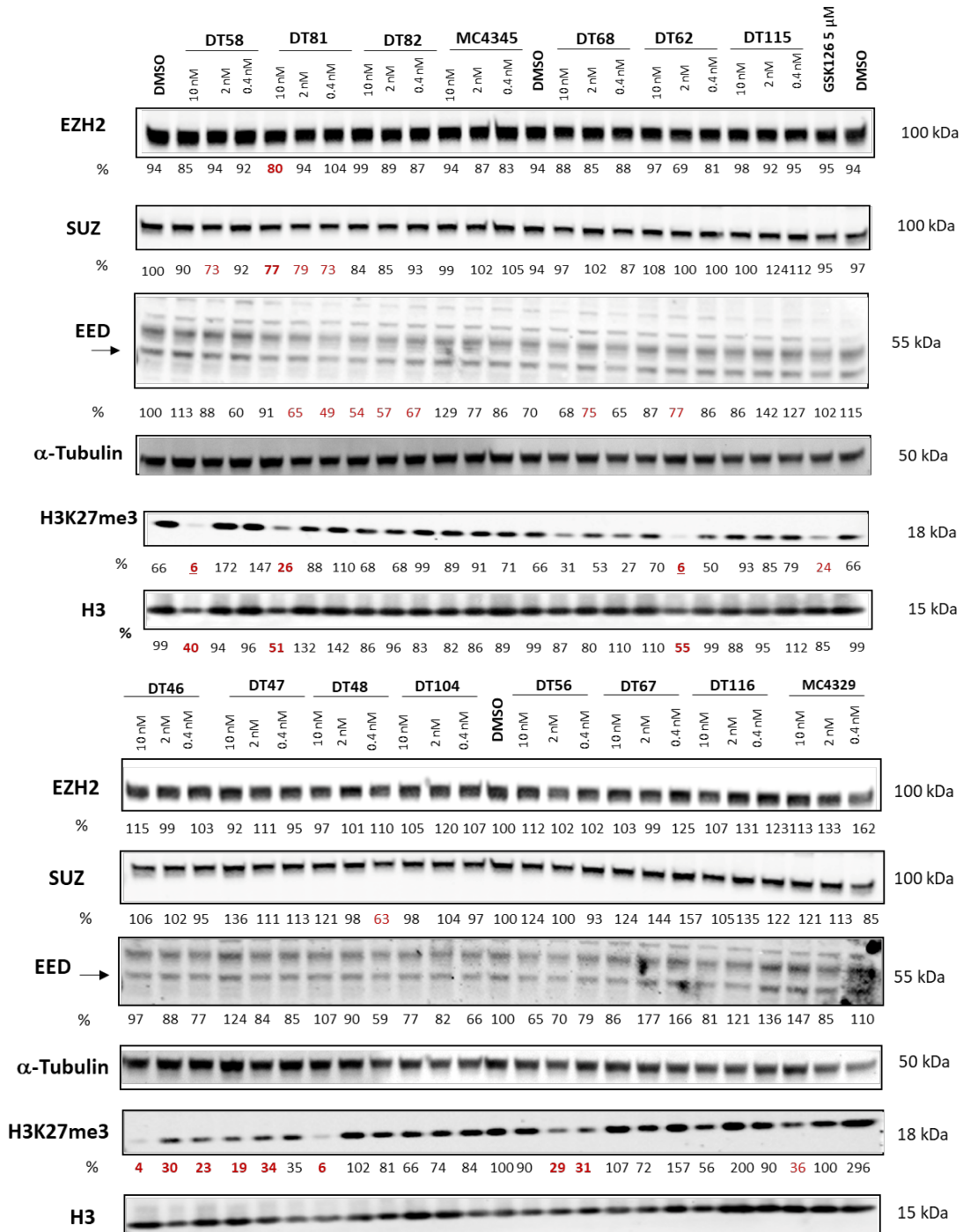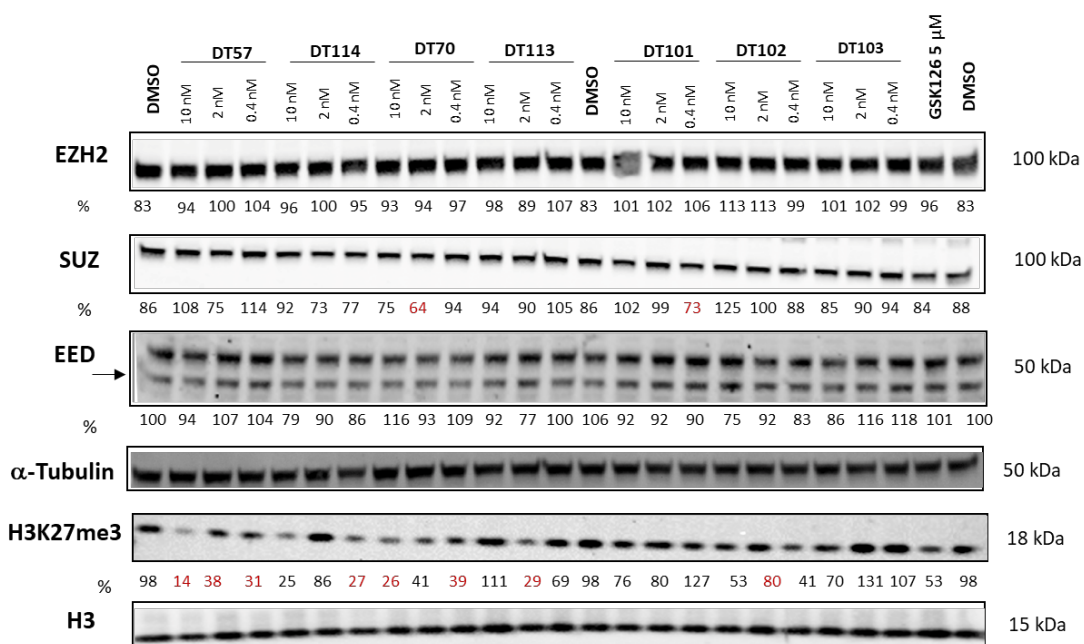
Figure 4.20. Second screening of all the synthetized EZH2 targeting PROTACs (Table 4.2). Western blot analysis of EZH2, EED, SUZ12, H3K27me3 and H3 levels following 16h treatment of HEK293 cells with indicated concentrations (10 nM, 2 nM, 0.4 nM) of all the synthetized CRBN and VHL based targeting PROTACs (Table 4.2).

These evidence confirmed that compound **DT81** is still able to induce a slight degradation of EZH2 and EED also at lower concentration (10 nM), while different compounds seem to be better degrader of SUZ12 at lower concentration such as **DT48, DT70, DT81, DT82**. Variability in H3K27me3 and H3 levels have been registered.

A third screening was conducted in order to evaluate the effect of all the EZH2 targeting PROTACs (Table 4.2) after a shorter treatment of 4h at 100 nM, 10 nM, 1 nM concentrations (Figure 4.21).
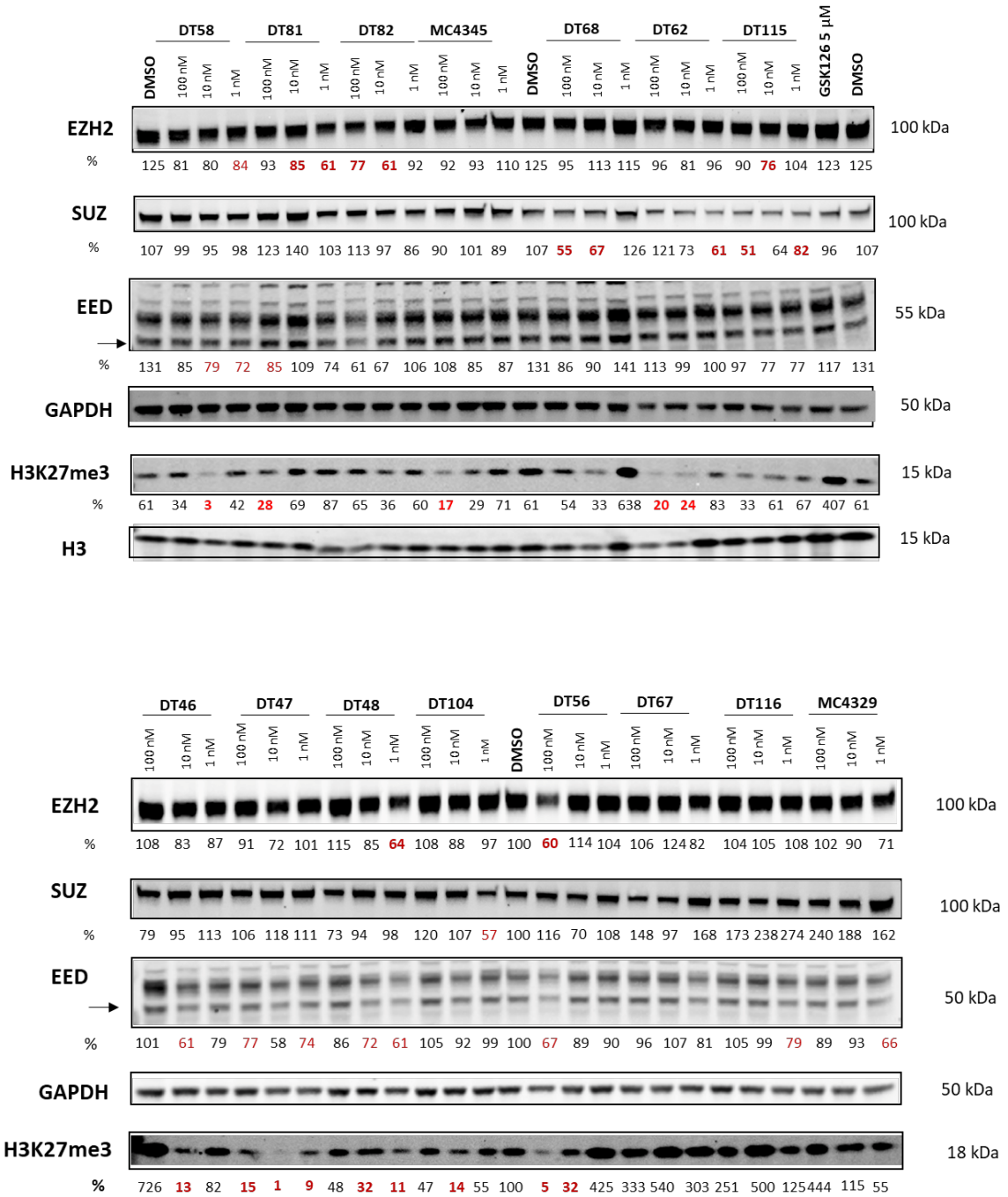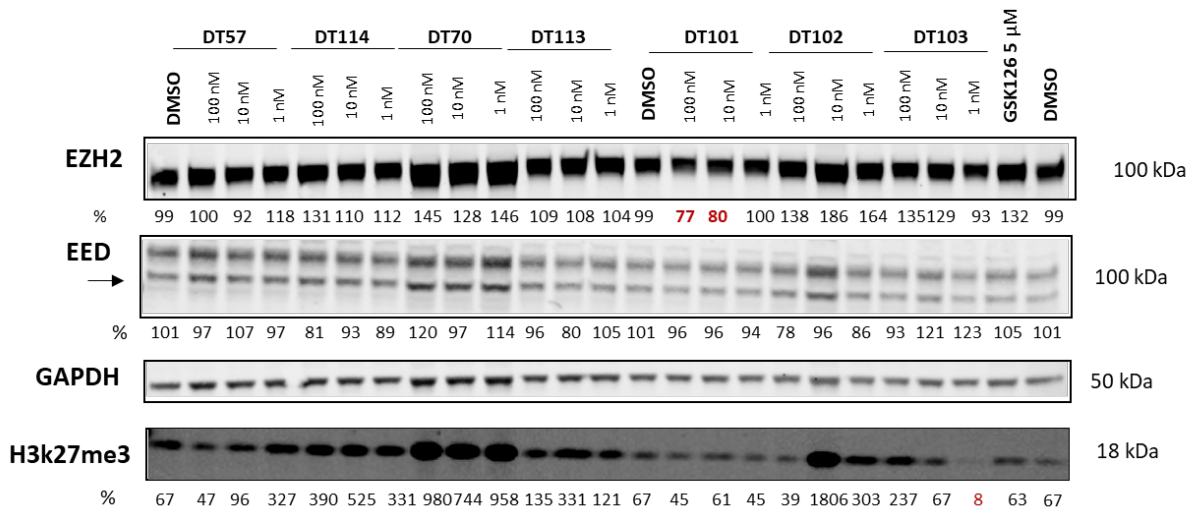
Figure 4.21. Third screening. Western blot analysis of EZH2, EED, SUZ12, H3K27me3 and H3 levels following 4h treatment of HEK293 cells with indicated concentrations (10 nM, 2 nM, 0.4 nM) of all the synthetized CRBN and VHL based targeting PROTACs (Table 4.2).

As shown in figure 4.21, degradations data between 20-40% has been registered for EZH2 (**DT81, DT82, DT48, DT56** and **DT101**), of 14-30% for EED (**DT46, DT47, DT48, DT56, DT81** and **DT82)** and of 40-50% for SUZ12 (**DT68** and **DT115)** at indicated concentrations of 10 nM, 2 nM, 0.4 nM.

The last screening conducted was focused on the comparison of the results collected from both HEK293 and HeLa cell lines after 24h treatment with all the synthetized EZH2 targeting PROTACs (Table 4.2) at single concentration of 200 nM (Figure 4.22)
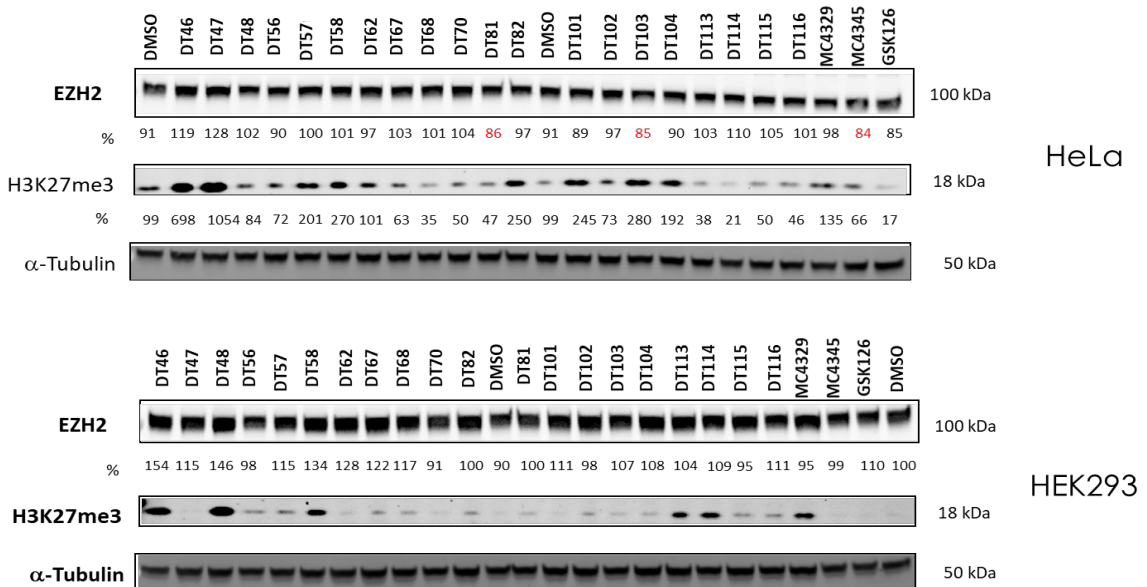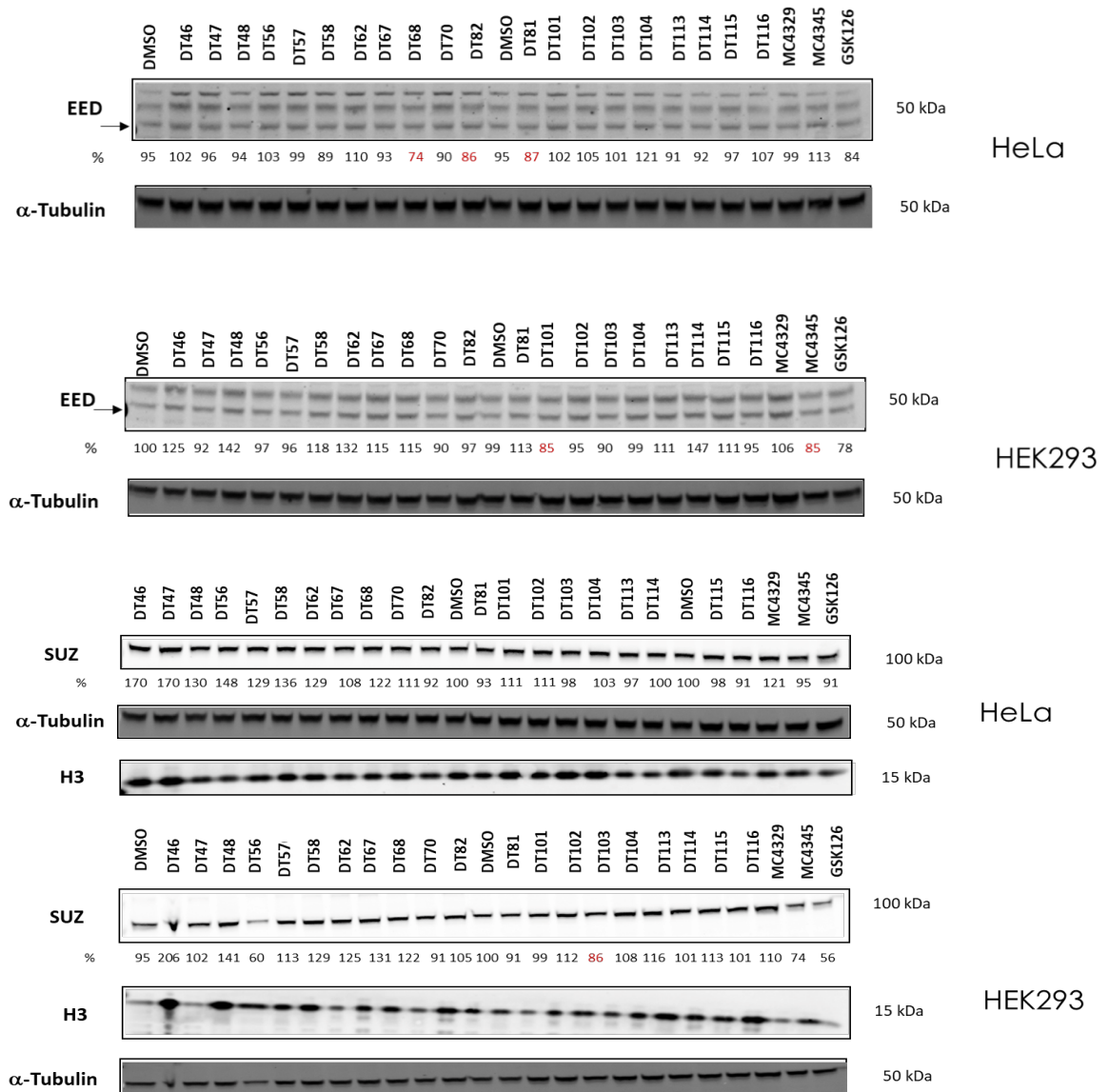
Figure 4.22. Fourth screening. Western blot analysis of EZH2, EED, SUZ12, H3K27me3 and H3 levels following 24h treatment of HEK293 and HeLa cell lines using 200 nM concentration of all the synthetized CRBN and VHL based targeting PROTACs (Table 4.2).

Unfortunately, in these conditions (24h treatment, concentration of 200 nM for each tested compound) no evidences of marked degradation of the targeted proteins have been registered in both cell lines, however **DT81, DT103** and **MC4345** showed a degradation of 15% for EZH2 and **DT68, DT82, DT81** of 15-30% for EED in HeLa cells; **MC4345** and **DT101** provided a degradation of 15% for EED in HEK293 cells and 26% SUZ12 degradation has also been collected for **DT103** in HEK293 cell line .
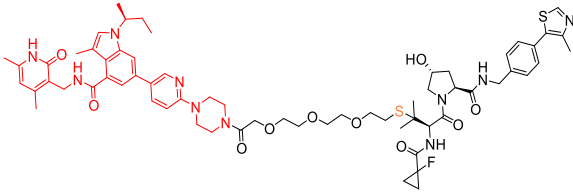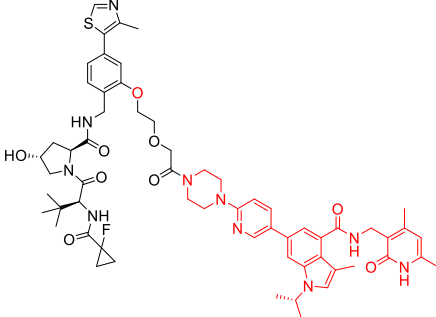
4.7 Conclusions and future perspectives

Taken together, despite this is an early state project, some considerations are necessary: 22 EZH2 targeting PROTACs have been synthetized (Table 4.2) and Western Blot analysis were conducted in order to evaluate the degradation of EZH2 and of the other components of the catalytic core of PRC2, including EED and SUZ12. H3K27me3 levels have been also monitored to collect informations about the modulation of the downstream effect mediated by the PRC2 complex. H3 levels have been used as reference (Figure 4.18-4.22).

The obtained results can be schematized as follows (Table 4.3, Figure 4.23):

- EZH2/EED/SUZ12 degradation (30-50%) have been registered for: **DT56** (5 μM, EZH2, EED16h treatment; SUZ 2nM 16h treatment) **DT103** (5 μM, EZH2, 16h treatment), **DT81** (5 μM, EZH2, EED, SUZ12 16h treatment), **DT82** (5 μM, EZH2,EED 16h treatment), **DT113** (2nM, EED, 16h treatment), **DT101** (10 nM, 2nM, EZH2, SUZ12, 4h treatment), **DT56** (100 nM, EZH2, 4h treatment), **DT48** (1nM, EZH2, SUZ12, 4h treatment).

- Strong decrease of H3K27me3 (40-95%) has been registered at concentration between 2 nM and 5 μM in both short (4h) or long (16 or 24h) treatments for: **DT82**, **DT115**, **MC4345**, **DT68**, **DT58** (also at 10 nM, 16h), **DT81** (also at10 nM, 16h), **DT62** (also at 2 nM, 16h), **DT103** (also at 1nM, 4h)

- Decrease of total level (50%) of H3 has been registered after 16h treatment of HEK293 cell line for compounds **DT58**, (10 nM), **DT81** (10 nM), **DT62** (2 nM).

BIOLOGICAL CHARACTERIZATION OF THE MOST PROMISING EZH2 TARGETING PROTACs

CODE	STRUCTURE	REGISTERED EFFECTS
90a **DT58**		EZH2[a]/EED[a]/SUZ12[b] degradation (30-50%) H3K27me3[b] (96%) H3 total level[d] (60%)
89c **DT81**		EZH2[a]/EED[a]/SUZ12[c] degradation (30-60%) H3K27me3[a] (40-95%) H3 total level[d] (50%)

87b **DT62**		EED[a]/SUZ12[e] degradation (40%) H3K27me3[b] (94%) H3 total level[b] (45%)
85c **DT115**		EZH2[a]/EED[a]/SUZ12[f] degradation (20-50%) H3K27me3[a] (85%)
85b **DT103**		EZH2[a]/EED[g] degradation (20%) H3K27me3[c] (92%)
89d **DT113**		EZH2[a]/EED[b]/SUZ12[h*] degradation (15-25%) H3K27me3[b] (70%)
89b **DT82**		EZH2[a]/EED[a]/SUZ12[c] degradation (30-40%) H3K27me3[a] (60%)
85a **MC4345**		EZH2[a]/EED[a]/SUZ12[e] degradation (25-50%) H3K27me3[i] (83%)
88b **DT48**		EZH2[e]/EED[e]/SUZ12[f] degradation (36-45%) H3K27me3[c] (90%)
87c **DT68**		EZH2[a]/EED[a]/SUZ12[c] degradation (36-50%) H3K27me3[a] (80%)

194

Compound	Structure	Activity
58a **DT101**		EZH2[f]/EED[g*] degradation (15-25%) H3K27me3[f] (60%)
90c **DT56**		EZH2[f]/EED[f] degradation (30-40%) H3K27me3[i] (70%)
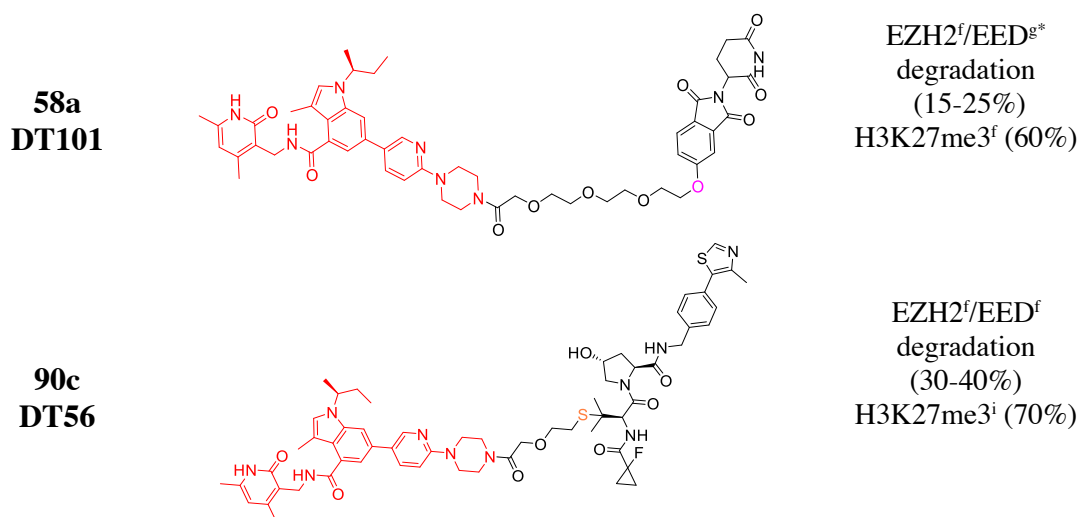
Table 4.3. Schematic representation of most interesting biological data (EZH2, EED, SUZ12 degradation and residual H3K27Me3 and H3 levels) collected for the best EZH2-targeting PROTACS synthetized: **90a DT58**, **89c DT81**, **87b DT62**, **85c DT115**, **85b DT103**, **89d DT113**, **89b DT82**, **85a MC4345**, **88b DT48**, **87c DT68**, **58a DT101**, **90c DT56**. a= 5μM, 16h; b= 2nM, 16h; c= 0.4nM, 15h; d= 10nM, 16, e= 1nM, 4h; f= 100nM, 4h; g= 200nM, 16h; h= 10nM, 16h; i= 10nM, 4h. All the results refer to HEK293 cell line, with the exeption of those with * that refer to HeLa cell line.
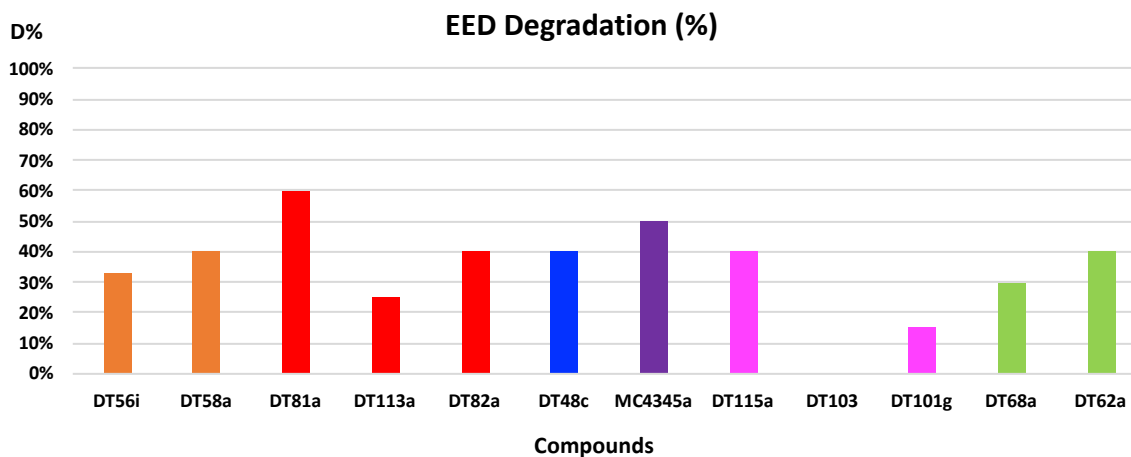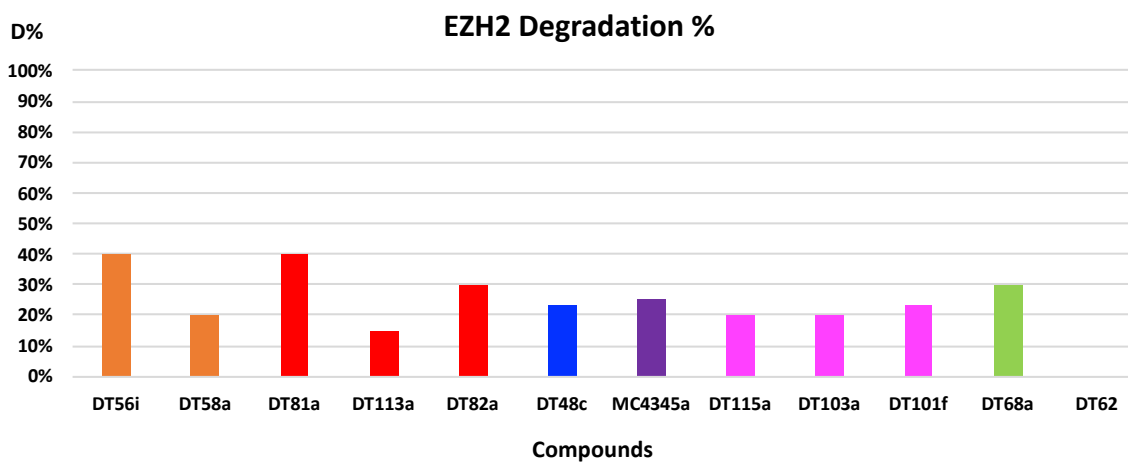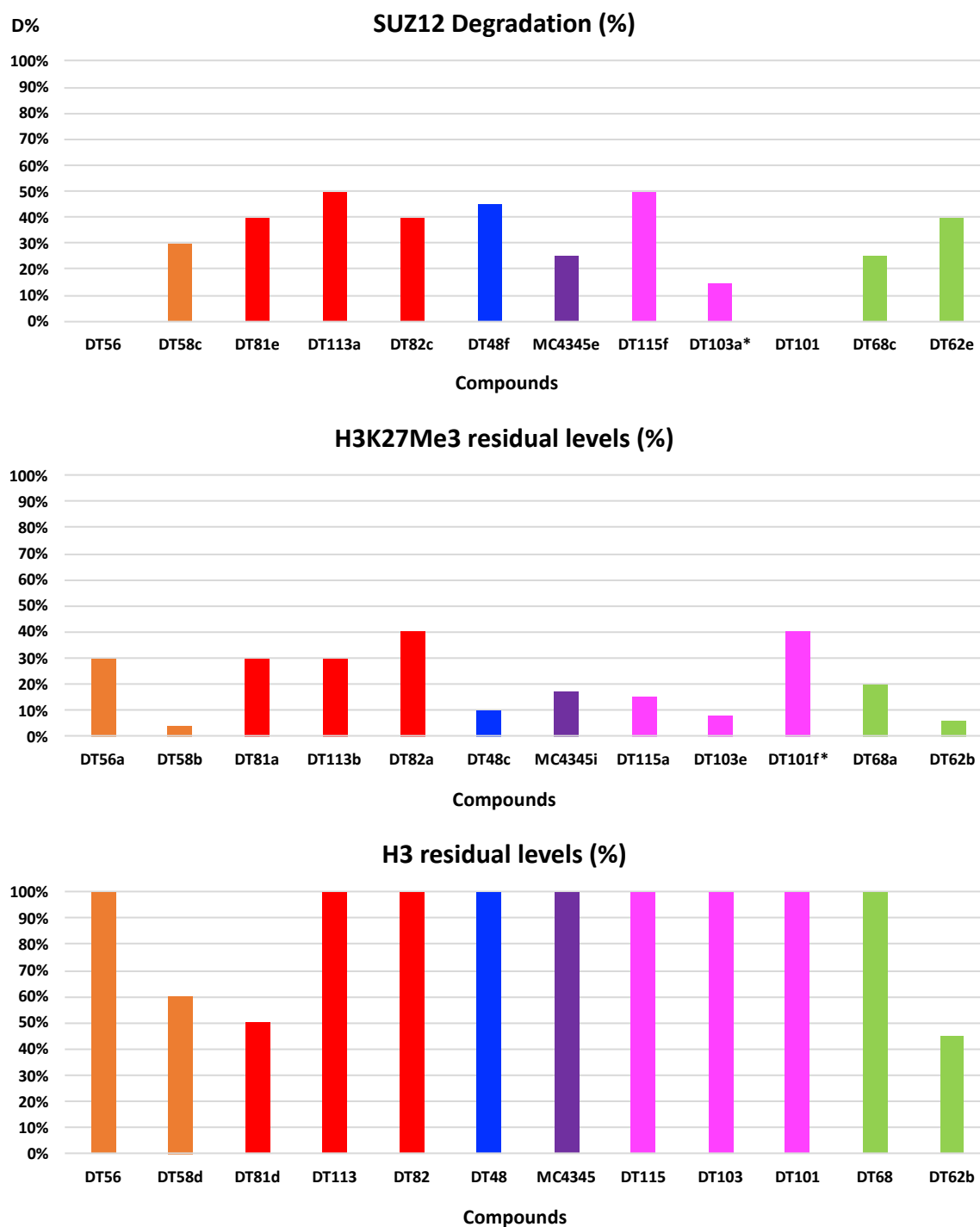
Figure 4.23. Graphical representation of most interesting biological data (EZH2, EED, SUZ12 degradation and residual H3K27Me3 and H3 levels) collected for the best EZH2-targeting PROTACS synthetized: **90a DT58**, **89c DT81**, **87b DT62**, **85c DT115**, **85b DT103**, **89d DT113**, **89b DT82**, **85a MC4345**, **88b DT48**, **87c DT68**, **58a DT101**, **90c DT56**. The different colours correlate with the relative derivatization point of the VHL (-SH, **37e**, orange; -OH red, **37c**, -NH$_2$, **37f**, blue) and CRBN (4-hydroxythalidomide, **36f**, purple; 5-hydroxythalidomide, **36g**, magenta; piperazine-thalidomide, **36d**, green) binders selected for PROTACs design. a= 5μM, 16h; b= 2nM, 16h; c= 0.4nM, 15h; d= 10nM, 16, e= 1nM, 4h; f= 100nM, 4h; g= 200nM, 16h; h= 10nM, 16h; i= 10nM, 4h. About the graph depicting the levels of H3, for compounds **DT113**, **DT82**, **DT48**, **MC4345**, **DT115**, **DT103**, **DT101** and **DT68** no concentrations have been indicated since no reduction in H3 levels was registered at any tested conditions. All the results refer to HEK293 cell line, with the exeption of those with * that refer to HeLa cell line.

The meaning covered by the strong variability of the downstream effect (H3K27me3 levels) collected for most of the compounds and in particular for **DT58, DT81, DT62, DT115, DT82, MC4345** and **DT68** is not yet clearly understood since the physiologically variability that have been registered after treatment of different wells of HEK293 cell line with DMSO (6 wells, DMSO1-6) using GSK126 at 5 μM (2 wells, GSK126 (1) and GSK126 (2)) and **DT58 90a** at 200 nM (2 wells, (**DT58** (1) and **DT58** (2)) as positive controls (Figure 4.23). Cell lysate have been collected and maintained separately for the consequent protein quantification and Western Blot as shown in Figure 4.24 which highlighted, in addition, variability of the total levels of H3 (as already registered after the 16h treatment of HEK293 with compounds **DT58**, (at 10nM), **DT81** (at 10nM), **DT62** (at 2nM), suggesting that the evaluation of these proteins level is intimately dependent on the cell cycle as well as on the lysis protocol adopted. Cell cycle synchronization and the application of a different protocol for the cell lysis could be interesting and promising factors to fully understand the alterations of the H3K27me3 pattern and H3 total levels potentially induced by the synthetized molecules.
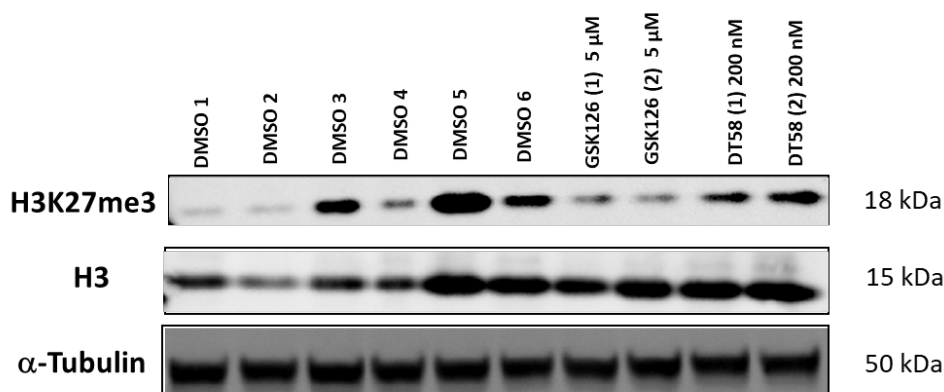
Figure 4.24. Western blot analysis showing the variability of H3K27me3 and H3 total levels after 24h treatment of HEK293 with **DMSO** (6 wells, **DMSO1-6**), **GSK126** at 5 μM (2 wells, **GSK126 (1)** and **GSK126 (2)**) and **DT58** at 200 nM (2 wells, (**DT58 (1)** and **DT58 (2)**) as controls positive controls.

If a strong decrease of the downstream effect (H3K27me3) will be registered using the just exposed precautions, the evaluation of the possible degradation of other members of the PRC2 complex, which may justify this evidence, could result a rational strategy.
In fact, as previously discussed, also other subunits of this multicomponent complex are fundamental for the catalysis of the methylation process, including AEBP2, which allows the binding with the methylated DNA (PRC2 has a strong tendency to be present on CpG island promoters of lowly transcribed and inactive genes) or RbAp464/48 (also known as RBBP4/7) which are required for PRC2 binding to unmodified nucleosomes (Figure 4.25). Considering the evidence reported to literature, potential degradation of these subunits, in addition to those within the catalytic core, would not ensure a full methyltransferase activity.
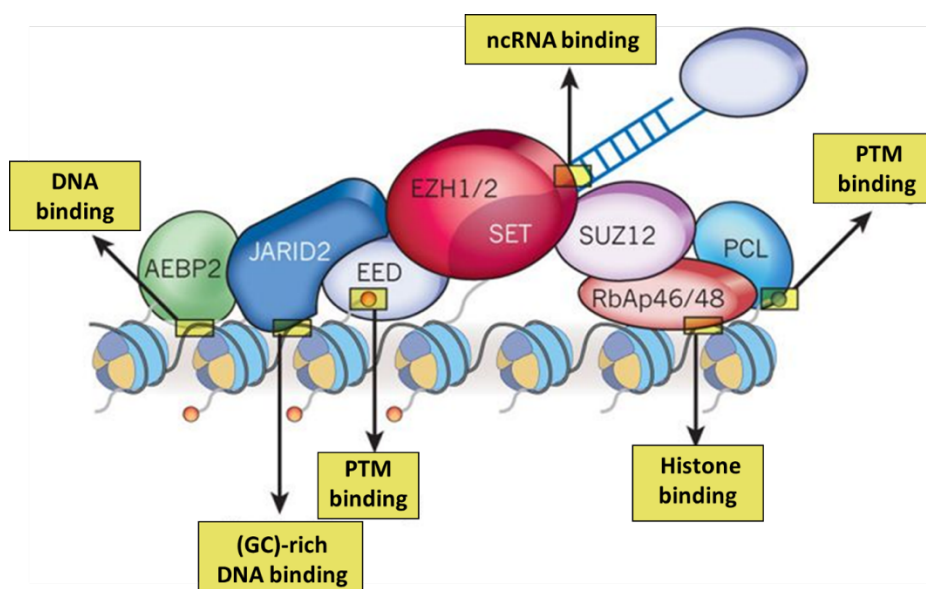
Figure 4.25. Schematization of PRC2 complex and of the role covered by each subunit. Adapted from Margueron *et al*. *Nature*, 2011, 469, p 343–349.[134]

From a chemical point of view, the collected results (Table 4.3, Figure 4.23) showed that compounds characterized by short linkers seem to be more effective in term of EZH2, EED, SUZ12 degradation but no preference between CRBN or VHL binder moiety (or nature of attachment points) can be safely highlighted. Although more information in term of both biological and biophysical assays would certainly be useful, at this early stage point is possible to identify **89c DT81** as the most promising compound of such series of EZH2 targeting PROTACs given it degradation results towards EZH2, EED and SUZ12, which resulted consistent after the various treatments conducted. In this framework, adopt an approach that maintains both the warheads (GSK126 **20** and the VHL binder **37c**) in order to evaluate the effects of the replacement of the linker typical of **89c DT81** with other (short) pegylated and non-pegylated linkers may be interesting. In fact, considering the main role that the linker covers in the establishment of a stable ternary complex, this step could result fundamental for the achievement of an efficient protein(s) degradation.

4.8 Methods

4.8.1 Cell Culture

HeLa (CCL-2) and HEK293 (CRL-1573) cells were purchased from ATCC and cultured in DMEM medium (Gibco) supplemented with 10% FBS, 100 μg/mL penicillin/streptomycin and L-glutamine. Cells were grown at 37 °C and 5% CO_2 and were kept no longer than 30 passages. All cell lines were routinely tested for mycoplasma contamination using MycoAlert kit from Lonza.

4.8.2 Evaluation of cellular activity of PROTACs

HeLa (5 x 10^5) and HEK293 (1 x 10^6) cells were seeded in standard 6-well plates (2 mL medium) overnight before treatment with compounds at the desired concentration, with a final DMSO concentration of 0.1% v/v. After the appropriate incubation time, cells were washed with DPBS (Gibco) and lysed using 85 μL RIPA buffer (Sigma-Aldrich) supplemented with cOmplete Mini EDTA-free protease inhibitor cocktail (Roche) and benzonase. Lysates were clarified by centrifugation (20000 *g*, 10 min, 4 °C) and the total protein content of the supernatant was quantified using a Bradford colorimetric assay. Samples were prepared using equal amounts of total protein and LDS sample buffer (Invitrogen).

4.8.3 Immunoblotting

Proteins were separated by SDS-PAGE on NuPage 4-12% Bis-Tris gels and transferred to Amersham Protran 0.45 NC nitrocellulose membranes (GE Healthcare) using wet transfer. Membranes were blocked using 5% w/v milk in Tris-buffered saline (TBS) with 0.1% Tween-20. Blots were probed using anti-EZH2 (Mouse IgG1, Primary antibodies, Cell Signaling, Cat. no. 5246, 1:100), Anti-EED (Sheep IgG1, primary antibodies, R&D Systems Cat. No. AF5827, 1:1000), Anti-SUZ12 (Rabbit IgG1, primary antibodies, Cell Signaling cat. No. D39F6, 1:1000), Anti-H3K27me3 (Rabbit IgG1, Primary antibodies, Cell Signaling, Cat. no. 9733, 1:1000), Anti-H3 Anti-H3 (Rabbit IgG1, Primary antibodies, Cell Signaling, Cat. no. 9715, 1:1000), Anti-GAPDH antibody (Rabbit IgG1, primary antibodies, abcam, cat no. ab181602) and anti-tubulin hFAB-rhodamine (BioRad, 12004166) primary antibodies, followed by incubation with secondary anti-Rabbit IRDye 800CW (ab216773) or anti-Sheep (STAR88A, Biorad) antibodies. Blots were developed using a Bio-Rad ChemiDoc MP Imaging System or the Amersham ECL Prime Western blotting detection kit and Amersham Hyperfilm ECL film, as appropriate. Band quantification was performed using the ImageJ software. Band intensities were normalized to the tubulin or GAPDH loading control and reported as % of the average 0.1% DMSO vehicle intensity. Degradation data was plotted and analysed using Prism (Graphpad, version 6).

Bibliography

(1) Goldberg, A. D.; Allis, C. D.; Bernstein, E. Epigenetics: A Landscape Takes Shape. *Cell* **2007**, *128* (4), 635–638. https://doi.org/10.1016/j.cell.2007.02.006.

(2) Jaenisch, R.; Bird, A. Epigenetic Regulation of Gene Expression: How the Genome Integrates Intrinsic and Environmental Signals. *Nat. Genet.* **2003**, *33* (3S), 245–254. https://doi.org/10.1038/ng1089.

(3) Berger, S. L.; Kouzarides, T.; Shiekhattar, R.; Shilatifard, A. An Operational Definition of Epigenetics. *Genes Dev.* **2009**, *23* (7), 781–783. https://doi.org/10.1101/gad.1787609.

(4) Pechalrieu, D.; Etievant, C.; Arimondo, P. B. DNA Methyltransferase Inhibitors in Cancer: From Pharmacology to Translational Studies. *Biochemical Pharmacology*. 2017. https://doi.org/10.1016/j.bcp.2016.12.004.

(5) Auclair, G.; Weber, M. Mechanisms of DNA Methylation and Demethylation in Mammals. *Biochimie* **2012**, *94* (11), 2202–2211. https://doi.org/10.1016/j.biochi.2012.05.016.

(6) Ehrlich, M. DNA Methylation in Cancer: Too Much, but Also Too Little. *Oncogene* **2002**, *21* (35), 5400–5413. https://doi.org/10.1038/sj.onc.1205651.

(7) Ben-Porath, I.; Cedar, H. Epigenetic Crosstalk. *Mol. Cell* **2001**, *8* (5), 933–935. https://doi.org/10.1016/S1097-2765(01)00399-9.

(8) Eden, S.; Hashimshony, T.; Keshet, I.; Cedar, H.; Thorne, D. W.; Ausio, J. DNA Methylation Models Histone Acetylation. *Chemtracts* **1999**, *12* (10), 718–723.

(9) Šestan, N. Methylation-Induced Repression— Minireview.Pdf. **1999**, *99*, 451–454.

(10) Bannister, A. J.; Zegerman, P.; Partridge, J. F.; Miska, E. A.; Thomas, J. O.; Allshire, R. C.; Kouzarides, T. Selective Recognition of Methylated Lysine 9 on Histone H3 by the HP1 Chromo Domain. *Nature* **2001**, *410* (6824), 120–124. https://doi.org/10.1038/35065138.

(11) Hon, G. C.; Hawkins, R. D.; Caballero, O. L.; Lo, C.; Lister, R.; Pelizzola, M.; Valsesia, A.; Ye, Z.; Kuan, S.; Edsall, L. E.; et al. Global DNA Hypomethylation Coupled to Repressive Chromatin Domain Formation and Gene Silencing in Breast Cancer. *Genome Res.* **2012**, *22* (2), 246–258. https://doi.org/10.1101/gr.125872.111.

(12) Lujambio, A.; Portela, A.; Liz, J.; Melo, S. A.; Rossi, S.; Spizzo, R.; Croce, C. M.; Calin, G. A.; Esteller, M. CpG Island Hypermethylation-Associated Silencing of Non-Coding RNAs Transcribed from Ultraconserved Regions in Human Cancer. *Oncogene* **2010**, *29* (48), 6390–6401. https://doi.org/10.1038/onc.2010.361.

(13) Baylin, S. B.; Jones, P. A. A Decade of Exploring the Cancer Epigenome - Biological and Translational Implications. *Nat. Rev. Cancer* **2011**, *11* (10), 726–734. https://doi.org/10.1038/nrc3130.A.

(14) Finley, A.; Copeland, R. A. Small Molecule Control of Chromatin Remodeling. *Chem. Biol.* **2014**, *21* (9), 1196–1210. https://doi.org/10.1016/j.chembiol.2014.07.024.

(15) Wu, J.; Grunstein, M. 25 Years after the Nucleosome Model: Chromatin Modifications. *Trends Biochem. Sci.* **2000**, *25* (12), 619–623. https://doi.org/10.1016/S0968-0004(00)01718-7.

(16) Luger, K.; Mäder, a W.; Richmond, R. K.; Sargent, D. F.; Richmond, T. J. Crystal Structure of the Nucleosome Core Particle at 2.8 A Resolution. *Nature* **1997**, *389* (6648), 251–260. https://doi.org/10.1038/38444.

(17) Taunton, J.; Hassig, C. A.; Schreiber, S. L. A Mammalian Histone Deacetylase Related to the Yeast Transcriptional Regulator Rpd3p. *Science (80-.)*. **1996**, *272* (5260), 408–411. https://doi.org/10.1126/science.272.5260.408.

(18) Brownell, J. E.; Zhou, J.; Ranalli, T.; Kobayashi, R.; Edmondson, D. G.; Roth, S. Y.; Allis, C. D. Tetrahymena Histone Acetyltransferase A: A Homolog to Yeast Gcn5p Linking Histone Acetylation to Gene Activation. *Cell* **1996**, *84* (6), 843–851. https://doi.org/10.1016/S0092-8674(00)81063-6.

(19) Dhalluin, C.; Carlson, J. E.; Zeng, L.; He, C.; Aggarwal, a K.; Zhou, M. M. Structure and Ligand of a Histone Acetyltransferase Bromodomain. *Nature* **1999**, *399* (6735), 491–496. https://doi.org/10.1038/20974.

(20) Filippakopoulos, P.; Picaud, S.; Mangos, M.; Keates, T.; Lambert, J. P.; Barsyte-Lovejoy, D.; Felletar, I.; Volkmer, R.; Müller, S.; Pawson, T.; et al. Histone Recognition and Large-Scale Structural Analysis of the Human Bromodomain Family. *Cell* **2012**, *149* (1), 214–231. https://doi.org/10.1016/j.cell.2012.02.013.

(21) Ruthenburg, A. J.; Li, H.; Patel, D. J.; David Allis, C. Multivalent Engagement of Chromatin Modifications by Linked Binding Modules. *Nat. Rev. Mol. Cell Biol.* **2007**, *8* (12), 983–994. https://doi.org/10.1038/nrm2298.

(22) Rothbart, S. B.; Strahl, B. D. Interpreting the Language of Histone and DNA Modifications. *Biochim. Biophys. Acta - Gene Regul. Mech.* **2014**, *1839* (8), 627–643. https://doi.org/10.1016/j.bbagrm.2014.03.001.

(23) Musselman, C. A.; Lalonde, M. E.; Cote, J.; Kutateladze, T. G. Perceiving the Epigenetic Landscape through Histone Readers. *Nat Struct Mol Biol* **2012**, *19* (12), 1218–1227. https://doi.org/10.1038/nsmb.2436.

(24) Singleton, M. R.; Wigley, D. B. Modularity and Specialization in Superfamily 1 and 2 Helicases. *Journal of Bacteriology*. 2002. https://doi.org/10.1128/JB.184.7.1819-1826.2002.

(25) Petty, E.; Pillus, L. Balancing Chromatin Remodeling and Histone Modifications in Transcription. *Trends in Genetics*. 2013. https://doi.org/10.1016/j.tig.2013.06.006.

(26) Clapier, C. R.; Cairns, B. R. The Biology of Chromatin Remodeling Complexes. *Annu. Rev. Biochem.* **2009**. https://doi.org/10.1146/annurev.biochem.77.062706.153223.

(27) Tang, L.; Nogales, E.; Ciferri, C. Structure and Function of SWI/SNF Chromatin Remodeling Complexes and Mechanistic Implications for Transcription. *Prog. Biophys. Mol. Biol.* **2010**, *102* (2–3), 122–128. https://doi.org/10.1016/j.pbiomolbio.2010.05.001.

(28) Welsby, I.; Hutin, D.; Leo, O. Complex Roles of Members of the ADP-Ribosyl Transferase Super Family in Immune Defences: Looking beyond PARP1. *Biochem. Pharmacol.* **2012**, *84* (1), 11–20. https://doi.org/10.1016/j.bcp.2012.02.016.

(29) Faraone-mennella, M. R. Chromatin Architecture and Functions : The Role (s) of Poly (ADP-RIBOSE) Polymerase and Poly (ADPribosyl) Ation of Nuclear Proteins 1. *Biochem. Cell Biol.* **2005**, No. 83, 396–404. https://doi.org/10.1139/O05-042.

(30) Rouleau, M.; Aubin, R.; Poirier, G. Poly(ADP-Ribosyl)Ated Chromatin Domains: Access Granted. *J Cell Sci* **2004**, *117* (Pt 6), 815–825. https://doi.org/10.1242/jcs.01080.

(31) Hemalatha, K.; Madhumitha, G. Inhibition of Poly (Adenosine Diphosphate-Ribose) Polymerase Using Quinazolinone Nucleus. *Appl. Microbiol. Biotechnol.* **2016**, 7799–7814. https://doi.org/10.1007/s00253-016-7731-1.

(32) Liscio, P.; Camaioni, E.; Carotti, A.; Pellicciari, R.; Macchiarulo, A. From Polypharmacology to Target Specificity : The Case of PARP Inhibitors. *Curr. Top. Med. Chem.* **2013**, *13*, 2939–2954.

(33) Huang, S.-M. a; Mishina, Y. M.; Liu, S.; Cheung, A.; Stegmeier, F.; Michaud, G.

a; Charlat, O.; Wiellette, E.; Zhang, Y.; Wiessner, S.; et al. Tankyrase Inhibition Stabilizes Axin and Antagonizes Wnt Signalling. *Nature* **2009**, *461* (7264), 614–620. https://doi.org/10.1038/nature08356.

(34) Quénet, D.; Ramy, R. El; Schreiber, V. The Role of Poly(ADP-Ribosyl)Ation in Epigenetic Events. *Int. J. Biochem.* **2009**, *41*, 60–65. https://doi.org/10.1016/j.biocel.2008.07.023.

(35) Krishnakumar, R.; Gamble, M. J.; Frizzell, K. M.; Berrocal, J. G.; Kininis, M.; Kraus, W. L. Reciprocal Binding of PARP-1 and Histone H1 at Promoters Specifies Transcriptional Outcomes. *Science (80-.).* **2008**, *319* (5864), 819–821. https://doi.org/10.1126/science.1149250.

(36) Kim, M. Y.; Mauro, S.; Gévry, N.; Lis, J. T.; Kraus, W. L. NAD+-Dependent Modulation of Chromatin Structure and Transcription by Nucleosome Binding Properties of PARP-1. *Cell* **2004**, *119* (6), 803–814. https://doi.org/10.1016/j.cell.2004.11.002.

(37) Guastafierro, T.; Cecchinelli, B.; Zampieri, M.; Reale, A.; Riggio, G.; Sthandier, O.; Zupi, G.; Calabrese, L.; Caiafa, P. CCCTC-Binding Factor Activates PARP-1 Affecting DNA Methylation Machinery. *J. Biol. Chem.* **2008**, *283* (32), 21873–21880. https://doi.org/10.1074/jbc.M801170200.

(38) Ferraris, D. V. Evolution of Poly(ADP-Ribose) Polymerase-1 (PARP-1) Inhibitors. from Concept to Clinic. *J. Med. Chem.* **2010**, *53* (12), 4561–4584. https://doi.org/10.1021/jm100012m.

(39) Hu, S.; Xie, Z.; Onishi, A.; Yu, X.; Jiang, L.; Lin, J.; Rho, H. sool; Woodard, C.; Wang, H.; Jeong, J. S.; et al. Profiling the Human Protein-DNA Interactome Reveals ERK2 as a Transcriptional Repressor of Interferon Signaling. *Cell* **2009**, *139* (3), 610–622. https://doi.org/10.1016/j.cell.2009.08.037.

(40) Dawson, M. A.; Bannister, A. J.; Göttgens, B.; Foster, S. D.; Bartke, T.; Green, A. R.; Kouzarides, T. JAK2 Phosphorylates Histone H3Y41 and Excludes HP1α from Chromatin. *Nature* **2009**, *461* (7265), 819–822. https://doi.org/10.1038/nature08448.

(41) Metzger, E.; Imhof, A.; Patel, D.; Kahl, P.; Hoffmeyer, K.; Friedrichs, N.; Müller, J. M.; Greschik, H.; Kirfel, J.; Ji, S.; et al. Phosphorylation of Histone H3T6 by PKCβI Controls Demethylation at Histone H3K4. *Nature* **2010**, *464* (7289), 792–796. https://doi.org/10.1038/nature08839.

(42) Baek, S. H. When Signaling Kinases Meet Histones and Histone Modifiers in the Nucleus. *Mol. Cell* **2011**, *42* (3), 274–284. https://doi.org/10.1016/j.molcel.2011.03.022.

(43) Zhou, W.; Wang, X.; Rosenfeld, M. G. Histone H2A Ubiquitination in Transcriptional Regulation and DNA Damage Repair. *Int. J. Biochem. Cell Biol.* **2009**, *41* (1), 12–15. https://doi.org/10.1016/j.biocel.2008.09.016.

(44) Minsky, N.; Shema, E.; Field, Y.; Schuster, M.; Segal, E.; Oren, M. Monoubiquitinated H2B Is Associated with the Transcribed Region of Highly Expressed Genes in Human Cells. *Nat. Cell Biol.* **2008**, *10* (4), 483–488. https://doi.org/10.1038/ncb1712.

(45) Weake, V. M.; Workman, J. L. Histone Ubiquitination: Triggering Gene Activity. *Mol. Cell* **2008**, *29* (6), 653–663. https://doi.org/10.1016/j.molcel.2008.02.014.

(46) Kim, J.; Guermah, M.; McGinty, R. K.; Lee, J. S.; Tang, Z.; Milne, T. A.; Shilatifard, A.; Muir, T. W.; Roeder, R. G. RAD6-Mediated Transcription-Coupled H2B Ubiquitylation Directly Stimulates H3K4 Methylation in Human Cells. *Cell* **2009**, *137* (3), 459–471. https://doi.org/10.1016/j.cell.2009.02.027.

(47) Lee, J. S.; Shukla, A.; Schneider, J.; Swanson, S. K.; Washburn, M. P.; Florens, L.; Bhaumik, S. R.; Shilatifard, A. Histone Crosstalk between H2B

Monoubiquitination and H3 Methylation Mediated by COMPASS. *Cell* **2007**, *131* (6), 1084–1096. https://doi.org/10.1016/j.cell.2007.09.046.

(48) Wang, H.; Zhai, L.; Xu, J.; Joo, H.-Y.; Jackson, S.; Erdjument-Bromage, H.; Tempst, P.; Xiong, Y.; Zhang, Y. Histone H3 and H4 Ubiquitylation by the CUL4-DDB-ROC1 Ubiquitin Ligase Facilitates Cellular Response to DNA Damage. *Mol. Cell* **2006**, *22* (3), 383–394. https://doi.org/10.1016/j.molcel.2006.03.035.

(49) Doil, C.; Mailand, N.; Bekker-Jensen, S.; Menard, P.; Larsen, D. H.; Pepperkok, R.; Ellenberg, J.; Panier, S.; Durocher, D.; Bartek, J.; et al. RNF168 Binds and Amplifies Ubiquitin Conjugates on Damaged Chromosomes to Allow Accumulation of Repair Proteins. *Cell* **2009**, *136* (3), 435–446. https://doi.org/10.1016/j.cell.2008.12.041.

(50) Moyal, L.; Lerenthal, Y.; Gana-Weisz, M.; Mass, G.; So, S.; Wang, S. Y.; Eppink, B.; Chung, Y. M.; Shalev, G.; Shema, E.; et al. Requirement of ATM-Dependent Monoubiquitylation of Histone H2B for Timely Repair of DNA Double-Strand Breaks. *Mol. Cell* **2011**, *41* (5), 529–542. https://doi.org/10.1016/j.molcel.2011.02.015.

(51) Shema, E.; Tirosh, I.; Aylon, Y.; Huang, J.; Ye, C.; Moskovits, N.; Raver-shapira, N.; Minsky, N.; Pirngruber, J.; Tarcic, G.; et al. The Histone H2B-Specific Ubiquitin Ligase RNF20 / HBRE1 Acts as a Putative Tumor Suppressor through Selective Regulation of Gene Expression. *Genes Dev.* **2008**, No. Pol II, 2664–2676. https://doi.org/10.1101/gad.1703008.as.

(52) Seeler, J.-S.; Dejean, A. Nuclear and Unclear Functions of SUMO. *Nat. Rev. Mol. Cell Biol.* **2003**, *4* (9), 690–699. https://doi.org/10.1038/nrm1200.

(53) Shen, Z.; Pardington-Purtymun, P. E.; Comeaux, J. C.; Moyzis, R. K.; Chen, D. J. UBL1, a Human Ubiquitin-like Protein Associating with Human RAD51/RAD52 Proteins. *Genomics* **1996**, *36* (2), 271–279. https://doi.org/10.1006/geno.1996.0462.

(54) Yang, M.; Hsu, C. T.; Ting, C. Y.; Liu, L. F.; Hwang, J. Assembly of a Polymeric Chain of SUMO1 on Human Topoisomerase I in Vitro. *J. Biol. Chem.* **2006**, *281* (12), 8264–8274. https://doi.org/10.1074/jbc.M510364200.

(55) Matic, I.; van Hagen, M.; Schimmel, J.; Macek, B.; Ogg, S. C.; Tatham, M. H.; Hay, R. T.; Lamond, A. I.; Mann, M.; Vertegaal, A. C. O. *In Vivo* Identification of Human Small Ubiquitin-like Modifier Polymerization Sites by High Accuracy Mass Spectrometry and an *in Vitro* to *in Vivo* Strategy. *Mol. Cell. Proteomics* **2008**, *7* (1), 132–144. https://doi.org/10.1074/mcp.M700173-MCP200.

(56) Wilkinson, K. A.; Henley, J. M. Targets and Consequences of Protein SUMOylation in Neurons. *Biochem. J.* **2010**, No. 428, 133–145. https://doi.org/10.1016/j.brainresrev.2010.04.002.

(57) Shiio, Y.; Eisenman, R. N. Histone Sumoylation Is Associated with Transcriptional Repression. *Proc. Natl. Acad. Sci. U. S. A.* **2003**, *100* (23), 13225–13230. https://doi.org/10.1073/pnas.1735528100.

(58) Nathan, D.; Ingvarsdottir, K.; Sterner, D. E.; Bylebyl, G. R.; Dokmanovic, M.; Dorsey, J. A.; Whelan, K. A.; Krsmanovic, M.; Lane, W. S.; Meluh, P. B.; et al. Histone Sumoylation Is a Negative Regulator in Saccharomyces Cerevisiae and Shows Dynamic Interplay with Positive-Acting Histone Modifications. *Genes Dev.* **2006**, *20* (8), 966–976. https://doi.org/10.1101/gad.1404206.

(59) Krishnan, S.; Horowitz, S.; Trievel, R. C. Structure and Function of Histone H3 Lysine 9 Methyltransferases and Demethylases. *ChemBioChem* **2011**, *12* (2), 254–263. https://doi.org/10.1002/cbic.201000545.

(60) Greer, E. L.; Shi, Y. Histone Methylation: A Dynamic Mark in Health, Disease and Inheritance. *Nat. Rev. Genet.* **2012**, *13* (5), 343–357.

https://doi.org/10.1038/nrg3173.

(61)   Zhang, Y.; Reinberg, D. Transcription Regulation by Histone Methylation: Interplay between Different Covalent Modifications of the Core Histone Tails. *Genes and Development*. 2001. https://doi.org/10.1101/gad.927301.

(62)   Kouzarides, T. Chromatin Modifications and Their Function. *Cell*. 2007. https://doi.org/10.1016/j.cell.2007.02.005.

(63)   Fortschegger, K.; Shiekhattar, R. Plant Homeodomain Fingers Form a Helping Hand for Transcription. *Epigenetics* **2011**. https://doi.org/10.4161/epi.6.1.13297.

(64)   Arrowsmith, C. H.; Bountra, C.; Fish, P. V.; Lee, K.; Schapira, M. Epigenetic Protein Families: A New Frontier for Drug Discovery. *Nat. Rev. Drug Discov.* **2012**, *11* (5), 384–400. https://doi.org/10.1038/nrd3674.

(65)   McGrath, J.; Trojer, P. Targeting Histone Lysine Methylation in Cancer. *Pharmacol. Ther.* **2015**, *150*, 1–22. https://doi.org/10.1016/j.pharmthera.2015.01.002.

(66)   Shi, Y. Histone Lysine Demethylases: Emerging Roles in Development, Physiology and Disease. *Nature Reviews Genetics*. 2007. https://doi.org/10.1038/nrg2218.

(67)   Hoffmann, I.; Roatsch, M.; Schmitt, M. L.; Carlino, L.; Pippel, M.; Sippl, W.; Jung, M. The Role of Histone Demethylases in Cancer Therapy. *Molecular Oncology*. 2012. https://doi.org/10.1016/j.molonc.2012.07.004.

(68)   Shi, Y.; Lan, F.; Matson, C.; Mulligan, P.; Whetstine, J. R.; Cole, P. A.; Casero, R. A.; Shi, Y. Histone Demethylation Mediated by the Nuclear Amine Oxidase Homolog LSD1. *Cell* **2004**, *119* (7), 941–953. https://doi.org/10.1016/j.cell.2004.12.012.

(69)   Feng, Q.; Wang, H.; Ng, H. H.; Erdjument-Bromage, H.; Tempst, P.; Struhl, K.; Zhang, Y. Methylation of H3-Lysine 79 Is Mediated by a New Family of HMTases without a SET Domain. *Curr. Biol.* **2002**, *12* (12), 1052–1058. https://doi.org/10.1016/S0960-9822(02)00901-6.

(70)   Herz, H. M.; Garruss, A.; Shilatifard, A. SET for Life: Biochemical Activities and Biological Functions of SET Domain-Containing Proteins. *Trends Biochem. Sci.* **2013**, *38* (12), 621–639. https://doi.org/10.1016/j.tibs.2013.09.004.

(71)   Chuikov, S.; Kurash, J. K.; Wilson, J. R.; Xiao, B.; Justin, N.; Ivanov, G. S.; McKinney, K.; Tempst, P.; Prives, C.; Gamblin, S. J.; et al. Regulation of P53 Activity through Lysine Methylation. *Nature* **2004**, *432* (7015), 353–360. https://doi.org/10.1038/nature03117.

(72)   Singer, M. S.; Kahana, A.; Wolf, A. J.; Meisinger, L. L.; Peterson, S. E.; Goggin, C.; Mahowald, M.; Gottschling, D. E. Identification of High-Copy Disruptors of Telomeric Silencing in Saccharomyces Cerevisiae. *Genetics* **1998**, *150* (2), 613–632.

(73)   Lacoste, N.; Utley, R. T.; Hunter, J. M.; Poirier, G. G.; C??t??, J. Disruptor of Telomeric Silencing-1 Is a Chromatin-Specific Histone H3 Methyltransferase. *J. Biol. Chem.* **2002**, *277* (34), 30421–30424. https://doi.org/10.1074/jbc.C200366200.

(74)   Van Leeuwen, F.; Gafken, P. R.; Gottschling, D. E. Dot1p Modulates Silencing in Yeast by Methylation of the Nucleosome Core. *Cell* **2002**, *109* (6), 745–756. https://doi.org/10.1016/S0092-8674(02)00759-6.

(75)   Ng, H. H.; Feng, Q.; Wang, H.; Erdjument-Bromage, H.; Tempst, P.; Zhang, Y.; Struhl, K. Lysine Methylation within the Globular Domain of Histone H3 by Dot1 Is Important for Telomeric Silencing and Sir Protein Association. *Genes Dev.* **2002**, *16* (12), 1518–1527. https://doi.org/10.1101/gad.1001502.

(76)   Min, J.; Feng, Q.; Li, Z.; Zhang, Y.; Xu, R. M. Structure of the Catalytic Domain

of Human Dot1L, a Non-SET Domain Nucleosomal Histone Methyltransferase. *Cell* **2003**, *112* (5), 711–723. https://doi.org/10.1016/S0092-8674(03)00114-4.

(77) Schubert, H. L.; Blumenthal, R. M.; Cheng, X. Many Paths to Methyltransfer: A Chronicle of Convergence. *Trends Biochem. Sci.* **2003**, *28* (6), 329–335. https://doi.org/10.1016/S0968-0004(03)00090-2.

(78) Barski, A.; Cuddapah, S.; Cui, K.; Roh, T. Y.; Schones, D. E.; Wang, Z.; Wei, G.; Chepelev, I.; Zhao, K. High-Resolution Profiling of Histone Methylations in the Human Genome. *Cell* **2007**, *129* (4), 823–837. https://doi.org/10.1016/j.cell.2007.05.009.

(79) Lee, J. S.; Smith, E.; Shilatifard, A. The Language of Histone Crosstalk. *Cell* **2010**, *142* (5), 682–685. https://doi.org/10.1016/j.cell.2010.08.011.

(80) Fraga, M. F.; Ballestar, E.; Villar-Garea, A.; Boix-Chornet, M.; Espada, J.; Schotta, G.; Bonaldi, T.; Haydon, C.; Ropero, S.; Petrie, K.; et al. Loss of Acetylation at Lys16 and Trimethylation at Lys20 of Histone H4 Is a Common Hallmark of Human Cancer. *Nat. Genet.* **2005**, *37* (4), 391–400. https://doi.org/10.1038/ng1531.

(81) Wang, Z.; Patel, D. J. Small Molecule Epigenetic Inhibitors Targeted to Histone Lysine Methyltransferases and Demethylases. *Q. Rev. Biophys.* **2013**, *46* (4), 349–373. https://doi.org/10.1017/S0033583513000085.

(82) Helin, K.; Dhanak, D. Chromatin Proteins and Modifications as Drug Targets. *Nature* **2013**, *502* (7472), 480–488. https://doi.org/10.1038/nature12751.

(83) Iwase, S.; Xiang, B.; Ghosh, S.; Ren, T.; Lewis, P. W.; Cochrane, J. C.; Allis, C. D.; Picketts, D. J.; Patel, D. J.; Li, H.; et al. ATRX ADD Domain Links an Atypical Histone Methylation Recognition Mechanism to Human Mental-Retardation Syndrome. *Nat. Struct. Mol. Biol.* **2011**, *18* (7), 769–776. https://doi.org/10.1038/nsmb.2062.

(84) Dillon, S. C.; Zhang, X.; Trievel, R. C.; Cheng, X. The SET-Domain Protein Superfamily: Protein Lysine Methyltransferases. *Genome Biol.* **2005**, *6* (8), 227. https://doi.org/10.1186/gb-2005-6-8-227.

(85) Krivtsov, A. V.; Armstrong, S. A. MLL Translocations, Histone Modifications and Leukaemia Stem-Cell Development. *Nat. Rev. Cancer* **2007**, *7* (11), 823–833. https://doi.org/10.1038/nrc2253.

(86) Rayasam, G. V.; Wendling, O.; Angrand, P.; Mark, M.; Niederreither, K.; Song, L.; Lerouge, T.; Hager, G. L.; Chambon, P.; Losson, R.; et al. NSD1 Is Essential for Early Post-Implantation Development and Has a Catalytically Active SET Domain. *EMBO J.* **2003**, *22* (12), 3153–3163. https://doi.org/10.1093/emboj/cdg288.

(87) Wang, G. G.; Cai, L.; Pasillas, M. P.; Kamps, M. P. NUP98–NSD1 Links H3K36 Methylation to Hox-A Gene Activation and Leukaemogenesis. *Nat. Cell Biol.* **2007**, *9* (7), 804–812. https://doi.org/10.1038/ncb1608.

(88) Kim, J.-Y.; Kee, H. J.; Choe, N.-W.; Kim, S.-M.; Eom, G.-H.; Baek, H. J.; Kook, H.; Kook, H.; Seo, S.-B. Multiple Myeloma-Related WHSC1/MMSET Isoform RE-IIBP Is a Histone Methyltransferase with Transcriptional Repression Activity. *Mol. Cell. Biol.* **2008**, *28* (6), 2023–2034. https://doi.org/10.1128/MCB.02130-07.

(89) Chen, M. W.; Hua, K. T.; Kao, H. J.; Chi, C. C.; Wei, L. H.; Johansson, G.; Shiah, S. G.; Chen, P. S.; Jeng, Y. M.; Cheng, T. Y.; et al. H3K9 Histone Methyltransferase G9a Promotes Lung Cancer Invasion and Metastasis by Silencing the Cell Adhesion Molecule Ep-CAM. *Cancer Res.* **2010**, *70* (20), 7830–7840. https://doi.org/10.1158/0008-5472.CAN-10-0833.

(90) Lawrence, M. S.; Stojanov, P.; Mermel, C. H.; Robinson, J. T.; Garraway, L. A.; Golub, T. R.; Meyerson, M.; Gabriel, S. B.; Lander, E. S.; Getz, G. Discovery and Saturation Analysis of Cancer Genes across 21 Tumour Types. *Nature* **2014**, *505*

(7484), 495–501. https://doi.org/10.1038/nature12912.

(91)   Shanower, G. A.; Muller, M.; Blanton, J. L.; Honti, V.; Gyurkovics, H.; Schedl, P. Characterization of the Grappa Gene, the Drosophila Histone H3 Lysine 79 Methyltransferase. *Genetics* **2005**, *169* (1), 173–184. https://doi.org/10.1534/genetics.104.033191.

(92)   Frederiks, F.; Tzouros, M.; Oudgenoeg, G.; van Welsem, T.; Fornerod, M.; Krijgsveld, J.; van Leeuwen, F. Nonprocessive Methylation by Dot1 Leads to Functional Redundancy of Histone H3K79 Methylation States. *Nat. Struct. Mol. Biol.* **2008**, *15* (6), 550–557. https://doi.org/10.1038/nsmb.1432.

(93)   Jones, B.; Su, H.; Bhat, A.; Lei, H.; Bajko, J.; Hevi, S.; Baltus, G. A.; Kadam, S.; Zhai, H.; Valdez, R.; et al. The Histone H3K79 Methyltransferase Dot1L Is Essential for Mammalian Development and Heterochromatin Structure. *PLoS Genet.* **2008**, *4* (9). https://doi.org/10.1371/journal.pgen.1000190.

(94)   Krogan, N. J.; Dover, J.; Wood, A.; Schneider, J.; Heidt, J.; Boateng, M. A.; Dean, K.; Ryan, O. W.; Golshani, A.; Johnston, M.; et al. The Paf1 Complex Is Required for Histone H3 Methylation by COMPASS and Dot1p: Linking Transcriptional Elongation to Histone Methylation. *Mol. Cell* **2003**, *11* (3), 721–729. https://doi.org/10.1016/S1097-2765(03)00091-1.

(95)   Jacinto, F. V; Ballestar, E.; Esteller, M. Impaired Recruitment of the Histone Methyltransferase DOT1L Contributes to the Incomplete Reactivation of Tumor Suppressor Genes upon DNA Demethylation. *Oncogene* **2009**, *28* (47), 4212–4224. https://doi.org/10.1038/onc.2009.267.

(96)   Krivtsov, A. V.; Feng, Z.; Lemieux, M. E.; Faber, J.; Vempati, S.; Sinha, A. U.; Xia, X.; Jesneck, J.; Bracken, A. P.; Silverman, L. B.; et al. H3K79 Methylation Profiles Define Murine and Human MLL-AF4 Leukemias. *Cancer Cell* **2008**, *14* (5), 355–368. https://doi.org/10.1016/j.ccr.2008.10.001.

(97)   Hess, J. L. MLL: A Histone Methyltransferase Disrupted in Leukemia. *Trends in Molecular Medicine*. 2004. https://doi.org/10.1016/j.molmed.2004.08.005.

(98)   Muntean, A. G.; Hess, J. L. The Pathogenesis of Mixed-Lineage Leukemia. *Annu. Rev. Pathol. Mech. Dis.* **2012**. https://doi.org/10.1146/annurev-pathol-011811-132434.

(99)   Tamai, H.; Inokuchi, K. 11q23/MLL Acute Leukemia : Update of Clinical Aspects. *Journal of clinical and experimental hematopathology : JCEH*. 2010. https://doi.org/10.3960/jslrt.50.91.

(100) Okada, Y.; Feng, Q.; Lin, Y.; Jiang, Q.; Li, Y.; Coffield, V. M.; Su, L.; Xu, G.; Zhang, Y. HDOT1L Links Histone Methylation to Leukemogenesis. *Cell* **2005**. https://doi.org/10.1016/j.cell.2005.02.020.

(101) Bernt, K. M.; Zhu, N.; Sinha, A. U.; Vempati, S.; Faber, J.; Krivtsov, A. V.; Feng, Z.; Punt, N.; Daigle, A.; Bullinger, L.; et al. MLL-Rearranged Leukemia Is Dependent on Aberrant H3K79 Methylation by DOT1L. *Cancer Cell* **2011**. https://doi.org/10.1016/j.ccr.2011.06.010.

(102) Nguyen, A. T.; Taranova, O.; He, J.; Zhang, Y. DOT1L, the H3K79 Methyltransferase, Is Required for MLL-AF9 - Mediated Leukemogenesis. *Blood* **2011**. https://doi.org/10.1182/blood-2011-02-334359.

(103) Chang, M. J.; Wu, H.; Achille, N. J.; Reisenauer, M. R.; Chou, C. W.; Zeleznik-Le, N. J.; Hemenway, C. S.; Zhang, W. Histone H3 Lysine 79 Methyltransferase Dot1 Is Required for Immortalization by MLL Oncogenes. *Cancer Res.* **2010**. https://doi.org/10.1158/0008-5472.CAN-10-3294.

(104) Chen, L.; Deshpande, A. J.; Banka, D.; Bernt, K. M.; Dias, S.; Buske, C.; Olhava, E. J.; Daigle, S. R.; Richon, V. M.; Pollock, R. M.; et al. Abrogation of MLL-AF10 and CALM-AF10-Mediated Transformation through Genetic Inactivation or

Pharmacological Inhibition of the H3K79 Methyltransferase Dot1l. *Leukemia* **2013**. https://doi.org/10.1038/leu.2012.327.

(105) Daigle, S. R.; Olhava, E. J.; Therkelsen, C. A.; Majer, C. R.; Sneeringer, C. J.; Song, J.; Johnston, L. D.; Scott, M. P.; Smith, J. J.; Xiao, Y.; et al. Selective Killing of Mixed Lineage Leukemia Cells by a Potent Small-Molecule DOT1L Inhibitor. *Cancer Cell* **2011**. https://doi.org/10.1016/j.ccr.2011.06.009.

(106) Deshpande, A. J.; Chen, L.; Fazio, M.; Sinha, A. U.; Bernt, K. M.; Banka, D.; Dias, S.; Chang, J.; Olhava, E. J.; Daigle, S. R.; et al. Leukemic Transformation by the MLL-AF6 Fusion Oncogene Requires the H3K79 Methyltransferase Dot1l. *Blood* **2013**. https://doi.org/10.1182/blood-2012-11-465120.

(107) Jo, S. Y.; Granowicz, E. M.; Maillard, I.; Thomas, D.; Hess, J. L. Requirement for Dot1l in Murine Postnatal Hematopoiesis and Leukemogenesis by MLL Translocation. *Blood* **2011**. https://doi.org/10.1182/blood-2010-12-327668.

(108) Sabatino, M.; Rotili, D.; Patsilinakos, A.; Forgione, M.; Tomaselli, D.; Alby, F.; Arimondo, P. B.; Mai, A.; Ragno, R. Disruptor of Telomeric Silencing 1-like (DOT1L): Disclosing a New Class of Non-Nucleoside Inhibitors by Means of Ligand-Based and Structure-Based Approaches. *J. Comput. Aided. Mol. Des.* **2018**. https://doi.org/10.1007/s10822-018-0096-z.

(109) Daigle, S. R.; Olhava, E. J.; Therkelsen, C. A.; Basavapathruni, A.; Jin, L.; Boriack-Sjodin, P. A.; Allain, C. J.; Klaus, C. R.; Raimondi, A.; Scott, M. P.; et al. Potent Inhibition of DOT1L as Treatment of MLL-Fusion Leukemia. *Blood* **2013**. https://doi.org/10.1182/blood-2013-04-497644.

(110) Godfrey, L.; Crump, N. T.; Thorne, R.; Lau, I. J.; Repapi, E.; Dimou, D.; Smith, A. L.; Harman, J. R.; Telenius, J. M.; Oudelaar, A. M.; et al. DOT1L Inhibition Reveals a Distinct Subset of Enhancers Dependent on H3K79 Methylation. *Nat. Commun.* **2019**. https://doi.org/10.1038/s41467-019-10844-3.

(111) Pray-Grant, M. G.; Daniel, J. A.; Schieltz, D.; Yates, J. R.; Grant, P. A. Chd1 Chromodomain Links Histone H3 Methylation with SAGA- and SLIK-Dependent Acetylation. *Nature* **2005**, *433* (7024), 434–438. https://doi.org/10.1038/nature03242.

(112) Lachner, M.; O'Carroll, D.; Rea, S.; Mechtler, K.; Jenuwein, T. Methylation of Histone H3 Lysine 9 Creates a Binding Site for HP1 Proteins. *Nature* **2001**, *410* (6824), 116–120. https://doi.org/10.1038/35065132.

(113) Fischle, W.; Wang, Y.; Jacobs, S. A.; Kim, Y.; Allis, C. D.; Khorasanizadeh, S. Molecular Basis for the Discrimination of Repressive Methyl-Lysine Marks in Histone H3 by Polycomb and HP1 Chromodomains. *Genes Dev.* **2003**, *17* (15), 1870–1881. https://doi.org/10.1101/gad.1110503.

(114) Min, J.; Zhang, Y.; Xu, R. Structural Basis for Specific Binding of Polycomb Chromodomain to Histone H3 Methylated at Lys 27 Structural Basis for Specific Binding of Polycomb Chromodomain to Histone H3 Methylated at Lys 27. **2003**, 1823–1828. https://doi.org/10.1101/gad.269603.

(115) Sanders, S. L.; Portoso, M.; Mata, J.; Bähler, J.; Allshire, R. C.; Kouzarides, T. Methylation of Histone H4 Lysine 20 Controls Recruitment of Crb2 to Sites of DNA Damage. *Cell* **2004**, *119* (5), 603–614. https://doi.org/10.1016/j.cell.2004.11.009.

(116) Wysocka, J.; Swigut, T.; Milne, T. A.; Dou, Y.; Zhang, X.; Burlingame, A. L.; Roeder, R. G.; Brivanlou, A. H.; Allis, C. D. WDR5 Associates with Histone H3 Methylated at K4 and Is Essential for H3 K4 Methylation and Vertebrate Development. *Cell* **2005**, *121* (6), 859–872. https://doi.org/10.1016/j.cell.2005.03.036.

(117) Martin, C.; Zhang, Y. The Diverse Functions of Histone Lysine Methylation. *Nat.*

Rev. **2005**, *6* (11), 838–849. https://doi.org/10.1038/nrm1761.

(118) Lewis, E. B. A Gene Complex Controlling Segmentation in Drosophila. In *Genes, Development, and Cancer: The Life and Work of Edward B. Lewis*; 2007. https://doi.org/10.1007/978-1-4020-6345-9_10.

(119) Whitcomb, S. J.; Basu, A.; Allis, C. D.; Bernstein, E. Polycomb Group Proteins: An Evolutionary Perspective. *Trends Genet.* **2007**. https://doi.org/10.1016/j.tig.2007.08.006.

(120) Scheuermann, J. C.; De Ayala Alonso, A. G.; Oktaba, K.; Ly-Hartig, N.; McGinty, R. K.; Fraterman, S.; Wilm, M.; Muir, T. W.; Müller, J. Histone H2A Deubiquitinase Activity of the Polycomb Repressive Complex PR-DUB. *Nature* **2010**. https://doi.org/10.1038/nature08966.

(121) Klymenko, T.; Papp, B.; Fischle, W.; Köcher, T.; Schelder, M.; Fritsch, C.; Wild, B.; Wilm, M.; Müller, J. A Polycomb Group Protein Complex with Sequence-Specific DNA-Binding and Selective Methyl-Lysine-Binding Activities. *Genes Dev.* **2006**. https://doi.org/10.1101/gad.377406.

(122) Simon, J. A.; Kingston, R. E. Mechanisms of Polycomb Gene Silencing: Knowns and Unknowns. *Nature Reviews Molecular Cell Biology*. 2009. https://doi.org/10.1038/nrm2763.

(123) Schuettengruber, B.; Cavalli, G. Recruitment of Polycomb Group Complexes and Their Role in the Dynamic Regulation of Cell Fate Choice. *Development*. 2009. https://doi.org/10.1242/dev.033902.

(124) Cao, R.; Wang, L.; Wang, H.; Xia, L.; Erdjument-Bromage, H.; Tempst, P.; Jones, R. S.; Zhang, Y. Role of Histone H3 Lysine 27 Methylation in Polycomb-Group Silencing. *Science (80-.).* **2002**. https://doi.org/10.1126/science.1076997.

(125) Agger, K.; Cloos, P. A. C.; Christensen, J.; Pasini, D.; Rose, S.; Rappsilber, J.; Issaeva, I.; Canaani, E.; Salcini, A. E.; Helin, K. UTX and JMJD3 Are Histone H3K27 Demethylases Involved in HOX Gene Regulation and Development. *Nature* **2007**. https://doi.org/10.1038/nature06145.

(126) Hong, S. H.; Cho, Y. W.; Yu, L. R.; Yu, H.; Veenstra, T. D.; Ge, K. Identification of JmjC Domain-Containing UTX and JMJD3 as Histone H3 Lysine 27 Demethylases. *Proc. Natl. Acad. Sci. U. S. A.* **2007**. https://doi.org/10.1073/pnas.0707292104.

(127) Lee, M. G.; Villa, R.; Trojer, P.; Norman, J.; Yan, K.-P.; Reinberg, D.; Croce, L. D.; Shiekhattar, R. Demethylation of H3K27 Regulates Polycomb Recruitment and H2A Ubiquitination. *Science (80-.).* **2007**, *318* (5849), 447–450. https://doi.org/10.1126/science.1149042.

(128) Lan, F.; Bayliss, P. E.; Rinn, J. L.; Whetstine, J. R.; Wang, J. K.; Chen, S.; Iwase, S.; Alpatov, R.; Issaeva, I.; Canaani, E.; et al. A Histone H3 Lysine 27 Demethylase Regulates Animal Posterior Development. *Nature* **2007**. https://doi.org/10.1038/nature06192.

(129) De Santa, F.; Totaro, M. G.; Prosperini, E.; Notarbartolo, S.; Testa, G.; Natoli, G. The Histone H3 Lysine-27 Demethylase Jmjd3 Links Inflammation to Inhibition of Polycomb-Mediated Gene Silencing. *Cell* **2007**, *130* (6), 1083–1094. https://doi.org/10.1016/j.cell.2007.08.019.

(130) Lulla, R. R.; Saratsis, A. M.; Hashizume, R. Mutations in Chromatin Machinery and Pediatric High-Grade Glioma. *Science Advances*. 2016. https://doi.org/10.1126/sciadv.1501354.

(131) Blackledge, N. P.; Farcas, A. M.; Kondo, T.; King, H. W.; McGouran, J. F.; Hanssen, L. L. P.; Ito, S.; Cooper, S.; Kondo, K.; Koseki, Y.; et al. Variant PRC1 Complex-Dependent H2A Ubiquitylation Drives PRC2 Recruitment and Polycomb Domain Formation. *Cell* **2014**. https://doi.org/10.1016/j.cell.2014.05.004.

(132) Cooper, S.; Dienstbier, M.; Hassan, R.; Schermelleh, L.; Sharif, J.; Blackledge, N. P.; DeMarco, V.; Elderkin, S.; Koseki, H.; Klose, R.; et al. Targeting Polycomb to Pericentric Heterochromatin in Embryonic Stem Cells Reveals a Role for H2AK119u1 in PRC2 Recruitment. *Cell Rep*. **2014**. https://doi.org/10.1016/j.celrep.2014.04.012.

(133) Holoch, D.; Margueron, R. Mechanisms Regulating PRC2 Recruitment and Enzymatic Activity. *Trends in Biochemical Sciences*. 2017. https://doi.org/10.1016/j.tibs.2017.04.003.

(134) Margueron, R.; Reinberg, D. The Polycomb Complex PRC2 and Its Mark in Life. *Nature*. 2011. https://doi.org/10.1038/nature09784.

(135) Margueron, R.; Li, G.; Sarma, K.; Blais, A.; Zavadil, J.; Woodcock, C. L.; Dynlacht, B. D.; Reinberg, D. Ezh1 and Ezh2 Maintain Repressive Chromatin through Different Mechanisms. *Mol. Cell* **2008**. https://doi.org/10.1016/j.molcel.2008.11.004.

(136) Cao, R.; Zhang, Y. SUZ12 Is Required for Both the Histone Methyltransferase Activity and the Silencing Function of the EED-EZH2 Complex. *Mol. Cell* **2004**. https://doi.org/10.1016/j.molcel.2004.06.020.

(137) Ketel, C. S.; Andersen, E. F.; Vargas, M. L.; Suh, J.; Strome, S.; Simon, J. A. Subunit Contributions to Histone Methyltransferase Activities of Fly and Worm Polycomb Group Complexes. *Mol. Cell. Biol.* **2005**. https://doi.org/10.1128/mcb.25.16.6857-6868.2005.

(138) Pasini, D.; Bracken, A. P.; Jensen, M. R.; Denchi, E. L.; Helin, K. Suz12 Is Essential for Mouse Development and for EZH2 Histone Methyltransferase Activity. *EMBO J*. **2004**. https://doi.org/10.1038/sj.emboj.7600402.

(139) He, A.; Shen, X.; Ma, Q.; Cao, J.; von Gise, A.; Zhou, P.; Wang, G.; Marquez, V. E.; Orkin, S. H.; Pu, W. T. PRC2 Directly Methylates GATA4 and Represses Its Transcriptional Activity. *Genes Dev*. **2012**. https://doi.org/10.1101/gad.173930.111.

(140) Vasanthakumar, A.; Xu, D.; Lun, A. T.; Kueh, A. J.; Gisbergen, K. P.; Iannarella, N.; Li, X.; Yu, L.; Wang, D.; Williams, B. R.; et al. A Non-canonical Function of Ezh2 Preserves Immune Homeostasis. *EMBO Rep*. **2017**. https://doi.org/10.15252/embr.201643237.

(141) Kim, K. H.; Roberts, C. W. M. Targeting EZH2 in Cancer. *Nature Medicine*. 2016. https://doi.org/10.1038/nm.4036.

(142) Zhang, Y.; Justin, N.; Wilson, J. R.; Gamblin, S. J. Comment on "Structural Basis of Histone H3K27 Trimethylation by an Active Polycomb Repressive Complex 2." *Science (80-.)*. **2016**, *354* (6319), 1543. https://doi.org/10.1126/science.aaf6236.

(143) Poepsel, S.; Kasinath, V.; Nogales, E. Cryo-EM Structures of PRC2 Simultaneously Engaged with Two Functionally Distinct Nucleosomes. *Nat. Struct. Mol. Biol.* **2018**. https://doi.org/10.1038/s41594-018-0023-y.

(144) Oksuz, O.; Narendra, V.; Lee, C. H.; Descostes, N.; LeRoy, G.; Raviram, R.; Blumenberg, L.; Karch, K.; Rocha, P. P.; Garcia, B. A.; et al. Capturing the Onset of PRC2-Mediated Repressive Domain Formation. *Mol. Cell* **2018**. https://doi.org/10.1016/j.molcel.2018.05.023.

(145) Margueron, R.; Justin, N.; Ohno, K.; Sharpe, M. L.; Son, J.; Drury, W. J.; Voigt, P.; Martin, S. R.; Taylor, W. R.; De Marco, V.; et al. Role of the Polycomb Protein EED in the Propagation of Repressive Histone Marks. *Nature* **2009**. https://doi.org/10.1038/nature08398.

(146) Højfeldt, J. W.; Laugesen, A.; Willumsen, B. M.; Damhofer, H.; Hedehus, L.; Tvardovskiy, A.; Mohammad, F.; Jensen, O. N.; Helin, K. Accurate H3K27 Methylation Can Be Established de Novo by SUZ12-Directed PRC2. *Nat. Struct.*

Mol. Biol. **2018**. https://doi.org/10.1038/s41594-018-0036-6.

(147) Nekrasov, M.; Wild, B.; Müller, J. Nucleosome Binding and Histone Methyltransferase Activity of Drosophila PRC2. *EMBO Rep*. **2005**. https://doi.org/10.1038/sj.embor.7400376.

(148) Mendenhall, E. M.; Koche, R. P.; Truong, T.; Zhou, V. W.; Issac, B.; Chi, A. S.; Ku, M.; Bernstein, B. E. GC-Rich Sequence Elements Recruit PRC2 in Mammalian ES Cells. *PLoS Genet*. **2010**. https://doi.org/10.1371/journal.pgen.1001244.

(149) Riising, E. M.; Comet, I.; Leblanc, B.; Wu, X.; Johansen, J. V.; Helin, K. Gene Silencing Triggers Polycomb Repressive Complex 2 Recruitment to CpG Islands Genome Wide. *Mol. Cell* **2014**. https://doi.org/10.1016/j.molcel.2014.06.005.

(150) Vizán, P.; Beringer, M.; Ballaré, C.; Di Croce, L. Role of PRC2-Associated Factors in Stem Cells and Disease. *FEBS J*. **2015**. https://doi.org/10.1111/febs.13083.

(151) Aranda, S.; Mas, G.; Di Croce, L. Regulation of Gene Transcription by Polycomb Proteins. *Sci. Adv*. **2015**. https://doi.org/10.1126/sciadv.1500737.

(152) Sanulli, S.; Justin, N.; Teissandier, A.; Ancelin, K.; Portoso, M.; Caron, M.; Michaud, A.; Lombard, B.; da Rocha, S. T.; Offer, J.; et al. Jarid2 Methylation via the PRC2 Complex Regulates H3K27me3 Deposition during Cell Differentiation. *Mol. Cell* **2015**. https://doi.org/10.1016/j.molcel.2014.12.020.

(153) Yap, D. B.; Chu, J.; Berg, T.; Schapira, M.; Cheng, S. W. G.; Moradian, A.; Morin, R. D.; Mungall, A. J.; Meissner, B.; Boyle, M.; et al. Somatic Mutations at EZH2 Y641 Act Dominantly through a Mechanism of Selectively Altered PRC2 Catalytic Activity, to Increase H3K27 Trimethylation. *Blood* **2011**. https://doi.org/10.1182/blood-2010-11-321208.

(154) Chang, C. J.; Hung, M. C. The Role of EZH2 in Tumour Progression. *British Journal of Cancer*. 2012. https://doi.org/10.1038/bjc.2011.551.

(155) Chase, A.; Cross, N. C. P. Aberrations of EZH2 in Cancer. *Clinical Cancer Research*. 2011. https://doi.org/10.1158/1078-0432.CCR-10-2156.

(156) Wang, C.; Liu, Z.; Woo, C. W.; Li, Z.; Wang, L.; Wei, J. S.; Marquez, V. E.; Bates, S. E.; Jin, Q.; Khan, J.; et al. EZH2 Mediates Epigenetic Silencing of Neuroblastoma Suppressor Genes CASZ1, CLU, RUNX3, and NGFR. *Cancer Res*. **2012**. https://doi.org/10.1158/0008-5472.CAN-11-0961.

(157) Kim, J.; Yu, J. Interrogating Genomic and Epigenomic Data to Understand Prostate Cancer. *Biochimica et Biophysica Acta - Reviews on Cancer*. 2012. https://doi.org/10.1016/j.bbcan.2011.12.003.

(158) Fujimoto, K.; Oimoto, N.; Katsuno, K.; Inouye, M. Effective Stabilisation of α-Helical Structures in Short Peptides with Acetylenic Cross-Linking Agents. *Chem. Commun*. **2004**, *4* (11), 1280–1281. https://doi.org/10.1039/b403615h.

(159) Nichol, J. N.; Dupéré-Richer, D.; Ezponda, T.; Licht, J. D.; Miller, W. H. H3K27 Methylation: A Focal Point of Epigenetic Deregulation in Cancer. In *Advances in Cancer Research*; 2016. https://doi.org/10.1016/bs.acr.2016.05.001.

(160) Kleer, C. G.; Cao, Q.; Varambally, S.; Shen, R.; Ota, I.; Tomlins, S. A.; Ghosh, D.; Sewalt, R. G. A. B.; Otte, A. P.; Hayes, D. F.; et al. EZH2 Is a Marker of Aggressive Breast Cancer and Promotes Neoplastic Transformation of Breast Epithelial Cells. *Proc. Natl. Acad. Sci. U. S. A*. **2003**, *100* (20), 11606–11611. https://doi.org/10.1073/pnas.1933744100.

(161) Varambally, S.; Dhanasekaran, S. M.; Zhou, M.; Barrette, T. R.; Kumar-Sinha, C.; Sanda, M. G.; Ghosh, D.; Pienta, K. J.; Sewalt, R. G. A. B.; Rubin, M. A.; et al. The Polycomb Group Protein EZH2 Is Involved in Progression of Prostate Cancer. *Nature* **2002**. https://doi.org/10.1038/nature01075.

(162) Bracken, A. P.; Pasini, D.; Capra, M.; Prosperini, E.; Colli, E.; Helin, K. EZH2 Is Downstream of the PRB-E2F Pathway, Essential for Proliferation and Amplified in Cancer. *EMBO J.* **2003**. https://doi.org/10.1093/emboj/cdg542.

(163) Bachmann, I. M.; Halvorsen, O. J.; Collett, K.; Stefansson, I. M.; Straume, O.; Haukaas, S. A.; Salvesen, H. B.; Otte, A. P.; Akslen, L. A. EZH2 Expression Is Associated with High Proliferation Rate and Aggressive Tumor Subgroups in Cutaneous Melanoma and Cancers of the Endometrium, Prostate, and Breast. *J. Clin. Oncol.* **2006**. https://doi.org/10.1200/JCO.2005.01.5180.

(164) Sauvageau, M.; Sauvageau, G. Polycomb Group Proteins: Multi-Faceted Regulators of Somatic Stem Cells and Cancer. *Cell Stem Cell.* 2010. https://doi.org/10.1016/j.stem.2010.08.002.

(165) Kamminga, L. M.; Bystrykh, L. V.; De Boer, A.; Houwer, S.; Douma, J.; Weersing, E.; Dontje, B.; De Haan, G. The Polycomb Group Gene Ezh2 Prevents Hematopoietic Stem Cell Exhaustion. *Blood* **2006**. https://doi.org/10.1182/blood-2005-09-3585.

(166) Herrera-Merchan, A.; Arranz, L.; Ligos, J. M.; de Molina, A.; Dominguez, O.; Gonzalez, S. Retraction: Ectopic Expression of the Histone Methyltransferase Ezh2 in Haematopoietic Stem Cells Causes Myeloproliferative Disease. *Nature communications.* 2017. https://doi.org/10.1038/ncomms14005.

(167) Vo, B. H. T.; Li, C.; Morgan, M. A.; Theurillat, I.; Finkelstein, D.; Wright, S.; Hyle, J.; Smith, S. M. C.; Fan, Y.; Wang, Y. D.; et al. Inactivation of Ezh2 Upregulates Gfi1 and Drives Aggressive Myc-Driven Group 3 Medulloblastoma. *Cell Rep.* **2017**. https://doi.org/10.1016/j.celrep.2017.02.073.

(168) Cardenas, H.; Zhao, J.; Vieth, E.; Nephew, K. P.; Matei, D. EZH2 Inhibition Promotes Epithelial-to-Mesenchymal Transition in Ovarian Cancer Cells. *Oncotarget* **2016**. https://doi.org/10.18632/oncotarget.11497.

(169) Honma, K.; Udono, H.; Kohno, T.; Yamamoto, K.; Ogawa, A.; Takemori, T.; Kumatori, A.; Suzuki, S.; Matsuyama, T.; Yui, K. Interferon Regulatory Factor 4 Negatively Regulates the Production of Proinflammatory Cytokines by Macropages in Response to LPS. *Proc. Natl. Acad. Sci. U. S. A.* **2005**. https://doi.org/10.1073/pnas.0504226102.

(170) Yoshida, H.; Nadanaka, S.; Sato, R.; Mori, K. XBP1 Is Critical to Protect Cells from Endoplasmic Reticulum Stress: Evidence from Site-2 Protease-Deficient Chinese Hamster Ovary Cells. *Cell Struct. Funct.* **2006**. https://doi.org/10.1247/csf.06016.

(171) Turner, C. A.; Mack, D. H.; Davis, M. M. Blimp-1, a Novel Zinc Finger-Containing Protein That Can Drive the Maturation of B Lymphocytes into Immunoglobulin-Secreting Cells. *Cell* **1994**. https://doi.org/10.1016/0092-8674(94)90321-2.

(172) Sciammas, R.; Davis, M. M. Modular Nature of Blimp-1 in the Regulation of Gene Expression during B Cell Maturation. *J. Immunol.* **2004**. https://doi.org/10.4049/jimmunol.172.9.5427.

(173) Alzrigat, M.; Párraga, A. A.; Agarwal, P.; Zureigat, H.; österborg, A.; Nahi, H.; Ma, A.; Jin, J.; Nilsson, K.; öberg, F.; et al. EZH2 Inhibition in Multiple Myeloma Downregulates Myeloma Associated Oncogenes and Upregulates MicroRNAs with Potential Tumor Suppressor Functions. *Oncotarget* **2017**. https://doi.org/10.18632/oncotarget.14378.

(174) Yan, J.; Ng, S. B.; Tay, J. L. S.; Lin, B.; Koh, T. L.; Tan, J.; Selvarajan, V.; Liu, S. C.; Bi, C.; Wang, S.; et al. EZH2 Overexpression in Natural Killer/T-Cell Lymphoma Confers Growth Advantage Independently of Histone Methyltransferase Activity. *Blood* **2013**. https://doi.org/10.1182/blood-2012-08-

450494.

(175) Xu, K.; Wu, Z. J.; Groner, A. C.; He, H. H.; Cai, C.; Lis, R. T.; Wu, X.; Stack, E. C.; Loda, M.; Liu, T.; et al. EZH2 Oncogenic Activity in Castration-Resistant Prostate Cancer Cells Is Polycomb-Independent. *Science (80-.).* **2012**. https://doi.org/10.1126/science.1227604.

(176) Kim, E.; Kim, M.; Woo, D. H.; Shin, Y.; Shin, J.; Chang, N.; Oh, Y. T.; Kim, H.; Rheey, J.; Nakano, I.; et al. Phosphorylation of EZH2 Activates STAT3 Signaling via STAT3 Methylation and Promotes Tumorigenicity of Glioblastoma Stem-like Cells. *Cancer Cell* **2013**. https://doi.org/10.1016/j.ccr.2013.04.008.

(177) McCabe, M. T.; Graves, A. P.; Ganji, G.; Diaz, E.; Halsey, W. S.; Jiang, Y.; Smitheman, K. N.; Ott, H. M.; Pappalardi, M. B.; Allen, K. E.; et al. Mutation of A677 in Histone Methyltransferase EZH2 in Human B-Cell Lymphoma Promotes Hypertrimethylation of Histone H3 on Lysine 27 (H3K27). *Proc. Natl. Acad. Sci. U. S. A.* **2012**. https://doi.org/10.1073/pnas.1116418109.

(178) Majer, C. R.; Jin, L.; Scott, M. P.; Knutson, S. K.; Kuntz, K. W.; Keilhack, H.; Smith, J. J.; Moyer, M. P.; Richon, V. M.; Copeland, R. A.; et al. A687V EZH2 Is a Gain-of-Function Mutation Found in Lymphoma Patients. *FEBS Lett.* **2012**. https://doi.org/10.1016/j.febslet.2012.07.066.

(179) Sneeringer, C. J.; Scott, M. P.; Kuntz, K. W.; Knutson, S. K.; Pollock, R. M.; Richon, V. M.; Copeland, R. A. Coordinated Activities of Wild-Type plus Mutant EZH2 Drive Tumor-Associated Hypertrimethylation of Lysine 27 on Histone H3 (H3K27) in Human B-Cell Lymphomas. *Proc. Natl. Acad. Sci. U. S. A.* **2010**. https://doi.org/10.1073/pnas.1012525107.

(180) Nikoloski, G.; Langemeijer, S. M. C.; Kuiper, R. P.; Knops, R.; Massop, M.; Tönnissen, E. R. L. T. M.; Van Der Heijden, A.; Scheele, T. N.; Vandenberghe, P.; De Witte, T.; et al. Somatic Mutations of the Histone Methyltransferase Gene EZH2 in Myelodysplastic Syndromes. *Nat. Genet.* **2010**. https://doi.org/10.1038/ng.620.

(181) Ntziachristos, P.; Tsirigos, A.; Vlierberghe, P. Van; Nedjic, J.; Trimarchi, T.; Flaherty, M. S.; Ferres-Marco, D.; Da Ros, V.; Tang, Z.; Siegle, J.; et al. Genetic Inactivation of the Polycomb Repressive Complex 2 in T Cell Acute Lymphoblastic Leukemia. *Nat. Med.* **2012**. https://doi.org/10.1038/nm.2651.

(182) Ernst, T.; Chase, A. J.; Score, J.; Hidalgo-Curtis, C. E.; Bryant, C.; Jones, A. V.; Waghorn, K.; Zoi, K.; Ross, F. M.; Reiter, A.; et al. Inactivating Mutations of the Histone Methyltransferase Gene EZH2 in Myeloid Disorders. *Nat. Genet.* **2010**. https://doi.org/10.1038/ng.621.

(183) Lee, T. I.; Jenner, R. G.; Boyer, L. A.; Guenther, M. G.; Levine, S. S.; Kumar, R. M.; Chevalier, B.; Johnstone, S. E.; Cole, M. F.; Isono, K. ichi; et al. Control of Developmental Regulators by Polycomb in Human Embryonic Stem Cells. *Cell* **2006**. https://doi.org/10.1016/j.cell.2006.02.043.

(184) Ezhkova, E.; Pasolli, H. A.; Parker, J. S.; Stokes, N.; Su, I. hsin; Hannon, G.; Tarakhovsky, A.; Fuchs, E. Ezh2 Orchestrates Gene Expression for the Stepwise Differentiation of Tissue-Specific Stem Cells. *Cell* **2009**. https://doi.org/10.1016/j.cell.2008.12.043.

(185) Shan, Y.; Liang, Z.; Xing, Q.; Zhang, T.; Wang, B.; Tian, S.; Huang, W.; Zhang, Y.; Yao, J.; Zhu, Y.; et al. PRC2 Specifies Ectoderm Lineages and Maintains Pluripotency in Primed but Not Naïve ESCs. *Nat. Commun.* **2017**. https://doi.org/10.1038/s41467-017-00668-4.

(186) Piunti, A.; Pasini, D. Epigenetic Factors in Cancer Development: Polycomb Group Proteins. *Futur. Oncol.* **2011**. https://doi.org/10.2217/fon.10.157.

(187) Chang, C. J.; Yang, J. Y.; Xia, W.; Chen, C. Te; Xie, X.; Chao, C. H.; Woodward,

W. A.; Hsu, J. M.; Hortobagyi, G. N.; Hung, M. C. EZH2 Promotes Expansion of Breast Tumor Initiating Cells through Activation of RAF1-β-Catenin Signaling. *Cancer Cell* **2011**. https://doi.org/10.1016/j.ccr.2010.10.035.

(188) Karantanos, T.; Chistofides, A.; Barhdan, K.; Li, L.; Boussiotis, V. A. Regulation of T Cell Differentiation and Function by EZH2. *Frontiers in Immunology*. 2016. https://doi.org/10.3389/fimmu.2016.00172.

(189) Caretti, G.; Di Padova, M.; Micales, B.; Lyons, G. E.; Sartorelli, V. The Polycomb Ezh2 Methyltransferase Regulates Muscle Gene Expression and Skeletal Muscle Differentiation. *Genes Dev*. **2004**. https://doi.org/10.1101/gad.1241904.

(190) Sher, F.; Rößler, R.; Brouwer, N.; Balasubramaniyan, V.; Boddeke, E.; Copray, S. Differentiation of Neural Stem Cells into Oligodendrocytes: Involvement of the Polycomb Group Protein Ezh2. *Stem Cells* **2008**. https://doi.org/10.1634/stemcells.2008-0121.

(191) Hwang, W. W.; Salinas, R. D.; Siu, J. J.; Kelley, K. W.; Delgado, R. N.; Paredes, M. F.; Alvarez-Buylla, A.; Oldham, M. C.; Lim, D. A. Distinct and Separable Roles for EZH2 in Neurogenic Astroglia. *Elife* **2014**. https://doi.org/10.7554/eLife.02439.001.

(192) Pereira, J. D.; Sansom, S. N.; Smith, J.; Dobenecker, M. W.; Tarakhovsky, A.; Livesey, F. J. Ezh2, the Histone Methyltransferase of PRC2, Regulates the Balance between Self-Renewal and Differentiation in the Cerebral Cortex. *Proc. Natl. Acad. Sci. U. S. A.* **2010**. https://doi.org/10.1073/pnas.1002530107.

(193) Acharyya, S.; Sharma, S. M.; Cheng, A. S.; Ladner, K. J.; He, W.; Kline, W.; Wang, H.; Ostrowski, M. C.; Huang, T. H.; Guttridge, D. C. TNF Inhibits Notch-1 in Skeletal Muscle Cells by Ezh2 and DNA Methylation Mediated Repression: Implications in Duchenne Muscular Dystrophy. *PLoS One* **2010**. https://doi.org/10.1371/journal.pone.0012479.

(194) Palacios, D.; Mozzetta, C.; Consalvi, S.; Caretti, G.; Saccone, V.; Proserpio, V.; Marquez, V. E.; Valente, S.; Mai, A.; Forcales, S. V.; et al. TNF/P38α/Polycomb Signaling to Pax7 Locus in Satellite Cells Links Inflammation to the Epigenetic Control of Muscle Regeneration. *Cell Stem Cell* **2010**. https://doi.org/10.1016/j.stem.2010.08.013.

(195) Chen, H.; Gu, X.; Su, I. H.; Bottino, R.; Contreras, J. L.; Tarakhovsky, A.; Kim, S. K. Polycomb Protein Ezh2 Regulates Pancreatic β-Cell Ink4a/Arf Expression and Regeneration in Diabetes Mellitus. *Genes Dev*. **2009**. https://doi.org/10.1101/gad.1742509.

(196) Zhou, J. X.; Dhawan, S.; Fu, H.; Snyder, E.; Bottino, R.; Kundu, S.; Kim, S. K.; Bhushan, A. Combined Modulation of Polycomb and Trithorax Genes Rejuvenates β Cell Replication. *J. Clin. Invest*. **2013**. https://doi.org/10.1172/JCI69468.

(197) Wei, Y.; Chen, Y. H.; Li, L. Y.; Lang, J.; Yeh, S. P.; Shi, B.; Yang, C. C.; Yang, J. Y.; Lin, C. Y.; Lai, C. C.; et al. CDK1-Dependent Phosphorylation of EZH2 Suppresses Methylation of H3K27 and Promotes Osteogenic Differentiation of Human Mesenchymal Stem Cells. *Nat. Cell Biol*. **2011**. https://doi.org/10.1038/ncb2139.

(198) Chen, Y. H.; Yeh, F. L.; Yeh, S. P.; Ma, H. T.; Hung, S. C.; Hung, M. C.; Li, L. Y. Myocyte Enhancer Factor-2 Interacting Transcriptional Repressor (MITR) Is a Switch That Promotes Osteogenesis and Inhibits Adipogenesis of Mesenchymal Stem Cells by Inactivating Peroxisome Proliferator-Activated Receptor γ-2. *J. Biol. Chem*. **2011**. https://doi.org/10.1074/jbc.M110.199612.

(199) Wang, L.; Jin, Q.; Lee, J. E.; Su, I. H.; Ge, K. Histone H3K27 Methyltransferase Ezh2 Represses Wnt Genes to Facilitate Adipogenesis. *Proc. Natl. Acad. Sci. U. S. A.* **2010**. https://doi.org/10.1073/pnas.1000031107.

(200) Blanquart, C.; Linot, C.; Cartron, P.-F.; Tomaselli, D.; Mai, A.; Bertrand, P. Epigenetic Metalloenzymes. *Curr. Med. Chem.* **2018**. https://doi.org/10.2174/0929867325666180706105903.

(201) Walport, L. J.; Hopkinson, R. J.; Schofield, C. J. Mechanisms of Human Histone and Nucleic Acid Demethylases. *Current Opinion in Chemical Biology*. 2012. https://doi.org/10.1016/j.cbpa.2012.09.015.

(202) Klose, R. J.; Kallin, E. M.; Zhang, Y. JmjC-Domain-Containing Proteins and Histone Demethylation. *Nat. Rev. Genet.* **2006**. https://doi.org/10.1038/nrg1945.

(203) Tsukada, Y. I.; Fang, J.; Erdjument-Bromage, H.; Warren, M. E.; Borchers, C. H.; Tempst, P.; Zhang, Y. Histone Demethylation by a Family of JmjC Domain-Containing Proteins. *Nature* **2006**. https://doi.org/10.1038/nature04433.

(204) Thinnes, C. C.; England, K. S.; Kawamura, A.; Chowdhury, R.; Schofield, C. J.; Hopkinson, R. J. Targeting Histone Lysine Demethylases - Progress, Challenges, and the Future. *Biochimica et Biophysica Acta - Gene Regulatory Mechanisms*. 2014. https://doi.org/10.1016/j.bbagrm.2014.05.009.

(205) Yang, Z.; Jiang, J.; Stewart, D. M.; Qi, S.; Yamane, K.; Li, J.; Zhang, Y.; Wong, J. AOF1 Is a Histone H3K4 Demethylase Possessing Demethylase Activity-Independent Repression Function. *Cell Res.* **2010**, *20* (3), 276–287. https://doi.org/10.1038/cr.2010.90.

(206) Fang, R.; Chen, F.; Dong, Z.; Hu, D.; Barbera, A. J.; Clark, E. A.; Fang, J.; Yang, Y.; Mei, P.; Rutenberg, M.; et al. LSD2/KDM1B and Its Cofactor NPAC/GLYR1 Endow a Structural and Molecular Model for Regulation of H3K4 Demethylation. *Mol. Cell* **2013**, *49* (3), 558–570. https://doi.org/10.1016/j.molcel.2012.11.019.

(207) Fang, R.; Barbera, A. J.; Xu, Y.; Rutenberg, M.; Leonor, T.; Bi, Q.; Lan, F.; Mei, P.; Yuan, G. C.; Lian, C.; et al. Human LSD2/KDM1b/AOF1 Regulates Gene Transcription by Modulating Intragenic H3K4me2 Methylation. *Mol. Cell* **2010**, *39* (2), 222–233. https://doi.org/10.1016/j.molcel.2010.07.008.

(208) Ciccone, D. N.; Su, H.; Hevi, S.; Gay, F.; Lei, H.; Bajko, J.; Xu, G.; Li, E.; Chen, T. KDM1B Is a Histone H3K4 Demethylase Required to Establish Maternal Genomic Imprints. *Nature* **2009**, *461* (7262), 415–418. https://doi.org/10.1038/nature08315.

(209) Takeuchi, T.; Takeuchi, T.; Katoh-fukui, Y.; Katoh-fukui, Y.; Tsuchiya, R.; Tsuchiya, R.; Sciences, L.; Sciences, L. Gene Trap Capture of a Novel Mouse Gene,. *Genes Dev.* **1995**, 1211–1222. https://doi.org/10.1101/gad.9.10.1211.

(210) Frescas, D.; Guardavaccaro, D.; Bassermann, F.; Koyama-Nasu, R.; Pagano, M. JHDM1B/FBXL10 Is a Nucleolar Protein That Represses Transcription of Ribosomal RNA Genes. *Nature* **2007**, *450* (7167), 309–313. https://doi.org/10.1038/nature06255.

(211) Wu, X.; Johansen, J. V.; Helin, K. Fbxl10/Kdm2b Recruits Polycomb Repressive Complex 1 to CpG Islands and Regulates H2A Ubiquitylation. *Mol. Cell* **2013**, *49* (6), 1134–1146. https://doi.org/10.1016/j.molcel.2013.01.016.

(212) Farcas, A. M.; Blackledge, N. P.; Sudbery, I.; Long, H. K.; McGouran, J. F.; Rose, N. R.; Lee, S.; Sims, D.; Cerase, A.; Sheahan, T. W.; et al. KDM2B Links the Polycomb Repressive Complex 1 (PRC1) to Recognition of CpG Islands. *Elife* **2012**, *2012* (1), 1–26. https://doi.org/10.7554/eLife.00205.

(213) Højfeldt, J. W.; Agger, K.; Helin, K. Histone Lysine Demethylases as Targets for Anticancer Therapy. *Nat. Rev. Drug Discov.* **2013**, *12* (12), 917–930. https://doi.org/10.1038/nrd4154.

(214) Yamane, K.; Toumazou, C.; Tsukada, Y. ichi; Erdjument-Bromage, H.; Tempst, P.; Wong, J.; Zhang, Y. JHDM2A, a JmjC-Containing H3K9 Demethylase, Facilitates Transcription Activation by Androgen Receptor. *Cell* **2006**, *125* (3),

483–495. https://doi.org/10.1016/j.cell.2006.03.027.

(215) Inagaki, T.; Tachibana, M.; Magoori, K.; Kudo, H.; Tanaka, T.; Okamura, M.; Naito, M.; Kodama, T.; Shinkai, Y.; Sakai, J. Obesity and Metabolic Syndrome in Histone Demethylase JHDM2a-Deficient Mice. *Genes to Cells* **2009**, *14* (8), 991–1001. https://doi.org/10.1111/j.1365-2443.2009.01326.x.

(216) Liu, Z.; Zhou, S.; Liao, L.; Chen, X.; Meistrich, M.; Xu, J. Jmjd1a Demethylase-Regulated Histone Modification Is Essential for CAMP-Response Element Modulator-Regulated Gene Expression and Spermatogenesis. *J. Biol. Chem.* **2010**, *285* (4), 2758–2770. https://doi.org/10.1074/jbc.M109.066845.

(217) Krieg, A. J.; Rankin, E. B.; Chan, D.; Razorenova, O.; Fernandez, S.; Giaccia, A. J. Regulation of the Histone Demethylase JMJD1A by Hypoxia-Inducible Factor 1 Enhances Hypoxic Gene Expression and Tumor Growth. *Mol. Cell. Biol.* **2010**, *30* (1), 344–353. https://doi.org/10.1128/MCB.00444-09.

(218) Park, S. J.; Kim, J. G.; Son, T. G.; Yi, J. M.; Kim, N. D.; Yang, K.; Heo, K. The Histone Demethylase JMJD1A Regulates Adrenomedullin-Mediated Cell Proliferation in Hepatocellular Carcinoma under Hypoxia. *Biochem. Biophys. Res. Commun.* **2013**, *434* (4), 722–727. https://doi.org/10.1016/j.bbrc.2013.03.091.

(219) Hu, Z.; Gomes, I.; Horrigan, S. K.; Kravarusic, J.; Mar, B.; Arbieva, Z.; Chyna, B.; Fulton, N.; Edassery, S.; Raza, a; et al. A Novel Nuclear Protein, 5qNCA (LOC51780) Is a Candidate for the Myeloid Leukemia Tumor Suppressor Gene on Chromosome 5 Band Q31. *Oncogene* **2001**, *20* (47), 6946–6954. https://doi.org/10.1038/sj.onc.1204850.

(220) Brauchle, M.; Yao, Z.; Arora, R.; Thigale, S.; Clay, I.; Inverardi, B.; Fletcher, J.; Taslimi, P.; Acker, M. G.; Gerrits, B.; et al. Protein Complex Interactor Analysis and Differential Activity of KDM3 Subfamily Members Towards H3K9 Methylation. *PLoS One* **2013**, *8* (4), 1–12. https://doi.org/10.1371/journal.pone.0060549.

(221) Braig, M.; Lee, S.; Loddenkemper, C.; Rudolph, C.; Peters, A. H. F. M.; Schlegelberger, B.; Stein, H.; Dörken, B.; Jenuwein, T.; Schmitt, C. A. Oncogene-Induced Senescence as an Initial Barrier in Lymphoma Development. *Nature* **2005**, *436* (7051), 660–665. https://doi.org/10.1038/nature03841.

(222) Rui, L.; Emre, N. C. T.; Kruhlak, M. J.; Chung, H. J.; Steidl, C.; Slack, G.; Wright, G. W.; Lenz, G.; Ngo, V. N.; Shaffer, A. L.; et al. Cooperative Epigenetic Modulation by Cancer Amplicon Genes. *Cancer Cell* **2010**, *18* (6), 590–605. https://doi.org/10.1016/j.ccr.2010.11.013.

(223) Benevolenskaya, E. V.; Murray, H. L.; Branton, P.; Young, R. A.; Kaelin, W. G. Binding of PRB to the PHD Protein RBP2 Promotes Cellular Differentiation. *Mol. Cell* **2005**, *18* (6), 623–635. https://doi.org/10.1016/j.molcel.2005.05.012.

(224) Schmitz, S. U.; Albert, M.; Malatesta, M.; Morey, L.; Johansen, J. V; Bak, M.; Tommerup, N.; Abarrategui, I.; Helin, K. Jarid1b Targets Genes Regulating Development and Is Involved in Neural Differentiation. *EMBO J.* **2011**, *30* (22), 4586–4600. https://doi.org/10.1038/emboj.2011.383.

(225) Lu, P. J.; Sundquist, K.; Baeckstrom, D.; Poulsom, R.; Hanby, A.; Meier-Ewert, S.; Jones, T.; Mitchell, M.; Pitha-Rowe, P.; Freemont, P.; et al. A Novel Gene (PLU-1) Containing Highly Conserved Putative DNA/Chromatin Binding Motifs Is Specifically up-Regulated in Breast Cancer. *J. Biol. Chem.* **1999**, *274* (22), 15633–15645. https://doi.org/10.1074/jbc.274.22.15633.

(226) Hayami, S.; Yoshimatsu, M.; Veerakumarasivam, A.; Unoki, M.; Iwai, Y.; Tsunoda, T.; Field, H. I.; Kelly, J. D.; Neal, D. E.; Yamaue, H.; et al. Overexpression of the JmjC Histone Demethylase KDM5B in Human Carcinogenesis: Involvement in the Proliferation of Cancer Cells through the

E2F/RB Pathway. *Mol. Cancer* **2010**, *9* (1), 59. https://doi.org/10.1186/1476-4598-9-59.

(227) Xiang, Y.; Zhu, Z.; Han, G.; Ye, X.; Xu, B.; Peng, Z.; Ma, Y.; Yu, Y.; Lin, H.; Chen, A. P.; et al. JARID1B Is a Histone H3 Lysine 4 Demethylase Up-Regulated in Prostate Cancer. *Proc. Natl. Acad. Sci. U. S. A.* **2007**, *104* (49), 19226–19231. https://doi.org/10.1073/pnas.0700735104.

(228) Yamane, K.; Tateishi, K.; Klose, R. J.; Fang, J.; Fabrizio, L. A.; Erdjument-Bromage, H.; Taylor-Papadimitriou, J.; Tempst, P.; Zhang, Y. PLU-1 Is an H3K4 Demethylase Involved in Transcriptional Repression and Breast Cancer Cell Proliferation. *Mol. Cell* **2007**, *25* (6), 801–812. https://doi.org/10.1016/j.molcel.2007.03.001.

(229) Roesch, A.; Fukunaga-Kalabis, M.; Schmidt, E. C.; Zabierowski, S. E.; Brafford, P. A.; Vultur, A.; Basu, D.; Gimotty, P.; Vogt, T.; Herlyn, M. A Temporarily Distinct Subpopulation of Slow-Cycling Melanoma Cells Is Required for Continuous Tumor Growth. *Cell* **2010**, *141* (4), 583–594. https://doi.org/10.1016/j.cell.2010.04.020.

(230) Smith, J. A.; White, E. A.; Sowa, M. E.; Powell, M. L. C.; Ottinger, M.; Harper, J. W.; Howley, P. M. Genome-Wide SiRNA Screen Identifies SMCX, EP400, and Brd4 as E2-Dependent Regulators of Human Papillomavirus Oncogene Expression. *Proc. Natl. Acad. Sci.* **2010**, *107* (8), 3752–3757. https://doi.org/10.1073/pnas.0914818107.

(231) De Santa, F.; Narang, V.; Yap, Z. H.; Tusi, B. K.; Burgold, T.; Austenaa, L.; Bucci, G.; Caganova, M.; Notarbartolo, S.; Casola, S.; et al. Jmjd3 Contributes to the Control of Gene Expression in LPS-Activated Macrophages. *EMBO J.* **2009**, *28* (21), 3341–3352. https://doi.org/10.1038/emboj.2009.271.

(232) Issaeva, I.; Zonis, Y.; Rozovskaia, T.; Orlovsky, K.; Croce, C. M.; Nakamura, T.; Mazo, A.; Eisenbach, L.; Canaani, E. Knockdown of ALR (MLL2) Reveals ALR Target Genes and Leads to Alterations in Cell Adhesion and Growth. *Mol. Cell. Biol.* **2007**, *27* (5), 1889–1903. https://doi.org/10.1128/MCB.01506-06.

(233) van Haaften, G.; Dalgliesh, G. L.; Davies, H.; Chen, L.; Bignell, G.; Greenman, C.; Edkins, S.; Hardy, C.; O'Meara, S.; Teague, J.; et al. Somatic Mutations of the Histone H3K27 Demethylase Gene UTX in Human Cancer. *Nat. Genet.* **2009**, *41* (5), 521–523. https://doi.org/10.1038/ng.349.

(234) Shmakova, A.; Batie, M.; Druker, J.; Rocha, S. Chromatin and Oxygen Sensing in the Context of JmjC Histone Demethylases. *Biochemical Journal*. 2014. https://doi.org/10.1042/BJ20140754.

(235) Crea, F.; Sun, L.; Mai, A.; Chiang, Y. T.; Farrar, W. L.; Danesi, R.; Helgason, C. D. The Emerging Role of Histone Lysine Demethylases in Prostate Cancer. *Molecular Cancer*. 2012. https://doi.org/10.1186/1476-4598-11-52.

(236) Shahbazian, M. D.; Grunstein, M. Functions of Site-Specific Histone Acetylation and Deacetylation. *Annu. Rev. Biochem.* **2007**, *76* (1), 75–100. https://doi.org/10.1146/annurev.biochem.76.052705.162114.

(237) Groth, A.; Rocha, W.; Verreault, A.; Almouzni, G. Chromatin Challenges during DNA Replication and Repair. *Cell* **2007**, *128* (4), 721–733. https://doi.org/10.1016/j.cell.2007.01.030.

(238) Schneider, A.; Chatterjee, S.; Bousiges, O.; Selvi, B. R.; Swaminathan, A.; Cassel, R.; Blanc, F.; Kundu, T. K.; Boutillier, A. L. Acetyltransferases (HATs) as Targets for Neurological Therapeutics. *Neurotherapeutics* **2013**, *10* (4), 568–588. https://doi.org/10.1007/s13311-013-0204-7.

(239) Davie, J. R. Covalent Modifications of Histones: Expression from Chromatin Templates. *Curr. Opin. Genet. Dev.* **1998**, *8* (2), 173–178.

https://doi.org/10.1016/S0959-437X(98)80138-X.

(240) Turner, B. M. Histone Acetylation and an Epigenetic Code. *BioEssays* **2000**, *22* (9), 836–845. https://doi.org/10.1002/1521-1878(200009)22:9<836::AID-BIES9>3.0.CO;2-X.

(241) Allis, C. D.; Berger, S. L.; Cote, J.; Dent, S.; Jenuwien, T.; Kouzarides, T.; Pillus, L.; Reinberg, D.; Shi, Y.; Shiekhattar, R.; et al. New Nomenclature for Chromatin-Modifying Enzymes. *Cell* **2007**, *131* (4), 633–636. https://doi.org/10.1016/j.cell.2007.10.039.

(242) Marmorstein, R.; Trievel, R. C. Histone Modifying Enzymes: Structures, Mechanisms, and Specificities. *Biochim. Biophys. Acta - Gene Regul. Mech.* **2009**, *1789* (1), 58–68. https://doi.org/10.1016/j.bbagrm.2008.07.009.

(243) Berndsen, C. E.; Denu, J. M. Catalysis and Substrate Selection by Histone/Protein Lysine Acetyltransferases. *Curr. Opin. Struct. Biol.* **2008**, *18* (6), 682–689. https://doi.org/10.1016/j.sbi.2008.11.004.

(244) Lee, K. K.; Workman, J. L. Histone Acetyltransferase Complexes: One Size Doesn't Fit All. *Nat. Rev. Mol. Cell Biol.* **2007**, *8* (4), 284–295. https://doi.org/10.1038/nrm2145.

(245) Dekker, F. J.; Haisma, H. J. Histone Acetyl Transferases as Emerging Drug Targets. *Drug Discov. Today* **2009**, *14* (19–20), 942–948. https://doi.org/10.1016/j.drudis.2009.06.008.

(246) Gu, W.; Roeder, R. G. Activation of P53 Sequence-Specific DNA Binding by Acetylation of the P53 C-Terminal Domain. *Cell* **1997**, *90* (4), 595–606. https://doi.org/10.1016/S0092-8674(00)80521-8.

(247) Dornan, D.; Shimizu, H.; Perkins, N. D.; Hupp, T. R. DNA-Dependent Acetylation of P53 by the Transcription Coactivator P300. *J. Biol. Chem.* **2003**, *278* (15), 13431–13441. https://doi.org/10.1074/jbc.M211460200.

(248) Zhang, Y. . et al. The Structure and Function of Histone Deacetylases: The Target for Anti-Cancer Therapy. *Curr Med Chem* **2008**, *15* (7), 2840–2849.

(249) RUIJTER, A. J. M. de; GENNIP, A. H. van; CARON, H. N.; KEMP, S.; KUILENBURG, A. B. P. van. Histone Deacetylases (HDACs): Characterization of the Classical HDAC Family. *Biochem. J.* **2003**, *370* (3), 737–749. https://doi.org/10.1042/bj20021321.

(250) Gregoretti, I. V.; Lee, Y. M.; Goodson, H. V. Molecular Evolution of the Histone Deacetylase Family: Functional Implications of Phylogenetic Analysis. *J. Mol. Biol.* **2004**, *338* (1), 17–31. https://doi.org/10.1016/j.jmb.2004.02.006.

(251) Kao, H. Y.; Lee, C. H.; Komarov, A.; Han, C. C.; Evans, R. M. Isolation and Characterization of Mammalian HDAC10, a Novel Histone Deacetylase. *J. Biol. Chem.* **2002**, *277* (1), 187–193. https://doi.org/10.1074/jbc.M108931200.

(252) Gao, L.; Cueto, M. A.; Asselbergs, F.; Atadja, P. Cloning and Functional Characterization of HDAC11, a Novel Member of the Human Histone Deacetylase Family. *J. Biol. Chem.* **2002**, *277* (28), 25748–25755. https://doi.org/10.1074/jbc.M111871200.

(253) Grozinger, C. M.; Hassig, C. a; Schreiber, S. L. Three Proteins Define a Class of Human Histone Deacetylases Related to Yeast Hda1p. *Proc. Natl. Acad. Sci. U. S. A.* **1999**, *96* (9), 4868–4873. https://doi.org/10.1073/pnas.96.9.4868.

(254) Yang, X.-J.; Seto, E. The Rpd3/Hda1 Family of Lysine Deacetylases: From Bacteria and Yeast to Mice and Men. *Nat. Rev. Mol. Cell Biol.* **2008**, *9* (3), 206–218. https://doi.org/10.1038/nrm2346.

(255) Marks, P. A.; Xu, W. S. Histone Deacetylase Inhibitors: Potential in Cancer Therapy. *J. Cell. Biochem.* **2009**, *107* (4), 600–608. https://doi.org/10.1002/jcb.22185.

(256) Newkirk, T. L.; Bowers, A. A.; Williams, R. M. Discovery, Biological Activity, Synthesis and Potential Therapeutic Utility of Naturally Occurring Histone Deacetylase Inhibitors. *Natural Product Reports*. 2009. https://doi.org/10.1039/b817886k.

(257) Ahringer, J. NuRD and SIN3: Histone Deacetylase Complexes in Development. *Trends Genet*. **2000**, *16* (8), 351–356. https://doi.org/10.1016/S0168-9525(00)02066-7.

(258) Huang, Y.; Myers, S. J.; Dingledine, R. Transcriptional Repression by REST: Recruitment of Sin3A and Histone Deacetylase to Neuronal Genes. *Nat Neurosci* **1999**, *2* (10), 867–872. https://doi.org/10.1038/13165.

(259) McKinsey, T. a; Zhang, C. L.; Lu, J.; Olson, E. N. Signal-Dependent Nuclear Export of a Histone Deacetylase Regulates Muscle Differentiation. *Nature* **2000**, *408* (6808), 106–111. https://doi.org/10.1038/35040593.

(260) Verdin, E.; Dequiedt, F.; Kasler, H. G. Class II Histone Deacetylases: Versatile Regulators. *Trends Genet*. **2003**, *19* (5), 286–293. https://doi.org/10.1016/S0168-9525(03)00073-8.

(261) Berdeaux, R.; Goebel, N.; Banaszynski, L.; Takemori, H.; Wandless, T.; Shelton, G. D.; Montminy, M. SIK1 Is a Class II HDAC Kinase That Promotes Survival of Skeletal Myocytes. *Nat. Med.* **2007**, *13* (5), 597–603. https://doi.org/10.1038/nm1573.

(262) Chang, S.; Bezprozvannaya, S.; Li, S.; Olson, E. N. An Expression Screen Reveals Modulators of Class II Histone Deacetylase Phosphorylation. *Proc. Natl. Acad. Sci. U. S. A.* **2005**, *102* (23), 8120–8125. https://doi.org/10.1073/pnas.0503275102.

(263) Yang, X. J.; Seto, E. Collaborative Spirit of Histone Deacetylases in Regulating Chromatin Structure and Gene Expression. *Curr. Opin. Genet. Dev.* **2003**, *13* (2), 143–153. https://doi.org/10.1016/S0959-437X(03)00015-7.

(264) Frye, R. A. Phylogenetic Classification of Prokaryotic and Eukaryotic Sir2-like Proteins. *Biochem. Biophys. Res. Commun.* **2000**, *273* (2), 793–798. https://doi.org/10.1006/bbrc.2000.3000.

(265) Chang, J. H.; Kim, H. C.; Hwang, K. Y.; Lee, J. W.; Jackson, S. P.; Bell, S. D.; Cho, Y. Structural Basis for the NAD-Dependent Deacetylase Mechanism of Sir2. *J. Biol. Chem.* **2002**, *277* (37), 34489–34498. https://doi.org/10.1074/jbc.M205460200.

(266) Brunmeir, R.; Lagger, S.; Seiser, C. Histone Deacetylase 1 and 2-Controlled Embryonic Development and Cell Differentiation. **2009**, *289* (April), 275–289. https://doi.org/10.1387/ijdb.082649rb.

(267) Weichert, W.; Ro, A.; Niesporek, S.; Noske, A.; Buckendahl, A.; Dietel, M.; Gekeler, V.; Boehm, M.; Beckers, T.; Denkert, C. Human Cancer Biology Class I Histone Deacetylase Expression Has Independent Prognostic Impact in Human Colorectal Cancer : Specific Role of Class I Histone Deacetylases In Vitro and In Vivo. **2008**, *14* (6), 1669–1678. https://doi.org/10.1158/1078-0432.CCR-07-0990.

(268) Glaser, K. B.; Li, J.; Staver, M. J.; Wei, R.; Albert, D. H.; Davidsen, S. K. Role of Class I and Class II Histone Deacetylases in Carcinoma Cells Using SiRNA. **2003**, *310*, 529–536. https://doi.org/10.1016/j.bbrc.2003.09.043.

(269) Senese, S.; Zaragoza, K.; Minardi, S.; Muradore, I.; Ronzoni, S.; Passafaro, A.; Bernard, L.; Draetta, G. F.; Alcalay, M.; Seiser, C.; et al. Role for Histone Deacetylase 1 in Human Tumor Cell Proliferation . **2007**, *27* (13), 4784–4795. https://doi.org/10.1128/MCB.00494-07.

(270) Huang, B. H.; Laban, M.; Leung, C.; Lee, L.; Lee, C. K.; Raju, G. C.; Hooi, S. C. Inhibition of Histone Deacetylase 2 Increases Apoptosis and P21 Cip1 / WAF1 Expression , Independent of Histone Deacetylase 1. **2005**, 395–404.

https://doi.org/10.1038/sj.cdd.4401567.

(271) Bhaskara, S.; Knutson, S. K.; Jiang, G.; Chandrasekharan, M. B.; Wilson, A. J.; Zheng, S.; Yenamandra, A.; Locke, K.; Yuan, J. L.; Bonine-Summers, A. R.; et al. Hdac3 Is Essential for the Maintenance of Chromatin Structure and Genome Stability. *Cancer Cell* **2010**, *18* (5), 436–447. https://doi.org/10.1016/j.ccr.2010.10.022.

(272) Moser, M. A.; Hagelkruys, A.; Seiser, C. Transcription and beyond: The Role of Mammalian Class I Lysine Deacetylases. *Chromosoma* **2014**, *123* (1–2), 67–78. https://doi.org/10.1007/s00412-013-0441-x.

(273) Decroos, C.; Bowman, C. M.; Moser, J. A. S.; Christianson, K. E.; Deardorff, M. A.; Christianson, D. W. Compromised Structure and Function of HDAC8 Mutants Identified in Cornelia de Lange Syndrome Spectrum Disorders. *ACS Chem. Biol.* **2014**. https://doi.org/10.1021/cb5003762.

(274) Song, S.; Wang, Y.; Xu, P.; Yang, R.; Ma, Z.; Liang, S.; Zhang, G. The Inhibition of Histone Deacetylase 8 Suppresses Proliferation and Inhibits Apoptosis in Gastric Adenocarcinoma. *Int. J. Oncol.* **2015**. https://doi.org/10.3892/ijo.2015.3182.

(275) Wang, Y.; Xu, P.; Yao, J.; Yang, R.; Shi, Z.; Zhu, X.; Feng, X.; Gao, S. MicroRNA-216b Is Down-Regulated in Human Gastric Adenocarcinoma and Inhibits Proliferation and Cell Cycle Progression by Targeting Oncogene HDAC8. *Targeted Oncology*. 2016. https://doi.org/10.1007/s11523-015-0390-9.

(276) Chakrabarti, A.; Oehme, I.; Witt, O.; Oliveira, G.; Sippl, W.; Romier, C.; Pierce, R. J.; Jung, M. HDAC8: A Multifaceted Target for Therapeutic Interventions. *Trends Pharmacol. Sci.* **2015**, *36* (7), 481–492. https://doi.org/10.1016/j.tips.2015.04.013.

(277) Marek, M.; Kannan, S.; Hauser, A. T.; Moraes Mourão, M.; Caby, S.; Cura, V.; Stolfa, D. A.; Schmidtkunz, K.; Lancelot, J.; Andrade, L.; et al. Structural Basis for the Inhibition of Histone Deacetylase 8 (HDAC8), a Key Epigenetic Player in the Blood Fluke Schistosoma Mansoni. *PLoS Pathog.* **2013**. https://doi.org/10.1371/journal.ppat.1003645.

(278) Stolfa, D. A.; Marek, M.; Lancelot, J.; Hauser, A. T.; Walter, A.; Leproult, E.; Melesina, J.; Rumpf, T.; Wurtz, J. M.; Cavarelli, J.; et al. Molecular Basis for the Antiparasitic Activity of a Mercaptoacetamide Derivative That Inhibits Histone Deacetylase 8 (HDAC8) from the Human Pathogen Schistosoma Mansoni. *J. Mol. Biol.* **2014**. https://doi.org/10.1016/j.jmb.2014.03.007.

(279) Parra, M.; Verdin, E. Regulatory Signal Transduction Pathways for Class IIa Histone Deacetylases. *Curr. Opin. Pharmacol.* **2010**, *10* (4), 454–460. https://doi.org/10.1016/j.coph.2010.04.004.

(280) McKinsey, T. A. Derepression of Pathological Cardiac Genes by Members of the CaM Kinase Superfamily. *Cardiovasc. Res.* **2007**, *73* (4), 667–677. https://doi.org/10.1016/j.cardiores.2006.11.036.

(281) Kawaguchi, Y.; Kovacs, J. J.; McLaurin, A.; Vance, J. M.; Ito, A.; Yao, T. P. The Deacetylase HDAC6 Regulates Aggresome Formation and Cell Viability in Response to Misfolded Protein Stress. *Cell* **2003**, *115* (6), 727–738. https://doi.org/10.1016/S0092-8674(03)00939-5.

(282) Pandey, U. B.; Nie, Z.; Batlevi, Y.; McCray, B. A.; Ritson, G. P.; Nedelsky, N. B.; Schwartz, S. L.; DiProspero, N. A.; Knight, M. A.; Schuldiner, O.; et al. HDAC6 Rescues Neurodegeneration and Provides an Essential Link between Autophagy and the UPS. *Nature* **2007**, *447* (7146), 860–864. https://doi.org/10.1038/nature05853.

(283) Lee, J. H.; Jeong, E. G.; Choi, M. C.; Kim, S. H.; Park, J. H.; Song, S. H.; Park, J.; Bang, Y. J.; Kim, T. Y. Inhibition of Histone Deacetylase 10 Induces Thioredoxin-

Interacting Protein and Causes Accumulation of Reactive Oxygen Species in SNU-620 Human Gastric Cancer Cells. *Mol. Cells* **2010**, *30* (2), 107–112. https://doi.org/10.1007/s10059-010-0094-z.

(284) Villagra, A.; Sotomayor, E. M.; Seto, E. Histone Deacetylases and the Immunological Network: Implications in Cancer and Inflammation. *Oncogene* **2010**, *29* (2), 157–173. https://doi.org/10.1038/onc.2009.334.

(285) Deubzer, H. E.; Schier, M. C.; Oehme, I.; Lodrini, M.; Haendler, B.; Sommer, A.; Witt, O. HDAC11 Is a Novel Drug Target in Carcinomas. *Int. J. Cancer* **2013**, *132* (9), 2200–2208. https://doi.org/10.1002/ijc.27876.

(286) Klar, A. J. S.; Fogel, S.; Macleod, K. Mar1 - A Regulator of the HMa and HMα Loci in Saccharomyces Cerevisiae. *Genetics* **1979**.

(287) Woodcock, C. L.; Ghosh, R. P. Chromatin Higher-Order Structure and Dynamics. *Cold Spring Harbor perspectives in biology*. 2010. https://doi.org/10.1101/cshperspect.a000596.

(288) Gottlieb, S.; Esposito, R. E. A New Role for a Yeast Transcriptional Silencer Gene, SIR2, in Regulation of Recombination in Ribosomal DNA. *Cell* **1989**. https://doi.org/10.1016/0092-8674(89)90681-8.

(289) Aparicio, O. M.; Billington, B. L.; Gottschling, D. E. Modifiers of Position Effect Are Shared between Telomeric and Silent Mating-Type Loci in S. Cerevisiae. *Cell* **1991**. https://doi.org/10.1016/0092-8674(91)90049-5.

(290) Braunstein, M.; Rose, A. B.; Holmes, S. G.; David Allis, C.; Broach, J. R. Transcriptional Silencing in Yeast Is Associated with Reduced Nucleosome Acetylation. *Genes Dev.* **1993**. https://doi.org/10.1101/gad.7.4.592.

(291) Brachmann, C. B.; Sherman, J. M.; Devine, S. E.; Cameron, E. E.; Pillus, L.; Boeke, J. D. The SIR2 Gene Family, Conserved from Bacteria to Humans, Functions in Silencing, Cell Cycle Progression, and Chromosome Stability. *Genes Dev.* **1995**. https://doi.org/10.1101/gad.9.23.2888.

(292) Derbyshire, M. K.; Weinstock, K. G.; Strathern, J. N. HST1, a New Member of the SIR2 Family of Genes. *Yeast* **1996**. https://doi.org/10.1002/(SICI)1097-0061(19960615)12:7<631::AID-YEA960>3.0.CO;2-8.

(293) Frye, R. A. Characterization of Five Human CDNAs with Homology to the Yeast SIR2 Gene: Sir2-like Proteins (Sirtuins) Metabolize NAD and May Have Protein ADP-Ribosyltransferase Activity. *Biochem. Biophys. Res. Commun.* **1999**. https://doi.org/10.1006/bbrc.1999.0897.

(294) Yamagata, K.; Goto, Y.; Nishimasu, H.; Morimoto, J.; Ishitani, R.; Dohmae, N.; Takeda, N.; Nagai, R.; Komuro, I.; Suga, H.; et al. Structural Basis for Potent Inhibition of SIRT2 Deacetylase by a Macrocyclic Peptide Inducing Dynamic Structural Change. *Structure* **2014**. https://doi.org/10.1016/j.str.2013.12.001.

(295) Tanno, M.; Sakamoto, J.; Miura, T.; Shimamoto, K.; Horio, Y. Nucleocytoplasmic Shuttling of the NAD + -Dependent Histone Deacetylase SIRT1. *J. Biol. Chem.* **2007**, *282* (9), 6823–6832. https://doi.org/10.1074/jbc.M609554200.

(296) North, B. J.; Verdin, E. Interphase Nucleo-Cytoplasmic Shuttling and Localization of SIRT2 during Mitosis. *PLoS One* **2007**, *2* (8). https://doi.org/10.1371/journal.pone.0000784.

(297) Osborne, B.; Cooney, G. J.; Turner, N. Are Sirtuin Deacylase Enzymes Important Modulators of Mitochondrial Energy Metabolism? *Biochim. Biophys. Acta - Gen. Subj.* **2014**, *1840* (4), 1295–1302. https://doi.org/10.1016/J.BBAGEN.2013.08.016.

(298) Yu, J.; Qin, B.; Wu, F.; Qin, S.; Nowsheen, S.; Shan, S.; Zayas, J.; Pei, H.; Lou, Z.; Wang, L. Regulation of Serine-Threonine Kinase Akt Activation by NAD+-Dependent Deacetylase SIRT7. *Cell Rep.* **2017**. https://doi.org/10.1016/j.celrep.2017.01.009.

(299) Pan, P. W.; Feldman, J. L.; Devries, M. K.; Dong, A.; Edwards, A. M.; Denu, J. M. Structure and Biochemical Functions of SIRT6. *J. Biol. Chem.* **2011**. https://doi.org/10.1074/jbc.M111.218990.

(300) Madsen, A. S.; Andersen, C.; Daoud, M.; Anderson, K. A.; Laursen, J. S.; Chakladar, S.; Huynh, F. K.; Colaço, A. R.; Backos, D. S.; Fristrup, P.; et al. Investigating the Sensitivity of NAD+-Dependent Sirtuin Deacylation Activities to NADH. *J. Biol. Chem.* **2016**. https://doi.org/10.1074/jbc.M115.668699.

(301) Haigis, M. C.; Mostoslavsky, R.; Haigis, K. M.; Fahie, K.; Christodoulou, D. C.; Murphy, A. J. J.; Valenzuela, D. M.; Yancopoulos, G. D.; Karow, M.; Blander, G.; et al. SIRT4 Inhibits Glutamate Dehydrogenase and Opposes the Effects of Calorie Restriction in Pancreatic β Cells. *Cell* **2006**. https://doi.org/10.1016/j.cell.2006.06.057.

(302) Anderson, K. A.; Huynh, F. K.; Fisher-Wellman, K.; Stuart, J. D.; Peterson, B. S.; Douros, J. D.; Wagner, G. R.; Thompson, J. W.; Madsen, A. S.; Green, M. F.; et al. SIRT4 Is a Lysine Deacylase That Controls Leucine Metabolism and Insulin Secretion. *Cell Metab.* **2017**. https://doi.org/10.1016/j.cmet.2017.03.003.

(303) Peng, C.; Lu, Z.; Xie, Z.; Cheng, Z.; Chen, Y.; Tan, M.; Luo, H.; Zhang, Y.; He, W.; Yang, K.; et al. The First Identification of Lysine Malonylation Substrates and Its Regulatory Enzyme. *Mol. Cell. Proteomics* **2011**. https://doi.org/10.1074/mcp.M111.012658.

(304) Du, J.; Zhou, Y.; Su, X.; Yu, J. J.; Khan, S.; Jiang, H.; Kim, J.; Woo, J.; Kim, J. H.; Choi, B. H.; et al. Sirt5 Is a NAD-Dependent Protein Lysine Demalonylase and Desuccinylase. *Science (80-.).* **2011**. https://doi.org/10.1126/science.1207861.

(305) Tan, M.; Peng, C.; Anderson, K. A.; Chhoy, P.; Xie, Z.; Dai, L.; Park, J.; Chen, Y.; Huang, H.; Zhang, Y.; et al. Lysine Glutarylation Is a Protein Posttranslational Modification Regulated by SIRT5. *Cell Metab.* **2014**. https://doi.org/10.1016/j.cmet.2014.03.014.

(306) Michishita, E.; McCord, R. A.; Berber, E.; Kioi, M.; Padilla-Nash, H.; Damian, M.; Cheung, P.; Kusumoto, R.; Kawahara, T. L. A.; Barrett, J. C.; et al. SIRT6 Is a Histone H3 Lysine 9 Deacetylase That Modulates Telomeric Chromatin. *Nature* **2008**. https://doi.org/10.1038/nature06736.

(307) Mostoslavsky, R.; Chua, K. F.; Lombard, D. B.; Pang, W. W.; Fischer, M. R.; Gellon, L.; Liu, P.; Mostoslavsky, G.; Franco, S.; Murphy, M. M.; et al. Genomic Instability and Aging-like Phenotype in the Absence of Mammalian SIRT6. *Cell* **2006**. https://doi.org/10.1016/j.cell.2005.11.044.

(308) Carafa, V.; Rotili, D.; Forgione, M.; Cuomo, F.; Serretiello, E.; Hailu, G. S.; Jarho, E.; Lahtela-Kakkonen, M.; Mai, A.; Altucci, L. Sirtuin Functions and Modulation: From Chemistry to the Clinic. *Clinical Epigenetics*. 2016. https://doi.org/10.1186/s13148-016-0224-3.

(309) Bitterman, K. J.; Anderson, R. M.; Cohen, H. Y.; Latorre-Esteves, M.; Sinclair, D. A. Inhibition of Silencing and Accelerated Aging by Nicotinamide, a Putative Negative Regulator of Yeast Sir2 and Human SIRT1. *J. Biol. Chem.* **2002**. https://doi.org/10.1074/jbc.M205670200.

(310) Schmidt, M. T.; Smith, B. C.; Jackson, M. D.; Denu, J. M. Coenzyme Specificity of Sir2 Protein Deacetylases. Implications for Physiological Regulation. *J. Biol. Chem.* **2004**. https://doi.org/10.1074/jbc.M407484200.

(311) Hoff, K. G.; Avalos, J. L.; Sens, K.; Wolberger, C. Insights into the Sirtuin Mechanism from Ternary Complexes Containing NAD+ and Acetylated Peptide. *Structure* **2006**. https://doi.org/10.1016/j.str.2006.06.006.

(312) Cen, Y.; Y. Youn, D.; A. Sauve, A. Advances in Characterization of Human Sirtuin Isoforms: Chemistries, Targets and Therapeutic Applications. *Curr. Med.*

Chem. **2011**. https://doi.org/10.2174/092986711795590084.

(313) Moniot, S.; Weyand, M.; Steegborn, C. Structures, Substrates, and Regulators of Mammalian Sirtuins - Opportunities and Challenges for Drug Development. *Front. Pharmacol*. **2012**. https://doi.org/10.3389/fphar.2012.00016.

(314) Sanders, B. D.; Jackson, B.; Marmorstein, R. Structural Basis for Sirtuin Function: What We Know and What We Don't. *Biochimica et Biophysica Acta - Proteins and Proteomics*. 2010. https://doi.org/10.1016/j.bbapap.2009.09.009.

(315) Chakrabarty, S. P.; Balaram, H. Reversible Binding of Zinc in Plasmodium Falciparum Sir2: Structure and Activity of the Apoenzyme. *Biochim. Biophys. Acta - Proteins Proteomics* **2010**. https://doi.org/10.1016/j.bbapap.2010.06.010.

(316) Min, J.; Landry, J.; Sternglanz, R.; Xu, R. M. Crystal Structure of a SIR2 Homolog-NAD Complex. *Cell* **2001**. https://doi.org/10.1016/S0092-8674(01)00317-8.

(317) Prasad, G. S.; Wahlberg, M.; Sridhar, V.; Sundaresan, V.; Yamaguchi, M.; Hatefi, Y.; Stout, C. D. Crystal Structures of Transhydrogenase Domain I with and without Bound NADH. *Biochemistry* **2002**. https://doi.org/10.1021/bi020251f.

(318) Jiang, H.; Khan, S.; Wang, Y.; Charron, G.; He, B.; Sebastian, C.; Du, J.; Kim, R.; Ge, E.; Mostoslavsky, R.; et al. SIRT6 Regulates TNF-α Secretion through Hydrolysis of Long-Chain Fatty Acyl Lysine. *Nature* **2013**. https://doi.org/10.1038/nature12038.

(319) Cosgrove, M. S.; Bever, K.; Avalos, J. L.; Muhammad, S.; Zhang, X.; Wolberger, C. The Structural Basis of Sirtuin Substrate Affinity. *Biochemistry* **2006**. https://doi.org/10.1021/bi0526332.

(320) Moniot, S.; Schutkowski, M.; Steegborn, C. Crystal Structure Analysis of Human Sirt2 and Its ADP-Ribose Complex. *J. Struct. Biol*. **2013**. https://doi.org/10.1016/j.jsb.2013.02.012.

(321) Jin, L.; Wei, W.; Jiang, Y.; Peng, H.; Cai, J.; Mao, C.; Dai, H.; Choy, W.; Bemis, J. E.; Jirousek, M. R.; et al. Crystal Structures of Human SIRT3 Displaying Substrate-Induced Conformational Changes. *J. Biol. Chem*. **2009**, *284* (36), 24394–24405. https://doi.org/10.1074/jbc.M109.014928.

(322) Zhao, X.; Allison, D.; Condon, B.; Zhang, F.; Gheyi, T.; Zhang, A.; Ashok, S.; Russell, M.; MacEwan, I.; Qian, Y.; et al. The 2.5 Å Crystal Structure of the SIRT1 Catalytic Domain Bound to Nicotinamide Adenine Dinucleotide (NAD +) and an Indole (EX527 Analogue) Reveals a Novel Mechanism of Histone Deacetylase Inhibition. *J. Med. Chem*. **2013**. https://doi.org/10.1021/jm301431y.

(323) Zhou, Y.; Zhang, H.; He, B.; Du, J.; Lin, H.; Cerione, R. A.; Hao, Q. The Bicyclic Intermediate Structure Provides Insights into the Desuccinylation Mechanism of Human Sirtuin 5 (SIRT5). *J. Biol. Chem*. **2012**. https://doi.org/10.1074/jbc.M112.384511.

(324) Feldman, J. L.; Dittenhafer-Reed, K. E.; Kudo, N.; Thelen, J. N.; Ito, A.; Yoshida, M.; Denu, J. M. Kinetic and Structural Basis for Acyl-Group Selectivity and NAD$^+$ Dependence in Sirtuin-Catalyzed Deacylation. *Biochemistry* **2015**. https://doi.org/10.1021/acs.biochem.5b00150.

(325) Finkel, T.; Deng, C. X.; Mostoslavsky, R. Recent Progress in the Biology and Physiology of Sirtuins. *Nature*. 2009. https://doi.org/10.1038/nature08197.

(326) Roth, M.; Chen, W. Y. Sorting out Functions of Sirtuins in Cancer. *Oncogene*. 2014. https://doi.org/10.1038/onc.2013.120.

(327) Martinez-Pastor, B.; Mostoslavsky, R. Sirtuins, Metabolism, and Cancer. *Front. Pharmacol*. **2012**. https://doi.org/10.3389/fphar.2012.00022.

(328) Yuan, H.; Su, L.; Chen, W. Y. The Emerging and Diverse Roles of Sirtuins in Cancer: A Clinical Perspective. *Onco. Targets. Ther*. **2013**.

https://doi.org/10.2147/OTT.S37750.

(329) Guarente, L. The Many Faces of Sirtuins: Sirtuins and the Warburg Effect. *Nat. Med.* **2014**. https://doi.org/10.1038/nm.3438.

(330) Eun, J. C.; Sang, J. N.; Keun, S. K.; Chan, Y. K.; Park, B. H.; Ho, S. P.; Lee, H.; Myoung, J. C.; Myoung, J. K.; Dong, G. L.; et al. Expression of DBC1 and SIRT1 Is Associated with Poor Prognosis of Gastric Carcinoma. *Clin. Cancer Res.* **2009**. https://doi.org/10.1158/1078-0432.CCR-08-3329.

(331) Stünkel, W.; Peh, B. K.; Tan, Y. C.; Nayagam, V. M.; Wang, X.; Salto-Tellez, M.; Ni, B. H.; Entzeroth, M.; Wood, J. Function of the SIRTI Protein Deacetylase in Cancer. *Biotechnol. J.* **2007**. https://doi.org/10.1002/biot.200700087.

(332) Huffman, D. M.; Grizzle, W. E.; Bamman, M. M.; Kim, J. S.; Eltoum, I. A.; Elgavish, A.; Nagy, T. R. SIRT1 Is Significantly Elevated in Mouse and Human Prostate Cancer. *Cancer Res.* **2007**. https://doi.org/10.1158/0008-5472.CAN-07-0085.

(333) Hida, Y.; Kubo, Y.; Murao, K.; Arase, S. Strong Expression of a Longevity-Related Protein, SIRT1, in Bowen's Disease. *Arch. Dermatol. Res.* **2007**. https://doi.org/10.1007/s00403-006-0725-6.

(334) Wang, R. H.; Sengupta, K.; Li, C.; Kim, H. S.; Cao, L.; Xiao, C.; Kim, S.; Xu, X.; Zheng, Y.; Chilton, B.; et al. Impaired DNA Damage Response, Genome Instability, and Tumorigenesis in SIRT1 Mutant Mice. *Cancer Cell* **2008**. https://doi.org/10.1016/j.ccr.2008.09.001.

(335) Araki, T.; Sasaki, Y.; Milbrandt, J. Increased Nuclear NAD Biosynthesis and SIRT1 Activation Prevent Axonal Degeneration. *Science (80-.).* **2004**. https://doi.org/10.1126/science.1098014.

(336) Li, X. H.; Chen, C.; Tu, Y.; Sun, H. T.; Zhao, M. L.; Cheng, S. X.; Qu, Y.; Zhang, S. Sirt1 Promotes Axonogenesis by Deacetylation of Akt and Inactivation of GSK3. *Molecular Neurobiology*. 2013. https://doi.org/10.1007/s12035-013-8437-3.

(337) Qin, W.; Yang, T.; Ho, L.; Zhao, Z.; Wang, J.; Chen, L.; Zhao, W.; Thiyagarajan, M.; MacGrogan, D.; Rodgers, J. T.; et al. Neuronal SIRT1 Activation as a Novel Mechanism Underlying the Prevention of Alzheimer Disease Amyloid Neuropathology by Calorie Restriction. *J. Biol. Chem.* **2006**. https://doi.org/10.1074/jbc.M602909200.

(338) Donmez, G.; Arun, A.; Chung, C. Y.; Mclean, P. J.; Lindquist, S.; Guarente, L. SIRT1 Protects against α-Synuclein Aggregation by Activating Molecular Chaperones. *J. Neurosci.* **2012**. https://doi.org/10.1523/JNEUROSCI.3442-11.2012.

(339) Jeong, J. K.; Moon, M. H.; Lee, Y. J.; Seol, J. W.; Park, S. Y. Autophagy Induced by the Class III Histone Deacetylase Sirt1 Prevents Prion Peptide Neurotoxicity. *Neurobiol. Aging* **2013**. https://doi.org/10.1016/j.neurobiolaging.2012.04.002.

(340) Jeong, H.; Cohen, D. E.; Cui, L.; Supinski, A.; Savas, J. N.; Mazzulli, J. R.; Yates, J. R.; Bordone, L.; Guarente, L.; Krainc, D. Sirt1 Mediates Neuroprotection from Mutant Huntingtin by Activation of the TORC1 and CREB Transcriptional Pathway. *Nat. Med.* **2012**. https://doi.org/10.1038/nm.2559.

(341) Yoon, M. J.; Yoshida, M.; Johnson, S.; Takikawa, A.; Usui, I.; Tobe, K.; Nakagawa, T.; Yoshino, J.; Imai, S. ichiro. SIRT1-Mediated ENAMPT Secretion from Adipose Tissue Regulates Hypothalamic NAD+ and Function in Mice. *Cell Metab.* **2015**. https://doi.org/10.1016/j.cmet.2015.04.002.

(342) Luo, J.; Nikolaev, A. Y.; Imai, S. ichiro; Chen, D.; Su, F.; Shiloh, A.; Guarente, L.; Gu, W. Negative Control of P53 by Sir2α Promotes Cell Survival under Stress. *Cell* **2001**. https://doi.org/10.1016/S0092-8674(01)00524-4.

(343) Vaziri, H.; Dessain, S. K.; Eaton, E. N.; Imai, S. I.; Frye, R. A.; Pandita, T. K.; Guarente, L.; Weinberg, R. A. HSIR2SIRT1 Functions as an NAD-Dependent P53 Deacetylase. *Cell* **2001**. https://doi.org/10.1016/S0092-8674(01)00527-X.

(344) Deng, C. X. SIRT1, Is It a Tumor Promoter or Tumor Suppressor? *International Journal of Biological Sciences*. 2009. https://doi.org/10.7150/ijbs.5.147.

(345) Bosch-Presegué, L.; Vaquero, A. The Dual Role of Sirtuins in Cancer. *Genes and Cancer*. 2011. https://doi.org/10.1177/1947601911417862.

(346) Cohen, H. Y.; Miller, C.; Bitterman, K. J.; Wall, N. R.; Hekking, B.; Kessler, B.; Howitz, K. T.; Gorospe, M.; De Cabo, R.; Sinclair, D. A. Calorie Restriction Promotes Mammalian Cell Survival by Inducing the SIRT1 Deacetylase. *Science (80-.)*. **2004**. https://doi.org/10.1126/science.1099196.

(347) Motta, M. C.; Divecha, N.; Lemieux, M.; Kamel, C.; Chen, D.; Gu, W.; Bultsma, Y.; McBurney, M.; Guarente, L. Mammalian SIRT1 Represses Forkhead Transcription Factors. *Cell* **2004**. https://doi.org/10.1016/S0092-8674(04)00126-6.

(348) Pruitt, K.; Zinn, R. L.; Ohm, J. E.; McGarvey, K. M.; Kang, S. H. L.; Watkins, D. N.; Herman, J. G.; Baylin, S. B. Inhibition of SIRT1 Reactivates Silenced Cancer Genes without Loss of Promoter DNA Hypermethylation. *PLoS Genet*. **2006**. https://doi.org/10.1371/journal.pgen.0020040.

(349) Jin, M. D.; Zhi, Y. W.; Dao, C. S.; Ru, X. L.; Sheng, Q. W. SIRT1 Interacts with P73 and Suppresses P73-Dependent Transcriptional Activity. *J. Cell. Physiol.* **2007**. https://doi.org/10.1002/jcp.20831.

(350) Derr, R. S.; van Hoesel, A. Q.; Benard, A.; Goossens-Beumer, I. J.; Sajet, A.; Dekker-Ensink, N. G.; de Kruijf, E. M.; Bastiaannet, E.; Smit, V. T. H. B. M.; van de Velde, C. J. H.; et al. High Nuclear Expression Levels of Histone-Modifying Enzymes LSD1, HDAC2 and SIRT1 in Tumor Cells Correlate with Decreased Survival and Increased Relapse in Breast Cancer Patients. *BMC Cancer*. 2014. https://doi.org/10.1186/1471-2407-14-604.

(351) Wilking, M. J.; Singh, C. K.; Nihal, M.; Ndiaye, M. A.; Ahmad, N. Sirtuin Deacetylases: A New Target for Melanoma Management. *Cell Cycle* **2014**. https://doi.org/10.4161/15384101.2014.949085.

(352) Harting, K.; Knöll, B. SIRT2-Mediated Protein Deacetylation: An Emerging Key Regulator in Brain Physiology and Pathology. *European Journal of Cell Biology*. 2010. https://doi.org/10.1016/j.ejcb.2009.11.006.

(353) Outeiro, T. F.; Kontopoulos, E.; Altmann, S. M.; Kufareva, I.; Strathearn, K. E.; Amore, A. M.; Volk, C. B.; Maxwell, M. M.; Rochet, J. C.; McLean, P. J.; et al. Sirtuin 2 Inhibitors Rescue α-Synuclein-Mediated Toxicity in Models of Parkinson's Disease. *Science (80-.)*. **2007**. https://doi.org/10.1126/science.1143780.

(354) Jing, E.; Gesta, S.; Kahn, C. R. SIRT2 Regulates Adipocyte Differentiation through FoxO1 Acetylation/Deacetylation. *Cell Metab*. **2007**. https://doi.org/10.1016/j.cmet.2007.07.003.

(355) Park, J. M.; Kim, T. H.; Jo, S. H.; Kim, M. Y.; Ahn, Y. H. Acetylation of Glucokinase Regulatory Protein Decreases Glucose Metabolism by Suppressing Glucokinase Activity. *Sci. Rep*. **2015**. https://doi.org/10.1038/srep17395.

(356) Someya, S.; Yu, W.; Hallows, W. C.; Xu, J.; Vann, J. M.; Leeuwenburgh, C.; Tanokura, M.; Denu, J. M.; Prolla, T. A. Sirt3 Mediates Reduction of Oxidative Damage and Prevention of Age-Related Hearing Loss under Caloric Restriction. *Cell* **2010**. https://doi.org/10.1016/j.cell.2010.10.002.

(357) Rangarajan, P.; Karthikeyan, A.; Lu, J.; Ling, E. A.; Dheen, S. T. Sirtuin 3 Regulates Foxo3a-Mediated Antioxidant Pathway in Microglia. *Neuroscience* **2015**. https://doi.org/10.1016/j.neuroscience.2015.10.048.

224

(358) Tao, R.; Coleman, M. C.; Pennington, J. D.; Ozden, O.; Park, S. H.; Jiang, H.; Kim, H. S.; Flynn, C. R.; Hill, S.; McDonald, W. H.; et al. Sirt3-Mediated Deacetylation of Evolutionarily Conserved Lysine 122 Regulates MnSOD Activity in Response to Stress. *Mol. Cell* **2010**. https://doi.org/10.1016/j.molcel.2010.12.013.

(359) Finley, L. W. S.; Haas, W.; Desquiret-Dumas, V.; Wallace, D. C.; Procaccio, V.; Gygi, S. P.; Haigis, M. C. Succinate Dehydrogenase Is a Direct Target of Sirtuin 3 Deacetylase Activity. *PLoS One* **2011**. https://doi.org/10.1371/journal.pone.0023295.

(360) Pannek, M.; Simic, Z.; Fuszard, M.; Meleshin, M.; Rotili, D.; Mai, A.; Schutkowski, M.; Steegborn, C. Crystal Structures of the Mitochondrial Deacylase Sirtuin 4 Reveal Isoform-Specific Acyl Recognition and Regulation Features. *Nat. Commun.* **2017**, *8* (1). https://doi.org/10.1038/s41467-017-01701-2.

(361) Han, Y.; Zhou, S.; Coetzee, S.; Chen, A. SIRT4 and Its Roles in Energy and Redox Metabolism in Health, Disease and During Exercise. *Front. Physiol.* **2019**, *10* (August). https://doi.org/10.3389/fphys.2019.01006.

(362) Miyo, M.; Yamamoto, H.; Konno, M.; Colvin, H.; Nishida, N.; Koseki, J.; Kawamoto, K.; Ogawa, H.; Hamabe, A.; Uemura, M.; et al. Tumour-Suppressive Function of SIRT4 in Human Colorectal Cancer. *Br. J. Cancer* **2015**. https://doi.org/10.1038/bjc.2015.226.

(363) Lu, W.; Zuo, Y.; Feng, Y.; Zhang, M. SIRT5 Facilitates Cancer Cell Growth and Drug Resistance in Non-Small Cell Lung Cancer. *Tumor Biol.* **2014**. https://doi.org/10.1007/s13277-014-2372-4.

(364) Etchegaray, J. P.; Chavez, L.; Huang, Y.; Ross, K. N.; Choi, J.; Martinez-Pastor, B.; Walsh, R. M.; Sommer, C. A.; Lienhard, M.; Gladden, A.; et al. The Histone Deacetylase SIRT6 Controls Embryonic Stem Cell Fate via TET-Mediated Production of 5-Hydroxymethylcytosine. *Nat. Cell Biol.* **2015**. https://doi.org/10.1038/ncb3147.

(365) Barber, M. F.; Michishita-Kioi, E.; Xi, Y.; Tasselli, L.; Kioi, M.; Moqtaderi, Z.; Tennen, R. I.; Paredes, S.; Young, N. L.; Chen, K.; et al. SIRT7 Links H3K18 Deacetylation to Maintenance of Oncogenic Transformation. *Nature* **2012**. https://doi.org/10.1038/nature11043.

(366) Lee, W. Y.; Lee, W. T.; Cheng, C. H.; Chen, K. C.; Chou, C. M.; Chung, C. H.; Sun, M. S.; Cheng, H. W.; Ho, M. N.; Lin, C. W. Repositioning Antipsychotic Chlorpromazine for Treating Colorectal Cancer by Inhibiting Sirtuin 1. *Oncotarget* **2015**. https://doi.org/10.18632/oncotarget.4768.

(367) Fried, H. M. Nutrient-Sensitive Mitochondrial NAD+ Levels Dictate Cell Survival. *Chemtracts* **2007**, *20* (4), 160–161. https://doi.org/10.1016/j.cell.2007.07.035.Nutrient-Sensitive.

(368) Schwer, B.; Eckersdorff, M.; Li, Y.; Silva, J. C.; Fermin, D.; Kurtev, M. V.; Giallourakis, C.; Comb, M. J.; Alt, F. W.; Lombard, D. B. Calorie Restriction Alters Mitochondrial Protein Acetylation. *Aging Cell.* 2009. https://doi.org/10.1111/j.1474-9726.2009.00503.x.

(369) Zhao, S.; Xu, W.; Jiang, W.; Yu, W.; Lin, Y.; Zhang, T.; Yao, J.; Zhou, L.; Zeng, Y.; Li, H.; et al. Regulation of Cellular Metabolism by Protein Lysine Acetylation. *Science (80-.).* **2010**. https://doi.org/10.1126/science.1179689.

(370) Navas-Enamorado, I.; Bernier, M.; Brea-Calvo, G.; de Cabo, R. Influence of Anaerobic and Aerobic Exercise on Age-Related Pathways in Skeletal Muscle. *Ageing Research Reviews.* 2017. https://doi.org/10.1016/j.arr.2017.04.005.

(371) Wang, M. S.; Wu, Y.; Culver, D. G.; Glass, J. D. Pathogenesis of Axonal Degeneration: Parallels between Wallerian Degeneration and Vincristine

Neuropathy. *Journal of Neuropathology and Experimental Neurology*. 2000. https://doi.org/10.1093/jnen/59.7.599.

(372) Schutkowski, M.; Fischer, F.; Roessler, C.; Steegborn, C. New Assays and Approaches for Discovery and Design of Sirtuin Modulators. *Expert Opinion on Drug Discovery*. 2014. https://doi.org/10.1517/17460441.2014.875526.

(373) Gertz, M.; Steegborn, C. Using Mitochondrial Sirtuins as Drug Targets: Disease Implications and Available Compounds. *Cellular and Molecular Life Sciences*. 2016. https://doi.org/10.1007/s00018-016-2180-7.

(374) Tennen, R. I.; Berber, E.; Chua, K. F. Functional Dissection of SIRT6: Identification of Domains That Regulate Histone Deacetylase Activity and Chromatin Localization. *Mech. Ageing Dev*. **2010**. https://doi.org/10.1016/j.mad.2010.01.006.

(375) Ahuja, N.; Schwer, B.; Carobbio, S.; Waltregny, D.; North, B. J.; Castronovo, V.; Maechler, P.; Verdin, E. Regulation of Insulin Secretion by SIRT4, a Mitochondrial ADP-Ribosyltransferase. *J. Biol. Chem*. **2007**. https://doi.org/10.1074/jbc.M705488200.

(376) North, B. J.; Marshall, B. L.; Borra, M. T.; Denu, J. M.; Verdin, E. *The Human Sir2 Ortholog, SIRT2, Is an NAD-Dependent Tubulin Deacetylase Mouse Sir2 Deacetylate the Transcription Factor Protein P53 and Suppress P53-Dependent Apoptosis in Re*; 2003.

(377) Verdin, E.; Dequiedt, F.; Fischle, W.; Frye, R.; Marshall, B.; North, B. Measurement of Mammalian Histone Deacetylase Activity. *Methods Enzymol*. **2003**. https://doi.org/10.1016/S0076-6879(03)77010-4.

(378) Wagner, G. R.; Bhatt, D. P.; O'Connell, T. M.; Thompson, J. W.; Dubois, L. G.; Backos, D. S.; Yang, H.; Mitchell, G. A.; Ilkayeva, O. R.; Stevens, R. D.; et al. A Class of Reactive Acyl-CoA Species Reveals the Non-Enzymatic Origins of Protein Acylation. *Cell Metab*. **2017**. https://doi.org/10.1016/j.cmet.2017.03.006.

(379) Mathias, R. A.; Greco, T. M.; Oberstein, A.; Budayeva, H. G.; Chakrabarti, R.; Rowland, E. A.; Kang, Y.; Shenk, T.; Cristea, I. M. Sirtuin 4 Is a Lipoamidase Regulating Pyruvate Dehydrogenase Complex Activity. *Cell* **2014**. https://doi.org/10.1016/j.cell.2014.11.046.

(380) Betsinger, C. N.; Cristea, I. M. Mitochondrial Function, Metabolic Regulation, and Human Disease Viewed through the Prism of Sirtuin 4 (SIRT4) Functions. *Journal of Proteome Research*. 2019. https://doi.org/10.1021/acs.jproteome.9b00086.

(381) Rauh, D.; Fischer, F.; Gertz, M.; Lakshminarasimhan, M.; Bergbrede, T.; Aladini, F.; Kambach, C.; Becker, C. F. W.; Zerweck, J.; Schutkowski, M.; et al. An Acetylome Peptide Microarray Reveals Specificities and Deacetylation Substrates for All Human Sirtuin Isoforms. *Nat. Commun*. **2013**, *4*, 1–10. https://doi.org/10.1038/ncomms3327.

(382) Heltweg, B.; Dequiedt, F.; Verdin, E.; Jung, M. Nonisotopic Substrate for Assaying Both Human Zinc and NAD+-Dependent Histone Deacetylases. *Anal. Biochem*. **2003**. https://doi.org/10.1016/S0003-2697(03)00276-8.

(383) Saunders, L. R.; Verdin, E. Sirtuins: Critical Regulators at the Crossroads between Cancer and Aging. *Oncogene*. 2007. https://doi.org/10.1038/sj.onc.1210616.

(384) Laurent, G.; German, N. J.; Saha, A. K.; de Boer, V. C. J.; Davies, M.; Koves, T. R.; Dephoure, N.; Fischer, F.; Boanca, G.; Vaitheesvaran, B.; et al. SIRT4 Coordinates the Balance between Lipid Synthesis and Catabolism by Repressing Malonyl CoA Decarboxylase. *Mol. Cell* **2013**. https://doi.org/10.1016/j.molcel.2013.05.012.

(385) Wu, T.; Liu, Y. H.; Fu, Y. C.; Liu, X. M.; Zhou, X. H. Direct Evidence of Sirtuin Downregulation in the Liver of Non-Alcoholic Fatty Liver Disease Patients. *Ann*.

Clin. Lab. Sci. **2014**.

(386) Osborne, B.; Bentley, N. L.; Montgomery, M. K.; Turner, N. The Role of Mitochondrial Sirtuins in Health and Disease. *Free Radical Biology and Medicine*. 2016. https://doi.org/10.1016/j.freeradbiomed.2016.04.197.

(387) Jeong, S. M.; Xiao, C.; Finley, L. W. S.; Lahusen, T.; Souza, A. L.; Pierce, K.; Li, Y. H.; Wang, X.; Laurent, G.; German, N. J.; et al. SIRT4 Has Tumor-Suppressive Activity and Regulates the Cellular Metabolic Response to Dna Damage by Inhibiting Mitochondrial Glutamine Metabolism. *Cancer Cell* **2013**. https://doi.org/10.1016/j.ccr.2013.02.024.

(388) Csibi, A.; Fendt, S. M.; Li, C.; Poulogiannis, G.; Choo, A. Y.; Chapski, D. J.; Jeong, S. M.; Dempsey, J. M.; Parkhitko, A.; Morrison, T.; et al. The MTORC1 Pathway Stimulates Glutamine Metabolism and Cell Proliferation by Repressing SIRT4. *Cell* **2013**. https://doi.org/10.1016/j.cell.2013.04.023.

(389) Huang, G.; Zhu, G. Sirtuin-4 (SIRT4), a Therapeutic Target with Oncogenic and Tumor-Suppressive Activity in Cancer. *OncoTargets and Therapy*. 2018. https://doi.org/10.2147/OTT.S157724.

(390) Huang, G.; Cheng, J.; Yu, F.; Liu, X.; Yuan, C.; Liu, C.; Chen, X.; Peng, Z. Clinical and Therapeutic Significance of Sirtuin-4 Expression in Colorectal Cancer. *Oncol. Rep.* **2016**. https://doi.org/10.3892/or.2016.4685.

(391) Chen, Z.; Lin, J.; Feng, S.; Chen, X.; Huang, H.; Wang, C.; Yu, Y.; He, Y.; Han, S.; Zheng, L.; et al. SIRT4 Inhibits the Proliferation, Migration, and Invasion Abilities of Thyroid Cancer Cells by Inhibiting Glutamine Metabolism. *Onco. Targets. Ther.* **2019**. https://doi.org/10.2147/OTT.S189536.

(392) Jeong, S. M.; Hwang, S.; Seong, R. H. SIRT4 Regulates Cancer Cell Survival and Growth after Stress. *Biochem. Biophys. Res. Commun.* **2016**. https://doi.org/10.1016/j.bbrc.2016.01.078.

(393) Lai, X.; Yu, Z.; Chen, X.; Huang, G. SIRT4 Is Upregulated in Chinese Patients with Esophageal Cancer. *Int. J. Clin. Exp. Pathol.* **2016**.

(394) Min, Z.; Gao, J.; Yu, Y. The Roles of Mitochondrial SIRT4 in Cellular Metabolism. *Frontiers in Endocrinology*. 2019. https://doi.org/10.3389/fendo.2018.00783.

(395) Nasrin, N.; Wu, X.; Fortier, E.; Feng, Y.; Baré, O. C.; Chen, S.; Ren, X.; Wu, Z.; Streeper, R. S.; Bordone, L. SIRT4 Regulates Fatty Acid Oxidation and Mitochondrial Gene Expression in Liver and Muscle Cells. *J. Biol. Chem.* **2010**. https://doi.org/10.1074/jbc.M110.124164.

(396) Hall, M.; Peters, G. Genetic Alterations of Cyclins, Cyclin-Dependent Kinases, and Cdk Inhibitors in Human Cancer. *Advances in Cancer Research*. 1996.

(397) Ho, L.; Titus, A. S.; Banerjee, K. K.; George, S.; Lin, W.; Deota, S.; Saha, A. K.; Nakamura, K.; Gut, P.; Verdin, E.; et al. SIRT4 Regulates ATP Homeostasis and Mediates a Retrograde Signaling via AMPK. *Aging (Albany. NY)*. **2013**. https://doi.org/10.18632/aging.100616.

(398) Luo, Y. X.; Tang, X.; An, X. Z.; Xie, X. M.; Chen, X. F.; Zhao, X.; Hao, D. L.; Chen, H. Z.; Liu, D. P. SIRT4 Accelerates Ang II-Induced Pathological Cardiac Hypertrophy by Inhibiting Manganese Superoxide Dismutase Activity. *Eur. Heart J.* **2017**. https://doi.org/10.1093/eurheartj/ehw138.

(399) Argmann, C.; Auwerx, J. Insulin Secretion: SIRT4 Gets in on the Act. *Cell*. 2006. https://doi.org/10.1016/j.cell.2006.08.031.

(400) Michishita, E.; Park, J. Y.; Burneskis, J. M.; Barrett, J. C.; Horikawa, I. Evolutionarily Conserved and Nonconserved Cellular Localizations and Functions of Human SIRT Proteins. *Mol. Biol. Cell* **2005**. https://doi.org/10.1091/mbc.E05-01-0033.

(401) Cosentino, C.; Grieco, D.; Costanzo, V. ATM Activates the Pentose Phosphate Pathway Promoting Anti-Oxidant Defence and DNA Repair. *EMBO J.* **2011**. https://doi.org/10.1038/emboj.2010.330.

(402) Lukey, M. J.; Wilson, K. F.; Cerione, R. A. Therapeutic Strategies Impacting Cancer Cell Glutamine Metabolism. *Future Medicinal Chemistry*. 2013. https://doi.org/10.4155/fmc.13.130.

(403) Verma, M.; Shulga, N.; Pastorino, J. G. Sirtuin-4 Modulates Sensitivity to Induction of the Mitochondrial Permeability Transition Pore. *Biochim. Biophys. Acta - Bioenerg.* **2013**. https://doi.org/10.1016/j.bbabio.2012.09.016.

(404) Lee, S. J.; Choi, S. E.; Jung, I. R.; Lee, K. W.; Kang, Y. Protective Effect of Nicotinamide on High Glucose/Palmitate-Induced Glucolipotoxicity to INS-1 Beta Cells Is Attributed to Its Inhibitory Activity to Sirtuins. *Arch. Biochem. Biophys.* **2013**. https://doi.org/10.1016/j.abb.2013.03.011.

(405) Bensaad, K.; Tsuruta, A.; Selak, M. A.; Vidal, M. N. C.; Nakano, K.; Bartrons, R.; Gottlieb, E.; Vousden, K. H. TIGAR, a P53-Inducible Regulator of Glycolysis and Apoptosis. *Cell* **2006**. https://doi.org/10.1016/j.cell.2006.05.036.

(406) DeBerardinis, R. J.; Lum, J. J.; Hatzivassiliou, G.; Thompson, C. B. The Biology of Cancer: Metabolic Reprogramming Fuels Cell Growth and Proliferation. *Cell Metabolism*. 2008. https://doi.org/10.1016/j.cmet.2007.10.002.

(407) Saggerson, D. Malonyl-CoA, a Key Signaling Molecule in Mammalian Cells. *Annu. Rev. Nutr.* **2008**. https://doi.org/10.1146/annurev.nutr.28.061807.155434.

(408) Kersten, S.; Rakhshandehroo, M.; Knoch, B.; Müller, M. Peroxisome Proliferator-Activated Receptor Alpha Target Genes. *PPAR Res.* **2010**. https://doi.org/10.1155/2010/612089.

(409) Parihar, P.; Solanki, I.; Mansuri, M. L.; Parihar, M. S. Mitochondrial Sirtuins: Emerging Roles in Metabolic Regulations, Energy Homeostasis and Diseases. *Experimental Gerontology*. 2015. https://doi.org/10.1016/j.exger.2014.12.004.

(410) Laurent, G.; de Boer, V. C. J.; Finley, L. W. S.; Sweeney, M.; Lu, H.; Schug, T. T.; Cen, Y.; Jeong, S. M.; Li, X.; Sauve, A. A.; et al. SIRT4 Represses Peroxisome Proliferator-Activated Receptor α Activity To Suppress Hepatic Fat Oxidation. *Mol. Cell. Biol.* **2013**. https://doi.org/10.1128/mcb.00087-13.

(411) Alam, N.; Saggerson, E. D. Malonyl-CoA and the Regulation of Fatty Acid Oxidation in Soleus Muscle. *Biochem. J.* **1998**. https://doi.org/10.1042/bj3340233.

(412) Winder, W. W.; Wilson, H. A.; Hardie, D. G.; Rasmussen, B. B.; Hutber, C. A.; Call, G. B.; Clayton, R. D.; Conley, L. M.; Yoon, S.; Zhou, B. Phosphorylation of Rat Muscle Acetyl-CoA Carboxylase by AMP-Activated Protein Kinase and Protein Kinase A. *J. Appl. Physiol.* **1997**. https://doi.org/10.1152/jappl.1997.82.1.219.

(413) Wang, Q.; Jiang, L.; Wang, J.; Li, S.; Yu, Y.; You, J.; Zeng, R.; Gao, X.; Rui, L.; Li, W.; et al. Abrogation of Hepatic ATP-Citrate Lyase Protects against Fatty Liver and Ameliorates Hyperglycemia in Leptin Receptor-Deficient Mice. *Hepatology* **2009**. https://doi.org/10.1002/hep.22774.

(414) Pebay-Peyroula, E.; Brandolin, G. Nucleotide Exchange in Mitochondria: Insight at a Molecular Level. *Current Opinion in Structural Biology*. 2004. https://doi.org/10.1016/j.sbi.2004.06.009.

(415) Zhou, Z. H.; McCarthy, D. B.; O'Connor, C. M.; Reed, L. J.; Stoops, J. K. The Remarkable Structural and Functional Organization of the Eukaryotic Pyruvate Dehydrogenase Complexes. *Proc. Natl. Acad. Sci. U. S. A.* **2001**. https://doi.org/10.1073/pnas.011597698.

(416) Fan, J.; Shan, C.; Kang, H. B.; Elf, S.; Xie, J.; Tucker, M.; Gu, T. L.; Aguiar, M.; Lonning, S.; Chen, H.; et al. Tyr Phosphorylation of PDP1 Toggles Recruitment

between ACAT1 and SIRT3 to Regulate the Pyruvate Dehydrogenase Complex. *Mol. Cell* **2014**. https://doi.org/10.1016/j.molcel.2013.12.026.

(417) Münzel, T.; Gori, T.; Keaney, J. F.; Maack, C.; Daiber, A. Pathophysiological Role of Oxidative Stress in Systolic and Diastolic Heart Failure and Its Therapeutic Implications. *European Heart Journal*. 2015. https://doi.org/10.1093/eurheartj/ehv305.

(418) Dai, D. F.; Johnson, S. C.; Villarin, J. J.; Chin, M. T.; Nieves-Cintrón, M.; Chen, T.; Marcinek, D. J.; Dorn, G. W.; Kang, Y. J.; Prolla, T. A.; et al. Mitochondrial Oxidative Stress Mediates Angiotensin II-Induced Cardiac Hypertrophy and Gαq Overexpression-Induced Heart Failure. *Circ. Res.* **2011**. https://doi.org/10.1161/CIRCRESAHA.110.232306.

(419) Loch, T.; Vakhrusheva, O.; Piotrowska, I.; Ziolkowski, W.; Ebelt, H.; Braun, T.; Bober, E. Different Extent of Cardiac Malfunction and Resistance to Oxidative Stress in Heterozygous and Homozygous Manganese-Dependent Superoxide Dismutase-Mutant Mice. *Cardiovasc. Res.* **2009**. https://doi.org/10.1093/cvr/cvp092.

(420) Nojiri, H.; Shimizu, T.; Funakoshi, M.; Yamaguchi, O.; Zhou, H.; Kawakami, S.; Ohta, Y.; Sami, M.; Tachibana, T.; Ishikawa, H.; et al. Oxidative Stress Causes Heart Failure with Impaired Mitochondrial Respiration. *J. Biol. Chem.* **2006**. https://doi.org/10.1074/jbc.M602118200.

(421) Shiomi, T.; Tsutsui, H.; Matsusaka, H.; Murakami, K.; Hayashidani, S.; Ikeuchi, M.; Wen, J.; Kubota, T.; Utsumi, H.; Takeshita, A. Overexpression of Glutathione Peroxidase Prevents Left Ventricular Remodeling and Failure after Myocardial Infarction in Mice. *Circulation* **2004**. https://doi.org/10.1161/01.CIR.0000109701.77059.E9.

(422) Frank, D.; Kuhn, C.; Van Eickels, M.; Gehring, D.; Hanselmann, C.; Lippl, S.; Will, R.; Katus, H. A.; Frey, N. Calsarcin-1 Protects against Angiotensin-II-Induced Cardiac Hypertrophy. *Circulation* **2007**. https://doi.org/10.1161/CIRCULATIONAHA.107.711317.

(423) Dai, D. F.; Rabinovitch, P. S.; Ungvari, Z. Mitochondria and Cardiovascular Aging. *Circulation Research*. 2012. https://doi.org/10.1161/CIRCRESAHA.111.246140.

(424) Hiroi, S.; Harada, H.; Nishi, H.; Satoh, M.; Nagai, R.; Kimura, A. Polymorphisms in the SOD2 and HLA-DRB1 Genes Are Associated with Nonfamilial Idiopathic Dilated Cardiomyopathy in Japanese. *Biochem. Biophys. Res. Commun.* **1999**. https://doi.org/10.1006/bbrc.1999.1036.

(425) Dos Santos, K. G.; Canani, L. H.; Gross, J. L.; Tschiedel, B.; Souto, K. E. P.; Roisenberg, I. The Catalase -262C/T Promoter Polymorphism and Diabetic Complications in Caucasians with Type 2 Diabetes. *Dis. Markers* **2006**.

(426) Sibbing, D.; Pfeufer, A.; Perisic, T.; Mannes, A. M.; Fritz-Wolf, K.; Unwin, S.; Sinner, M. F.; Gieger, C.; Gloeckner, C. J.; Wichmann, H. E.; et al. Mutations in the Mitochondrial Thioredoxin Reductase Gene TXNRD2 Cause Dilated Cardiomyopathy. *Eur. Heart J.* **2011**. https://doi.org/10.1093/eurheartj/ehq507.

(427) Schmitt, J. P.; Kamisago, M.; Asahi, M.; Hua Li, G.; Ahmad, F.; Mende, U.; Kranias, E. G.; MacLennan, D. H.; Seidman, J. G.; Seidman, C. E. Dilated Cardiomyopathy and Heart Failure Caused by a Mutation in Phospholamban. *Science (80-.)*. **2003**. https://doi.org/10.1126/science.1081578.

(428) Sundaresan, N. R.; Gupta, M.; Kim, G.; Rajamohan, S. B.; Isbatan, A.; Gupta, M. P. Sirt3 Blocks the Cardiac Hypertrophic Response by Augmenting Foxo3a-Dependent Antioxidant Defense Mechanisms in Mice. *J. Clin. Invest.* **2009**. https://doi.org/10.1172/JCI39162.

(429) Choi, Y. L.; Tsukasaki, K.; O'Neill, M. C.; Yamada, Y.; Onimaru, Y.; Matsumoto, K.; Ohashi, J.; Yamashita, Y.; Tsutsumi, S.; Kaneda, R.; et al. A Genomic Analysis of Adult T-Cell Leukemia. *Oncogene* **2007**. https://doi.org/10.1038/sj.onc.1209898.

(430) Garber, M. E.; Troyanskaya, O. G.; Schluens, K.; Petersen, S.; Thaesler, Z.; Pacyna-Gengelbach, M.; Van De Rijn, M.; Rosen, G. D.; Perou, C. M.; Whyte, R. I.; et al. Diversity of Gene Expression in Adenocarcinoma of the Lung. *Proc. Natl. Acad. Sci. U. S. A.* **2001**. https://doi.org/10.1073/pnas.241500798.

(431) Fu, L.; Dong, Q.; He, J.; Wang, X.; Xing, J.; Wang, E.; Qiu, X.; Li, Q. SIRT4 Inhibits Malignancy Progression of NSCLCs, through Mitochondrial Dynamics Mediated by the ERK-Drp1 Pathway. *Oncogene* **2017**. https://doi.org/10.1038/onc.2016.425.

(432) Chen, X.; Lai, X.; Wu, C.; Tian, Q.; Lei, T.; Pan, J.; Huang, G. Decreased SIRT4 Protein Levels in Endometrioid Adenocarcinoma Tissues Are Associated with Advanced AJCC Stage. *Cancer Biomarkers* **2017**. https://doi.org/10.3233/CBM-160419.

(433) Jeong, S. M.; Lee, A.; Lee, J.; Haigis, M. C. SIRT4 Protein Suppresses Tumor Formation in Genetic Models of Myc-Induced B Cell Lymphoma. *J. Biol. Chem.* **2014**. https://doi.org/10.1074/jbc.M113.525949.

(434) Shi, Q.; Liu, T.; Zhang, X.; Geng, J.; He, X.; Nu, M.; Pang, D. Decreased Sirtuin 4 Expression Is Associated with Poor Prognosis in Patients with Invasive Breast Cancer. *Oncol. Lett.* **2016**. https://doi.org/10.3892/ol.2016.5021.

(435) Seder, C. W.; Hnrtojo, W.; Lin, L.; Silvers, A. L.; Wang, Z.; Thomas, D. G.; Giordano, T. J.; Chen, G.; Chang, A. C.; Orringer, M. B.; et al. Upregulated INHBA Expression May Promote Cell Proliferation and Is Associated with Poor Survival IN Lung Adenocarcinoma1 Www.Neoplasia.Com. *Neoplasia* **2009**. https://doi.org/10.1593/neo.81582.

(436) Colombo, S. L.; Palacios-Callender, M.; Frakich, N.; Carcamo, S.; Kovacs, I.; Tudzarova, S.; Moncada, S. Molecular Basis for the Differential Use of Glucose and Glutamine in Cell Proliferation as Revealed by Synchronized HeLa Cells. *Proc. Natl. Acad. Sci. U. S. A.* **2011**. https://doi.org/10.1073/pnas.1117500108.

(437) Gao, P.; Tchernyshyov, I.; Chang, T. C.; Lee, Y. S.; Kita, K.; Ochi, T.; Zeller, K. I.; De Marzo, A. M.; Van Eyk, J. E.; Mendell, J. T.; et al. C-Myc Suppression of MiR-23a/b Enhances Mitochondrial Glutaminase Expression and Glutamine Metabolism. *Nature* **2009**. https://doi.org/10.1038/nature07823.

(438) Chen, Y.; Wang, H.; Luo, G.; Dai, X. SIRT4 Inhibits Cigarette Smoke Extracts-Induced Mononuclear Cell Adhesion to Human Pulmonary Microvascular Endothelial Cells via Regulating NF-KB Activity. *Toxicol. Lett.* **2014**. https://doi.org/10.1016/j.toxlet.2014.02.022.

(439) Liu, B.; Che, W.; Xue, J.; Zheng, C.; Tang, K.; Zhang, J.; Wen, J.; Xu, Y. SIRT4 Prevents Hypoxia-Induced Apoptosis in H9c2 Cardiomyoblast Cells. *Cell. Physiol. Biochem.* **2013**. https://doi.org/10.1159/000354469.

(440) Ciccia, A.; Elledge, S. J. The DNA Damage Response: Making It Safe to Play with Knives. *Molecular Cell*. 2010. https://doi.org/10.1016/j.molcel.2010.09.019.

(441) Negrini, S.; Gorgoulis, V. G.; Halazonetis, T. D. Genomic Instability an Evolving Hallmark of Cancer. *Nature Reviews Molecular Cell Biology*. 2010. https://doi.org/10.1038/nrm2858.

(442) Jeong, S. M.; Haigis, M. C. Sirtuins in Cancer: A Balancing Act between Genome Stability and Metabolism. *Molecules and Cells*. 2015. https://doi.org/10.14348/molcells.2015.0167.

(443) Komlos, D.; Mann, K. D.; Zhuo, Y.; Ricupero, C. L.; Hart, R. P.; Liu, A. Y. C.;

Firestein, B. L. Glutamate Dehydrogenase 1 and SIRT4 Regulate Glial Development. *Glia* **2013**. https://doi.org/10.1002/glia.22442.

(444) Shih, J.; Liu, L.; Mason, A.; Higashimori, H.; Donmez, G. Loss of SIRT4 Decreases GLT-1-Dependent Glutamate Uptake and Increases Sensitivity to Kainic Acid. *J. Neurochem.* **2014**. https://doi.org/10.1111/jnc.12942.

(445) Wong, D. W.; Soga, T.; Parhar, I. S. Aging and Chronic Administration of Serotonin-Selective Reuptake Inhibitor Citalopram Upregulate Sirt4 Gene Expression in the Preoptic Area of Male Mice. *Front. Genet.* **2015**. https://doi.org/10.3389/fgene.2015.00281.

(446) Robertson, K. D.; Jones, P. A. DNA Methylation: Past, Present and Future Directions. *Carcinogenesis* **2000**, *21* (3), 461–467. https://doi.org/10.1093/carcin/21.3.461.

(447) Okano, M.; Bell, D. W.; Haber, D. A.; Li, E. DNA Methyltransferases Dnmt3a and Dnmt3b Are Essential for de Novo Methylation and Mammalian Development. *Cell* **1999**, *99* (3), 247–257. https://doi.org/10.1016/S0092-8674(00)81656-6.

(448) Xu, F.; Mao, C.; Ding, Y.; Rui, C.; Wu, L.; Shi, A.; Zhang, H.; Zhang, L.; Xu, Z. Molecular and Enzymatic Profiles of Mammalian DNA Methyltransferases: Structures and Targets for Drugs. *Curr. Med. Chem.* **2010**, *17* (33), 4052–4071. https://doi.org/10.1016/j.bbi.2008.05.010.

(449) Lopez, M.; Halby, L.; Arimondo, P. B. *DNA Methyltransferases - Role and Function*; 2016; Vol. 945. https://doi.org/10.1007/978-3-319-43624-1.

(450) Gros, C.; Fahy, J.; Halby, L.; Dufau, I.; Erdmann, A.; Gregoire, J. M.; Ausseil, F.; Vispé, S.; Arimondo, P. B. DNA Methylation Inhibitors in Cancer: Recent and Future Approaches. *Biochimie* **2012**, *94* (11), 2280–2296. https://doi.org/10.1016/j.biochi.2012.07.025.

(451) Lucidi, A. . T. D. . R. D. . M. A. DNA Methylation: Biological Implications and Modulation of Its Aberrant Dysregulation Springer Editor. In *The DNA, RNA, and Histone Methylomes*; Springer Editor, Ed.; 2019. https://doi.org/10.1007/978-3-030-14792-1_12.

(452) Lister, R.; Pelizzola, M.; Dowen, R. H.; Hawkins, R. D.; Hon, G.; Tonti-Filippini, J.; Nery, J. R.; Lee, L.; Ye, Z.; Ngo, Q.-M.; et al. Human DNA Methylomes at Base Resolution Show Widespread Epigenomic Differences. *Nature* **2009**, *462* (7271), 315–322. https://doi.org/10.1038/nature08514.

(453) Laurent, L.; Wong, E.; Li, G.; Laurent, L.; Wong, E.; Li, G.; Huynh, T.; Tsirigos, A.; Ong, C. T.; Low, H. M.; et al. Dynamic Changes in the Human Methylome during Differentiation Dynamic Changes in the Human Methylome during Differentiation. **2010**, 320–331. https://doi.org/10.1101/gr.101907.109.

(454) Portela, A.; Esteller, M. Epigenetic Modifications and Human Disease. *Nat. Biotechnol.* **2010**, *28* (10), 1057–1068. https://doi.org/10.1038/nbt.1685.

(455) Irizarry, R. A.; Ladd-Acosta, C.; Wen, B.; Wu, Z.; Montano, C.; Onyango, P.; Cui, H.; Gabo, K.; Rongione, M.; Webster, M.; et al. The Human Colon Cancer Methylome Shows Similar Hypo- and Hypermethylation at Conserved Tissue-Specific CpG Island Shores. *Nat. Genet.* **2009**, *41* (2), 178–186. https://doi.org/10.1038/ng.298.

(456) Hellman, A.; Chess, A. Gene Body-Specific Methylation on the Active X Chromosome. *Science (80-.).* **2007**, *315* (5815), 1141–1143. https://doi.org/10.1126/science.1136352.

(457) Zilberman, D.; Gehring, M.; Tran, R. K.; Ballinger, T.; Henikoff, S. Genome-Wide Analysis of Arabidopsis Thaliana DNA Methylation Uncovers an Interdependence between Methylation and Transcription. *Nat. Genet.* **2007**, *39* (1), 61–69. https://doi.org/10.1038/ng1929.

(458) Wu, X.; Zhang, Y. TET-Mediated Active DNA Demethylation: Mechanism, Function and Beyond. *Nature Reviews Genetics*. 2017. https://doi.org/10.1038/nrg.2017.33.

(459) Tahiliani, M.; Koh, K. P.; Shen, Y.; Pastor, W. A.; Bandukwala, H.; Brudno, Y.; Agarwal, S.; Iyer, L. M.; Liu, D. R.; Aravind, L.; et al. Conversion of 5-Methylcytosine to 5-Hydroxymethylcytosine in Mammalian DNA by MLL Partner TET1. *Science (80-.).* **2009**. https://doi.org/10.1126/science.1170116.

(460) He, Y. F.; Li, B. Z.; Li, Z.; Liu, P.; Wang, Y.; Tang, Q.; Ding, J.; Jia, Y.; Chen, Z.; Li, N.; et al. Tet-Mediated Formation of 5-Carboxylcytosine and Its Excision by TDG in Mammalian DNA. *Science (80-.).* **2011**. https://doi.org/10.1126/science.1210944.

(461) Spruijt, C. G.; Gnerlich, F.; Smits, A. H.; Pfaffeneder, T.; Jansen, P. W. T. C.; Bauer, C.; Münzel, M.; Wagner, M.; Müller, M.; Khan, F.; et al. Dynamic Readers for 5-(Hydroxy)Methylcytosine and Its Oxidized Derivatives. *Cell* **2013**. https://doi.org/10.1016/j.cell.2013.02.004.

(462) Hashimoto, H.; Liu, Y.; Upadhyay, A. K.; Chang, Y.; Howerton, S. B.; Vertino, P. M.; Zhang, X.; Cheng, X. Recognition and Potential Mechanisms for Replication and Erasure of Cytosine Hydroxymethylation. *Nucleic Acids Res*. **2012**. https://doi.org/10.1093/nar/gks155.

(463) Mellén, M.; Ayata, P.; Heintz, N. 5-Hydroxymethylcytosine Accumulation in Postmitotic Neurons Results in Functional Demethylation of Expressed Genes. *Proc. Natl. Acad. Sci. U. S. A.* **2017**. https://doi.org/10.1073/pnas.1708044114.

(464) Melamed, P.; Yosefzon, Y.; David, C.; Tsukerman, A.; Pnueli, L. Tet Enzymes, Variants, and Differential Effects on Function. *Frontiers in Cell and Developmental Biology*. 2018. https://doi.org/10.3389/fcell.2018.00022.

(465) Esteller, M. Cancer Epigenomics: DNA Methylomes and Histone-Modification Maps. *Nat. Rev. Genet.* **2007**, *8* (4), 286–298. https://doi.org/10.1038/nrg2005.

(466) Razin, A.; Cedar, H. DNA Methylation and Gene Expression. *Microbiol. Rev.* **1991**, *55* (3), 451–458. https://doi.org/10.1002/wsbm.64.

(467) Comb, M.; Goodman, H. M. CpG Methylation Inhibits Proenkephalin Gene Expression and Binding of the Transcription Factor AP-2. *Nucleic Acids Res.* **1990**, *18* (13), 3975–3982. https://doi.org/10.1093/nar/18.13.3975.

(468) Taverna, S. D.; Li, H.; Ruthenburg, A. J.; Allis, C. D.; Patel, D. J. How Chromatin-Binding Modules Interpret Histone Modifications: Lessons from Professional Pocket Pickers. *Nat. Struct. Mol. Biol.* **2007**, *14* (11), 1025–1040. https://doi.org/10.1038/nsmb1338.

(469) Yun, M.; Wu, J.; Workman, J. L.; Li, B. Readers of Histone Modifications. *Cell Res.* **2011**, *21* (4), 564–578. https://doi.org/10.1038/cr.2011.42.

(470) Patel, D. J.; Wang, Z. Readout of Epigenetic Modifications. *Annu. Rev. Biochem.* **2013**, *82*, 81–118. https://doi.org/10.1146/annurev-biochem-072711-165700.

(471) Hughes, R. M.; Wiggins, K. R.; Khorasanizadeh, S.; Waters, M. L. Recognition of Trimethyllysine by a Chromodomain Is Not Driven by the Hydrophobic Effect. *Proc. Natl. Acad. Sci.* **2007**, *104* (27), 11184–11188. https://doi.org/10.1073/pnas.0610850104.

(472) Li, H.; Fischle, W.; Wang, W.; Duncan, E. M.; Liang, L.; Murakami-Ishibe, S.; Allis, C. D.; Patel, D. J. Structural Basis for Lower Lysine Methylation State-Specific Readout by MBT Repeats of L3MBTL1 and an Engineered PHD Finger. *Mol. Cell* **2007**, *28* (4), 677–691. https://doi.org/10.1016/j.molcel.2007.10.023.

(473) Owen, D. J.; Ornaghi, P.; Yang, J. C.; Lowe, N.; Evans, P. R.; Ballario, P.; Neuhaus, D.; Filetici, P.; Travers, a a. The Structural Basis for the Recognition of Acetylated Histone H4 by the Bromodomain of Histone Acetyltransferase Gcn5p.

EMBO J. **2000**, *19* (22), 6141–6149. https://doi.org/10.1093/emboj/19.22.6141.

(474) Morinière, J.; Rousseaux, S.; Steuerwald, U.; Soler-López, M.; Curtet, S.; Vitte, A.-L.; Govin, J.; Gaucher, J.; Sadoul, K.; Hart, D. J.; et al. Cooperative Binding of Two Acetylation Marks on a Histone Tail by a Single Bromodomain. *Nature* **2009**, *461* (7264), 664–668. https://doi.org/10.1038/nature08397.

(475) Gallenkamp, D.; Gelato, K. A.; Haendler, B.; Weinmann, H. Bromodomains and Their Pharmacological Inhibitors. *ChemMedChem* **2014**, *9* (3), 438–464. https://doi.org/10.1002/cmdc.201300434.

(476) Jung, M.; Gelato, K. A.; Fernández-Montalván, A.; Siegel, S.; Haendler, B. Targeting BET Bromodomains for Cancer Treatment. *Epigenomics*. 2015. https://doi.org/10.2217/epi.14.91.

(477) Tomaselli, D.; Lucidi, A.; Rotili, D.; Mai, A. Epigenetic Polypharmacology: A New Frontier for Epi-Drug Discovery. *Med. Res. Rev.* **2019**, No. October 2018. https://doi.org/10.1002/med.21600.

(478) Yoo, J.; Choi, S.; Medina-Franco, J. L. Molecular Modeling Studies of the Novel Inhibitors of DNA Methyltransferases SGI-1027 and CBC12: Implications for the Mechanism of Inhibition of DNMTs. *PLoS One* **2013**. https://doi.org/10.1371/journal.pone.0062152.

(479) Fahy, J.; Jeltsch, A.; Arimondo, P. B. DNA Methyltransferase Inhibitors in Cancer: A Chemical and Therapeutic Patent Overview and Selected Clinical Studies. *Expert Opinion on Therapeutic Patents*. 2012. https://doi.org/10.1517/13543776.2012.729579.

(480) Santi, D. V.; Garrett, C. E.; Barr, P. J. On the Mechanism of Inhibition of DNA-Cytosine Methyltransferases by Cytosine Analogs. *Cell*. 1983.

(481) Mai, A.; Massa, S.; Rotili, D.; Cerbara, I.; Valente, S.; Pezzi, R.; Simeoni, S.; Ragna, R. Histone Deacetylation in Epigenetics: An Attractive Target for Anticancer Therapy. *Medicinal Research Reviews*. 2005. https://doi.org/10.1002/med.20024.

(482) Faria Freitas, M.; Cuendet, M.; Bertrand, P. HDAC Inhibitors: A 2013–2017 Patent Survey. *Expert Opinion on Therapeutic Patents*. 2018. https://doi.org/10.1080/13543776.2018.1459568.

(483) Zwergel, C.; Valente, S.; Jacob, C.; Mai, A. Emerging Approaches for Histone Deacetylase Inhibitor Drug Discovery. *Expert Opinion on Drug Discovery*. 2015. https://doi.org/10.1517/17460441.2015.1038236.

(484) Stazi, G.; Zwergel, C.; Mai, A.; Valente, S. EZH2 Inhibitors: A Patent Review (2014-2016). *Expert Opinion on Therapeutic Patents*. 2017. https://doi.org/10.1080/13543776.2017.1316976.

(485) Fioravanti, R.; Stazi, G.; Zwergel, C.; Valente, S.; Mai, A. Six Years (2012–2018) of Researches on Catalytic EZH2 Inhibitors: The Boom of the 2-Pyridone Compounds. *Chemical Record*. 2018. https://doi.org/10.1002/tcr.201800091.

(486) Kaniskan, H. Ü.; Konze, K. D.; Jin, J. Selective Inhibitors of Protein Methyltransferases. *J. Med. Chem.* **2015**. https://doi.org/10.1021/jm501234a.

(487) Stein, E. M.; Garcia-Manero, G.; Rizzieri, D. A.; Tibes, R.; Berdeja, J. G.; Savona, M. R.; Jongen-Lavrenic, M.; Altman, J. K.; Thomson, B.; Blakemore, S. J.; et al. The DOT1L Inhibitor Pinometostat Reduces H3K79 Methylation and Has Modest Clinical Activity in Adult Acute Leukemia. *Blood* **2018**. https://doi.org/10.1182/blood-2017-12-818948.

(488) Campbell, C. T.; Haladyna, J. N.; Drubin, D. A.; Thomson, T. M.; Maria, M. J.; Yamauchi, T.; Waters, N. J.; Olhava, E. J.; Pollock, R. M.; Smith, J. J.; et al. Mechanisms of Pinometostat (EPZ-5676) Treatment–Emergent Resistance in MLL-Rearranged Leukemia. *Mol. Cancer Ther.* **2017**.

https://doi.org/10.1158/1535-7163.MCT-16-0693.

(489) Binda, C.; Valente, S.; Romanenghi, M.; Pilotto, S.; Cirilli, R.; Karytinos, A.; Ciossani, G.; Botrugno, O. A.; Forneris, F.; Tardugno, M.; et al. Biochemical, Structural, and Biological Evaluation of Tranylcypromine Derivatives as Inhibitors of Histone Demethylases LSD1 and LSD2. *J. Am. Chem. Soc.* **2010**. https://doi.org/10.1021/ja101557k.

(490) Zheng, Y. C.; Ma, J.; Wang, Z.; Li, J.; Jiang, B.; Zhou, W.; Shi, X.; Wang, X.; Zhao, W.; Liu, H. M. A Systematic Review of Histone Lysine-Specific Demethylase 1 and Its Inhibitors. *Med. Res. Rev.* **2015**. https://doi.org/10.1002/med.21350.

(491) Rotili, D.; Mai, A. Targeting Histone Demethylases: A New Avenue for the Fight against Cancer. *Genes and Cancer* **2011**. https://doi.org/10.1177/1947601911417976.

(492) Gerhart, S. V.; Kellner, W. A.; Thompson, C.; Pappalardi, M. B.; Zhang, X. P.; Montes De Oca, R.; Penebre, E.; Duncan, K.; Boriack-Sjodin, A.; Le, B.; et al. Activation of the P53-MDM4 Regulatory Axis Defines the Anti-Tumour Response to PRMT5 Inhibition through Its Role in Regulating Cellular Splicing. *Sci. Rep.* **2018**. https://doi.org/10.1038/s41598-018-28002-y.

(493) Brand, M.; Measures, A. M.; Wilson, B. G.; Cortopassi, W. A.; Alexander, R.; Höss, M.; Hewings, D. S.; Rooney, T. P. C.; Paton, R. S.; Conway, S. J. Small Molecule Inhibitors of Bromodomain - Acetyl-Lysine Interactions. *ACS Chemical Biology*. 2015. https://doi.org/10.1021/cb500996u.

(494) Filippakopoulos, P.; Knapp, S. Targeting Bromodomains: Epigenetic Readers of Lysine Acetylation. *Nature Reviews Drug Discovery*. 2014. https://doi.org/10.1038/nrd4286.

(495) Brown, R.; Curry, E.; Magnani, L.; Wilhelm-Benartzi, C. S.; Borley, J. Poised Epigenetic States and Acquired Drug Resistance in Cancer. *Nature Reviews Cancer*. 2014. https://doi.org/10.1038/nrc3819.

(496) Easwaran, H.; Tsai, H. C.; Baylin, S. B. Cancer Epigenetics: Tumor Heterogeneity, Plasticity of Stem-like States, and Drug Resistance. *Molecular Cell*. 2014. https://doi.org/10.1016/j.molcel.2014.05.015.

(497) Zeller, C.; Brown, R. Therapeutic Modulation of Epigenetic Drivers of Drug Resistance in Ovarian Cancer. *Therapeutic Advances in Medical Oncology*. 2010. https://doi.org/10.1177/1758834010375759.

(498) Peixoto, P.; Renaude, E.; Boyer-Guittaut, M.; Hervouet, E. Epigenetics, a Key Player of Immunotherapy Resistance. *Cancer Drug Resist.* **2018**. https://doi.org/10.20517/cdr.2018.17.

(499) Biersack, B. Alkylating Anticancer Agents and Their Relations to MicroRNAs. *Cancer Drug Resist.* **2019**, 1–17. https://doi.org/10.20517/cdr.2019.09.

(500) White, J. C.; Pucci, P.; Crea, F. The Role of Histone Lysine Demethylases in Cancer Cells' Resistance to Tyrosine Kinase Inhibitors. *Cancer Drug Resist.* **2019**, 20517. https://doi.org/10.20517/cdr.2019.16.

(501) Ponnusamy, L.; Mahalingaiah, P. K. S.; Chang, Y.-W.; Singh, K. P. Role of Cellular Reprogramming and Epigenetic Dysregulation in Acquired Chemoresistance in Breast Cancer. *Cancer Drug Resist.* **2019**. https://doi.org/10.20517/cdr.2018.11.

(502) Jia, Z.-H.; Wang, X.-G.; Zhang, H. Overcome Cancer Drug Resistance by Targeting Epigenetic Modifications of Centrosome. *Cancer Drug Resist.* **2019**. https://doi.org/10.20517/cdr.2018.010.

(503) Schwarzenbach, H.; Gahan, P. B. Resistance to Cis- and Carboplatin Initiated by Epigenetic Changes in Ovarian Cancer Patients. *Cancer Drug Resist.* **2019**.

https://doi.org/10.20517/cdr.2019.010.

(504) Meyer, L. K.; Hermiston, M. L. The Epigenome in Pediatric Acute Lymphoblastic Leukemia: Drug Resistance and Therapeutic Opportunities. *Cancer Drug Resist.* **2019**. https://doi.org/10.20517/cdr.2019.11.

(505) Seno, A.; Mizutani, A.; Aizawa, K.; Onoue, R.; Masuda, J.; Ochi, N.; Taniguchi, S.; Sota, T.; Hiramoto, Y.; Michiue, T.; et al. Daunorubicin Can Eliminate IPS-Derived Cancer Stem Cells via ICAD/CAD-Independent DNA Fragmentation. *Cancer Drug Resist.* **2019**. https://doi.org/10.20517/cdr.2019.01.

(506) Wilting, R. H.; Dannenberg, J. H. Epigenetic Mechanisms in Tumorigenesis, Tumor Cell Heterogeneity and Drug Resistance. *Drug Resist. Updat.* **2012**. https://doi.org/10.1016/j.drup.2012.01.008.

(507) Benedetti, R.; Conte, M.; Iside, C.; Altucci, L. Epigenetic-Based Therapy: From Single- to Multi-Target Approaches. *International Journal of Biochemistry and Cell Biology*. 2015. https://doi.org/10.1016/j.biocel.2015.10.016.

(508) Chou, T. C. Theoretical Basis, Experimental Design, and Computerized Simulation of Synergism and Antagonism in Drug Combination Studies. *Pharmacological Reviews*. 2006. https://doi.org/10.1124/pr.58.3.10.

(509) Webster, R.; Castellano, J. M.; Onuma, O. K. Putting Polypills into Practice: Challenges and Lessons Learned. *The Lancet*. 2017. https://doi.org/10.1016/S0140-6736(17)30558-5.

(510) Mroz, E. A.; Rocco, J. W. The Challenges of Tumor Genetic Diversity. *Cancer*. 2017. https://doi.org/10.1002/cncr.30430.

(511) Anighoro, A.; Bajorath, J.; Rastelli, G. Polypharmacology: Challenges and Opportunities in Drug Discovery. *Journal of Medicinal Chemistry*. 2014. https://doi.org/10.1021/jm5006463.

(512) Dumbrava, E. I.; Meric-Bernstam, F. Personalized Cancer Therapy- Leveraging a Knowledge Base for Clinical Decision-Making. *Cold Spring Harbor Molecular Case Studies*. 2018. https://doi.org/10.1101/mcs.a001578.

(513) Knight, Z. A.; Lin, H.; Shokat, K. M. Targeting the Cancer Kinome through Polypharmacology. *Nature Reviews Cancer*. 2010. https://doi.org/10.1038/nrc2787.

(514) Kozikowski, A.; Butler, K. Chemical Origins of Isoform Selectivity in Histone Deacetylase Inhibitors. *Curr. Pharm. Des.* **2008**. https://doi.org/10.2174/138161208783885353.

(515) Lai, C. J.; Bao, R.; Tao, X.; Wang, J.; Atoyan, R.; Qu, H.; Wang, D. G.; Yin, L.; Samson, M.; Forrester, J.; et al. CUDC-101, a Multitargeted Inhibitor of Histone Deacetylase, Epidermal Growth Factor Receptor, and Human Epidermal Growth Factor Receptor 2, Exerts Potent Anticancer Activity. *Cancer Res.* **2010**. https://doi.org/10.1158/0008-5472.CAN-09-3360.

(516) Zhang, L.; Zhang, Y.; Mehta, A.; Boufraqech, M.; Davis, S.; Wang, J.; Tian, Z.; Yu, Z.; Boxer, M. B.; Kiefer, J. A.; et al. Dual Inhibition of HDAC and EGFR Signaling with CUDC-101 Induces Potent Suppression of Tumor Growth and Metastasis in Anaplastic Thyroid Cancer. *Oncotarget* **2015**. https://doi.org/10.18632/oncotarget.3268.

(517) Galloway, T. J.; Wirth, L. J.; Colevas, A. D.; Gilbert, J.; Bauman, J. E.; Saba, N. F.; Raben, D.; Mehra, R.; Ma, A. W.; Atoyan, R.; et al. A Phase I Study of CUDC-101, a Multitarget Inhibitor of HDACs, EGFR, and HER2, in Combination with Chemoradiation in Patients with Head and Neck Squamous Cell Carcinoma. *Clin. Cancer Res.* **2015**. https://doi.org/10.1158/1078-0432.CCR-14-2820.

(518) Shimizu, T.; LoRusso, P. M.; Papadopoulos, K. P.; Patnaik, A.; Beeram, M.; Smith, L. S.; Rasco, D. W.; Mays, T. A.; Chambers, G.; Ma, A.; et al. Phase I First-

in-Human Study of CUDC-101, a Multitargeted Inhibitor of HDACs, EGFR, and HER2 in Patients with Advanced Solid Tumors. *Clin. Cancer Res.* **2014**. https://doi.org/10.1158/1078-0432.CCR-14-0570.

(519) Courtney, K. D.; Corcoran, R. B.; Engelman, J. A. The PI3K Pathway as Drug Target in Human Cancer. *Journal of Clinical Oncology*. 2010. https://doi.org/10.1200/JCO.2009.25.3641.

(520) Chen, Y.; Peubez, C.; Smith, V.; Xiong, S.; Kocsis-Fodor, G.; Kennedy, B.; Wagner, S.; Balotis, C.; Jayne, S.; Dyer, M. J. S.; et al. CUDC-907 Blocks Multiple pro-Survival Signals and Abrogates Microenvironment Protection in CLL. *J. Cell. Mol. Med.* **2019**. https://doi.org/10.1111/jcmm.13935.

(521) Sun, K.; Atoyan, R.; Borek, M. A.; Dellarocca, S.; Samson, M. E. S.; Ma, A. W.; Xu, G. X.; Patterson, T.; Tuck, D. P.; Viner, J. L.; et al. Dual HDAC and PI3K Inhibitor CUDC-907 down Regulates MYC and Suppresses Growth of MYC-Dependent Cancers. *Mol. Cancer Ther.* **2017**. https://doi.org/10.1158/1535-7163.MCT-16-0390.

(522) Oki, Y.; Kelly, K. R.; Flinn, I.; Patel, M. R.; Gharavi, R.; Ma, A.; Parker, J.; Hafeez, A.; Tuck, D.; Younes, A. CUDC-907 in Relapsed/Refractory Diffuse Large B-Cell Lymphoma, Including Patients with MYC-Alterations: Results from an Expanded Phase I Trial. *Haematologica* **2017**. https://doi.org/10.3324/haematol.2017.172882.

(523) Rask-Andersen, M.; Zhang, J.; Fabbro, D.; Schiöth, H. B. Advances in Kinase Targeting: Current Clinical Use and Clinical Trials. *Trends in Pharmacological Sciences*. 2014. https://doi.org/10.1016/j.tips.2014.09.007.

(524) Daub, H. Quantitative Proteomics of Kinase Inhibitor Targets and Mechanisms. *ACS Chem. Biol.* **2015**. https://doi.org/10.1021/cb5008794.

(525) Cai, X.; Zhai, H. X.; Wang, J.; Forrester, J.; Qu, H.; Yin, L.; Lai, C. J.; Bao, R.; Qian, C. Discovery of 7-(4-(3-Ethynylphenylamino)-7-Methoxyquinazolin-6-Yloxy)-N- Hydroxyheptanamide (CUDC-101) as a Potent Multi-Acting HDAC, EGFR, and HER2 Inhibitor for the Treatment of Cancer. *J. Med. Chem.* **2010**. https://doi.org/10.1021/jm901453q.

(526) Pei, Y.; Liu, K. W.; Wang, J.; Garancher, A.; Tao, R.; Esparza, L. A.; Maier, D. L.; Udaka, Y. T.; Murad, N.; Morrissy, S.; et al. HDAC and PI3K Antagonists Cooperate to Inhibit Growth of MYC-Driven Medulloblastoma. *Cancer Cell* **2016**. https://doi.org/10.1016/j.ccell.2016.02.011.

(527) Younes, A.; Berdeja, J. G.; Patel, M. R.; Flinn, I.; Gerecitano, J. F.; Neelapu, S. S.; Kelly, K. R.; Copeland, A. R.; Akins, A.; Clancy, M. S.; et al. Safety, Tolerability, and Preliminary Activity of CUDC-907, a First-in-Class, Oral, Dual Inhibitor of HDAC and PI3K, in Patients with Relapsed or Refractory Lymphoma or Multiple Myeloma: An Open-Label, Dose-Escalation, Phase 1 Trial. *Lancet Oncol.* **2016**. https://doi.org/10.1016/S1470-2045(15)00584-7.

(528) Ahuja, N.; Sharma, A. R.; Baylin, S. B. Epigenetic Therapeutics: A New Weapon in the War Against Cancer. *Annu. Rev. Med.* **2016**. https://doi.org/10.1146/annurev-med-111314-035900.

(529) Bondeson, D. P.; Mares, A.; Smith, I. E. D.; Ko, E.; Campos, S.; Miah, A. H.; Mulholland, K. E.; Routly, N.; Buckley, D. L.; Gustafson, J. L.; et al. Catalytic in Vivo Protein Knockdown by Small-Molecule PROTACs. *Nat. Chem. Biol.* **2015**. https://doi.org/10.1038/nchembio.1858.

(530) Toure, M.; Crews, C. M. Small-Molecule PROTACS: New Approaches to Protein Degradation. *Angewandte Chemie - International Edition*. 2016. https://doi.org/10.1002/anie.201507978.

(531) Tinworth, C. P.; Lithgow, H.; Churcher, I. Small Molecule-Mediated Protein

Knockdown as a New Approach to Drug Discovery. *MedChemComm*. 2016. https://doi.org/10.1039/c6md00347h.

(532) Neklesa, T. K.; Winkler, J. D.; Crews, C. M. Targeted Protein Degradation by PROTACs. *Pharmacology and Therapeutics*. 2017. https://doi.org/10.1016/j.pharmthera.2017.02.027.

(533) Collins, I.; Wang, H.; Caldwell, J. J.; Chopra, R. Chemical Approaches to Targeted Protein Degradation through Modulation of the Ubiquitin-Proteasome Pathway. *Biochemical Journal*. 2017. https://doi.org/10.1042/BCJ20160762.

(534) Itoh, Y. Chemical Protein Degradation Approach and Its Application to Epigenetic Targets. *Chemical Record*. 2018. https://doi.org/10.1002/tcr.201800032.

(535) Guo, J.; Liu, J.; Wei, W. Degrading Proteins in Animals: "PROTAC"Tion Goes in Vivo. *Cell Research*. 2019. https://doi.org/10.1038/s41422-019-0144-9.

(536) An, S.; Fu, L. Small-Molecule PROTACs: An Emerging and Promising Approach for the Development of Targeted Therapy Drugs. *EBioMedicine*. 2018. https://doi.org/10.1016/j.ebiom.2018.09.005.

(537) Zou, Y.; Ma, D.; Wang, Y. The PROTAC Technology in Drug Development. *Cell Biochem. Funct.* **2019**, *37* (1), 21–30. https://doi.org/10.1002/cbf.3369.

(538) Dang, C. V; Reddy, E. P.; Shokat, K. M.; Soucek, L. Drugging the "undruggable" Cancer Targets What Would You Say Are the Key so-Called Undruggable Targets in Cancer (and Why)? HHS Public Access. *Nat Rev Cancer* **2017**. https://doi.org/10.1038/nrc.2017.36.

(539) Galdeano, C.; Gadd, M. S.; Soares, P.; Scaffidi, S.; Van Molle, I.; Birced, I.; Hewitt, S.; Dias, D. M.; Ciulli, A. Structure-Guided Design and Optimization of Small Molecules Targeting the Protein-Protein Interaction between the von Hippel-Lindau (VHL) E3 Ubiquitin Ligase and the Hypoxia Inducible Factor (HIF) Alpha Subunit with in Vitro Nanomolar Affinities. *J. Med. Chem.* **2014**. https://doi.org/10.1021/jm5011258.

(540) Crew; Andrew P.; et al. Compounds and Methods for the Targeted Degradation of Androgen Receptor. US2018/99940, 2018.

(541) Girardini, M.; Maniaci, C.; Hughes, S. J.; Testa, A.; Ciulli, A. Cereblon versus VHL: Hijacking E3 Ligases against Each Other Using PROTACs. *Bioorganic Med. Chem.* **2019**, *27* (12), 2466–2479. https://doi.org/10.1016/j.bmc.2019.02.048.

(542) Hughes, S. J.; Ciulli, A. Molecular Recognition of Ternary Complexes: A New Dimension in the Structure-Guided Design of Chemical Degraders. *Essays in Biochemistry*. 2017. https://doi.org/10.1042/EBC20170041.

(543) Jaakkola, P.; Mole, D. R.; Tian, Y. M.; Wilson, M. I.; Gielbert, J.; Gaskell, S. J.; Von Kriegsheim, A.; Hebestreit, H. F.; Mukherji, M.; Schofield, C. J.; et al. Targeting of HIF-α to the von Hippel-Lindau Ubiquitylation Complex by O 2 -Regulated Prolyl Hydroxylation. *Science (80-.)*. **2001**. https://doi.org/10.1126/science.1059796.

(544) Hon, W. C.; Wilson, M. I.; Harlos, K.; Claridge, T. D. W.; Schofield, C. J.; Pugh, C. W.; Maxwell, P. H.; Ratcliffe, P. J.; Stuart, D. I.; Jones, E. Y. Structural Basis for the Recognition of Hydroxyproline in HIF-1α by PVHL. *Nature* **2002**. https://doi.org/10.1038/nature00767.

(545) Min, J. H.; Yang, H.; Ivan, M.; Gertler, F.; Kaelin, W. G.; Pavietich, N. P. Structure of an HIF-1α-PVHL Complex: Hydroxyproline Recognition in Signaling. *Science (80-.)*. **2002**. https://doi.org/10.1126/science.1073440.

(546) Wu, D.; Potluri, N.; Lu, J.; Kim, Y.; Rastinejad, F. Structural Integration in Hypoxia-Inducible Factors. *Nature* **2015**. https://doi.org/10.1038/nature14883.

(547) Kaelin, W. G.; Ratcliffe, P. J. Oxygen Sensing by Metazoans: The Central Role of the HIF Hydroxylase Pathway. *Molecular Cell*. 2008.

https://doi.org/10.1016/j.molcel.2008.04.009.

(548)   Schofield, C. J.; Ratcliffe, P. J. Oxygen Sensing by HIF Hydroxylases. *Nature Reviews Molecular Cell Biology*. 2004. https://doi.org/10.1038/nrm1366.

(549)   Semenza, G. L. Life with Oxygen. *Science*. 2007. https://doi.org/10.1126/science.1147949.

(550)   Soares, P.; Gadd, M. S.; Frost, J.; Galdeano, C.; Ellis, L.; Epemolu, O.; Rocha, S.; Read, K. D.; Ciulli, A. Group-Based Optimization of Potent and Cell-Active Inhibitors of the von Hippel-Lindau (VHL) E3 Ubiquitin Ligase: Structure-Activity Relationships Leading to the Chemical Probe (2S,4R)-1-((S)-2-(1-Cyanocyclopropanecarboxamido)-3,3-Dimethylbutanoyl)-4-Hydr. *J. Med. Chem.* **2018**, *61* (2), 599–618. https://doi.org/10.1021/acs.jmedchem.7b00675.

(551)   Buckley, D. L.; Van Molle, I.; Gareiss, P. C.; Tae, H. S.; Michel, J.; Noblin, D. J.; Jorgensen, W. L.; Ciulli, A.; Crews, C. M. Targeting the von Hippel-Lindau E3 Ubiquitin Ligase Using Small Molecules to Disrupt the VHL/HIF-1α Interaction. *J. Am. Chem. Soc.* **2012**. https://doi.org/10.1021/ja209924v.

(552)   Frost, J.; Galdeano, C.; Soares, P.; Gadd, M. S.; Grzes, K. M.; Ellis, L.; Epemolu, O.; Shimamura, S.; Bantscheff, M.; Grandi, P.; et al. Potent and Selective Chemical Probe of Hypoxic Signalling Downstream of HIF-α Hydroxylation via VHL Inhibition. *Nat. Commun.* **2016**. https://doi.org/10.1038/ncomms13312.

(553)   Briggs, C. R. S.; O'Hagan, D.; Howard, J. A. K.; Yufit, D. S. The C-F Bond as a Tool in the Conformational Control of Amides. *J. Fluor. Chem.* **2003**. https://doi.org/10.1016/S0022-1139(02)00243-9.

(554)   Banks, J. W.; Batsanov, A. S.; Howard, J. A. K.; O'Hagan, D.; Rzepa, H. S.; Martin-Santamaria, S. The Preferred Conformation of α-Fluoroamides. *J. Chem. Soc. Perkin Trans. 2* **1999**. https://doi.org/10.1039/a907452j.

(555)   Maniaci, C.; Hughes, S. J.; Testa, A.; Chen, W.; Lamont, D. J.; Rocha, S.; Alessi, D. R.; Romeo, R.; Ciulli, A. Homo-PROTACs: Bivalent Small-Molecule Dimerizers of the VHL E3 Ubiquitin Ligase to Induce Self-Degradation. *Nat. Commun.* **2017**. https://doi.org/10.1038/s41467-017-00954-1.

(556)   Zoppi, V.; Hughes, S. J.; Maniaci, C.; Testa, A.; Gmaschitz, T.; Wieshofer, C.; Koegl, M.; Riching, K. M.; Daniels, D. L.; Spallarossa, A.; et al. Iterative Design and Optimization of Initially Inactive Proteolysis Targeting Chimeras (PROTACs) Identify VZ185 as a Potent, Fast, and Selective von Hippel-Lindau (VHL) Based Dual Degrader Probe of BRD9 and BRD7. *J. Med. Chem.* **2019**, *62* (2), 699–726. https://doi.org/10.1021/acs.jmedchem.8b01413.

(557)   Gadd, M. S.; Testa, A.; Lucas, X.; Chan, K. H.; Chen, W.; Lamont, D. J.; Zengerle, M.; Ciulli, A. Structural Basis of PROTAC Cooperative Recognition for Selective Protein Degradation. *Nat. Chem. Biol.* **2017**. https://doi.org/10.1038/nchembio.2329.

(558)   Chan, K. H.; Zengerle, M.; Testa, A.; Ciulli, A. Impact of Target Warhead and Linkage Vector on Inducing Protein Degradation: Comparison of Bromodomain and Extra-Terminal (BET) Degraders Derived from Triazolodiazepine (JQ1) and Tetrahydroquinoline (I-BET726) BET Inhibitor Scaffolds. *J. Med. Chem.* **2018**. https://doi.org/10.1021/acs.jmedchem.6b01912.

(559)   Remillard, D.; Buckley, D. L.; Paulk, J.; Brien, G. L.; Sonnett, M.; Seo, H. S.; Dastjerdi, S.; Wühr, M.; Dhe-Paganon, S.; Armstrong, S. A.; et al. Degradation of the BAF Complex Factor BRD9 by Heterobifunctional Ligands. *Angew. Chemie - Int. Ed.* **2017**. https://doi.org/10.1002/anie.201611281.

(560)   Bobbin, M. L.; Rossi, J. J. RNA Interference (RNAi)-Based Therapeutics: Delivering on the Promise? *Annu. Rev. Pharmacol. Toxicol.* **2016**, *56* (1), 103–122. https://doi.org/10.1146/annurev-pharmtox-010715-103633.

(561) Zengerle, M.; Chan, K. H.; Ciulli, A. Selective Small Molecule Induced Degradation of the BET Bromodomain Protein BRD4. *ACS Chem. Biol.* **2015**. https://doi.org/10.1021/acschembio.5b00216.

(562) Winter, G. E.; Buckley, D. L.; Paulk, J.; Roberts, J. M.; Souza, A.; Dhe-Paganon, S.; Bradner, J. E. Phthalimide Conjugation as a Strategy for in Vivo Target Protein Degradation. *Science (80-.).* **2015**. https://doi.org/10.1126/science.aab1433.

(563) Lu, J.; Qian, Y.; Altieri, M.; Dong, H.; Wang, J.; Raina, K.; Hines, J.; Winkler, J. D.; Crew, A. P.; Coleman, K.; et al. Hijacking the E3 Ubiquitin Ligase Cereblon to Efficiently Target BRD4. *Chem. Biol.* **2015**. https://doi.org/10.1016/j.chembiol.2015.05.009.

(564) Sakamoto, K. M.; Kim, K. B.; Kumagai, A.; Mercurio, F.; Crews, C. M.; Deshaies, R. J. Protacs: Chimeric Molecules That Target Proteins to the Skp1-Cullin-F Box Complex for Ubiquitination and Degradation. *Proc. Natl. Acad. Sci. U. S. A.* **2001**. https://doi.org/10.1073/pnas.141230798.

(565) Frances Potjewyd, Anne-Marie W. Turner, Joshua Beri, Justin M. Rectenwald, Jacqueline L. Norris-Drouin, Stephanie H. Cholensky, David M. Margolis, Kenneth H. Pearce, Laura E. Herring, L. I. J. Degradation of Polycomb Repressive Complex 2 with an EED-Targeted Bivalent Chemical Degrader. *BIORXYV* **2019**. https://doi.org/10.1101/676965.

(566) W., Q.; K., Z.; J., G.; Y., H.; Y., W.; H., Z.; M., Z.; J., Z.; Z., Y.; L., L.; et al. An Allosteric PRC2 Inhibitor Targeting the H3K27me3 Binding Pocket of EED. *Nature Chemical Biology*. 2017.

(567) Valenzuela-Fernández, A.; Cabrero, J. R.; Serrador, J. M.; Sánchez-Madrid, F. HDAC6: A Key Regulator of Cytoskeleton, Cell Migration and Cell-Cell Interactions. *Trends in Cell Biology*. 2008. https://doi.org/10.1016/j.tcb.2008.04.003.

(568) Yang, K.; Song, Y.; Xie, H.; Wu, H.; Wu, Y. T.; Leisten, E. D.; Tang, W. Development of the First Small Molecule Histone Deacetylase 6 (HDAC6) Degraders. *Bioorganic Med. Chem. Lett.* **2018**. https://doi.org/10.1016/j.bmcl.2018.05.057.

(569) Jang, S.; Yu, X. M.; Odorico, S.; Clark, M.; Jaskula-Sztul, R.; Schienebeck, C. M.; Kupcho, K. R.; Harrison, A. D.; Winston-Mcpherson, G. N.; Tang, W.; et al. Novel Analogs Targeting Histone Deacetylase Suppress Aggressive Thyroid Cancer Cell Growth and Induce Re-Differentiation. *Cancer Gene Ther.* **2015**. https://doi.org/10.1038/cgt.2015.37.

(570) Jaskula-Sztul, R.; Eide, J.; Tesfazghi, S.; Dammalapati, A.; Harrison, A. D.; Yu, X. M.; Scheinebeck, C.; Winston-McPherson, G.; Kupcho, K. R.; Robers, M. B.; et al. Tumor-Suppressor Role of Notch3 in Medullary Thyroid Carcinoma Revealed by Genetic and Pharmacological Induction. *Mol. Cancer Ther.* **2015**. https://doi.org/10.1158/1535-7163.MCT-14-0073.

(571) Mori, T.; Ito, T.; Liu, S.; Ando, H.; Sakamoto, S.; Yamaguchi, Y.; Tokunaga, E.; Shibata, N.; Handa, H.; Hakoshima, T. Structural Basis of Thalidomide Enantiomer Binding to Cereblon. *Sci. Rep.* **2018**. https://doi.org/10.1038/s41598-018-19202-7.

(572) Bondeson, D. P.; Smith, B. E.; Burslem, G. M.; Buhimschi, A. D.; Hines, J.; Jaime-Figueroa, S.; Wang, J.; Hamman, B. D.; Ishchenko, A.; Crews, C. M. Lessons in PROTAC Design from Selective Degradation with a Promiscuous Warhead. *Cell Chem. Biol.* **2018**. https://doi.org/10.1016/j.chembiol.2017.09.010.

(573) Zhou, B.; Hu, J.; Xu, F.; Chen, Z.; Bai, L.; Fernandez-Salas, E.; Lin, M.; Liu, L.; Yang, C. Y.; Zhao, Y.; et al. Discovery of a Small-Molecule Degrader of Bromodomain and Extra-Terminal (BET) Proteins with Picomolar Cellular

Potencies and Capable of Achieving Tumor Regression. *J. Med. Chem.* **2018**. https://doi.org/10.1021/acs.jmedchem.6b01816.

(574) An, Z.; Lv, W.; Su, S.; Wu, W.; Rao, Y. Developing Potent PROTACs Tools for Selective Degradation of HDAC6 Protein. *Protein Cell* **2019**, *10* (8), 606–609. https://doi.org/10.1007/s13238-018-0602-z.

(575) Bergman, J. A.; Woan, K.; Perez-Villarroel, P.; Villagra, A.; Sotomayor, E. M.; Kozikowski, A. P. Selective Histone Deacetylase 6 Inhibitors Bearing Substituted Urea Linkers Inhibit Melanoma Cell Growth. *J. Med. Chem.* **2012**. https://doi.org/10.1021/jm301098e.

(576) Pais, T. F.; Szego, É. M.; Marques, O.; Miller-Fleming, L.; Antas, P.; Guerreiro, P.; De Oliveira, R. M. H.; Kasapoglu, B.; Outeiro, T. F. The NAD-Dependent Deacetylase Sirtuin 2 Is a Suppressor of Microglial Activation and Brain Inflammation. *EMBO J.* **2013**. https://doi.org/10.1038/emboj.2013.200.

(577) Bael, N. S.; Swanson, M. J.; Vassilev, A.; Howard, B. H. Human Histone Deacetylase SIRT2 Interacts with the Homeobox Transcription Factor HOXA10. *J. Biochem.* **2004**. https://doi.org/10.1093/jb/mvh084.

(578) Park, S. H.; Zhu, Y.; Ozden, O.; Kim, H. S.; Jiang, H.; Deng, C. X.; Gius, D.; Vassilopoulos, A. SIRT2 Is a Tumor Suppressor That Connects Aging, Acetylome, Cell Cycle Signaling, and Carcinogenesis. *Translational Cancer Research*. 2012. https://doi.org/10.3978/j.issn.2218-676X.2012.05.01.

(579) Kim, H. S.; Vassilopoulos, A.; Wang, R. H.; Lahusen, T.; Xiao, Z.; Xu, X.; Li, C.; Veenstra, T. D.; Li, B.; Yu, H.; et al. SIRT2 Maintains Genome Integrity and Suppresses Tumorigenesis through Regulating APC/C Activity. *Cancer Cell* **2011**. https://doi.org/10.1016/j.ccr.2011.09.004.

(580) Schiedel, M.; Herp, D.; Hammelmann, S.; Swyter, S.; Lehotzky, A.; Robaa, D.; Oláh, J.; Ovádi, J.; Sippl, W.; Jung, M. Chemically Induced Degradation of Sirtuin 2 (Sirt2) by a Proteolysis Targeting Chimera (PROTAC) Based on Sirtuin Rearranging Ligands (SirReals). *J. Med. Chem.* **2018**. https://doi.org/10.1021/acs.jmedchem.6b01872.

(581) Belkina, A. C.; Denis, G. V. BET Domain Co-Regulators in Obesity, Inflammation and Cancer. *Nature Reviews Cancer*. 2012. https://doi.org/10.1038/nrc3256.

(582) Raina, K.; Lu, J.; Qian, Y.; Altieri, M.; Gordon, D.; Rossi, A. M. K.; Wang, J.; Chen, X.; Dong, H.; Siu, K.; et al. PROTAC-Induced BET Protein Degradation as a Therapy for Castration-Resistant Prostate Cancer. *Proc. Natl. Acad. Sci. U. S. A.* **2016**. https://doi.org/10.1073/pnas.1521738113.

(583) Gosmini, R.; Nguyen, V. L.; Toum, J.; Simon, C.; Brusq, J. M. G.; Krysa, G.; Mirguet, O.; Riou-Eymard, A. M.; Boursier, E. V.; Trottet, L.; et al. The Discovery of I-BET726 (GSK1324726A), a Potent Tetrahydroquinoline ApoA1 up-Regulator and Selective BET Bromodomain Inhibitor. *J. Med. Chem.* **2014**. https://doi.org/10.1021/jm5010539.

(584) Wyce, A.; Ganji, G.; Smitheman, K. N.; Chung, C. wa; Korenchuk, S.; Bai, Y.; Barbash, O.; Le, B. C.; Craggs, P. D.; McCabe, M. T.; et al. BET Inhibition Silences Expression of MYCN and BCL2 and Induces Cytotoxicity in Neuroblastoma Tumor Models. *PLoS One* **2013**. https://doi.org/10.1371/journal.pone.0072967.

(585) Qin, C.; Hu, Y.; Zhou, B.; Fernandez-Salas, E.; Yang, C. Y.; Liu, L.; McEachern, D.; Przybranowski, S.; Wang, M.; Stuckey, J.; et al. Discovery of QCA570 as an Exceptionally Potent and Efficacious Proteolysis Targeting Chimera (PROTAC) Degrader of the Bromodomain and Extra-Terminal (BET) Proteins Capable of Inducing Complete and Durable Tumor Regression. *J. Med. Chem.* **2018**. https://doi.org/10.1021/acs.jmedchem.8b00506.

(586) N.H., T.; N.C.O., T.; R.K., P.; Humphreys P.G. AO - Humphreys, P. G. O. http://orcid. org/000.-0002-8614-7155. Clinical Progress and Pharmacology of Small Molecule Bromodomain Inhibitors. *Curr. Opin. Chem. Biol.* **2016**.

(587) Zoppi, V.; Hughes, S. J.; Maniaci, C.; Testa, A.; Gmaschitz, T.; Wieshofer, C.; Koegl, M.; Riching, K. M.; Daniels, D. L.; Spallarossa, A.; et al. Iterative Design and Optimization of Initially Inactive Proteolysis Targeting Chimeras (PROTACs) Identify VZ185 as a Potent, Fast, and Selective von Hippel-Lindau (VHL) Based Dual Degrader Probe of BRD9 and BRD7. *J. Med. Chem.* **2019**. https://doi.org/10.1021/acs.jmedchem.8b01413.

(588) Le Douarin, B.; Zechel, C.; Garnier, J. M.; Lutz, Y.; Tora, L.; Pierrat, P.; Heery, D.; Gronemeyer, H.; Chambon, P.; Losson, R. The N-Terminal Part of TIF1, a Putative Mediator of the Ligand-Dependent Activation Function (AF-2) of Nuclear Receptors, Is Fused to B-Raf in the Oncogenic Protein T18. *EMBO J.* **1995**. https://doi.org/10.1002/j.1460-2075.1995.tb07194.x.

(589) Allton, K.; Jain, A. K.; Herz, H. M.; Tsai, W. W.; Sung, Y. J.; Qin, J.; Bergmann, A.; Johnson, R. L.; Barton, M. C. Trim24 Targets Endogenous P53 for Degradation. *Proc. Natl. Acad. Sci. U. S. A.* **2009**. https://doi.org/10.1073/pnas.0813177106.

(590) Tsai, W. W.; Wang, Z.; Yiu, T. T.; Akdemir, K. C.; Xia, W.; Winter, S.; Tsai, C. Y.; Shi, X.; Schwarzer, D.; Plunkett, W.; et al. TRIM24 Links a Non-Canonical Histone Signature to Breast Cancer. *Nature* **2010**. https://doi.org/10.1038/nature09542.

(591) Zhan, Y.; Kost-Alimova, M.; Shi, X.; Leo, E.; Bardenhagen, J. P.; Shepard, H. E.; Appikonda, S.; Vangamudi, B.; Zhao, S.; Tieu, T. N.; et al. Development of Novel Cellular Histone-Binding and Chromatin-Displacement Assays for Bromodomain Drug Discovery. *Epigenetics and Chromatin* **2015**. https://doi.org/10.1186/s13072-015-0026-4.

(592) Gechijian, L. N.; Buckley, D. L.; Lawlor, M. A.; Reyes, J. M.; Paulk, J.; Ott, C. J.; Winter, G. E.; Erb, M. A.; Scott, T. G.; Xu, M.; et al. Functional TRIM24 Degrader via Conjugation of Ineffectual Bromodomain and VHL Ligands Article. *Nat. Chem. Biol.* **2018**. https://doi.org/10.1038/s41589-018-0010-y.

(593) Nagy, Z.; Tora, L. Distinct GCN5/PCAF-Containing Complexes Function as Co-Activators and Are Involved in Transcription Factor and Global Histone Acetylation. *Oncogene* **2007**, *26* (37), 5341–5357. https://doi.org/10.1038/sj.onc.1210604.

(594) Sun, X. J.; Man, N.; Tan, Y.; Nimer, S. D.; Wang, L. The Role of Histone Acetyltransferases in Normal and Malignant Hematopoiesis. *Frontiers in Oncology*. 2015. https://doi.org/10.3389/fonc.2015.00108.

(595) Mateo, F.; Vidal-Laliena, M.; Pujol, M. J.; Bachs, O. Acetylation of Cyclin A: A New Cell Cycle Regulatory Mechanism. *Biochemical Society Transactions*. 2010. https://doi.org/10.1042/BST0380083.

(596) Li, P.; Zheng, Y.; Chen, X. Drugs for Autoimmune Inflammatory Diseases: From Small Molecule Compounds to Anti-TNF Biologics. *Frontiers in Pharmacology*. 2017. https://doi.org/10.3389/fphar.2017.00460.

(597) Tanaka, T.; Narazaki, M.; Kishimoto, T. Immunotherapeutic Implications of IL-6 Blockade for Cytokine Storm. *Immunotherapy*. 2016. https://doi.org/10.2217/imt-2016-0020.

(598) Humphreys, P. G.; Bamborough, P.; Chung, C. W.; Craggs, P. D.; Gordon, L.; Grandi, P.; Hayhow, T. G.; Hussain, J.; Jones, K. L.; Lindon, M.; et al. Discovery of a Potent, Cell Penetrant, and Selective P300/CBP-Associated Factor (PCAF)/General Control Nonderepressible 5 (GCN5) Bromodomain Chemical

Probe. *J. Med. Chem.* **2017**. https://doi.org/10.1021/acs.jmedchem.6b01566.

(599) Bassi, Z. I.; Fillmore, M. C.; Miah, A. H.; Chapman, T. D.; Maller, C.; Roberts, E. J.; Davis, L. C.; Lewis, D. E.; Galwey, N. W.; Waddington, K. E.; et al. Modulating PCAF/GCN5 Immune Cell Function through a PROTAC Approach. *ACS Chem. Biol.* **2018**, *13* (10), 2862–2867. https://doi.org/10.1021/acschembio.8b00705.

(600) Deshaies, R. J. Protein Degradation: Prime Time for PROTACs. *Nature Chemical Biology*. 2015. https://doi.org/10.1038/nchembio.1887.

(601) Huang, G.; Zhu, G. Sirtuin-4 (SIRT4), a Therapeutic Target with Oncogenic and Tumor-Suppressive Activity in Cancer. *Onco. Targets. Ther.* **2018**, *11*, 3395–3400. https://doi.org/10.2147/OTT.S157724.

(602) Bonkowski, M. S.; Sinclair, D. A. Slowing Ageing by Design: The Rise of NAD+ and Sirtuin-Activating Compounds. *Nature Reviews Molecular Cell Biology*. 2016. https://doi.org/10.1038/nrm.2016.93.

(603) Anderson, K. A.; Madsen, A. S.; Olsen, C. A.; Hirschey, M. D. Metabolic Control by Sirtuins and Other Enzymes That Sense NAD+, NADH, or Their Ratio. *Biochimica et Biophysica Acta - Bioenergetics*. 2017. https://doi.org/10.1016/j.bbabio.2017.09.005.

(604) Liu, C.; Zhu, X.; Zhang, P.; Yang, H.; Zhu, C.; Fu, H. Axially Chiral Cyclic Diphosphine Ligand-Enabled Palladium-Catalyzed Intramolecular Asymmetric Hydroarylation. *iScience* **2018**. https://doi.org/10.1016/j.isci.2018.11.018.

(605) Tang, S.; Xie, X.; Wang, X.; He, L.; Xu, K.; She, X. Concise Total Syntheses of (+)-Strictifolione and (6 R)-6-[(4 R,6 R)-4,6-Dihydroxy-10-Phenyldec-1-Enyl]-5,6-Dihydro-2 H -Pyran-2-One. *J. Org. Chem.* **2010**. https://doi.org/10.1021/jo101875w.

(606) Chen, Lei; Sun, Guodong; Han, Xiaodong; Li, Shun; Zeng, Jiebin; Wang, Zhongqing; Luo, Z. Sacubitril Intermediate and Preparation Method Thereof. US 20180362439 A1 20181220, 2018.

(607) Pivazyan, V. A.; Ghazaryan, E. A.; Shainova, R. S.; Tamazyan, R. A.; Ayvazyan, A. G.; Yengoyan, A. P. Synthesis and Growth Stimulant Properties of 2-Acetyl-3,7-Dimethyl-5H-Thiazolo[3,2-a]Pyrimidin-5-One Derivatives. *J. Chem.* **2017**. https://doi.org/10.1155/2017/8180913.

(608) Qin, H.; Liu, C.; Guo, Y.; Wang, R.; Zhang, J.; Ma, L.; Zhang, Z.; Wang, X.; Cui, Y.; Liu, J. Synthesis and Biological Evaluation of Novel C5 Halogen-Functionalized S-DABO as Potent HIV-1 Non-Nucleoside Reverse Transcriptase Inhibitors. *Bioorganic Med. Chem.* **2010**. https://doi.org/10.1016/j.bmc.2010.03.025.

(609) Mai, A.; Artico, M.; Sbardella, G.; Quartarone, S.; Massa, S.; Loi, A. G.; De Montis, A.; Scintu, F.; Putzolu, M.; La Colla, P. Dihydro(Alkylthio)(Naphthylmethyl)Oxopyrimidines: Novel Non-Nucleoside Reverse Transcriptase Inhibitors of the S-DABO Series. *J. Med. Chem.* **1997**. https://doi.org/10.1021/jm960802y.

(610) Rodriguez, A. L.; Tamrazi, A.; Collins, M. L.; Katzenellenbogen, J. A. Design, Synthesis, and in Vitro Biological Evaluation of Small Molecule Inhibitors of Estrogen Receptor α Coactivator Binding. *J. Med. Chem.* **2004**. https://doi.org/10.1021/jm030404c.

(611) J., L.; Y., Q.; M., A.; H., D.; J., W.; K., R.; J., H.; J.D., W.; A.P., C.; K., C. Hijacking the E3 Ubiquitin Ligase Cereblon to Efficiently Target BRD4. *Chemistry and Biology*. 2015.

(612) Zoppi, V.; Hughes, S. J.; Maniaci, C.; Testa, A.; Gmaschitz, T.; Wieshofer, C.; Koegl, M.; Riching, K. M.; Daniels, D. L.; Spallarossa, A.; et al. Iterative Design

and Optimization of Initially Inactive Proteolysis Targeting Chimeras (PROTACs) Identify VZ185 as a Potent, Fast, and Selective von Hippel-Lindau (VHL) Based Dual Degrader Probe of BRD9 and BRD7. *J. Med. Chem.* **2019**, *62* (2), 699–726. https://doi.org/10.1021/acs.jmedchem.8b01413.

(613) Fang, Y.; Liao, G.; Yu, B. Targeting Histone Lysine Demethylase LSD1/KDM1A as a New Avenue for Cancer Therapy. *Curr. Top. Med. Chem.* **2019**. https://doi.org/10.2174/1568026611911190725094910.

(614) Majello, B.; Gorini, F.; Saccà, C. D.; Amente, S. Expanding the Role of the Histone Lysine-Specific Demethylase Lsd1 in Cancer. *Cancers (Basel).* **2019**. https://doi.org/10.3390/cancers11030324.

(615) Peng, B.; Shi, R.; Jiang, W.; Ding, Y.-H.; Dong, M.-Q.; Zhu, W.-G.; Xu, X. Phosphorylation of LSD1 by PLK1 Promotes Its Chromatin Release during Mitosis. *Cell Biosci.* **2017**. https://doi.org/10.1186/s13578-017-0142-x.

(616) Han, X.; Gui, B.; Xiong, C.; Zhao, L.; Liang, J.; Sun, L.; Yang, X.; Yu, W.; Si, W.; Yan, R.; et al. Destabilizing LSD1 by Jade-2 Promotes Neurogenesis: An Antibraking System in Neural Development. *Mol. Cell* **2014**. https://doi.org/10.1016/j.molcel.2014.06.006.

(617) Feng, J.; Xu, G.; Liu, J.; Zhang, N.; Li, L.; Ji, J.; Zhang, J.; Zhang, L.; Wang, G.; Wang, X.; et al. Phosphorylation of LSD1 at Ser112 Is Crucial for Its Function in Induction of EMT and Metastasis in Breast Cancer. *Breast Cancer Res. Treat.* **2016**. https://doi.org/10.1007/s10549-016-3959-9.

(618) Luo, H.; Shenoy, A. K.; Li, X.; Jin, Y.; Jin, L.; Cai, Q.; Tang, M.; Liu, Y.; Chen, H.; Reisman, D.; et al. MOF Acetylates the Histone Demethylase LSD1 to Suppress Epithelial-to-Mesenchymal Transition. *Cell Rep.* **2016**. https://doi.org/10.1016/j.celrep.2016.05.050.

(619) Amente, S.; Lania, L.; Majello, B. The Histone LSD1 Demethylase in Stemness and Cancer Transcription Programs. *Biochimica et Biophysica Acta - Gene Regulatory Mechanisms.* 2013. https://doi.org/10.1016/j.bbagrm.2013.05.002.

(620) Sehrawat, A.; Gao, L.; Wang, Y.; Bankhead, A.; McWeeney, S. K.; King, C. J.; Schwartzman, J.; Urrutia, J.; Bisson, W. H.; Coleman, D. J.; et al. LSD1 Activates a Lethal Prostate Cancer Gene Network Independently of Its Demethylase Function. *Proc. Natl. Acad. Sci. U. S. A.* **2018**. https://doi.org/10.1073/pnas.1719168115.

(621) Theisen, E. R.; Gajiwala, S.; Bearss, J.; Sorna, V.; Sharma, S.; Janat-Amsbury, M. Reversible Inhibition of Lysine Specific Demethylase 1 Is a Novel Anti-Tumor Strategy for Poorly Differentiated Endometrial Carcinoma. *BMC Cancer* **2014**. https://doi.org/10.1186/1471-2407-14-752.

(622) Fiskus, W.; Sharma, S.; Shah, B.; Portier, B. P.; Devaraj, S. G. T.; Liu, K.; Iyer, S. P.; Bearss, D.; Bhalla, K. N. Highly Effective Combination of LSD1 (KDM1A) Antagonist and Pan-Histone Deacetylase Inhibitor against Human AML Cells. *Leukemia* **2014**. https://doi.org/10.1038/leu.2014.119.

(623) Wu, Y.; Wang, Y.; Yang, X. H.; Kang, T.; Zhao, Y.; Wang, C.; Evers, B. M.; Zhou, B. P. The Deubiquitinase USP28 Stabilizes LSD1 and Confers Stem-Cell-like Traits to Breast Cancer Cells. *Cell Rep.* **2013**. https://doi.org/10.1016/j.celrep.2013.08.030.

(624) Zheng, Y. C.; Yu, B.; Chen, Z. S.; Liu, Y.; Liu, H. M. TCPs: Privileged Scaffolds for Identifying Potent LSD1 Inhibitors for Cancer Therapy. *Epigenomics.* 2016. https://doi.org/10.2217/epi-2015-0002.

(625) Mohammad, H. P.; Smitheman, K. N.; Kamat, C. D.; Soong, D.; Federowicz, K. E.; VanAller, G. S.; Schneck, J. L.; Carson, J. D.; Liu, Y.; Butticello, M.; et al. A DNA Hypomethylation Signature Predicts Antitumor Activity of LSD1 Inhibitors

in SCLC. *Cancer Cell* **2015**. https://doi.org/10.1016/j.ccell.2015.06.002.

(626) Lv, T.; Yuan, D.; Miao, X.; Lv, Y.; Zhan, P.; Shen, X.; Song, Y. Over-Expression of LSD1 Promotes Proliferation, Migration and Invasion in Non-Small Cell Lung Cancer. *PLoS One* **2012**. https://doi.org/10.1371/journal.pone.0035065.

(627) Magliulo, D.; Bernardi, R.; Messina, S. Lysine-Specific Demethylase 1A as a Promising Target in Acute Myeloid Leukemia. *Frontiers in Oncology*. 2018. https://doi.org/10.3389/fonc.2018.00255.

(628) Mould, D. P.; Alli, C.; Bremberg, U.; Cartic, S.; Jordan, A. M.; Geitmann, M.; Maiques-Diaz, A.; McGonagle, A. E.; Somervaille, T. C. P.; Spencer, G. J.; et al. Development of (4-Cyanophenyl)Glycine Derivatives as Reversible Inhibitors of Lysine Specific Demethylase 1. *J. Med. Chem.* **2017**. https://doi.org/10.1021/acs.jmedchem.7b00462.

(629) Tahiliani, M.; Mei, P.; Fang, R.; Leonor, T.; Rutenberg, M.; Shimizu, F.; Li, J.; Rao, A.; Shi, Y. The Histone H3K4 Demethylase SMCX Links REST Target Genes to X-Linked Mental Retardation. *Nature* **2007**. https://doi.org/10.1038/nature05823.

(630) Castermans, D.; Vermeesch, J. R.; Fryns, J. P.; Steyaert, J. G.; Van de Ven, W. J. M.; Creemers, J. W. M.; Devriendt, K. Identification and Characterization of the TRIP8 and REEP3 Genes on Chromosome 10q21.3 as Novel Candidate Genes for Autism. *Eur. J. Hum. Genet.* **2007**. https://doi.org/10.1038/sj.ejhg.5201785.

(631) Laumonnier, F.; Holbert, S.; Ronce, N.; Faravelli, F.; Lenzner, S.; Schwartz, C. E.; Lespinasse, J.; Van Esch, H.; Lacombe, D.; Goizet, C.; et al. Mutations in PHF8 Are Associated with X Linked Mental Retardation and Cleft Lip/Cleft Palate. *J. Med. Genet.* **2005**. https://doi.org/10.1136/jmg.2004.029439.

(632) Qiu, J.; Shi, G.; Jia, Y.; Li, J.; Wu, M.; Li, J.; Dong, S.; Wong, J. The X-Linked Mental Retardation Gene PHF8 Is a Histone Demethylase Involved in Neuronal Differentiation. *Cell Res.* **2010**. https://doi.org/10.1038/cr.2010.81.

(633) Hopkinson, R. J.; Tumber, A.; Yapp, C.; Chowdhury, R.; Aik, W. S.; Che, K. H.; Li, X. S.; Kristensen, J. B. L.; King, O. N. F.; Chan, M. C.; et al. 5-Carboxy-8-Hydroxyquinoline Is a Broad Spectrum 2-Oxoglutarate Oxygenase Inhibitor Which Causes Iron Translocation. *Chem. Sci.* **2013**. https://doi.org/10.1039/c3sc51122g.

(634) Kruidenier, L.; Chung, C. W.; Cheng, Z.; Liddle, J.; Che, K.; Joberty, G.; Bantscheff, M.; Bountra, C.; Bridges, A.; Diallo, H.; et al. A Selective Jumonji H3K27 Demethylase Inhibitor Modulates the Proinflammatory Macrophage Response. *Nature*. 2012. https://doi.org/10.1038/nature11262.

(635) Pattabiraman, D. R.; McGirr, C.; Shakhbazov, K.; Barbier, V.; Krishnan, K.; Mukhopadhyay, P.; Hawthorne, P.; Trezise, A.; Ding, J.; Grimmond, S. M.; et al. Interaction of C-Myb with P300 Is Required for the Induction of Acute Myeloid Leukemia (AML) by Human AML Oncogenes. *Blood* **2014**. https://doi.org/10.1182/blood-2012-02-413187.

(636) Zor, T.; De Guzman, R. N.; Dyson, H. J.; Wright, P. E. Solution Structure of the KIX Domain of CBP Bound to the Transactivation Domain of C-Myb. *J. Mol. Biol.* **2004**. https://doi.org/10.1016/j.jmb.2004.01.038.

(637) Uttarkar, S.; Piontek, T.; Dukare, S.; Schomburg, C.; Schlenke, P.; Berdel, W. E.; Muller-Tidow, C.; Schmidt, T. J.; Klempnauer, K. H. Small-Molecule Disruption of the Myb/P300 Cooperation Targets Acute Myeloid Leukemia Cells. *Mol. Cancer Ther.* **2016**. https://doi.org/10.1158/1535-7163.MCT-16-0185.

(638) Kauppi, M.; Murphy, J. M.; De Graaf, C. A.; Hyland, C. D.; Greig, K. T.; Metcalf, D.; Hilton, A. A.; Nicola, N. A.; Kile, B. T.; Hilton, D. J.; et al. Point Mutation in the Gene Encoding P300 Suppresses Thrombocytopenia in Mpl/Mice. *Blood* **2008**. https://doi.org/10.1182/blood-2007-10-119677.

(639) Papathanasiou, P.; Tunningley, R.; Pattabiraman, D. R.; Ye, P.; Gonda, T. J.; Whittle, B.; Hamilton, A. E.; Cridland, S. O.; Lourie, R.; Perkins, A. C. A Recessive Screen for Genes Regulating Hematopoietic Stem Cells. *Blood* **2010**. https://doi.org/10.1182/blood-2010-04-269951.

(640) Uttarkar, S.; Frampton, J.; Klempnauer, K. H. Targeting the Transcription Factor Myb by Small-Molecule Inhibitors. *Experimental Hematology*. 2017. https://doi.org/10.1016/j.exphem.2016.12.003.

(641) Bowers, E. M.; Yan, G.; Mukherjee, C.; Orry, A.; Wang, L.; Holbert, M. A.; Crump, N. T.; Hazzalin, C. A.; Liszczak, G.; Yuan, H.; et al. Virtual Ligand Screening of the P300/CBP Histone Acetyltransferase: Identification of a Selective Small Molecule Inhibitor. *Chem. Biol.* **2010**. https://doi.org/10.1016/j.chembiol.2010.03.006.

(642) Gao, X. N.; Lin, J.; Ning, Q. Y.; Gao, L.; Yao, Y. S.; Zhou, J. H.; Li, Y. H.; Wang, L. L.; Yu, L. A Histone Acetyltransferase P300 Inhibitor C646 Induces Cell Cycle Arrest and Apoptosis Selectively in AML1-ETO-Positive AML Cells. *PLoS One* **2013**. https://doi.org/10.1371/journal.pone.0055481.

(643) Van Den Bosch, T.; Boichenko, A.; Leus, N. G. J.; Ourailidou, M. E.; Wapenaar, H.; Rotili, D.; Mai, A.; Imhof, A.; Bischoff, R.; Haisma, H. J.; et al. The Histone Acetyltransferase P300 Inhibitor C646 Reduces Pro-Inflammatory Gene Expression and Inhibits Histone Deacetylases. *Biochem. Pharmacol.* **2016**. https://doi.org/10.1016/j.bcp.2015.12.010.

(644) Fang, F.; Li, G.; Jing, M.; Xu, L.; Li, Z.; Li, M.; Yang, C.; Liu, Y.; Qian, G.; Hu, X.; et al. C646 Modulates Inflammatory Response and Antibacterial Activity of Macrophage. *Int. Immunopharmacol.* **2019**. https://doi.org/10.1016/j.intimp.2019.105736.

(645) Morin, R. D.; Mendez-Lago, M.; Mungall, A. J.; Goya, R.; Mungall, K. L.; Corbett, R. D.; Johnson, N. A.; Severson, T. M.; Chiu, R.; Field, M.; et al. Frequent Mutation of Histone-Modifying Genes in Non-Hodgkin Lymphoma. *Nature* **2011**. https://doi.org/10.1038/nature10351.

(646) Morin, R. D.; Johnson, N. A.; Severson, T. M.; Mungall, A. J.; An, J.; Goya, R.; Paul, J. E.; Boyle, M.; Woolcock, B. W.; Kuchenbauer, F.; et al. Somatic Mutations Altering EZH2 (Tyr641) in Follicular and Diffuse Large B-Cell Lymphomas of Germinal-Center Origin. *Nat. Genet.* **2010**, *42* (2), 181–185. https://doi.org/10.1038/ng.518.

(647) Pasqualucci, L.; Trifonov, V.; Fabbri, G.; Ma, J.; Rossi, D.; Chiarenza, A.; Wells, V. A.; Grunn, A.; Messina, M.; Elliot, O.; et al. Analysis of the Coding Genome of Diffuse Large B-Cell Lymphoma. *Nat. Genet.* **2011**. https://doi.org/10.1038/ng.892.

(648) Gan, L.; Yang, Y.; Li, Q.; Feng, Y.; Liu, T.; Guo, W. Epigenetic Regulation of Cancer Progression by EZH2: From Biological Insights to Therapeutic Potential. *Biomarker Research*. 2018. https://doi.org/10.1186/s40364-018-0122-2.

(649) Lee, S. T.; Li, Z.; Wu, Z.; Aau, M.; Guan, P.; Karuturi, R. K. M.; Liou, Y. C.; Yu, Q. Context-Specific Regulation of NF-KB Target Gene Expression by EZH2 in Breast Cancers. *Mol. Cell* **2011**. https://doi.org/10.1016/j.molcel.2011.08.011.

(650) Kim, J.; Lee, Y.; Lu, X.; Song, B.; Fong, K. W.; Cao, Q.; Licht, J. D.; Zhao, J. C.; Yu, J. Polycomb- and Methylation-Independent Roles of EZH2 as a Transcription Activator. *Cell Rep.* **2018**. https://doi.org/10.1016/j.celrep.2018.11.035.

(651) Wilson, B. G.; Roberts, C. W. M. SWI/SNF Nucleosome Remodellers and Cancer. *Nature Reviews Cancer*. 2011. https://doi.org/10.1038/nrc3068.

(652) Kim, K. H.; Kim, W.; Howard, T. P.; Vazquez, F.; Tsherniak, A.; Wu, J. N.; Wang, W.; Haswell, J. R.; Walensky, L. D.; Hahn, W. C.; et al. SWI/SNF-Mutant Cancers

Depend on Catalytic and Non-Catalytic Activity of EZH2. *Nature Medicine*. 2015. https://doi.org/10.1038/nm.3968.

(653) Kim, W.; Bird, G. H.; Neff, T.; Guo, G.; Kerenyi, M. A.; Walensky, L. D.; Orkin, S. H. Targeted Disruption of the EZH2-EED Complex Inhibits EZH2-Dependent Cancer. *Nat. Chem. Biol.* **2013**. https://doi.org/10.1038/nchembio.1331.

(654) Bitler, B. G.; Aird, K. M.; Garipov, A.; Li, H.; Amatangelo, M.; Kossenkov, A. V.; Schultz, D. C.; Liu, Q.; Shih, I. M.; Conejo-Garcia, J. R.; et al. Synthetic Lethality by Targeting EZH2 Methyltransferase Activity in ARID1A-Mutated Cancers. *Nat. Med.* **2015**. https://doi.org/10.1038/nm.3799.

(655) Wang, X.; Cao, W.; Zhang, J.; Yan, M.; Xu, Q.; Wu, X.; Wan, L.; Zhang, Z.; Zhang, C.; Qin, X.; et al. A Covalently Bound Inhibitor Triggers EZH 2 Degradation through CHIP -mediated Ubiquitination . *EMBO J.* **2017**. https://doi.org/10.15252/embj.201694058.

(656) Whitesell, L.; Lindquist, S. L. HSP90 and the Chaperoning of Cancer. *Nature Reviews Cancer*. 2005. https://doi.org/10.1038/nrc1716.

(657) Ferreira, J. V.; Fofo, H.; Bejarano, E.; Bento, C. F.; Ramalho, J. S.; Girao, H.; Pereira, P. STUB1/CHIP Is Required for HIF1A Degradation by Chaperone-Mediated Autophagy. *Autophagy* **2013**. https://doi.org/10.4161/auto.25190.

(658) Baker, T.; Nerle, S.; Pritchard, J.; Zhao, B.; Rivera, V. M.; Garner, A.; Gonzalvez, F. Acquisition of a Single EZH2 D1 Domain Mutation Confers Acquired Resistance to EZH2-Targeted Inhibitors. *Oncotarget* **2015**. https://doi.org/10.18632/oncotarget.5066.

(659) Bisserier, M.; Wajapeyee, N. Mechanisms of Resistance to Ezh2 Inhibitors in Diffuse Large B-Cell Lymphomas. *Blood* **2018**. https://doi.org/10.1182/blood-2017-08-804344.

(660) Gibaja, V.; Shen, F.; Harari, J.; Korn, J.; Ruddy, D.; Saenz-Vash, V.; Zhai, H.; Rejtar, T.; Paris, C. G.; Yu, Z.; et al. Development of Secondary Mutations in Wild-Type and Mutant EZH2 Alleles Cooperates to Confer Resistance to EZH2 Inhibitors. *Oncogene* **2016**. https://doi.org/10.1038/onc.2015.114.

(661) McCabe, M. T.; Ott, H. M.; Ganji, G.; Korenchuk, S.; Thompson, C.; Van Aller, G. S.; Liu, Y.; Pietra, A. Della; LaFrance, L. V.; Mellinger, M.; et al. EZH2 Inhibition as a Therapeutic Strategy for Lymphoma with EZH2-Activating Mutations. *Nature*. 2012. https://doi.org/10.1038/nature11606.

(662) Song, X.; Gao, T.; Wang, N.; Feng, Q.; You, X.; Ye, T.; Lei, Q.; Zhu, Y.; Xiong, M.; Xia, Y.; et al. Selective Inhibition of EZH2 by ZLD1039 Blocks H3K27methylation and Leads to Potent Anti-Tumor Activity in Breast Cancer. *Sci. Rep.* **2016**. https://doi.org/10.1038/srep20864.

(663) Zeng, D.; Liu, M.; Pan, J. Blocking EZH2 Methylation Transferase Activity by GSK126 Decreases Stem Cell-like Myeloma Cells. *Oncotarget* **2017**. https://doi.org/10.18632/oncotarget.13773.

(664) Bratkowski, M.; Yang, X.; Liu, X. An Evolutionarily Conserved Structural Platform for PRC2 Inhibition by a Class of Ezh2 Inhibitors. *Sci. Rep.* **2018**. https://doi.org/10.1038/s41598-018-27175-w.